Synthesis and Study of Long Pyridyl-Endcapped Oligoynes on the Way to Carbyne

by

Yueze Gao

A thesis submitted in partial fulfillment of the requirements for the degree of

Doctor of Philosophy

Department of Chemistry
University of Alberta

Abstract

The versatility of elemental carbon is revealed not only in the formation of diverse structures of organic compounds but also in its all-carbon forms, carbon allotropes, which feature unique properties. During the last 35 years, the discovery and synthesis of new carbon allotropes have made it a reality to uncover the unique properties of these new forms of carbon. The *sp*-carbon allotrope, commonly referred to as carbyne, however, is effectively absent from this list, and intense discussion continues over its very existence. Throughout the past 60 years, oligoynes and polyynes have been targeted as model systems toward carbyne.

This thesis deals with the synthesis, characterization, and properties of pyridyl-endcapped oligo-/polyynes. Chapter 1 introduces recent developments in carbon-rich compounds. Then, this chapter reviews the state-of-the-art synthetic methods for assembling oligo-/polyynes, focusing on the formation of "long" derivatives that are at least the length of an octayne. The synthesis of shorter oligoynes is also briefly discussed with the introduction of commonly used methods, such as the Hay, Eglinton–Galbraith, and Cadiot–Chodkiewicz coupling reactions. Finally, the properties of oligo-/polyynes are summarized and discussed, with the purpose of providing insights into understanding and predicting the characteristics of carbyne.

Chapter 2 focuses on the development of pyridyl-endcapped oligoynes (PEOs), and the fundamental goal has been the use of PEOs as a model to study carbyne. The chemical stabilization of oligoynes by sterically encumbered endgroups, particularly the 3,5-bis(3,5-di-*tert*-butylphenyl)pyridyl group, is key to assemble an extended series of stable oligoynes. Versatile synthetic strategies toward elongation of the *sp*-carbon chains have been developed, resulting in a

series of stable PEOs that consists of as many as 48 contiguous *sp*-carbons. Spectroscopic and X-ray crystallographic analyses show that endgroups influence the properties of oligoyne derivatives, but this effect diminishes as length increases toward the polyyne/carbyne limit. For instance, with UV-vis spectroscopy, molecular symmetry clearly documents the evolution of characteristics from oligoynes to polyynes. The combined experimental data are used to refine predictions for the $D_{\infty h}$ structure of carbyne.

When oligo- and polyynes are formed under Hay conditions, unusual byproducts resulting from the loss of alkyne units from the desired oligo-/polyyne are sometimes observed, particularly in the synthesis of longer derivatives. Chapter 3 deals with a mechanistic study of alkyne loss under the typical oxidative coupling conditions. A pentayne precursor with ^{13}C labelling has been designed and synthesized, and its subsequent coupling reactions are examined. The mass spectrometric and NMR spectroscopic analyses support that the terminal alkyne unit is being removed from the carbon chain during the course of the oxidative coupling reaction. Two plausible mechanisms are provided suggesting pathways that might be responsible for the C–C bond cleavage. Finally, suggestions for methods to avoid/suppress the loss of alkyne unit are discussed.

Chapter 4 deals with the synthesis and characterization of a series of platinum complexes coordinated to the terminal pyridyl groups of PEOs. This chapter provides preliminary results in exploring the relationship between axial chirality and the helical frontier molecular orbitals of oligoynes.

Chapter 5 presents the hierarchical synthesis of three porphyrin and four bisporphyrin derivatives. This strategy relies on the incorporation linkers based on azo moieties appended with

pyridyl and/or acetylenic groups that facilitate axial coordination to Ga- and Ru-metalloporphyrins. These porphyrinic systems allow for a quantitative analysis of the effects of diamagnetic anisotropy (DA) on the ligand, arising from the porphyrin, using ^{1}H NMR spectroscopic and X-ray crystallographic analyses. A simple power-law relationship between the proton chemical shift of ligand protons and distance from the porphyrin core is experimentally outlined, which confirms previous theoretical predictions and shows that the limit of DA is about 2 nm. Photophysical properties of the azo-linked porphyrins are analyzed by UV-vis spectroscopy, showing that appreciable *cis-trans* isomerization is not observed for azo ligands bound only to Ga-porphyrins. Incorporation of Ru-porphyrins to an azo ligand facilitates photoswitching behavior, but the process faces competition from decarbonylation of the Ru-porphyrin, and appreciable switching is only documented for **GaL1Ru**.

Chapter 6 gives a summary and outlook for the topics discussed in this thesis, including a discussion of some future directions. Finally, Chapter 7 provides the experimental details and supporting spectra discussed in this thesis.

Preface

Parts of Chapter 2 of this thesis have been published as Y. Gao, Y. Hou, F. Gordillo Gámez, M. Ferguson, J. Casado, R. R. Tykwinski, *"The loss of endgroup effects in long pyridyl-endcapped oligoynes on the way to carbyne,"* *Nat. Chem.* **2020**, *12*, 1143–1149. R. R. Tykwinski and I wrote the paper with the contribution of J. Casado. R. R. Tykwinski and I designed the molecules. I was responsible for the syntheses and characterization of all the new compounds and carried out all room temperature data collections, thermal analyses, and data analyses. Y. Hou carried out the scale-up syntheses of the precursors of **Py**[2b]** series. J. Casado and F. Gordillo Gámez carried out low temperature absorption and Raman spectroscopy. M. Ferguson conducted X-ray crystallographic characterization and refinement.

Chapter 5 of this thesis has been published as Y. Gao, V. Walter, M. J. Ferguson, Rik R. Tykwinski, *"Hierarchical synthesis, structure, and photophysical properties of gallium- and ruthenium-porphyrins with axially bonded azo dyes,"* *Chem. Eur. J.* **2020** (in press, DOI: 10.1002/chem.202002030). R. R. Tykwinski and I wrote the paper. R. R. Tykwinski, V. Walter, and I designed the molecules. I was responsible for the syntheses and characterization of all the new compounds and carried out all data collections and data analyses. M. Ferguson conducted X-ray crystallographic characterization and refinement.

Chapter 3 of this thesis is my original work, as well as the literature review in Chapter 1. Parts of Chapter 4 of this thesis are a joint project, with the contributions of M. Krempe and J. L. Marshall. These chapters have not been published.

Acknowledgements

the thesis edits. Furthermore, I would like to thank the administrative services at the University of Alberta. Special thanks to Anita Weiler for her professionalism and excellent job in helping me with the move from FAU to U of A.

Finally, I want to thank my wife Dan Yang for her full support, understanding, patience, and love. I need to thank Dan for her professional advice and technological support during my research. Special thanks to my parents and the whole family for their endless support.

Table of Contents

List of Figures

noncovalent bonding with fullerene and b) a PEO endcapped with platinum cationic species. .103

List of Schemes

List of Tables

List of Abbreviations

Å	Ångstrom
$[\alpha]_D$	specific rotation (sodium D Line)
AMT	active metal template
APPI	atmospheric pressure photoionization
aq	aqueous
Ar group	aromatic group
BJ	break junction
BLA	bond length alternation
bp	boiling point
Bpin	bis(pinacolato)diboron
br	broad
calcd	calculated
CCDC	Cambridge Crystallographic Data Center
CD	circular dichroism
CIF	crystallographic information file
cm	centimeter(s)
CSD	Cambridge Structural Database
d	day(s)
d	doublet (spectral)
DA	diamagnetic anisotropy
DDQ	2,3-dichloro-5,6-dicyanobenzoquinone
DFT	density functional theory
DIPEA	diisopropylethylamine
DMBP	6,6'-dimethyl-2,2'-bipyridine
DMF	*N,N*-dimethylformamide
dp	decomposition point
DSC	differential scanning calorimetry
dtBBP	4,4'-di-*t*-butyl-2,2'-bipyridine
ECL	effective conjugation length

equiv	equivalent(s)
ESI	electrospray ionization
Et	ethyl
Et$_2$O	diethyl ether
EtOAc	ethyl acetate
EtOH	ethanol
eV	electron volts
FBWr	Fritsch–Buttenberg–Wiechell rearrangement
FMOs	frontier molecular orbitals
FTIR	Fourier transform infrared spectroscopy
g	gram(s)
h	hour(s)
HMBC	heteronuclear multiple bond correlation
HOMO	highest occupied molecular orbital
HOPG	highly ordered pyrolytic graphite
HSQC	heteronuclear single quantum coherence
Hz	hertz
i	*iso*
*i*Pr	*iso*-propyl
IR	infrared spectroscopy
kcal	kilocalorie(s)
L	liter(s)
LiHMDS	lithium hexamethyldisilazide
LUMO	lowest unoccupied molecular orbital
m	multiplet
MALDI	matrix-assisted laser desorption ionization
Me	methyl
Me$_3$O•BF$_4$	trimethyloxonium tetrafluoroborate
mg	milligram(s)
MHz	megahertz

mL	milliliter(s)
mmol	millimole(s)
mol	mole(s)
mp	melting point
MS	mass spectrometry
m/z	mass-to-charge ratio
NBS	*N*-bromosuccinimide
n-BuLi	*n*-butyllithium
NIS	*N*-iodosuccinimide
nm	nano meter
NICS	nucleus-independent chemical shift
NMR	nuclear magnetic resonance
ORTEP	Oak Ridge thermal ellipsoid plot
p	*para*
p-Tol	*para*-toluene
PEOs	pyridyl-endcapped oligoynes
Ph	phenyl
ppm	parts per million
PSS	photostationary state
Py	pyridine
R_f	retention factor
rt	room temperature
s	singlet
s	strong
satd	saturated
SCAs	synthetic carbon allotropes
sh	shoulder
STM	scanning tunneling microscopy
t	triplet
t-Bu	*tert*-butyl

TATA	triazatriangulenium
TBAF	tetrabutylammonium fluoride
TDA-1	tris[2-(2-methoxyethoxy)ethyl]amine
TES	triethylsilyl
TFA	trifluoroacetic acid
THF	tetrahydrofuran
TIPS	triisopropylsilyl
TLC	thin layer chromatography
TMEDA	*N,N,N',N'*-tetramethylethylenediamine
TMS	trimethylsilyl
tpfpp	5,10,15,20-tetrakis(pentafluorophenyl)porphyrin
Tr*	supertrityl [tris(3,5-di-*t*-butylphenyl)methyl]
UV-vis	ultraviolet-visible
vw	very weak
w	weak

CHAPTER 1 – Introduction to Oligoynes, Polyynes, and Carbyne

1.1   Introduction to carbon-rich compounds and materials

1.1.1 Synthetic carbon allotropes (SCAs)

Carbon-rich molecules and materials have been studied extensively and developed,[1] in particular, since the discovery of fullerene in 1985.[2] The last 35 years have thus seen the advance of carbon chemistry from fullerene chemistry to other fundamental milestones, such as graphene,[3] carbon nanotubes,[4] and graphyne/graphdiyne.[5] Synthetic chemists have been attracted to these carbon allotropes by the allure of developing multi-step synthesis and the potential properties of new forms of carbon. Building blocks and model compounds have been designed and synthesized to yield these new carbon forms and/or investigate their properties. During the course of targeting the synthetic carbon allotropes (SCAs), new synthetic methods are being developed simultaneously, and the unique properties of new building blocks/models are being uncovered.[6] For example, graphene nanoribbons (GNRs),[7] cycloparaphenylenes (CPPs),[8] and radiaannulene oligomers[9] have been developed. More specific examples include using a bottom-up strategy to form non-planar polyphenylene precursors from small molecules, then these precursors are planarized via intramolecular cyclodehydrogenation to yield corresponding GNRs with a well-defined structure.[10] Furthermore, a series of size-controlled molecules CPPs was reported first in 2008, representing a milestone in "carbon" chemistry.[11] Subsequently, a rational bottom-up approach, allowing synthesis of nanotubes with uniform diameters, has been reported using the well-defined CPPs as templates.[12] Finally, the so-called radiaannulenes have been assembled by iterative acetylenic coupling reactions and used to model 6,6,12-graphyne.[9]

1.1.2 *sp*-Carbon allotrope: Carbyne

It is worth noting that the new allotropes discussed so far are composed of sp^2-carbon, and mostly constructed of sp^2-carbon. Specifically, graphene and carbon nanotubes are composed of sp^2-carbon, while graphyne/graphdiyne are constructed with a variable ratio of sp-carbon/sp^2-carbon. The other well-known carbon allotrope, diamond, is made up of pure sp^3-hybridized carbon. As

the hardest naturally occurring material, the sp^3-carbon is organized in a tetrahedral arrangement, forming a three-dimensional network of 6-membered rings. With different arrangements of carbon resulting in significant differences of characteristics, one may wonder what the sp-hybridized carbon allotrope is like and what properties an allotrope of sp-carbon might display.

The carbon allotrope with an infinite chain of sp-hybridized carbon is known as carbyne. It is straightforward to propose two structural forms of carbyne, with closed-shell electronic structures, a polyynic form, and a cumulenic form (Figure 1.1). The polyynic form contains alternating single and triple carbon-carbon bonds, while the cumulenic form is composed of contiguous double bonds. Structurally, the polyynic form (C–C≡C) is expected to maintain bond length alternation (BLA), while the cumulenic form (C=C=C) is not. Electronically, carbyne is expected to be a semiconductor in the polyynic form, with a band gap of ca. 2.2 eV,[13] while in the cumulenic form, carbyne is expected to be metallic.[14] The structure of carbyne is dominated by the so-called Peierls distortion[15] at the infinite length making the polyynic form more possible than the cumulenic form.[16] The existence of carbyne, however, has been controversial over the years, and the "real" structure of carbyne is unknown.[16-17]
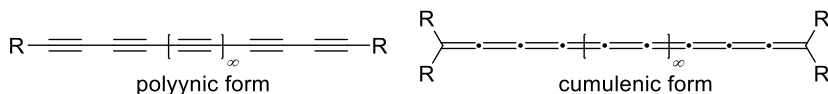
Figure 1.1. Carbyne in polyynic form and cumulenic form.

Although there remains contention over its existence, theoretical/computational work predicts that carbyne will be an intriguing material. For example, carbyne has been theoretically predicted to show unusual mechanical performance, with a nominal Young modulus of 32.7 TPa.[18] Young's modulus (expressed as stress/strain in Pa or N/m^2) quantifies the stiffness of an elastic material through the measurement of the amount of deformation (strain, expressed as $\Delta L/L$) of an elastic material under a given load (stress in N/m^2). As a comparison, well-performing materials of carbon-fiber-reinforced plastics and diamond have a rather small Young modulus of 0.1–0.23[19] and 1.22 TPa, respectively.[18] Carbyne might also be attractive as a scaffold for storage of hydrogen with an estimated surface area up to ca. 13000 m^2/g that is four times larger than that of graphene (ca. 2700 m^2/g).[20] For example, calcium-decorated carbyne complex is calculated to adsorb ca. 8 weight % of hydrogen.[20]

Heat control through an engineering material is essential in electronic and optoelectronic devices, and the development of well-performing conducting materials is of importance toward the miniaturization of integrated circuits.[21] Thermal conductivity of a single carbyne chain in the polyynic and cumulenic form is expected to exceed 54 and 148 kW/m•K, respectively, at room temperature. As a comparison, the value of copper is 0.4 kW/m•K,[22] and other modern materials, such as graphene and nanotubes, show values of 5 and 3.5 kW/m•K, respectively.[23] To test these predicted properties experimentally would require the successful synthesis of oligo-/polyynes as models of carbyne.

Toward the study of carbyne, many series of model compounds with different endgroups have been developed. In the literature, the terminology of oligoyne and polyyne is not differentiated clearly, and the terminology that is used often reflects traditional "habits" of a particular research group. This terminology should, however, be defined, and for this thesis the following definitions will be used. The transition of an oligoyne to a polyyne should be recognized by means of a characterization that shows the loss of an endgroup effect. Or, to put it another way, the properties of an oligoyne change as a function of molecular length, whereas those of a polyyne have reached an asymptotic limit and do not.

1.1.3 Molecular wires

Oligo-/polyynes are composed of a rigid and approximately cylindrical π-delocalization of two degenerate π-electron systems over the *sp*-carbon chain and with nearly unhindered rotation about the *sp*-carbon chain.[24] These features make them ideal molecular wires,[25] which can function as building blocks and self-assembly for nanoscale devices.[26] In particular, oligo-/polyynes are good candidates as molecular wires that have been studied widely in STM-break junction devices in terms of single-molecule conductance.[27] Studies have revealed that the length of single molecules is critical to charge transport,[28] while the endgroups terminating the *sp*-carbon chains as anchoring groups being interfaced to two metal electrodes are also important in charge transport.[29] Therefore, the strategy to synthesize oligo-/polyynes with different lengths and the choice of endgroups are both of importance toward the study of single-molecule conductance. Thus, in many respects, oligo-/polyynes are desired synthetically as carbon-rich materials in modelling the potential properties of carbyne and/or to function as building blocks toward nanoscale devices.

1.2 Synthetic methods for oligo- and polyynes: The octaynes

One of the major goals of my project is to synthesize long oligo-/polyynes, so that these oligo-/polyynes can be used as a model to extrapolate the potential properties of carbyne. Therefore, the introduction of the synthetic methods for assembling oligo-/polyynes will focus on the formation of long oligo-/polyynes R–(C≡C)$_n$–R (**R[n]**, $n \geq 8$), where "R" is the endgroup terminating the sp-carbon chain and "n" is the number of alkyne units. As a starting point, however, the most commonly used methods for the synthesis of short oligoynes R–(C≡C)$_n$–R (**R[n]**, $n < 8$), such as the Hay coupling, Eglinton–Galbraith coupling, and Cadiot–Chodkiewicz coupling will be introduced first. Several recently developed methods will also be briefly described. To facilitate a comparison amongst methods, the synthesis of "short" octaynes R–(C≡C)$_8$–R (**R[8]**) will be discussed first in detail. Then, the application of these synthetic methods to longer derivatives **R[n]**, $n \geq 10$, will be presented as a function of terminal endgroups in the subsequent section (Section 1.3).

1.2.1 Synthesis of octaynes using homocoupling reactions

Acetylenic coupling reactions begin in 1869 with the discovery by Carl Glaser that copper phenylacetylide undergoes oxidative dimerization to produce diphenylbutadiyne in the presence of air; this is now known as Glaser homocoupling reaction (Scheme 1.1a).[30] The prototype of this reaction uses ammonium hydroxide as a base, in a solvent such as ethanol. An important improvement of the Glaser homocoupling reaction was reported in 1956 by Eglinton and Galbraith, who showed that an excess of Cu(OAc)$_2$ and pyridine in the presence of oxygen could perform the oxidative dimerization of terminal alkynes to give a diyne (Scheme 1.1b, path B).[31] In 1962, another milestone in the oxidative dimerization of terminal alkynes was reported, which is now known as the Hay homocoupling reaction (Scheme 1.1b, path C).[32] The Hay homocoupling uses a catalytic amount of CuCl and the organic base tetramethylethylenediamine (TMEDA) in the presence of oxygen. This reaction can be run in a wide variety of solvents because of the good solubility of the TMEDA-bound cuprous derivatives. Both Eglinton–Galbraith and Hay homocoupling reactions still are used widely in the modern synthesis of oligoynes. Beyond these basic routes, other adaptions of existing methods also have been developed in homocoupling reactions of terminal alkynes, such as the palladium-catalyzed system,[33] the copper-catalyzed system mediated with blue-light,[34] and others.[35] All of these methods, and others,[36] contribute

to the broad diversity of methods in the toolbox to make 1,3-diynes.
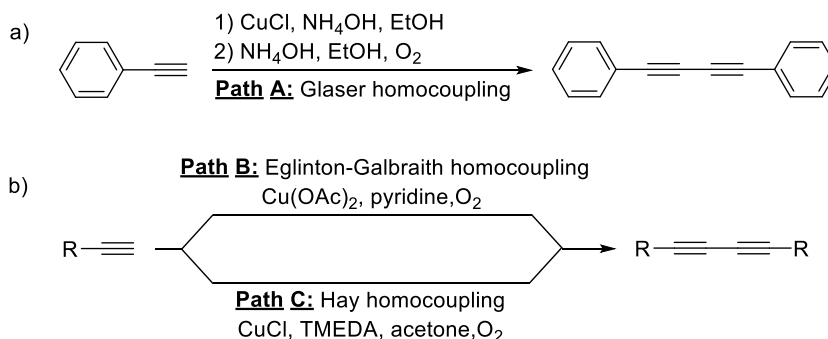
Scheme 1.1. a) Glaser homocoupling reaction. b) Eglinton–Galbraith homocoupling reaction and Hay homocoupling reaction.

A diverse toolbox has been developed for the synthesis of 1,3-diynes, while limited options are available for the synthesis of longer oligoynes, especially as one reaches the octayne derivatives R–(C≡C)$_8$–R (**R[8]**). Before proceeding to octayne synthesis, it is helpful to offer a couple of words describing the overall process. Many reactions to form octaynes rely on dimerization of the corresponding tetraynes. Because terminal oligoynes (i.e., oligoynes terminated with a hydrogen atom) are usually unstable to isolation,[37] a trialkylsilyl group is commonly used as a terminus to stabilize the *sp*-hybridized carbon framework. The trialkylsilyl "protecting group" must be removed prior to the homocoupling reaction or sometimes during the reaction (i.e., in situ desilylation). The removal of the protecting group and the subsequent termination of the oligoyne chain with a hydrogen atom is generally called "deprotection". In the specific case of desilylation, this process is most commonly accomplished by treating the trimethylsilyl-endcapped oligoyne with a base in MeOH, often either NaOH/MeOH or K$_2$CO$_3$/MeOH. These conditions also will remove the triethylsilyl group, while the more resilient triisopropylsilyl group is typically removed via reaction with a fluoride source, e.g., CsF or tetrabutylammonium fluoride (TBAF), in wet THF as a proton source.[38]

Hay homocoupling is the most popular and common method toward making octaynes, and the synthesis of octaynes with *sp*^{3}-carbon endgroups has been reported using this method. For example, Tykwinski and co-workers have described that the Hay homocoupling reaction successfully affords the octaynes **_t_Bu[8]**[39] and **Ad[8]**[40] in 61 and 75% yields, respectively (Scheme 1.2). It is noted that the yields are calculated from the corresponding trialkylsilyl-

protected tetrayne, as the terminal tetrayne is not stable to isolation. Hoheisel and Frauenrath have reported that tetrayne desilylation in the presence of AgNO$_3$/MeOH, followed by the Hay homocoupling protocol gives octayne **Glu[8]** in 58% yield.[41] The Hay homocoupling protocol has been used to give **Tr*[8]** in 97% yield (based on the isolated terminal tetrayne).[42] In this example, the terminal tetrayne is stable to isolation as a result of the bulky nature of **Tr*** endgroup, which provides a significant stabilizing effect to the *sp*-carbon rod (*vide infra*).

octayne	*t*Bu[8]	Ad[8]	Glu[8]	Tr*[8]
SiX$_3$	SiMe$_3$	SiMe$_3$	SiMe$_3$	Si*i*Pr$_3$
desilylation	in situ	in situ	AgNO$_3$,CH$_2$Cl$_2$/MeOH	CsF, THF/H$_2$O
octayne yield	61%	75%	58%	97%*
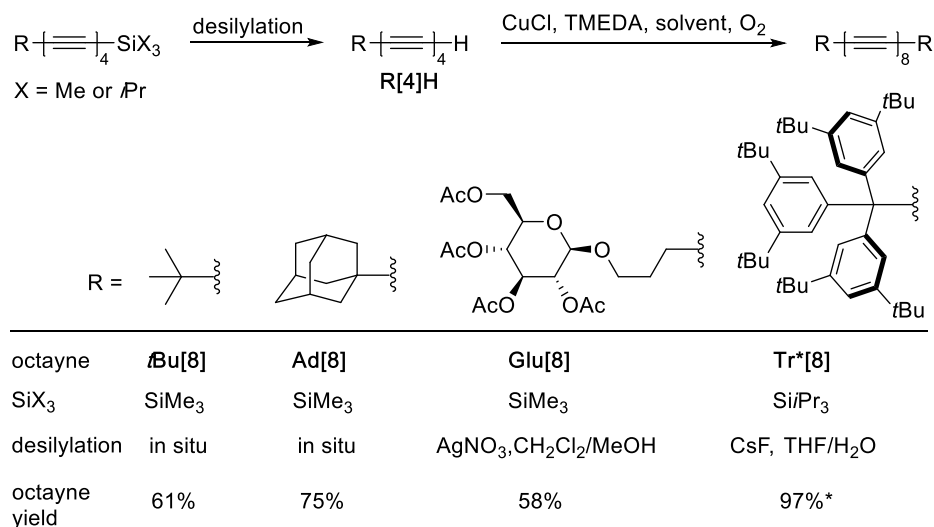
Scheme 1.2. Hay homocoupling reactions for ***t*Bu[8]**, **Ad[8]**, **Tr*[8]**, and **Glu[8]**. *Yields are calculated from the corresponding terminal oligoynes, otherwise, yields are calculated over two steps from the corresponding trialkylsilyl-protected tetraynes.

octayne	**Py(Ph)[8]**	**Ph(F)[8]**	**Mes[8]**	**Ph(OSi)[8]**
SiX$_3$	SiEt$_3$	Si*i*Pr$_3$	SiEt$_3$	SiMe$_3$
desilylation	CsF, THF/H$_2$O	TBAF, THF	NaOH, MeOH	K$_2$CO$_3$, MeOH/THF
octayne yield	6%	19%	25%	9%
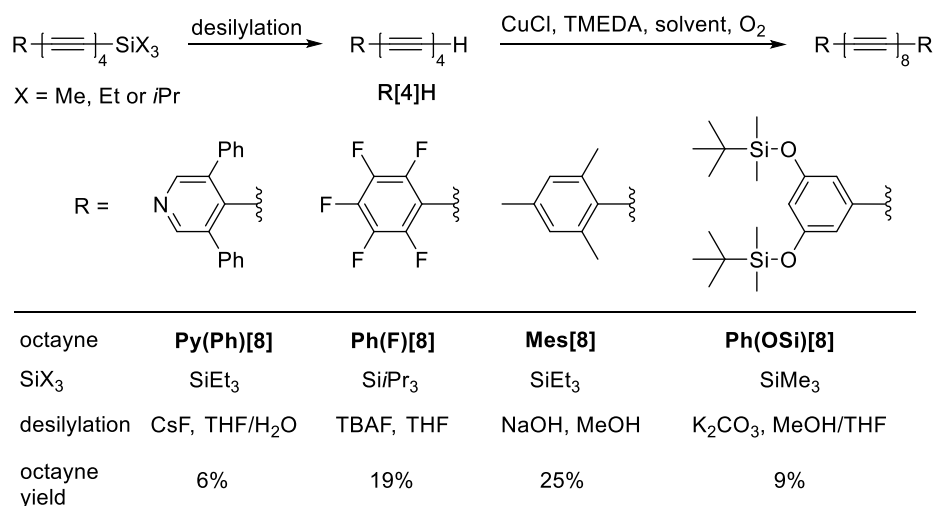
Scheme 1.3. Hay homocoupling reactions for **Py(Ph)[8]**, **Ph(F)[8]**, **Mes[8]**, and **Ph(OSi)[8]**.

There are several examples of the synthesis of octaynes **R[8]** featuring *sp*^{2}-carbon

endgroups based on the Hay homocoupling reaction. A sequence of desilylation and subsequent homocoupling reactions using CuCl and TMEDA under aerobic conditions gives **Py(Ph)[8]**,[43] **Ph(F)[8]**,[44] **Mes[8]**,[45] and **Ph(OSi)[8]**[46] in 6–25% yields (Scheme 1.3). Comparing with the synthesis of octaynes **R[8]** with sp^3-carbon endgroups (*vide supra*), the yields of the octaynes endcapped with sp^2-carbon groups are typically lower (58–97% vs. 6–25%). The low yields obtained for these sp^2-carbon endcapped octaynes are attributed to the instability of the terminal tetraynes.

The synthesis of silyl- and platinum-atom endcapped octaynes **TES[8]**, **Pt(tol)[8]**, and **Pt(PhF)[8]** has been accomplished via Hay homocoupling reactions. Octayne **TES[8]** is obtained from the oxidative dimerization of terminal tetrayne **TES[4]H**, which is deprotected partially from the double-TES endcapped **TES[4]** using NaOH; the yield of **TES[8]** is not reported.[47] Gladysz and co-workers have pioneered the synthesis of metal-endcapped oligo-/polyynes and applied the Hay homocoupling reaction to the formation of Pt-endcapped octaynes **Pt(tol)[8]**[48] and **Pt(PhF)[8]**[49] in 70 and 92% yields, respectively (Scheme 1.4). It is worth mentioning that the formation of **Pt(tol)[8]** and **Pt(PhF)[8]** is performed in "one-port". Desilylation of the triethylsilyl-protected tetrayne is accomplished by using TBAF in wet THF, followed by the addition of trimethylsilyl chloride as a fluoride ion scavenger. Finally, the addition of the Hay catalyst effects formation of the homocoupling products.

octayne	TES[8]	Pt(tol)[8]	Pt(PhF)[8]
desilylation	NaOH, MeOH	TBAF, THF	TBAF, THF
octayne yield	—	70%	92%
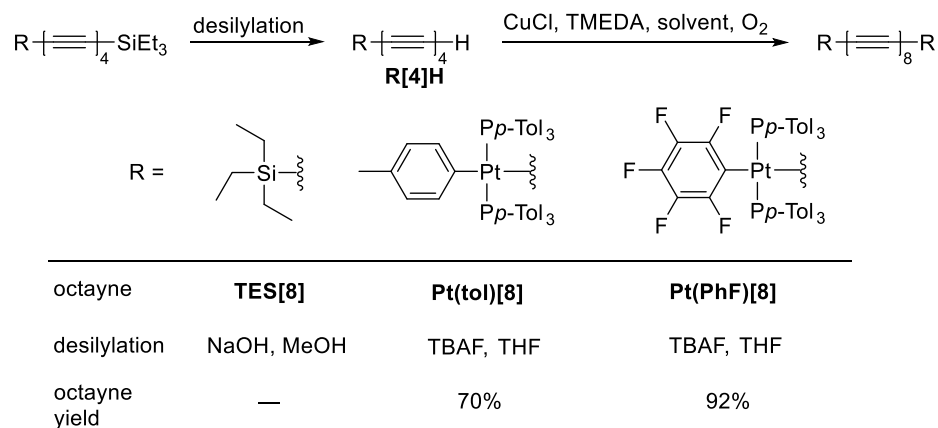
Scheme 1.4. Hay homocoupling reactions for **TES[8]**, **Pt(tol)[8]**, and **Pt(PhF)[8]**.

The Eglinton–Galbraith homocoupling reaction has also been used in the formation of octaynes **R[8]**. Gladysz and co-workers have reported that a sequence of desilylation and

homocoupling forms **Re[8]** in 67% yield (based on **Re[4]H**).[50] In this case, **Re[4]H** can be isolated as a stable solid. In the case of the porphyrin derivative **Por[8]** the trimethylsilyl-protected tetrayne undergoes in situ desilylation under the conditions of the Eglinton–Galbraith reaction, and the subsequent homocoupling reaction gives the Ni-porphyrin endcapped octayne **Por[8]** (Scheme 1.5a).[51] Alternatively, the tetrayne endcapped with a carboxyl group can also be used as a precursor to a terminal tetrayne, which liberates CO_2 in a decarboxylation reaction using tetraamminecopper sulfate ($[Cu(NH_3)_4]SO_4$), as in the formation of the ferrocenyl derivative **Fc[8]**. With the terminal tetrayne in hand, the Eglinton–Galbraith homocoupling protocol provides **Fc[8]** in 84% yield (based on the isolated terminal tetrayne).[52]

octayne	**Re[8]**	**Por[8]**	**Fc[8]**
X group	SiMe$_3$	SiMe$_3$	COOH
deprotection	TBAF, THF	in situ	[Cu(NH$_3$)$_4$]SO$_4$, acetone
octayne yield	67%*	—	84%*
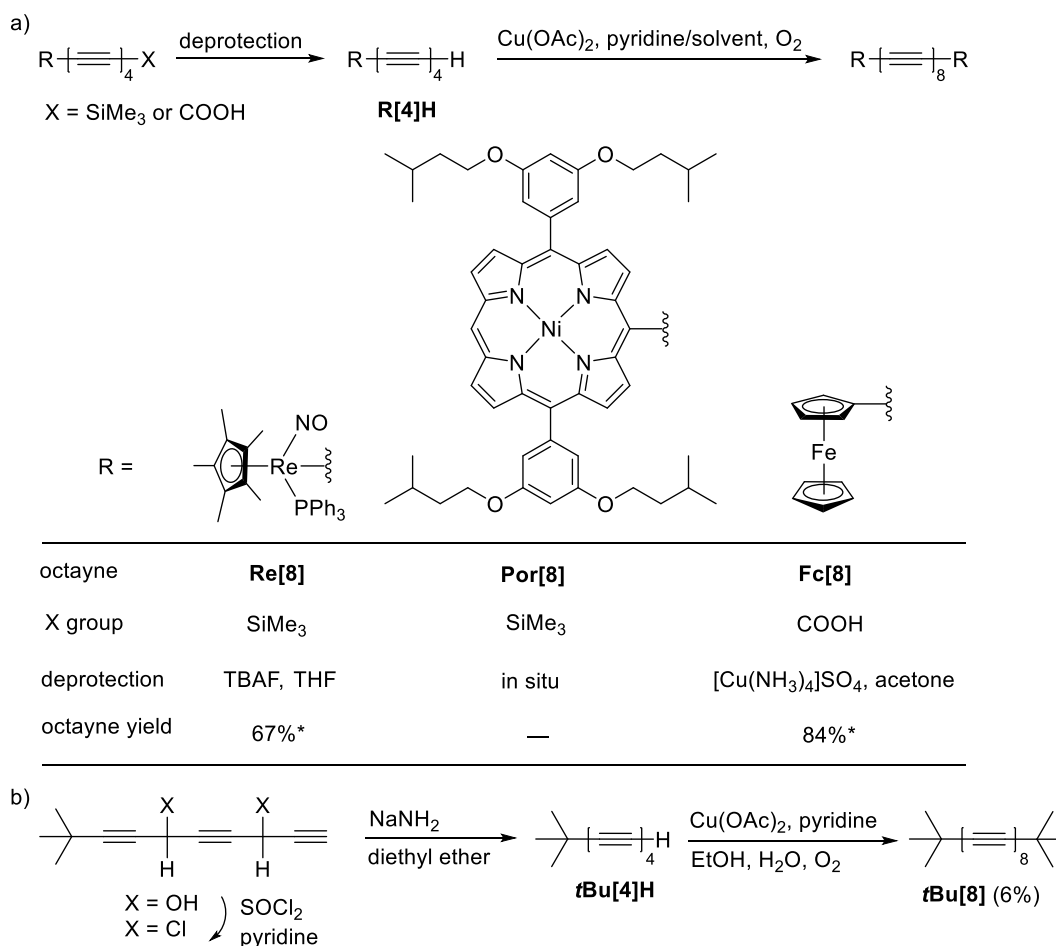
Scheme 1.5. a) Eglinton–Galbraith homocoupling reactions for **Re[8]**, **Fc[8]**, **Por[8]**, and b) *t*Bu[8]. *Yields are calculated from the corresponding terminal tetraynes, otherwise, yields are calculated over two steps from the corresponding protected oligoynes.

Jones and co-workers have reported the synthesis of the octayne *t*Bu[8].[53] As shown in

Scheme 1.5b, dehydrohalogenation from the glycol using thionyl chloride and pyridine gives the corresponding dichloride precursor. Exhaustive elimination of the dichloride using sodium amide gives the terminal tetrayne, and an Eglinton–Galbraith homocoupling reaction forms the targeted octayne *t*Bu[8] in 6% yield (based on the glycol).
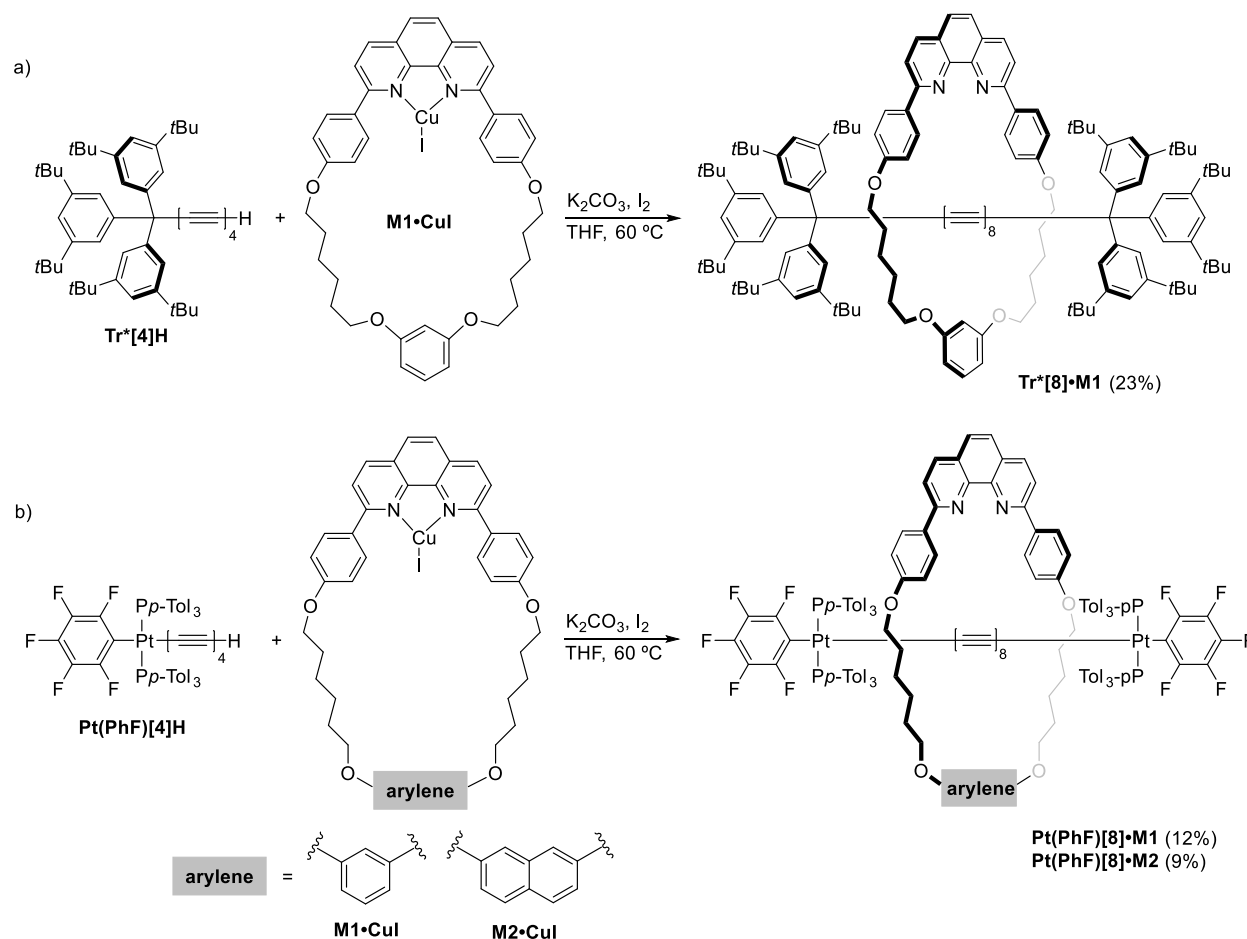
Scheme 1.6. a) Cu(I)-template homocoupling reactions for **Tr*[8]·M1**, and b) **Pt(PhF)[8]·M1** and **Pt(PhF)[8]·M2**.

Recently, an active metal template strategy has been successfully applied to form octaynes via a homocoupling reaction. In this approach, the Cu(I)-template is first formed through the reaction of CuI and a phenanthroline-based macrocycle (e.g., **M1** or **M2**). This template directs the catalytic homocoupling of two terminal tetraynes through the cavity of the macrocycle to form an octayne rotaxane. The resulting ocatyne rotaxane exhibits enhanced thermal stability compared with the identical, unthreaded octayne, as a result of better steric protection of the *sp*-carbon chains from intermolecular reactions, based on shielding from the macrocycle.[54] More specifically, the

9

reaction of the terminal tetrayne **Tr*[4]H** in the presence of the Cu(I)-template complexes **M1·CuI**, the base K_2CO_3, and the oxidant I_2 gives the octayne rotaxane **Tr*[8]·M1** in 23% yield (Scheme 1.6a).[54c] An analogous protocol has been applied to the synthesis of **Pt(PhF)[8]·M1** and **Pt(PhF)[8]·M2** in 12 and 9% yields, respectively (Scheme 1.6b).[54b] It is worth noting that the constitution and size of macrocycles can be adjusted to provide different cavities suitable for encapsulation of *sp*-carbon rods, based on the type of the stopper present (i.e., the endgroup).

1.2.2 Synthesis of octaynes using heterocoupling reactions

Hay and Eglinton–Galbraith coupling protocols can be potentially applied to synthesis of unsymmetrical oligoynes and/or odd-numbered oligoynes using two different terminal acetylene starting materials. These reactions usually do not, however, show selectivity toward the desired unsymmetrical oligoynes versus the two possible homocoupling products, although exceptions exist (Scheme 1.7a).[55] It has been confirmed that the more acidic of the two precursors reacts faster, leading to a disproportionately high yield of this homocoupling oligoyne. For example, Bohlmann and co-workers have demonstrated that the reaction of 1-phenyl-1,3-butadiyne and pent-2-ene-4-yn-1-ol produces predominantly the symmetrical product **Ph[4]**, with trace amounts of the heterocoupling products (Scheme 1.7b).[56]
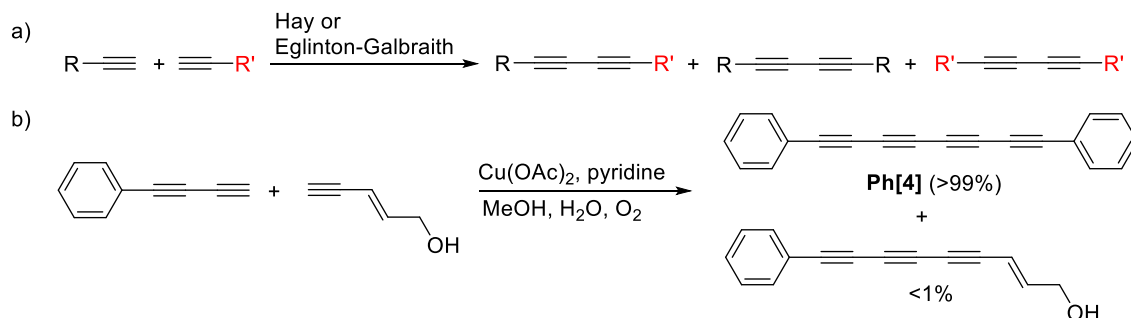
Scheme 1.7. a) Homocoupling and heterocoupling products produced from Hay or Eglinton–Galbraith reactions. b) A homocoupling product is produced predominantly from the more acidic acetylenic reagent reported by Bohlmann.

Toward solutions to this challenge, an excess of the less precious acetylenic reagent (i.e., cheaper or more easily made) can be used to bias the reaction toward the unsymmetrical derivative. The Hay coupling protocol gives the unsymmetrical octayne **Pt(tol)[8]TES** in 1% yield using terminal diyne **Pt(tol)[2]H** and a large excess (18 equiv) of the four-carbon building block $SiEt_3$–$(C≡C)_2$–H (**TES[2]H**) as starting materials.[48] The major products of the reaction include the tetrayne **Pt(tol)[4]TES** and hexayne **Pt(tol)[6]TES** in 29 and 30% yields, respectively (Scheme

1.8a). Chalifoux and Tykwinski have reported a modified Eglinton–Galbraith protocol, which is applied using the terminal tetrayne **Tr*[4]H** and an excess (5 equiv) of a 8-carbon building block *i*Pr$_3$Si–(C≡C)$_4$–SiMe$_3$ (**TIPS[4]TMS**) in the presence of excess Cu(OAc)$_2$·H$_2$O, K$_2$CO$_3$, and 2,6-lutidine. The trimethylsilyl group is removed under the reaction conditions, and this in situ approach thus avoids isolation of the unstable terminal tetrayne *i*Pr$_3$Si–(C≡C)$_4$–H. The subsequent heterocoupling reaction gives **Tr*[8]TIPS** in 77% yield (Scheme 1.8b).[42]
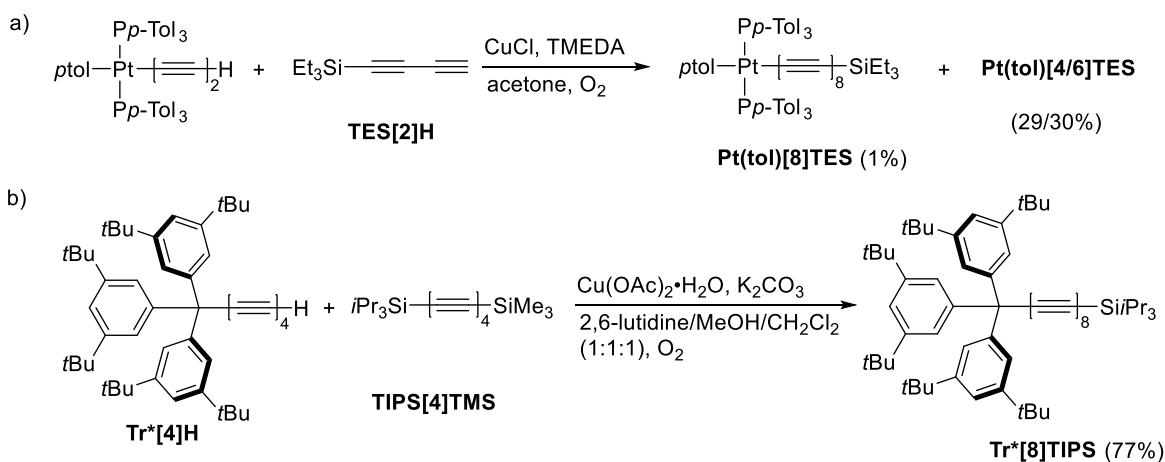
Scheme 1.8. a) Hay coupling reactions for **Pt(tol)[8]TES**. b) Modified Eglinton–Galbraith heterocoupling for **Tr*[8]TIPS**.

To overcome the selectivity issues with use of either the Hay or Eglinton–Galbraith reactions, Cadiot and Chodkiewicz developed a heterocoupling reaction in 1955 to form unsymmetrical oligoynes.[57] The Cadiot–Chodkiewicz heterocoupling reaction relies on the reaction of a terminal alkyne with a bromo-, iodo-, or chloro-alkyne derivative catalyzed by a Cu(I) salt to give the unsymmetrical oligoyne (Scheme 1.9a). The unsymmetrical oligoyne is typically the major product, although homocoupling of the alkynyl halide often complicates the reaction. Pd-assisted Cadiot–Chodkiewicz heterocoupling reactions have also been reported,[58] and reaction of a terminal alkyne and a bromo- or iodoalkyne occurs in the presence of catalytic CuI and a palladium salt, such as Pd(PPh$_3$)$_4$ (Scheme 1.9b).

An interesting adaptation of the Cadiot–Chodkiewicz reaction allows for the iterative elongation of oligoynes. Reaction of a terminal alkyne (or oligoyne) with a trialkylsilyl-terminated bromoalkyne results in chain extension via the Cadiot–Chodkiewicz heterocoupling reaction (Scheme 1.9c). The oligoyne product thus features a trialkylsilyl group, and repeating the

desilylation and heterocoupling sequence affords the next longer homologue. This iterative protocol of desilylation and subsequent heterocoupling reactions has been pioneered by Walton and co-workers[45, 59] and is often used to provide oligoynes bearing terminal trialkylsilyl protecting groups.[42, 46] Finally, other heterocoupling methods have also been reported, such as a Negishi-like coupling using a palladium catalyst,[60] a gold-catalyzed protocol,[61] a nickel/copper-cocatalyzed aerobic method,[62] and a copper-catalyzed reaction promoted by blue-light.[63]
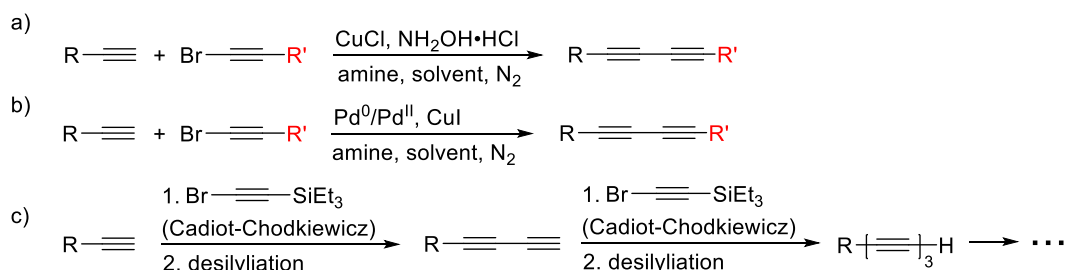
Scheme 1.9. a) Cadiot–Chodkiewicz heterocoupling reaction. b) Pd-assisted Cadiot–Chodkiewicz heterocoupling reaction. c) Iterative protocol of making longer oligoynes using Cadiot–Chodkiewicz heterocoupling reaction.

Hirsch and co-workers have reported an alkyl-bridged octayne **Ph(*t*Bu)(*O*-alkyl)[8]** in 1% yield, based on a Pd/Cu catalyzed heterocoupling reaction with a bromodiyne as a key step (Scheme 1.10a).[58c] Bruce and co-workers have reported an elegant synthesis of an octayne endcapped with tricobalt carbonyl clusters (**Co₃C[8]**). A double heterocoupling reaction occurs between the polyynyl gold complex[64] and the diiodotetrayne **I[4]I**[58d, 65] in the presence of Pd(PPh₃)₄ and CuI, giving the product **Co₃C[8]** in 86% yield (Scheme 1.10b).[66]
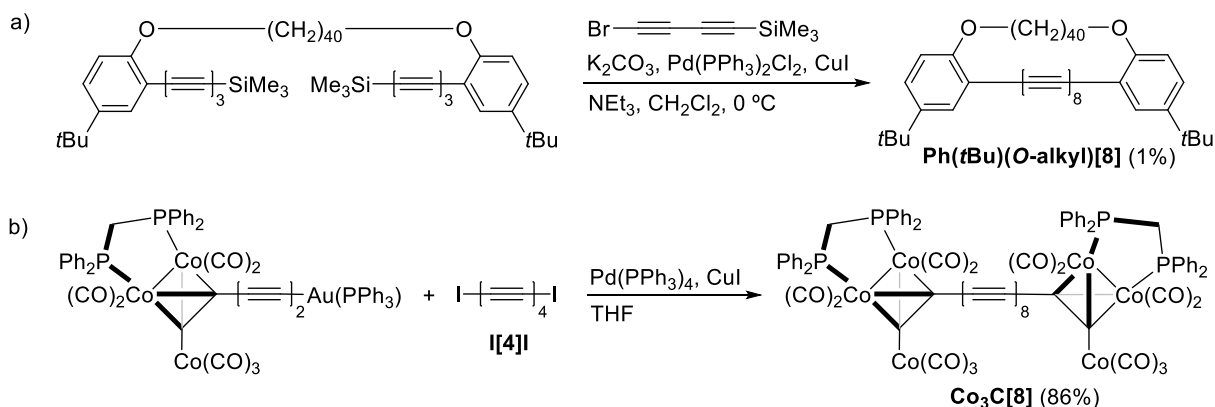
Scheme 1.10. a) Pd/Cu-catalyzed heterocoupling reaction toward **Ph(*t*Bu)(alkyl)[8]**, and b) **Co₃C[8]**.

1.2.3 Alternative methods toward octaynes

A number of methods have been developed toward the synthesis of oligoynes that have separated

themselves from the most established homocoupling and heterocoupling methodologies. Examples of the syntheses of the octaynes will be provided here. These methods include, but are not limited to, the Fritsch-Buttenberg-Wiechell rearrangement (FBWr),[67] the use of a masked alkyne,[66, 68] laser ablation,[69] graphite vapor deposition,[70] as well as atomic manipulation on the surface.[71]

The application of FBWr to the synthesis of oligoynes was first reported in 2000 by the research group of Tykwinski.[67a] This method is useful to make both unsymmetrical and symmetrical oligoynes. In general, the lithium-bromine exchange between a dibromoolefin and nBuLi forms a carbenoid species, and 1,1-elimination of LiBr concurrent with 1,2-migration of one of the pendent alkynes yields the desired oligoyne. A less polar solvent, i.e., with poor solvating ability, such as hexanes or toluene, reportedly favors this reaction through facilitating the 1,1-elimination and migration.[67a] A double FBWr has been used to form the octaynes **Ad[8]**, **Ph[8]**, and **TIPS[8]** in 38, 13 and 10% yields, respectively (Scheme 1.11).[72]
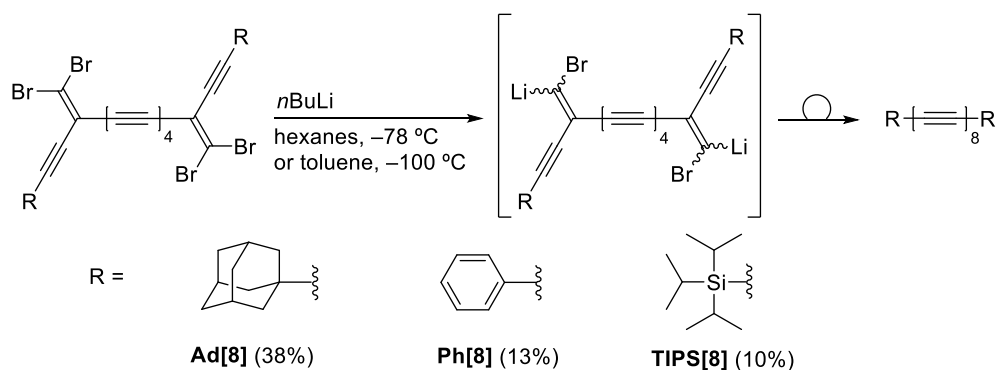
Scheme 1.11. Synthesis of **Ad[8]**, **Ph[8]**, and **TIPS[8]** using the FBW rearrangement.

There are abundant masking groups used as precursors of alkynes and oligoynes, such as cobalt complexes,[68c, 68h, 73] propellane,[68g] indan,[68b, 68e] and the CO moiety.[68d] Anderson and co-workers have reported that oxidative decomplexation of cobalt carbonyl complexes using iodide gives **TIPS[8]** in 45% yield (Scheme 1.12a).[68h]

Oligoynes can be formed by laser ablation of carbon sources, such as carbon nanotubes, graphite, and solvent molecules, to give the parent oligoynes **H[n]**.[69] These methods typically give oligoynes up to a length of $n = 8$, and are often separated by HPLC. Hirsch and co-workers have reported the synthesis of **CN[8]** by vaporizing graphite under Krätschmer–Huffman conditions[74] in the presence of cyanogen gas.[70a] This method results in a mixture of **CN[n]** ($n =$ 3–9), and **CN[8]** can be separated by preparative HPLC (Scheme 1.12b).

Scheme 1.12. a) Synthesis of **TIPS[8]** by unmasking of cobalt complex. b) Synthesis of **CN[8]** using cyanogen and vaporized graphite. c) On-surface synthesis of **Ph[8]** by atomic manipulation.

On-surface formation of oligoynes via skeletal rearrangement or extrusion of carbon monoxide induced by atomic manipulation has been reported at the single-molecule level.[71] A recent breakthrough using this approach is the formation of the *sp*-hybridized molecular carbon allotrope cyclo[18]carbon on the surface of bilayer NaCl, as reported by Anderson and co-workers (not shown).[71a] In the given example (Scheme 1.12c), a vinyl radical intermediate is formed by the cleavage of a C–Br bond through the application of voltage pulses using scanning tunneling microscopy (STM). An additional voltage pulse then cleaves the remaining C–Br bond, which triggers the 1,2-shift to yield **Ph[8]** on the surface. This atomic manipulation strategy can synthesize oligoynes in a single-molecule level; this study also provides structural insight into the reaction intermediates, which could also be observed.

1.3 Synthesis of long oligo-/polyynes (*n* > 8) with *sp*³-carbon endgroups

This section reviews the synthesis of long oligo-/polyyne derivatives **R[*n*]** (*n* > 8). The oligo-/polyyne derivatives discussed herein are classified by endgroup according to the atom directly bonded with the terminal *sp*-carbon chain of the oligo-/polyynes. This affords two distinct classes of oligo-/polyynes. First are endgroups based on *sp*³-carbon that do not afford appreciable π-electron communication with the *sp*-carbon chain. Second are endgroups derived from *sp*²-carbon endgroups that offer the potential for conjugation between the endgroup and *sp*-carbon chain. The

14

synthetic strategy to each long oligo-/polyyne will be discussed in this section. Long oligo-/polyyne derivatives with transition metal endgroups will not be discussed.

1.3.1 *t*-Butyl-endcapped oligoynes (*t*Bu[10] and *t*Bu[12])

The synthesis of *t*-butyl-endcapped oligoynes *t*Bu[*n*] dates back to 1953, and Bohlmann reports the synthesis of *t*Bu[*n*] up to *n* = 7.[75] Subsequently, Jones and co-workers extended the *t*Bu[*n*] series up to *n* = 10, the decayne *t*Bu[10].[53] As shown in Scheme 1.13a, a double 1,4-elimination of the dichloro precursor using alkaline alumina affords the terminal pentayne. Subsequently, an Eglinton–Galbraith homocoupling reaction gives the targeted decayne *t*Bu[10] in 39% yield (based on the diol precursor). Alternatively, the dichloro precursor could be dehydrohalogenated in situ under the Eglinton–Galbraith coupling conditions and directly converted into the decayne, giving *t*Bu[10] in 24% yield.
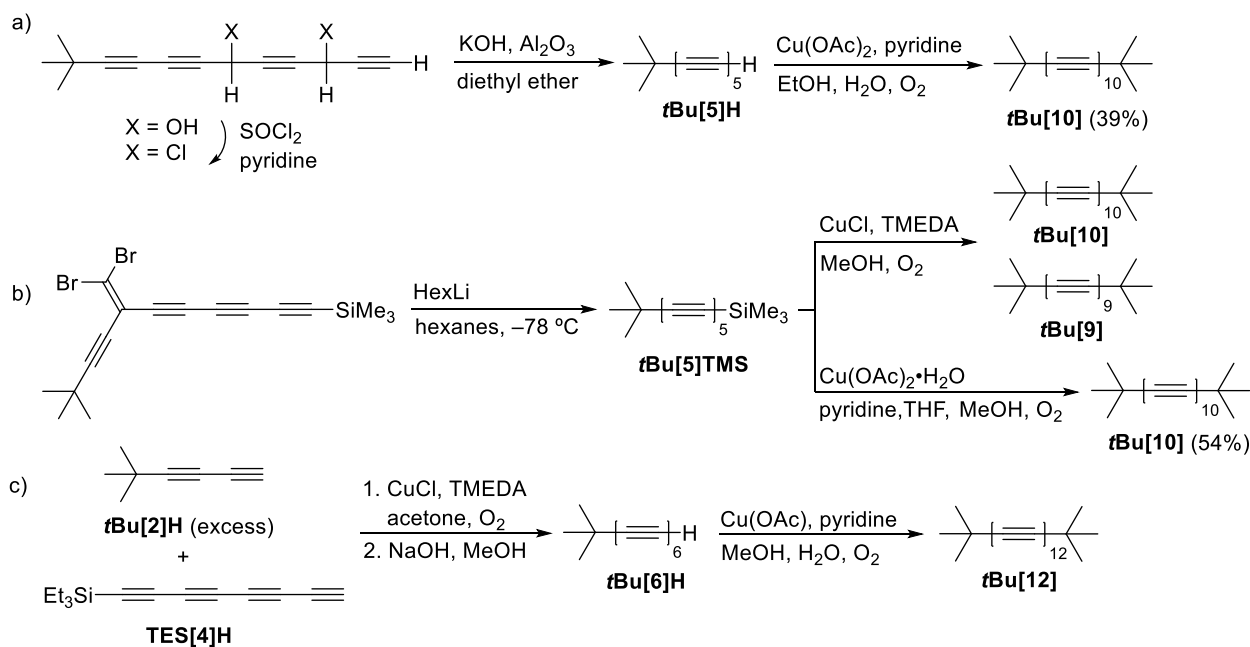
Scheme 1.13. a) Synthesis of *t*Bu[10] reported by Jones and co-workers. b) Synthesis of *t*Bu[10] using Hay coupling reactions and Eglinton–Galbraith coupling reactions. c) Synthesis of *t*Bu[12] reported by Walton and co-workers.

Recently, the synthesis of *t*Bu[10] has been reevaluated by combining the use of FBWr and homocoupling protocols [39] As shown in Scheme 1.13b, the FBW rearrangement gives the silyl-protected pentayne *t*Bu[5]TMS. Then, this pentayne is directly subjected to conditions of the Hay homocoupling reaction, during which the trimethylsilyl group is removed in situ, resulting in the

formation of the terminal pentayne, which goes on to give decayne *t*Bu[10]. Interestingly, the Hay homocoupling gives not only the desired decayne *t*Bu[10] as a major product but also a small amount of nonayne *t*Bu[9]. The formation of nonayne *t*Bu[9] highlights a challenge when synthesizing longer oligoynes, typically **R[*n*]** (*n* ≥ 10), in which by-products are observed that result from the loss of C2 units from the oligoyne framework, i.e., the apparent loss of alkyne units. The homocoupling reaction conditions often need to be optimized to avoid the problem of loss of C2 units. In the case of *t*Bu[10], Eglinton–Galbraith homocoupling conditions circumvent the problem and give the desired decayne *t*Bu[10] in 54% yield.[39] Noteworthy, the decayne *t*Bu[10] is stable under ambient conditions, facilitating characterization by NMR spectroscopy, mass spectrometric analysis, and X-ray crystallography.

As shown in Scheme 1.13c, Hay coupling using triethylsilyl-protected terminal tetrayne **TES[4]H** and an excess of *t*Bu-endcapped terminal diyne *t*Bu[2]H (5.6 equiv) results in the formation of the desired unsymmetrical hexayne *t*Bu[6]TES, as reported by Walton and co-workers.[47] Although this hexayne is not separated from the resulting mixture of the homocoupling byproducts, the resulting terminal hexayne *t*Bu[6]H can be separated by chromatography. The subsequent Hay coupling using *t*Bu[6]H gives only trace quantities of the desired dodecayne *t*Bu[12] (not shown). On the other hand, the Eglinton–Galbraith homocoupling reaction and associated work-up gives red-brown needles, proposed to be *t*Bu[12] on the basis of UV-vis spectroscopic analysis. The product *t*Bu[12] is reported to decompose gradually to a black solid over 8 min at rt.

1.3.2 Adamantyl-endcapped oligoynes (Ad[10] and Ad[12])

Adamantyl-endcapped oligoynes (**Ad[*n*]**) have been reported by Tykwinski and co-workers.[40, 76] The FBWr protocol, Hay homocoupling, and Eglinton–Galbraith homocoupling have all been exploited toward the synthesis of **Ad[10]** (Scheme 1.14). Starting from a stable dibromoolefin, deprotection gives the terminal triyne, which is used in a Hay coupling to form the desired tetrabromoolefin in 60% yield. A two-fold FBWr affords the final decayne **Ad[10]** as an orange solid in 3% yield after work-up and purification (Scheme 1.14a). This is the first successful example of the direct synthesis of a decayne by a FBWr, albeit the yield is low. The direct synthesis of **Ad[10]** has also been investigated using homocoupling reactions in order to improve the yield (Scheme 1.14b). A FBWr gives the trimethylsilyl-protected pentayne **Ad[5]TMS**, which is not

stable in its neat form and thus carried forward in solution to the subsequent homocoupling step. In situ removal of the trimethylsilyl group, followed by the Hay homocoupling reaction at 0 °C affords the desired decayne **Ad[10]** in 29% yield, mixed with a small amount of nonayne **Ad[9]**. Alternatively, Eglinton–Galbraith homocoupling circumvents the loss of an alkyne unit and affords **Ad[10]** in 29% yield. Compound **Ad[10]** is reportedly stable as a solid and has been characterized by NMR spectroscopy and mass spectrometric analysis.
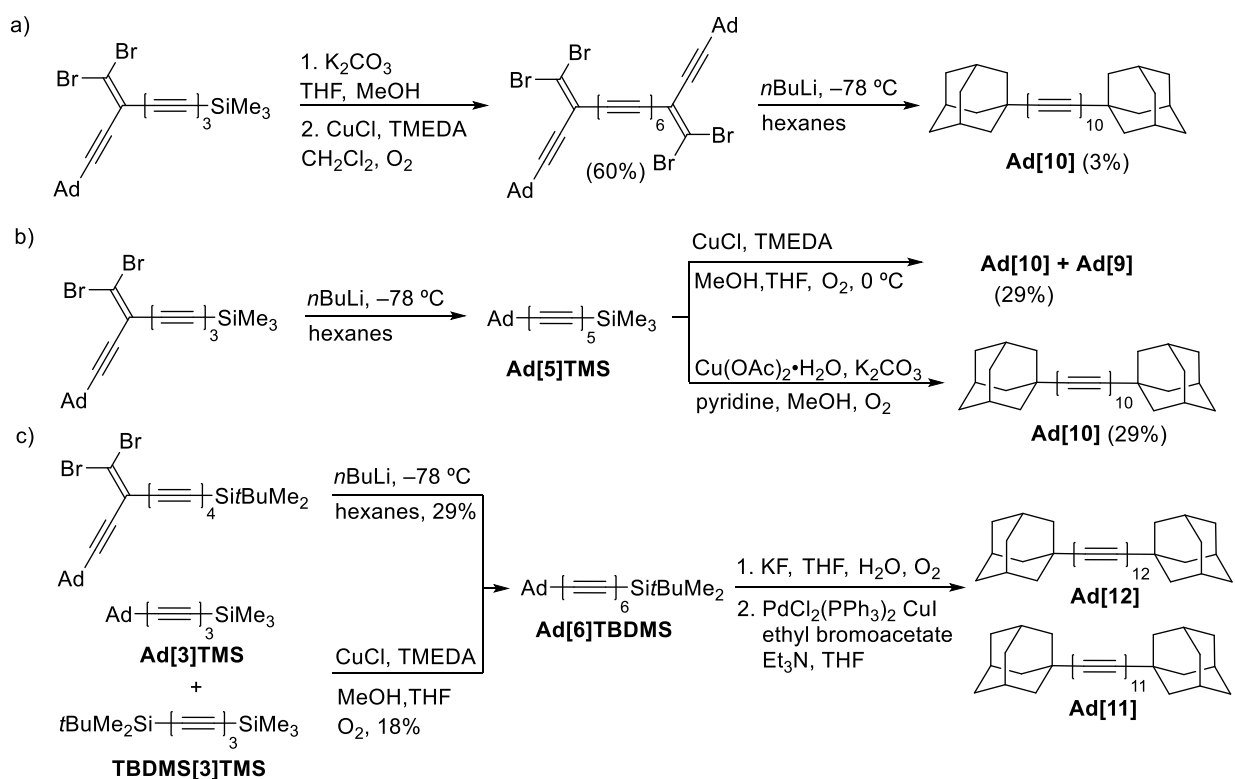
Scheme 1.14. a) Synthesis of **Ad[10]** using two-fold FBW rearrangement. b) Synthesis of **Ad[10]** using Hay and Eglinton–Galbraith coupling reactions. c) Synthesis of **Ad[12]** using Pd/Cu-catalyzed homocoupling.

Toward the synthesis of **Ad[12]**, the hexayne **Ad[6]TBDMS** is synthesized as a precursor by two different methods (Scheme 1.14c). One method uses a FBWr, affording **Ad[6]TBDMS** in 29% yield. The other method uses two different triynes **Ad[3]TMS** and **TBDMS[3]TMS**, which both undergoe in situ desilylation, and the subsequent homocoupling reaction gives **Ad[6]TBDMS** in 18% yield. Potassium fluoride in wet THF is then used to remove the *tert*-butyldimethylsilyl protecting group. Cu-catalyzed homocoupling at –40 °C gives the dodecayne **Ad[12]**, as well as a considerable amount of undecayne **Ad[11]** (not shown). A modified system using Pd/Cu catalysis,

17

on the other hand, forms the desired dodecayne **Ad[12]**, albeit with minor contamination with undecayne **Ad[11]**. As a neat solid, dodecayne **Ad[12]** quickly decomposes to a black, insoluble solid over seconds, but it can be stable for a few days when stored in solution at temperatures below –20 °C.

1.3.3 Triarylmethyl-endcapped oligo-/polyynes (Tr*[n], n = 10, 12, 14, 16, 18, 20, 22)

The tris(3,5-di-t-butylphenyl)methyl (**Tr***) endcapped oligo-/polyynes, **Tr*[n]**, have been synthesized and well-characterized up to $n = 22$, and **Tr*[22]** represents the longest oligo-/polyyne formed to date via a multi-step synthesis that has been reported.[42] The formation of **Tr*[22]** is a milestone in the synthesis of long oligo-/polyynes. The successful formation of the **Tr*[n]** series relies not only on the choice of the sterically demanding triarylmethyl endgroup, but also on the synthetic strategy.

Table 1.1. Synthesis of oligoynes **Tr*[c]TIPS** as precursors.
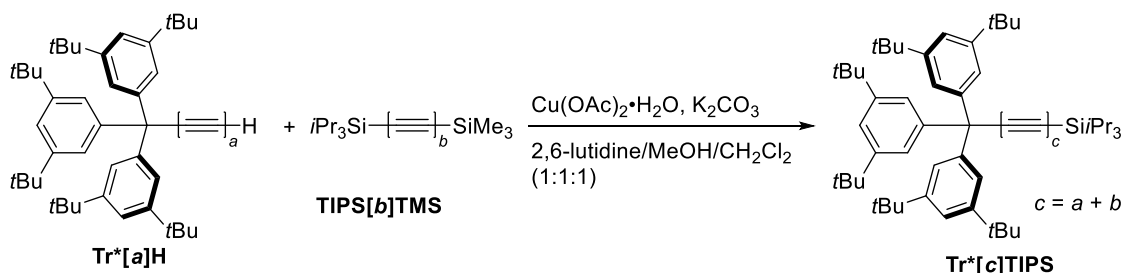
Tr*[a]H	TIPS[b]TMS	Tr*[c]TIPS %yield
(a = 2)	(b = 3)	(c = 5), 84
(a = 3)	(b = 3)	(c = 6), 63
(a = 3)	(b = 4)	(c = 7), 73
(a = 4)	(b = 4)	(c = 8), 77
(a = 5)	(b = 4)	(c = 9), 42
(a = 6)	(b = 4)	(c = 10), 52
(a = 7)	(b = 4)	(c = 11), 35

Unsymmetrical oligoynes **Tr*[c]TIPS** (c = 5–11) have been synthesized as precursors to the symmetrical oligo-/polyynes **Tr*[n]** (n = 10, 12, 14, 16, 18, 20, 22). Starting from terminal

oligoynes **Tr*[*a*]H**, longer derivatives **Tr*[*c*]TIPS** can be built up through the iterative reaction, with either a three-carbon building block **TIPS[3]TMS** or a four-carbon building block **TIPS[4]TMS** (Table 1.1). Specifically, oligoynes **Tr*[*c*]TIPS** are formed via the reaction of terminal oligoynes **Tr*[*a*]H** with an excess of **TIPS[3]TMS** or **TIPS[4]TMS** in the presence of excess $Cu(OAc)_2 \cdot H_2O$, K_2CO_3, and 2,6-lutidine. This protocol avoids the isolation of unstable terminal oligoynes (**TIPS[3]H** and **TIPS[4]H**) by the in situ removal of the trimethylsilyl group.

With **Tr*[*c*]TIPS** (c = 5–11) in hand, a sequence of desilylation (CsF, THF/H_2O) and homocoupling reactions allows the formation of **Tr*[*n*]** (n = 10, 12, 14, 16, 18, 20, 22). When using the typical Eglinton–Galbraith conditions ($Cu(OAc)_2 \cdot H_2O$, pyridine, and THF), the decayne **Tr*[10]** and dodecayne **Tr*[12]** are afforded in modest isolated yields of 26 and 41%, respectively. A critical change of the base from pyridine to the less nucleophilic 2,6-lutidine greatly improves the isolated yield and gives the decayne **Tr*[10]** and dodecayne **Tr*[12]** in isolated yields of 74 and 86%, respectively (Scheme 1.15). This modified Eglinton–Galbraith protocol is general and afforded members of the series in 18–90% yields. The products **Tr*[10–22]** are isolated as yellow, orange, or red solids that are stable under ambient conditions.
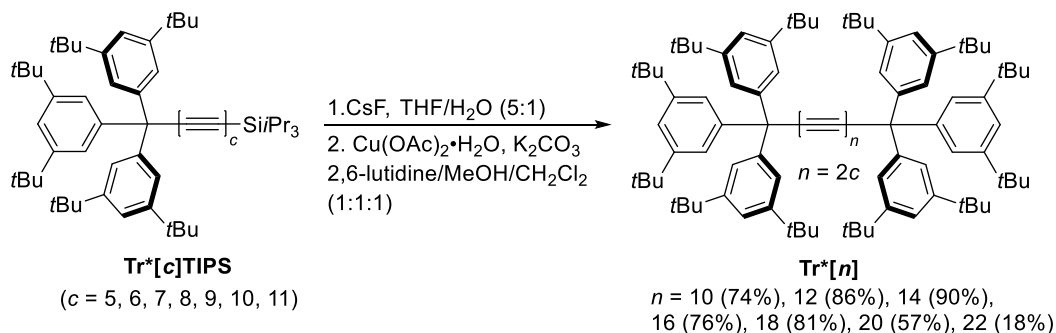
Scheme 1.15. Synthesis of **Tr*[*n*]** using modified Eglinton–Galbraith homocoupling reaction.

1.3.4 Glycoside-endcapped oligoynes (Glu[10] and Glu[12])

Glycoside-endcapped oligoynes have been reported by Frauenrath and co-workers and used as amphiphiles in the investigation of self-assembly behavior in aqueous media.[77] The formation of suitable pentayne and hexayne precursors featuring triisopropylsilyl protecting group is successfully accomplished via a Negishi heterocoupling reaction (not shown). With the penta- and hexayne precursors in hand, desilylation (AgF or CsF) followed by modified Glaser and Eglinton–Galbraith homocoupling reactions afford the decayne **Glu[10]** and dodecayne **Glu[12]**,

19

respectively (Scheme 1.16).
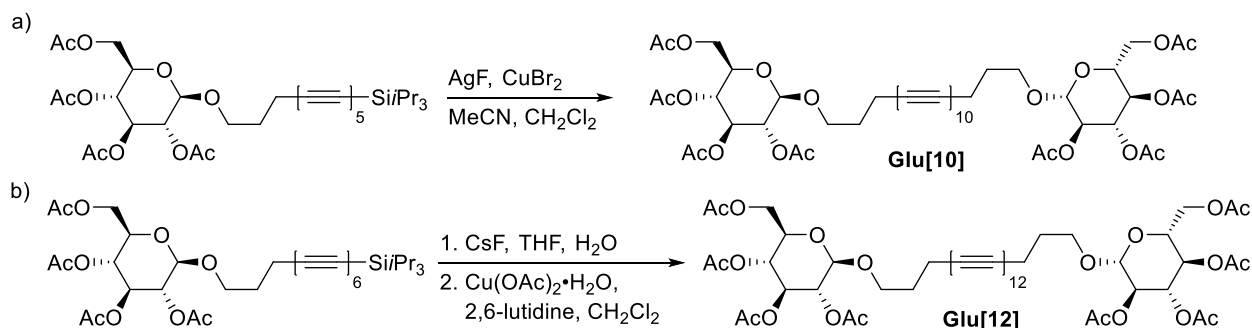
Scheme 1.16. a) Synthesis of **Glu[10]** using a modified Glaser homocoupling reaction. b) Synthesis of **Glu[12]** using modified Eglinton–Galbraith homocoupling reaction.

1.4 Synthesis of long oligoynes ($n > 8$) with sp^2-carbon endgroups

1.4.1 Aryl-substitute-endcapped and dendrimer-endcapped oligoynes (Ph(OSi)[10] and Dendrimer[10])

The syntheses of aryl and dendrimer-endcapped decaynes (**Ph(OSi)[10]** and **Dendrimer[10]**) were reported by Hirsch in 2002 (Scheme 1.17).[46] Through the introduction of large and bulky endgroups, it has been hypothesized that the intermolecular distance between sp-carbon chains would be increased, providing kinetic stability to the products. This work features the synthesis of two decaynes, **Ph(OSi)[10]** and **Dendrimer[10]**. In both cases, a trimethylsilyl-protecting group is removed from a pentayne precursor to provide the terminal pentayne in solution, which is then subjected to standard Hay homocoupling conditions, giving the desired decaynes. As described for other syntheses of decaynes (*vide supra*), shorter oligoynes are also formed during the synthesis via the loss of alkyne units. It is worth noting that this was the first study to demonstrate the issue of loss of alkyne units during an oxidative homocoupling reaction and, to date, a mechanistic study of this process has not been reported. The mixture of **Ph(OSi)[8–10]** is not separated following the homocoupling reaction, but the individual products are identified by mass spectrometric analysis. On the other hand, small amounts of pure **Dendrimer[10]** could be isolated by HPLC and characterized by MS and UV-vis spectroscopic analysis.
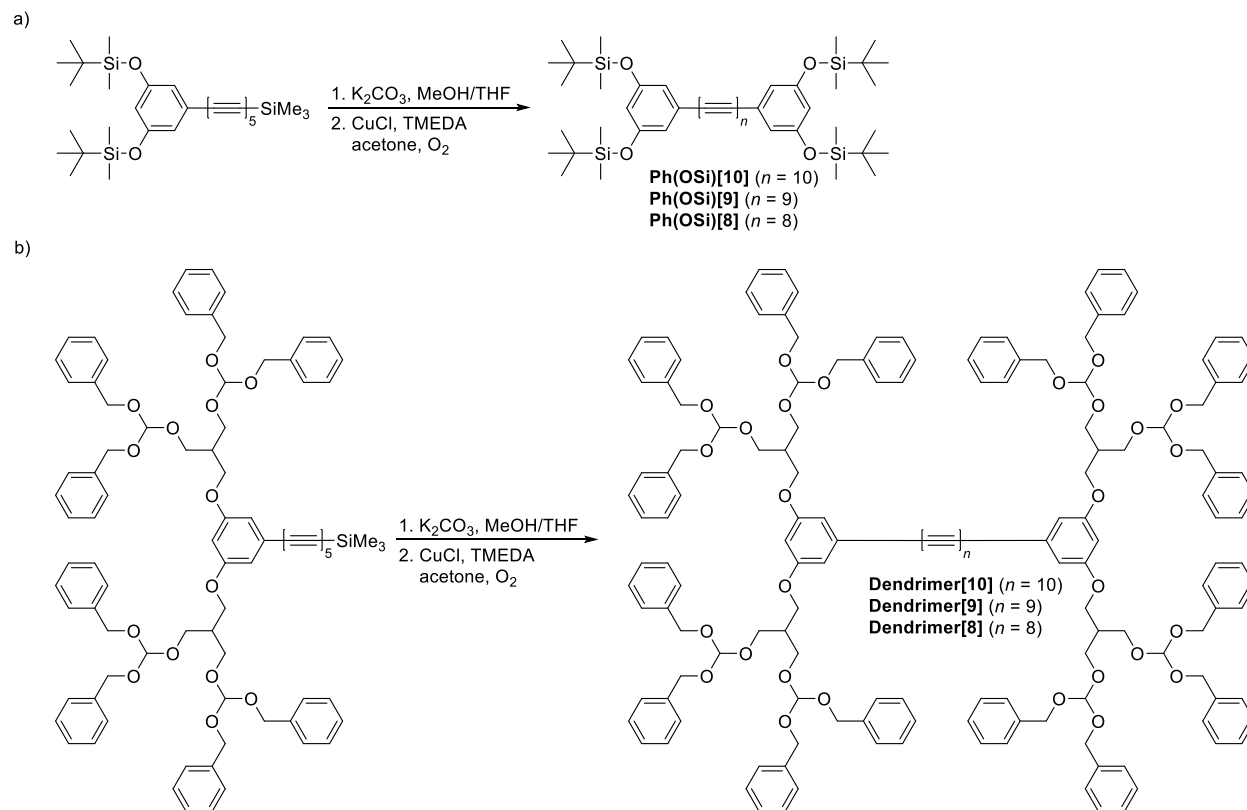
Scheme 1.17. a) Synthesis of **Ph(OSi)[10]** accompanied with shorter **Ph(OSi)[8/9]** using a Hay homocoupling reaction. b) Synthesis of **Dendrimer[10]** accompanied with shorter **Dendrimer[8/9]** using a Hay homocoupling reaction.

1.4.2 The 3,5-bis(trifluoromethyl)phenyl-endcapped oligoyne (Ph(CF₃)[12])

The first, and only, aryl-endcapped dodecayne described to date, **Ph(CF₃)[12]**, has been synthesized and reported by Cox and co-workers in 2007.[78] Formation of **Ph(CF₃)[12]** avoids formation and handling of unstable terminal alkynes as precursors through a masking strategy. Specifically, acetylene formation is achieved through desilylation of vinyl chlorides that results in beta-elimination. Thus, using four equivalents of tetrabutylammonium fluoride (TBAF), the 3,5-bis(trifluoromethyl)phenyl endcapped dodecayne **Ph(CF₃)[12]** is successfully obtained (Scheme 1.18). Unfortunately, the dodecayne **Ph(CF₃)[12]** undergoes extensive decomposition even at low concentrations (10^{-6} M) in CH_2Cl_2, and characterization is limited by the instability of this compound. Formation of the dodecayne is, nevertheless, supported by UV-vis spectroscopic and MALDI-TOF MS analyses.
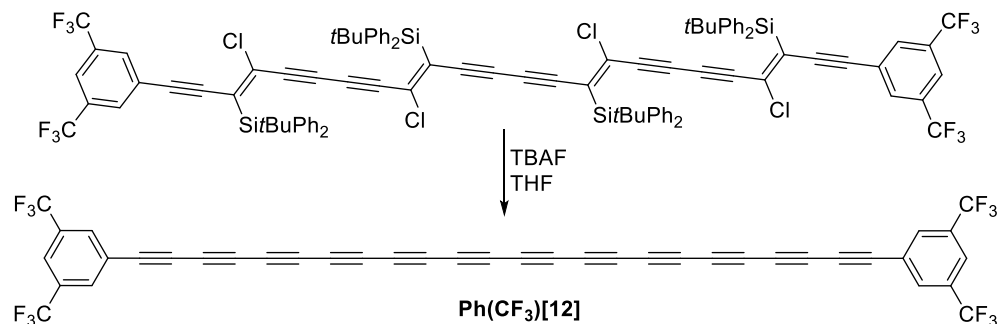
Scheme 1.18. Synthesis of a dodecayne **Ph(CF3)[12]** using elimination strategy reported by Cox and co-workers.

It is noted that oligoynes endcapped with sp^3-carbon based groups have been synthesized up to the length of $n = 22$ alkyne units, while those endcapped with aryl groups (sp^2-carbon) have been achieved only up to $n = 12$ alkyne units, albeit with limited stability (*vide supra*). It is not clear if the diminished stability arises from conjugation of the sp-carbon chain with the endgroup or from reduced steric shielding of the oligoyne from the planar aryl-groups. Given that hyperconjugation of the sp-carbon chain with the sp^3-carbon-endcapped oligoynes exists, and these derivatives are stable, it is intriguing to determine if/how conjugation of the sp-carbon chain with an endgroup is a critical factor that influences the stability of an oligoyne (as suggested by the instability of aryl-endcapped derivatives). Synthetically, this is a significant concern toward achieving long oligoynes ($n > 12$) endcapped with sp^2-carbon based groups. Alternatively, many studies have established that steric shielding of the oligoyne framework, especially the 'protection' of the end-most acetylene moieties, is a key component to providing kinetically stable oligoynes from reactions.[79] Thus, an interplay between electronic and steric factors appears to exist toward ensuring extended oligoynes, and the successful design of an endgroup should make the synthesis of a long oligo-/polyyne innately possible.

1.5 Properties of oligo-/polyynes

With successful syntheses of long oligo-/polyynes ($n \geq 10$), it becomes possible to extrapolate properties as a function of length toward understanding and predicting the characteristics of carbyne. Through the use of ^{13}C NMR and UV-vis spectroscopy, as well as bond length analysis (via X-ray crystallographic data), structural information of carbyne can be predicted. This section will provide examples of detailed characterization of oligo-/polyyne series, and comparisons as a function of endgroups are used to help outline an emerging picture of the properties of carbyne.

1.5.1 ^{13}C NMR spectroscopy

The available ^{13}C NMR spectroscopic data of the longest representative oligoynes, including *t*Bu[10],[39] Ad[10],[76] Glu[12],[80] and Tr*[22][42], as measured in CDCl$_3$, has been summarized in Table 1.2. For comparison, **Re[10]**[50] in CD$_2$Cl$_2$, **Pt(tol)[14]**[48a] in acetone-d$_6$, and computed **H[10]** have also been included.

Table 1.2. ^{13}C NMR alkyne carbon resonances for oligoynes *t*Bu[10], Ad[10], Glu[12], TIPS[10], Tr*[22], Re[10], Pt(tol)[14], and H[10].

oligoyne	Alkyne carbon chemical shifts in CDCl$_3$ (ppm)
*t*Bu[10][a]	89.6, 64.3, 63.8, 63.5, 63.5, 63.0, 62.6, 62.1, 61.6, 61.4
Ad[10][a]	89.2, 64.7, 63.9, 63.7, 63.5, 63.1, 62.6, 62.1, 61.6, 61.5
Glu[12][a]	81.6, 66.2, 64.0, 63.8, 63.7, 63.5, 63.2, 62.9, 62.5, 61.4, 60.5
Tr*[22][a]	87.35, 68.66, 64.60, 64.27, 64.14, 64.00, 63.91, 63.83, 63.77, 63.72, 63.66, 63.61, 63.54, 63.44, 63.33, 63.15, 62.93, 62.64, 62.58, 62.29, 62.10
TIPS[10][a]	89.3, 88.8, 63.8, 63.6, 63.5, 63.2, 62.9, 62.5, 62.2, 61.0
Re[10][b]	127.3, 113.2, 67.0, 66.6, 66.5, 65.5, 65.4, 65.3, 64.9, 64.8
Pt(tol)[14][c]	126.0, 95.0, 67.8, 66.9, 65.4, 64.5, 63.7, 63.1, 62.5, 61.8, 61.0, 60.0, 58.8, 55.3
H[10][d]	73.46, 71.05, 66.29, 66.14, 66.10, 65.92, 65.68, 65.41, 65.12, 64.86

^{a} Measured in CDCl$_3$. ^{b}Measured in CD$_2$Cl$_2$. ^{c}Measured in acetone-d$_6$.^{d}Computed values.

According to previous studies via ^{13}C labelling and two-dimensional NMR spectroscopy, the most downfield resonance for each oligoyne stems from the terminal alkyne moiety (R–C≡C–(C≡C)$_{n–2}$–C≡C–R).[72b, 81] For the oligo-/polyynes endcapped with metal-atoms (**Re[10]** and **Pt(tol)[14]**), this statement is also true, which is supported with the ^{13}C NMR assignment of the terminal alkyne moiety via the analysis of the coupling constants through the terminal alkyne and the endgroup moieties, i.e., the correlation between carbon and phosphorus atoms $J_{C–P}$.[48a, 50] For non-metal endcapped oligo-/polyynes, additional resonances appear within a narrow range of 61–65 ppm. The literature suggests, through the analysis of ^{13}C NMR for metal-atom endcapped **Re[10]** and **Pt(tol)[14]**, that the presumable chemical shift of carbyne would be in the narrow range of either 64–67 or 60–63 ppm, respectively; this data highlights the potential influence of the metal

endgroups.[48a, 50] The data for oligoynes endcapped with non-metal groups (i.e., sp^3-carbon and silyl) shows approximate convergence values of 63.5 ppm for **tBu[10]**, 63.7 ppm for **Ad[10]**, 63.6 ppm for **TIPS[10]**, 63.8 ppm for **Glu[12]**, and 63.7 ppm for **Tr*[22]**. The analysis of nucleus independent chemical shifts (NICS) for H-endcapped oligoynes (**H[n]**) indicates that no additive or multiplicative effects exist along the chain.[82] This computational study implies that the convergence chemical shifts would not be affected by the incorporation of additional sp-carbons. Therefore, a good approximation of the ^{13}C NMR spectroscopic chemical shift for carbyne would likely be in the confined range of 63–64 ppm. Furthermore, this presumed chemical shift of carbyne indicates that the structure of carbyne should be polyynic, thus, Peierls distortion[15] remains.

1.5.2 UV-vis spectroscopy

UV-vis spectroscopy provides insight into many aspects of the electronic properties of oligo-/polyynes. On one hand, there are usually clear trends in wavelength of the lowest energy UV-vis absorption observed in the spectra of oligoynes (λ_{max}), and λ_{max} changes as a function of molecular length. On the other hand, UV-vis spectra of oligoynes also feature characteristic, sharp bands that include vibrational fine structure, which provide valuable structural data. As the number of alkyne units (n) is increased for a series of oligoynes, the λ_{max} values steadily red shift. It is reasonable to examine the UV-vis data as a function of increasing length n to map the transitions from an oligoyne to a polyyne as the effective conjugation length (ECL) is reached (ECL is also referred to as the saturation length, i.e., when a value saturates as a function of molecular length). Or to put it another way, beyond the ECL, further extension of the chain length yields no additional change in λ_{max} (and λ_{sat} has been reached). While the analysis of the relationships between n and λ offers clues to the potential properties of carbyne, when properties are independent of both chain length and terminal functionality, the ability to synthesize longer polyynes is undoubtedly needed for more accurate predictions.

UV-vis spectra for oligoynes usually exhibit two regions of absorption, namely the region of λ_{main} that has a strong high energy absorption and the region of λ_{weak} that has a lower energy and greatly diminished intensity. Generally, these two distinct regions can be observed in short oligoynes, with the exception H-endcapped oligoynes (**H[n]**) [47, 69a, 69b] and cyano-endcapped oligoyne (**CN[n]**), both with $D_{\infty h}$ molecular symmetry.[70a] According to recent computational

24

studies and experimental observations, λ_{main} is strongly dipole allowed, while λ_{weak} is increasingly forbidden as a function of n as the molecular pseudosymmetry approaches $D_{\infty h}$.[83] Therefore, the molar absorption ε of λ_{main} steadily increases with molecular length, while ε of λ_{weak} steadily decreases. The vanishing absorption intensity of λ_{weak} thus represents an observable index that reflects the transition from an oligoyne to a polyyne as increasing n and demonstrates the loss of endgroup effects.

In the analysis of UV-vis absorption data, the intense maxima of λ_{main} with the lowest energy absorption, $\lambda_{max(main)}$, has typically been plotted as a function of $1/n$ (Figure 1.2), using an empirical function of the form:[46, 50, 72b]

$$\lambda_{(n)} = k(1/n) + b \qquad \text{equation (1)}$$

where n is the number of alkyne units, $\lambda_{(n)}$ is λ_{max} for an oligoyne of length n, the y-intercept b is the value of λ_∞ as $1/n \to 0$, and the factor 'k' reflects how fast the oligoyne approaches to carbyne. An absorption wavelength of $\lambda_{sat} = b$ can be extrapolated as a prediction for $n = \infty$, representing a prediction for polyynes and carbyne. Using $\lambda_{max(main)}$ values of oligoynes, the analyses using equation (1) give values for **TIPS[n]** at $\lambda_{sat(main)} = 570$ nm,[72b] **Pt(tol)[n]** at $\lambda_{sat(main)} = 573$ nm,[48a] **Re[n]** at $\lambda_{sat(main)} = 565$ nm,[50] **Glu[n]** at $\lambda_{sat(main)} = 561$ nm,[80] and **Tr*[n]** at $\lambda_{sat(main)} = 564$ nm (see Table 1.3).[42] In a similar manner, the values of using $\lambda_{max(weak)}$ have been fit for two series of oligoynes, giving values for **Glu[n]** of $\lambda_{sat(weak)} = 810$ nm and for **Tr*[n]** of $\lambda_{sat(weak)} = 756$ nm, respectively (Table 1.3).[80]

A second empirical relationship has been used to analyze UV-vis data based on the power-law form:[72b]

$$E_g = 1/\lambda_{(n)} = an^{-x} \qquad \text{equation (2)}$$

where E_g is the energy gap in cm^{-1} calculated from λ_{max}, n is the number of alkyne units, $\lambda_{(n)}$ is λ_{max} for an oligoyne of length n, and the factor 'a' is the constant slope. When x = 0.5, equation (2) can become $\lambda_{(n)}^2 = an$, which is commonly called the 'Lewis–Calvin law' observed in polyenic compounds.[84] Using equation (2) for the analysis of $\lambda_{max(main)}$ values of **TIPS[n]** gives the best fit of $E_g = 1/\lambda_{(n)} = 64900n^{-0.379\pm0.002}$. Thus, $n = 32$ when $\lambda_{max(main)} = \lambda_{sat(main)} = 570$ nm (*vide supra*), which predicts the progression of the absorption wavelength $\lambda_{max(main)}$ reaches saturation at ECL of 32 alkyne units.
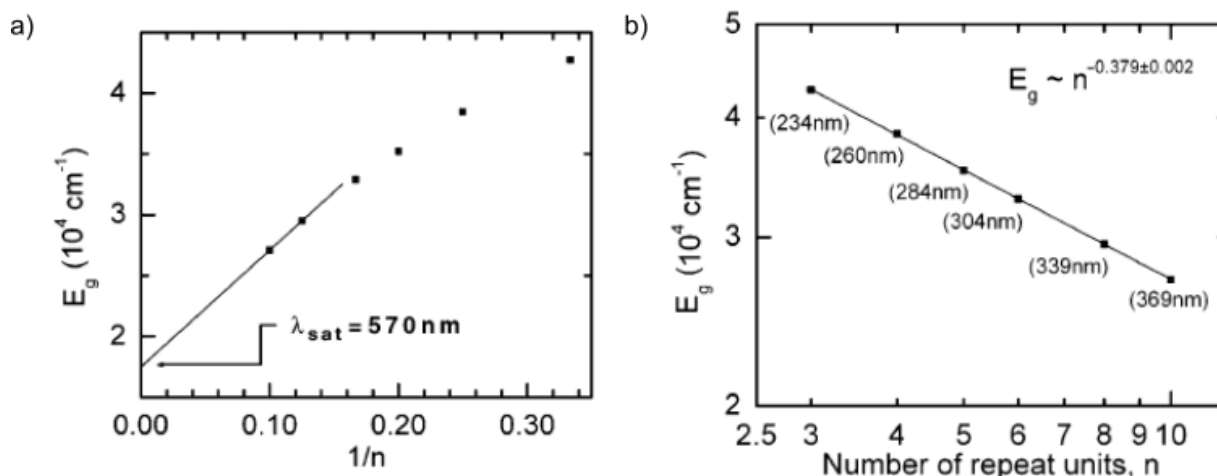
Figure 1.2. a): Plots of E_g values in cm^{-1} at $\lambda_{max(main)}$ versus $1/n$ for **TIPS[n]** using equation (1). b): Power-law plot of E_g values in cm^{-1} at $\lambda_{max(main)}$ versus n for **TIPS[n]** using equation (2). (Reprinted with permission from American Chemical Society: *J. Am. Chem. Soc.* **2005**, *127*, 2666−2676).

Table 1.3. Summary of λ_{sat} values predicted by two methods from oligoynes.

oligoyne	$\lambda_{sat(main)}{}^a$		$\lambda_{sat(weak)}{}^b$	reference
	eq (1)	eq (3)	eq (1)	
TIPS[n]	570^c	$-^i$	$-^i$	[72b]
Pt(tol)[n]	573^d	$-^i$	$-^i$	[48a]
Re[n]	565^e	$-^i$	$-^i$	[50]
Glu[n]	561^f	$-^i$	810^f	[80]
Tr*[n]	564^g	485^h	756^f	[42, 80]

^{a}Analysis with $\lambda_{max(main)}$ absorptions. ^{b}Analysis with $\lambda_{max(weak)}$ absorptions. ^{c}For $n = 8, 10$. ^{d}For $n = 6, 8, 10, 12, 14$. ^{e}For $n = 3, 4, 5, 6, 8, 10$. ^{f}For $n = 4, 6, 8, 10, 12$. ^{g}For $n = 10, 12, 14, 16, 18, 20, 22$. ^{h}For $n = 4, 6, 8, 10, 12, 14, 16, 18, 20, 22$. ^{i}Not reported or insufficient data.

It is noted, however, that the convergence length should be reached at an oligomer length n, far less than infinity for conjugated systems in general and oligoynes in particular.[42, 85] Thus, there are nonnegligible deviations from the necessary linear plot of λ_{max} versus $1/n$. As an alternative, Meier has reported a protocol[85a] that accounts for the effective conjugation length of oligoynes and offers a better estimate using an exponential function expressed by:

$$\lambda_{(n)} = \lambda_\infty - (\lambda_\infty - \lambda_1)\, e^{-k(n-1)} \qquad \text{equation (3)}$$

where n is the number of alkyne units, $\lambda_{(n)}$ is λ_{max} for an oligoyne of length n (thus λ_1 is λ_{max} of the

monomer with $n = 1$), and λ_∞ is the limiting value as $n \to \infty$. The factor "k" provides an indication of how fast saturation (convergence) is approached. Finally, λ_{sat} is defined by fulfilment of the relationship $\lambda_\infty - \lambda_{(n)} \leq 1$ nm. The use of Meier equation (3) predicts a $\lambda_{sat(main)}$ for carbyne of 485 nm (2.56 eV) at $n = 48$ for **Tr*[n]** (Figure 1.3). From the known experimental data, the analysis of $\lambda_{sat(main)}$ for **Tr*[n]** offers the most accurate prediction showing that carbyne has a finite bandgap of ca. 2.56 eV.
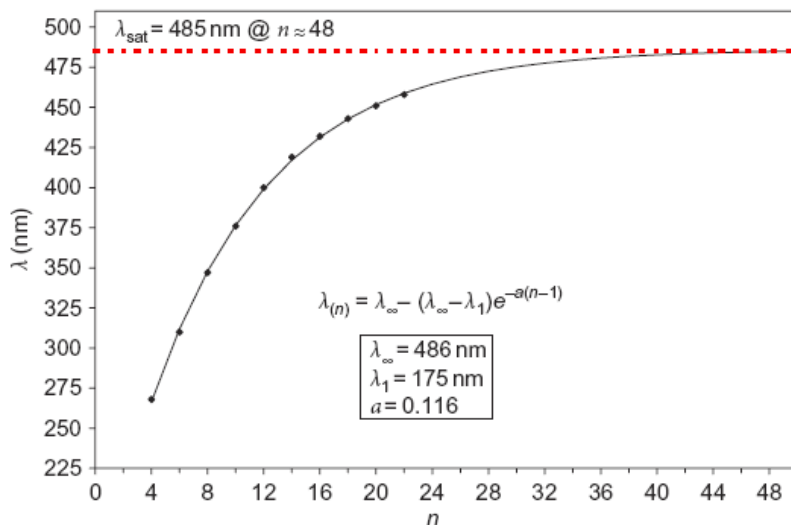
Figure 1.3. Convergence of $\lambda_{max(main)}$ in the **Tr*[n]** series using equation (3). (Reprinted with permission from Springer nature: *Nat. Chem.* **2010**, *2*, 967–971).

1.5.3 X-ray crystallographic analysis

X-ray crystallographic analysis is essential to determine the structural properties of oligoynes in the solid-state. A fundamental analysis of bond lengths of an oligoyne backbone is necessary to uncover if the single and triple bonds lengths finally converge to one value at the ECL. This analysis is based on bond length alteration (BLA) of oligoynes, which is the difference in the bond length between the single and triple bonds and reflects the band gap of a 1-D conjugated system.[13, 85b] A cumulenic form of carbyne is expected with BLA = 0,[86] while a polyynic form will have a non-zero BLA value,[87] which is also referred to as Peierls distortion i.e., Peierls distortion suggests that the structure maintains a sequence of long (single) and short (triple) bonds.[15] Recently, BLA of oligoynes has been widely investigated through theoretical calculations[13, 88] and experimentally via analysis of X-ray crystallographic data.[39, 89] The chain conformation of oligoynes is also interesting to examine. Bending of an oligoyne framework occurs with some extent of deviation from linearity and is often observed, presumably due to crystal packing

effects.[72b, 89]

The longest oligoyne that has been realized by X-ray crystallography is the decayne ***t*Bu[10]**.[39] X-ray crystallography analysis for the series ***t*Bu[*n*]** (n = 2, 3, 4, 8, 10) has been reported. This analysis allows experimental consideration of BLA values change as a function of molecular length n. BLA values reportedly reach a limiting value of 0.135 Å at n = 10 to 12 in the ***t*Bu[*n*]** series.[39] Computationally, the **H[*n*]** series predicts a limiting BLA value of 0.139 Å.[90] Both analyses suggest the reduction of BLA value as a function of n does not reach zero and approaches saturation at relatively short oligoyne lengths. These consistent data allow an extrapolation toward carbyne that would contain contiguous alternating single and triple bonds, and Peierls distortion will be upheld. More details will be discussed in subsequent chapters.

1.6 Conclusions

Successful strategies have been developed for the synthesis of long oligoynes, R–(C≡C)$_n$–R (**R[*n*]**, n ≥ 8). A number of methods have been improved to offer promising results for reaction yield of oligoynes, such as the Hay coupling reaction. In many cases, however, loss of alkyne units during the oxidative coupling reactions remains an issue to overcome, although this problem can sometimes be avoided or suppressed by the optimization of reaction parameters such as temperature.

The choice of an endgroup is a key to the stability of oligoynes, and a clever endgroup design thus offers appreciable advances in the stability of oligo-/polyynes as a function of length. With a series of long oligo-/polyyne in hand, the combination of spectroscopic and physical analyses gives a reasonable prediction for the properties of polyynes and carbyne that cannot yet be synthesized. For example, the ^{13}C NMR chemical shift for carbyne is expected to be in the range of 63–64 ppm, while carbyne is predicted to maintain a finite optical gap of 485 nm (2.56 eV) at ECL of n = 48, based on analyses of the strongest, λ_{main} absorptions in the UV-vis spectra. On the other hand, the weaker, lower energy absorption, λ_{weak} would suggest a lower optical energy gap, but extrapolation of the absorption data for λ_{weak} to make an reliable estimate for carbyne is not yet possible due to a lack of suitable oligo-/polyynes. Finally, using solid-state analysis based on X-ray crystallographic data, BLA values of carbyne are predicted to be ca. 0.135–0.139 Å, with the ECL of ca. n = 10 to 12. Syntheses and analyses reported to date converge on one common conclusion: Chemists must improve the rational synthesis of polyynes in order to better model the

properties of carbyne.

1.7 Motivation

The last three decades have witnessed the rapid development of carbon-rich compounds and materials, with the discovery and potential applications of their exceptional properties.[91] Carbon is one of the most versatile elements in the periodic table, and the synthesis of new forms of carbon, so-called "synthetic carbon allotropes (SCAs)",[6] is an extensive research area. The *sp*-carbon allotrope, commonly referred to as carbyne, however, is absent, and intense discussion exists over its existence.[16-17, 92] The central point of debate is likely the instability of carbyne. The past 60 years are rich in the synthesis of oligo-/polyynes, and some of these studies have provided useful model systems toward understanding the potential of carbyne.[42, 72b]

In 2010, a remarkable chain of 44 *sp*-hybridized carbon atoms was realized by Chalifoux and Tykwinski (Figure 1.4).[42] The carbon chain of **Tr*[22]** is terminated with sp^3-carbon endgroups, namely bulky triarylmethyl groups. The well-developed synthesis of **Tr*[n]** (*n* = 4–22), as described in the introduction, affords a series of monodisperse oligomers with defined molecular length, which is important because it would be possible to extrapolate the properties of these oligoynes to that of carbyne. Recently, in 2016, carbon chains composed of more than 6000 carbon atoms have been formed in double-walled carbon nanotubes, albeit with random lengths.[92] These encapsulated carbon chains represent the closest achievement yet reported toward the synthesis of a stable sample of carbyne.
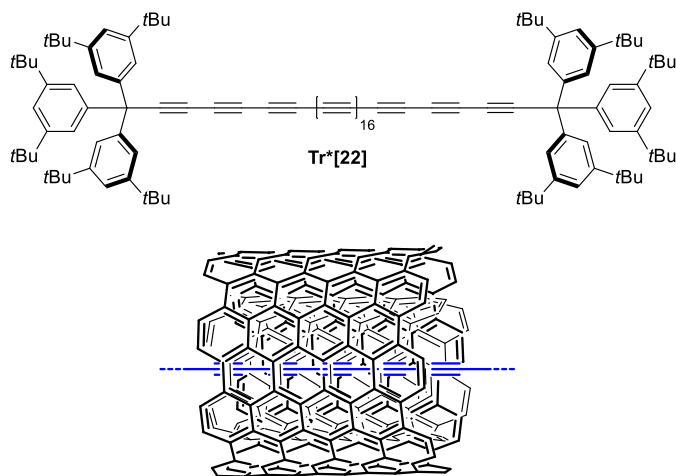
Figure 1.4. Molecular structure of **Tr*[22]** and long linear carbon chains encapsulated in double-walled carbon nanotubes.

In the absence of experimental studies of carbyne, chemists extrapolate its potential characteristics through the examination of homologous series of oligoynes. Before considering an authentic sample of carbyne (purely *sp*-carbon chain without an endgroup), a polyyne should be more easily achieved. However, the transition of an oligoyne (showing properties linked to length) to a polyyne (properties independent of length) has not been detailed experimentally. Thus, progress toward carbyne is, to some extent, linked to the synthesis of polyynes. Thus, a primary goal of this thesis is the formation of a series of oligoynes and polyynes as suitable model compounds, such that the properties of carbyne could be better predicted as a function of molecular length.

The fundamental study of oligo-/polyynes is important, not only in the aspect of modelling the potential properties of carbyne but also in uncovering the unique properties of oligoynes, e.g., as molecular wires. Oligoynes consist of a rigid and approximately cylindrical π-system, with a nearly unhindered rotation about the *sp*-carbon chain, which makes them potentially ideal molecules as wires.[25, 43] To achieve the goal of molecular wires, the design of oligoynes endcapped with anchoring groups is required. Thus, pyridyl-endcapped oligoynes (PEOs) have been developed, and the PEOs without steric protecting groups are known up to the length of a hexayne.[93] PEOs modified in the 3- and 5-positions of the pyridyl ring with phenyl groups offer steric shielding of the *sp*-carbon core and can be up to the length of an octayne (Figure 1.5).[43] For example, without any steric protection, **Py[6]** is unstable as a solid, while the introduction of phenyl groups renders **Py*[8]** stable in the solid state. Motivated by the fact that a bulky endgroup can stabilize PEOs, the goal of this project is to synthesize a series of long PEOs with good stability, based on increasing the steric shielding offered by the pendent aryl group in **Py**[*n*].

Py[*n*] (*n* = 2,4,6)   Py*[*n*] (*n* = 2,4,6,8)   Py**[*n*] (this work)
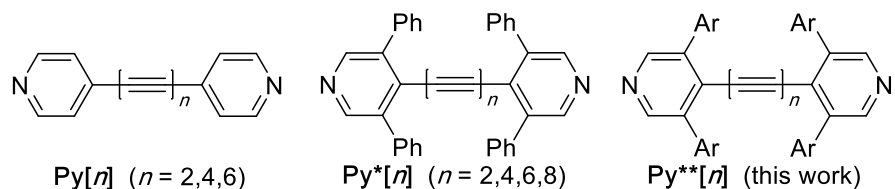
Figure 1.5. Known structures of PEOs **Py[*n*]** and **Py*[*n*]**; PEOs developed herein **Py**[*n*].

As discussed in the introduction, many products from the syntheses of long oligoynes R–(C≡C)$_n$–R ($n \geq 10$) show loss of alkyne units when using Hay homocoupling.[39, 72] The activation of a C–C bond by copper salts is rare and exciting.[94] This phenomenon motivated me to confirm

and study the loss of an alkyne unit, while determining which alkyne unit is being removed from the carbon chain. Thus, a mechanistic study of alkyne loss during the Hay homocoupling reaction has been targeted. A ^{13}C labeled pentayne has been designed as a key intermediate (Scheme 1.19), and its subsequent homocoupling reaction will be examined.
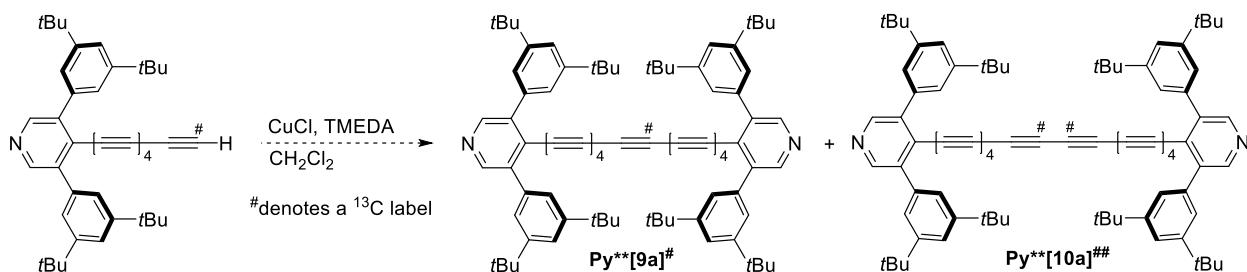
Scheme 1.19. A ^{13}C labeled pentayne under Hay homocoupling conditions.

Because pyridyl can serve as an anchoring group to, for example, metal electrodes, PEOs have been designed as molecular wires and studied by scanning tunneling microscopes in break junction (STM-BJ) devices.[24a, 27] Beyond metal electrodes, graphene as an ideal low-dimensional electrode material has been extensively developed on single-molecule junctions.[95] Unfortunately, pyridyl groups do not effectively anchor to a graphene electrode based on noncovalent interactions alone. A hypothesis was formulated that coordination of PEOs to cationic platinum atoms could enhance the association between PEOs and graphene electrodes. Therefore, model compounds have been synthesized to test this hypothesis (Figure 1.6a).
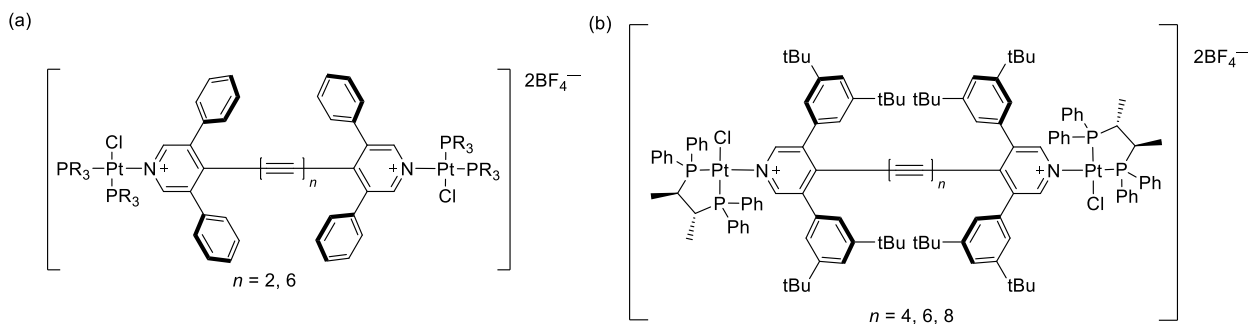
Figure 1.6. Structures of (a) achiral Pt-PEOs complexes, and (b) chiral Pt-PEOs complexes.

Beyond molecular wires, recent computational reports predict that oligoynes should display axial chirality via the helical arrangement of their frontier molecular orbitals.[18, 96] Therefore, a series of chiral PEOs bound as Pt-complexes bearing chiraphos ligands has been

31

designed and synthesized. These molecules are studied toward establishing whether, or not, the predicted chiral characteristics of oligoynes might be confirmed experimentally (Figure 1.6b).

Along the way toward functionalization and application, the ability to combine molecular wires with chromophores has led to work in photochemistry. For example, alkynes and oligoynes can play a role in the attachment of switchable systems to a surface toward the formation of functional nanosystems.[97] A "platform approach" has been developed by a number of researchers, including the work by Herges and co-workers that allows for the organization of free-standing molecules on a surface, based on the design and synthesis of planar triazatriangulenium (TATA) groups as the platform (Figure 1.7a).[98] Motivated by the platform approach, it is hypothesized that porphyrins could serve in a similar manner since porphyrins are a class of flat, π-rich molecules. With the goal of creating functional platforms, a hierarchical assembly based on a gallium-porphyrin as a platform, combined with PEOs as linkers is targeted (Figure 1.7b).[99] The modular method should allow the hierarchal synthesis of porphyrins bearing axially bounded azo groups, which are multicomponent and photoswitchable systems that are also suitable as molecular wires.

Figure 1.7. a) Schematic view of the platform approach using gold (111) as a surface and triazatriangulenium (TATA) as a platform anchoring with an azobenzene functional group using acetylide linker.[100] The platform approach is potentially applied for porphyrin systems. b) The synthetic scheme of the formation of the multidimensional gallium-acetylide porphyrin complex.

1.8 References

[1] a) X. Y. Wang, X. L. Yao, K. Mullen, *Sci. China Chem.* **2019**, *62*, 1099–1144; b) Y. Segawa, D. R. Levine, K. Itami, *Acc. Chem. Res.* **2019**, *52*, 2760–2767.

[2] H. W. Kroto, J. R. Heath, S. C. Obrien, R. F. Curl, R. E. Smalley, *Nature* **1985**, *318*, 162–163.

[3] K. S. Novoselov, A. K. Geim, S. V. Morozov, D. Jiang, Y. Zhang, S. V. Dubonos, I. V. Grigorieva, A. A. Firsov, *Science* **2004**, *306*, 666–669.

[4] a) R. H. Baughman, A. A. Zakhidov, W. A. de Heer, *Science* **2002**, *297*, 787–792; b) Y. N. Xia, P. D. Yang, Y. G. Sun, Y. Y. Wu, B. Mayers, B. Gates, Y. D. Yin, F. Kim, Y. Q. Yan, *Adv. Mater.* **2003**, *15*, 353–389.

[5] a) C. S. Huang, Y. J. Li, N. Wang, Y. R. Xue, Z. C. Zuo, H. B. Liu, Y. L. Li, *Chem. Rev.* **2018**, *118*, 7744–7803; b) X. Gao, H. B. Liu, D. Wang, J. Zhang, *Chem. Soc. Rev.* **2019**, *48*, 908–936.

[6] A. Hirsch, *Nat. Mater.* **2010**, *9*, 868–871.

[7] J. M. Cai, P. Ruffieux, R. Jaafar, M. Bieri, T. Braun, S. Blankenburg, M. Muoth, A. P. Seitsonen, M. Saleh, X. L. Feng, K. Mullen, R. Fasel, *Nature* **2010**, *466*, 470–473.

[8] E. R. Darzi, R. Jasti, *Chem. Soc. Rev.* **2015**, *44*, 6401–6410.

[9] M. D. Kilde, A. H. Murray, C. L. Andersen, F. E. Storm, K. Schmidt, A. Kadziola, K. V. Mikkelsen, F. Hampel, O. Hammerich, R. R. Tykwinski, M. B. Nielsen, *Nat. Commun.* **2019**, *10*, 3714.

[10] A. Narita, X. Feng, Y. Hernandez, S. A. Jensen, M. Bonn, H. Yang, I. A. Verzhbitskiy, C. Casiraghi, M. R. Hansen, A. H. Koch, G. Fytas, O. Ivasenko, B. Li, K. S. Mali, T. Balandina, S. Mahesh, S. De Feyter, K. Mullen, *Nat. Chem.* **2014**, *6*, 126–132.

[11] R. Jasti, J. Bhattacharjee, J. B. Neaton, C. R. Bertozzi, *J. Am. Chem. Soc.* **2008**, *130*, 17646–17647.

[12] H. Omachi, T. Nakayama, E. Takahashi, Y. Segawa, K. Itami, *Nat. Chem.* **2013**, *5*, 572–576.

[13] S. Yang, M. Kertesz, *J. Phys. Chem. A* **2006**, *110*, 9771–9774.

[14] J. A. Januszewski, R. R. Tykwinski, *Chem. Soc. Rev.* **2014**, *43*, 3184–3203.

[15] R. Hoffmann, *Angew. Chem. Int. Ed. Engl.* **1987**, *26*, 846–878.

[16] C. S. Casari, A. Milani, *Mrs Commun.* **2018**, *8*, 207–219.

[17] a) B. Pan, J. Xiao, J. Li, P. Liu, C. Wang, G. Yang, *Sci. Adv.* **2015**, *1*, e1500857; b) P. Tarakeshwar, P. R. Buseck, H. W. Kroto, *J. Phys. Chem. Lett.* **2016**, *7*, 1675–1681.

[18] M. Liu, V. I. Artyukhov, H. Lee, F. Xu, B. I. Yakobson, *ACS Nano* **2013**, *7*, 10075–10082.

[19] L. P. Kobets, I. S. Deev, *Compos. Sci. Technol.* **1998**, *57*, 1571–1580.

[20] P. B. Sorokin, H. Lee, L. Y. Antipina, A. K. Singh, B. I. Yakobson, *Nano Lett.* **2011**, *11*, 2660–2665.

[21] A. Malhotra, M. Maldovan, *Nanotechnology* **2019**, *30*, 372002.

[22] Y. Zhang, H. L. Zhang, J. H. Wu, X. T. Wang, *Scr. Mater.* **2011**, *65*, 1097–1100.

[23] M. Wang, S. Lin, *Sci. Rep.* **2015**, *5*, 18122.

[24] a) C. Wang, A. S. Batsanov, M. R. Bryce, S. Martín, R. J. Nichols, S. J. Higgins, V. M.

García-Suárez, C. J. Lambert, *J. Am. Chem. Soc.* **2009**, *131*, 15647–15654; b) P. Moreno-Garcia, M. Gulcur, D. Z. Manrique, T. Pope, W. J. Hong, V. Kaliginedi, C. C. Huang, A. S. Batsanov, M. R. Bryce, C. Lambert, T. Wandlowski, *J. Am. Chem. Soc.* **2013**, *135*, 12228–12240.

[25] C. S. Casari, M. Tommasini, R. R. Tykwinski, A. Milani, *Nanoscale* **2016**, *8*, 4414–4435.

[26] D. M. Guldi, H. Nishihara, L. Venkataraman, *Chem. Soc. Rev.* **2015**, *44*, 842–844.

[27] a) D. C. Milan, M. Krempe, A. K. Ismael, L. D. Movsisyan, M. Franz, I. Grace, R. J. Brooke, W. Schwarzacher, S. J. Higgins, H. L. Anderson, C. J. Lambert, R. R. Tykwinski, R. J. Nichols, *Nanoscale* **2017**, *9*, 355–361; b) P. Moreno-Garcia, M. Gulcur, D. Z. Manrique, T. Pope, W. J. Hong, V. Kaliginedi, C. C. Huang, A. S. Batsanov, M. R. Bryce, C. Lambert, T. Wandlowski, *J. Am. Chem. Soc.* **2013**, *135*, 12228–12240.

[28] a) X. Zhao, C. Huang, M. Gulcur, A. S. Batsanov, M. Baghernejad, W. Hong, M. R. Bryce, T. Wandlowski, *Chem. Mater.* **2013**, *25*, 4340–4347; b) A. Shah, B. Adhikari, S. Martic, A. Munir, S. Shahzad, K. Ahmad, H. B. Kraatz, *Chem. Soc. Rev.* **2015**, *44*, 1015–1027.

[29] E. Leary, A. La Rosa, M. T. Gonzalez, G. Rubio-Bollinger, N. Agrait, N. Martin, *Chem. Soc. Rev.* **2015**, *44*, 920–942.

[30] C. Glaser, *Ber. Dtsch. Chem. Ges.* **1869**, 422–424.

[31] G. Eglinton, A. R. Galbraith, *Chem. Ind. (London)* **1956**, 737–738.

[32] A. S. Hay, *J. Org. Chem.* **1962**, *27*, 3320–3321.

[33] a) J. H. Li, Y. Liang, Y. X. Xie, *J. Org. Chem.* **2005**, *70*, 4393–4396; b) A. Toledo, I. Funes-Ardoiz, F. Maseras, A. C. Albeniz, *Acs Catal.* **2018**, *8*, 7495–7506.

[34] A. Sagadevan, V. P. Charpe, K. C. Hwang, *Catal. Sci. Technol.* **2016**, *6*, 7688–7692.

[35] a) P. Siemsen, R. C. Livingston, F. Diederich, *Angew. Chem. Int. Ed.* **2000**, *39*, 2632–2657; b) A. Studer, M. Maji, *Synthesis* **2009**, 2467–2470; c) M. S. Maji, T. Pfeifer, A. Studer, *Angew. Chem. Int. Ed.* **2008**, *47*, 9547–9550.

[36] a) E. H. Smith, J. Whittall, *Organometallics* **1994**, *13*, 5169–5172; b) S. Oae, Y. Inubushi, M. Yoshihara, *Phosphorus Sulfur* **1995**, *103*, 101–110.

[37] a) K. West, C. Wang, A. S. Batsanov, M. R. Bryce, *J. Org. Chem.* **2006**, *71*, 8541–8544; b) C. Wang, A. S. Batsanov, K. West, M. R. Bryce, *Org. Lett.* **2008**, *10*, 3069–3072; c) K. West, L. N. Hayward, A. S. Batsanov, M. R. Bryce, *Eur. J. Org. Chem.* **2008**, 5093–5098.

[38] a) J. Anthony, A. M. Boldi, Y. Rubin, M. Hobi, V. Gramlich, C. B. Knobler, P. Seiler, F. Diederich, *Helv. Chim. Acta* **1995**, *78*, 13–45; b) R. Eastmond, T. R. Johnson, D. R. M. Walton, *J. Organomet. Chem.* **1973**, *50*, 87–92.

[39] W. A. Chalifoux, R. McDonald, M. J. Ferguson, R. R. Tykwinski, *Angew. Chem. Int. Ed.* **2009**, *48*, 7915–7919.

[40] W. A. Chalifoux, M. J. Ferguson, R. McDonald, F. Melin, L. Echegoyen, R. R. Tykwinski, *J. Phys. Org. Chem.* **2012**, *25*, 69–76.

[41] T. N. Hoheisel, H. Frauenrath, *Org. Lett.* **2008**, *10*, 4525–4528.

[42] W. A. Chalifoux, R. R. Tykwinski, *Nat. Chem.* **2010**, *2*, 967–971.

[43] M. Krempe, R. Lippert, F. Hampel, I. Ivanovic-Burmazovic, N. Jux, R. R. Tykwinski, *Angew. Chem. Int. Ed.* **2016**, *55*, 14802–14806.

[44] J. Kendall, R. McDonald, M. J. Ferguson, R. R. Tykwinski, *Org. Lett.* **2008**, *10*, 2163–2166.

[45] T. R. Johnson, D. R. M. Walton, *Tetrahedron* **1972**, *28*, 5221–5236.

[46] T. Gibtner, F. Hampel, J. P. Gisselbrecht, A. Hirsch, *Chem. Eur. J.* **2002**, *8*, 408–432.

[47] R. Eastmond, D. R. M. Walton, T. R. Johnson, *Tetrahedron* **1972**, *28*, 4601–4616.

[48] a) Q. L. Zheng, J. C. Bohling, T. B. Peters, A. C. Frisch, F. Hampel, J. A. Gladysz, *Chem. Eur. J.* **2006**, *12*, 6486–6505; b) Q. L. Zheng, J. A. Gladysz, *J. Am. Chem. Soc.* **2005**, *127*, 10508–10509.

[49] W. Mohr, J. Stahl, F. Hampel, J. A. Gladysz, *Chem. Eur. J.* **2003**, *9*, 3324–3340.

[50] R. Dembinski, T. Bartik, B. Bartik, M. Jaeger, J. A. Gladysz, *J. Am. Chem. Soc.* **2000**, *122*, 810–822.

[51] K. Nakamura, T. Fujimoto, S. Takara, K.-i. Sugiura, H. Miyasaka, T. Ishii, M. Yamashita, Y. Sakata, *Chem. Lett.* **2003**, *32*, 694–695.

[52] K. Schlögl, W. Steyrer, *J. Organomet. Chem.* **1966**, *6*, 399–411.

[53] E. Jones, H. Lee, M. Whiting, *J. Chem. Soc.* **1960**, 3483–3489.

[54] a) M. Franz, J. A. Januszewski, F. Hampel, R. R. Tykwinski, *Eur. J. Org. Chem.* **2019**, 3503–3512; b) H. Amini, Z. Baranova, N. Weisbach, S. Gauthier, N. Bhuvanesh, J. H. Reibenspies, J. A. Gladysz, *Chem. Eur. J.* **2019**, *25*, 15896–15914; c) L. D. Movsisyan, M. Franz, F. Hampel, A. L. Thompson, R. R. Tykwinski, H. L. Anderson, *J. Am. Chem. Soc.* **2016**, *138*, 1366–1376; d) M. Franz, J. A. Januszewski, D. Wendinger, C. Neiss, L. D. Movsisyan, F. Hampel, H. L. Anderson, A. Gorling, R. R. Tykwinski, *Angew. Chem. Int. Ed.* **2015**, *54*, 6645–6649.

[55] a) D. Chakraborty, S. Nandi, D. Mullangi, S. Haldar, C. P. Vinod, R. Vaidhyanathan, *ACS Appl. Mater. Interfaces* **2019**, *11*, 15670–15679; b) L. Su, J. Dong, L. Liu, M. Sun, R. Qiu, Y. Zhou, S. F. Yin, *J. Am. Chem. Soc.* **2016**, *138*, 12348–12351; c) M. K. Holganza, L. Trigoura, S. Elfarra, Y. Seo, J. Oiler, Y. Xing, *Tetrahedron Lett.* **2019**, *60*, 1179–1181.

[56] F. Bohlmann, H. Schönowsky, E. Inhoffen, G. Grau, *Chem. Ber.* **1964**, *97*, 794–800.

[57] W. Chodkiewicz, P. Cadiot, *C. R. Hebd. Seances Acad. Sci.* **1955**, *241*, 1055–1057.

[58] a) B. Pigulski, N. Gulia, S. Szafert, *Chem. Eur. J.* **2015**, *21*, 17769–17778; b) N. Gulia, B. Pigulski, S. Szafert, *Organometallics* **2015**, *34*, 673–682; c) C. Klinger, O. Vostirowsky, A. Hirsch, *Eur. J. Org. Chem.* **2006**, 1508–1524; d) R. C. DeCicco, A. Black, L. Li, N. S. Goroff, *Eur. J. Org. Chem.* **2012**, 4699–4704.

[59] R. Eastmond, D. R. M. Walton, *Tetrahedron* **1972**, *28*, 4591–4599.

[60] E. Métay, Q. Hu, E.-i. Negishi, *Org. Lett.* **2006**, *8*, 5773–5776.

[61] H. H. Peng, Y. M. Xi, N. Ronaghi, B. L. Dong, N. G. Akhmedov, X. D. Shi, *J. Am. Chem. Soc.* **2014**, *136*, 13174–13177.

[62] W. Y. Yin, C. He, M. Chen, H. Zhang, A. W. Lei, *Org. Lett.* **2009**, *11*, 709–712.

[63] A. Sagadevan, P. C. Lyu, K. C. Hwang, *Green Chem.* **2016**, *18*, 4526–4530.

[64] A. B. Antonova, M. I. Bruce, B. G. Ellis, M. Gaudio, P. A. Humphrey, M. Jevric, G. Melino, B. K. Nicholson, G. J. Perkins, B. W. Skelton, B. Stapleton, A. H. White, N. N. Zaitseva, *Chem. Commun.* **2004**, 960–961.

[65] K. Gao, N. S. Goroff, *J. Am. Chem. Soc.* **2000**, *122*, 9320–9321.

[66] M. I. Bruce, N. N. Zaitseva, B. K. Nicholson, B. W. Skelton, A. H. White, *J. Organomet. Chem.* **2008**, *693*, 2887–2897.

[67] a) S. Eisler, R. R. Tykwinski, *J. Am. Chem. Soc.* **2000**, *122*, 10736–10737; b) E. Jahnke, R. R. Tykwinski, *Chem. Commun.* **2010**, *46*, 3235–3249.

[68] a) F. Diederich, Y. Rubin, C. B. Knobler, R. L. Whetten, K. E. Schriver, K. N. Houk, Y. Li, *Science* **1989**, *245*, 1088–1090; b) Y. Rubin, F. Diederich, *J. Am. Chem. Soc.* **1989**, *111*, 6870–6871; c) Y. Rubin, C. B. Knobler, F. Diederich, *J. Am. Chem. Soc.* **1990**, *112*, 1607–1617; d) S. W. Mcelvany, M. M. Ross, N. S. Goroff, F. Diederich, *Science* **1993**, *259*, 1594–1596; e) Y. Tobe, T. Fujii, K. Naemura, *J. Org. Chem.* **1994**, *59*, 1236–1237; f) Y. Tobe, T. Fujii, H. Matsumoto, K. Naemura, Y. Achiba, T. Wakabayashi, *J. Am. Chem. Soc.* **1996**, *118*, 2758–2759; g) Y. Tobe, R. Umeda, N. Iwasa, M. Sonoda, *Chem. Eur. J.* **2003**, *9*, 5549–5559; h) D. R. Kohn, P. Gawel, Y. Y. Xiong, K. E. Christensen, H. L. Anderson, *J. Org. Chem.* **2018**, *83*, 2077–2086.

[69] a) J. Zhao, Y. Zhang, Y. Fang, Z. Fan, G. Ma, Y. Liu, X. Zhao, *Chem. Phys. Lett.* **2017**, *682*, 96–100; b) J. H. Park, W. C. Mitchel, H. E. Smith, L. Grazulis, K. G. Eyink, *Carbon* **2010**, *48*, 1670–1673; c) M. Tsuji, T. Tsuji, S. Kuboyama, S.-H. Yoon, Y. Korai, T. Tsujimoto, K. Kubo, A. Mori, I. Mochida, *Chem. Phys. Lett.* **2002**, *355*, 101–108.

[70] a) G. Schermann, T. Grösser, F. Hampel, A. Hirsch, *Chem. Eur. J.* **1997**, *3*, 1105–1112; b) T. Grösser, A. Hirsch, *Angew. Chem. Int. Ed. Engl.* **1993**, *32*, 1340–1342.

[71] a) K. Kaiser, L. M. Scriven, F. Schulz, P. Gawel, L. Gross, H. L. Anderson, *Science* **2019**, *365*, 1299–1301; b) N. Pavlicek, P. Gawel, D. R. Kohn, Z. Majzik, Y. Y. Xiong, G. Meyer, H. L. Anderson, L. Gross, *Nat. Chem.* **2018**, *10*, 853–858.

[72] a) T. Luu, E. Elliott, A. D. Slepkov, S. Eisler, R. McDonald, F. A. Hegmann, R. R. Tykwinski, *Org. Lett.* **2005**, *7*, 51–54; b) S. Eisler, A. D. Slepkov, E. Elliott, T. Luu, R. McDonald, F. A. Hegmann, R. R. Tykwinski, *J. Am. Chem. Soc.* **2005**, *127*, 2666–2676.

[73] M. M. Haley, B. L. Langsdorf, *Chem. Commun.* **1997**, 1121–1122.

[74] W. Krätschmer, L. D. Lamb, K. Fostiropoulos, D. R. Huffman, *Nature* **1990**, *347*, 354–358.

[75] F. Bohlmann, *Chem. Ber.* **1953**, *86*, 657–667.

[76] A. Lucotti, M. Tommasini, D. Fazzi, M. Del Zoppo, W. A. Chalifoux, M. J. Ferguson, G. Zerbi, R. R. Tykwinski, *J. Am. Chem. Soc.* **2009**, *131*, 4239–4244.

[77] S. Schrettl, E. Contal, T. N. Hoheisel, M. Fritzsche, S. Balog, R. Szilluweit, H. Frauenrath, *Chem. Sci.* **2015**, *6*, 564–574.

[78] S. M. E. Simpkins, M. D. Weller, L. R. Cox, *Chem. Commun.* **2007**, 4035–4037.

[79] B. Pigulski, N. Gulia, S. Szafert, *Eur. J. Org. Chem.* **2019**, 1420–1445.

[80] J. Zirzlmeier, S. Schrettl, J. C. Brauer, E. Contal, L. Vannay, É. Brémond, E. Jahnke, D. M. Guldi, C. Corminboeuf, R. R. Tykwinski, H. Frauenrath, *Nat. Commun.* **2020**, *11*, 4797.

[81] R. R. Tykwinski, T. Luu, *Synthesis* **2012**, *44*, 1915–1922.

[82] A. Ehnbom, M. B. Hall, J. A. Gladysz, *Org. Lett.* **2019**, *21*, 753–757.

[83] a) Y. Nagano, T. Ikoma, K. Akiyama, S. Tero-Kubota, *J. Am. Chem. Soc.* **2003**, *125*, 14103–14112; b) D. Fazzi, F. Scotognella, A. Milani, D. Brida, C. Manzoni, E. Cinquanta, M. Devetta, L. Ravagnan, P. Milani, F. Cataldo, L. Lüer, R. Wannemacher, J. Cabanillas-

Gonzalez, M. Negro, S. Stagira, C. Vozzi, *Phys. Chem. Chem. Phys.* **2013**, *15*, 9384–9391.

[84] G. N. Lewis, M. Calvin, *Chem. Rev.* **1939**, *25*, 273–328.

[85] a) H. Meier, U. Stalmach, H. Kolshorn, *Acta Polym.* **1997**, *48*, 379–384; b) S. Yang, M. Kertesz, *J. Phys. Chem. A* **2008**, *112*, 146–151.

[86] M. Weimer, W. Hieringer, F. D. Sala, A. Görling, *Chem. Phys.* **2005**, *309*, 77–87.

[87] a) L. Shi, P. Rohringer, M. Wanko, A. Rubio, S. Waßerroth, S. Reich, S. Cambré, W. Wenseleers, P. Ayala, T. Pichler, *Phys. Rev. Mater.* **2017**, *1*, 075601; b) M. Kertesz, C. H. Choi, S. Yang, *Chem. Rev.* **2005**, *105*, 3448–3481.

[88] C. D. Zeinalipour-Yazdi, D. P. Pullman, *J. Phys. Chem. B* **2008**, *112*, 7377–7386.

[89] S. Szafert, J. A. Gladysz, *Chem. Rev.* **2006**, *106*, PR1–PR33.

[90] S. Yang, M. Kertesz, V. Zólyomi, J. Kürti, *J. Phys. Chem. A* **2007**, *111*, 2434–2441.

[91] a) D. R. Dreyer, R. S. Ruoff, C. W. Bielawski, *Angew. Chem. Int. Ed.* **2010**, *49*, 9336–9344; b) E. Frackowiak, *Phys. Chem. Chem. Phys.* **2007**, *9*, 1774–1785; c) E. Frackowiak, F. Béguin, *Carbon* **2001**, *39*, 937–950; d) H. Shi, G. Wen, Y. Nie, G. Zhang, H. Duan, *Nanoscale* **2020**, *12*, 5261–5285; e) D. G. Papageorgiou, Z. Li, M. Liu, I. A. Kinloch, R. J. Young, *Nanoscale* **2020**, *12*, 2228–2267.

[92] L. Shi, P. Rohringer, K. Suenaga, Y. Niimi, J. Kotakoski, J. C. Meyer, H. Peterlik, M. Wanko, S. Cahangirov, A. Rubio, Z. J. Lapin, L. Novotny, P. Ayala, T. Pichler, *Nat. Mater.* **2016**, *15*, 634–640.

[93] C. Wang, H. Jia, H. Li, Y. Wang, *Jilin Huagong Xueyuan Xuebao* **2012**, *20*, 33–36.

[94] a) P. Sivaguru, Z. K. Wang, G. Zanoni, X. H. Bi, *Chem. Soc. Rev.* **2019**, *48*, 2615–2656; b) K. Wu, C. Song, D. Cui, *Chinese J. Org. Chem.* **2017**, *37*, 586–602; c) D. S. Kim, W. J. Park, C. H. Jun, *Chem. Rev.* **2017**, *117*, 8977–9015.

[95] Y. Li, C. Yang, X. Guo, *Acc. Chem. Res.* **2020**, *53*, 159–169.

[96] C. H. Hendon, D. Tiana, A. T. Murray, D. R. Carbery, A. Walsh, *Chem. Sci.* **2013**, *4*, 4278–4284.

[97] A. Goulet-Hanssens, F. Eisenreich, S. Hecht, *Adv. Mater.* **2020**, e1905966.

[98] A. Schlimm, R. Low, T. Rusch, F. Rohricht, T. Strunskus, T. Tellkamp, F. Sonnichsen, U. Manthe, O. Magnussen, F. Tuczek, R. Herges, *Angew. Chem. Int. Ed.* **2019**, *58*, 6574–6578.

[99] V. Walter, Y. Gao, N. Grzegorzek, M. Krempe, F. Hampel, N. Jux, R. R. Tykwinski, *Angew. Chem. Int. Ed.* **2019**, *58*, 494–498.

[100] M. Hammerich, R. Herges, *J. Org. Chem.* **2015**, *80*, 11233–11236.

CHAPTER 2 – The Loss of Endgroup Effects in Long Pyridyl-Endcapped Oligoynes on the Way to Carbyne[*]

2.1 Introduction

In order to exploit the potential of the most versatile element of the periodic table, the creation of new forms of carbon, so-called "synthetic carbon allotropes (SCAs)",[1] has become a focus of many research efforts. The formation of a cyclic oligoyne[2] and graphynes,[3] are salient recent examples, complementing more common reports about synthetic (nano)graphenes,[4] nanodiamonds,[5] and nanorings/-tubes.[6]

Throughout the past 60 years, oligo- and polyynes, which can be differentiated by the presence and lack of endgroup effects, respectively, have been targeted as representatives of the SCA composed of *sp*-hybridized carbon, commonly referred to as carbyne.[7] Carbyne might be the strongest known material[8] or the ideal molecular wire,[7d] but experimental confirmation of these predictions remains elusive due to a lack of synthetically accessible oligo-/polyynes. There are numerous reports of the synthesis of oligoynes composed of up to 14 contiguous alkyne units.[7a, 9] Few examples beyond this length have been isolated, as highlighted in Chapter 1, although oligo-/polyynes endcapped with sterically demanding triarylmethyl groups have been characterized up to 22 alkynes (**Tr*[*n*]** Figure 2.1a).[10] Polyynes composed of hundreds to thousands of alkynes have been formed inside carbon nanotubes (albeit with random lengths).[11]

Studies to date have clearly established that steric shielding of the oligoyne framework is a key component to providing kinetically stable products,[10] and "protection" of the end-most alkyne units from reactions emerges as a vital consideration.[12] It can be noted that the products arising from the decomposition of oligoynes have never been conclusively identified, but empirical evidence overwhelming confirms that the larger the endgorup the more stable the oligoyne. This protection scheme is considered for pyridyl-endcapped oligoynes (PEOs), with the goal to stabilize PEOs as molecular wires in, for example, STM break-junction devices.[13] Stabilization is necessary since the construction of unfunctionalized PEOs is limited to the di- and tetraynes **Py[2]**

---

and **Py[4]**,[14] while **Py[6]** is too unstable to be fully characterized (Figure 2.1b).[15] Modification of PEOs through incorporation of phenyl groups at the 3- and 5-positions of pyridyl endgroup provides derivatives **Py*[*n*]** up to the octayne **Py*[8]**.[16] The stability of **Py*[8]** is consistent with limits encountered with other studied oligoynes,[10, 17] and only one aryl-endcapped derivative beyond the length of 10 alkyne units has been characterized (albeit limited).[18] Kinetic instability of aryl functionalized oligoynes has thus been a bottleneck in answering both fundamental and applied questions.
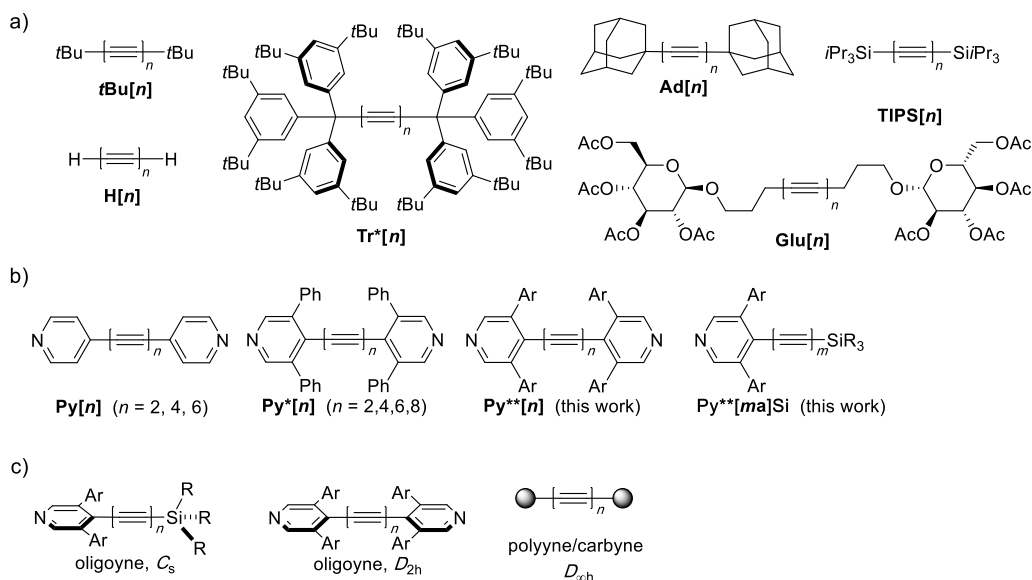
Figure 2.1. a) Molecular structures of previously reported oligoyne series discussed in this chapter, **tBu[*n*]**, **H[*n*]**, **Tr*[*n*]**, **Ad[*n*]**, **TIPS[*n*]**, and **Glu[*n*]**. b) Known PEOs **Py[*n*]** and **Py*[*n*]** and those discussed herein **Py**[*n*]**, along with precursors **Py**[*m*a]Si**. c) A comparison of symmetry between oligoynes and polyynes/carbyne.

Guided by the hypothesis that bulky endgroups are requisite to achieve stable derivatives, in the present work, I have designed PEOs with functionality at the 3- and 5-positions of the pyridyl ring (**Py**[*n*]**, Figure 2.1b). A series of di- and tetraynes was synthesized and used to evaluate stability versus endgroup functionalization. Ultimately, 3,5-di-*t*ert-butylphenyl groups were identified as the most promising, and the challenging syntheses were developed and optimized for long oligoyne derivatives. These efforts culminated in the formation of an unsymmetrical dodecayne **Py**[12a]Si** as a stable solid, which is the longest unsymmetrical oligoyne that has been reported to date, and a stable tetracosayne **Py**[24a]** (48 *sp*-carbons), which is three times the length of previous PEOs and nearly twice as long as any reported diaryl oligoyne.

Electronic absorption spectra of these new oligo-/polyynes confirm a remarkable trend. Namely, the spectra document the presence and subsequent loss of low energy transitions (λ_{weak})

as a function of length. These absorptions are clearly present in the spectra of the unsymmetrical oligoynes **Py**[ma]Si** (m = 3, 4, 5, 6, 8, 9, 12) due to lower pseudo-Cs symmetry (C_1 without a reflection plane) and shorter **Py**[na]** (n = 2, 4, 6, 8, 10) due to pseudo-D_{2h} symmetry in the co-planar form (D_{2d} with orthogonal endgroups or D_2 in other cases), but they gradually "disappear" as oligoyne length is increased and the molecules approach the $D_{\infty h}$ symmetry of carbyne (Figure 2.1c). The absorbance loss of the λ_{weak} transitions outlines the loss of endgroup effects and the transition from oligoynes to polyynes as a function of length. Likewise, ^{13}C NMR, Raman, and UV-vis spectroscopy, as well as solid-state analyses (bond length alternation, BLA) confirm similar saturation behavior as a function of molecular length, consistent with the transition from oligoynes to the limiting regime dominated by Peierls distortion, i.e., polyynes. Together, these analyses offer a refined description of expected physical and electronic properties of the allotrope carbyne, based on experimental evidence.

2.2 Synthesis of short pyridyl-endcapped oligoynes (Py**[2a–e] and Py**[4a–d])

A library of five diynes (**Py**[2a–e]**) and four tetraynes (**Py**[4a–d]**) have been successfully synthesized, while the efforts to synthesize **Py**[4e]**, **Py**[2f]**, and **Py**[4f]** failed (*vide infra*). These available PEOs (**Py**[2a–e]** and **Py**[4a–d]**) with five endgroups (**a–e**) were thus studied as model compounds to guide optimization of the kinetic stability so that an optimal endgroup could be selected toward the extension of the carbon chain. Initially, six endgroups were chosen for the assembly of PEOs, and the six endgroups are 3,5-bis(3,5-di-*tert*-butylphenyl)pyridine (**a**), 3,5-bis(4-*tert*-butylphenyl)pyridine (**b**), 3,5-(2-tolyl)pyridine (**c**), 3,5-(7-*tert*-butylpyrene-2-yl)pyridine (**d**), 3,5-(pyrene-2-yl)pyridine (**e**), and 3,5-bis(2,6-di-methylphenyl)pyridine (**f**), respectively. As a consequence, five endgroups (**a–e**) have been successfully incorporated in PEOs (Figure 2.2).
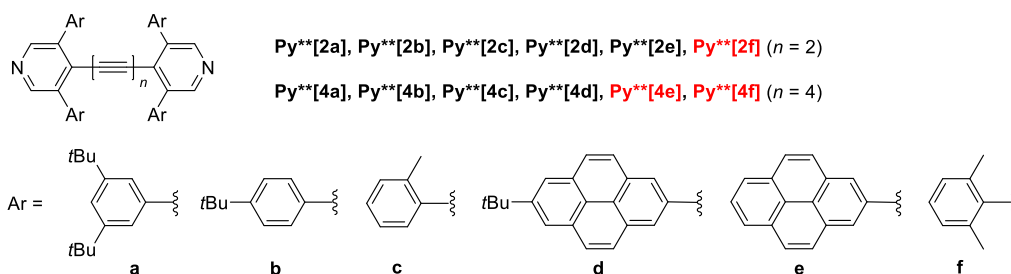
Figure 2.2. Molecular structures of the diynes **Py**[2a–f]** and the tetraynes **Py**[4a–f]**. The synthesis of the compounds in red were unsuccessful.

2.2.1 Synthesis of 3,5-dibromo-1-methyl-4-pyridone

The synthesis of pyridyl-endcapped di- and tetraynes begins with the formation of the reported compound 3,5-dibromo-1-methyl-4-pyridone **2.3**.[19] The synthesis of compound **2.3** was adapted from a reported methylation method using the known compound 3,5-dibromo-4-pyridone **2.2** as a precursor.[20] Compound **2.2** is afforded from a commercially available 4-pyridone (**2.1**), either under acidic or basic conditions with the addition of bromine.[20-21] In my synthesis, compound **2.1** was treated with KOH in water, followed by the addition of bromine. Workup gave **2.2** in 83% with a scale of 10 g. The methylation of compound **2.2** using methyl iodide in the presence of K_2CO_3 in DMF afforded the desired compound **2.3** in good yield (Scheme 2.1). Noted herein is that only the *N*-methylated product (**2.3**) was obtained, while *O*-methylated product was not observed, as has been reported for a similar compound.[22]
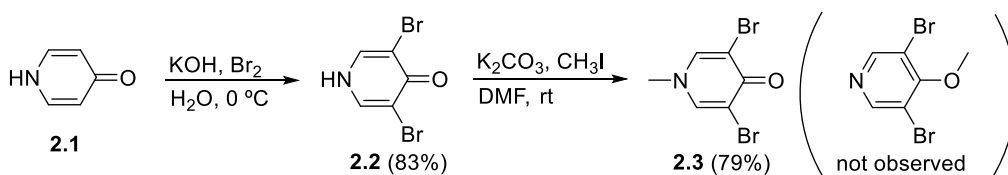
Scheme 2.1. Synthesis of 3,5-dibromo-1-methyl-4-pyridone **2.3**.

2.2.2 Synthesis of boronic ester

Suzuki cross-coupling reactions are envisioned to introduce the functional groups to the dibromo precursor **2.3**, and thus the respective boronic esters are needed. Boronic acid pinacol esters of 2-(3,5-di-*tert*-butylphenyl)-4,4,5,5-tetramethyl-1,3,2-dioxaborolane **Bpin(a)**, 2-(4-*tert*-butylphenyl)-4,4,5,5-tetramethyl-1,3,2-dioxaborolane **Bpin(b)**, 2-(2-methylphenyl)-4,4,5,5-tetramethyl-1,3,2-dioxaborolane **Bpin(c)**, and 2-(2,6-di-methylphenyl)-4,4,5,5-tetramethyl-1,3,2-dioxaborolane **Bpin(f)** were formed by adaptations of a known procedure.[23] In general, the Miyaura borylation reaction was applied to the corresponding aryl bromide and bis(pinacolato)diboron in the presence of Pd(dppf)Cl2 and KOAc. Workup and solvent removal afforded the desired boronic esters in good yields (Scheme 2.2).
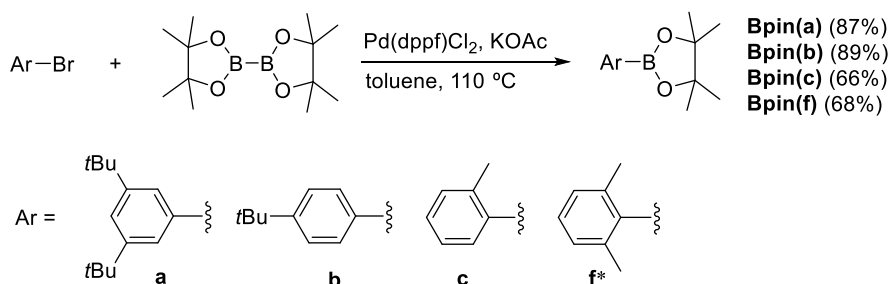
Scheme 2.2. Synthesis of **Bpin(a)**, **Bpin(b)**, **Bpin(c)**, and **Bpin(f)**. *The reaction was conducted in a DMF solution.

The selective C–H borylation of pyrene and its derivatives in the 2- and 2,7-positions has been well developed by Marder and co-workers.[24] The regiospecific C–H borylation of pyrene and 2-*tert*-butylpyrene[25] in the presence of (1,5-cyclooctadiene)(methoxy)iridium dimer, [Ir(μ-OMe)cod]₂ and 4,4'-di-tert-butyl-2,2'-bipyridine (dtBBP) as catalysts gave the desired products of 2-[7-(*tert*-butyl)pyren-2-yl]-4,4,5,5-tetramethyl-1,3,2-dioxaborolane **Bpin(d)** and 2-pyren-2-yl-4,4,5,5-tetramethyl-1,3,2-dioxaborolane **Bpin(e)** in acceptable yields (Scheme 2.3).
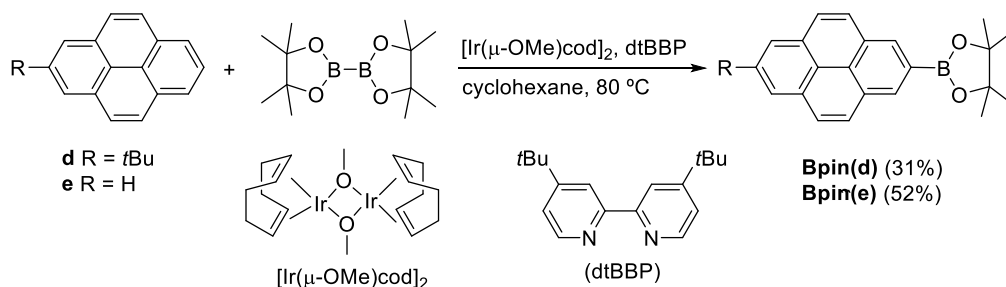
Scheme 2.3. Synthesis of **Bpin(d)** and **Bpin(e)**.

2.2.3 Synthesis of terminal monoynes and diynes

Suzuki cross-coupling reactions using **2.3** were optimized, and using Ar-Bpin, Pd(PPh₃)₄, and Cs₂CO₃ in toluene/EtOH (4:1) at 80 °C gave **2.4a–e** in good yields (Scheme 2.4a). Surprisingly, all attempts to incorporate the 2,6-dimethylphenyl to give **2.4f** failed, presumably due to the reduced reactivity of the boronic ester arising from steric hinderance from the two *ortho* methyl groups. The bromination of 4-pyridone derivatives **2.4a–e** in neat PBr₃ at 150–170 °C afforded **2.5a–e** in moderate to good yields; thus, the pyridyl groups are formed in this step. The proposed mechanism is shown in Figure 2.3. The 4-pyridone **2.4a–e** has a ketone group, and the double bond of the ketone is weakened due to the conjugation with the vinylogous amine. This weakened double bond is supported by the infrared spectrum showing a strong stretching signal of the ketone at 1640–1645 cm⁻¹. Nucleophilic attack on PBr₃ gives the intermediate **A**, followed by attack of the bromide anion to the 4-position of **A**, with the subsequent elimination of a phosphenous bromide

giving the intermediate **B**. The proposed intermediates **A** and **B** are supported by MS analysis. During the optimization process, MS characterization of the reaction mixture shows strong signals for intermediates **A** and **B**. Strong signals are observed for $[M]^+$ at m/z 550.3 and 674.5, respectively, for the intermediate **A** and **B** of the series **a** in the electrospray ionization (ESI) mass analysis. Finally, the demethylation of the intermediate **B** and loss of bromomethane forms the final products **2.5a–e**. A similar bromination reaction was previously reported showing that 4-pyridone derivatives could be reacted with phosphorus oxybromide ($POBr_3$) to give the brominated products.[26]
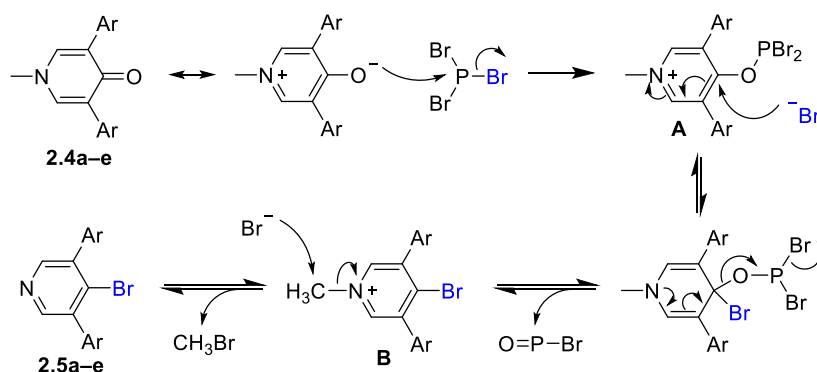
Figure 2.3. The proposed mechanism of bromination of compounds **2.4a–e** using PBr₃.

With the brominated derivatives **2.5a–e** in hand, Sonogashira cross-coupling reactions with 2-methyl-3-butyn-2-ol, Pd(PPh₃)₄, CuI, in Et₃N, at 80 °C gave **2.6a–e** in good yields. The use of 2-hydroxylpropyl ($-C(CH_3)_2OH$) as a protecting group facilitates the separation of the cross-coupling products on chromatographic supports through the introduction of a functional group with higher polarity. Subsequently, the desired terminal monoynes **2.7a–e** were obtained by alkyne deprotection with NaOH in the presence of tris[2-(2-methoxyethoxy)ethyl]amine (TDA-1) as a phase transfer catalyst. The use of TDA-1 was key to deprotection, and, for example, only a trace amount of **2.7a** was produced in the absence of TDA-1. The importance of TDA-1 will be discussed below.

Next, the elongation of the *sp*-carbon chain in **2.7a–e** was investigated by means of oxidative cross-coupling reactions. In initial efforts, two-carbon building blocks, Br–C≡C–SiMe₃ (**2.10**) and Br–C≡C–SiEt₃ (**2.11**),[27] were used in the Cadiot–Chodkiewicz cross-coupling reactions (Scheme 2.4b). The reaction of **2.7a** with **2.10** and **2.11** under Cadiot–Chodkiewicz conditions at rt gave only low yields (ca. 10%–20%) as monitored by ¹H NMR spectroscopy. The

desired product was not separated because the polarity of the starting terminal monoyne is similar to that of the silyl-protected diyne. Furthermore, it is likely that the steric bulk of the endgroup retards the cross-coupling reaction and results in low yields at low temperature (reaction at higher temperature was not attempted). To make separation easier and improve the reaction yield, Br–C≡C–C(CH$_3$)$_2$OH (4-bromo-2-methyl-3-butyn-2-ol, **2.12**)[28] was then applied in order to take advantage of the polarity difference between starting material and product. The reaction of **2.7a** and **2.12** at 80 °C, followed by workup and purification, gave **2.8a** as a colourless solid in 79% yield. Cadiot–Chodkiewicz cross-coupling reactions of **2.7b–d** with **2.12** gave the corresponding unsymmetrical diynes **2.8a–d** in 63%–75% yields (Scheme 2.4a). Compound **2.7e** was insufficiently soluble in common solvents to accomplish the cross-coupling reaction to **2.8e**. An alternate route to **2.8e** was attempted, using a Sonogashira cross-coupling reaction with **2.5e** and HC≡C–C≡C–SiiPr$_3$ (**2.16**); but it also failed presumably due to the poor solubility of **2.5e** in Et$_3$N.
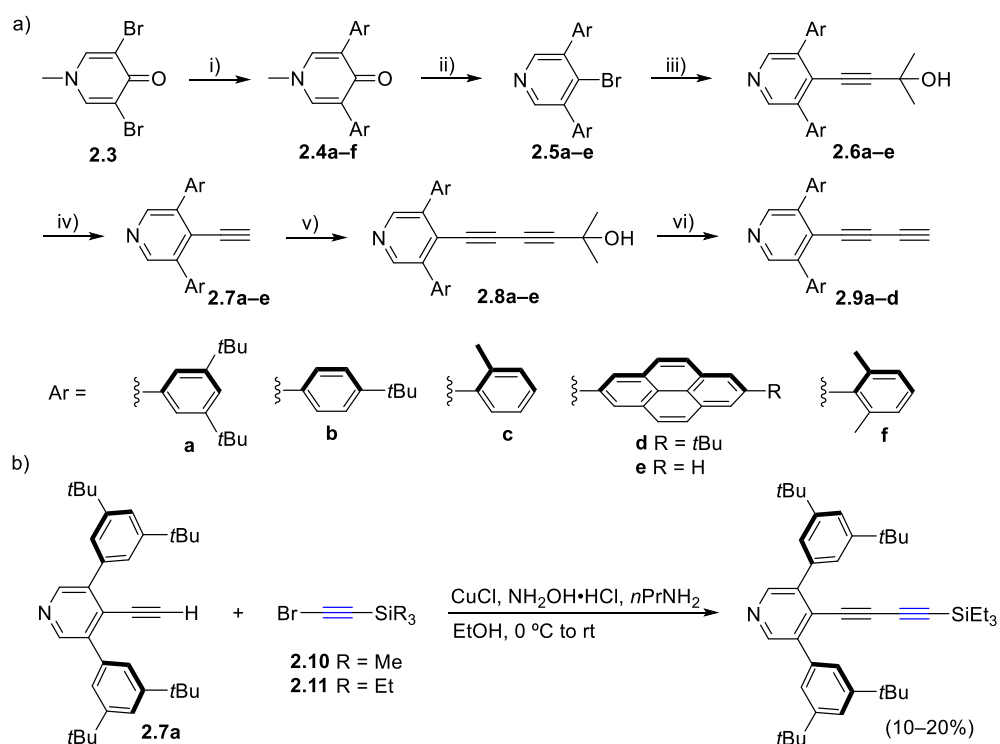
Scheme 2.4. a) Synthesis of terminal monoynes and diynes. Reagents, conditions, and yields: i) **Bpin(a–f)**, Pd(PPh$_3$)$_4$, Cs$_2$CO$_3$, toluene/EtOH (4:1), 80 °C; **2.4a** 88%, **2.4b** 86%, **2.4c** 83%, **2.4d** 75%, **2.4e** 69%, **2.4f** 0%; ii) PBr$_3$, 150 °C for **2.4a–c**, **2.4e**, and 170 °C for **2.4d**; **2.5a** 93%, **2.5b** 85%, **2.5c** 70%, **2.5d** 51%, **2.5e** 59%; iii) 2-Methylbut-3-yn-2-ol, Pd(PPh$_3$)$_4$, CuI, Et$_3$N, 80 °C; **2.6a** 71%, **2.6b** 72%, **2.6c** 58%, **2.6d** 75%, **2.6e** 65%; iv) NaOH, TDA-1, toluene, 110 °C; **2.7a** 93%, **2.7b** 95%, **2.7c** 87%, **2.7d** 94%, **2.7e** 74%; v) 4-Bromo-2-methyl-3-butyn-2-ol, CuCl, NH$_2$OH·HCl, nPrNH$_2$, EtOH, 0 °C to rt for **2.7b** and **2.7c**, and 0 °C to 80 °C for **2.7a** and **2.7d**; **2.8a** 79%, **2.8b** 75%, **2.8c** 73%, **2.8d** 63%, **2.8e** 0%; vi) NaOH, TDA-1, toluene, rt for **2.8a–c**, and 110 °C for **2.8d**; **2.9a** 89%, **2.9b** 73%, **2.9d** 58%. b) Synthesis of diynes using **2.10** and **2.11**.

The subsequent deprotection of **2.8a–c** was accomplished at rt in good yields in the presence of TDA-1, while no product was produced at rt without TDA-1. To the best of our knowledge, this is the first case where 4-aryl-2-methyl-3-butyn-2-ol can be cleaved at rt. As stated in 1985 by Havens, "*Acetone, the byproduct, must be removed by distillation to shift the equilibrium toward the arylacetylene*".[29] Following this precedent, deprotection is usually furnished at a high temperature (usually reflux in toluene) to afford the terminal monoynes and diynes. In the present case, the phase transfer catalyst TDA-1 plays an influential role in performing the deprotection at rt for arylacetylenes that are longer than monoynes, although the exact role has not yet been determined. The deprotection reaction to form **2.9d** was, unexpectedly, not successful at rt, and it should be done at reflux in toluene.

Two common diynes (**2.13** and **2.15**), endcapped with a phenyl group and a TIPS group, respectively, were also investigated toward optimization of this deprotection method. The reactions were conducted in dry toluene at rt in the presence of NaOH and TDA-1, and purification by column chromatography afforded the corresponding terminal diynes **2.14** and **2.16** in acceptable yields (Scheme 2.5). The successful deprotection at rt is important for a number of reasons: 1) stability is a big concern when exposing terminal arylacetylenes containing more than two alkyne units to reactions at high temperature, 2) as a protecting group, the 2-hydroxy-2-propyl group facilitates purification because of the greater polarity in comparison to, for example, trialkylsilyl groups, and 3) the combination of NaOH and TDA-1 appears to have great potential as a general method for deprotection of other substrates and for longer oligoynes.
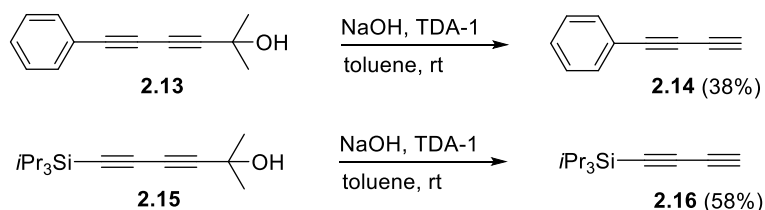
Scheme 2.5. Investigation of the method of deprotection of 4-aryl-2-methyl-3-butyn-2-ol.

Following deprotection, butadiynes **2.9a**,**b**,**d** are stable products under ambient conditions in the solid-state, while **2.9c** discolors to a black solid upon precipitation and, therefore, must be kept in a solution. The reaction yield of **2.9c** could not be determined, and it was used directly for the next step, following purification.

Next, diynes and tetraynes were then targeted through oxidative homocoupling reactions. Initial attempts with **2.7a** showed that only a trace of the desired diyne **Py**[2a]** was formed when the reaction was performed using either Hay[30] or Eglinton–Galbraith[31] homocoupling conditions at rt. On the other hand, Eglinton–Galbraith reactions at a reaction temperature of 100 °C smoothly gave **Py**[2a]** and were subsequently used to complete the other series of four diynes **Py**[2b–e]**. The analogous reaction at rt using diynes **2.9a–d** gave tetraynes **Py**[4a–d]** (Scheme 2.6). The inefficiency of homocoupling toward diynes could be due to steric effects arising from the endgroups, and the reactions thus require higher temperatures. The endgroups have less of an influence when forming the longer tetraynes, and these reactions proceed at rt.
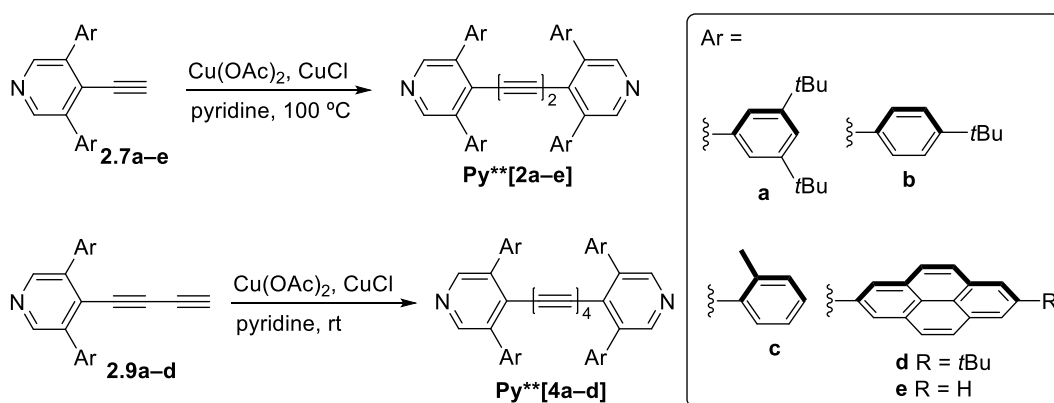
Scheme 2.6. Synthesis of pyridyl-endcapped di- and tetraynes. Yields: **Py**[2a]** 70%, **Py**[2b]** 91%, **Py**[2c]** 83%, **Py**[2d]** 95%, **Py**[2e]** 80%; **Py**[4a]** 84%, **Py**[4b]** 92%, **Py**[4c]** 69%,[#] **Py**[4d]** 93%; [#]the yield of **Py**[4c]** is over the two steps.

2.3 Endgroup choice

The diynes and tetraynes **Py**[2a–e]** and **Py**[4a–d]**, respectively, are all stable in the presence of air, light, and moisture under ambient conditions, and differential scanning calorimetry (DSC) has been used to evaluate thermal stability (Table 2.1). The onset decomposition temperature of **Py**[2a]** (404 °C) is significantly higher than either **Py[2]** (209 °C) or **Py*[2]** (314 °C). Furthermore, the onset decomposition temperature of **Py**[4a]** (309 °C) is also higher than **Py[4]** (160 °C) and **Py*[4]** (235 °C). While those of **Py**[2b–e]** (335–363 °C) and **Py**[4b–d]** (224–245 °C) are marginally higher than those of **Py*[2]** and **Py*[4]**, respectively. Thus, **Py**[2a]** and **Py**[4a]** present the most remarkable thermal stability in comparison to that of **Py*[2]** and **Py*[4]**, as well as **Py**[2b–e]** and **Py**[4b–d]**, respectively.

Table 2.1. Melting and decomposition points of di- and tetraynes determined by differential scanning calorimetry (DSC).

diynes	mp (°C)	dp[a] (°C)	tetraynes	mp (°C)	dp[a] (°C)
Py[2]	207	209[16]	**Py[4]**	–[b]	160[13a]
Py*[2]	193	314[16]	**Py*[4]**	–[b]	235[16]
Py[2a]**	360	404	**Py**[4a]**	298	309
Py[2b]**	286	341	**Py**[4b]**	–[b]	245
Py[2c]**	212	335	**Py**[4c]**	–[b]	241
Py[2d]**	–[b]	344	**Py**[4d]**	–[b]	224
Py[2e]**	–[b]	363			

[a]Onset temperature for decomposition. [b]No observed melting point.

As just described, a clear stabilizing effect is found by increasing steric bulk in the 3- and 5-pyridyl positions as one considers decomposition points in the progression of the series from **Py[n]**, **Py*[n]**, and **Py**[n]** (Table 2.1). In addition, **Py**[2a]** and **Py**[4a]** show melting points at 360 °C and 298 °C, respectively, and the former is, remarkably, stable as a liquid up to its decomposition point at 404 °C. For tetrayne **Py**[4a]** the window is narrower (mp 298 °C, dp 309 °C). The DSC analyses indicate that the modification of the pyridyl group in the 3- and 5-positions can be a successful strategy toward the improvement of the thermal stability.

X-ray crystallography provides an empirical analysis of factors that should influence stability. A comparison of solid-state structures for diynes **Py**[2a,c,e]** confirms that the 3,5-bis(3,5-di-*tert*-butylphenyl)pyridyl groups offer the most significant shielding of the acetylenic framework (see Figure 2.13). Shielding of the endmost acetylenes becomes more obvious in tetrayne derivative **Py**[4a]**. Thus, in order to elongate the linear carbon chain, PEOs incorporating 3,5-bis(3,5-di-*tert*-butylphenyl)pyridyl endgroups have been selected.

2.4 Synthesis of silyl-protected oligoynes as precursors (Py**[*m*a]Si, *m* = 3, 4, 5, 6, 8, 9, and 12)

With a viable protecting group strategy in hand, attention turned to chain extension (Scheme 2.7, 2.8). Our strategy was modeled after a sequential method of desilylation and subsequent coupling reactions to provide an extended *sp*-carbon chain, as pioneered by Walton and co-workers[32] and developed successfully by many research groups recently.[10, 17b, 33] The diyne **2.9a** was used with the two-carbon building block Br–C≡C–SiEt$_3$ (**2.11**, 5 equiv) in a Cadiot–Chodkiewicz reaction to

give triyne **Py**[3a]Si** in 86% yield. Desilylation of **Py**[3a]Si** using CsF in a solution of THF/H$_2$O (5/1) gave the terminal triyne, which was then used in a Cadiot–Chodkiewicz cross-coupling with an excess of **2.11** to give tetrayne **Py**[4a]Si** in 72% yield over the two steps (Scheme 2.7).
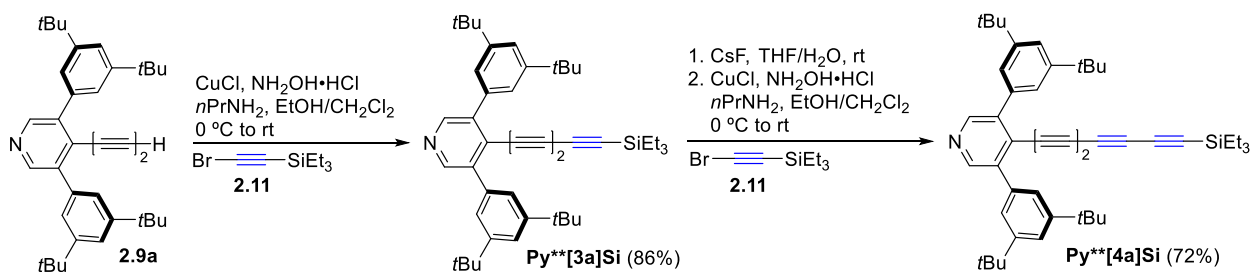
Scheme 2.7. Synthesis of silyl-protected oligoynes as precursors (**Py**[3/4a]Si**) using Cadiot–Chodkiewicz reactions.

Toward longer derivatives, Hay reactions, Eglinton–Galbraith reactions, and the modified Eglinton–Galbraith reactions[10] between **2.9a** and H–[C≡C]$_3$–SiiPr$_3$ (**2.18**) have been explored. As previously reported, triyne **2.18** was obtained from the known building block Me$_3$Si–[C≡C]$_3$–SiiPr$_3$ (**2.17**)[34] by selectively removing the trimethylsilyl group (Scheme 2.8). Following desilylation and workup, a solution of the only moderately stable terminal triyne **2.18** was carried on to an Eglinton–Galbraith reaction using Cu(OAc)$_2$ and pyridine (or 2,6-lutidine in the case of a modified Eglinton–Galbraith reaction), which resulted in the formation of pentayne **Py**[5a]Si** in 12% yield (20% yield in the modified Eglinton–Galbraith reaction). The purification is, however, tedious, and careful separation of the product is necessary by column chromatography. Due to the low yields and tedious purification, efforts were then turned to the use of a Hay reaction, which gratifyingly gave the product in ca. 50% yield. The formation of the tetrayne **Py**[4a]TIPS** (i.e., the apparent loss of an alkyne unit) was also observed from the reaction (Scheme 2.8), by mass spectrometric analysis and proton NMR analysis (ca. 15% yield relative to the pentayne **Py**[5a]Si**. The resulting mixture, unfortunately, could not be separated by either recrystallization or column chromatography. The loss of an alkyne unit during an oxidative coupling reaction has been observed by others in the synthesis of longer oligoynes (typically longer than an octayne).[17b, 35] In the present case, it is reasonable to assume that the loss of an alkyne unit stems from the six-carbon building block **2.18** during the course of the Hay oxidative coupling process. This statement is supported with the evidence that no by-product of loss of an alkyne unit was observed for the

formation of **Py**[4a]** from the homocoupling of **2.9a** as well as the formation of the triyne **Py**[3a]Si** from **2.9a**. The issue of loss of alkyne units will be addressed in Chapter 3.
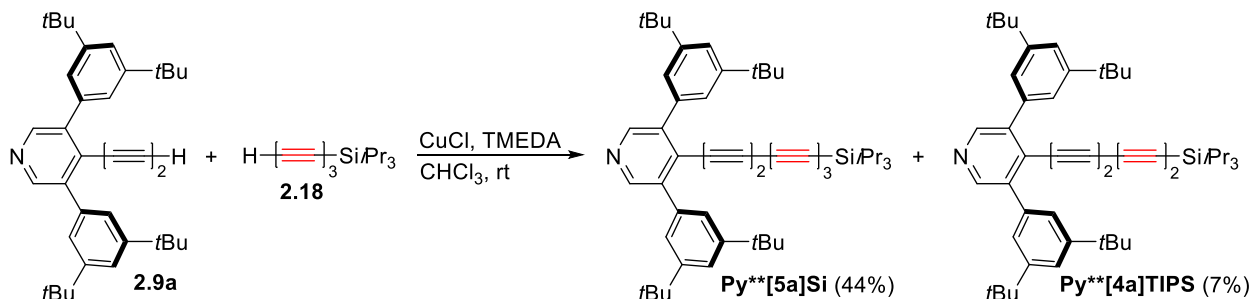
Scheme 2.8. The attempt of synthesis of **Py**[5a]Si** using a Hay reaction as well as the accompanying **Py**[4a]TIPS** as a byproduct.

To circumvent the competitive reaction resulting in loss of an alkyne unit, a new six-carbon building block I–[C≡C]$_3$–SiiPr$_3$ (**2.19**) was designed and synthesized from **2.17**. In this case, it was envisioned that Pd-catalysis could be used, rather than Cu. Removal of the TMS group from **2.17** using K$_2$CO$_3$ in EtOAc/MeOH and subsequent iodination of the intermediate **2.18** using *N*-iodosuccinimide (NIS) afforded **2.19** in 85% yield over the two steps (Scheme 2.9). Compound **2.19** is isolated as a neat oil that decomposes overnight under refrigeration at 4 °C, but it can be stored in a solution of hexanes for weeks without noticeable change.
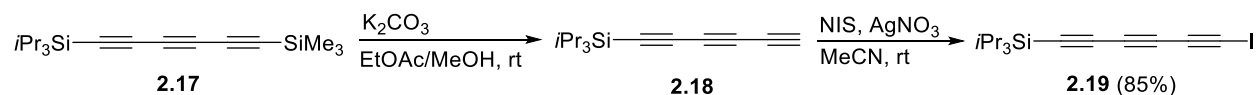
Scheme 2.9. Synthesis of six-carbon building block **2.19**.

With the new building block **2.19** in hand, the cross-coupling reaction between **2.9a** and **2.19** (ca. 5 equiv) in the presence of Pd(PPh$_3$)$_2$, CuI, and NEt$_3$ gave pentayne **Py**[5a]Si** in 48% yield and without loss of alkyne units. Subsequently, octayne **Py**[8a]Si** was obtained from **Py**[5a]Si** in 40% yield using an analogous protocol of desilylation, followed by coupling with **2.19**, while diisopropylethylamine (DIPEA) was used as base rather than Et$_3$N. DIPEA was used based on the observation that a significant amount of decomposition of the terminal pentayne occurred in the presence of Et$_3$N. Starting with **Py**[3a]Si**, the sequential process of desilylation and cross-coupling reaction with **2.19** gave hexayne **Py**[6a]Si** in 65% yield. In a similar manner,

nonayne **Py**[9a]Si** was obtained in 36% yield from **Py**[6a]Si**, and dodecayne **Py**[12a]Si** was obtained in 24% yield from **Py**[9a]Si**, as shown in Scheme 2.10.
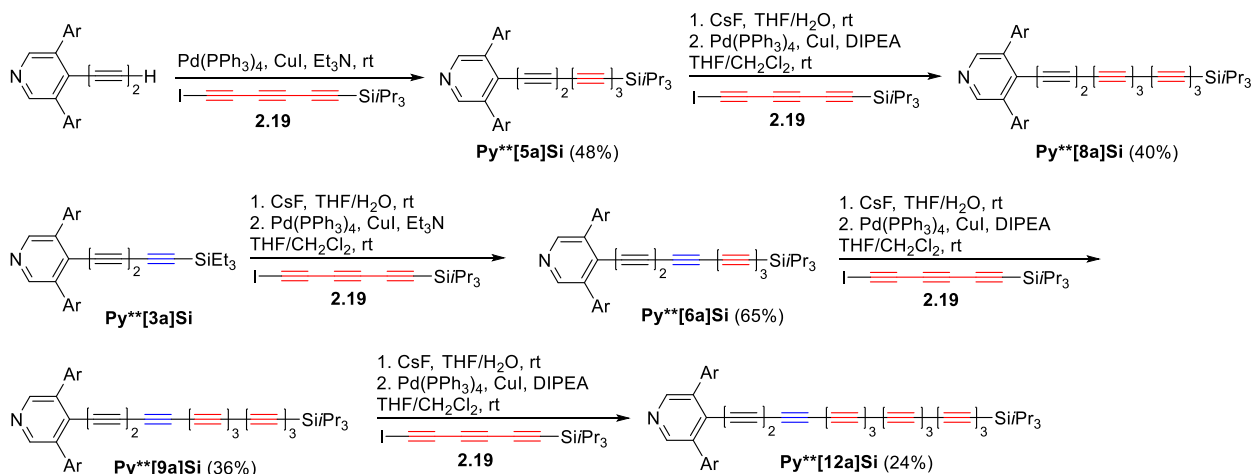
Scheme 2.10. Synthesis of silyl-protected oligoynes as precursors (**Py**[*m*a]Si**); Ar = 3,5-bis(3,5-di-*tert*-butylphenyl), DIPEA = diisopropylethylamine.

Hexayne **Py**[6a]Si** is isolated as a yellow solid, while longer derivatives **Py**[*m*a]Si** (*m* = 8, 9, 12) are obtained as orange solids after recrystallization from CH_2Cl_2/MeOH. All the silyl-protected oligoynes **Py**[*m*a]Si** are stable under ambient conditions as solids and in solution. It is worth highlighting that nonayne **Py**[9a]Si** and dodecayne **Py**[12a]Si** are the longest of all known heteroaromatic endcapped oligoynes synthesized and characterized to date.

2.5 Synthesis of pyridyl-endcapped oligoynes (Py**[*n*a], *n* = 6, 8, 10, 12, 16, and 24)

With precursors **Py**[*m*a]Si** in hand, a sequence of desilylation and oxidative homocoupling reactions were applied to provide **Py**[*n*a]**. As described in Chapter 1, numerous oligoynes have been synthesized, mostly based on the widely known Hay and Eglinton–Galbraith reactions.[17a, 35-36] Nevertheless, optimizations of these general reactions were needed, especially for the homocoupling reactions of terminal oligoynes that is longer than a tetrayne (Scheme 2.11).

The overall process for oligoyne formation included removal of the trialkylsilyl protecting group, followed by oxidative homocoupling. The desilylation of the triyne **Py**[3a]Si** and tetrayne **Py**[4a]Si** using CsF in THF/H_2O (5:1) was complete in 20–30 min, as monitored by TLC analysis. The homo-coupled products **Py**[6a]** and **Py**[8a]** were formed from terminal

50

oligoynes by a Hay coupling reaction at rt (**Method A**). Column chromatography and subsequent recrystallization from CH_2Cl_2/MeOH afforded **Py**[6a]** and **Py**[8a]** as orange solids in 84 and 69% yields, respectively. The homocoupling conditions of **Method A** were, however, ineffective toward forming **Py**[10a]**, giving shorter oligoynes as byproducts as a result of the loss of alkyne units (ca. 10%, Table 2.2). A literature precedent suggested modification of the Eglinton–Galbraith homocoupling and using 2,6-lutidine as the base rather than pyridine (**Method D**, Table 2.2),[10] but this alternation gave low yield with the current system. Motivated by the recent formation of polyyne rotaxane molecules, based on the presence of phenanthroline group in the macrocycle that functions as a ligand in Cu-catalyzed homocoupling reactions of oligoynes,[37] an analogous protocol using 4,4'-di-*tert*-butyl-2,2'-bipyridine (dtBBP) and 6,6'-dimethyl-2,2'-bipyridine (DMBP) was explored (Scheme 2.12).

Precursor	Method	Py**[*na*]	yield
Py**[3a]Si	A	6	84%
Py**[4a]Si	A	8	69%
Py**[5a]Si	B	10	64%
Py**[6a]Si	C	12	70%
Py**[8a]Si	B	16	57%
Py**[12a]Si	A	24	28%
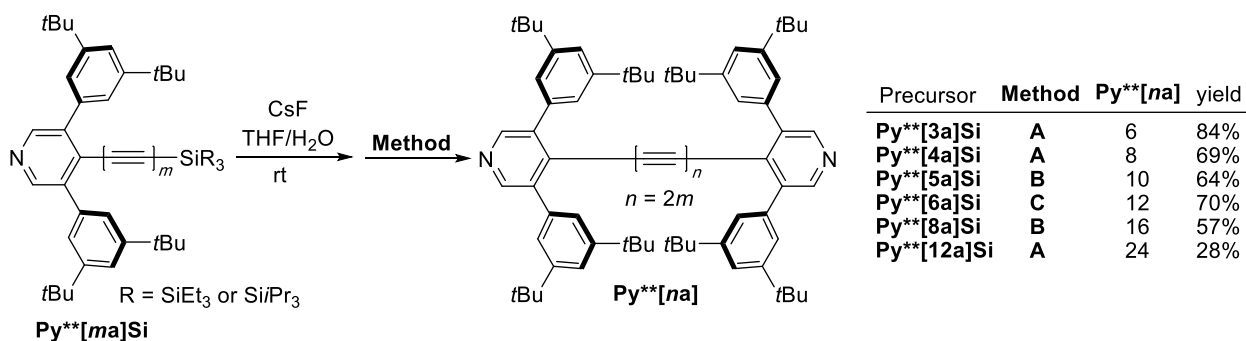
Scheme 2.11. Synthesis of **Py**[*na*]** from **Py**[*ma*]Si**. **Method A**) CuCl, TMEDA, CH_2Cl_2/THF, O_2; **Method B**) CuCl, 4,4'-di-*t*-butyl-2,2'-bipyridine (dtBBP), 6,6'-dimethyl-2,2'-bipyridine (DMBP), CH_2Cl_2/THF, O_2; **Method C**) CuCl, dtBBP CH_2Cl_2/EtOAc/THF, O_2.

The Eglinton–Galbraith homocoupling reaction was tested with the substrate **2.9a** using dtBBP and DMBP as a base/ligand. The homo-coupled product **Py**[4a]** was observed in this reaction (by TLC analysis) when using dtBBP and either CuCl or Cu(OAc)$_2$ (entry 1 and 2, Scheme 2.12), while no product was observed in the presence of DMBP (entry 3 and 4, Scheme 2.12). Empirically, the reaction appears much faster using CuCl than Cu(OAc)$_2$, as monitored by TLC analysis. The reaction using CuCl was complete in ca. 5 h, but more than half of **2.9a** remained unreacted after a reaction time of ca. 15 h when using Cu(OAc)$_2$. Therefore, the combination of CuCl and dtBBP was deemed to be more efficient in this homocoupling reaction.
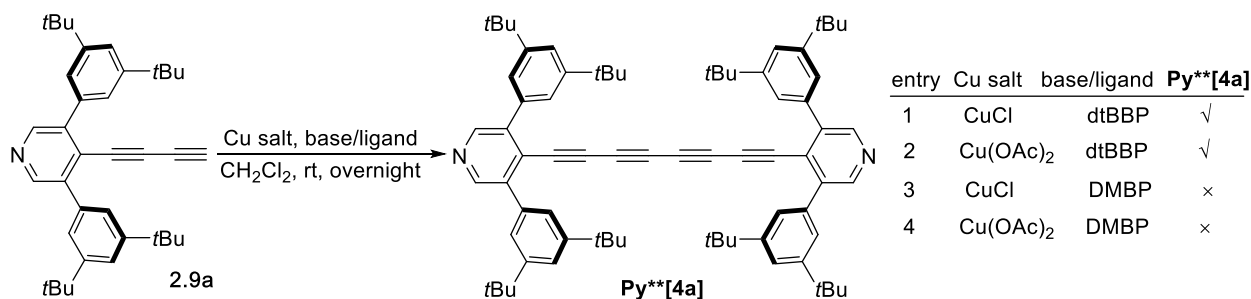
Scheme 2.12. Screening of homocoupling conditions for **2.9a**.

Table 2.2. Summary of homocoupling syntheses resulting in loss of alkyne units.

Target oligoyne	Method	Combined yield	Product (ratio)[a]
Py**[10a]	b	53%	**Py**[10a/9a/8a]** (100/5/5)
	c	64%	**Py**[10a/9a/8a]** (100/2/trace)
	d	70%	**Py**[10a/9a/8a]** (100/8/trace)
	e	17%	**Py**[10a/9a/8a]** (100/4/trace)
Py**[12a]	b	56%	**Py**[12a/11a/10a]** (100/8/3)
	d	70%	**Py**[12a/11a]** (100/trace)
	e	4%	**Py**[12a/11a/10a]** (100/2/1)
Py**[16a]	c	57%	**Py**[16a/15a]** (100/3–5)
	d	58%	**Py**[16a/15a]** (100/11)
Py**[24a]	b	28%	**Py**[24a/23a]** (100/trace)
	c	—[b]	**Py**[12–24a]**

[a]Ratios are estimated based on mass spectral analysis relative to target oligoyne. [b]Not determined.
[b]**Method A**), CuCl, TMEDA, CH$_2$Cl$_2$/THF, O$_2$, 0 °C for **Py**[10a]** and **Py**[12a]**; CuCl, TMEDA, CH$_2$Cl$_2$/THF, O$_2$, 0 °C → rt for **Py**[24a]**; [c]**Method B**), CuCl, 4,4'-di-*t*-butyl-2,2'-bipyridine (dtBBP), 6,6'-dimethyl-2,2'-bipyridine (DMBP), CH$_2$Cl$_2$/THF, O$_2$, rt; [d]**Method C**), CuCl, dtBBP, CH$_2$Cl$_2$/EtOAc/THF, O$_2$, rt; [e]**Method D**), Cu(OAc)$_2$, 2,6-lutidine, CH$_2$Cl$_2$/THF, O$_2$, rt.

These conditions (**Method C**) were applied to the formation of **Py**[10a]**, **Py**[12a]** and **Py**[16a]**. While **Method C** gave the products in good yields of 58–70%, only **Py**[12a]** could be obtained pure after workup. On the other hand, oligoynes of **Py**[9a]** and **Py**[15a]** (ca. 10%) were observed during the synthesis of **Py**[10a]** and **Py**[16a]**, respectively, based on the mass spectrometric analysis. When using **Method B** in the presence of both dtBBP and DMBP, however, the loss of alkyne units was significantly suppressed and only about 2–5% of shorter oligoynes relative to the target oligoynes were observed (Table 2.2). Finally, pure **Py**[24a]** was produced in 28% yield using **Method A** at 0 °C, while **Method B** gave complicated mixtures of oligoynes (from a decayne to the tetracosayne) due to the loss of alkyne units.

Thus, while the desired oligo-/polyynes **Py**[*n*a]** up to $n = 24$ could be synthesized and isolated with acceptable purity, no method appears to be general for all lengths. Most frustratingly, there does not seem to be a relationship between oligoyne length, the Method, and the success of the reaction. Additional optimization is thus necessary to extend this methodology beyond molecular lengths described above.

It is worth noting that oligo-/polyynes **Py**[6a]–Py**[24a]** are bench-stable, confirming the premise that the bulky endgroups can afford persistent derivatives. Compound **Py**[24a]** slowly decomposed as a solid at room temperature over a period of hours (monitored by the changes in the UV-vis). When **Py**[24a]** was stored in a solution of EtOAc/CH_2Cl_2 at 5 °C, however, the sample was reasonably stable and slowly discolored over three days as a dark solid precipitated.

2.6 ^{13}C NMR spectroscopic analysis

Oligoynes **Py**[*m*a]Si** and **Py**[*n*a]** are sufficiently stable and soluble for ^{13}C NMR spectroscopic analysis, while the analysis for **Py**[24a]** did not give meaningful results due to the greatly diminished solubility of this sample (Figure 2.4). The ^{13}C NMR spectra for oligoynes **Py**[*m*a]Si** and **Py**[*n*a]**, highlighting resonances for the alkyne carbons, are shown in Figure 2.4a and 2.4b and summarized in Table 2.3 and 2.4. The spectra of oligoynes up to the octayne for **Py**[*m*a]Si** feature unique resonances for each *sp*-hybridized carbon, while spectra for both nonayne **Py**[9a]Si** and dodecayne **Py**[12a]Si** show two degenerate signals. Similarly, oligoynes **Py**[12a]** and **Py**[16a]** show one and two degenerate signals, respectively. The preliminary identification of individual signals has been attempted by either ^{13}C labeling experiments or heteronuclear multiple bond correlation (HMBC) analysis.[35, 38] Herein, two HMBC experiments result in tentative assignment of the two terminal *sp*-hybridized carbons. As in the examples of compound **Py**[4a]Si** and **Py**[4a]** shown in Figure 2.4c and 2.4d, the correlation between H_a (δ 8.66) and C1 (δ 73.1) in a 'w' shape through four bonds is stronger than the correlation between H_a and C2 (δ 83.6) through five bonds. The proton H_b (δ 0.64) from the methylene group of TES group correlates C8 (δ 88.1) through three bonds, while the correlation of C7 was not observed. This assignment has been confirmed by ^{13}C labelling experiment and will be discussed in Chapter 3. The results outline that the alkyne carbon resonances of outermost *sp*-hybridized carbons shift downfield more than that of the inner carbons.
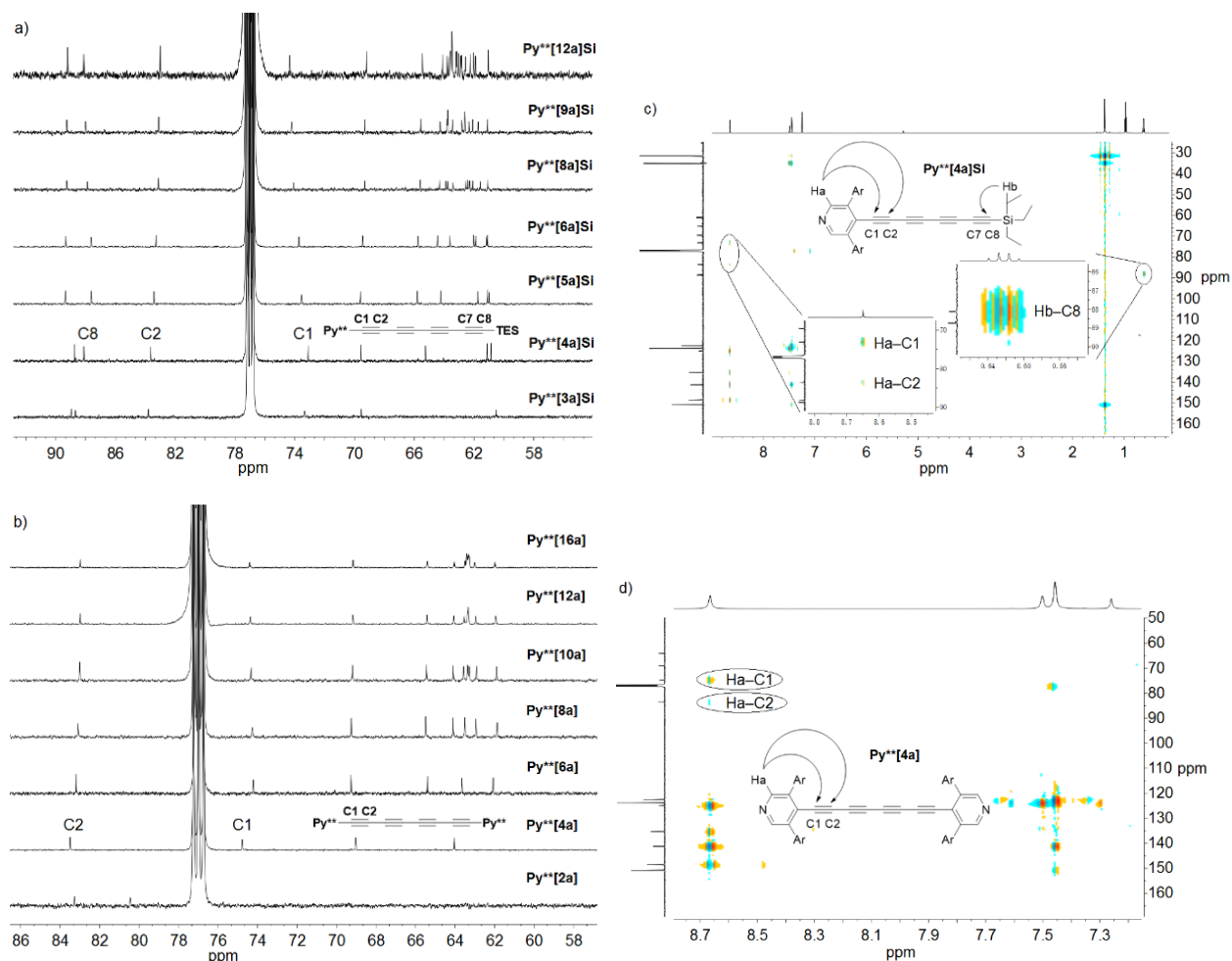
Figure 2.4. a) and b) ^{13}C NMR spectra highlighting alkyne carbon resonances for oligoynes **Py******[ma]Si** and **Py******[na]**, respectively (in CDCl$_3$); c) and d) ^{1}H–^{13}C HMBC spectra of oligoynes **Py******[4a]Si** and **Py******[4a]**, respectively (in CDCl$_3$).

As molecular length increases, additional carbon resonances appear within a narrow range of 62–65 ppm for **Py******[16a]** and 61–66 ppm for compound **Py******[12a]Si**. Finally, the carbon resonances converge toward a value of 63.4 ppm and 63.6 ppm for **Py******[na]** and **Py******[ma]Si**, respectively. The convergence value of 63.4 ppm for **Py******[na]** and 63.6 ppm for **Py******[ma]Si** are nearly identical to the value of 63.7 ppm observed for the **Tr*****[n]**[10] and **tBu[n]**[17a] series that are endcapped by sp^3-carbon moieties. Thus, in all cases ^{13}C NMR spectroscopy suggests a polyyynic framework at extended lengths, i.e., Peierls distortion is operative and carbyne would be composed of alternating single and triple bonds. Furthermore, the spectroscopic similarities between the two series **Tr*****[n]** and **Py******[na]** confirm that endgroups exert a minimal effect on the ^{13}C NMR spectroscopic signature for carbyne, as would be expected.

Table 2.3. ^{13}C NMR alkyne carbon resonances for oligoynes **Py**[*m*a]Si**.

oligoyne	Alkyne carbon chemical shifts in $CDCl_3$ (ppm)
Py**[3a]Si	89.0, 88.7, 83.8, 73.3, 69.6, 60.5
Py**[4a]Si	88.7, 88.1, 83.6, 73.1, 69.6, 65.3, 61.1, 60.9
Py**[5a]Si	89.4, 87.6, 83.4, 73.6, 69.6, 65.8, 64.2, 61.7, 61.09, 60.98
Py**[6a]Si	89.3, 87.6, 83.3, 73.7, 69.5, 65.8, 64.4, 63.6, 62.0, 61.9, 61.2, 61.1
Py**[8a]Si	89.3, 87.9, 83.1, 74.1, 69.3, 65.6, 64.3, 63.9, 63.8, 63.4, 62.5, 62.4, 62.3, 62.1, 61.6, 61.1
Py**[9a]Si	89.2, 88.0, 83.1, 74.2, 69.3, 65.6, 64.3, 63.8, 63.7, 63.4, 62.8, 62.6, 62.3, 62.1, 61.7, 61.1
Py**[12a]Si	89.2, 88.1, 83.0, 74.3, 69.2, 65.5, 64.1, 63.8, 63.7, 63.60, 63.57, 63.5, 63.20, 63.15, 63.0, 62.9, 62.8, 62.6, 62.3, 62.0. 61.9, 61.0

Table 2.4. ^{13}C NMR alkyne carbon resonances for oligoynes **Py**[*n*a]**.

polyynes	Alkyne carbon chemical shifts in $CDCl_3$ (ppm)
Py**[2a]	83.3, 80.5
Py**[4a]	83.5, 74.8, 69.0, 64.0
Py**[6a]	83.2, 74.2, 69.3, 65.4, 63.7, 62.1
Py**[8a]	83.1, 74.3, 69.3, 65.5, 64.1, 63.5, 63.0, 61.9
Py**[10a]	83.0, 74.3, 69.2, 65.5, 64.1, 63.6, 63.4, 63.3, 62.9, 61.9
Py**[12a]	83.0, 74.4, 69.2, 65.4, 64.1, 63.5, 63.4, 63.34, 63.31, 63.0, 61.9
Py**[16a]	83.0, 74.4, 69.2, 65.4, 64.0, 63.5, 63.41, 63.38, 63.37, 63.32, 63.29, 63.27, 63.0, 62.0

2.7 UV-vis spectroscopic analysis

As 1-D conjugated systems, oligoynes are expected to show a correlation between the molecular length, electronic absorptions (e.g., the "optical energy gap", based on λ_{max} as the lowest-energy transition observed in the electronic absorption spectra[39]), and bond length alternation (BLA = the bond length difference between consecutive single and triple bonds).[40] Theoretical and experimental studies have predicted that neither the optical energy gap nor BLA for polyynes/carbyne will be zero,[10, 40b, 41] i.e., Peierls distortion is maintained.[42]

2.7.1 UV-vis spectra of Py**[*m*a]Si and Py**[*n*a]

The quantitative UV-vis spectra of oligo-/polyynes **Py****[*m*a]Si and **Py****[*n*a] have been measured in CH_2Cl_2 at room temperature (Figure 2.5 and 2.6), and the relevant UV-vis data have been listed in Table 2.5. Toward achieving a better resolution, oligo-/polyynes **Py****[*n*a] have also been measured in 2-MeTHF at 80 K (Figure 2.7). The UV-vis spectra of oligo-/polyynes **Py****[*m*a]Si and **Py****[*n*a] exhibit two regions of absorption, as has been commonly observed for other analogs,[17b] namely, a region of intense absorption, λ_{main}, at higher energy and a region of lower intensity signal, λ_{weak}, at lower energy. The spectra of **Py****[*m*a]Si with $m \geq 4$ show several intense absorptions, characteristic of vibrational fine structure of oligoynes, in the region of λ_{main}, with the most significant absorbance extending to 410 nm for the longest derivative **Py****[12a]Si. The absorbances in this region are less resolved compared with those of sp^3-carbon-endcapped oligo-/polyynes,[10, 17a] presumably due to the conjugation of the carbon chain with the sp^2-endgroup. Furthermore, a series of weaker absorptions in the region of λ_{weak} is well-resolved, with the lowest energy values ($\lambda_{max(weak)}$), ranging from $\lambda_{max(weak)}$ = 360 nm for **Py****[3a]Si to $\lambda_{max(weak)}$ = 564 nm for **Py****[12a]Si. The molar extinction absorbance in the λ_{main} region increases with chain length to the value of 390000 $M^{-1}cm^{-1}$ for **Py****[12a]Si. The extinctions of $\lambda_{max(weak)}$ are, on the other hand, relatively weak and steadily decrease in intensity from 15100 $M^{-1}cm^{-1}$ for **Py****[3a]Si to 643 $M^{-1}cm^{-1}$ for **Py****[12a]Si (Table 2.5). The spectra of oligo-/polyynes **Py****[*n*a] with $n \geq 6$ show several intense maxima, λ_{main}, with lowest energy values ($\lambda_{max(main)}$) that extend to 473 nm for the longest derivative **Py****[24a] at rt. In addition to λ_{main}, a series of weaker absorptions, λ_{weak}, is also clearly observed at lower energy for oligoynes up to **Py****[16a], which range from $\lambda_{max(weak)}$ = 421 nm for **Py****[4a] to $\lambda_{max(weak)}$ = 593 nm for **Py****[16a]. By the length of **Py****[24a], however, λ_{weak} absorptions are no longer discernable. The λ_{weak} absorptions at 80 K are slightly better resolved and red-shifted at lower temperature (see Figure 2.7).
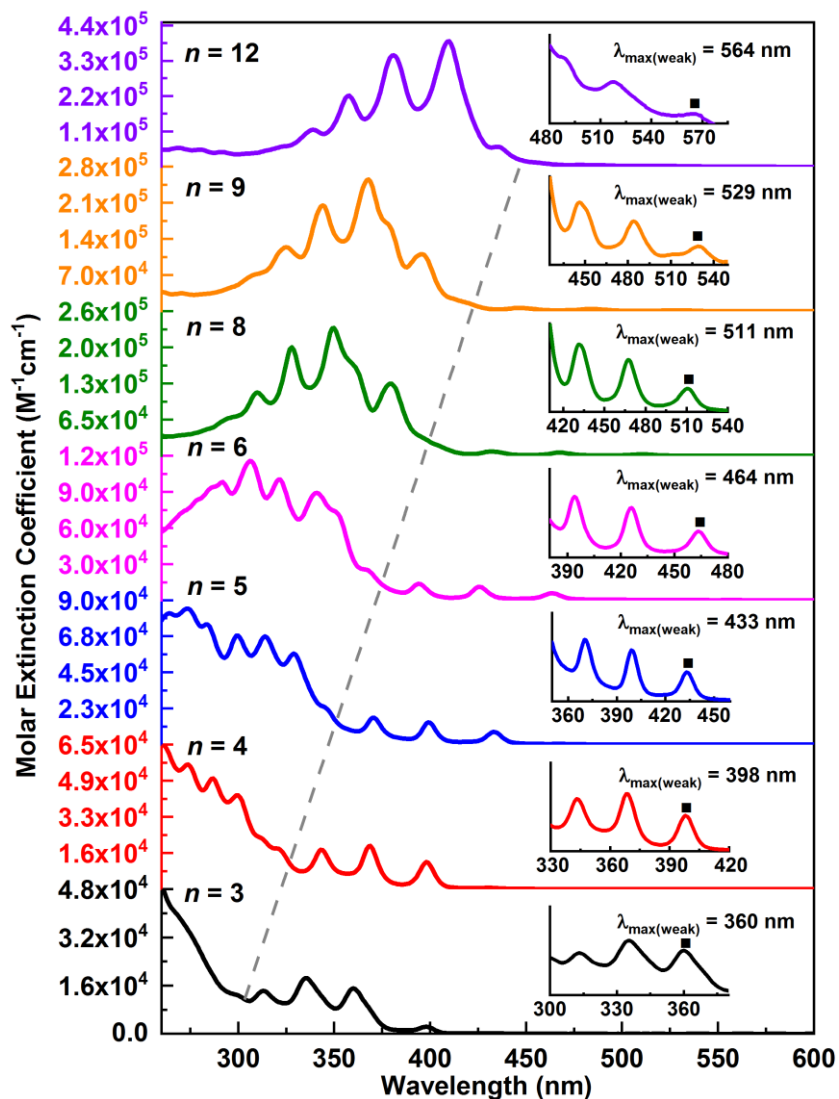
Figure 2.5. UV-vis spectra of **Py**[*m*a]Si** oligoynes as measured in CH_2Cl_2 at room temperature. The dashed line is a guide for the eye to separate the spectra into two regions, λ_{main} at higher energy and λ_{weak} at lower energy. The lowest energy absorption, $\lambda_{max(weak)}$, of each derivative is labeled with a black square in the accompanying expansion.

Table 2.5. Relevant UV-vis data for **Py**[_m_a]Si** and **Py**[_n_a]** series.

Py**[_n_a]	$\lambda_{max(weak)}$ [nm]	ε [M^{-1}cm^{-1}]	Py**[_m_a]Si	$\lambda_{max(weak)}$ [nm]	ε [M^{-1}cm^{-1}]
Py**[4a]	421	16900	**Py**[3a]Si**	360	15100
Py**[6a]	477	9460	**Py**[4a]Si**	398	12100
Py**[8a]	520	3960	**Py**[5a]Si**	433	7850
Py**[10a]	550	1900	**Py**[6a]Si**	464	5880
Py**[12a]	571	879	**Py**[8a]Si**	511	2620
Py**[16a]	593	505	**Py**[9a]Si**	529	1870
Py**[24a]	_a_	_a_	**Py**[12a]Si**	564	643

[a]Not observed.
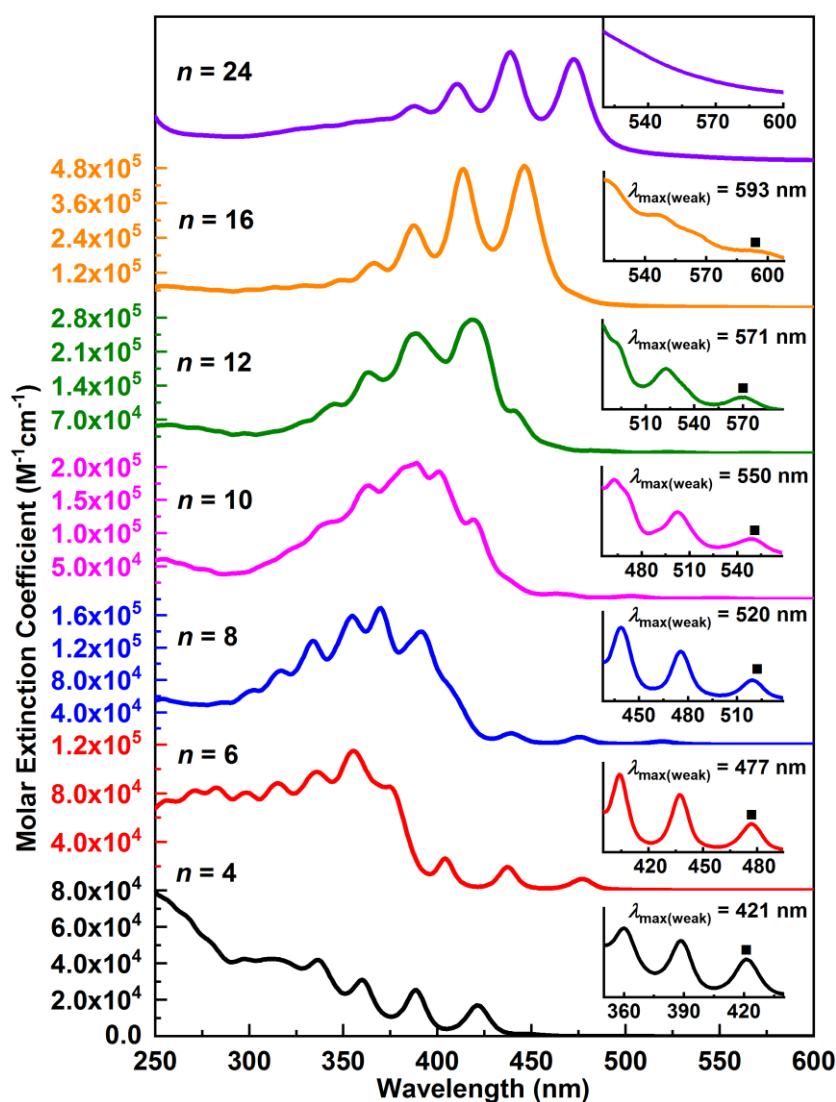
Figure 2.6. UV-vis spectra of **Py**[_n_a]** oligoynes as measured in CH_2Cl_2 at room temperature. The lowest energy absorption, $\lambda_{max(weak)}$, for each derivative is labeled in the accompanying expansion with a black square; note that the absorbance intensities for **Py**[24a]** are in arbitrary units.
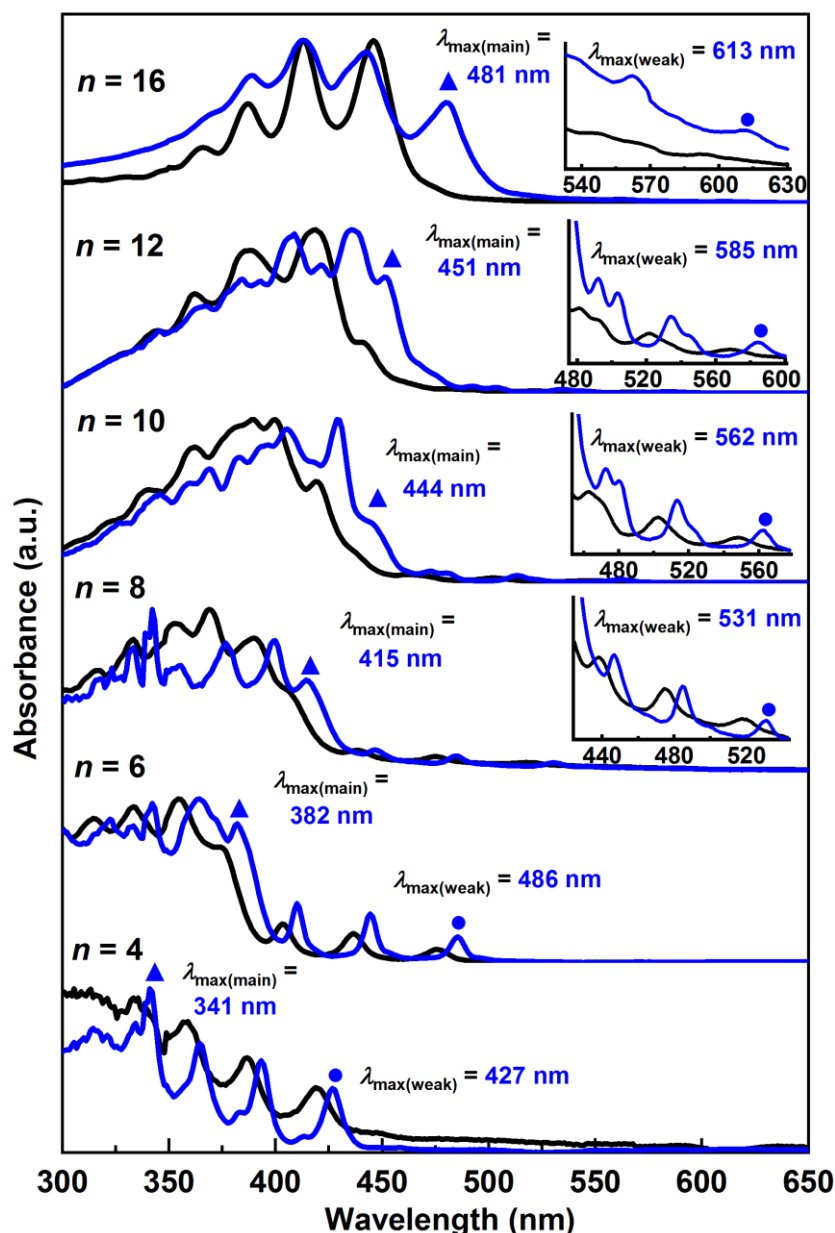
Figure 2.7. UV-vis spectra of **Py**[*n*a]** oligoynes as measured in 2-MeTHF at rt (black) and at 80 K (blue). a.u. = arbitrary units (λ_{max} absorption peak at lowest energy in the region of λ_{weak} is labelled with a blue circle for each derivative). The choice of the λ_{max} absorption peak for the high energy in the region of λ_{main} is potentially problematic given the presence of overlapping peaks. In this figure, the lowest energy absorption in the region of λ_{main} that is clearly resolved is labelled with a blue triangle for each derivative; these values are for demonstration purposes only.

It is well established that the lowest energy wavelength of significant absorption (λ_{max}) shows a steady shift to lower energy as a function of oligoyne length.[36] Previous work has linked λ_{max} to the HOMO $\rightarrow$ LUMO excitation of oligoynes, but the origin of λ_{max} for oligoynes via UV-

vis analyses has recently been challenged, based predominantly on molecular symmetry.[39b, 43] Previous studies have predicted that the low energy HOMO–LUMO transition involved in the excitation to the first singlet excited state of an oligoyne ($S_0 \rightarrow S_1$) is formally electric dipole forbidden by symmetry and, therefore, an optical dark state. On the other hand, at shorter wavelength than $S_0 \rightarrow S_1$, a weakly allowed excitation is expected (λ_{weak}), and calculations for aryl endcapped oligoynes show that the absorbance of the λ_{weak} bands should diminish as molecular length is increased.[43b, 43c] Finally, the spectra of oligoynes and polyynes are dominated by strong, higher energy, electric dipole allowed absorptions (λ_{main}). These predictions are strikingly confirmed by the **Py**[na]** oligo-/polyynes. In the case of "shorter" derivatives, pseudo symmetry (Figure 2.1c) is reduced through the presence of endgroups giving "intense" λ_{weak} absorptions (a lower energy HOMO $\rightarrow$ LUMO excitation is not found). On the other hand, the absorbance of λ_{weak} signal decreases dramatically versus length as the influence of the endgroups is diminished and the oligoynes tend toward the $D_{\infty h}$ symmetry expected of polyynes and carbyne (Figure 2.5 and 2.6). Ultimately, the λ_{weak} absorptions are no longer experimentally observed for **Py**[24a]**, confirming that the properties of oligoynes are tending toward those of polyynes. Exponential fitting of molar absorptivity of $\lambda_{max(weak)}$ versus length is consistent with the loss of these absorbances by the length of **Py**[24a]** (Figure 2.10). In the **Py**[ma]Si** series, a steady decrease of the absorption in the λ_{weak} region as a function of polyynic length was also observed, but the signal can still be discernible, which means that up to the length of **Py**[12a]Si**, the **Py**[ma]Si** series ($m \leq 12$) is still an oligoyne with the effect of endgroup.

2.7.2 Linear fitting of λ_{max}

Numerous studies have used λ_{max} as a predictive tool for the optical energy gap of long polyynes and, ultimately, carbyne. Based on the premise that λ_{max} should reach a saturation limit with an asymptotic plateau (λ_{sat}), the limiting value of λ_{max} at the saturation limit would be a reasonable estimate for carbyne. The intense maxima of λ_{main} and λ_{weak} with the lowest energy values, $\lambda_{max(main)}$ and $\lambda_{max(weak)}$, respectively are plotted as a function of $1/n$, using a linear function of the form[17b, 35, 44].

$$\lambda_{(n)} = k(1/n) + b \qquad \text{equation (1)}$$

where n is the number of acetylenic units, $\lambda_{(n)}$ is λ_{max} for an oligoyne of length n, the y-intercept b

is the λ_∞ as $n \to 0$, and the factor 'k' reflects how fast the oligoyne approaches to carbyne. UV-vis spectroscopic data of $\lambda_{max(weak)}$ for **Py**[na]** and **Py**[ma]Si** have been plotted in Figure 2.8 using equation (1) and summarized in Table 2.6. Likewise, UV-vis spectroscopic data of $\lambda_{max(main)}$ for oligoynes **tBu[n]** and **Ad[n]** have been plotted in Figure 2.9 using equation (1) and summarized in Table 2.6. The analysis of both $\lambda_{max(weak)}$ and $\lambda_{max(main)}$ for **Glu[n]** and **Tr*[n]** has been reported in the literature[10, 39b] and summarized in Table 2.7. The linear fitting equation (1) gives $\lambda_{sat(main)}$ of 498 nm for **tBu[n]**, 512 nm for **Ad[n]**, 561 nm for **Glu[n]**, and 564 nm for **Tr*[n]**, respectively. Apparently, although excellent correlation is fitted for each series, the prediction of $\lambda_{sat(main)}$ is dependent on different endgroups. In a similar manner, the linear fitting gives $\lambda_{sat(weak)}$ of 810 nm for **Glu[n]**, 756 nm for **Tr*[n]**, 663 nm for **Py**[na]**, and 662 nm for **Py**[ma]Si**, respectively. As analyzed above, this commonly used plotting has shown defects in predicting the optical gap for carbyne (*vide infra*).

Table 2.6. UV-vis spectroscopic data of $\lambda_{max(main)}$ and $\lambda_{max(weak)}$ for oligoynes **tBu[n]**,[17a, 32] **Ad[n]**,[45] **Glu[n]**,[39b] **Tr*[n]**,[10, 39b] **Py**[na]**, and **Py**[ma]Si**.

n	tBu[n][a]	Ad[n][b]	Glu[n][c]		Tr*[n][a]		Py**[na][c]	Py**[ma]Si[c]
	$\lambda_{max(main)}$	$\lambda_{max(main)}$	$\lambda_{max(main)}$	$\lambda_{max(weak)}$	$\lambda_{max(main)}$	$\lambda_{max(weak)}$	$\lambda_{max(weak)}$	$\lambda_{max(weak)}$
3	213	—[d]	—[d]	—[d]	—[d]	—[d]	—[d]	360
4	240	250	242	347	268	368	421	398
5	266	276	—[d]	—[d]	—[d]	—[d]	—[d]	433
6	289	300	292	430	310	443	477	464
8	330	340	334	487	347	495	520	511
9	—[d]	—[d]	—[d]	—[d]	—[d]	—[d]	—[d]	529
10	362	373	367	523	376	508	550	—[d]
12	387	398	393	564	400	—[d]	571	564
14	—[d]	—[d]	—[d]	—[d]	419	—[d]	—[d]	—[d]
16	—[d]	—[d]	—[d]	—[d]	432	—[d]	593	—[d]
18	—[d]	—[d]	—[d]	—[d]	443	—[d]	—[d]	—[d]
20	—[d]	—[d]	—[d]	—[d]	451	—[d]	—[d]	—[d]
22	—[d]	—[d]	—[d]	—[d]	458	—[d]	—[d]	—[d]
24	—[d]	—[d]	—[d]	—[d]	—[d]	—[d]	—[d]	—[d]

[a]Measured in hexanes, [b]measured in THF, [c]measured in CH_2Cl_2, [d]not reported or not observed.

Table 2.7. Summary of λ_{sat} values predicted by two methods from oligo-/polyynes.

oligoyne	$\lambda_{sat(main)}$[a]		$\lambda_{sat(weak)}$[b]		reference
	eq (1)	eq (2)	eq (1)	eq (2)	
*t*Bu[*n*]	498[c]	501[d]	—[f]	—[f]	[17a, 32]
Ad[*n*]	512[c]	502[e]	—[f]	—[f]	[45]
Glu[*n*]	561[g]	502[g]	810[g]	649[g]	[39b]
Tr*[*n*]	564[h]	485[i]	756[g]	—[f]	[10, 39b]
Py**[*n*a]	—[j]	—[j]	663[k]	617[l]	
			687[k,m]	643[l,m]	
Py**[*m*a]Si	—[j]	—[j]	662[n]	621[o]	

[a]Analysis with $\lambda_{max(main)}$ absorptions. [b]Analysis with $\lambda_{max(weak)}$ absorptions. [c]For n = 8, 10, 12. [d]For n = 3, 4, 5, 6, 8, 10, 12. [e]For n = 4, 5, 6, 8, 10, 12. [f]Not reported or insufficient data. [g]For n = 4, 6, 8, 10, 12. [h]For n = 10, 12, 14, 16, 18, 20, 22. [i]For n = 4, 6, 8, 10, 12, 14, 16, 18, 20, 22. [j]Analysis of $\lambda_{sat(main)}$ is not straightforward for **Py**[*n*a] and **Py**[*m*a]Si derivatives. [k]For n = 6, 8, 10, 12, 16. [l]For n = 4, 6, 8, 10, 12, 16. [m]Measurements at 80 K. [n]For n = 6, 8, 9, 12. [o]For n = 3, 4, 5, 6, 8, 9, 12.
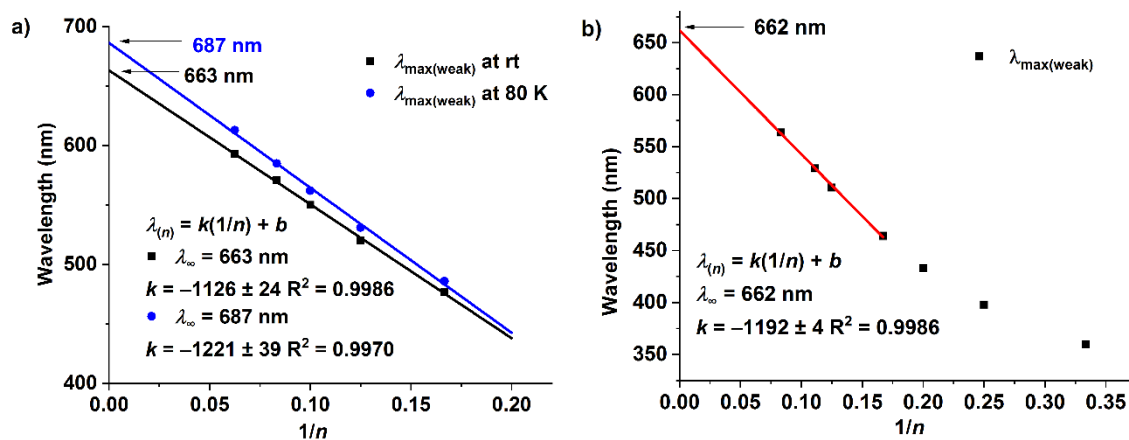
Figure 2.8. Plots of $\lambda_{max(weak)}$ versus $1/n$ using equation (1) for a) **Py**[*n*a] as measured in CH_2Cl_2 at rt (black) and in 2-MeTHF at 80 K (blue), where n is the number of triple bonds, and b) **Py**[*m*a]Si as measured in CH_2Cl_2 at rt, where n is the number of triple bonds.
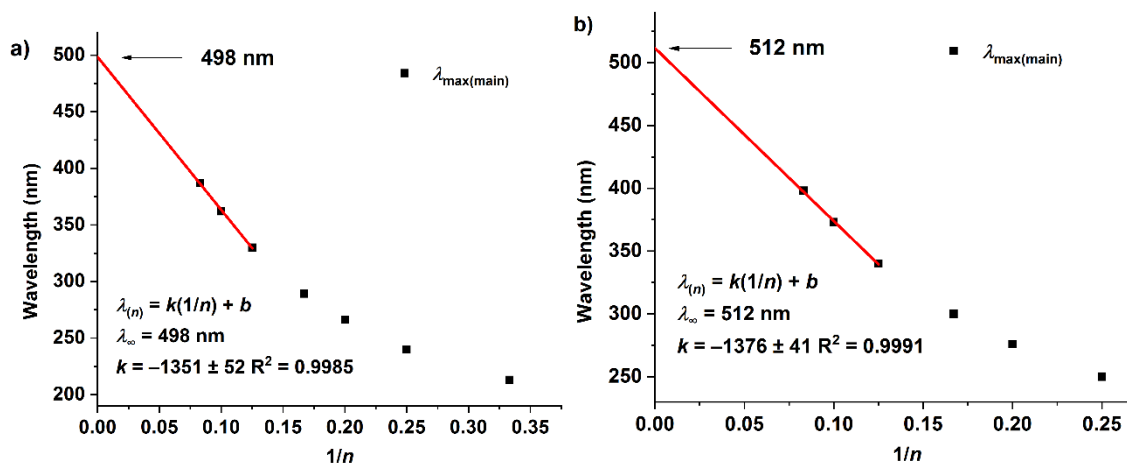
Figure 2.9. Plots of $\lambda_{\text{max(main)}}$ versus $1/n$ using equation (1) for a) **tBu[n]** as measured in hexanes at rt, where n is the number of triple bonds, and b) **Ad[n]** as measured in THF at rt, where n is the number of triple bonds.

2.7.3 Exponential fitting of λ_{max}

As discussed in Section 2.6.2, there exists a problem with estimations based on λ_{max} versus $1/n$, which has been previously discussed for conjugated molecules in general[46] and oligoynes specifically.[10] Namely, the analysis of λ_{max} versus $1/n$ rests on the assumption that λ_{max} decreases in energy uniformly as a function of length, even though it is well established that conjugated organic oligomers reach a convergent limit (i.e., saturation or effective conjugation length) at lengths much shorter than infinity.[47] To account for the saturation length in oligoynes, an alternative analysis has been outlined by Meier[46] using an exponential function of the form:

$$\lambda_{(n)} = \lambda_\infty - (\lambda_\infty - \lambda_1)e^{-k(n-1)} \qquad \text{equation (2)}$$

where n is the number of alkyne units, $\lambda_{(n)}$ is λ_{max} for an oligoyne of length n (thus λ_1 is λ_{max} of the monomer with $n = 1$, calculated according to equation (2), and λ_∞ is the limiting value as $n \to \infty$). The factor "k" provides an indication of how fast saturation (convergence) is approached. Finally, λ_{sat} is defined by fulfilment of the relationship $\lambda_\infty - \lambda_{(n)} \leq 1$.

Analysis of $\lambda_{\text{max(weak)}}$ values for **Py**[na]** using the Meier protocol gives $\lambda_{\text{sat(weak)}} = 617$ nm and 643 nm at room temperature and 80 K, respectively (Figure 2.10, Table 2.7). This analysis predicts the convergence of $\lambda_{\text{max(weak)}}$ at values of $\lambda_{\text{sat(weak)}} = 617$ and 643 nm (rt and 80 K, respectively) at a length of ca. $n = 34$ and 37 (rt and 80 K, respectively), i.e., the polyyne limit (Figure 2.10, Table 2.7). Analysis of $\lambda_{\text{max(weak)}}$ values for the **Py**[ma]Si** series using the Meier protocol gives $\lambda_{\text{sat(weak)}} = 621$ nm at a length of ca. $n = 36$ (Figure 2.11, Table 2.7), which is consistent with the consequence of $\lambda_{\text{sat(weak)}} = 617$ nm at a length of ca. $n = 34$ for **Py**[na]** series.

$\lambda_{\text{sat(weak)}}$ of 649 nm for **Glu[n]** (Figure 2.12, Table 2.7), 617 nm for **Py**[na]**, and 621 nm for **Py**[ma]Si**, at n = 42, 34, and 36, with k = 0.152, 0.176, and 0.170, respectively are obtained. The values of k reflect that **Py**[na]** and **Py**[ma]Si** reach saturation more quickly than **Glu[n]**. Given that **Py**[ma]Si** and **Glu[n]** are analyzed up to the same length (n up to 12) and the k value of the former is bigger, therefore, the former should give a more accurate prediction, and this statement agrees with the prediction given by **Py**[na]** (n up to 16) that both **Py**[na]** and **Py**[ma]Si** give close predictions. Molar absorptivity of $\lambda_{\text{max(weak)}}$ versus length n can also be analyzed by adaption of equation (2) to give the form:

$$\varepsilon_{(n)} = \varepsilon_1 e^{-k(n-1)} \quad \text{equation (3)}$$

Equation (3) tends to ε_∞ = 0 as a function of length for λ_{weak} transitions, as expected for carbyne, and the convergence of molar absorptivity of the λ_{weak} transitions is greatly diminished at lengths $n \geq 20$ (Figure 2.10 and 2.11). Finally, the λ_{weak} absorbance of **Py**[24]** in the UV-vis spectra is no longer discernible, which supports the loss of endgroup effects, thus the properties of oligoynes are tending toward that of polyyne.
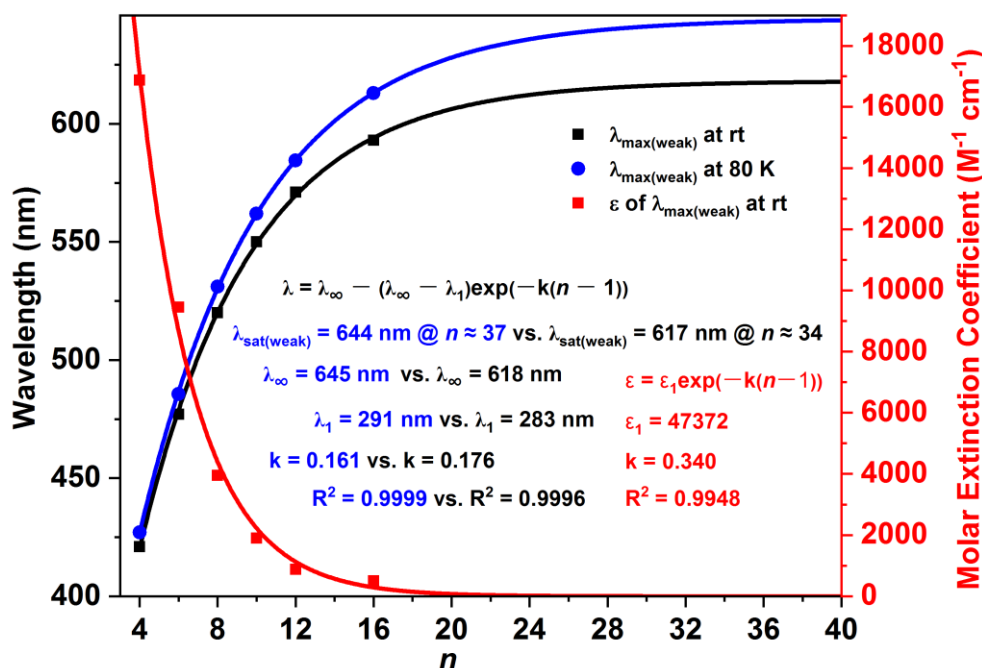
Figure 2.10. Convergence, according to equation (2), of $\lambda_{\text{max(weak)}}$ as a function of oligoyne length n in the series **Py**[na]** at low (blue) and room (black) temperature and convergence of molar absorptivity of the $\lambda_{\text{max(weak)}}$ according to equation (3) in red.
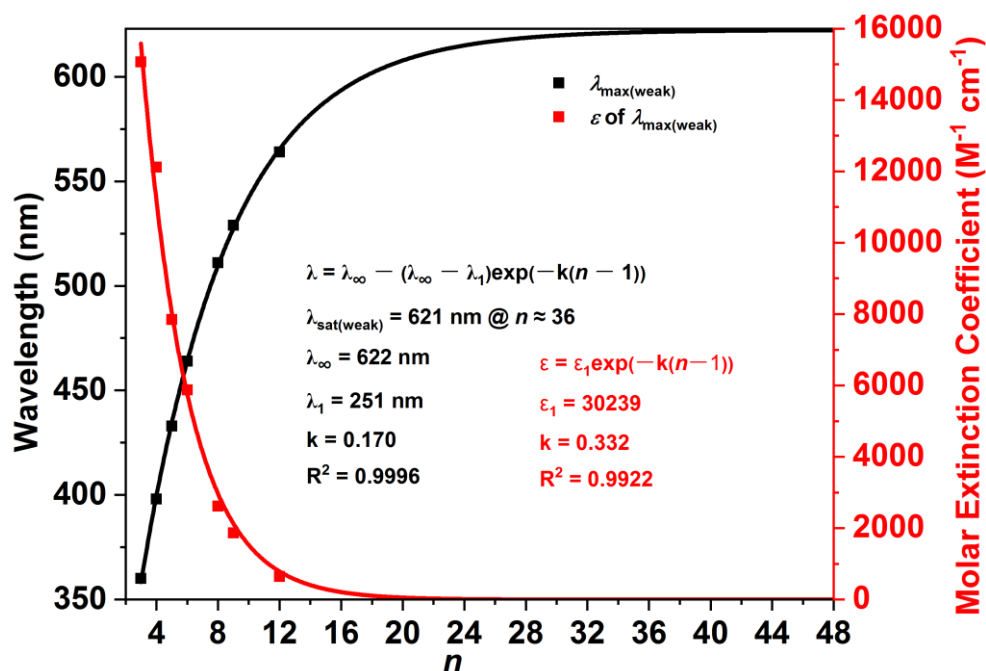
Figure 2.11. Convergence, according to equation (2), of $\lambda_{max(weak)}$ as a function of oligoyne length n in the series **Py**[ma]Si** at rt and convergence of molar absorptivity of the $\lambda_{max(weak)}$ according to equation (3).
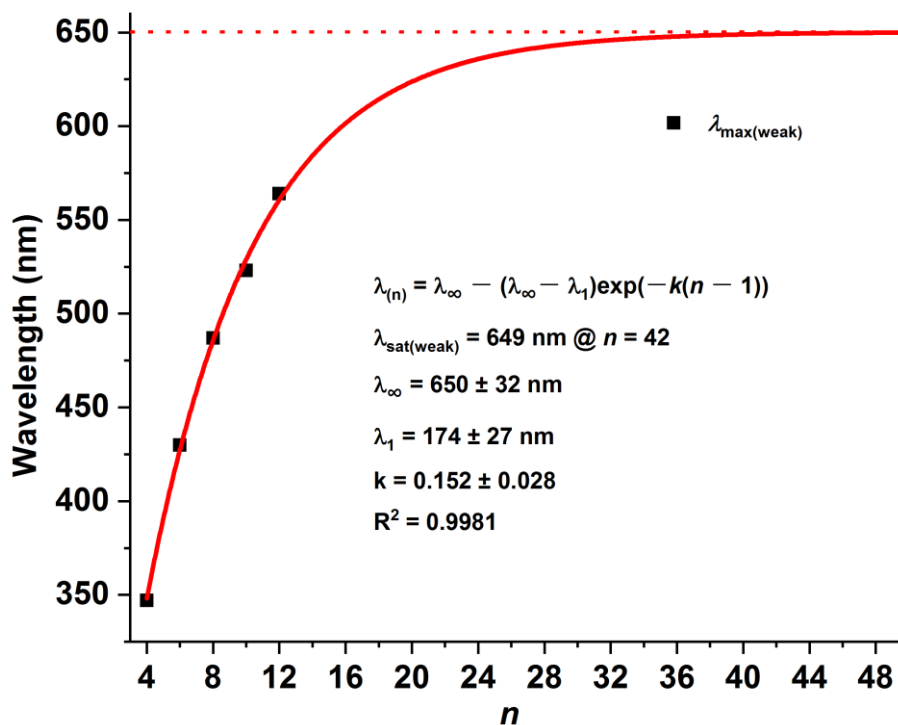
Figure 2.12. Convergence, according to equation (2), of $\lambda_{max(weak)}$ as a function of oligoyne length n in the series **Glu[n]**.

The values derived from **Py**[na]** using Meier's equation are the most accurate estimation

to date for the optical gap of carbyne (617 nm/2.01 eV at rt), based on the analysis of $\lambda_{\max(\text{weak})}$ and confirm that carbyne should maintain a sizable band gap and Peierls distortion will be upheld. It should be noted that even though λ_{weak} transitions are greatly diminished at lengths $n \geq 20$ (Figure 2.10), they should be rendered partially allowed through even minor deviations from an ideal, linear geometry, as has been previously established for oligoynes.[48]

2.8 X-ray crystallographic analysis

X-ray crystallographic analysis has been successful for diyne **Py**[2a]**, tetrayne **Py**[4a]**, hexayne **Py**[6a]** (two polymorphs in triclinic and monoclinic crystal system, **Py**[6a]ᵗ** and **Py**[6a]ᵐ** respectively), and octayne **Py**[8a]** (Figure 2.13). The solid-state structure of octayne **Py**[8a]** deserves mention, given that it represents that of the longest aryl-endcapped oligoyne reported to date, and only the third octayne to be described without metal endgroups. Crystals suitable for X-ray crystallographic analysis were also obtained for compounds **Py**[4a]Si**, **Py**[2c]**, and **Py**[2e]**. Oak Ridge Thermal Ellipsoid Plot (ORTEP) representations for selected compounds **Py**[2a–8a]**, **Py**[4a]Si** (two crystallographically independent molecules of **Py**[4a]SiA** and **Py**[4a]SiB**, respectively), **Py**[2c]**, and **Py**[2e]** are shown in Figure 2.14. Selected solid-state packing and key intermolecular interactions, such as CH/π_{sp} interactions are shown in Figure 2.15.

2.8.1 X-ray crystallographic structures

The first thing that is clear from the crystallographic analyses is the steric shielding afforded by the Py** endgroups (Figure 2.13). Secondly, all **Py**[na]** oligoynes are essentially linear, with average C≡C–C(sp) angles of 178.8° for **Py**[2a]**, 177.2° for **Py**[4a]**, 178.5° for **Py**[6a]ᵗ**, 178.7° for **Py**[6a]ᵐ**, and 178.6°for **Py**[8a]**. The terminal pyridyl rings are nearly coplanar in the solid-state, with torsional angles between planes of the six C/N atoms of the pyridyl ring, all between 0–7° for $n = 2, 4, 8$, while the angle is 26° for both polymorphs of $n = 6$. The crystal structure of **Py**[8a]** is the longest aryl-endcap oligoyne that has been reported to date. Comparing with the other octaynes reported in the literature,[17a, 35, 37a] **Py**[8a]** has the most linear chain conformation.
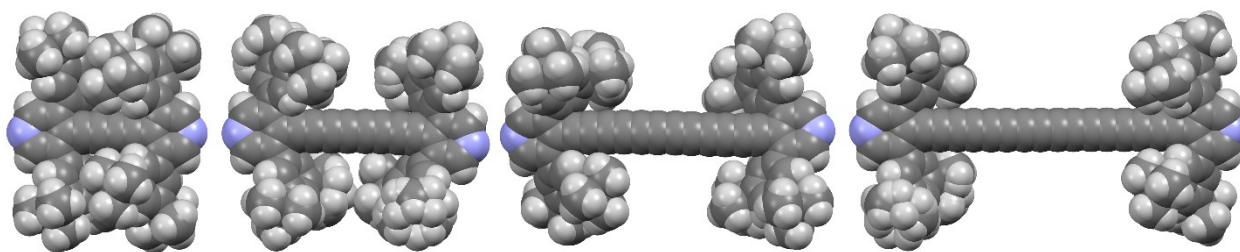
Figure 2.13. X-ray crystallographic structures for **Py**[2a]**, **Py**[4a]**, **Py**[6a]**[t], and **Py**[8a]** shown as space filling model.

Moving away from the series **Py**[*n*a]**, the average C≡C–C(*sp*) angles for **Py**[4a]SiA**, **Py**[4a]SiB**, and **Py**[2e]**, at 173.5°, 170.8°, and 174.9°, respectively, are smaller than for **Py**[2a–8a]**. In particular, the angle of C(6A)–C(7A)≡C(8A), C(6B)–C(7B)≡C(8B), and C(2)–C(3)≡C(4) of **Py**[4a]SiA**, **Py**[4a]SiB**, and **Py**[2e]** are reduced to 170.2(6)°, 164.7(7)°, and 173.9(3)°, respectively, indicating that the conformation of the carbon chain deviates significantly from linearity (atom labels can be found in Figure 2.14g–i), presumably due to crystal packing forces as has been documented.[7c]
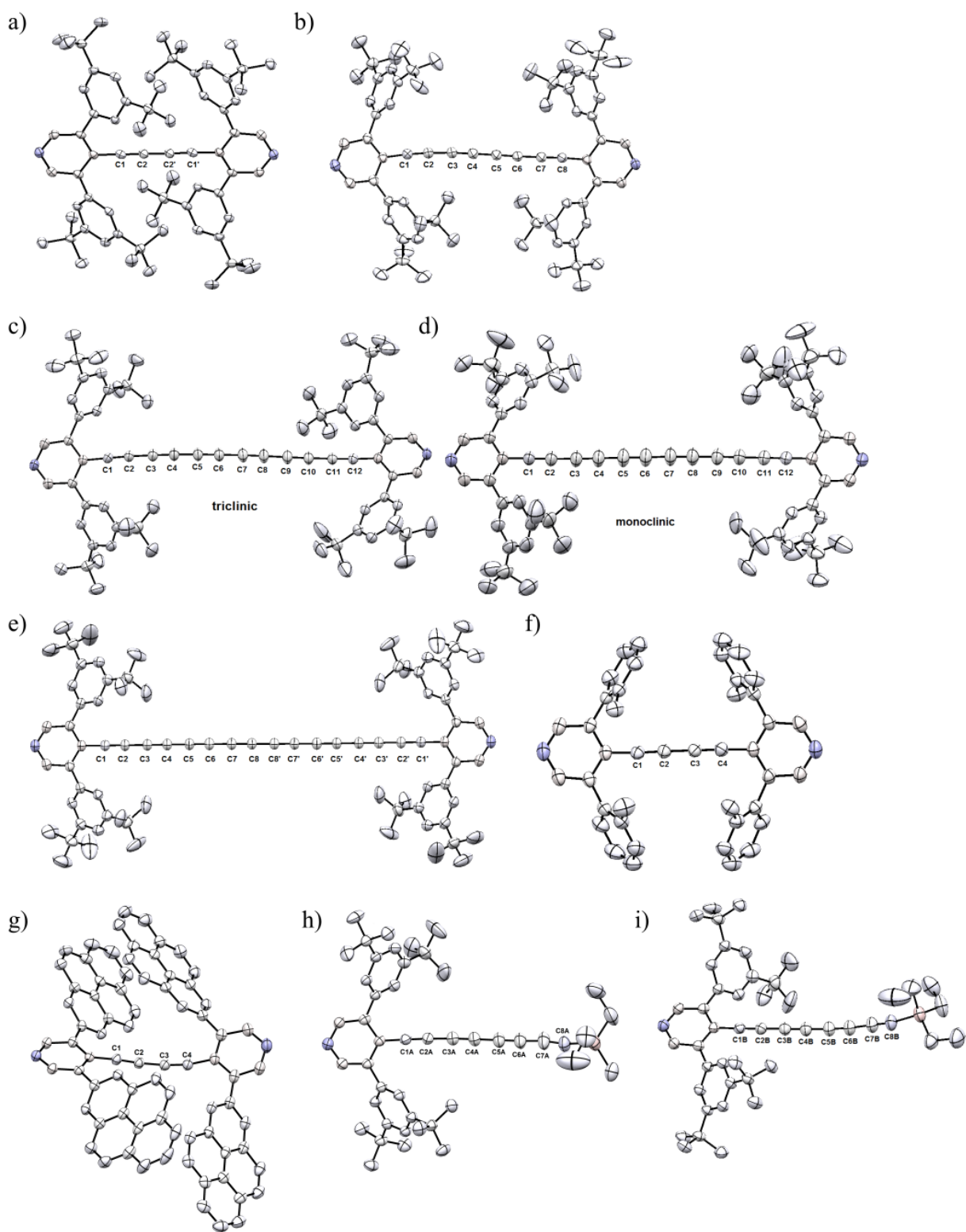
Figure 2.14. ORTEP representations for a) **Py**[2a]**, b) **Py**[4a]**, c) **Py**[6a]^t**, d) **Py**[6a]^m**, e) **Py**[8a]**, f) **Py**[2c]**, g) **Py**[2e]**, h) **Py**[4a]SiA**, and i) **Py**[4a]SiB** (ellipsoids shown at 50% probability).

Two primary types of noncovalent interactions involving the pyrene groups can be observed in the solid-state for **Py**[2e]**. These are the intramolecular face-to-face and edge-to-face interactions, and these two interactions are also involved in intermolecular packing (Figure 2.15). The shortest intramolecular and intermolecular carbon-to-carbon distance in the face-to-face mode between two pyrene groups is 3.445(4) Å and 3.426(3) Å, respectively (Figure 2.16a and b). Furthermore, the distance between the carbon atoms from one pyrene group to the plane of the other pyrene group (the plane is generated using all 16 atoms from the pyrene group) is in the range of 3.197–4.201 Å (intramolecular) and 3.384–3.621 Å (intermolecular). The intramolecular and intermolecular edge-to-face interactions can be easily visualized with the interactions of CH group from one pyrene group to the other pyrene group. In particular, the intramolecular CH/π_{pyrene} interactions are found at the 4- and 5-position of one pyrene group to the other pyrene plane (generated using all 16 atoms) with a distance of 2.698 Å and 2.839 Å, respectively (Figure 2.16c). On the other hand, the intermolecular CH/π_{pyrene} short contacts are found in the range of 2.754–2.925 Å (Figure 2.16d). Interestingly, the oligoyne framework of **Py**[2e]** appears bent to accommodate these secondary interactions (*vide supra*).
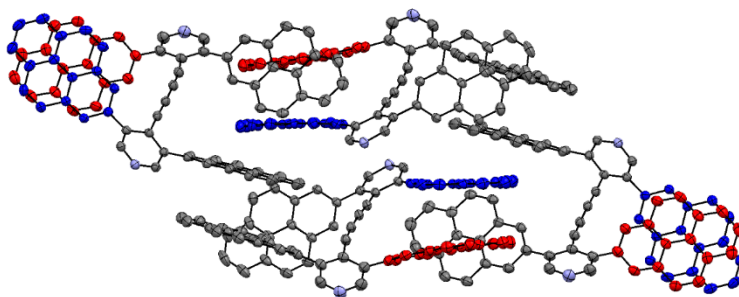
Figure 2.15. Crystal packing diagram of compound **Py**[2e]** highlighting face-to-face and edge-to-face interactions.
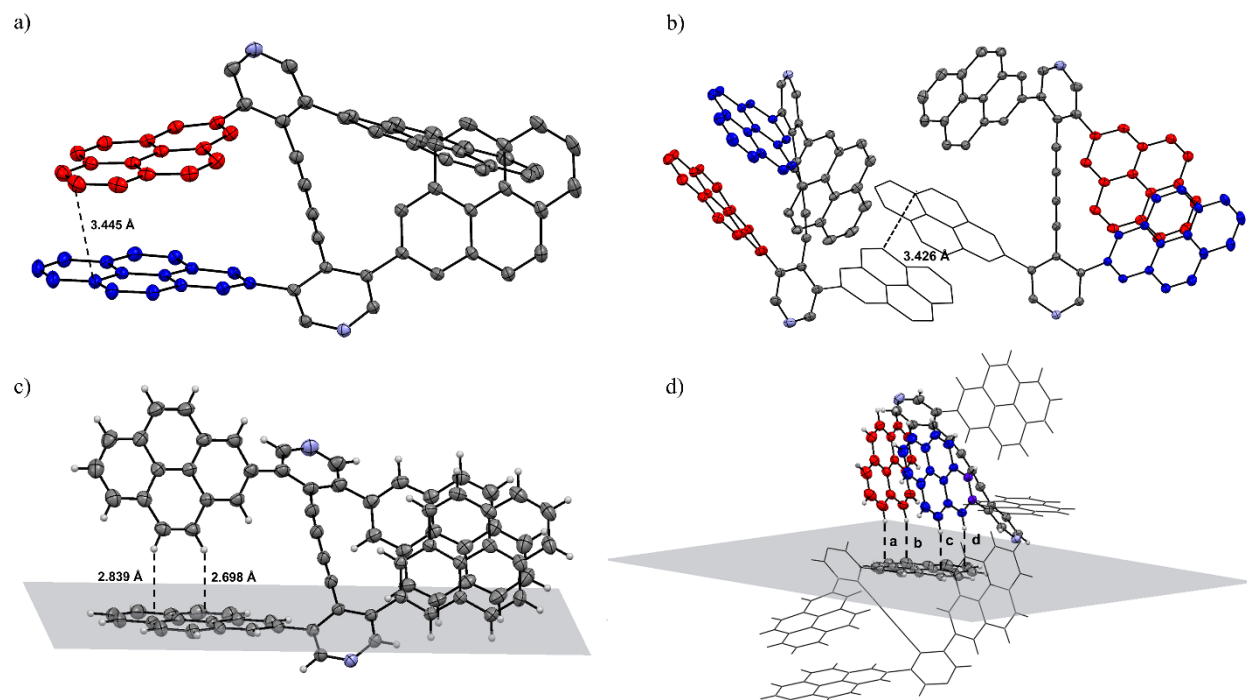
Figure 2.16. a) Intramolecular and b) intermolecular face-to-face interactions of **Py**[2e]**, with the shortest carbon-to-carbon distance of 3.445 (4) Å and 3.426 (3) Å. c) Intramolecular edge-to-face interactions expressed by CH/π_{pyrene} (the plane of pyrene is generated with all 16 carbon atoms) short contacts with the distance of 2.698 Å and 2.839 Å, and d) intermolecular CH/π_{pyrene} short contacts with the distances of a: 2.925 Å; b: 2.795 Å; c: 2.754 Å; d: 2.830 Å.

CH/π interactions involving sp^2-hybridized systems are common and have received much attention.[49] On the other hand, CH/π_{sp} interactions are rarely discussed for oligoynes and only a few examples are reported. In particular, a number of CH/π_{sp} interactions are described in the solid-state for oligoyne rotaxanes between the CH moiety of the macrocycle and the C_{sp} moiety of the oligoyne thread in the encapsulated rotaxane.[37a] The *tert*-butyl moiety from the endgroup and the π–system of *sp*-carbon chains interacts in the solid-state via CH/C_{sp} short contacts in the **Py**[na]** series. A search of the Cambridge Structural Database (CSD) revealed that *tert*-butyl group and *sp*-carbon chains (longer than a tetrayne; 12 hits) typically interact with $CH\cdots C_{sp}$ distances in the range of 2.642–2.885 Å. In **Py**[4a]**, CH/C_{sp} interactions for C4, C5, and C7 have $CH\cdots C_{sp}$ distances of 2.787, 2.799, and 2.770 Å, respectively (Figure 2.17a). No CH/C_{sp} interaction is found in **Py**[6a]ᵐ**, and only one type of CH/C_{sp} interaction is found in **Py**[6a]ᵗ** for the innermost *sp*-carbon C7, with a distance of 2.882 Å (Figure 2.17b). The CH/C_{sp} interactions in **Py**[8a]** are found for C2 (C2'), C3 (C3'), C6 (C6'), and C7 (C7'), and the $CH\cdots C_{sp}$ distances are in the range of 2.699–2.883 Å (Figure 2.17c).
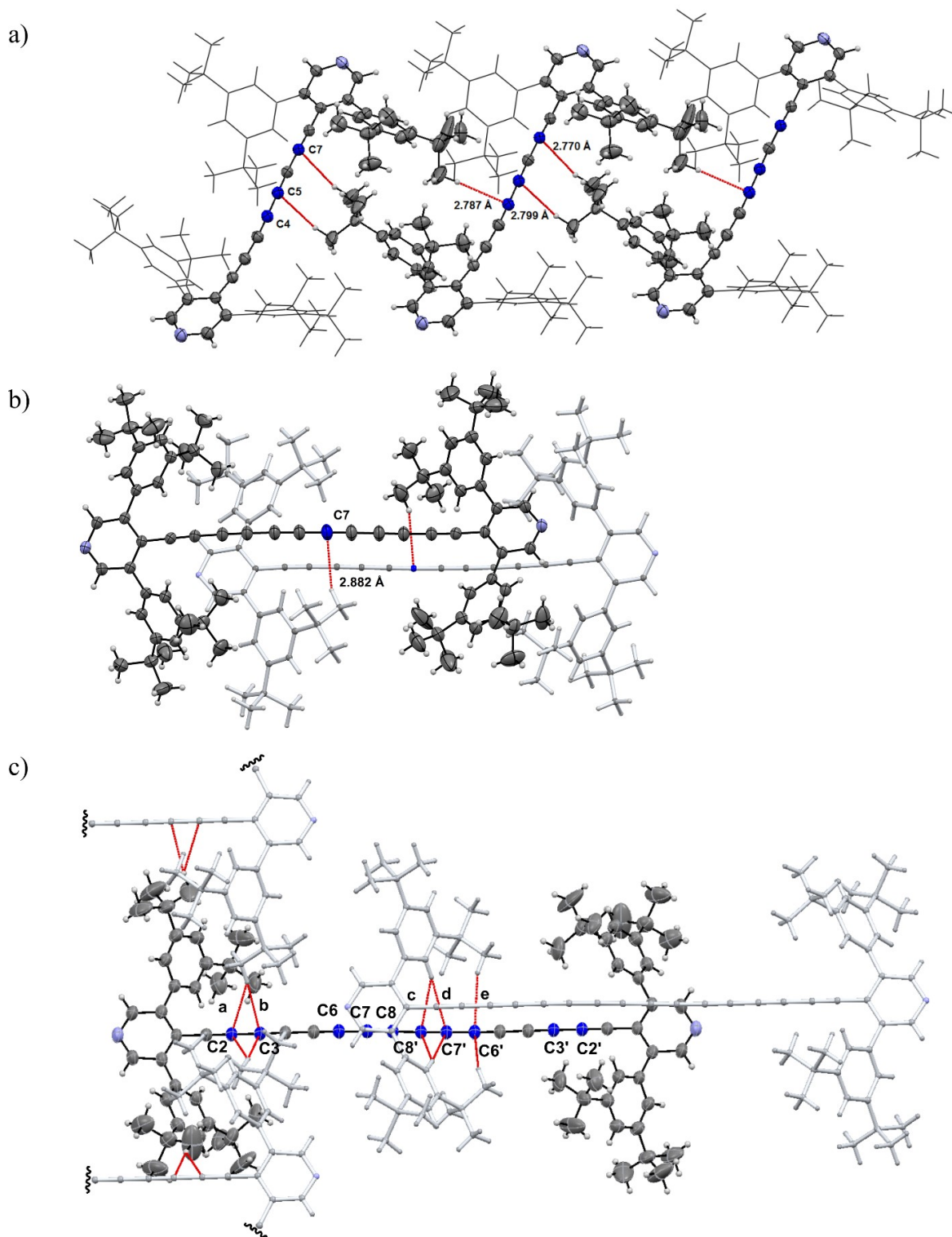
Figure 2.17. X-ray crystal structures with CH/C_{sp} short contacts. a) **Py******[4a]**; d(CH/C_{sp}): CH/C4: 2.787 Å; CH/C5: 2.799 Å; CH/C7: 2.770 Å. b) **Py******[6a]**[t]; d(CH/C_{sp}): CH/C7: 2.882 Å. c) **Py******[8a]**; d(CH/C_{sp}): a: 2.783 Å; b: 2.699 Å; c: 2.807 Å; d: 2.881 Å; e: 2.883 Å.

The solid-state packing for **Py******[na]** is shown in Figure 2.18–2.21. An obvious trend is

that the distance of *sp*-carbon chains between neighboring oligoynes decreases as a function of molecular length. For example, the closest inter-*sp*-chain distance is 7.287(3) Å for **Py**[2a]**, 6.574(3) Å for **Py**[4a]**, 3.782(4) Å for **Py**[6a]ᵐ**, 3.677(3) Å for **Py**[6a]ᵗ**, and 3.457 Å for **Py**[8a]** (distances are atom to atom). For **Py**[6a]ᵐ** and **Py**[6a]ᵗ**, neighboring molecules pack to form centrosymmetric, dimeric pairs, with inter 1,4- and 1,6-C_{sp} distances 3.782(4) Å and 3.677(3) Å, respectively (Figure 2.20). These intermolecular distances are in the range required for topochemical polymerization of oligoynes (ca. 4 Å). It is, however, not possible for topochemical polymerization to take place, because the distance between the dimeric pairs is 7–8 Å, which is too far away for polymerization. Furthermore, the distance of inter C1–C8' for **Py**[8a]** is only 3.457 Å (Figure 2.21a), which is seemingly conducive for topochemical polymerization. The translational period *d'*, however, is about 11 Å, and the angle γ between the oligoyne rod and the translational vector is about 25° (Figure 2.21b); these are too far away from that required for topochemical polymerization of the oligoynes (ca. *d'* = 4.7 to 5.2 Å, γ = ca. 45°).[50] These facts make topochemical polymerization unlikely and help illustrate the steric protection offered by the endgroups.
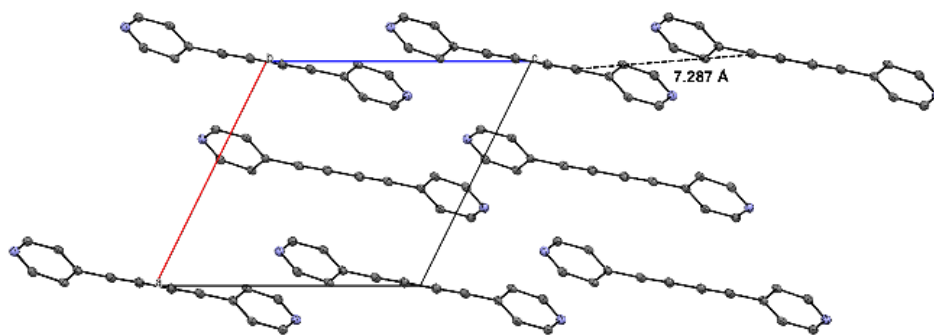
Figure 2.18. Crystal packing diagram of **Py**[2a]** as viewed along the crystallographic b-axis (hydrogen atoms and 3,5-bis(3,5-di-*t*ert-butylphenyl) groups omitted for clarity). The closest inter-*sp*-chain distance is 7.287(3) Å (distances are atom to atom).
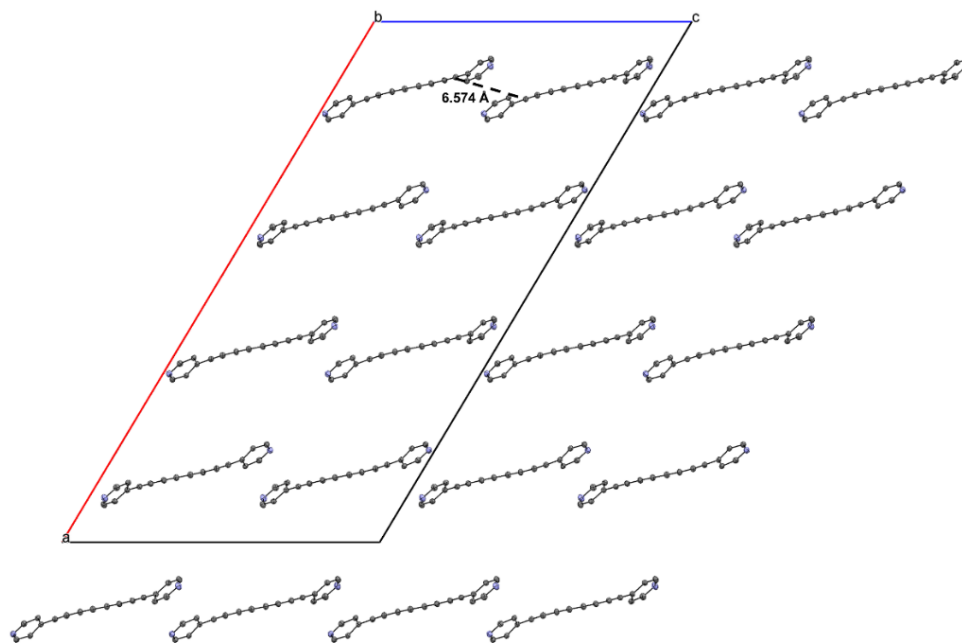
Figure 2.19. Crystal packing diagram of **Py**[4a]** as viewed along the crystallographic b-axis (hydrogen atoms and 3,5-bis(3,5-di-*t*ert-butylphenyl) groups omitted for clarity). The closest inter-*sp*-chain distance is 6.574(3) Å (distances are atom to atom).

a)

b)
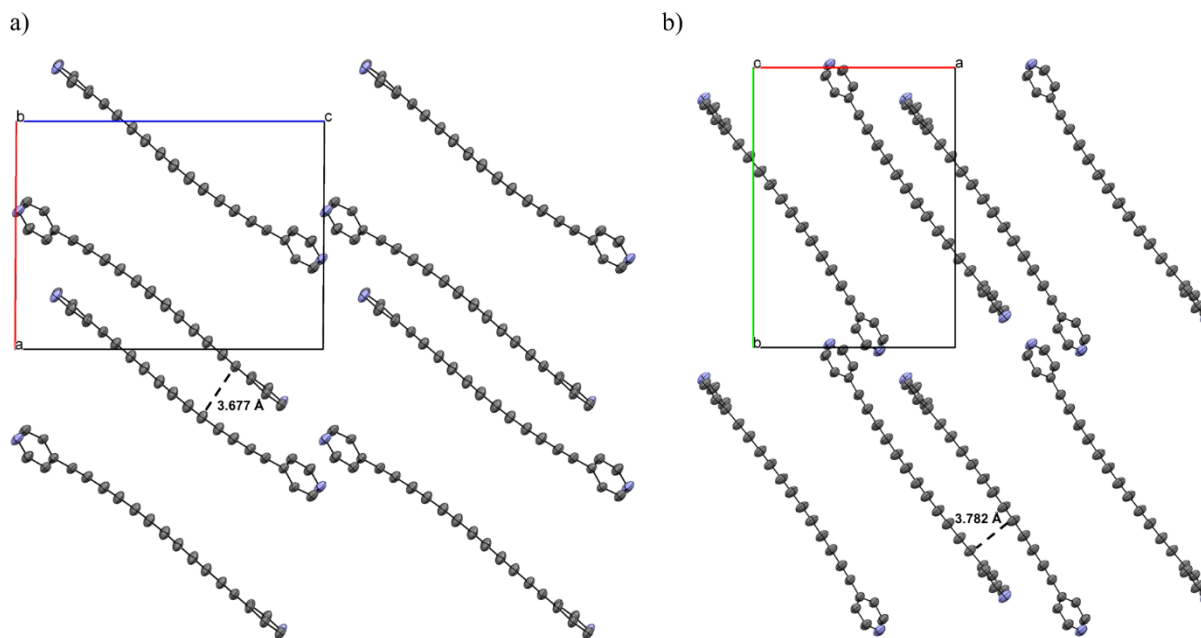
Figure 2.20. a) Crystal packing diagram of **Py**[6a]ᵗ** and b) of **Py**[6a]ᵐ** as viewed along the crystallographic b- and c-axis, respectively (hydrogen atoms and 3,5-bis(3,5-di-*t*ert-butylphenyl) groups omitted for clarity). The closest inter-*sp*-chain distance is 3.677(4) Å and 3.782(3) Å, respectively (distances are atom to atom).
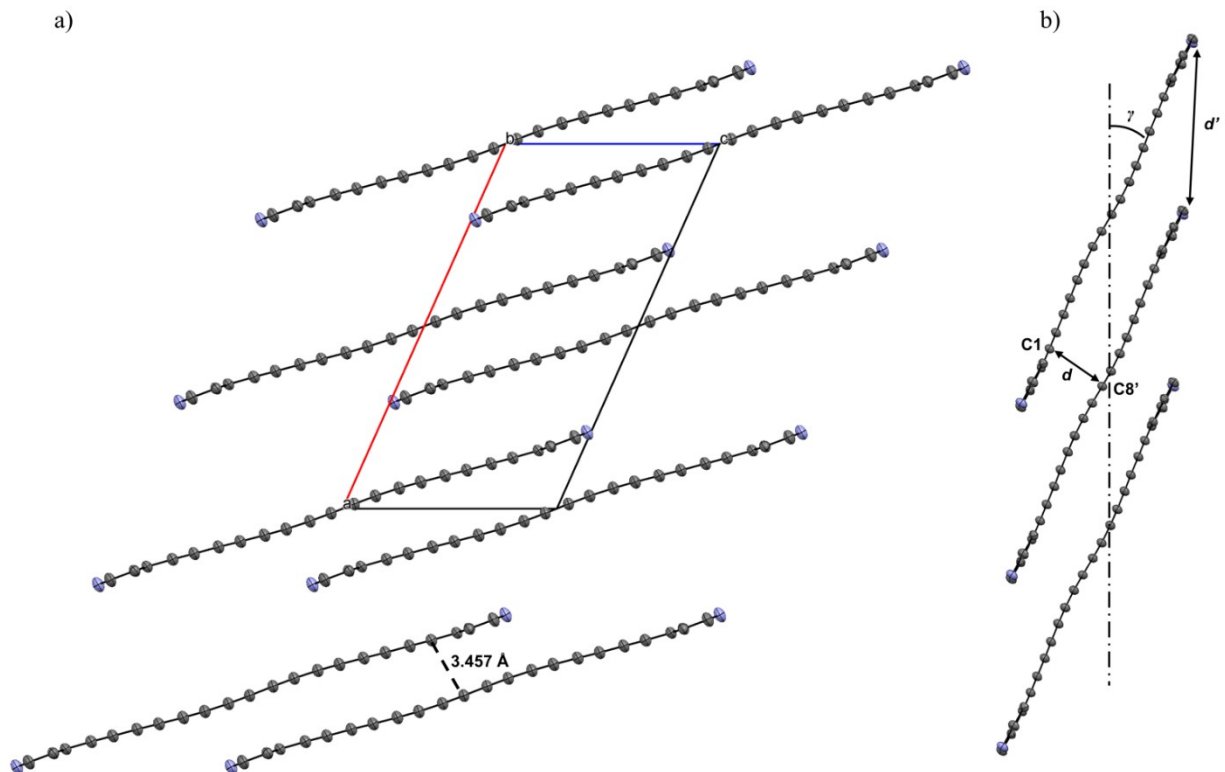
Figure 2.21. a) Crystal packing diagram of **Py**[8a]** as viewed along the crystallographic b-axis (hydrogen atoms and 3,5-bis(3,5-di-*t*ert-butylphenyl) groups omitted for clarity). The closest inter-*sp*-chain distance is 3.457 Å (distances are atom to atom). b) Schematic representation of parameters for topochemical polymerization for **Py**[8a]**. The translational period *d'*, atom-to-atom distance is about 11 Å and the angle γ between the oligoyne rod and the translational vector is about 25°.

2.8.2 BLA analysis

Bond length alternation for **Py**[na]** (summarized in Table 2.8) has been examined on the basis of the definition proposed by Brédas and co-workers,[51] as the difference between the average lengths of the carbon–carbon single and triple bonds (defined here as BLA_{avg}). Plots of experimental BLA_{avg} data versus $1/n$ suggest a value of 0.134 Å for **Py**[na]** at the asymptotic limit (i.e., at infinite length, Figure 2.22a), nearly identical to that predicted on the basis of experimental data for **tBu[n]** (0.136 Å)[17a] and calculated values for **H[n]** (0.130 Å).[52]

By adapting equation (2), BLA_{avg} values as a function of length is expressed by equation (4):

$$\delta_{(n)} = \delta_\infty - (\delta_\infty - \delta_1)e^{-k(n-1)} \qquad \text{equation (4)}$$

which predicates slightly higher BLA_{avg} values at the convergence length of 0.140 Å (**Py**[na]**), 0.146 Å (**tBu[n]**), and 0.136 Å (**H[n]**), as shown in Figure 2.22b. Thus, irrespective of the fitting

protocol, BLA$_{avg}$ values are clearly approaching saturation by approximately the length of ca. $n = 10$ to 12, as has been previously predicted by theory.[53] The experimental BLA$_{avg}$ values for **Py**[na]** and ***t*Bu[n]** corroborate that the influence of the endgroups, i.e., conjugated pyridyl or non-conjugated *tert*-butyl groups, appears minimal and disappears as a function of length (although analysis of longer oligoynes would be needed to confirm this premise). The experimental values are also consistent with the limiting values predicted for H–(C≡C)$_\infty$–H (BLA$_{avg}$ = 0.136 Å),[52] which represent oligoynes with $D_{\infty h}$ symmetry.

Table 2.8. Summary of BLA (Å) data for oligoynes **Py**[na]**.

oligoyne	C—C (avg)	C≡C (avg)	BLA$_{avg}$
Py**[2a]	1.370	1.204	0.166
Py**[4a]	1.358	1.208	0.150
Py**[6a][t]	1.355	1.206	0.149
Py**[6a][m]	1.349	1.208	0.141
Py**[6a]$_{avg}$[a]	1.352	1.207	0.145
Py**[8a]	1.352	1.211	0.141

[a]Average value from the two polymorphs.
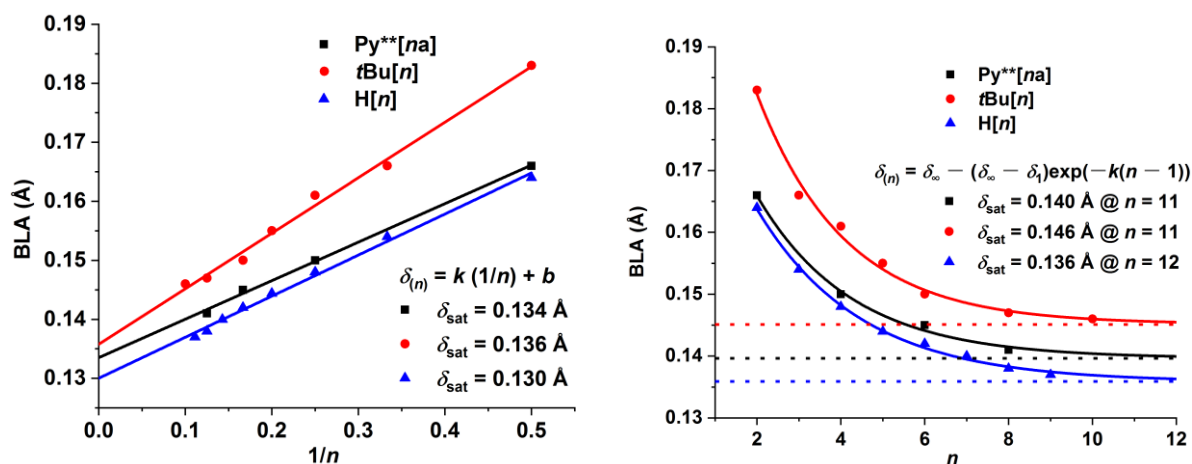
Figure 2.22. a) Plots of BLA$_{avg}$ versus $1/n$ for **Py**[na]**, ***t*Bu[n]**, and **H[n]**, where n is the number of triple bonds. The linear fitting uses the equation of $\delta_{(n)} = k(1/n) + b$, where $k = 0.065 \pm 0.002$, $b = 0.134 \pm 0.001$ for **Py**[na]**; $k = 0.094 \pm 0.004$, $b = 0.136 \pm 0.001$ for ***t*Bu[n]**; $k = 0.071 \pm 0.002$, $b = 0.130 \pm 0.001$ for **H[n]**. b) Convergence of experimental BLA$_{avg}$ values for **Py**[na]** and ***t*Bu[n]**, and calculated values for **H[n]** according to equation (4), where $\delta_\infty = 0.140 \pm 0.002$, $k = 0.443 \pm 0.094$, $\delta_1 = 0.181 \pm 0.004$ for **Py**[na]**; $\delta_\infty = 0.145 \pm 0.002$, $k = 0.478 \pm 0.060$, $\delta_1 = 0.205 \pm 0.005$ for ***t*Bu[n]**; $\delta_\infty = 0.136 \pm 0.001$, $k = 0.407 \pm 0.027$, $\delta_1 = 0.178 \pm 0.001$ for **H[n]**; δ_{sat} is defined by fulfilment of the relationship $\delta_{(n)} - \delta_\infty \leq 0.0005$ Å.

2.9 Raman analysis

The occurrence of strong Raman bands associated to the BLA oscillation is a common feature in oligoynes, and the energy/wavenumber of the Raman line moves consistently to lower values as BLA decreases.[54] In collaboration with the group of Prof. Juan Casado (University of Malaga), Raman spectra of **Py**[2a–16a]** in the solid-state have been recorded and show that the collective symmetric stretching CC vibration [$v_{C\equiv C}$] dominates the spectrum of all compounds (Figure 2.23a). Vibrational energies (wavenumbers) as a function of length display a downshift of 282 cm^{-1} from **Py**[2a]** ($v_{C\equiv C}$ = 2204 cm^{-1}) to **Py**[16a]** ($v_{C\equiv C}$ = 1922 cm^{-1}). An analysis of the saturation behavior can be done by adapting equation (2) to the form:

$$v_{(n)} = v_\infty - (v_\infty - v_1)e^{-k(n-1)} \qquad \text{equation (5)}$$

and predicts a convergence limit of the Raman shifts at ca. $n = 37$ (Figure 2.23b). This prediction is in very good agreement with the convergence limit of $n = 34$, calculated for the band gap saturation from $v_{sat(weak)}$. In addition, the wavenumber at saturation ($n = 37$) from equation (5) is 1886 cm^{-1}, which is in excellent accord with the Raman band measured for carbyne encapsulated in carbon nanotubes that is reported in the range 1850–1880 cm^{-1}.[55]

a)   b)
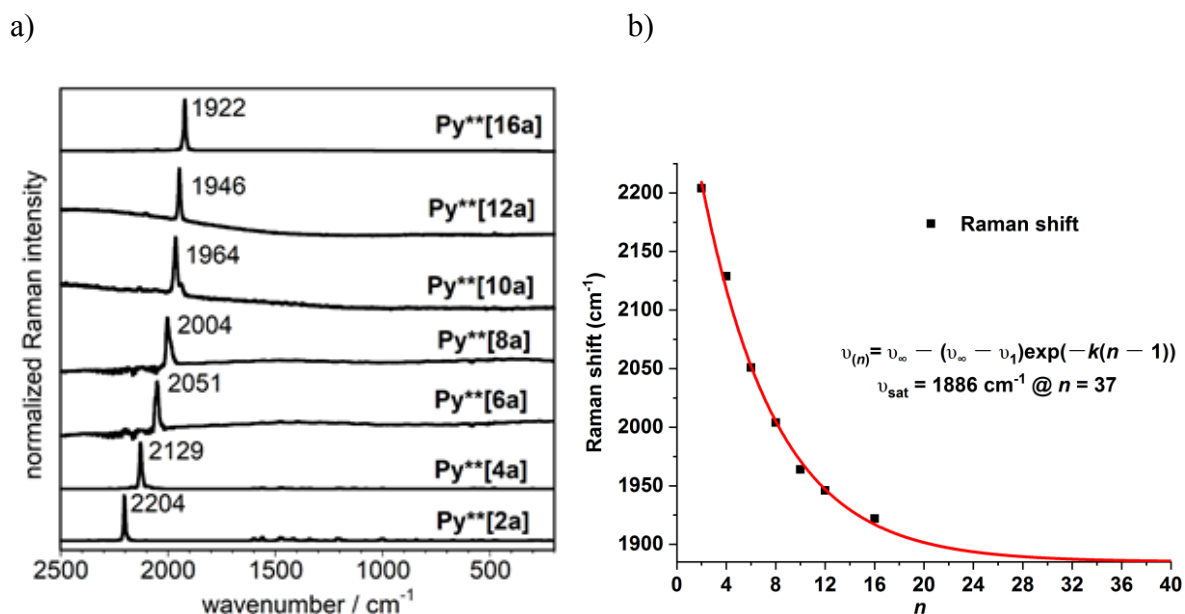
Figure 2.23. a) Solid-state FT-Raman spectra of **Py**[na]** at room temperature. b) Convergence of the Raman shifts for **Py**[na]** according to equation (5), where v_∞ = 1885 ± 14, v_1 = 2268 ± 12, k = 0.166 ± 0.017; insufficient quantities of **Py**[24a]** were available for Raman analysis.

The saturation behavior of the Raman shifts *vs* length for the longest compounds reveals a

permanent/constant dimerization effect in the repeating unit (C≡C–C), which is the structural manifestation of the Peierls distortion (i.e., such as the BLA) that is typical when a polyyne regime far from the oligomer behavior is reached.

2.10 Conclusions

The studies described in this chapter outline a successful stabilization strategy for pyridyl-endcapped oligoynes (PEOs) through substitution of the terminal pyridyl rings. Preliminary studies of di- and tetraynes with strategically substituted pyridines suggest that 3,5-bis(3,5-di-*tert*-butylphenyl)pyridyl endgroups are the most efficient, and this endgroup has been incorporated into extended oligoynes that includes the longest, monodisperse, isolable polyyne known to date **Py**[24a]**. The successful synthesis of **Py**[16a]** and **Py**[24a]** demonstrates that functionalized and stable oligoynes of many nanometers in length can be designed and realized and these molecules are suitable for applications in e.g., molecular electronics (the length of **Py**[24a]** is estimated as 6.9 nm, N to N).

Physical and spectroscopic analyses of the series **Py**[*m*a]Si** and **Py**[*n*a]** confirm that endgroups influence the properties of the shorter molecules, i.e., oligoynes. In particular, endgroups in oligoynes reduce pseudo-symmetry that is manifested as a series of low intensity electronic absorptions (λ_{weak}). The λ_{weak} absorptions gradually become forbidden and ultimately "disappear" in the longest member of this series of molecules, polyyne **Py**[24a]**. When extrapolated to infinite length, the physical and spectroscopic data are consistent with the prediction that carbyne is a polyyne-like material with a finite bandgap of ca. λ_{sat} 617 nm (2.01 eV) based on analysis of $\lambda_{max(weak)}$. Even though λ_{weak} transitions are diminished at lengths $n \geq 20$, they should remain partially allowed through minor deviations from an ideal, linear geometry. Convergence of experimental values for ^{13}C NMR, UV-vis and Raman spectroscopies, as well as BLA (via X-ray crystallography) consistently predict the carbyne limit will be reached by ca. $n =$ 34–37 alkyne units (i.e., the complete disappearance of endgroup effects). These combined analyses offer the most complete and reliable predictions for the experimental properties of polyynes and carbyne.

2.11 References

[1]   A. Hirsch, *Nat. Mater.* **2010**, *9*, 868–871.

[2]   K. Kaiser, L. M. Scriven, F. Schulz, P. Gawel, L. Gross, H. L. Anderson, *Science* **2019**, *365*, 1299–1301.

[3]   a) M. D. Kilde, A. H. Murray, C. L. Andersen, F. E. Storm, K. Schmidt, A. Kadziola, K. V. Mikkelsen, F. Hampel, O. Hammerich, R. R. Tykwinski, M. B. Nielsen, *Nat. Commun.* **2019**, *10*, 3714; b) D. Malko, C. Neiss, F. Viñes, A. Görling, *Phys. Rev. Lett.* **2012**, *108*, 086804.

[4]   X. Y. Wang, X. L. Yao, K. Mullen, *Sci. China Chem.* **2019**, *62*, 1099–1144.

[5]   H. Schwertfeger, A. A. Fokin, P. R. Schreiner, *Angew. Chem. Int. Ed.* **2008**, *47*, 1022–1036.

[6]   E. R. Darzi, R. Jasti, *Chem. Soc. Rev.* **2015**, *44*, 6401–6410.

[7]   a) W. A. Chalifoux, R. R. Tykwinski, *C. R. Chimie* **2009**, *12*, 341–358; b) R. R. Tykwinski, *Chem. Rec.* **2015**, *15*, 1060–1074; c) S. Szafert, J. A. Gladysz, *Chem. Rev.* **2006**, *106*, PR1–PR33; d) C. S. Casari, M. Tommasini, R. R. Tykwinski, A. Milani, *Nanoscale* **2016**, *8*, 4414–4435; e) F. Banhart, *ChemTexts* **2020**, *6*, 3–10.

[8]   M. Liu, V. I. Artyukhov, H. Lee, F. Xu, B. I. Yakobson, *ACS Nano* **2013**, *7*, 10075–10082.

[9]   a) Q. Zheng, J. C. Bohling, T. B. Peters, A. C. Frisch, F. Hampel, J. A. Gladysz, *Chem. Eur. J.* **2006**, *12*, 6486–6505; b) N. Weisbach, H. Kuhn, H. Amini, A. Ehnbom, F. Hampel, J. H. Reibenspies, M. B. Hall, J. A. Gladysz, *Organometallics* **2019**, *38*, 3294–3310.

[10]   W. A. Chalifoux, R. R. Tykwinski, *Nat. Chem.* **2010**, *2*, 967–971.

[11]   L. Shi, P. Rohringer, K. Suenaga, Y. Niimi, J. Kotakoski, J. C. Meyer, H. Peterlik, M. Wanko, S. Cahangirov, A. Rubio, Z. J. Lapin, L. Novotny, P. Ayala, T. Pichler, *Nat. Mater.* **2016**, *15*, 634–639.

[12]   B. Pigulski, N. Gulia, S. Szafert, *Eur. J. Org. Chem.* **2019**, 1420–1445.

[13]   a) C. Wang, A. S. Batsanov, M. R. Bryce, S. Martín, R. J. Nichols, S. J. Higgins, V. M. García-Suárez, C. J. Lambert, *J. Am. Chem. Soc.* **2009**, *131*, 15647–15654; b) D. C. Milan, M. Krempe, A. K. Ismael, L. D. Movsisyan, M. Franz, I. Grace, R. J. Brooke, W. Schwarzacher, S. J. Higgins, H. L. Anderson, C. J. Lambert, R. R. Tykwinski, R. J. Nichols, *Nanoscale* **2017**, *9*, 355–361.

[14]   P. Moreno-Garcia, M. Gulcur, D. Z. Manrique, T. Pope, W. J. Hong, V. Kaliginedi, C. C. Huang, A. S. Batsanov, M. R. Bryce, C. Lambert, T. Wandlowski, *J. Am. Chem. Soc.* **2013**, *135*, 12228–12240.

[15]   C. Wang, H. Jia, H. Li, Y. Wang, *Jilin Huagong Xueyuan Xuebao* **2012**, *20*, 33–36.

[16]   M. Krempe, R. Lippert, F. Hampel, I. Ivanovic-Burmazovic, N. Jux, R. R. Tykwinski, *Angew. Chem. Int. Ed.* **2016**, *55*, 14802–14806.

[17]   a) W. A. Chalifoux, R. McDonald, M. J. Ferguson, R. R. Tykwinski, *Angew. Chem. Int. Ed.* **2009**, *48*, 7915–7919; b) T. Gibtner, F. Hampel, J. P. Gisselbrecht, A. Hirsch, *Chem. Eur. J.* **2002**, *8*, 408–432.

[18]   S. M. E. Simpkins, M. D. Weller, L. R. Cox, *Chem. Commun.* **2007**, 4035–4037.

[19]   X. Yi, J. Chen, X. Xu, Y. Ma, *Synth. Commun.* **2017**, *47*, 872–877.

[20]   a) A. C. Spivey, T. Fekner, S. E. Spey, *J. Org. Chem.* **2000**, *65*, 3154–3159; b) O. S. Tee, M.

Paventi, *Can. J. Chem.* **1983**, *61*, 2556–2562.

[21] L. Robke, T. Rodrigues, P. Schröder, D. J. Foley, G. J. L. Bernardes, L. Laraia, H. Waldmann, *Tetrahedron* **2018**, *74*, 4531–4537.

[22] C. Eidamshaus, H.-U. Reissig, *Eur. J. Org. Chem.* **2011**, 6056–6069.

[23] J. Ranta, T. Kumpulainen, H. Lemmetyinen, A. Efimov, *J. Org. Chem.* **2010**, *75*, 5178–5194.

[24] a) D. N. Coventry, A. S. Batsanov, A. E. Goeta, J. A. Howard, T. B. Marder, R. N. Perutz, *Chem. Commun.* **2005**, 2172–2174; b) A. G. Crawford, Z. Liu, I. A. Mkhalid, M. H. Thibault, N. Schwarz, G. Alcaraz, A. Steffen, J. C. Collings, A. S. Batsanov, J. A. Howard, T. B. Marder, *Chem. Eur. J.* **2012**, *18*, 5022–5035.

[25] Y. Hashikawa, M. Murata, A. Wakamiya, Y. Murata, *J. Am. Chem. Soc.* **2017**, *139*, 16350–16358.

[26] H.-J. Knops, L. Born, *Tetrahedron Lett.* **1983**, *24*, 2973–2976.

[27] X. Nie, G. Wang, *J. Org. Chem.* **2006**, *71*, 4734–4741.

[28] M. Turlington, Y. Du, S. G. Ostrum, V. Santosh, K. Wren, T. Lin, M. Sabat, L. Pu, *J. Am. Chem. Soc.* **2011**, *133*, 11780–11794.

[29] S. J. Havens, P. M. Hergenrother, *J. Org. Chem.* **1985**, *50*, 1763–1765.

[30] A. S. Hay, *J. Org. Chem.* **1962**, *27*, 3320–3321.

[31] G. Eglinton, A. R. Galbraith, *Chem. Ind. (London)* **1956**, 737–738.

[32] T. R. Johnson, D. R. M. Walton, *Tetrahedron* **1972**, *28*, 5221–5236.

[33] H. Amini, Z. Baranova, N. Weisbach, S. Gauthier, N. Bhuvanesh, J. H. Reibenspies, J. A. Gladysz, *Chem. Eur. J.* **2019**, *25*, 15896–15914.

[34] P. Bichler, W. A. Chalifoux, S. Eisler, A. L. K. Shi Shun, E. T. Chernick, R. R. Tykwinski, *Org. Lett.* **2009**, *11*, 519–522.

[35] S. Eisler, A. D. Slepkov, E. Elliott, T. Luu, R. McDonald, F. A. Hegmann, R. R. Tykwinski, *J. Am. Chem. Soc.* **2005**, *127*, 2666–2676.

[36] R. R. Tykwinski, W. Chalifoux, S. Eisler, A. Lucotti, M. Tommasini, D. Fazzi, M. Del Zoppo, G. Zerbi, *Pure Appl. Chem.* **2010**, *82*, 891–904.

[37] a) L. D. Movsisyan, M. Franz, F. Hampel, A. L. Thompson, R. R. Tykwinski, H. L. Anderson, *J. Am. Chem. Soc.* **2016**, *138*, 1366–1376; b) M. Franz, J. A. Januszewski, F. Hampel, R. R. Tykwinski, *Eur. J. Org. Chem.* **2019**, 3503–3512.

[38] R. R. Tykwinski, T. Luu, *Synthesis* **2012**, *44*, 1915–1922.

[39] a) J.-L. Bredas, *Mater. Horiz.* **2014**, *1*, 17–19; b) J. Zirzlmeier, S. Schrettl, J. C. Brauer, E. Contal, L. Vannay, É. Brémond, E. Jahnke, D. M. Guldi, C. Corminboeuf, R. R. Tykwinski, H. Frauenrath, *Nat. Commun.* **2020**, *11*, 4797.

[40] a) A. Milani, M. Tommasini, G. Zerbi, *J. Raman Spectrosc.* **2009**, *40*, 1931–1934; b) M. Kertesz, C. H. Choi, S. Yang, *Chem. Rev.* **2005**, *105*, 3448–3481.

[41] L. Shi, P. Rohringer, M. Wanko, A. Rubio, S. Waßerroth, S. Reich, S. Cambré, W. Wenseleers, P. Ayala, T. Pichler, *Phys. Rev. Mater.* **2017**, *1*, 075601.

[42] R. Hoffmann, *Angew. Chem. Int. Ed. Engl.* **1987**, *26*, 846–878.

[43] a) L. D. Movsisyan, M. D. Peeks, G. M. Greetham, M. Towrie, A. L. Thompson, A. W. Parker, H. L. Anderson, *J. Am. Chem. Soc.* **2014**, *136*, 17996–18008; b) D. Fazzi, F. Scotognella, A.

Milani, D. Brida, C. Manzoni, E. Cinquanta, M. Devetta, L. Ravagnan, P. Milani, F. Cataldo, L. Lüer, R. Wannemacher, J. Cabanillas-Gonzalez, M. Negro, S. Stagira, C. Vozzi, *Phys. Chem. Chem. Phys.* **2013**, *15*, 9384–9391; c) Y. Nagano, T. Ikoma, K. Akiyama, S. Tero-Kubota, *J. Am. Chem. Soc.* **2003**, *125*, 14103–14112.

[44] R. Dembinski, T. Bartik, B. Bartik, M. Jaeger, J. A. Gladysz, *J. Am. Chem. Soc.* **2000**, *122*, 810–822.

[45] W. A. Chalifoux, M. J. Ferguson, R. McDonald, F. Melin, L. Echegoyen, R. R. Tykwinski, *J. Phys. Org. Chem.* **2012**, *25*, 69–76.

[46] H. Meier, U. Stalmach, H. Kolshorn, *Acta Polym.* **1997**, *48*, 379–384.

[47] R. E. Martin, F. Diederich, *Angew. Chem. Int. Ed.* **1999**, *38*, 1350–1377.

[48] A. Lucotti, M. Tommasini, D. Fazzi, M. Del Zoppo, W. A. Chalifoux, M. J. Ferguson, G. Zerbi, R. R. Tykwinski, *J. Am. Chem. Soc.* **2009**, *131*, 4239–4244.

[49] M. Nishio, *Phys. Chem. Chem. Phys.* **2011**, *13*, 13873–13900.

[50] K. Fahsi, J. Deschamps, K. Chougrani, L. Viau, B. Boury, A. Vioux, A. van der Lee, S. G. Dutremez, *CrystEngComm* **2013**, *15*, 4261–4279.

[51] R. L. Gieseking, C. Risko, J.-L. Brédas, *J. Phys. Chem. Lett.* **2015**, *6*, 2158–2162.

[52] C. D. Zeinalipour-Yazdi, D. P. Pullman, *J. Phys. Chem. B* **2008**, *112*, 7377–7386.

[53] S. Yang, M. Kertesz, *J. Phys. Chem. A* **2006**, *110*, 9771–9774.

[54] N. R. Agarwal, A. Lucotti, D. Fazzi, M. Tommasini, C. Castiglioni, W. A. Chalifoux, R. R. Tykwinski, *J. Raman Spectrosc.* **2013**, *44*, 1398–1410.

[55] L. Shi, P. Rohringer, K. Suenaga, Y. Niimi, J. Kotakoski, J. C. Meyer, H. Peterlik, M. Wanko, S. Cahangirov, A. Rubio, Z. J. Lapin, L. Novotny, P. Ayala, T. Pichler, *Nat. Mater.* **2016**, *15*, 634–640.

CHAPTER 3 – Mechanistic Study of Alkyne Fragmentation in Oligoynes via ^{13}C Labelling

3.1 Introduction

The oxidative acetylenic coupling reactions of terminal alkynes have proven to be robust methods to form diynes. This methodology has been conveniently employed on numerous occasions towards the synthesis of complex structures, such as natural products,[1] annulenes,[2] and graphdiyne.[3] More recently, these methods have become crucial for the assembly of conjugated materials, including conjugated polymers[4] and oligo-/polyynes.[5]
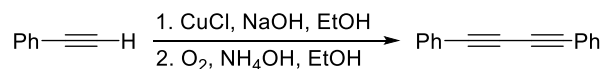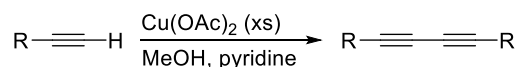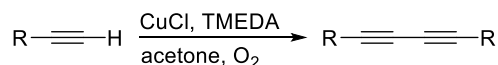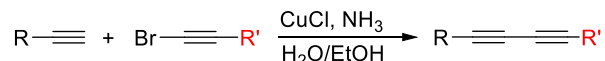
Figure 3.1. Acetylenic coupling reactions.

Oxidative acetylenic coupling had its beginning in 1869, when Carl Glaser reported that copper phenylacetylide underwent oxidative dimerization to give diphenyl-1,3-butadiyne in the presence of air (Figure 3.1a).[6] This original procedure was not broadly utilized predominantly because it required the isolation of the initial copper acetylide as prescribed by Glaser. Whereas, a modification introduced by Eglinton and Galbraith nearly a century later in 1956 was adopted widely as a method of choice (Figure 3.1b).[7] In the 1960s, the Hay coupling was introduced and was a significant improvement to existing methods for the synthesis of oligoynes via oxidative acetylenic homocoupling (Figure 3.1c).[8] These improvements were largely attributed to milder conditions of the reaction and the solubility of the catalyst system in a broader range of solvents,

such as acetone and CH_2Cl_2. Furthermore, in 1955, Cadiot and Chodkiewicz developed a hetereocoupling reaction in order to synthesize unsymmetrical diynes (Figure 3.1d).[9]

These Cu-catalyzed, oxidative acetylenic coupling reactions have been widely applied to the syntheses of oligo-/polyynes via carbon–carbon bond formation. Tykwinski and co-workers[10] as well as others[11] recently have reported that when oligo- and polyynes are formed under Hay conditions, unusual products are sometimes observed, particularly in the synthesis of longer derivatives (Figure 3.2).
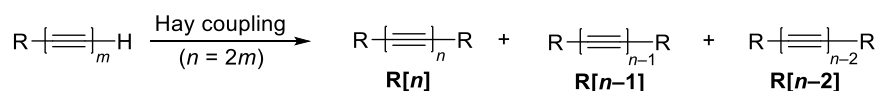
Figure 3.2. Illustration of loss of alkyne units under Hay coupling.

The general scheme is outlined in Figure 3.2. The observed oligoyne byproducts result from the loss of alkyne units from the desired products, presumably under copper catalysis. For example, the attempted synthesis of a decayne also affords the nonayne and sometimes octayne as byproducts. Using Hay conditions (CuCl, TMEDA, solvent, O_2), a range of oligoyne systems have produced this behavior, including *t*Bu[*n*],[10b] **Ad[*n*]**,[10a] **TIPS[*n*]**,[10c] **Ph(OSi)[*n*]**,[11] **Dendrimer[*n*]**,[11] and **Py**[*n*a]** (Figure 3.3).
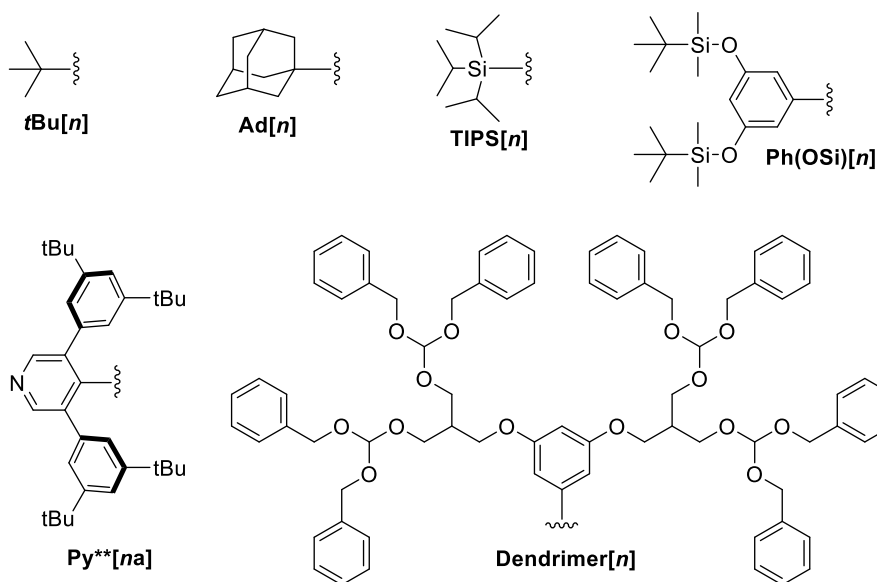
Figure 3.3. The oligo-/polyynes that have been reported showing loss of alkyne units.

In the case of targeting the decayne **TIPS[10]**, the formation of the nonayne byproduct

could be suppressed through conducting the reaction at lower temperature (–10 °C versus rt),[10c] while for **Ad[*n*]**, alkyne loss could be avoided using Eglinton–Galbraith instead of Hay coupling conditions.[10a] As discussed in Chapter 2, while synthesizing the **Py**[*n*a]** series, it was observed that both Hay and Eglinton–Galbraith reactions resulted in alkyne cleavage, which posed serious synthetic challenges.

The activation of C–C bond is usually challenging due to the inertness and lack of selectivity, yet the past decades have seen many advances in particular transition metal-catalyzed oxidative cleavage reactions.[12] Systems containing strained C–C bond in the starting substrates, such as cyclopropane and cyclobutane, have been a common substrate to facilitate the cleavage of C–C bond.[12b, 13] On the other hand, unstrained C–C bond cleavage via Cu-catalyzed aerobic oxidation reactions has become an interesting subject given the cheap source of Cu and molecular oxygen; C(CO)–C bond cleavage is particularly studied.[14] The activation of C(*sp*)–C(*sp*) bond under Cu-catalyzed aerobic conditions has not been explicitly documented, but appears possible when including the C(*sp*)–C(*sp*) bond in the elongated oligoynes, i.e., the loss of alkyne units in oligoynes.[10-11] Given that the C–C bond is one of the most robust in organic chemistry and that the cleavage of the C–C bond using Cu-catalysts is uncommon and synthetically challenging; [10-11] the potential for C–C bond cleavage in oxidative acetylenic coupling reactions intrigues us.

The project described in this chapter is driven primarily by several questions: (1) Is the Hay coupling the only reaction resulting in the loss of alkyne units during the expansion of the oligo-/polyyne framework? (2) Which alkyne units are being removed from the *sp*-carbon chain? (3) What causes the alkyne loss to take place? (4) Are there synthetic methods to prevent the loss of alkynes? To answer these questions, the Hay, Eglinton–Galbraith, and Cadiot–Chodkiewicz coupling reactions have been applied to various oligoyne precursors regarding to the loss of alkyne units. Furthermore, a pentayne has been synthesized with the terminal carbon in the *sp*-carbon chain isotopically labeled with a ^{13}C atom. By subjecting the coupling products of the labeled pentayne to mass spectrometric and ^{13}C NMR spectroscopic analyses, the loss of the terminal alkyne unit during the reaction can be verified. Two plausible mechanisms have been proposed herein as well as methods to prevent this reaction pathway to enable more facile formation of extended polyynes.

3.2 Synthesis of ^{13}C-labeled pentayne Py**[5a]Si$^{\#}$

The loss of the alkyne unit taking place in the terminal position during the Hay homocoupling reaction is a reasonable hypothesis. To probe this hypothesis, a ^{13}C-labeled pentayne (**Py**[5a]Si$^{\#}$**, $^{\#}$denotes ^{13}C labelling atom) with the ^{13}C atom in the terminal position is desired. A Cadiot–Chodkiewicz heterocoupling between the terminal tetrayne (**Py**[4a]H**) and a two-carbon building block containing ^{13}C label (**3.7**) could give the target pentayne (Scheme 3.1a). The synthesis of tetrayne (**Py**[4a]H**) from triethylsilyl-protected tetrayne (**Py**[4a]Si**) has already been described in Chapter 2. Thus, in this project, the ^{13}C-labeled two-carbon building block (**3.7**) becomes the preliminary target. If the loss of alkyne unit did not take place in the terminal position during the Hay homocoupling reaction, then a ^{13}C-labeled pentayne (**Py**[5a]Si$^{2\#}$**) could be synthesized placing the ^{13}C atom in the second alkyne position. This synthesis would require more of the precious building block containing the ^{13}C atom because a ^{13}C-labeled tetrayne (**Py**[4a]Si$^{\#}$**) should be used as a starting material (Scheme 3.1b). By using a heterocoupling reaction, i.e., the Cadiot–Chodkiewicz coupling reaction of **3.7** and **Py**** endcapped oligoynes, a ^{13}C atom could be synthetically placed in any alkyne position.
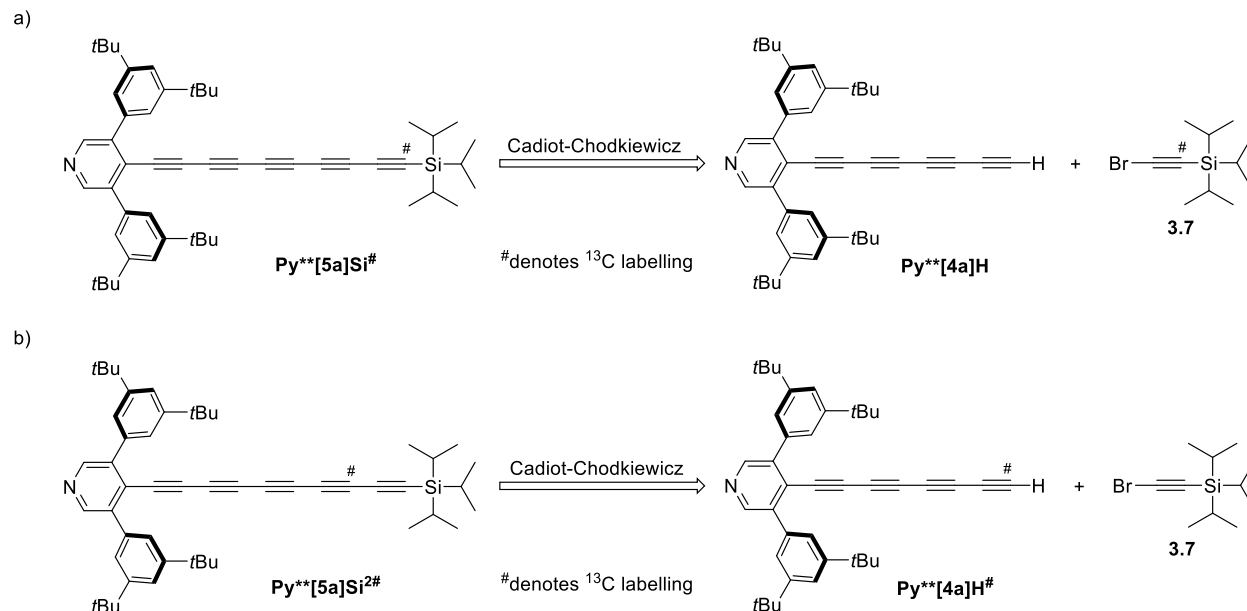
Scheme 3.1. Retrosynthesis of ^{13}C-labeled pentaynes.

3.2.1 Synthesis of ^{13}C-labeled building block

The synthesis of ^{13}C-labeled triisopropylsilylacetylene (**3.6**) was adapted from known methods,[15] and converted to **3.7**, as described for the ^{12}C isotopomer.[16] The reported method was used to

synthesize a 20% ^{13}C-enriched triisopropylsilylacetylene, and the synthesis of 100% ^{13}C-labeled **3.6** is described herein (Scheme 3.2).
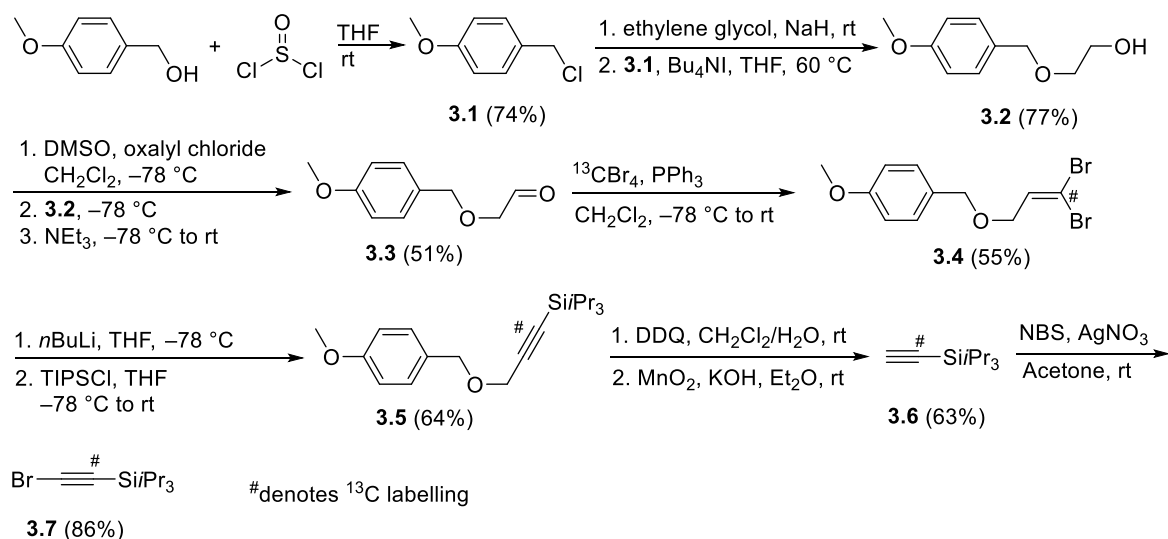
Scheme 3.2. Synthesis of ^{13}C-labeled building block **3.7**.

Chlorination of anisyl alcohol by thionyl chloride afforded anisyl chloride (**3.1**) in a good yield. Then, the deprotonation of ethylene glycol (3 equiv) by sodium hydride gave the respective sodium salt, which reacted with anisyl chloride via a S$_N$2 reaction to afford compound **3.2** in 77% yield. Subsequently, compound **3.2** was oxidized under Swern conditions to give the aldehyde **3.3**. The reaction of ^{13}CBr$_4$ and triphenylphosphine formed an ylide, which was added to the obtained aldehyde affording dibromoolefin **3.4** through a Ramirez reaction. This reaction should be run at a low temperature (–78 °C to rt) for 4–5 h to help suppress the Appel side reaction that was observed to take place in the benzylic ether position. The reagent used in the Ramirez reaction, ^{13}CBr$_4$, can be purchased; however, it is rather expensive (500 mg/$571 CAD from Millipore Sigma). Alternatively, the reagent can be synthesized from the more affordable ^{13}CH$_3$I (5 g/$643 CAD from Millipore Sigma) by using a reported method as shown in Scheme 3.3 (1 g of ^{13}CH$_3$I can make 1–1.2 g of ^{13}CBr$_4$).[17] With **3.4** in hand, the formation of the alkyne **3.5** was through two possible pathways. One such route would be via the elimination of HBr by *n*BuLi to yield a bromoalkyne intermediate, and a subsequent lithium-bromo exchange afforded a lithium acetylide intermediate, which was quenched with TIPS-Cl to give the desired product **3.5**. The other possibility was that the lithium-bromo exchange took place at first to form a carbenoid species, and 1,1-elimination of LiBr concurrent with 1,2-migration gave the terminal alkyne intermediate;

this intermediate was deprotonated by *n*BuLi and quenched subsequently with TIPS-Cl to give the desired product **3.5**. Treating **3.5** with 2,3-dichloro-5,6-dicyanobenzoquinone (DDQ) gave the desired propargylic alcohol, and a byproduct anisyl aldehyde. Finally, the oxidation of the propargylic alcohol by MnO_2/KOH and the subsequent release of carbon dioxide afforded the desired TIPS-acetylene **3.6** containing the ^{13}C labeled atom. Bromination of **3.6** with *N*-bromosuccinimide (NBS) gave the ^{13}C-labeled building block **3.7** (Scheme 3.2).
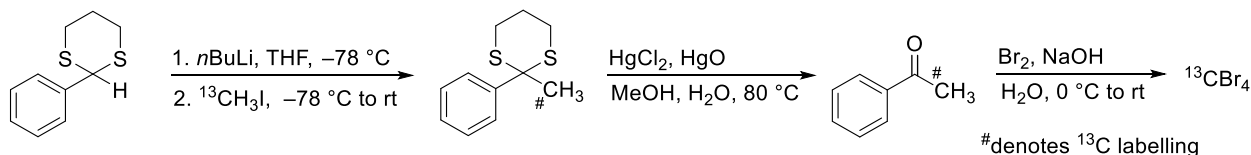
Scheme 3.3. Synthesis of [13]CBr_4.

3.2.2 Synthesis of Py**[5a]Si[#]

The synthesis of **Py**[4a]Si** has already been described in Chapter 2. With **Py**[4a]Si** in hand, the desilylation using CsF in THF/H_2O gave the terminal tetrayne (**Py**[4a]H**). The Pd-assisted Cadiot–Chodkiewicz heterocoupling reaction of **3.7** and **Py**[4a]H** in the presence of Pd(PPh_3)_4, CuI, and diisopropylethylamine (DIPEA) gave the ^{13}C-labeled pentayne **Py**[5a]Si[#]** in 18% yield (Scheme 3.4).
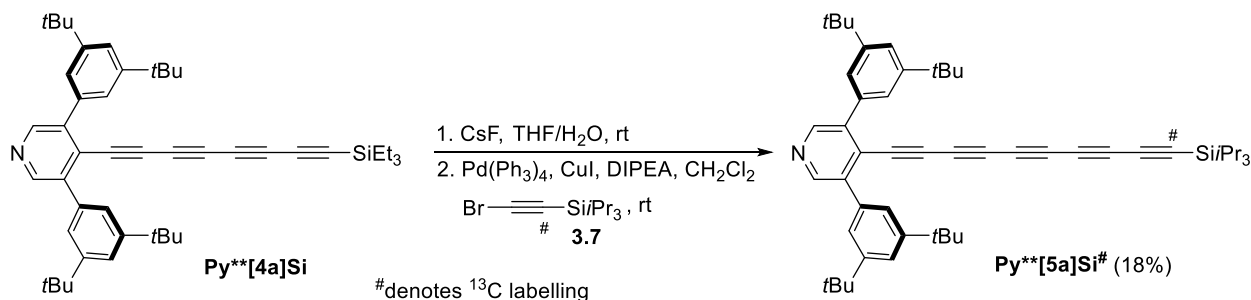
Scheme 3.4. Synthesis of ^{13}C-labeled **Py**[5a]Si[#]** using Pd-assisted Cadiot–Chodkiewicz heterocoupling.

3.3 Observations of loss of alkyne units

3.3.1 Loss of an alkyne unit in the Cadiot–Chodkiewicz heterocoupling

Using a typical Cadiot–Chodkiewicz heterocoupling condition (CuCl, hydroxylamine hydrochloride, and *n*-propylamine), the reaction of **Py**[4a]H** (desilylated product from **Py**[4a]Si**) and the ^{13}C-labeled building block **3.7** gave the expected ^{13}C-labeled pentayne **Py**[5a]Si[#]** in 10% yield and a ^{13}C-labeled tetrayne **Py**[4a]Si[#]** in 2% yield, i.e., 20% of

Py**[4a]Si# relative to **Py**[5a]Si#** (Scheme 3.5). The mixture of **Py**[5a]Si#** and **Py**[4a]Si#** cannot be separated by either silica-gel chromatography or recrystallization method. Thus, mass spectrometric and ^{1}H NMR spectroscopic analyses are used to determine the ratio of the mixture (*vide infra*).
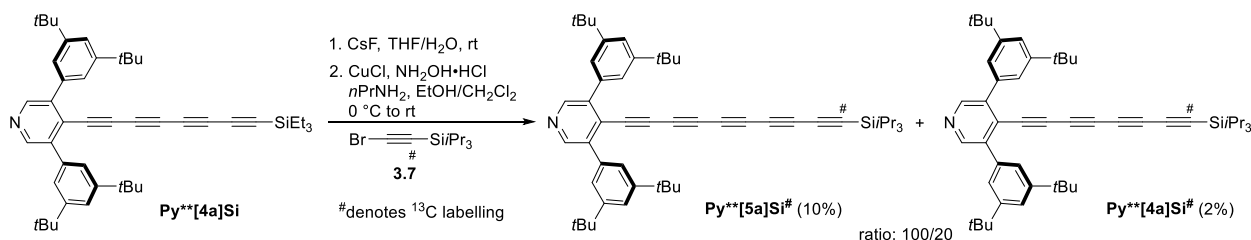
Scheme 3.5. Loss of an alkyne unit in the synthesis of ^{13}C-labeled **Py**[5a]Si#** using Cadiot–Chodkiewicz heterocoupling.

Strong signals at *m/z* 733.4996 and 709.4992 are observed in the matrix-assisted laser desorption/ionization (MALDI) HRMS analysis (Figure 3.4). These signals are assigned for [M+H]$^+$ for **Py**[5a]Si#** and **Py**[4a]Si#**, respectively. The ratio of the abundance at *m/z* 733.4996 and 709.4992 is about 100:20. The analysis of MALDI-HRMS supports that the loss of an alkyne unit has occurred in the Cadiot–Chodkiewicz heterocoupling reaction.

Sum Formula	Sigma	m/z	Err [ppm]	Mean Err [ppm]	Err [mDa]	rdb	N Rule	e⁻
C 49 H 66 N 1 Si 1 ^13C 1	0.042	709.49926	0.05	-1.05	0.03	19.50	-	even
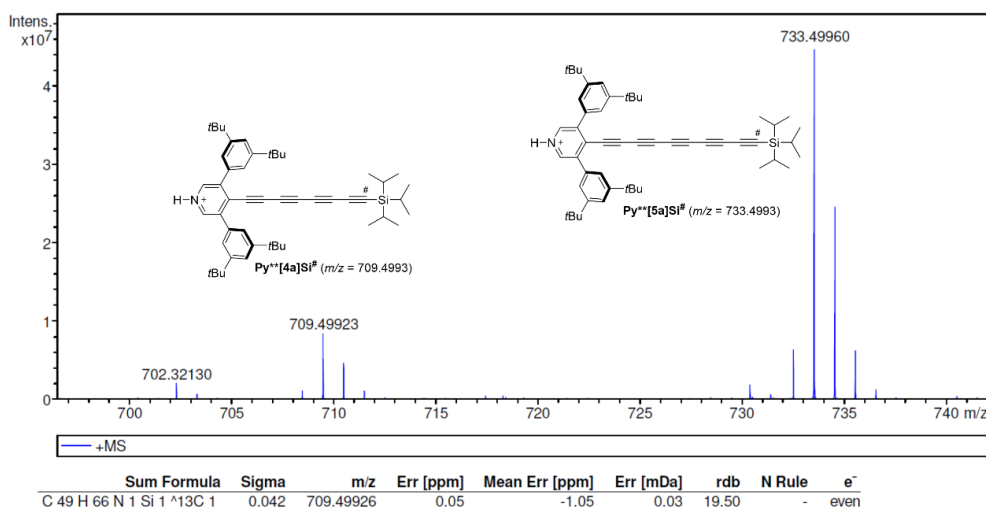
Figure 3.4. MALDI-HRMS analysis showing a mixture of **Py**[5a]Si#** and **Py**[4a]Si#**, supporting the loss of alkyne unit during the Cadiot–Chodkiewicz heterocoupling.

The isolated product from the Cadiot–Chodkiewicz heterocoupling was also analyzed by ^{1}H NMR and ^{13}C NMR spectroscopies in CDCl$_3$. Two sets of signals have appeared in the ^{1}H NMR spectrum, including one set of signals assigned to **Py**[5a]Si#** and an additional set of signals

assigned to **Py**[4a]Si#** (Figure 3.5a). The integral of the protons of **Py**[4a]Si#** is about 20% of that for **Py**[5a]Si#**, which is consistent with the abundance ratio observed in the MALDI-HRMS analysis. The ^{13}C NMR spectrum of the mixture clearly shows the ^{13}C-labeled atom with the resonances of **Py**[5a]Si#** at 87.6 ppm as the most significant signal and **Py**[4a]Si#** at 87.5 ppm as a less significant signal, respectively (Figure 3.5b). These analyses, to the best of my knowledge, show the first observation of loss of an alkyne unit in the Cadiot–Chodkiewicz heterocoupling reaction to date.
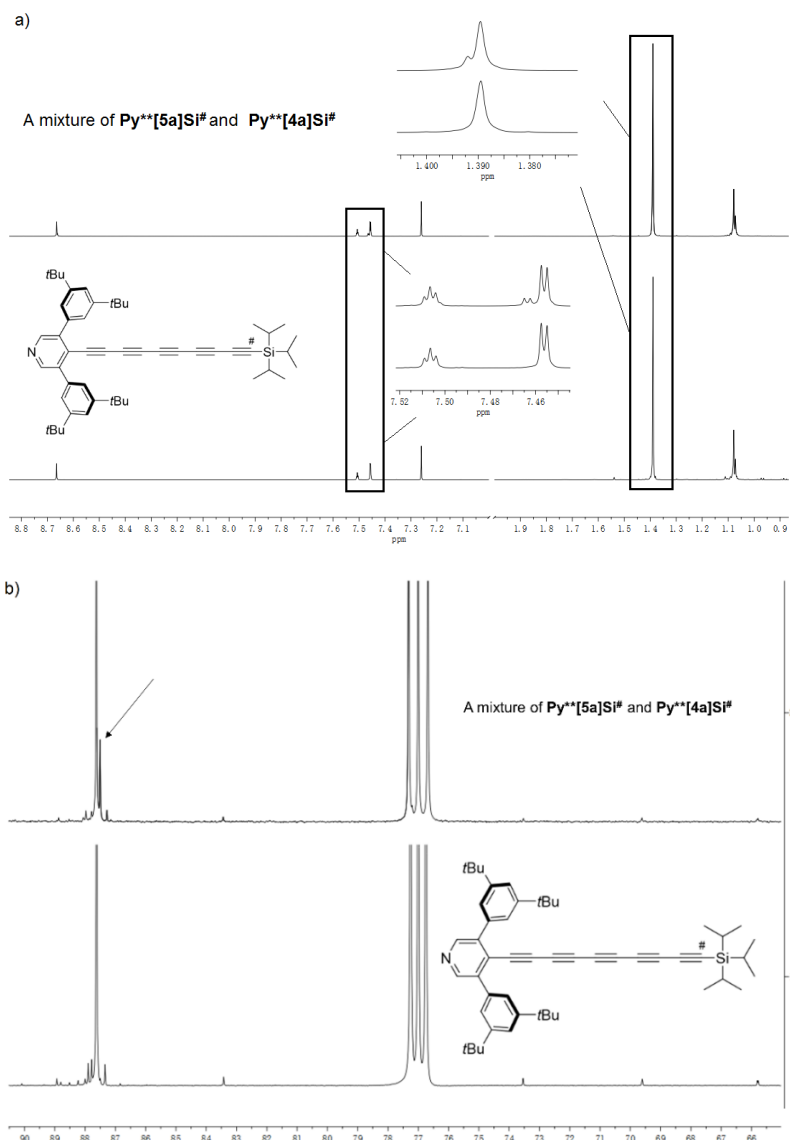
Figure 3.5. a) Comparison of ^{1}H NMR spectra of a mixture of **Py**[5a]Si#** and **Py**[4a]Si#** (top spectrum) as well as the pure **Py**[5a]Si#** (bottom spectrum) as measured in CDCl$_3$. b) Comparison of ^{13}C NMR spectra of a mixture of **Py**[5a]Si#** and **Py**[4a]Si#** (top spectrum) as well as the pure **Py**[5a]Si#** (bottom spectrum) as measured in CDCl$_3$. The arrow indicates the resonance signal of the ^{13}C-labeled atom from **Py**[4a]Si#**.

Comparison of the ^{13}C NMR spectra for the ^{13}C-labeled **Py**[5a]Si$^\#$** and the unlabeled **Py**[5a]Si** provides the evidences for the assignment of each individual carbon for C4–C10 (the *sp*-carbons are labeled as C1–C10 shown in Figure 3.6). At the end of the chain, C10 is the ^{13}C-labeled carbon, C9 is next to C10, and a "ABq" pattern has been resolved for C9 and C10 with the coupling constant of $^1J_{CC}$ = 145.6 Hz. According to the significance of coupling between the ^{13}C-labelling C10 and other carbons in the carbon chain, the coupling constants from large to small reflect the distance between the individual carbons and C10 from small to large. Therefore, the chemical shifts at 87.6 (C10), 89.4 (C9, ABq, $^1J_{CC}$ = 145.6 Hz), 61.09 (C8, d, $^2J_{CC}$ = 15.5 Hz), 64.2 (C7, d, $^3J_{CC}$ = 12.3 Hz), 61.7 (C6, d, $^4J_{CC}$ = 5.5 Hz), 65.8 (C5, d, $^5J_{CC}$ = 3.5 Hz), and 60.98 (C4, d, $^6J_{CC}$ = 2.4 Hz) ppm are assigned. Using the 2D heteronuclear multiple bond correlation NMR spectroscopic analysis, C1 is determined to correspond to the signal at 73.5 ppm and C2 at 83.4 ppm (Chapter 2). Finally, C3 should be the remaining signal at 69.6 ppm (Figure 3.6). Therefore, all the *sp*-carbons C1–C10 are assigned.
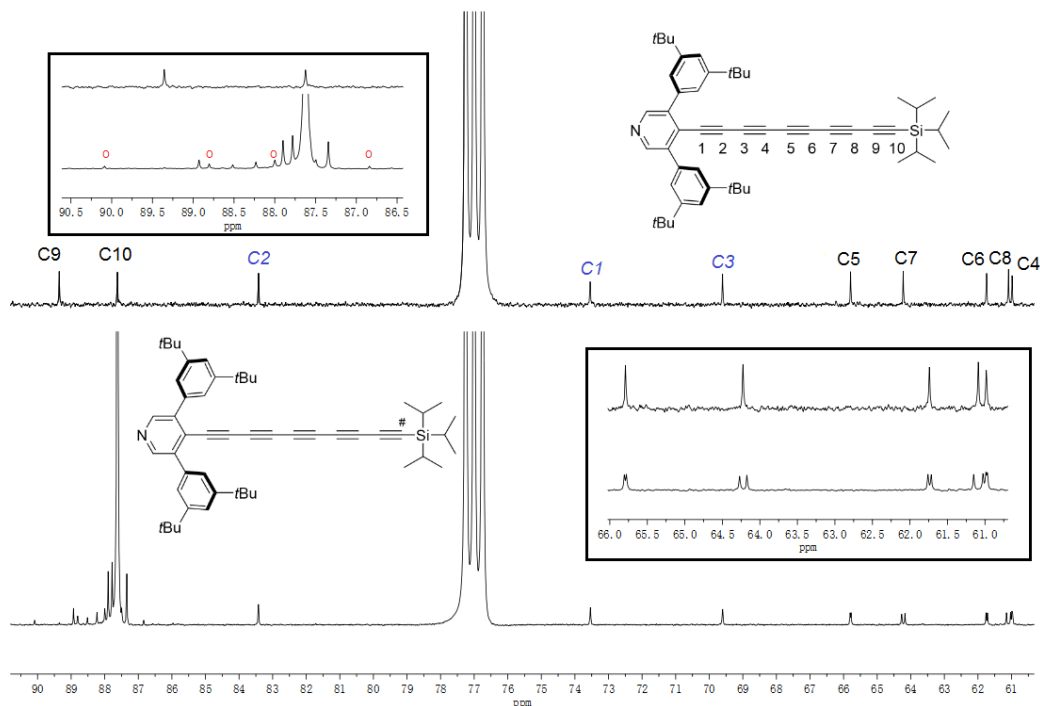
Figure 3.6. Comparison of ^{13}C NMR spectra for unlabeled **Py**[5a]Si** (top spectrum) and ^{13}C-labeled **Py**[5a]Si$^\#$** (bottom spectrum) as measured in CDCl$_3$. The box on the up left is the expansion area from 86.5–90.5 ppm, 'o' denotes parts of ABq pattern of C10 and C9; the box on the bottom right is the expansion area from 61–66 ppm, the doublets of each signal helps the assignment of carbon 4–8.

3.3.2 Loss of an alkyne unit in the Hay coupling

Loss of alkyne units has been observed previously in Hay coupling reactions.[10-11] The process of loss of the alkyne moiety is an interesting, yet poorly understood, example of carbon–carbon bond activation.[12b, 13, 18] Herein, the Hay coupling reaction is reexamined through ^{13}C-labelling experiments. The precursor **Py**[5a]Si#** was labeled by a ^{13}C atom in the terminal position adjacent to the silyl atom, and the synthesis has already been described in Section 3.2.2. With **Py**[5a]Si#** in hand, the deprotection reaction gave the terminal pentayne **Py**[5a]H#** in the presence of CsF in THF/H$_2$O (5:1). Then, **Py**[5a]H#** was subjected to Hay reaction conditions (CuCl, TMEDA, CH$_2$Cl$_2$, O$_2$), which gave a decayne **Py**[10a]##** and a nonayne **Py**[9a]#** in ca. 45 and 2% yield, respectively (Scheme 3.6). Silica-gel chromatography and recrystallization (CH$_2$Cl$_2$/MeOH) proved inefficient for the separation of **Py**[10a]##** and **Py**[9a]#**. Mass spectrometric and ^{13}C NMR spectroscopic analyses are used to determine the ratio of the mixture (*vide infra*).
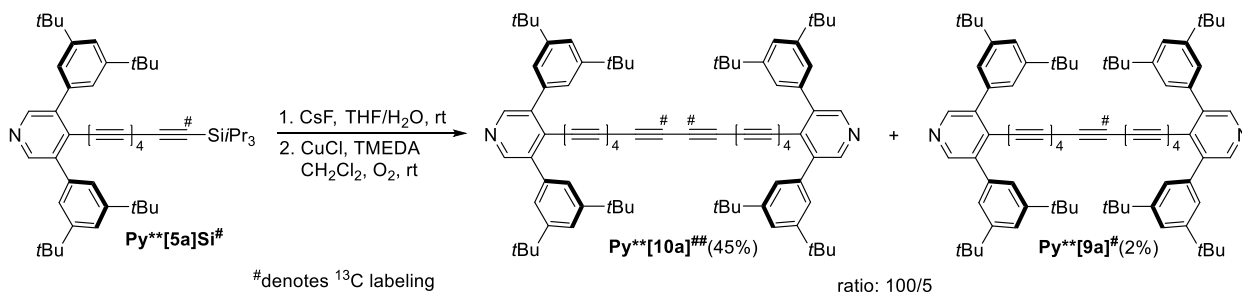
Scheme 3.6. Hay coupling reaction for ^{13}C-labeled **Py**[5a]Si#** results in a mixture of **Py**[9a]#** and **Py**[10a]##**.

Strong signals at *m/z* 576.3579 and 563.8563 are observed in the electrospray ionization (ESI) HRMS analysis (Figure 3.7 and 3.8). These signals are assigned for [M + 2H]$^{2+}$ for **Py**[10a]##** (C$_{84}$^{13}C$_2$H$_{90}$N$_2$) and **Py**[9a]#** (C$_{83}$^{13}CH$_{90}$N$_2$), respectively. This result is critical to support that the nonayne has one ^{13}C-labeled atom in the molecular fragment, which confirms that the loss of an alkyne unit takes place in the terminal position. Furthermore, the ratio of the abundance at *m/z* 576.3579 and 563.8563 is about 100:5.
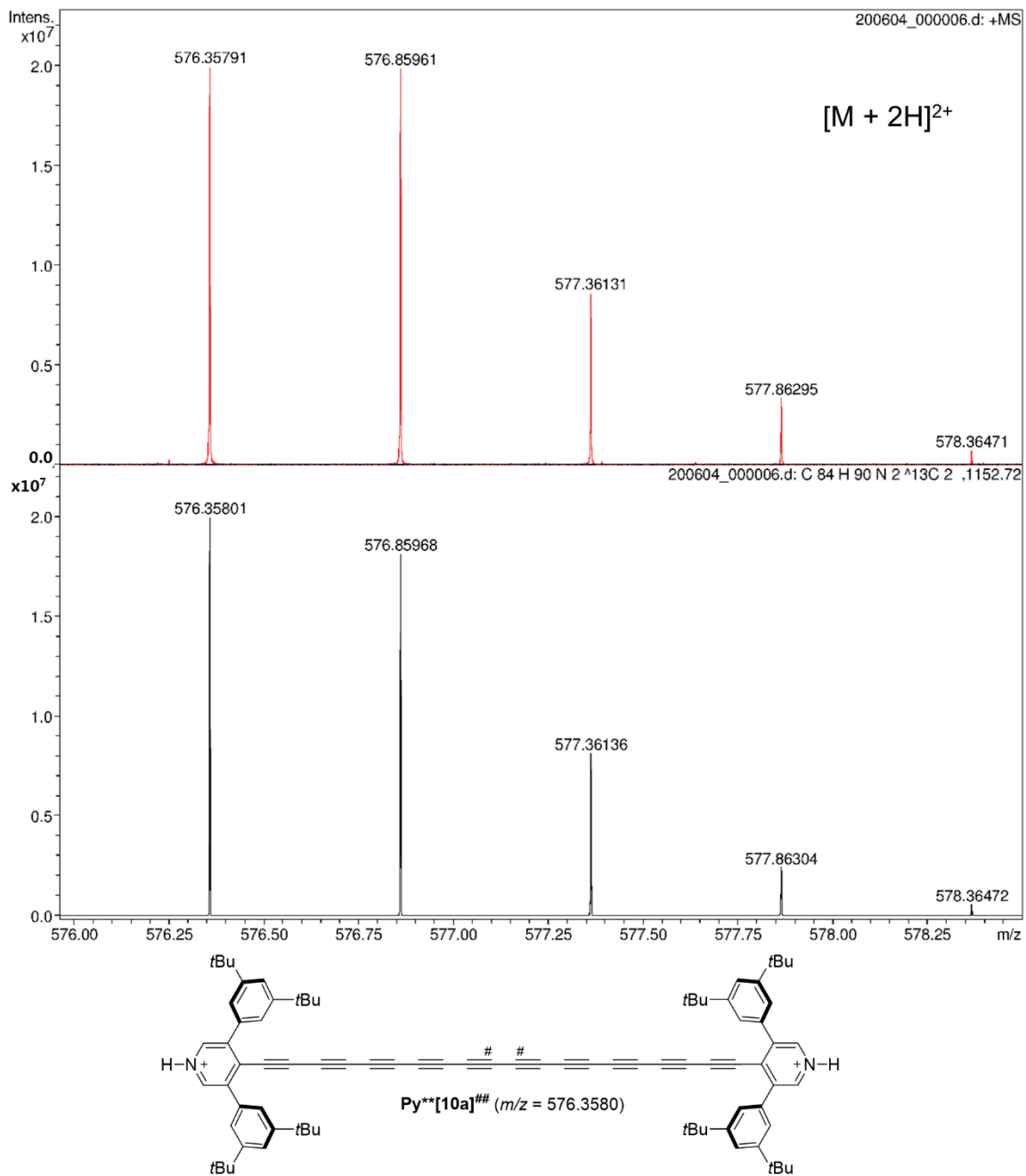
Figure 3.7. Comparison of ESI spectra of the experimental (top) and simulated (bottom) isotope patterns for **Py**[10a]##** as [M + 2H]2+.
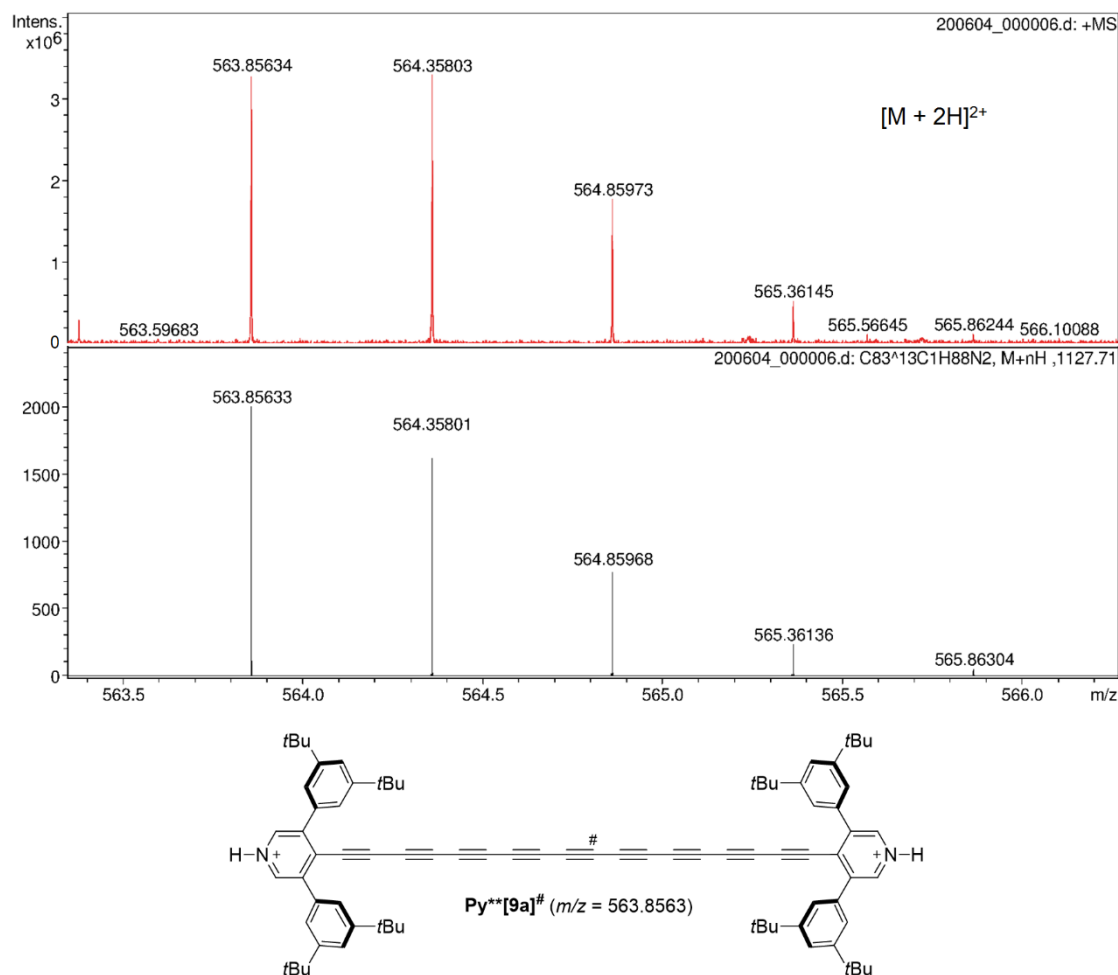
Figure 3.8. Comparison of ESI spectra of the experimental (top) and simulated (bottom) isotope patterns for **Py**[9a]**[#] as $[M + 2H]^{2+}$.

The mixture of **Py**[10a]**[##] and **Py**[9a]**[#] only shows one set of signals in the ^{1}H NMR (700 MHz) spectrum. The ^{13}C NMR spectrum clearly shows the most intense resonance, with a chemical shift at 63.6 ppm assigned as the ^{13}C-labeled atom of **Py**[10a]**[##] (Figure 3.9). A less intense resonance, with a chemical shift at 63.5 ppm, is assigned as the ^{13}C-labeled atom of **Py**[9a]**[#], which is ca. five times bigger than the un-labeled individual *sp*-carbon. Therefore, the mass and ^{13}C NMR spectroscopic analyses unambiguously document the loss of an alkyne unit in the terminal position of the pentayne precursor in the formation of **Py**[10a]**[##] in the Hay homocoupling reaction.

Finally, the chemical shift of the central carbon (^{13}C-labeled atom) at 63.5 ppm is consistent with the convergence of carbon resonances at a value of 63.4 ppm and 63.6 ppm for **Py**[na]** and

Py**[*m*a]Si, respectively, as the previous study described in Chapter 2. These values are nearly identical to the value of 63.7 ppm observed for the **Tr*[*n*]**[19] and ***t*Bu[*n*]**[10b] series that are endcapped by sp^3-carbon moieties.
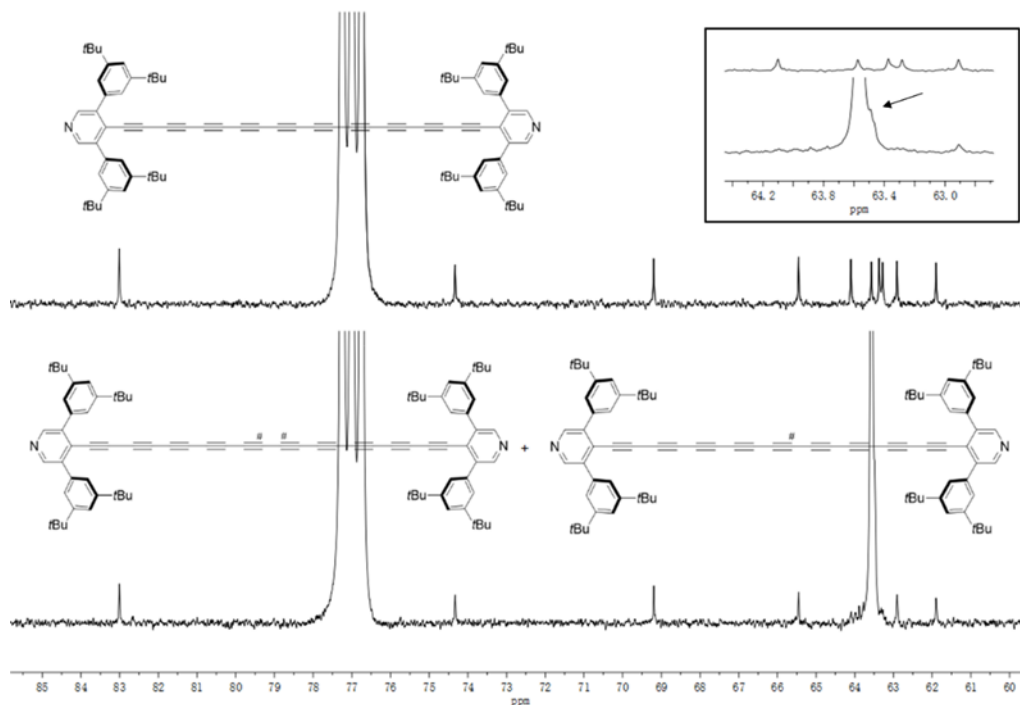
Figure 3.9. Comparison of ^{13}C NMR spectra of unlabeled **Py**[10a]** (top spectrum) and a mixture of ^{13}C-labeled **Py**[10a]**[##] and **Py**[9a]**[#] (bottom spectrum), as measured in CDCl3. In the box, the arrow indicates the resonance of the ^{13}C-labeled atom from **Py**[9a]**[#].

As already described in Chapter 2, the Hay coupling reaction of **Py**[2a]H** and **TIPS[3]H** resulted in a mixture of two products, a pentayne **Py**[5a]Si** and a tetrayne **Py**[4a]Si** in ca. 43 and 8% yield, respectively (Scheme 3.7).
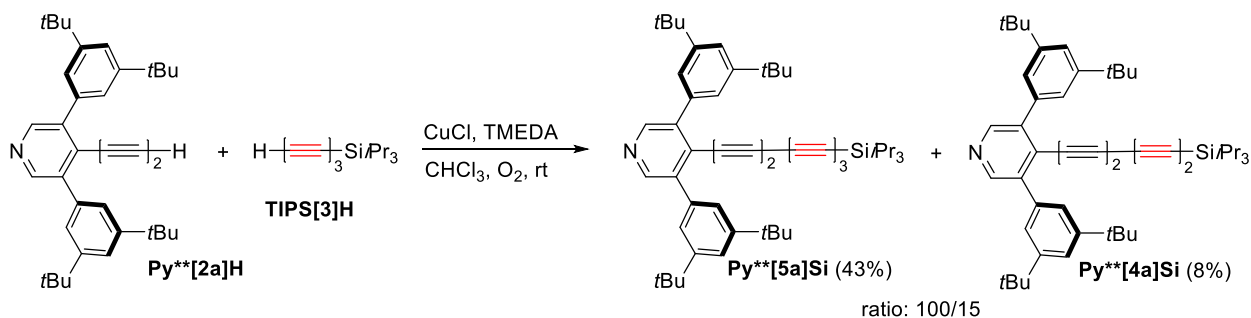
Scheme 3.7. Hay coupling reaction for **Py**[2a]H** and **TIPS[3]H** results in a mixture of **Py**[5a]Si** and **Py**[4a]Si**.

Strong signals for [M + H]$^+$ at *m/z* 732.4959 and 708.4959 for **Py**[5a]Si** and **Py**[4a]Si**, respectively, are observed in the ESI-HRMS analysis (Figure 3.10). The ratio of the abundance at *m/z* 733.4996 and 707.4992 is about 100:15. The mixture was measured by ^{1}H NMR spectroscopy in CDCl$_3$. An additional set of signals, aside from that of **Py**[5a]Si**, has appeared in the ^{1}H NMR spectrum (Figure 3.11). The percentage of the additional signals is about 15% relative to that of **Py**[5a]Si**, which is consistent with the ratio observed in the ESI-HRMS analysis. The combined spectroscopic analyses of ESI-HRMS and ^{1}H NMR support that the loss of an alkyne unit has occurred in the formation of **Py**[5a]Si** in the Hay coupling reaction. This observation suggests that the loss of an alkyne unit can occur for a triyne, which is the shortest oligoyne that has been observed with a loss of an alkyne unit in the Hay coupling reaction.

Formula Calculator Results

Formula	Ion Species	Mass	Calc. Mass	m/z	Calc. m/z	Diff (mDa)	Diff (ppm)	DBE	Ion	Score
C52 H65 N Si	C52 H66 N Si	731.4885	731.4886	732.4957	732.4959	0.18	0.25	22	(M+H)+	99.15

Figure 3.10. Mass analysis supporting loss of an alkyne unit during the synthesis of **Py**[5a]Si** from **Py**[2a]H** and **TIPS[3]H** (identity of signal at *m/z* 686.3086 not determined).

Figure 3.11. ^{1}H NMR spectrum supporting the presence of **Py**[4a]Si** during the synthesis of **Py**[5a]Si** from **Py**[2a]H** and **TIPS[3]H** (1 and 2 denote residual solvent signals of CH_2Cl_2 and MeOH, respectively; these solvents were used for recrystallization).

3.3.3 Loss of an alkyne unit in the Eglinton–Galbraith coupling

Loss of an alkyne unit in Eglinton–Galbraith coupling reaction has not been conducted via a ^{13}C-labelling experiment. The alkyne fragmentation in the Eglinton–Galbraith coupling reaction has been described in Chapter 2. Herein, this reaction is discussed in detail. The deprotection reaction of a pentayne **Py**[5a]Si** gave the terminal pentayne **Py**[5a]H** by using CsF in THF/H$_2$O. Then the terminal pentayne **Py**[5a]H** was subjected to the Eglinton–Galbraith coupling condition (Cu(OAc)$_2$, 2,6-lutidine, CH$_2$Cl$_2$, air) giving a decayne **Py**[10a]** and a nonayne **Py**[9a]** in ca. 16 and 1% yield, respectively (Scheme 3.8), as determined by ESI-MS spectrometry.
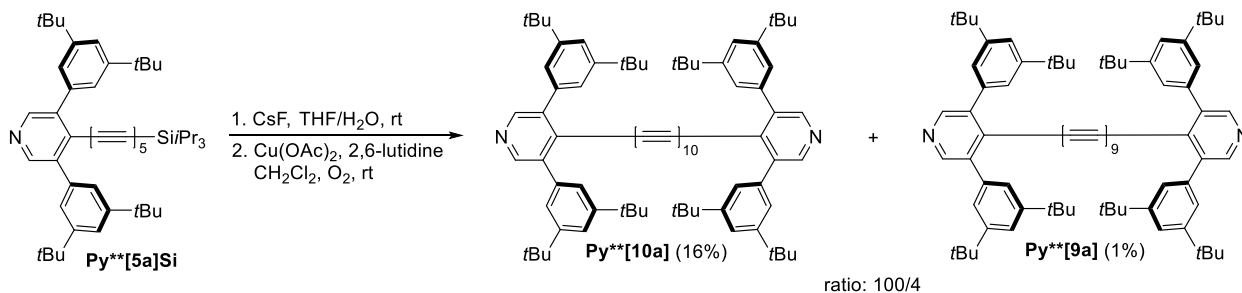
Scheme 3.8. Eglinton–Galbraith coupling results in a mixture of **Py**[10a]** and **Py**[9a]**.

3.4 Proposed mechanisms of the loss of an alkyne unit

Two mechanisms are proposed herein to potentially explain pathways that may be operative during the loss of an alkyne unit in the copper-catalyzed oxidative homocoupling reactions. The key step of the loss of an alkyne unit in particular is discussed. The mechanisms are described with the use of the ^{13}C-labeled pentayne **Py**[5a]H$^{#}$** as the reactant, TMEDA as a ligand and base, CuX (X = Cl, Br, I, OAc) as a source of copper catalyst, and molecular oxygen from the air as an oxidant.

Before discussing a mechanism for the loss of an alkyne in the Hay reaction, it is instructive to consider the mechanism of the Hay coupling for oxidative homocoupling of acetylenes. A summary of the most commonly accepted mechanistic aspects typically described in the literature is shown in Scheme 3.9A. Direct deprotonation of an alkyne by an amine base is not possible, and thus prior coordination of a copper salt is necessary to facilitate deprotonation in Step (i). Ligand exchange with a Cu(II)-TMEDA complex occurs twice, Steps (ii) and (iii), followed by a reductive elimination to give the "homocoupled" product in Step (iv).

Proposed Mechanism 1 for the loss of an acetylene unit is described schematically in Scheme 3.9B and can be described as a retro-Hay coupling. While π-coordination of the pentayne **Py**[5a]H$^{#}$** is likely, this has not been established. Thus, the initial reaction is the oxidative insertion of Cu(I) into the C–C single bond at the termini of the pentayne, Step (iv'). It seems likely that the electronic makeup of the *sp*-carbon chain must be of paramount importance in this process for the selective insertion of the copper atom at this bond. Namely, this step (the oxidative addition) is not observed for shorter oligoynes, and products consistent with insertion of copper into other C–C single bonds in the oligoyne chain have not been observed. The subsequent step frees up the acetylide unit (^{13}C-labeled) via ligand exchange from the dimeric intermediate, Step (iii'), and subsequent protonation presumably affords acetylene that is ultimately lost to solution or as a gas. A second ligand exchange introduces a pentayne into the Cu-dimer, followed by reductive elimination to form nonayne **Py**[9a]$^{#}$** as well as regenerating Cu(I) (which can be oxidized to C(II) by oxygen present in the solution).

A

base

(i)

(ii)

(iii)

(iv)

e.g.,
TMEDA

B

(iv')

(iii')

(iii)

(iv)

+ 2 Cu$^+$

tBu tBu

tBu tBu

= Py**

#denotes ^{13}C labelling
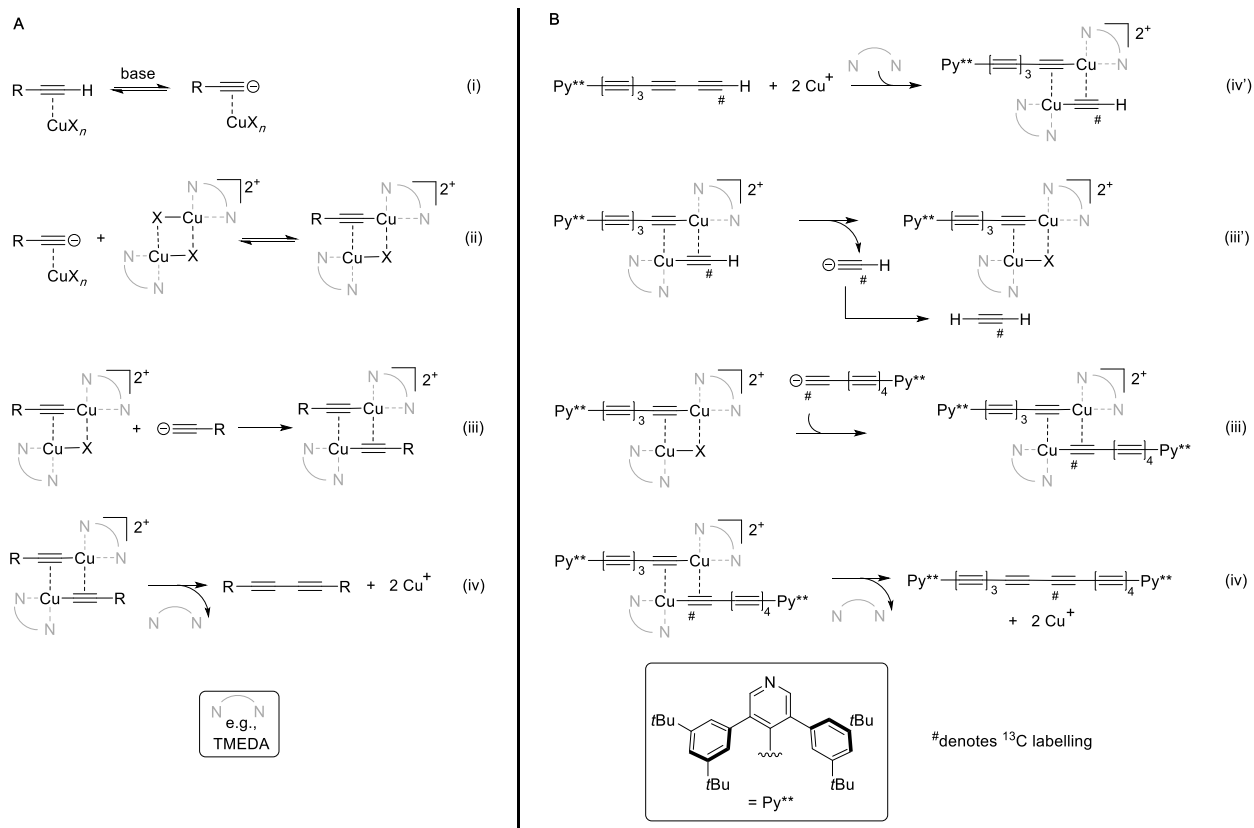
Scheme 3.9. Hay homocoupling reaction mechanism and retro-Hay coupling mechanism for the formation of **Py**[9a]**[#]** with the loss of an alkyne unit.

Proposed Mechanism 2 (Scheme 3.10) describes an addition/elimination process that is also initiated by π-coordination of copper that facilitates deprotonation by the amine base and results in formation of the copper acetylide complex in Step (i). The subsequent nucleophilic attack in Step (ii) at the most electrophilic *sp*-carbon is directed by proximity to the Cu-complex, giving the Cu-alkylidene product.[20] Subsequent collapse of this intermediate Cu-alkylidene in Step (iii) releases the tetrayne as an acetylide, presumably due to its propensity as a better leaving group. The other product from Step (iii) is the Cu-acetylide bearing the nucleophile, which is subsequently lost to solution due to its reduced acidity relative to the pentayne starting material (this product has not been experimentally observed in our reactions, but would not likely be stable).[21] In Step (iii), the source of the nucleophile could be an acetylide anion, X (X = Cl, OAc), a hydroxide anion, or the base/ligand used in the reaction, e.g., pyridine used in the Eglinton–Galbraith reaction. Then, the tetrayne acetylide is captured in the steps of the Hay mechanism with **Py**[5a]H**[#]**, step (iv), followed by the reductive elimination to form the nonayne **Py**[9a]**[#]** in step (v).
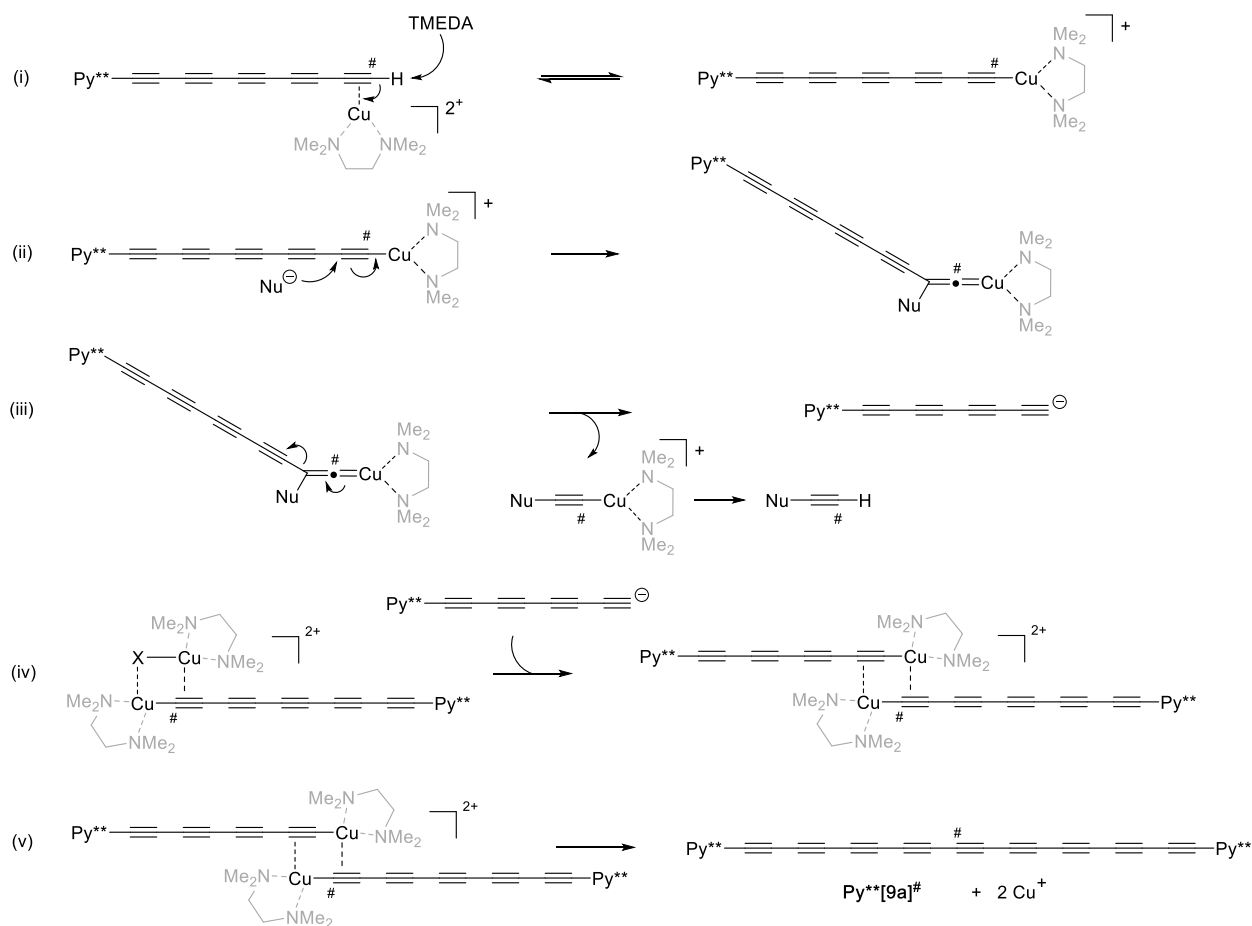
Scheme 3.10. A plausible mechanism for the formation of **Py**[9a]#** with the loss of an alkyne unit.

3.5 Methods to avoid or suppress the loss of alkyne unit

Loss of alkyne units has been observed in the Cadiot–Chodkiewicz, Eglinton–Galbraith, and Hay coupling reactions. As has been described previously, methods have been developed to avoid or suppress the loss of alkyne units during these reactions. Typical examples are summarized in this section to guide researchers to select the optimal methods towards the synthesis of longer oligo-/polyynes.

A typical Cadiot–Chodkiewicz heterocoupling reaction (CuCl, hydroxylamine hydrochloride, and *n*-propylamine) forms a mixture of **Py**[5a]Si#** and **Py**[4a]Si#** from **Py**[4a]H** and compound **3.7** (Scheme 3.11a). However, a Pd-assisted Cadiot–Chodkiewicz heterocoupling protocol (CuI, Pd(PPh₃)₄, and diisopropylethylamine) provides the desired pentayne **Py**[5a]Si#** and avoids the loss of an alkyne unit. When conducting the Hay coupling reaction to prepare the ¹²C-isotopomer **Py**[5a]Si** from **Py**[2a]H** and H–(C≡C)₃–TIPS, a

mixture of **Py**[5a]Si** and **Py**[4a]Si** was obtained, with a ratio of 100/15. Gratifyingly, the use of an iodine terminated building block, I–(C≡C)₃–TIPS, in the Pd-assisted Cadiot–Chodkiewicz heterocoupling reaction produced pure **Py**[5a]Si** in 48% isolated yield (Scheme 3.11b). Therefore, the Pd-assisted Cadiot–Chodkiewicz heterocoupling seemingly appears to be a useful method to avoid the loss of alkyne units.
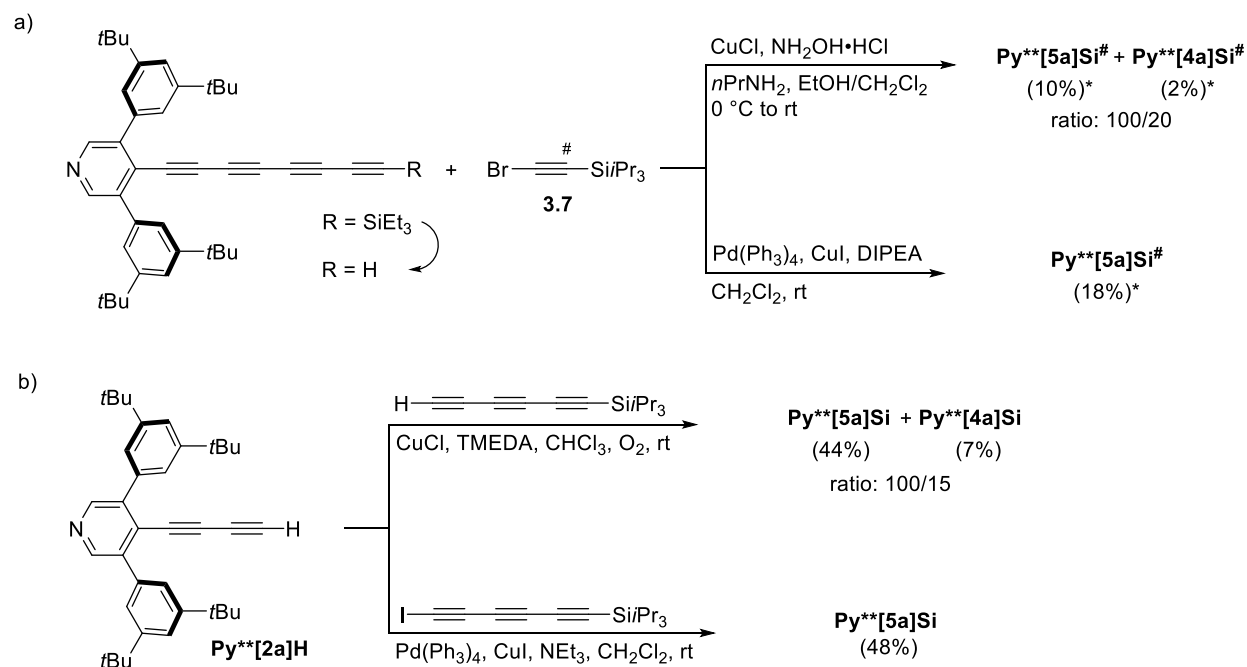
Scheme 3.11. Schematic demonstration of the synthesis of a) **Py**[5a]Si**[#] in the Cadiot–Chodkiewicz heterocoupling reactions and b) **Py**[5a]Si** in the Hay coupling and the Pd-assisted Cadiot–Chodkiewicz heterocoupling reactions. [#]Indicates 13C-labeling. [*]Yields are calculated based on the silyl-protected tetraynes.

In the homocoupling reactions, a mixture of **Py**[10a]**[##] and **Py**[9a]**[#] (ratio: 100/5) is formed from **Py**[5a]H**[#] under the typical Hay homocoupling conditions (TMEDA, CuCl, CH₂Cl₂, O₂). By changing the ligand and base from TMEDA to 4,4'-di-*tert*-butyl-2,2'-bipyridine (dtBBP) and 6,6'-dimethyl-2,2'-bipyridine (DMBP), respectively, the modified coupling reaction gives a mixture of **Py**[10a]** and **Py**[9a]** (ratio: 100/2). In comparison to previously established conditions, the loss of an alkyne unit is supressed and only traces of the nonayne are observed in the reaction mixture (Scheme 3.12). Further, the yield of the desired decayne is increased from 45 to 63% concomitantly. There are no general guidelines, however, given **Py**[24a]** can be synthesized without the observation of loss of an alkyne unit by using the Hay conditions.
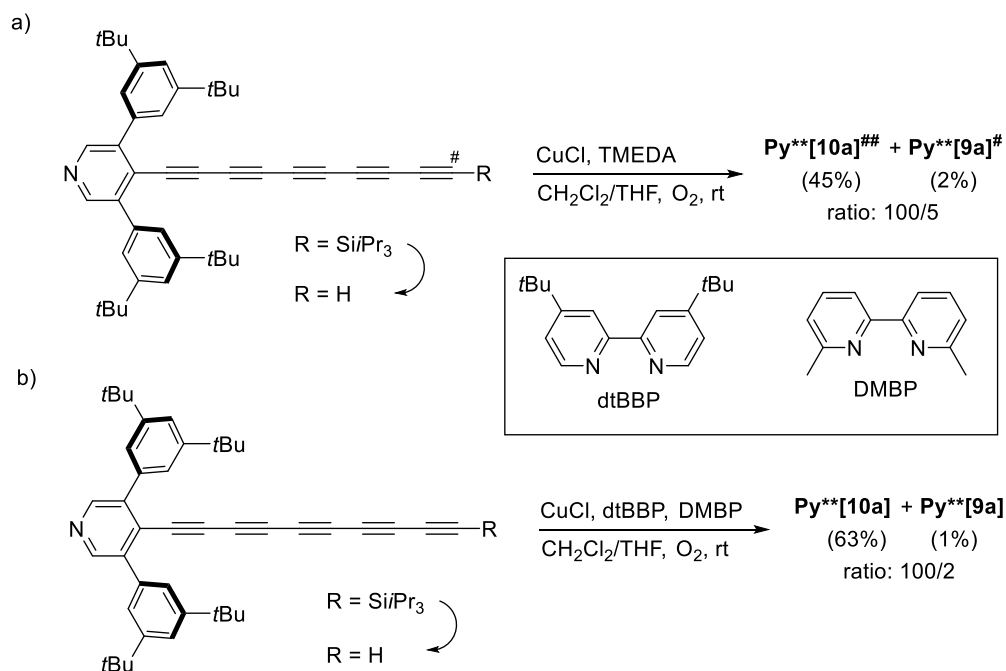
Scheme 3.12. Schematic demonstration of the synthesis of a) **Py**[10a]**[##] in the Hay homocoupling reaction and b) **Py**[10a]** in the modified coupling reactions. Yields are calculated based on the silyl-protected pentaynes.

3.6 Conclusions

By synthesizing a target ^{13}C-labeled precursor, the alkyne cleavage has been observed in the Cadiot–Chodkiewicz and Hay coupling reactions. Loss of alkyne units taking place in the terminal position has been unambiguously confirmed by mass spectrometric and NMR spectroscopic analyses in these coupling reactions. Two plausible mechanisms are provided to help rationalize the C–C bond activation; however, a more rigorous mechanistic study must be conducted to confirm the true underlying reaction pathway. To suppress the observed side reactions that were investigated in this chapter, several optimized methods were established. By utilizing a modified Pd-assisted Cadiot–Chodkiewicz coupling reaction or modifying the ligand and base used in the Hay coupling, alkyne cleavage could be minimized, and yields of the desired product were increased concomitantly by ca. 4–18%. In the future, the Eglinton–Galbraith coupling reaction will be investigated through ^{13}C-labeling experiments to gain more insights into the process of alkyne fragmentations. Using different endgroups of the oligoyne precursors to change the electronic makeup of the carbon chain should help understand the process of alkyne fragmentations. Nevertheless, optimizations of the coupling reactions are needed to avoid/suppress both the alkyne loss and improve the yields of the desired products.

3.7 References

[1]   A. L. K. Shi Shun, R. R. Tykwinski, *Angew. Chem. Int. Ed.* **2006**, *45*, 1034–1057.

[2]   J. A. Marsden, G. J. Palmer, M. M. Haley, *Eur. J. Org. Chem.* **2003**, 2355–2369.

[3]   X. Gao, H. B. Liu, D. Wang, J. Zhang, *Chem. Soc. Rev.* **2019**, *48*, 908–936.

[4]   S. E. Allen, R. R. Walvoord, R. Padilla-Salinas, M. C. Kozlowski, *Chem. Rev.* **2013**, *113*, 6234–6458.

[5]   a) W. A. Chalifoux, R. R. Tykwinski, *C. R. Chimie* **2009**, *12*, 341–358; b) R. R. Tykwinski, W. Chalifoux, S. Eisler, A. Lucotti, M. Tommasini, D. Fazzi, M. Del Zoppo, G. Zerbi, *Pure Appl. Chem.* **2010**, *82*, 891–904.

[6]   C. Glaser, *Ber. Dtsch. Chem. Ges.* **1869**, 422–424.

[7]   G. Eglinton, A. R. Galbraith, *Chem. Ind. (London)* **1956**, 737–738.

[8]   A. S. Hay, *J. Org. Chem.* **1962**, *27*, 3320–3321.

[9]   W. Chodkiewicz, P. Cadiot, *C. R. Hebd. Seances Acad. Sci.* **1955**, *241*, 1055–1057.

[10]   a) W. A. Chalifoux, M. J. Ferguson, R. McDonald, F. Melin, L. Echegoyen, R. R. Tykwinski, *J. Phys. Org. Chem.* **2012**, *25*, 69–76; b) W. A. Chalifoux, R. McDonald, M. J. Ferguson, R. R. Tykwinski, *Angew. Chem. Int. Ed.* **2009**, *48*, 7915–7919; c) S. Eisler, A. D. Slepkov, E. Elliott, T. Luu, R. McDonald, F. A. Hegmann, R. R. Tykwinski, *J. Am. Chem. Soc.* **2005**, *127*, 2666–2676.

[11]   T. Gibtner, F. Hampel, J. P. Gisselbrecht, A. Hirsch, *Chem. Eur. J.* **2002**, *8*, 408–432.

[12]   a) P. Sivaguru, Z. K. Wang, G. Zanoni, X. H. Bi, *Chem. Soc. Rev.* **2019**, *48*, 2615–2656; b) L. Souillart, N. Cramer, *Chem. Rev.* **2015**, *115*, 9410–9464; c) C. H. Jun, *Chem. Soc. Rev.* **2004**, *33*, 610–618.

[13]   C. T. To, K. S. Chan, *Eur. J. Org. Chem.* **2019**, 6581–6591.

[14]   a) W. Zhou, W. Y. Fan, Q. J. Jiang, Y. F. Lang, N. Jiao, *Org. Lett.* **2015**, *17*, 2542–2545; b) C. Tang, N. Jiao, *Angew. Chem. Int. Ed.* **2014**, *53*, 6528–6532; c) A. Maji, S. Rana, Akanksha, D. Maiti, *Angew. Chem. Int. Ed.* **2014**, *53*, 2428–2432; d) X. Huang, X. Li, M. Zou, S. Song, C. Tang, Y. Yuan, N. Jiao, *J. Am. Chem. Soc.* **2014**, *136*, 14858–14865; e) W. Zhou, Y. Yang, Y. Liu, G.-J. Deng, *Green Chem.* **2013**, *15*, 76–80; f) C. Zhang, P. Feng, N. Jiao, *J. Am. Chem. Soc.* **2013**, *135*, 15257–15262; g) L. Zhang, X. Bi, X. Guan, X. Li, Q. Liu, B. D. Barry, P. Liao, *Angew. Chem. Int. Ed.* **2013**, *52*, 11303–11307.

[15]   J. P. Brand, J. Charpentier, J. Waser, *Angew. Chem. Int. Ed.* **2009**, *48*, 9346–9349.

[16]   R. Frei, J. Waser, *J. Am. Chem. Soc.* **2013**, *135*, 9620–9623.

[17]   R. A. Seburg, J. A. Hodges, R. J. McMahon, *Helv. Chim. Acta* **2009**, *92*, 1626–1643.

[18]   a) K. Wu, C. Song, D. Cui, *Chinese J. Org. Chem.* **2017**, *37*, 586–602; b) D. S. Kim, W. J. Park, C. H. Jun, *Chem. Rev.* **2017**, *117*, 8977–9015.

[19]   W. A. Chalifoux, R. R. Tykwinski, *Nat. Chem.* **2010**, *2*, 967–971.

[20]   a) J. Wang, X. Cao, S. Lv, C. Zhang, S. Xu, M. Shi, J. Zhang, *Nat. Commun.* **2017**, *8*, 14625; b) I. V. Shishkov, F. Rominger, P. Hofmann, *Organometallics* **2009**, *28*, 1049–1059; c) B. F. Straub, P. Hofmann, *Angew. Chem.* **2001**, *113*, 1328–1330.

[21]   F. Bohlmann, H. Schönowsky, E. Inhoffen, G. Grau, *Chem. Ber.* **1964**, *97*, 794–800.

CHAPTER 4 – A Series of Platinum Complexes Coordinated to Oligoynes

4.1 Introduction

Pyridyl end-capped oligoynes (PEOs) have been studied as molecular wires in terms of single-molecule conductance for over a decade.[1] PEOs incorporate pyridine as endgroups that can serve as an anchor to gold electrodes, facilitating the study of single-molecule conductance by scanning tunneling microscope break junction (STM-BJ) technology.[1-2] STM-BJ has become a powerful tool to study electron transport between electrodes and molecules.[3] The properties of electron transport through a single or, at most, a few molecules are sensitive to the contacts formed between the anchoring group and the electrode.[2-3] As an alternative to a gold electrode, a graphene electrode can be stable up to high temperature and has been extensively developed to date.[4] A recent example using fullerene as an anchor toward a graphene electrode via noncovalent bonding[4c] has been reported for the fabrication of single-molecule junctions (Figure 4.1a). The potential applications using PEOs as molecular wires would be boosted if PEOs could contact not only with the gold electrode, but also with more demanding graphene electrodes. Pure PEOs wires, however, are not able to show a strong binding affinity toward a graphene electrode, presumably due to the limited interactions between the pyridyl endgroup and the graphene electrode.[5] The connection of PEOs and graphene electrodes could be enhanced by the introduction of columbic interactions with a cationic species appended to the pyridyl endgroup. The introduction of platinum(II) cations to PEOs will form a square planar geometry about the electron-deficient Pt center, which could facilitate the noncovalent bonding to a planar surface of the graphene electrode (Figure 4.1b). Therefore, a series of cationic platinum complexes coordinated with PEOs has been designed and synthesized as model compounds to allow testing of this hypothesis.
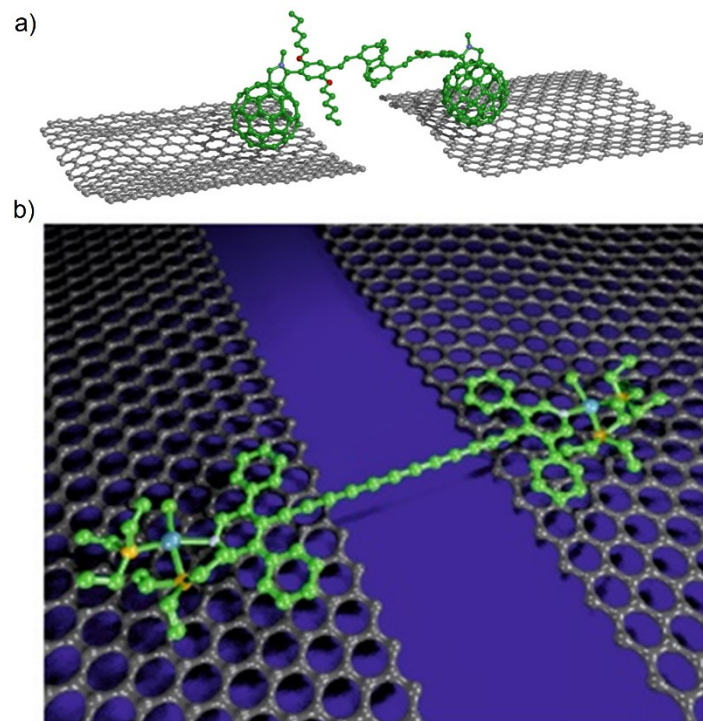
Figure 4.1. Illustration of a) a single-molecule junction between graphene electrodes through noncovalent bonding with fullerene (reprinted with permission from American Chemical Society: *Nano Lett.* **2015**, *15*, 3512−3518) and b) a PEO endcapped with platinum cationic species (reprinted from the reference [5]).

Beyond offering more efficient molecular wires, coordination of PEOs to Pt can offer other interesting opportunities. Recent computational reports predict that oligo-/polyynes and cumulenes could display axial chirality and the helical arrangement of their frontier molecular orbitals (FMOs).[6] The introduction of chirality to a molecular wire is of interest as the introduction of circular currents might be potentially useful in a molecular-wire device.[6d] As an example shown in Figure 4.2, methyl sulfide endcapped triyne (**SMe[3]**) displays helical frontier orbitals when rotating the molecular axis along the *sp*-carbon chain from 180/0° (C_{2h}/C_{2v} symmetry) to other torsional angles (C_2 symmetry).[6a, 6e] The helical orbitals on the *sp*-carbon chain immediately appear from the expected rectilinear orbital shape by rotating the endgroup through a reduction of molecular symmetry, e.g., from a coplanar geometry with a C_{2h} (or C_{2v}) symmetry to a non-coplanar geometry with a C_2 symmetry.[6a] Such a reduction of molecular symmetry can arise from axial chirality (by rotating the endgroup) or through a smart design of the endgroups, e.g., the introduction of chiral/asymmetrical endgroups. The single-bond rotation between the endgroup and the carbon chain to provide axial chirality is facile and not particularly practical in

103

synthetic experiments due to the low rotation barrier around the *sp*-carbon chain.[7] A smart design of the endgroup could be more feasible to introduce axial chirality through lowering the molecular symmetry of an oligoyne.
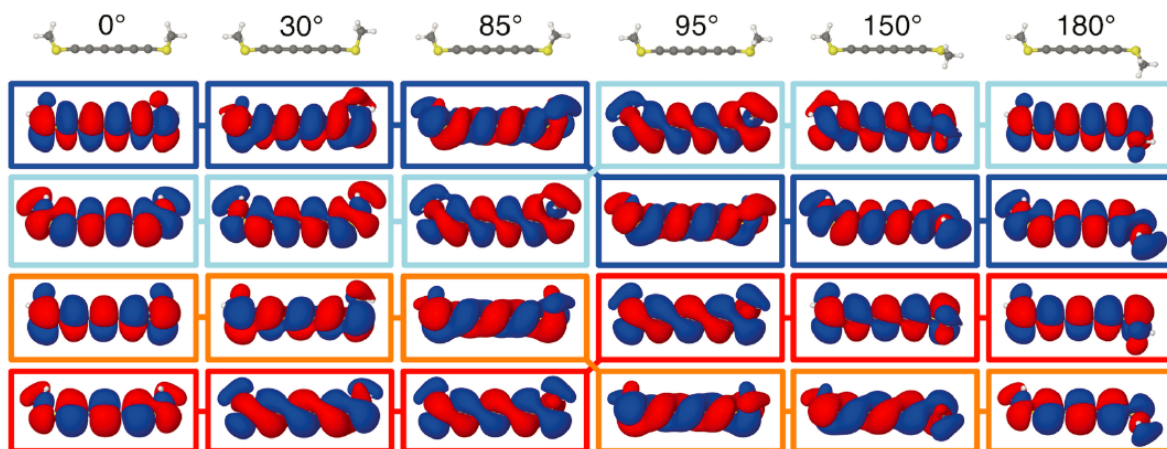
Figure 4.2. Frontier molecular orbitals (LUMO+1, LUMO, HOMO, HOMO−1 from top to bottom) of methyl sulfide endcapped triyne at dihedral orbitals of 0°, 30°, 85°, 95°, 150°, and 180°, respectively. (reprinted with permission from American Chemical Society: *J. Phys. Chem. C* **2020**, *124*, 18968−18982)

A preliminary model, analogous to the above-mentioned cationic PEOs coordinated with a chiral platinum complex, is proposed (Figure 4.3). The introduction of a chiral phosphorus ligand lowers the molecular symmetry from D_{2h} (or D_{2v}/D_2) of the naked oligoyne to the C_2 symmetry of the oligoyne platinum complex. Additionally, the electronic interaction between the platinum moiety and the oligoyne backbone is limited, as established through X-ray crystallographic and UV-vis spectroscopic analyses, which means that chirality of the hexayne **Py*[6]** moiety is electronically independent of the Pt-center. Preliminary experiments of Pyridyl-endcapped hexaynes coordinated with a chiral platinum complex to form **(R,R,R,R)-Py*[6]Pt** and **(S,S,S,S)-Py*[6]Pt** (Figure 4.3) have been designed and synthesized previously in our group.[5] Preliminary calculations show that **(S,S,S,S)-Py*[6]Pt** displays the helical orbitals of LUMO.[8] The circular dichroism (CD) spectra show the chiral characters of the oligoynes and offer the first experimental confirmation of the theoretical prediction that the helical arrangement of FMOs can produce axial chirality (Figure 4.4).[9] The formation of the Pt complexes coordinated to **Py*[n]** series is limited up to a hexayne, because low production yield of the octayne **Py*[8]** (6%) as the longest oligoyne in this series limits its use in the complexation reaction.[10] The octayne **Py**[8a]** (69%) in my synthesis can be conveniently obtained as described in Chapter 2. Thus, the **Py**[na]** series

(Figure 4.5) has been chosen for the complexation reactions.
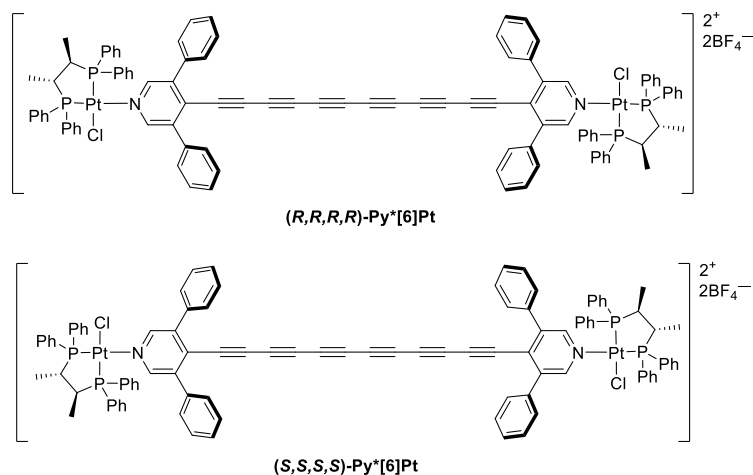
Figure 4.3. Molecular structures of **(R,R,R,R)-Py*[6]Pt** and **(S,S,S,S)-Py*[6]Pt**.
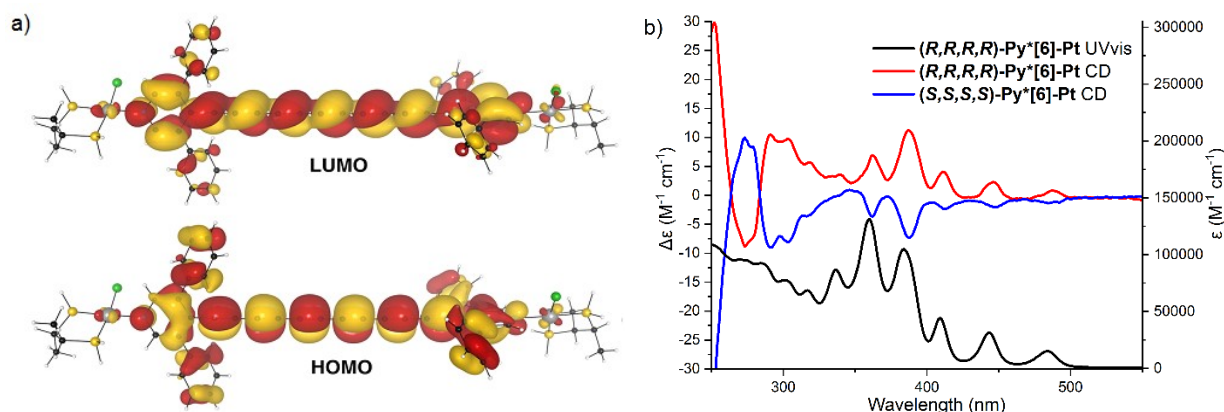
Figure 4.4. a) Preliminary calculations of HOMO and LUMO of **(S,S,S,S)-Py*[6]Pt** (ref: [5]). b) CD spectra of **(R,R,R,R)-Py*[6]Pt** and **(S,S,S,S)-Py*[6]Pt** and UV-vis spectra of **(R,R,R,R)-Py*[6]Pt**.

4.2 Synthesis of PEO-Pt complexes

As proposed in the introduction, cationic platinum complexes coordinated with PEOs (PEO-Pt) are desired. The primary purpose has been to enhance the binding affinity of the endgroups toward graphene electrodes in single-molecular junctions. Initially, the secondary purpose was to investigate the influences of chirality on the oligoyne core, and this aspect has now become a major focus of the project. There are many PEOs with different endgroups available as candidates, as has been presented in Chapter 2. Based on the consideration of the stability of the PEOs and the steric effects of the endgroups toward graphene, the previously reported diyne **Py*[2]**[10] and hexayne **Py*[6]**[10] have been tested as the backbone of PEO-Pt complexes. Physical and electronic trends as a function of molecular length are expected when studying the chirality of PEOs; thus, a series

of **Py**[4a, 6a, 8a]** is used as the backbones (Figure 4.5).

The synthesis of dihalo-bis-ligandplatinum (II) complexes (Pt-dimers) has been known for over half a century (Figure 4.5),[11] and these Pt-dimers can be an excellent source to coordinate with PEOs to form the PEO-Pt complexes due to the noncoordinating feature of the tetrafluoroborate anion. Herein, the syntheses of the Pt-dimers will be briefly discussed, and the straightforward method for the complexation of the PEOs and the Pt-dimers will be provided.
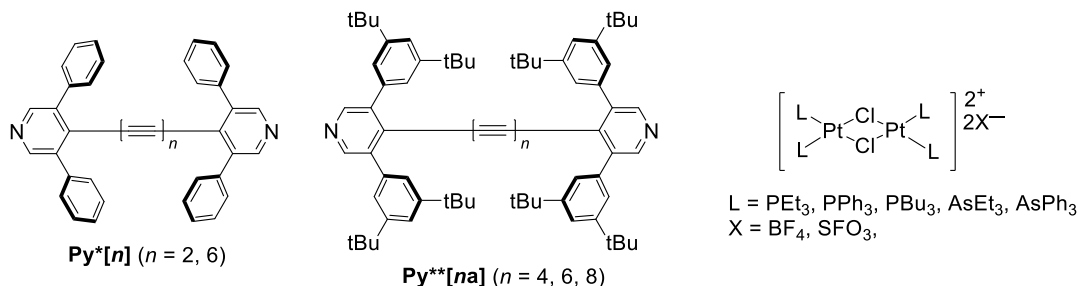
Figure 4.5. Molecular structures of **Py*[2]**, **Py*[6]**, **Py**[2a]**, **Py**[6a]**, **Py**[8a]**, and Pt-dimers.

4.2.1 Synthesis of achiral Pt-dimers as precursors

The synthesis of Pt-dimers **4.1** and **4.2** has been reported previously.[11a, 11b, 12] The use of a strong electrophile, trimethyloxonium tetrafluoroborate ($Me_3O \cdot BF_4$), allows abstraction of a chloride anion from cis-$PtCl_2(PEt_3)_2$ and cis-$PtCl_2(PPh_3)_2$ to form a "monomer" as an intermediate. Subsequently, given the unstable nature of the intermediate, dimerization occurs to give Pt-dimer **4.1** and **4.2** bridged by halide atoms in 80 and 85% yield, respectively (Scheme 4.1).
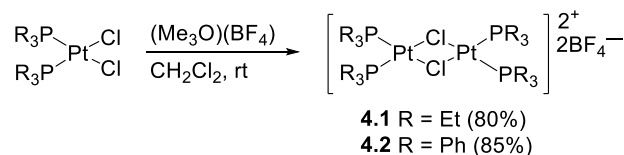
Scheme 4.1. Synthesis of achiral Pt-dimers of **4.1** and **4.2**.

Toward forming chiral dimers **4.5** and **4.6**, analogs of **4.1** and **4.2**, complexes **4.3** and **4.4** were first synthesized as starting materials. The synthesis of halide bridged Pt-dimers with four stereocenters, compound **4.5** (*R,R,R,R*-configuration) and **4.6** (*S,S,S,S*-configuration), was then accomplished by adopting known procedures.[11a, 11b] The replacement of the weak benzonitrile ligand from cis-$PtCl_2(PhCN)_2$ with bidentate (2R,3R)-(+)-2,3-bis(diphenylphosphino)butane ((*R,R*)-chiraphos) and (2S,3S)-(−)-2,3-bis(diphenylphosphino)butane ((*S,S*)-chiraphos) introduces chirality to the platinum complex to give **4.3** and **4.4**. Similar to the synthesis of **4.1** and **4.2**,

$Me_3O \cdot BF_4$ facilitated the dimerization formation with replacement of the chloride ligand with a noncoordinating tetrafluoroborate anion. Workup and recrystallization ($CH_2Cl_2/Et_2O/hexanes$) gave the homochiral Pt-dimers **4.5** and **4.6** in good yields (Scheme 4.2).
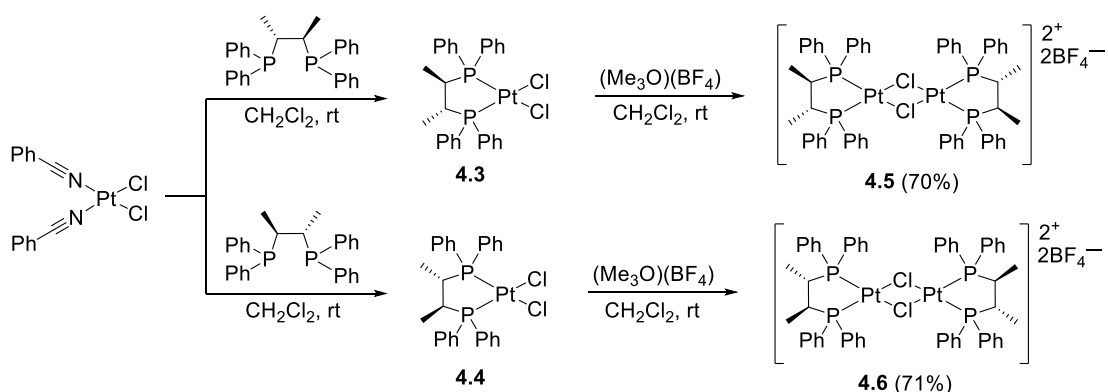
Scheme 4.2. Synthesis of chiral Pt-dimers of **4.5** and **4.6**.

4.2.2 Synthesis of achiral PEO-Pt complexes

The complexation of diyne **Py*[2]** with achiral Pt-dimers **4.1** and **4.2** gave **(Et)-Py*[2]Pt** and **(Ph)-Py*[2]Pt** in 63 and 97% yields, respectively, after recrystallizations from $CH_2Cl_2/EtOAc$. Similarly, the complexation of hexayne **Py*[6]** with **4.1** and **4.2** separately gave **(Et)-Py*[6]Pt**, and **(Ph)-Py*[2]Pt** in 92 and 70% yields after recrystallization from $CH_2Cl_2/toluene$ and $CH_2Cl_2/EtOAc$, respectively. The appearance of diyne **Py*[2]** and hexayne **Py*[6]** is a colorless and a yellow-brown solid, respectively. After the complexation with Pt-dimers, compound **(Et)-Py*[2]Pt** and **(Ph)-Py*[2]Pt** became a colorless to a light yellow-brown solid and compound **(Et)-Py*[6]Pt** and **(Ph)-Py*[6]Pt** became a brown solid. These complexes are all stable under ambient conditions.
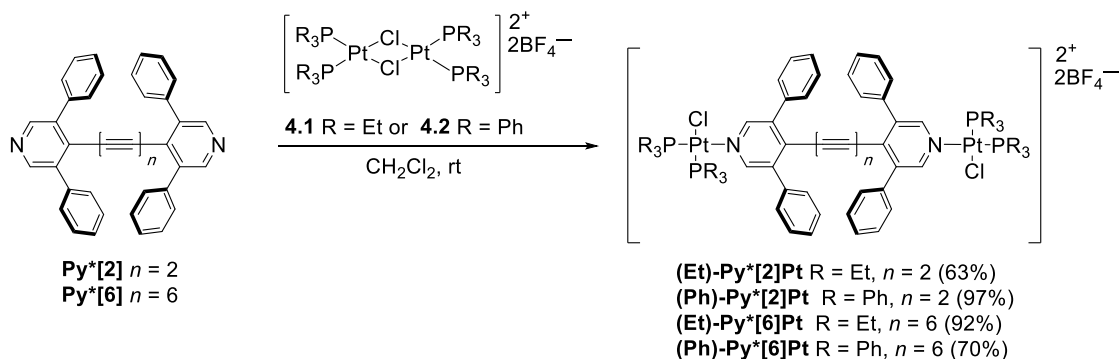
Scheme 4.3. Synthesis of achiral diyne and hexayne Pt-dimers of **(Et)-Py*[2]Pt**, **(Ph)-Py*[2]Pt**, **(Et)-Py*[6]Pt**, and **(Ph)-Py*[6]Pt**.

4.2.3 Synthesis of chiral PEO-Pt complexes

The complexation of the (*R,R,R,R*)-Pt-dimers (**4.5**) with **Py**[4a]**, **Py**[6a]**, and **Py**[8a]** gave homochiral (*R,R,R,R*)-PEO-Pt complexes (***R,R,R,R***)-**Py**[4a]Pt**, (***R,R,R,R***)-**Py**[6a]Pt**, and (***R,R,R,R***)-**Py**[8a]Pt**, respectively, after recrystallizations from CH₂Cl₂/EtOAc/hexanes. Similarly, the homochiral (*S,S,S,S*)-PEO-Pt complex (***S,S,S,S***)-**Py**[6a]Pt** was obtained from the complexation of the (*S,S,S,S*)-Pt-dimers (**4.6**) with **Py**[6a]** (Scheme 4.4).
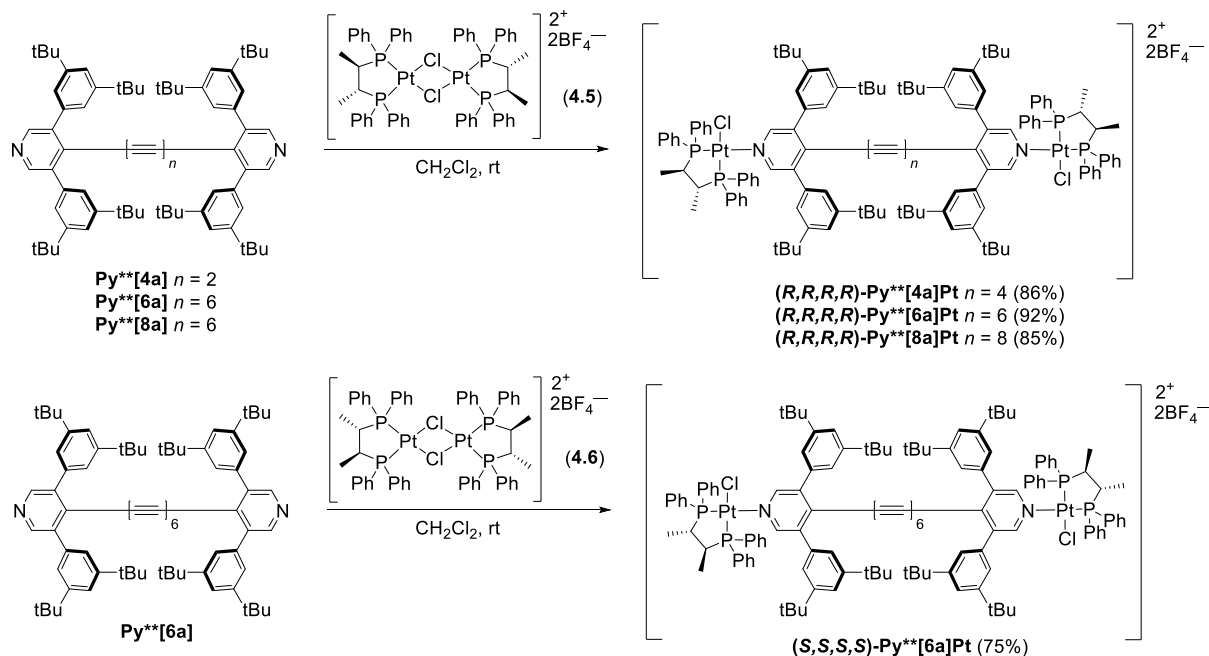
Scheme 4.4. Syntheses of chiral PEO-Pt complexes of (***R,R,R,R***)-**Py**[4a,6a,8a]Pt** and (***S,S,S,S***)-**Py**[6a]Pt**.

4.3 Discussion

The alkyne carbon resonances in the ^{13}C NMR spectra for **Py*[6]** and **Py**[6a]** have been highlighted and compared, as shown in Figure 4.6. As expected, the chemical shifts of the alkyne carbons for the ligands, **Py*[6]** and **Py**[6a]**, are similar. The HMBC analyses have helped assign the chemical shifts at ca. 83 and 74 ppm as carbons C2 and C1, respectively, as has been discussed in Chapter 2. In (***R,R,R,R***)-**Py*[6]Pt** (Figure 4.6d), complexation of the PEO ligand to the Pt moiety results in downfield shifts of C2 and upfield shift of C1 to ca. 87 and 72 ppm, respectively. The difference in chemical shifts of C1 and C2 is not surprising, given the formation of the cationic complex upon binding to Pt. To examine the nature of this effect, spectra of hexayne **Py*[6]** were obtained in a solution containing 1 equivalent of trifluoroacetic acid (TFA, **Py*[6]·TFA**; Figure 4.6b). Upon protonation, resonances for C1 and C2 shifts upfield and downfield, respectively, and

this trend is further accentuated by addition of a second equivalent of TFA (**Py*[6]•2TFA**; Figure 4.6c).　providing a clear trend in the chemical shifts as a function of cationic structure (Figure 4.6, dashed line). Thus, a comparison of the spectrum of **(R,R,R,R)-Py*[6]Pt** to that of **Py*[6]•2TFA** suggests that the shifts in ^{13}C NMR resonances of C1 and C2 of **(R,R,R,R)-Py*[6]Pt** are due simply to the formation of a cationic species. Namely, the chemical shifts of alkynyl carbons C1 and C2 for **Py[6]•2TFA** show only minor deviations from those of the **(R,R,R,R)-Py*[6]** ($\Delta\delta$ of 0.7 for C2, 0.4 for C1 and 0.6–0.1 for C3–6). The minimal observed differences in the chemical shift between **Py[6]•2TFA** and **(R,R,R,R)-Py*[6]** suggest that the coordination of the cationic Pt-complex is analogous to that of protonation, and it has little effect on the electronic structure of the alkyne chain, confirmed by resonance of the remaining *sp*-carbons C3–C6. This premise is further supported by the spectra of achiral model compounds **(Et)-Py*[6]Pt** and **(Ph)-Py*[6]Pt**, which are nearly identical to those of their chiral cousins **(R,R,R,R)-Py*[6]** and **(S,S,S,S)-Py*[6]**.
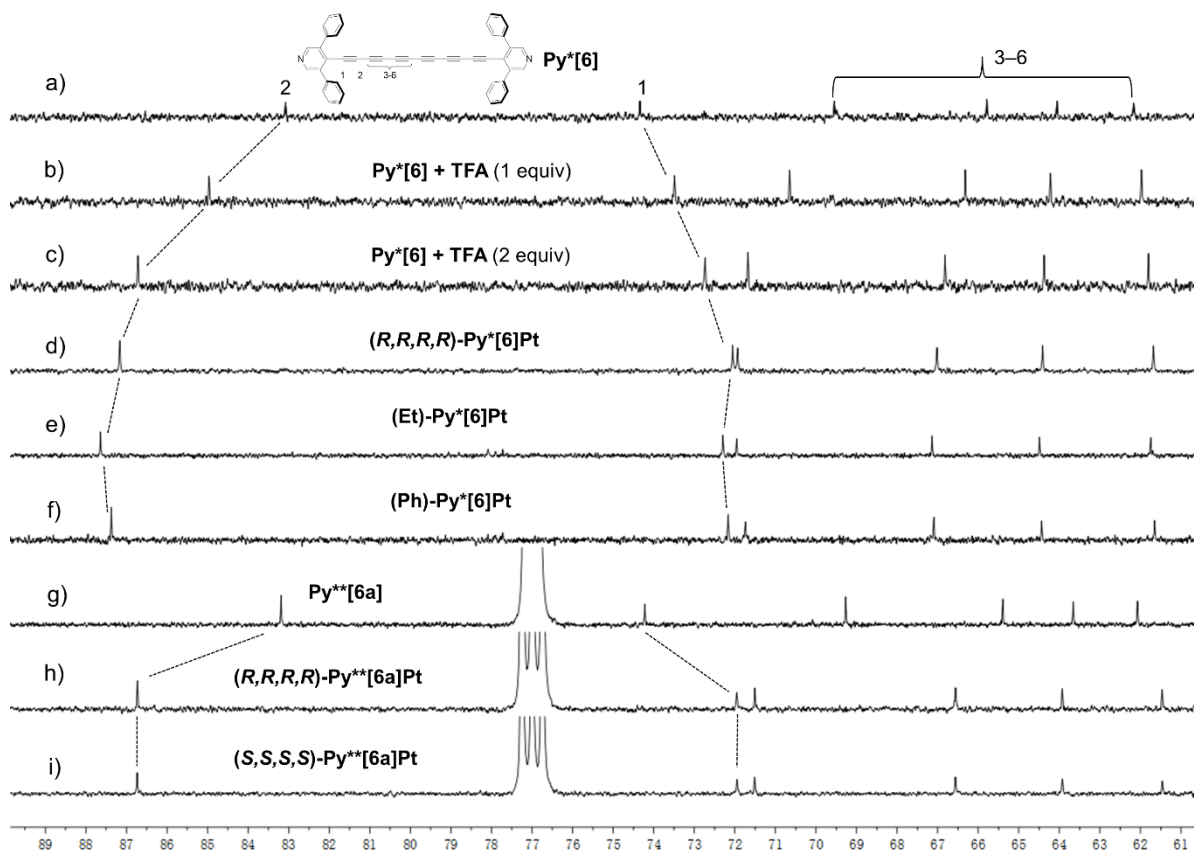
Figure 4.6. Comparison of the ^{13}C NMR spectra of **Py*[6]**, **Py*[6]** + TFA (1 equiv), **Py*[6]** + TFA (2 equiv), **(Et)-Py*[6]Pt**, and **(Ph)-Py*[6]Pt** in CD$_2$Cl$_2$, as well as **Py**[6a]**, **(R,R,R,R)-Py**[6a]Pt**, and **(S,S,S,S)-Py**[6a]Pt** in CDCl$_3$.

The complexation of the ligands, **Py**[4a]** and **Py**[8a]** to the Pt complex results in downfield shift of C2 and upfield shift of C1 to the same extent as discussed above for **Py*[6]** and **Py**[6a]** series (Figure 4.7 and 4.8).
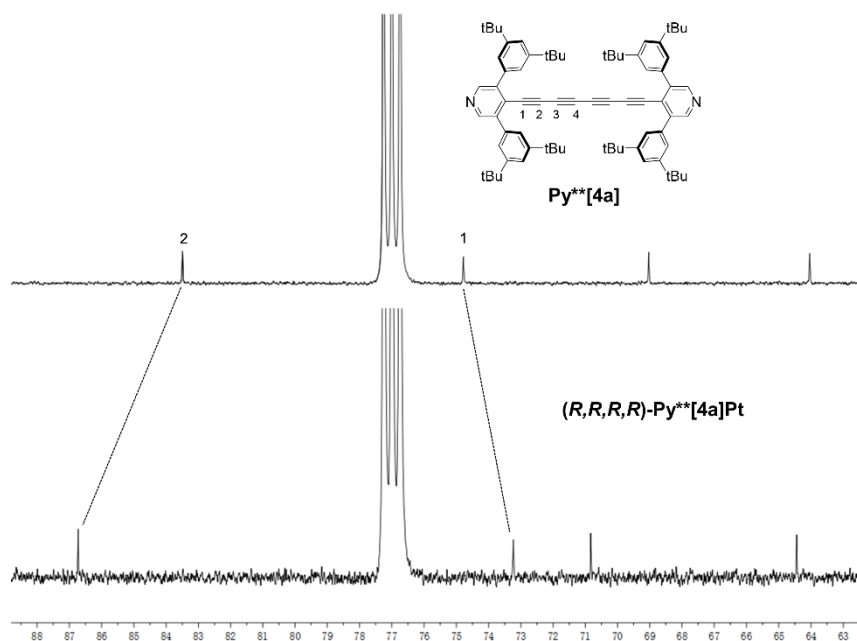
Figure 4.7. Comparison of the ^{13}C NMR spectra of **Py**[4a]** and **(R,R,R,R)-Py**[4a]Pt** in CDCl$_3$.
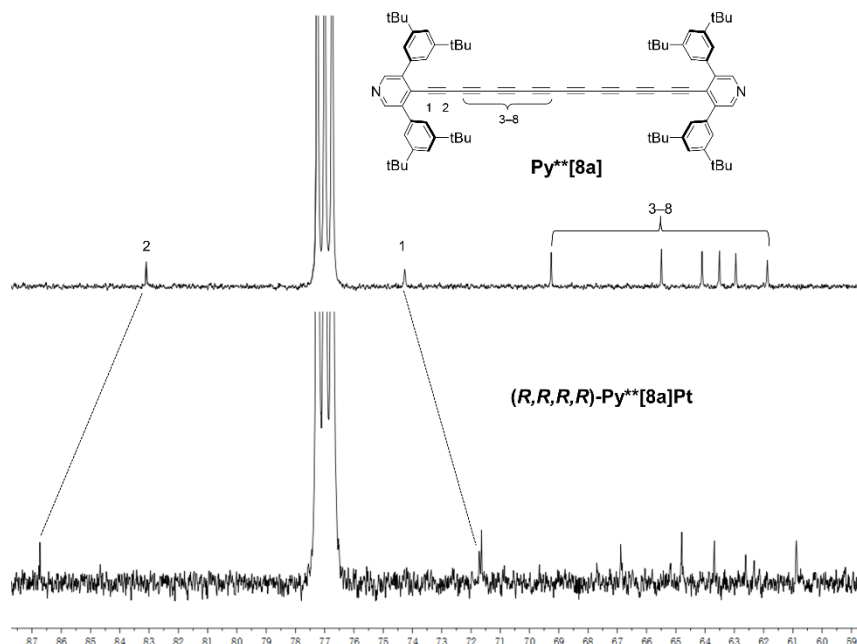
Figure 4.8. Comparison of the ^{13}C NMR spectra of **Py**[8a]** and **(R,R,R,R)-Py**[8a]Pt** in CDCl$_3$.

The electronic absorption spectra of **Py*[6]**, homochiral complexes **(R,R,R,R)-Py*[6]Pt**

and **(S,S,S,S)-Py*[6]Pt**, as well as achiral complexes **(Et)-Py*[6]Pt** and **(Ph)-Py*[6]Pt** are shown in Figure 4.9 and highlight the distinct vibronic fine structures in the low energy region (390–490 nm) of the spectra that is characteristic of diaryl polyynes.[13] Furthermore, these vibrational bands offer a convenient signature for absorptions derived from the hexayne chromophore because these transitions are significantly red-shifted from any that arise from either the platinum complex or the phenyl moieties of the pyridyl endgroups. The electronic absorption spectra of **(R,R,R,R)-Py*[6]Pt** and **(S,S,S,S)-Py*[6]Pt** are identical, as is expected for enantiomers, while all significant absorptions are red-shifted 10 nm relative to that of **Py*[6]**, as a result of coordination of the pyridinium moiety to the cationic platinum center. The red-shift upon metal complexation is also consistent with the analogous red shift signals of **Py*[6]•TFA** (500 equiv), formed upon protonation of **Py*[6]** with TFA, indicating that the electronic effects of platinum coordination on the electronic structure of the polyyne unit is limited (Figure 4.9). This premise is further supported by the spectra of achiral model compounds **(Et)-Py*[6]Pt** and **(Ph)-Py*[6]Pt**, which are nearly identical to those of their chiral cousins **(R,R,R,R)-Py*[6]Pt** and **(S,S,S,S)-Py*[6]Pt**.
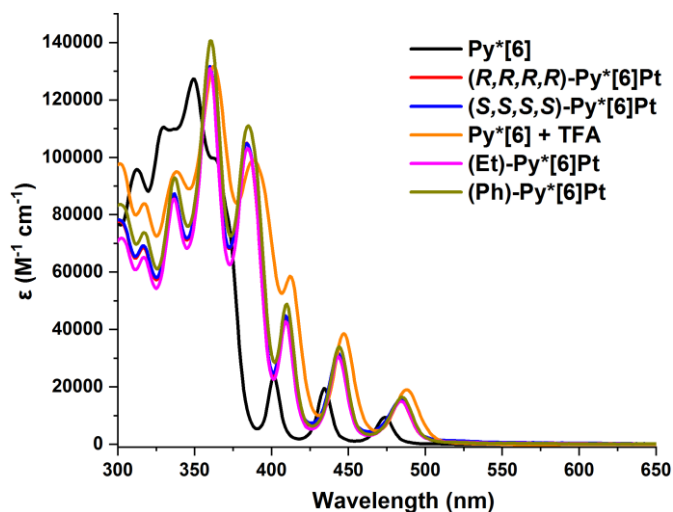
Figure 4.9. Electronic spectra of **Py*[6]**, the homochiral complexes **(R,R,R,R)-Py*[6]Pt** and **(S,S,S,S)-Py*[6]Pt**, and protonated pyridyl polyyne **Py[6] + TFA** (500 equiv), as well as the achiral complexes **(Et)-Py*[6]Pt** and **(Ph)-Py*[6]Pt** (the spectrum of **(R,R,R,R)-Py*[6]Pt** in red is not completely observable due to overlap with the identical spectrum with **(S,S,S,S)-Py*[6]Pt** in blue; the spectrum of **Py[6] + TFA** used excess TFA (500 equiv) and has been normalized against **(R,R,R,R)-Py*[6]Pt**).

The UV-vis absorption spectra of the homochiral complexes **(R,R,R,R)-Py**[4a,6a,8a]Pt** and **(S,S,S,S)-Py**[6a]Pt** are shown in Figure 4.10. The molar extinction absorbance increases as

a function of molecular length in the λ_{main} region (the high energy region, see the definition in Chapter 2) and decreases as a function of molecular length in the λ_{weak} region (the low energy region, see the definition in Chapter 2). The extinction values of these complexes have a similar trend to that of their ligands. It is noted that the calculation of the molar extinction absorbance of the enantiomers **(R,R,R,R)-Py**[6a]Pt** and **(S,S,S,S)-Py**[6a]Pt** is not identical (with an error of ca. 15%) presumably due to the deviations of their mass measurements.
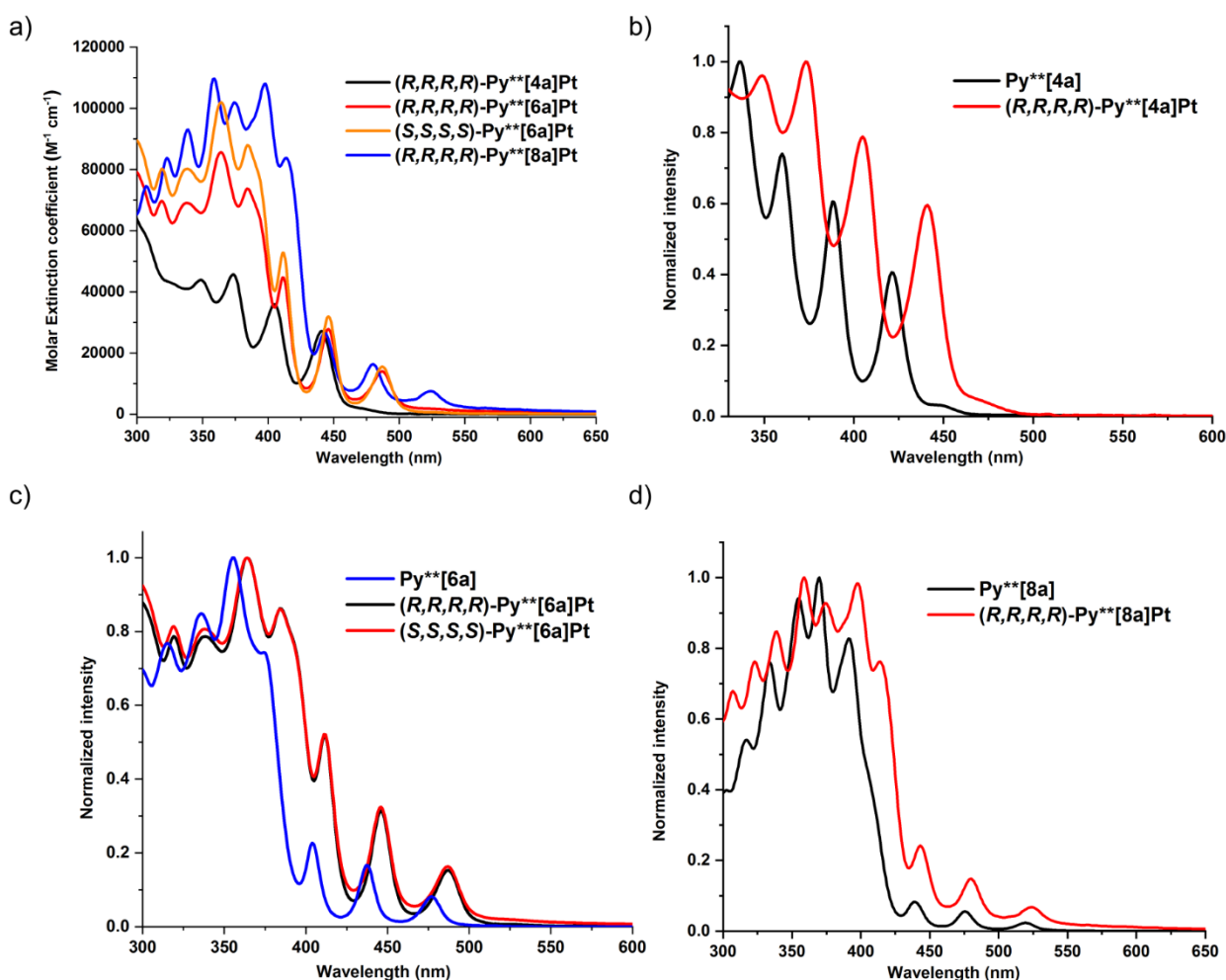
Figure 4.10. a) Electronic spectra of complexes **(R,R,R,R)-Py**[4a,6a,8a]Pt** and **(S,S,S,S)-Py**[6a]Pt**. b) The normalized UV-vis spectra of ligand **Py**[4a]** and the complex **(R,R,R,R)-Py**[4a]Pt**. c) The normalized UV-vis spectra of ligand **Py**[6a]** and the complexes **(R,R,R,R)-Py**[6a]Pt** and **(S,S,S,S)-Py**[6a]Pt**. d) The normalized UV-vis spectra of ligand **Py**[8a]** and the complex **(R,R,R,R)-Py**[8a]Pt**.

The comparison of the lowest energy (λ_{max}) in the electronic spectra of the homochiral complexes, **(R,R,R,R)-Py**[4a,6a,8a]Pt** and **(S,S,S,S)-Py**[6a]Pt**, to their ligands, **Py**[4a–8a]**,

shows red shift in the range of 5 to 20 nm. To be more specific, λ_{max} of the tetrayne complex **(R,R,R,R)-Py**[4a]Pt** is 441 nm, which is 20 nm red-shifted from 421 nm of its tetrayne ligand **Py**[4a]** (Figure 4.10b). λ_{max} = 487 nm for hexayne complexes **(R,R,R,R)-Py**[6a]Pt** and **(S,S,S,S)-Py**[6a]Pt** which is 11 nm red-shifted from 476 nm of the hexayne ligand **Py**[6a]** (Figure 4.10c). Finally, λ_{max} = 524 nm for the octayne complex **(R,R,R,R)-Py**[8a]Pt**, which is 5 nm red-shifted from 519 nm of the octayne ligand **Py**[8a]** (Figure 4.10d). The difference in λ_{max} values between the complexes and the naked oligoynes decreases as increasing the molecular length. This trend implies that the influence of cationic Pt center on the electronic structure of the alkyne chain decreases as the molecular length increases.

Finally, a preliminary CD spectroscopic measurement of the complex **(R,R,R,R)-Py**[6a]Pt** did not give a cotton signal in the range of 350–600 nm, presumably due to the low concentration that was used. The measurement was at a concentration ca. 0.01 mM, and the cuvette length was 5 mm.

4.4 Conclusions

Two hypotheses are provided. The first hypothesis is that the introduction of platinum cationic species to pyridyl-endcapped oligoynes (PEOs) can facilitate the non-covalent bonding between PEOs-Pt and graphene electrodes. The second hypothesis is that the introduction of chiral platinum complexes to PEOs could help understand the axial chirality of the PEOs backbone. Theoretically, the axial chirality can be visualized through the display of helical orbitals of the carbon chain; experimentally, the axial chirality can be observed through such as circular dichroism spectroscopic analysis. Toward each hypothesis, PEOs-Pt complexes have been designed and synthesized as models.

Due to limited time before the writing of this thesis, the project exploring PEO-Pt complexes has not yet been finished, and the characterization of these complexes is limited. This characterization includes mass spectrometric analyses and ^{1}H, ^{13}C, ^{31}P, ^{11}B, ^{19}F NMR spectroscopic analyses. The detailed characterization has been summarized in the experimental chapter (Chapter 7). While critical experiments, including the constructions and measurements of single-molecule junction, X-ray crystallographic analysis, UV-vis spectroscopic analysis, CD spectroscopic analysis, and theoretical calculations must be conducted in the future.

4.5 References

[1]   a) D. C. Milan, M. Krempe, A. K. Ismael, L. D. Movsisyan, M. Franz, I. Grace, R. J. Brooke, W. Schwarzacher, S. J. Higgins, H. L. Anderson, C. J. Lambert, R. R. Tykwinski, R. J. Nichols, *Nanoscale* **2017**, *9*, 355–361; b) C. Wang, A. S. Batsanov, M. R. Bryce, S. Martín, R. J. Nichols, S. J. Higgins, V. M. García-Suárez, C. J. Lambert, *J. Am. Chem. Soc.* **2009**, *131*, 15647–15654.

[2]   P. Moreno-Garcia, M. Gulcur, D. Z. Manrique, T. Pope, W. J. Hong, V. Kaliginedi, C. C. Huang, A. S. Batsanov, M. R. Bryce, C. Lambert, T. Wandlowski, *J. Am. Chem. Soc.* **2013**, *135*, 12228–12240.

[3]   E. Leary, A. La Rosa, M. T. Gonzalez, G. Rubio-Bollinger, N. Agrait, N. Martin, *Chem. Soc. Rev.* **2015**, *44*, 920–942.

[4]   a) F. Prins, A. Barreiro, J. W. Ruitenberg, J. S. Seldenthuis, N. Aliaga-Alcalde, L. M. Vandersypen, H. S. van der Zant, *Nano Lett.* **2011**, *11*, 4607–4611; b) Y. Li, C. Yang, X. Guo, *Acc. Chem. Res.* **2020**, *53*, 159–169; c) K. Ullmann, P. B. Coto, S. Leitherer, A. Molina-Ontoria, N. Martin, M. Thoss, H. B. Weber, *Nano Lett.* **2015**, *15*, 3512–3518; d) Y. Cao, S. Dong, S. Liu, L. He, L. Gan, X. Yu, M. L. Steigerwald, X. Wu, Z. Liu, X. Guo, *Angew. Chem. Int. Ed.* **2012**, *51*, 12228–12232.

[5]   M. Krempe, Pyridyl polyynes: synthesis and investigation toward stabilized molecular wires, PhD thesis, 2016, University of Erlangen-Nuremberg.

[6]   a) M. H. Garner, W. Bro-Jørgensen, G. C. Solomon, *J. Phys. Chem. C* **2020**, *124*, 18968–18982; b) M. H. Garner, C. Corminboeuf, *Org. Lett.* **2020**, *22*, 8028–8033; c) Y. Orimoto, Y. Aoki, A. Imamura, *J. Phys. Chem. C* **2019**, *123*, 11134–11139; d) M. H. Garner, A. Jensen, L. O. H. Hyllested, G. C. Solomon, *Chem. Sci.* **2019**, *10*, 4598–4608; e) M. H. Garner, R. Hoffmann, S. Rettrup, G. C. Solomon, *ACS Cent. Sci.* **2018**, *4*, 688–700; f) Y. Aoki, Y. Orimoto, A. Imamura, *ACS Cent. Sci.* **2018**, *4*, 664–665; g) A. Imamura, Y. Aoki, *Chem. Phys. Lett.* **2013**, *590*, 136–140; h) C. H. Hendon, D. Tiana, A. T. Murray, D. R. Carbery, A. Walsh, *Chem. Sci.* **2013**, *4*, 4278–4284; i) Y.-D. Guo, X.-H. Yan, Y. Xiao, *RSC Advances* **2013**, *3*, 16672–16680.

[7]   a) M. D. Peeks, P. Neuhaus, H. L. Anderson, *Phys. Chem. Chem. Phys.* **2016**, *18*, 5264–5274; b) J. A. Sebree, T. S. Zwier, *Phys. Chem. Chem. Phys.* **2012**, *14*, 173–183; c) P. W. Thulstrup, S. V. Hoffmann, B. K. Hansen, J. Spanget-Larsen, *Phys. Chem. Chem. Phys.* **2011**, *13*, 16168–16174.

[8]   Preliminary calculations from Chris Hendon and Aron Walsh.

[9]   Unpublished results, contributions from J. L. Marshall, Y. Gao, M. Krempe, R. Crespo-Otero, A. Walsh, M. J. Ferguson, R. McDonald, F. Hampel, C. H. Hendon, R. R. Tykwinski.

[10]   M. Krempe, R. Lippert, F. Hampel, I. Ivanovic-Burmazovic, N. Jux, R. R. Tykwinski, *Angew. Chem. Int. Ed.* **2016**, *55*, 14802–14806.

[11]   a) P. M. Treichel, K. P. Wagner, W. J. Knebel, *Inorg. Chim. Acta* **1972**, *6*, 674–676; b) C. Eaborn, N. Farrell, J. L. Murphy, A. Pidcock, *J. Chem. Soc., Dalton Trans.* **1976**, 58–67; c) F. Morandini, G. Consiglio, O. Piccolo, *Inorg. Chim. Acta* **1982**, *57*, 15–19.

[12] W. J. Cherwinski, H. C. Clark, *Can. J. Chem.* **1969**, *47*, 2665–2669.

[13] a) T. Luu, E. Elliott, A. D. Slepkov, S. Eisler, R. McDonald, F. A. Hegmann, R. R. Tykwinski, *Org. Lett.* **2005**, *7*, 51–54; b) T. Gibtner, F. Hampel, J. P. Gisselbrecht, A. Hirsch, *Chem. Eur. J.* **2002**, *8*, 408–432; c) R. R. Tykwinski, W. Chalifoux, S. Eisler, A. Lucotti, M. Tommasini, D. Fazzi, M. Del Zoppo, G. Zerbi, *Pure Appl. Chem.* **2010**, *82*, 891–904.

CHAPTER 5 – Hierarchical Synthesis, Structure, and Photophysical Properties of Gallium- and Ruthenium-Porphyrins with Axially Bonded Azo Dyes[*]

5.1 General introduction to azo compounds

Azobenzene derivatives have been developed as photoresponsive triggers in molecular machines,[1] biological systems,[2] and many other areas in which bistability is important.[3] In particular, the switchable nature of the azo group facilitates control of molecular configuration, and this property allows a desired function to be fine-tuned.[4] Finally, the attachment of multicomponent, switchable systems, such as an azo dye, to a surface is highly desirable to form functional nanosystems.[3a]

5.1.1 General methods of the synthesis of azo compounds

With the idea to use azo compounds as a functional molecular component, I will first introduce general synthetic methods of azo compounds. There have been numerous reports of methods to synthesize azo compounds, and the azo coupling reaction, the Mills reaction, and the oxidation of anilines are particularly described herein, given that these methods are widely used.[5]

In a typical azo coupling reaction, a primary amine is transformed to a diazonium salt in the presence of nitrous acid, which is usually formed in situ from $NaNO_2$ and HCl. After the addition of an aromatic nucleophile such as phenol, an azo compound is formed (Scheme 5.1). Nucleophilic aromatics are usually required to be activated by the introduction of electron donor groups to facilitate the coupling reaction. The substitution at the *para* position of the activated aromatic is preferred, unless this position is occupied, in which case the azo coupling reaction would occur at the *ortho* position. Additionally, the azo coupling reaction is pH dependent since a strong acid would protonate the primary amine, hindering the formation of the diazonium salt, while a slightly alkaline solution would facilitate the formation of more nucleophilic phenoxide species.
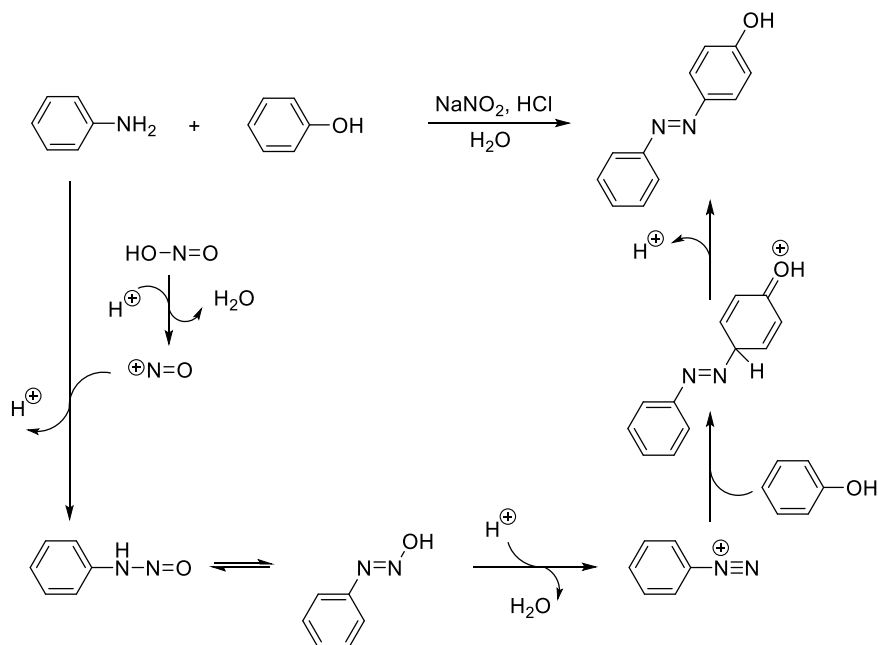
Scheme 5.1. Mechanism of an azo coupling reaction.

The reaction of nitroso derivatives and anilines in the presence of acetic acid is referred to as the Mills reaction. The nitroso derivatives are usually prepared from a primary amine or hydroxylamine under oxidation conditions, using tert-butyl hypochlorite, ferric chloride, or other oxidants.[5a, 6] Overoxidation to nitro derivatives should be avoided during the synthesis of nitroso derivatives; usually, low temperature and high dilution are applied. In particular, aniline reacts with acetic acid to form acetanilide, which works as a nucleophile to react with the nitroso derivative. The loss of acetic acid forms the corresponding azo compound (Scheme 5.2). Aromatic nitroso derivatives can also be produced from aromatic nitro derivatives in the presence of NaOH, K_2CO_3, and TDA-1 (tris[2-(2-methoxyethoxy)ethyl]amine) in xylene at reflux.[7] This method has been chosen for my synthesis and will be described in detail in Section 5.2. The Mills condition can tolerate many substituents, and the activation of a substrate is not required, so this reaction offers promise of the formation of a variety of azo compounds.[5]
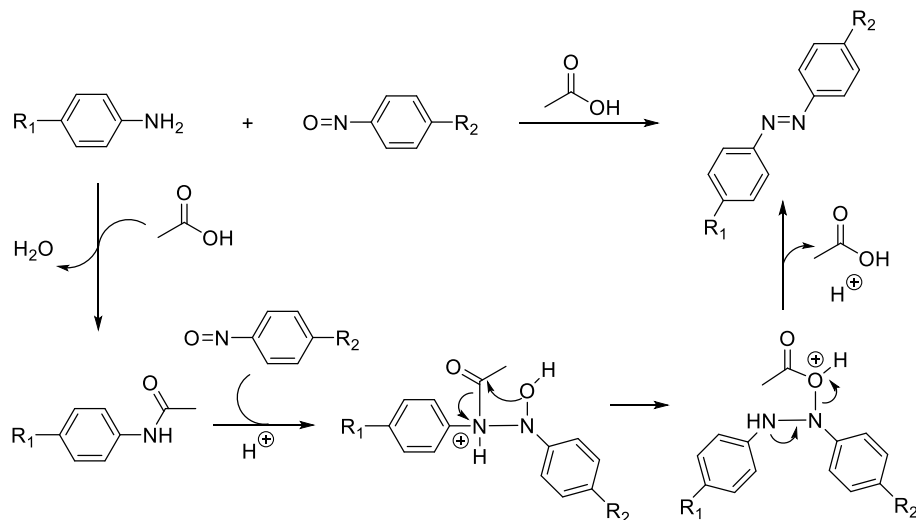
Scheme 5.2. Mechanism of a Mills reaction.

Oxidation of aniline derivatives has been a useful method to obtain symmetrical azo compounds.[5b] It has been reported that numerous oxidants can be applied in the formation of azo compounds.[5b] Usually these oxidants are stoichiometric and environmentally unfriendly.[5] Recently Zhang and co-workers used CuBr as the catalyst and O_2 as the oxidant in the presence of pyridine to synthesize azo compounds.[8] A plausible mechanism is provided by Zhang and co-workers, as shown in Scheme 5.3. The copper(I) salt is oxidized to the peroxo-dicopper(II) complex (**A**) by molecular oxygen. Then, the aromatic amine is oxidized by complex **A** through a single electron transfer process to a radical cation **B**, followed by coupling with another equivalent of the aromatic amine, forming an intermediate **C** with a three-electron sigma bond as reported in the literature.[8] Subsequently, compound **C** donates two protons and another electron through reaction with **A**, forming hydrazine **D**, which is then oxidized to the target azo compound. This method is used to synthesize my azo compounds and will further be described in Section 5.2.
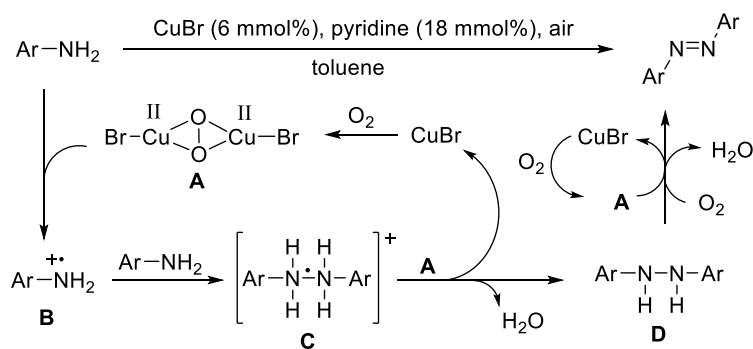
Scheme 5.3. Proposed mechanism of the oxidation of amines into azo compound.

5.1.2 Mechanism of photoisomerization of azobenzene

The *trans*-isomer of azobenzene (***trans*-AB**) has a planar conformation in its lowest energy state, with C_{2h} symmetry, as investigated by X-ray and computational results.[9] The planarity is severely distorted for the *cis*-isomer (***cis*-AB**), with a dihedral angle of 53.3° between the planes formed from two phenyl moieties.[10] Theories about the mechanism of photoisomerization, such as the rotation mechanism, inversion mechanism, concerted-inversion mechanism, and inversion-assisted rotation mechanism, have been proposed and argued.[11] Herein, the two most widely studied mechanisms are provided, based on the azobenzene model, as shown in Scheme 5.4.
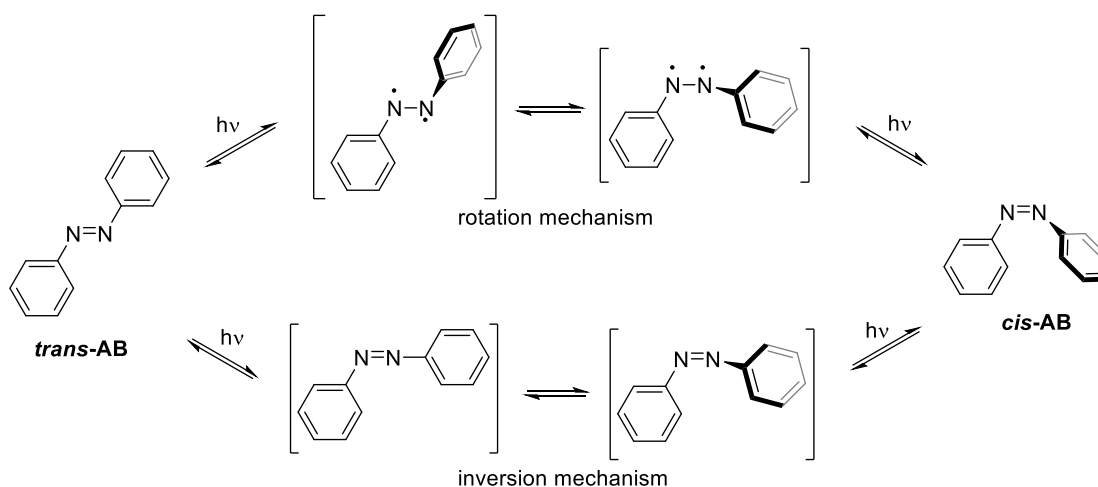
Scheme 5.4. Proposed mechanism of the rotation and inversion pathways of the *trans*/*cis* isomerization of azobenzene (**AB**).

The rotation mechanism involves breaking the π-bond of the N=N moiety so that free rotation around the N–N single bond eventually furnishes the isomerization. This process includes the change of the C–N–N–C dihedral angle, while the N–N–C angle stays at about 120°. For the inversion pathway, one nitrogen atom adapts *sp*-hybridization, generating a linear conformation with a N=N–C of 180°, during which the C–N=N–C dihedral angle stays at 0°. Eventually, the isomerization is completed along with the rehybridization to sp^2.

5.1.3 Azo compounds as a functional moiety on surface

A switchable system containing an azo compound on a surface can form a functional nanosystem. As an elegant example, a "platform approach" has been developed by Herges and co-workers that allows for the organization of free-standing molecules on a Au surface, based on the design and synthesis of triazatriangulenium (TATA) moieties as the platform.[12] As an alternative to the use

of triazatriangulenes as platforms,[13] porphyrins are flat, π-rich molecules, and they are well-known in constructing a self-assembly on surfaces such as highly ordered pyrolytic graphite (HOPG) and metals.[14] Furthermore, metalloporphyrins can be readily modified through coordination of ligands to metal ions in the axial position.[15] Thus, the platform approach toward functional molecular nanostructures could be potentially advanced through the development of versatile protocols using porphyrins as platforms.

An intriguing system was recently reported by Hopkins and co-workers, in which Ga-porphyrins were successfully assembled on the surface of HOPG.[16] This study utilized a simple metal acetylide ligand, which was placed in an orthogonal orientation to the surface through bonding to the platform. Intrigued by the concept of hierarchical assembly building from Ga-porphyrins, we have devised a protocol that allows a range of acetylides to be appended as ligands via axial bonding to a Ga-porphyrin.[17] The conjugation length and electronic composition of the ligands could be controlled through the selection of the alkyne chosen to form the acetylide, which allows the strategic placement of further functionality above the surface.

Building on the concept of Ga-porphyrins as a platform, the attachment of photoresponsive groups as axial ligands was envisioned toward systems suitable for free standing surface functionalization. There have been reported examples of photoswitches attached to porphyrins, particularly by the work of Herges and co-workers.[18] Furthermore, the tethering of two porphyrins with an azo-bridge via either a *meso-meso*- or β-β-linkage has also been explored,[19] as well as the supramolecular axial coordination of metalloporphyrins.[20] The direct attachment of an azo-switch via an axial covalent bond to a porphyrin is, however, rare and, to the best of my knowledge, this motif is limited to phosphorus porphyrins reported by Reddy et al.[21] and a Rh-porphyrin by Yao et al.[22]

Herein, I will present our strategy to use axial bonding between the metal atom of a Ga-porphyrin and acetylide ligands bearing an azo moiety toward creating a platform for switchable systems. The method is modular, allowing the hierarchical elaboration to form an unsymmetrical bisporphyrin via a coordination bond between an azo-pyridyl ligand and a Ru-porphyrin. Alternatively, symmetrical bisporphyrins can be assembled through bridging either two Ga-porphyrins between a diacetylenic azo linker or two Ru-porphyrins between a bipyridyl linker.

5.2 Synthesis of *trans*-ligands of L1–L5

The assembly of the desired porphyrinic systems required ligands *trans*-L1–L5 (Scheme 5.5 and 5.6). The synthesis of ligand *trans*-L1 began with the preparation of 4-acetamido-pyridine (**5.1**) using 4-aminopyridine and isopropenyl acetate, as reported in the literature (Scheme 5.5a).[23] Then, the Mills reaction[7] of **5.1** and 1-bromo-4-nitrobenzene produced the azo compound **5.2** in a moderate yield. Subsequent Sonogashira cross-coupling[24] of **5.2** with 2-methyl-3-butyn-2-ol gave **5.3**. The use of 2-methyl-3-butyn-2-ol as the alkyne source was required for the synthesis of ligand **5.3** since incomplete conversion during the Sonogashira cross-coupling of **5.2** and trimethylsilylacetylene led to a problematic separation and low yields. Liberation of the acetylene group was accomplished via reaction of **5.3** with NaOH in toluene (110 °C) and furnished the desired ligand *trans*-L1. Following an analogous strategy, the known azo compound **5.5**[25] was subjected to a Sonogashira cross-coupling reaction with trimethylsilylacetylene to give **5.6**, followed by deprotection with K_2CO_3 to give ligand *trans*-L2 in excellent yield (Scheme 5.5b).
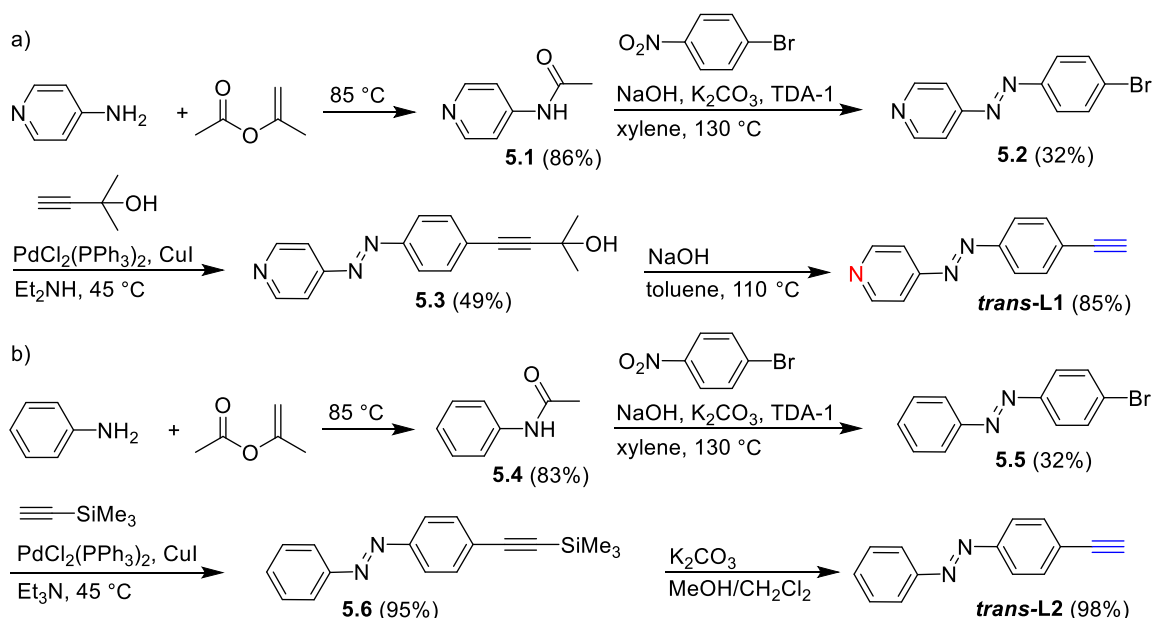
Scheme 5.5. Synthesis of azo ligands a) *trans*-L1 and b) *trans*-L2.

The synthesis of ligands *trans*-L3[26], *trans*-L4[27], and *trans*-L5[28] has been reported in the literature. A brief description of these syntheses is presented herein (Scheme 5.6). Oxidation of 4-iodoaniline using CuCl and pyridine in the air furnished the synthesis of azo compound **5.7** in a moderate yield of 44%. Then, **5.7** was subjected to a Sonogashira double cross-coupling

reaction with trimethylsilylacetylene, giving compound **5.8**. Subsequent deprotection using tetrabutylammonium fluoride (TBAF) in wet THF gratifyingly furnished the synthesis of ***trans*-L3** in excellent yield (Scheme 5.6a). Oxidation of 4-aminopyridine using sodium hypochlorite gave ***trans*-L4** (Scheme 5.6b). Finally, using an analogous strategy, a Sonogashira cross-coupling of **5.9**[28] with 2-methyl-3-butyn-2-ol gave **5.10**, which was deprotected to give the model compound ***trans*-L5** (Scheme 5.6c).
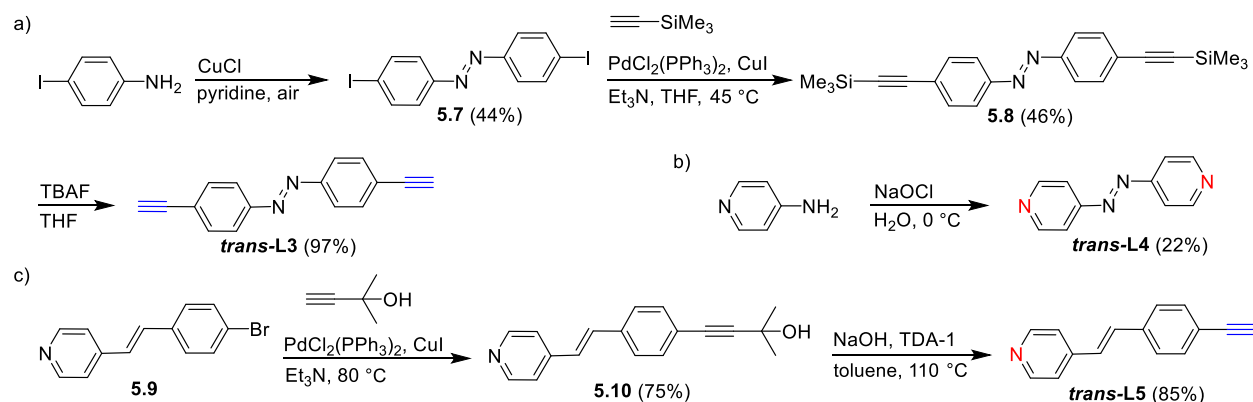
Scheme 5.6. Synthesis of azo ligands a) **L3** and b) **L4**, as well as c) the model ligand **L5**.

5.3 Synthesis of gallium- and ruthenium-porphyrins with axially bonded azo dyes

5.3.1 Synthesis of starting porphyrins

Ga(tpfpp)Cl (**5.11**) was synthesized as described in the literature.[29] Ru(tpfpp)(CO)(MeCN) (**5.12**) was formed by stirring Ru(tpfpp)(CO)[30] in a MeCN solution through adaption of a procedure reported in the literature.[17] Ru(tpfpp)(CO)(pyridine) (**5.13**) was formed from **5.12** via reaction with pyridine through adaption of the procedure reported in the literature (Figure 5.1).[31]
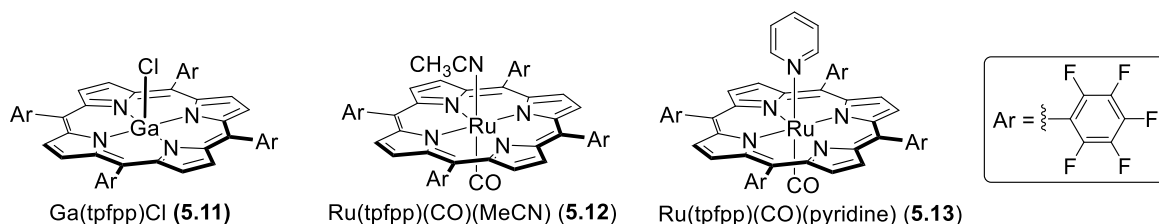
Figure 5.1. Molecular structures of **5.11–5.13**.

5.3.2 Synthesis of *trans*-L1–L5 containing porphyrins

Initial attempts to assemble **GaL1** (see Scheme 5.7 for structure) used *n*BuLi to form the acetylide

from ***trans*-L1** (5 equiv), followed by reaction with Ga(tpfpp)Cl (**5.11**).[29] This approach, however, was unsuccessful and led to a complex, unidentifiable mixture. Ligand ***trans*-L1** could be recovered from the resulting reaction mixture, but the desired product could not be isolated chromatographically (silica gel, alumina, or size exclusion). On the other hand, using lithium bis(trimethylsilyl)amide (LiHMDS) smoothly gave the acetylide from ***trans*-L1**, which was then treated with porphyrin **5.11** in a solution of THF, and isolation of the product by size exclusion chromatography gave **GaL1** in good yield (Scheme 5.7). It is noted that the incorporation of perfluorophenyl groups in the *meso*-positions of the porphyrin increases the persistence of the resulting complexes in comparison to nonfluorinated arenes, as a result of a stronger metal–acetylide bond.[17]

As a model compound for comparison to **GaL1** that does not contain the coordinating pyridyl ligand, complex **GaL2** was prepared in 93% yield via lithiation of ***trans*-L2** with *n*BuLi and addition to porphyrin **5.11** in a solution of toluene (Scheme 5.7). Both compounds **GaL1** and **GaL2** are stable solids that slowly hydrolyze in solution to liberate the free azo ligand, presumably due to the presence of adventitious water.
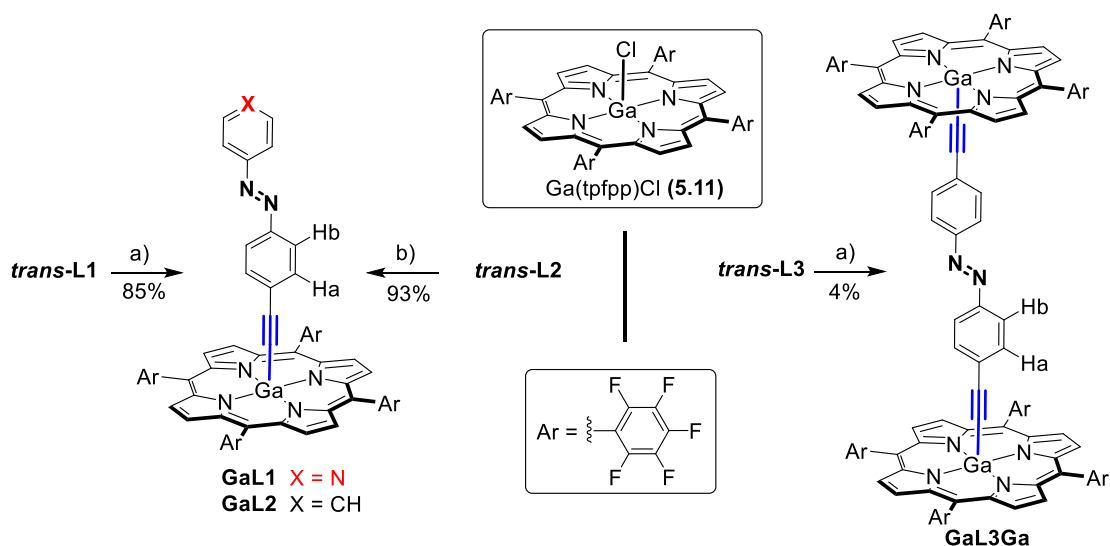
Scheme 5.7. Synthesis of porphyrins **GaL1**, **GaL2**, and **GaL3Ga**. Reagents and conditions: a) LiHMDS, then Ga(tpfpp)Cl (**5.11**), THF, –78 °C to rt; b) *n*BuLi in hexanes, then **5.11**, toluene/THF (5:2), –78 to 50 °C.

As observed in efforts to form **GaL1**, using *n*BuLi to form the acetylide of ***trans*-L3** and subsequent reaction with porphyrin **5.11** failed to give the target complex **GaL3Ga**. Formation of

GaL3Ga was, however, successful using LiHMDS to form the acetylide, although only very low yields could be isolated pure (4%; Scheme 5.7). In attempts toward optimization, the deprotonation process was examined through formation of the acetylide with either *n*BuLi or LiHMDS and quenching with D_2O (Figure 5.2). The former reaction gave an unidentified mixture of products, based on the analysis of proton integration (with non-integer protons) in the ^1H NMR spectrum; the triplet and quintet patterns in the ^1H NMR spectrum seems to indicate the incorporation of the butyl group into one product of the mixture. The later reaction gave deuterated *trans*-L3, based on the loss of the acetylide proton signal in the spectrum, suggesting that the deuterated acetylide had been formed successfully. Nevertheless, the reaction to form **GaL3Ga** could not be easily optimized, and additional efforts were abandoned.
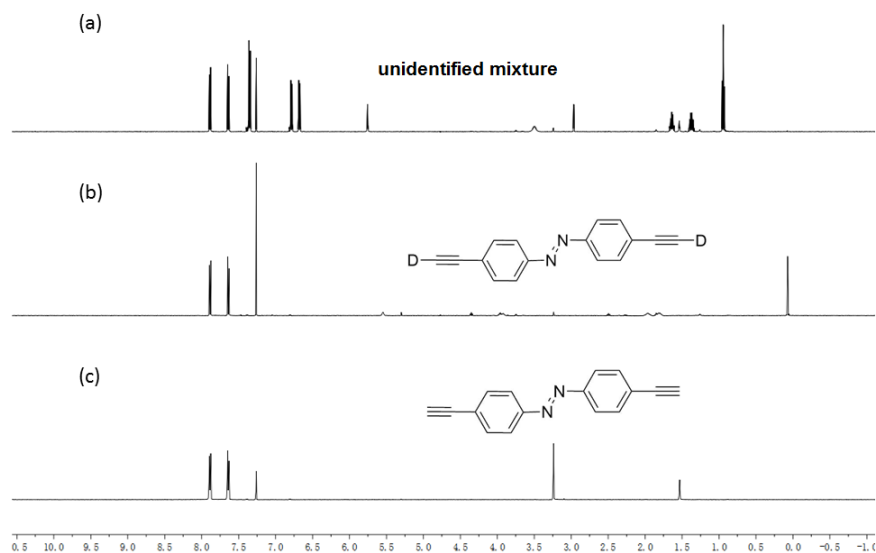
Figure 5.2. ^1H NMR spectra (in $CDCl_3$) of: (a) *trans*-L3 following deprotonation using *n*BuLi (2.2 equiv) and subsequent quenching by addition of D_2O, (b) *trans*-L3 following deprotonation using LiHMDS (2.2 equiv) and subsequent quenching by addition of D_2O, and (c) *trans*-L3.

The pyridyl groups in ligands *trans*-L1 and *trans*-L4 allow for an alternative approach toward a platform design beyond σ-acetylide complexes, namely through a coordinative self-assembly between the pyridyl group and a second metalloporphyrin. A Ru-metalloporphyrin with a CO ligand was chosen since pyridyl coordination to the metalloporphyrin is known to be strong and ligand-exchange slow,[32] which is advantageous when constructing porphyrin assemblies in solution (Scheme 5.8).[33] Thus, **RuL1** and **RuL4Ru** were formed by the complexation of Ru(tpfpp)(CO)(MeCN) (**5.12**) with *trans*-L1 and *trans*-L4, respectively, and the products were

purified by column chromatography and isolated in good yields. Finally, the strategic expansion of the framework of the **GaL1** was then targeted, and the bimetallic porphyrin system **GaL1Ru** was formed through the reaction of platform **GaL1** with porphyrin **5.12** in toluene (Scheme 5.8). The product could be isolated pure by size-exclusion chromatography to give **GaL1Ru** in 44% yield as a dark red solid that was stable >1 year when stored either as a solid at rt or as a frozen solution in benzene under refrigeration (–20 °C). Finally, **GaL5Ru** was formed from *trans*-**L5** for use as a model compound, in which the ligand lacks the azo moiety for comparisons to compound **GaL1Ru** (Scheme 5.8).

Scheme 5.8. Synthesis of porphyrins **RuL1**, **RuL4**, **GaL1Ru**, and **GaL5Ru**. Reagents and conditions: a) Ru(tpfpp)(CO)(MeCN) (**5.12**), CH₂Cl₂, rt; b) **5.12**, toluene, 50 °C; c) LiHMDS, then Ga(tpfpp)Cl (**5.11**), THF, –78 °C to rt.

5.4 Structural characterization of the porphyrin complexes

The formation of **GaL1**, **GaL2**, **GaL3Ga**, **GaL1Ru**, **GaL5Ru**, **RuL1**, and **RuL4Ru** has been confirmed by mass spectrometry (MS) combined with ^{1}H, ^{13}C, ^{19}F, and 2D (^{1}H–^{1}H COSY, HSQC, HMBC) NMR spectroscopic analyses. A common feature of the spectroscopic characterization of all axial-bonded complexes is the dramatic "upfield" shift of the aryl protons of the ligands (Ha–Hd) in the ^{1}H NMR spectra, as a result of diamagnetic shielding from the porphyrin (see Schemes 5.7 and 5.8 for proton labelling). Furthermore, individual resonances of all five fluorine atoms of the *meso*-pentafluorophenyl groups are found in the ^{19}F NMR spectra, with the expected F–F coupling. Inequivalence of the fluorine atoms of the *meso*-aryl groups is significant, as it confirms that dissociation of the axial acetylide from the Ga-porphyrin does not occur (at least on the timescale of the NMR experiments). Finally, strong signals are observed for [M]$^+$ at *m/z* 1247.0402,

1246.0439, and 2310.0063 for **GaL1**, **GaL2**, and **GaL3Ga**, respectively, in the atmospheric pressure photoionization (APPI) HRMS analysis. Complexes **GaL1Ru**, **RuL1**, and **RuL4Ru**, on the other hand, show loss of the Ru-porphyrin moiety under APPI MS analysis, along with fragmentation patterns consistent with their proposed structure. Interestingly, under matrix-assisted laser desorption/ionization (MALDI) HRMS analysis using *trans*-2-[3-(4-*tert*-butylphenyl)-2-methyl-2-propenylidene]malononitrile (DCTB) as matrix, two strong signals are observed for the complex **GaL5Ru**. One signal is observed for $[M - (CO)]^+$ at *m/z* 2318.9969, and the other signal is observed for $[M - (CO) + DCTB]^+$ at *m/z* 2569.1484.

It is noted that UV-vis and NMR spectroscopic characterization, supported by X-ray crystallography, conclusively corroborates the clean conversion of the *trans*-ligand to the *trans*-isomer of **GaL1**, **GaL2**, **GaL3Ga**, **GaL1Ru**, **GaL5Ru**, **RuL1**, and **RuL4Ru**. The configuration of ligands **L1**–**L5** as the pure *trans*-isomers has been established by their ^{1}H NMR spectra that show only one set of AA'BB' resonances for each ligand. Upon irradiation of *trans*-**L1** and *trans*-**L2** at 365 nm, a new set of resonances appears and finally reaches PSS, as shown in the ^{1}H NMR spectra (see the experimental section in Chapter 7). Furthermore, characteristic UV-vis spectroscopic changes are observed as a function of irradiation time, with the corresponding decrease in the π–π* transition, which are completely consistent with literature reports (see detailed discussions in Section 5.4.4).[34] Likewise, as synthesized from isomerically pure ligands, the platforms **GaL1**, **RuL1**, **GaL2**, **GaL1Ru, GaL3Ga**, **RuL4Ru**, and **GaL5Ru** are also isolated as pure *trans*-isomers, as established by their ^{1}H NMR spectra showing only one set of AA'XX' resonances, consistent with that observed for the unbound ligand. Furthermore, X-ray crystallographic analysis of **RuL1** and **RuL4Ru** corroborate the *trans*-configuration (see detailed discussions in Section 5.4.1).

5.4.1 X-ray crystallographic analysis

X-ray crystallographic analysis has been successful for **RuL1** and **RuL4Ru**, confirming both the proposed structure and stereochemistry about the azo moiety (Figure 5.3). In both molecules, the Ru-porphyrin features a six-coordinate geometry, with slightly distorted octahedral geometry. The carbon and nitrogen framework of porphyrin ring is essentially planar in both cases, and the mean deviations from the least-squares planes (porphyrin-*N,N,N,N*-plane) fall within the range of –0.106(9) to 0.078(7) Å for **RuL1** and –0.220(5) to 0.039(4) Å for **RuL4Ru**. The Ru atom is

situated above this plane by 0.061(2) Å and 0.0718(10) Å for **RuL1** and **RuL4Ru**, respectively. The axial pyridyl ligands are close to perpendicular to the porphyrin rings, with N(py)–Ru–N(pyrrole) angles ranging from 87.61(16)° to 88.74(16)° for **RuL1** and 86.12(8)° to 89.31(8)° for **RuL4Ru**. Furthermore, the N(py)–Ru–C(CO) angles of **RuL1** and **RuL4Ru** are nearly linear at 177.6(2)° and 179.22(11)°, respectively. With respect to the ligand, the dihedral angle between the pyridyl and the phenylene ring of *trans*-**L1** is only 13.9(2)°, while the two pyridyl rings of *trans*-**L4** are coplanar (as determined by planes generated from the six atoms of the aryl groups of the linkers). Finally, the solid-state structures highlight that the presence of the CO ligand complicates the use of Ru-porphyrins as part of a platform strategy, although the photochemical removal of the CO group is possible (*vide infra*).[20g, 35]
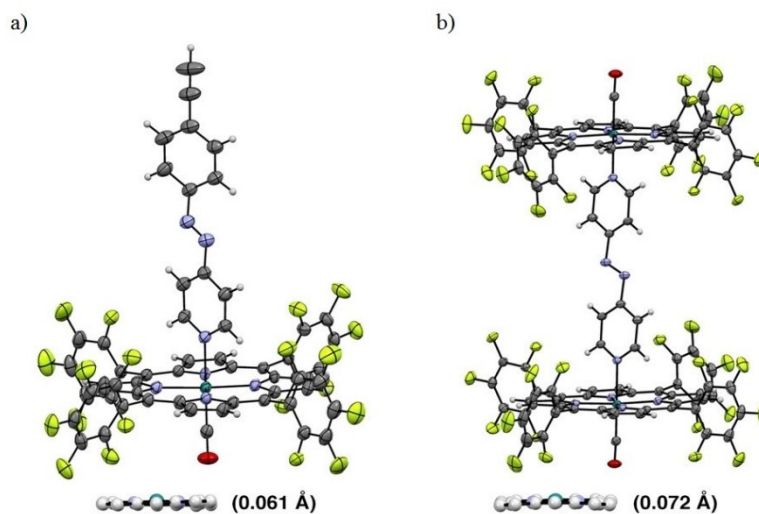
Figure 5.3. Top: ORTEP drawing of a) **RuL1** and b) **RuL4Ru**. Bottom: Side view of the porphyrin rings and the displacement (Å) of the Ru atom out of the plane of the porphyrin for a) **RuL1** and b) **RuL4Ru**. Thermal ellipsoids drawn at 30% probability; gray carbon, red oxygen, lime green fluorine, purple nitrogen, white hydrogen, green ruthenium; CCDC 1999060 (**RuL1**) 1999059 (**RuL4Ru**).

5.4.2 ^{1}H NMR characterization

The β-protons of the Ga-porphyrins of **GaL1** and **GaL2** are easily assigned as the most downfield singlets, with an integration of 8H and an identical chemical shift at δ 8.94. The resonances of the β-protons are shifted very slightly upfield to δ 8.86 in sandwiched complexes of **GaL1Ru** and **GaL3Ga** upon addition of the second porphyrin. Likewise, the chemical shift of the β-protons for the Ru-porphyrins of **GaL1Ru** (δ 8.54) and **RuL4Ru** (δ 8.52) are shifted slightly upfield from

those of **RuL1** (δ 8.65) by a similar amount (ca. 0.1 ppm). Thus, the β-protons appear to experience a slight effect from diamagnetic anisotropy (DA) over a distance of almost 1.3 nm from the second porphyrin, as estimated from the crystal structure of **RuL4Ru** (see Figure 5.6b for details).

The assignment of individual protons of the azo ligands used in the formation of the platforms is reasonably straightforward. A comparison of coupling patterns and constants allows separation into independent spin systems, H_a/H_b and H_c/H_d, while HMBC experiments reveal ^3J correlations between H_a and the neighboring acetylenic carbon that allow the distinction between H_a and H_b (see the experimental section in Chapter 7 for spectra and details). In the case of ***trans*-L2**, COSY experiments show that the correlation of $H_d \leftrightarrow H_p$ (H_p the proton at the *para* position of ***trans*-L2**) is stronger than that of $H_c \leftrightarrow H_p$, providing the identification of H_c and H_d, while analysis of HSQC and HMBC spectra of ***trans*-L1** allows distinction of H_c and H_d (Figure 5.4).
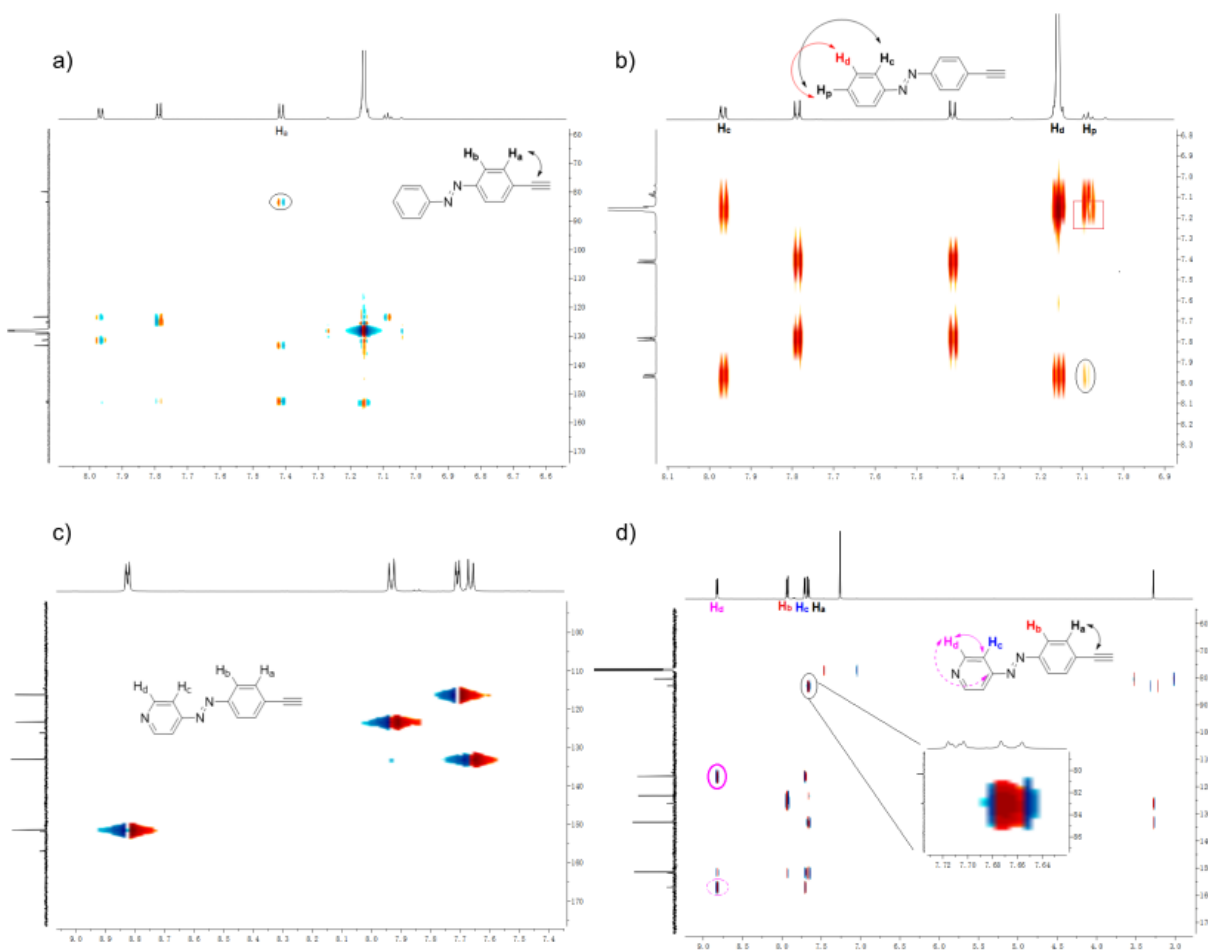
Figure 5.4. a) ^1H–^{13}C HMBC and b) ^1H–^1H COSY spectra of ***trans*-L2** in C_6D_6. c) ^1H–^{13}C HSQC and d) ^1H–^{13}C HMBC spectra of ***trans*-L1** in CDCl$_3$.

The protons H_a–H_d of ligands of metalloporphyrins are consistently shifted upfield in comparison to those of the free azo ligands, respectively, as expected due to the DA of the metalloporphyrins (Table 5.1). For example, protons H_a–H_d of free ligand *trans*-**L1** are found at δ 7.37, 7.68, 7.38, 8.63, respectively, and they are shifted to δ 7.05, 6.95, 5.01, and 1.74, respectively, in **RuL1**. A comparison of **GaL1** and **GaL2** to the free ligands *trans*-**L1** and *trans*-**L2** verifies that the influence of the Ga-porphyrin on each ligand is nearly the same. Protons H_a/H_b are shifted from δ 7.37/7.68 and 7.40/7.78 in *trans*-**L1** and *trans*-**L2**, respectively, to δ 5.40/5.43 and 6.72/6.82 for **GaL1** and **GaL2**, respectively.

Table 5.1. Selected ^{1}H NMR chemical shifts of *trans*-**L1**, **GaL1**, **RuL1**, **GaL1Ru**, *trans*-**L2**, **GaL2**, *trans*-**L3**, **GaL3Ga** in C$_6$D$_6$, and *trans*-**L4**, **RuL4Ru** (ppm, in CDCl$_3$).

proton	L1	GaL1	RuL1	GaL1Ru	L2	GaL2	L3	GaL3Ga	L4[a]	RuL4Ru[a]
H$_a$	7.37	5.40	7.05	5.09	7.40	5.43	7.39	5.20	–	–
H$_b$	7.68	6.72	6.95	6.00	7.78	6.82	7.73	6.37	–	–
H$_c$	7.38	6.99	5.01	4.62	7.96	7.57	–	–	7.74	5.03
H$_d$	8.63	8.38	1.74	1.49	7.15[b]	6.94	–	–	8.88	1.32
β-H	–	8.94	8.65	8.86/8.54	–	8.94	–	8.86	–	8.52

[a] measured in CDCl$_3$, [b] Signals are coincident with C$_6$D$_6$.

The "sandwich" structure of **GaL1Ru**, **GaL3Ga**, and **RuL4Ru** provides a stronger shielding environment to the ligand when the second porphyrin is added. For example, signals for H_a–H_d of **GaL1Ru** at δ 5.09, 6.00, 4.62, and 1.49 are shifted upfield when compared with **GaL1** (δ 5.40, 6.72, 6.99, and 8.38) and **RuL1** (δ 7.05, 6.95, 5.01, and 1.74), which show that the effects on proton resonances resulting from the Ga-porphyrin and Ru-porphyrin are approximately cumulative (see Figure 5.5 and Table 5.2 for details). To be more specific, the $\Delta\delta$ values between **GaL1** and **L1** ($\delta_{L1} - \delta_{GaL1}$) for protons H_a–H_d are 1.97, 0.96, 0.39, and 0.25 ppm, respectively; the $\Delta\delta$ values between **RuL1** and **L1** ($\delta_{L1} - \delta_{RuL1}$) for protons H_a–H_d are 0.32, 0.73, 2.37, and 6.89 ppm, respectively; the $\Delta\delta$ values between **GaRuL1** and **L1** ($\delta_{L1} - \delta_{GaL1Ru}$) for protons H_a–H_d are 2.28, 1.68, 2.76, and 7.14 ppm, respectively. Thus, the sum of ($\delta_{L1} - \delta_{GaL1}$) and ($\delta_{L1} - \delta_{RuL1}$) is essentially the same with ($\delta_{L1} - \delta_{GaL1Ru}$) (2.29, 1.69, 2.76, and 7.14 ppm vs. 2.28, 1.68, 2.76, and 7.14 ppm).
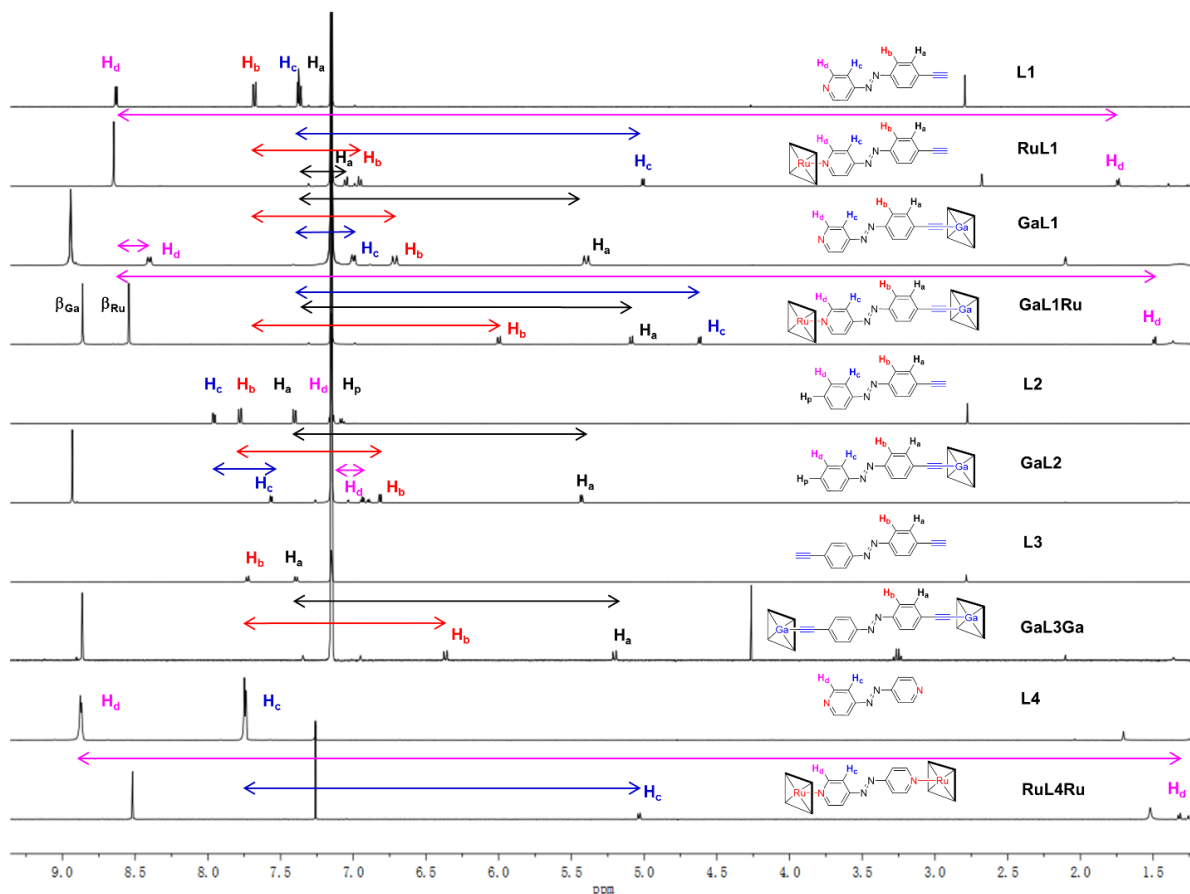
Figure 5.5. ^{1}H NMR spectra of *trans*-**L1**, **RuL1**, **GaL1**, **GaL1Ru**, *trans*-**L2**, **GaL2**, *trans*-**L3**, and **GaL3Ga** in C_6D_6 and *trans*-**L4** and **RuL4Ru** in $CDCl_3$. Arrows designate the change of chemical shift between free ligand and the resulting porphyrin complex.

Table 5.2. Differences of chemical shifts ($\Delta\delta$ in ppm) of protons H_a–H_d as measured in C_6D_6.[a]

$\Delta\delta$ (ppm)	H_a	H_b	H_c	H_d
$\delta_{L2} - \delta_{GaL2}$	1.97	0.96	0.39	0.21
$\delta_{L1} - \delta_{GaL1}$	1.97	0.96	0.39	0.25
$\delta_{L1} - \delta_{RuL1}$	0.32	0.73	2.37	6.89
$(\delta_{L1} - \delta_{GaL1}) + (\delta_{L1} - \delta_{RuL1})$	2.29	1.69	2.76	7.14
$\delta_{L1} - \delta_{GaL1Ru}$	2.28	1.68	2.76	7.14
$\delta_{L3} - \delta_{GaL3Ga}$	2.19	1.37	–	–
$\delta_{L4} - \delta_{RuL4Ru}$	–	–	2.71	7.56

[a]All ligands are the *trans*-isomer.

5.4.3 Diamagnetic anisotropy analysis

It is interesting to consider the development of a simple, predictive analysis for the cumulative

effects from DA on chemical shifts of ligand protons as a function of distance, r, of the proton from the porphyrins. This general topic has been discussed in the literature, and these studies suggest that such estimates can be complicated by both orientation of the proton in the "shielding cone" of the porphyrin and its distance from the porphyrin.[36] More recently, however, Stanger has shown that, based on $NICS_{\pi,zz}$ calculations, at a distance r greater than 2 Å, the maximum DA is found approximately at the geometrical center above the aromatic molecule.[37] Adapting the proposal of Stanger to the analysis of experimental chemical shifts suggests that the effect of DA can be approximated through the relationship of $\Delta\delta(r)$, where r is the distance of the proton from the plane of the aromatic system. The experimental data for chemical shifts would thus fit to a two-parameter power law of the form:

$$\Delta\delta(r) = ka^r \qquad \text{eq (1)}$$

where $\Delta\delta(r)$ represents the change in chemical shift in the presence of DA at a distance r from the porphyrin, 'a' and 'k' are fitting parameters, and 'k' indicates how fast the anisotropy effect decays versus the distance. Importantly, as $r \to \infty$, a limiting value of $\Delta\delta_\infty = 0$ is achieved, and the effects of DA would no longer discernible by the NMR measurement.[38]

The effects of DA arising from a Ru-porphyrin could be evaluated using **RuL1** and considering the difference in chemical shift between the free ligand and the porphyrin complexes, $\Delta\delta$ (in ppm) as a function of the distance (r in Å) of protons to the porphyrin plane. Values of r are obtained by calculating the distance between protons H_a–H_e and a plane generated from 24 carbon and nitrogen atoms of Ru-porphyrin in the solid-state structure (Figure 5.6).
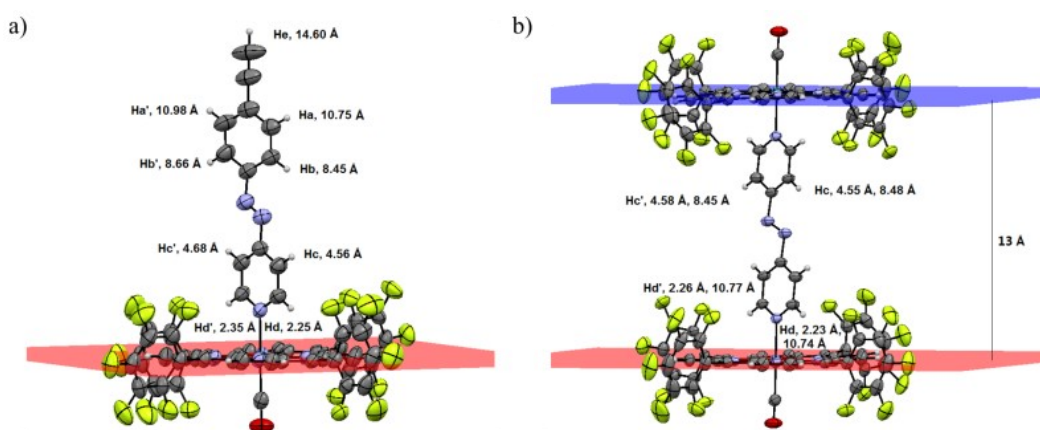
Figure 5.6. X-ray crystallographic structure of a) **RuL1** and b) **RuL4Ru** and the labels of the distance between protons and the plane of Ru-porphyrin ring (a plane generated from the porphyrin ring of 24 atoms).

Using $\Delta\delta$ and r values for **RuL1**, analysis using eq (1) gives $a = 0.61 \pm 0.03$ and $k = 22.75 \pm 2.64$ for experimental data measured in CDCl$_3$ (see Figure 5.7 and Table 5.3 for details). As a test, using the parameters from eq (1), eq (2) was given in the below form and applied to the sandwich **RuL4Ru** system:

$$\Delta\delta'(r) = \Delta\delta(r_1) + \Delta\delta(r_2) = 22.75(0.61^{r_1} + 0.61^{r_2}) \qquad \text{eq (2)}$$

where $\Delta\delta'(r)$ represents the change in chemical shifts in the presence of DA at a distance r_1 from a porphyrin and a distance r_2 from anther porphyrin. The calculated values for protons ($\Delta\delta'$) in **RuL4Ru** were obtained by summing the contributions to diamagnetic shielding from the two Ru-porphyrins ($\Delta\delta(r_1)$ and $\Delta\delta(r_2)$), based on eq (2), and using X-ray data to estimate r (i.e., $\Delta\delta' = \Delta\delta(r_1) + \Delta\delta(r_2)$, see Table 5.4 for details). The analysis using eq (2) for **RuL4Ru** predicts upfield shifts of $\Delta\delta' = 7.48$ and 2.73 ppm for protons H_d and H_c, respectively, which match well with the experimentally measured values of 7.56 and 2.71 ppm, respectively. The slight deviations between calculated and experimental chemical shifts likely arise from the estimation of r using X-ray crystallographic data, which offers only a static analysis for a clearly dynamic system (e.g., via bond bending) in solution. The fit to eq (1) provides a quantitative analysis and nicely verifies the additive effect of the two porphyrin rings although both constants a and k would be expected to vary with substrate and ligand. Finally, taking into account of the accuracy of the NMR spectroscopy (±0.001 ppm), the anisotropy effect would be predicted to disappear at distances greater than ca. 20.0 Å.[38]
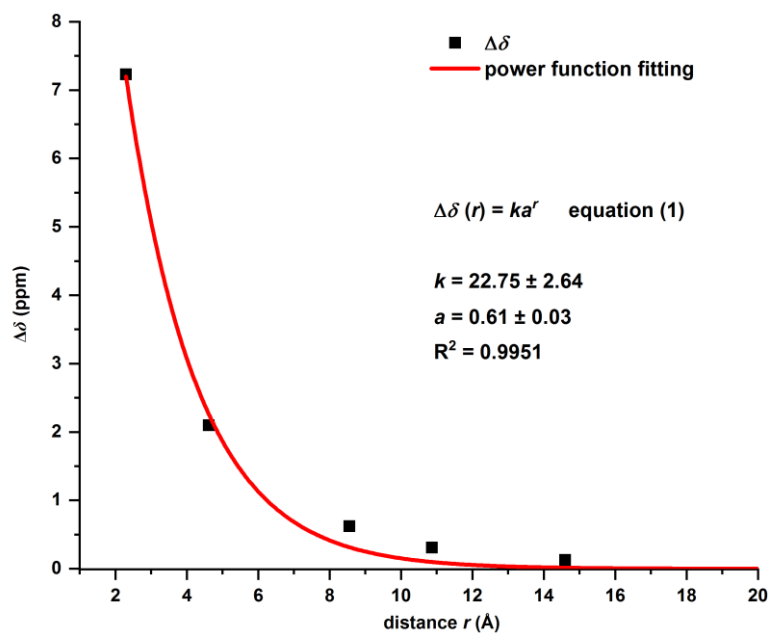
Figure 5.7. Fitting of $\Delta\delta(r)$ ($\Delta\delta = \delta(r)_{\text{L1}} - \delta(r)_{\text{RuL1}}$, at distance r), as measured in CDCl$_3$, where r is the distance measured between the proton and the plane of the Ru-porphyrin ring (a plane generated from the porphyrin ring of 24 atoms).

Table 5.3. $\Delta\delta(r)^a$ as a function of distance r between protons H$_a$–H$_e$ and the plane^b of the Ru-porphyrin ring according to eq (1).

proton	Distance r (Å)	$\Delta\delta(r)$ exp (ppm)	$\Delta\delta(r)$ calc (ppm)	Error
H$_e$	14.60	0.13	0.02	0.11
H$_a$	10.87^c	0.31	0.10	0.21
H$_b$	8.56^c	0.62	0.31	0.31
H$_c$	4.62^c	2.10	2.26	0.16
H$_d$	2.30^c	7.23	7.20	0.03

$^a\Delta\delta(r) = \delta(r)_{\text{L1}} - \delta(r)_{\text{RuL1}}$, difference in chemical shifts of analogous protons of **RuL1** and *trans*-**L1** in ppm as measured in CDCl$_3$. ^{b}A plane generated from the porphyrin ring of 24 atoms. ^{c}The averaged length of two individual protons.

Table 5.4. $\Delta\delta(r)^a$ as a function of distances r_1 and r_2 between protons and planes of the two Ru-porphyrin rings according to eq (2).

	distance r_1 (Å)[b]	$\Delta\delta(r_1)$ (ppm)[d]	distance r_2 (Å)[c]	$\Delta\delta(r_2)$ (ppm)[d]	$\Delta\delta'_{calc}$ (ppm)[e]	$\Delta\delta_{exp}$ (ppm)
$H_c/H_{c'}$	4.57	2.38	8.47	0.35	2.73	2.71
$H_d/H_{d'}$	2.28	7.37	10.76	0.11	7.48	7.56

[a]$\Delta\delta(r) = \delta(r)_{L4} - \delta(r)_{RuL4Ru}$, for chemical shifts of analogous protons of **RuL4Ru** and **trans-L4** in ppm, as measured in CDCl$_3$. [b]The averaged distance r to one porphyrin ring. [c]The averaged distance r to the other porphyrin ring. [d]The calculated $\Delta\delta(r_1)$ and $\Delta\delta(r_2)$ uses equation (2); the calculation is shown below: [e]$\Delta\delta'_{cal} = \Delta\delta(r_1) + \Delta\delta(r_2)$. For protons Hc/c': $\Delta\delta(4.57$ Å$) = 22.75*(0.61)^{4.57} = 2.38$ ppm; $\Delta\delta(8.47$ Å$) = 22.75*(0.61)^{8.47} = 0.35$ ppm; $\Delta\delta'_{calc} = 2.73$ ppm. For protons Hd/d': $\Delta\delta(2.28$ Å$) = 22.75*(0.61)^{2.28} = 7.37$ ppm; $\Delta\delta(10.76$ Å$) = 22.75*(0.61)^{10.76} = 0.11$ ppm; $\Delta\delta'_{calc} = 7.48$ ppm.

5.4.4 Photoswitching in ligand *trans*-L1 and *trans*-L2

Azobenzene derivatives are designed to show photoswitching under UV-vis irradiation,[34] and the investigation here begins with ***trans*-L1** and ***trans*-L2**, in order to establish a reference point for analysis of optoelectronic properties.[39] Ligands ***trans*-L1** and ***trans*-L2** show similar energies for the π–π* ($\lambda_{max} = 333$ nm) and n–π* ($\lambda_{max} = 450$ nm) bands, while the molar absorptivity of the π–π* band and n–π* band of ***trans*-L1** are weaker than those of ***trans*-L2**. Selective irradiation of either ***trans*-L1** or ***trans*-L2** at 365 nm affects reversible *trans-cis* switching. Upon irradiation at 450 nm, the photostationary state (PSS) affects reversible *cis-trans* switching. The PSS is rapidly reached (2–5 min) for ***trans*-L1** and ***trans*-L2** upon irradiation at 365 nm, while the reverse reaction is slower (4–4.5 h) upon irradiation at 450 nm. The intensity of absorptions centered at 333 nm of ***trans*-L1** and ***trans*-L2** is decreased upon isomerization to the *cis*-isomers, while that of peaks centered at 262 and 450 nm, characteristic of the *cis*-isomer, is increased (Figure 5.8). Irradiation of ***trans*-L1** and ***trans*-L2** at 365 nm in an NMR tube produced predominantly ***cis*-L1** and ***cis*-L2** at the PSS (63 and 90% yield, respectively), while subsequent irradiation of the resulting *cis/trans*-isomeric mixture at 450 nm reversed the switching to return to primarily ***trans*-L1** and ***trans*-L2** at the PSS (92 and 85% yield, respectively).
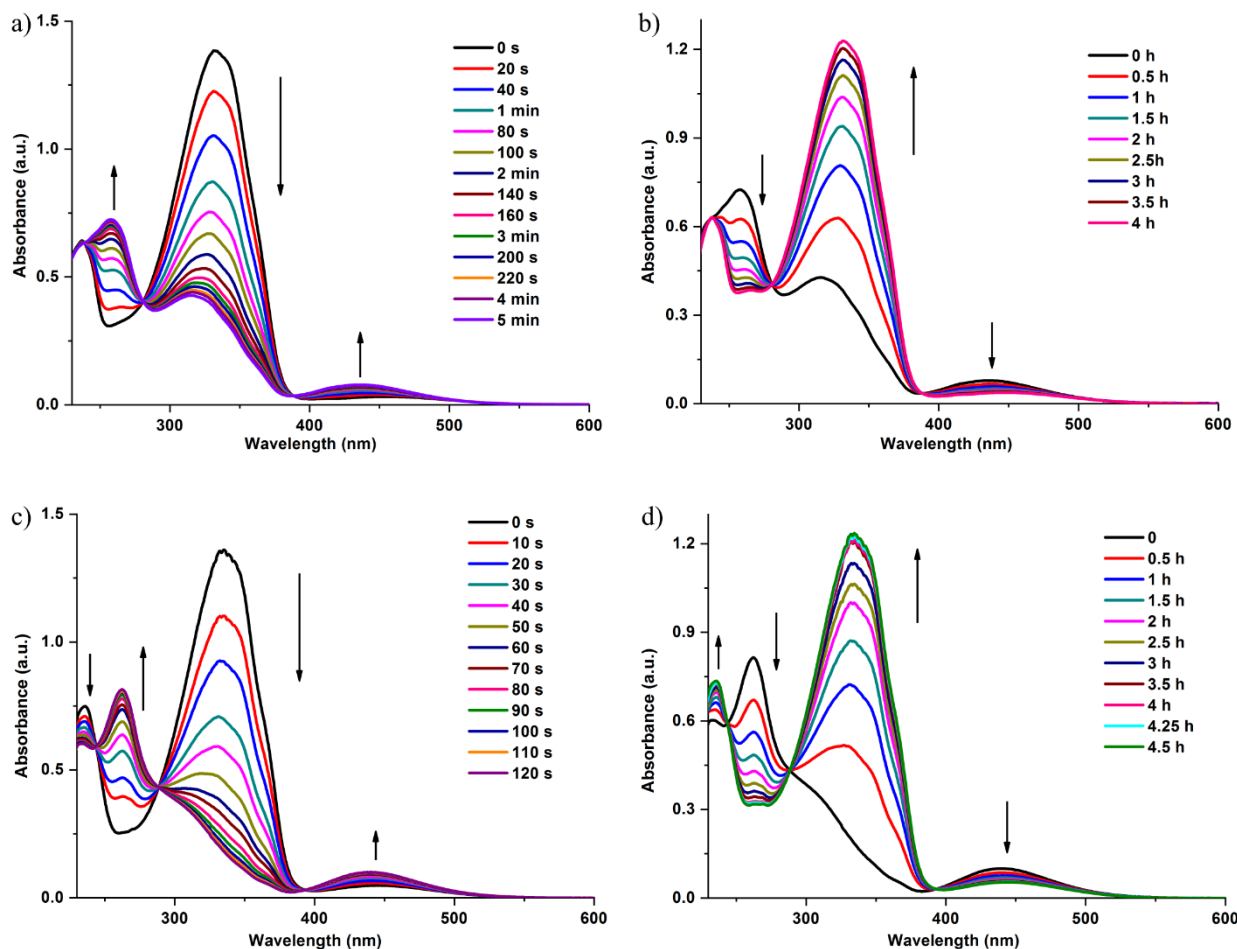
Figure 5.8. UV-vis spectra changes of a) ***trans*-L1** in THF upon irradiation at 365 nm until the PSS is reached, and b) the mixture ***cis*-/*trans*-L1** resulting from the PSS upon irradiation at 450 nm; c) ***trans*-L2** in THF upon irradiation at 365 nm and d) the mixture ***cis*-/*trans*-L2** resulting from the PSS upon irradiation at 450 nm.

5.4.5 UV-vis analysis in platforms with Ga- and/or Ru-porphyrins

Appending ***trans*-L1–L4** as axial ligands to either Ga- or Ru-porphyrins has little effect on the ground-state electronic makeup of either the ligand or the metalloporphyrin, and absorption spectra of the *trans*-complexes are effectively a sum of their parts. Noticeable features from the spectra of **GaL1**, **RuL1**, **GaL1Ru**, **GaL2**, **GaL3Ga**, **RuL4Ru**, and **GaL5Ru** include Soret bands at 404–405 nm and at 422 nm for Ru- and Ga-porphyrins, respectively (Figure 5.9a). The UV-vis spectrum of mixed-metal bisporphyrin **GaL1Ru** in CH_2Cl_2 shows two completely separate Soret bands centered at 405 nm ($\varepsilon = 398000$ $M^{-1}cm^{-1}$) and 422 nm ($\varepsilon = 505000$ $M^{-1}cm^{-1}$) assigned to the Ru- and Ga-porphyrins, respectively (Figure 5.9a). The two separate Soret bands are also observed for **GaL5Ru** in CH_2Cl_2, centered at 406 nm ($\varepsilon = 426000$ $M^{-1}cm^{-1}$) and 422 nm ($\varepsilon = 478000$ $M^{-1}cm^{-1}$). Split Soret bands have been reported by Osuka and co-workers for a series of *meso-meso*-linked

bisporphyrins, derived from exciton coupling.[40] It is unlikely that exitonic coupling is operative in **GaL1Ru**, however, as the Ru-porphyrin and Ga-porphyrin have quite independent absorptions and little electronic communication in the ground state. More specifically, a linear combination of the spectra of **GaL1Ru** and **L1** is essentially equivalent to the summation of the spectra of **GaL1** and **RuL1** (Figure 5.9b).
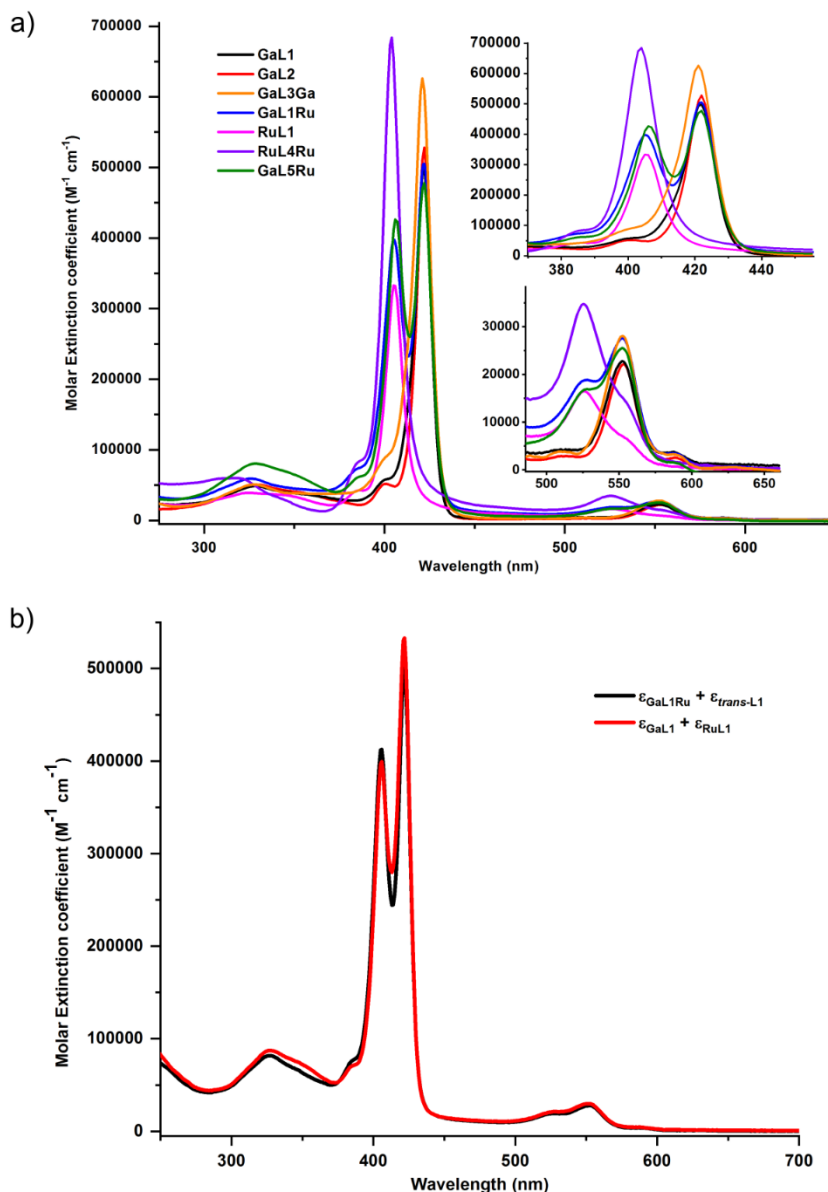
Figure 5.9. a) Quantitative UV-vis spectra of **GaL1**, **GaL2**, **GaL3Ga**, **GaL1Ru**, **GaL5Ru**, **RuL1**, and **RuL4Ru** in CH$_2$Cl$_2$ solutions. b) Comparison of quantitative absorbance of (ε_{GaL1Ru} + $\varepsilon_{trans\text{-}L1}$) and ($\varepsilon_{GaL1}$ + ε_{RuL1}), as measured in CH$_2$Cl$_2$, demonstrating that Ga-porphyrin has little electronic communication with Ru-porphyrin in the **GaL1Ru** complex at the ground state.

5.4.6 Photoswitching in platforms with either Ga- or Ru-porphyrins

Azo ligands appended to metalloporphyrins are expected to undergo photoisomerization.[1b, 4b, 19a] Unfortunately, the photoisomerization of platforms *trans*-**GaL1** and *trans*-**GaL2** was essentially suppressed upon irradiation at 365 nm. Ruthenium complexes with azo dyes have been reported to be photoswitchable,[41] suggesting that systems based on axial bonding to a Ru-porphyrin might be more efficiently switched. Upon irradiation at 360 nm in toluene solution, *trans*-**RuL1** and *trans*-**RuL4Ru** exhibit obvious changes in their UV-vis spectra. Specifically, irradiation of *trans*-**RuL1** and *trans*-**RuL4Ru** at 360 nm results in a reduction of the Soret bands at the PSS (centered at 407 nm and 405 nm and reduced ca. 15% and 13%, respectively), and the concurrent emergence of a broad absorption between 560–800 nm (see Figures 5.10 and 5.11 for details). The PSS is reached by 130 min for **RuL1** and 210 min for **RuL4Ru**, which is significantly longer than that for the unbound ligands *trans*-**L1** and *trans*-**L2** (*vide supra*). The new, broad absorption at low energy was tentatively assigned as a metal-to-axial ligand charge-transfer (MLCT) band, as has been suggested by Marvaud and Launay for Ru-porphyrins with axially bonded 4,4'-azopyridines.[20g] The thermal reversibility of the switching was then explored. After reaching the PSS, irradiation was discontinued, and the resulting solutions of **RuL1** and **RuL4Ru** were allowed to stand in the dark. This resulted in a slight recovery of the initial UV-vis spectrum of both platforms *trans*-**RuL1** and *trans*-**RuL4Ru**, but the switching processes was mainly irreversible under thermal conditions (see Figures 5.10 and 5.11 for details).
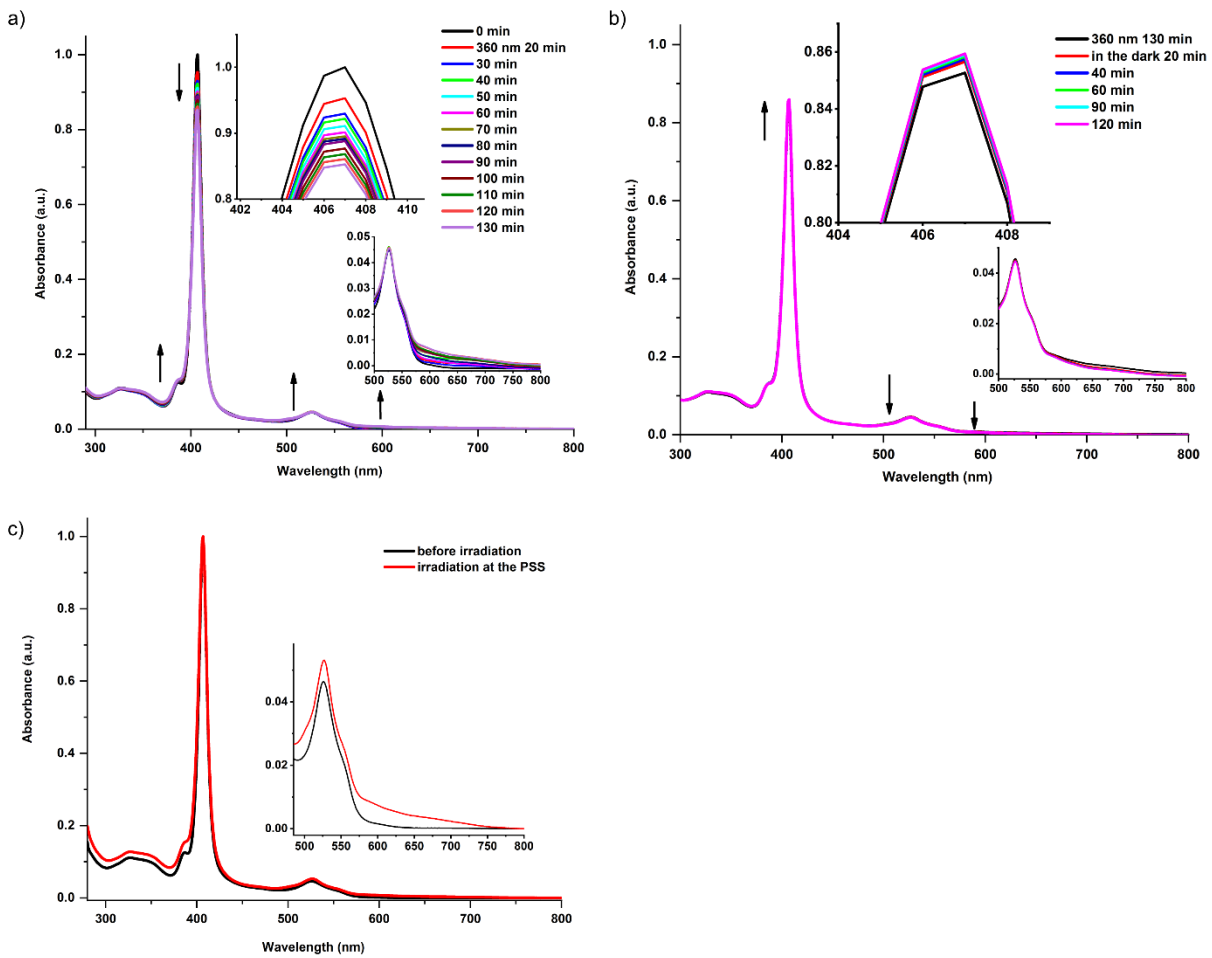
Figure 5.10. UV-vis spectra changes of **RuL1** in toluene a) upon irradiation at 360 nm and b) after reaching PSS upon standing in the dark. c) Comparison of UV-vis spectra changes of **RuL1** in toluene before irradiation and after reaching the PSS.
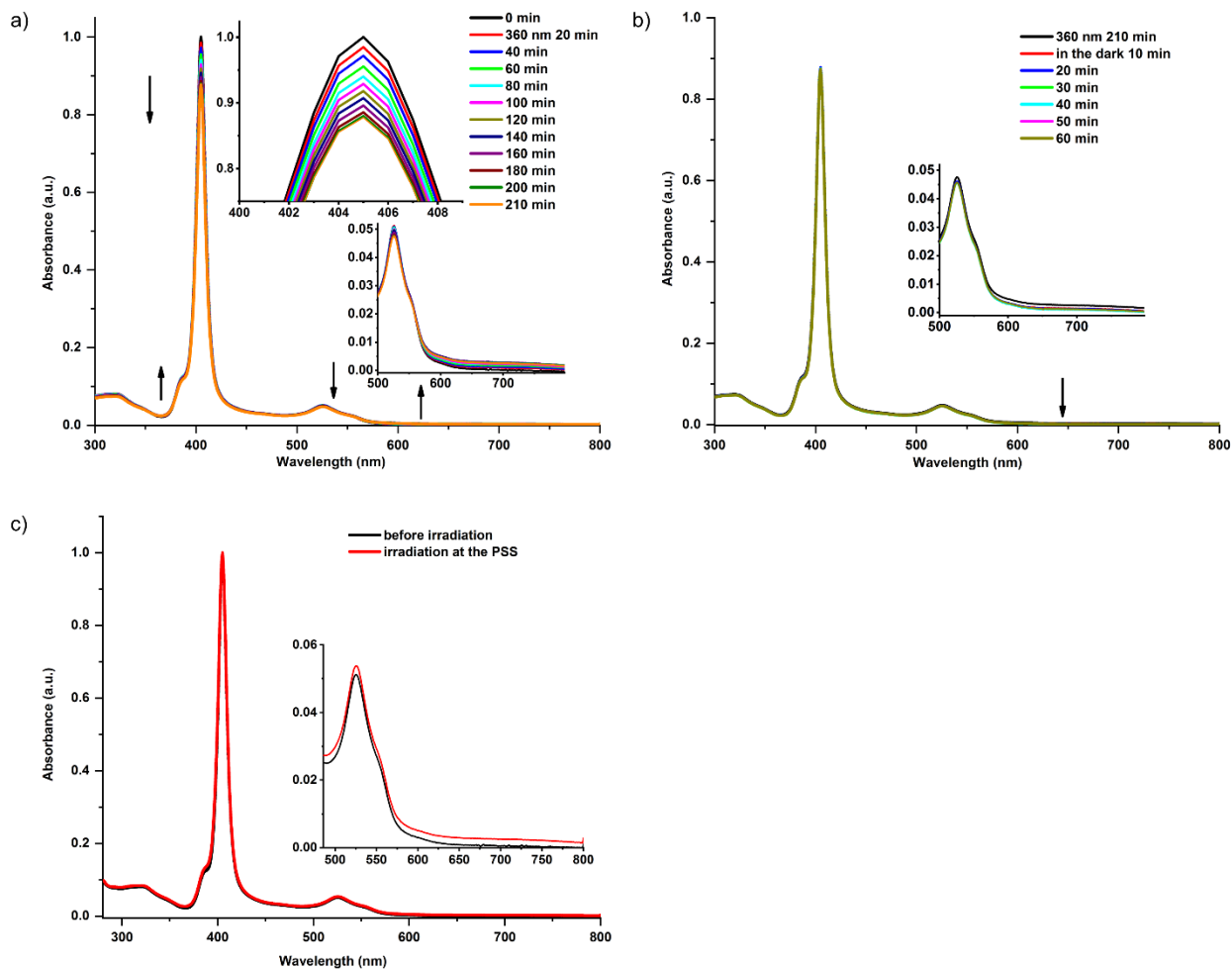
Figure 5.11. UV-vis spectra changes of **RuL4Ru** in toluene a) upon irradiation at 360 nm and b) after reaching PSS upon standing in the dark. c) Comparison of UV-vis spectra changes of **RuL4Ru** in toluene before irradiation and after reaching the PSS.

To probe the origin of the low energy bands from photoisomerization, a control experiment was designed based on **RuL1**. A mixture of *trans/cis*-**L1** at the PSS was obtained by the irradiation of a pure *trans*-**L1**. This isomeric mixture of *trans/cis*-**L1** was then titrated to a solution of porphyrin **5.12** in toluene. Indeed, the product formed showed a weak and broad peak at 600–800 nm that increased in intensity as a function of the concentration of *trans/cis*-**L1**, suggesting the formation of a mixture of *trans/cis*-**RuL1** (see Figure 5.12a). As a comparison, *trans*-**L1** was also titrated to a solution of porphyrin **5.12** in toluene under analogous conditions (see Figure 5.12b). The intensity of the low energy band in this second control experiment was, however, weaker than that produced by direct irradiation of **RuL1** (see comparison in Figure 5.13). Therefore, emergence of the low energy band during the photoirradiation of *trans*-**RuL1** is most reasonably assigned to

a combination of photo-decarbonation and the photoisomerization to the *cis*-**RuL1**.
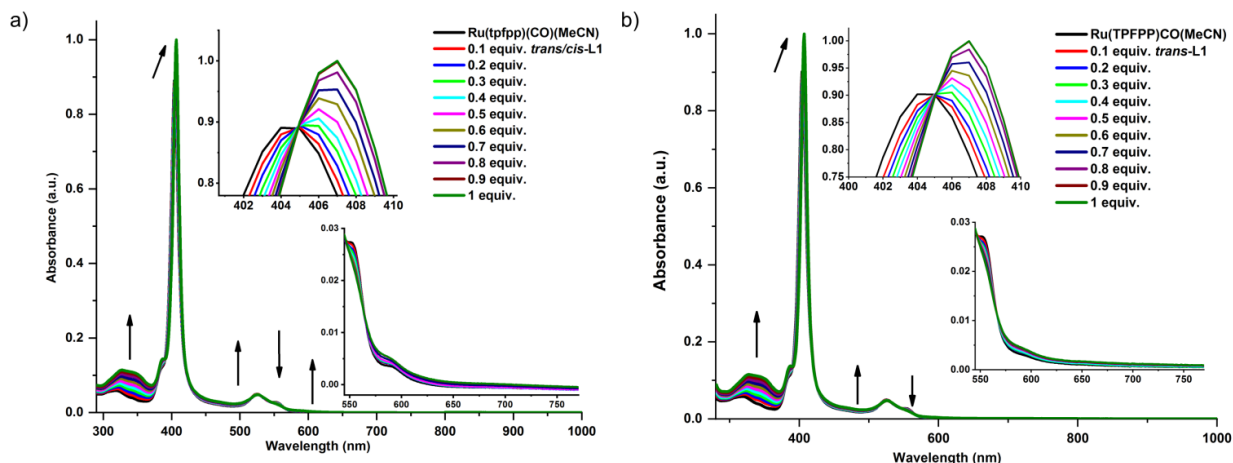
Figure 5.12. a) UV-vis spectra changes acquired upon the titration of Ru(tpfpp)(CO)(MeCN) (**5.12**) with *trans/cis*-**L1** in toluene. b) UV-Vis spectra changes acquired upon the titration of Ru(tpfpp)(CO)(MeCN) (**5.12**) with *trans*-**L1** in toluene.
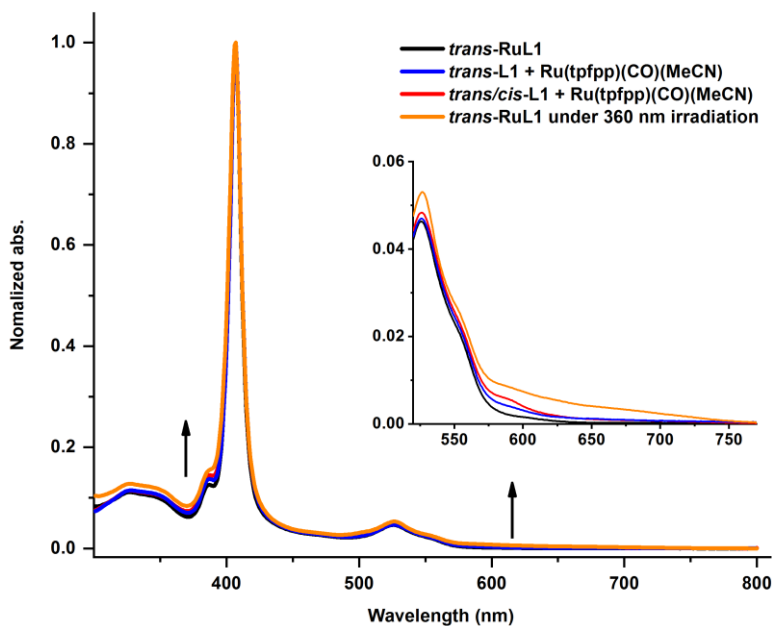
Figure 5.13. Comparison of normalized UV-vis absorption spectra of *trans*-**RuL1** and *trans*-**RuL1** upon irradiation of 360 nm at PSS, as well as the solution of Ru(tpfpp)(CO)(MeCN) (**5.12**) titrated with of *trans/cis*-**L1** and *trans/cis*-**L1** (1 equiv) in toluene.

The inability to achieve reversible switching for **RuL1** and **RuL4Ru** suggested that competing photochemical processes were occurring. It was thus hypothesized that the switching experiments were complicated by photochemical decarbonylation, which is known for Ru-porphyrins and Ru-complexes,[20g, 35b, 35c, 42] and this possibility will be discussed below.

In view of the lack of switching observed for **GaL1** combined with the partial switching

established for **RuL1** and **RuL4Ru** (*vide supra*), the photoisomerization of **GaL1Ru** inherently presented an interesting option since it featured a combination of the two structural motifs. Irradiation of ***trans*-GaL1Ru** at 365 nm in a solution of hexanes results in a reduction (27%) and broadening in the Soret band arising from the Ru-porphyrin, while little change in the Soret band of the Ga-porphyrin is observed (Figure 5.14b). Concurrently, a new absorption centered at 500 nm appears as well as a broad peak at 560–800 nm (as had been observed for **RuL1** and **RuL4Ru** and assigned as a MLCT band). The PSS was reached after irradiation for 2 h. Attempts to reverse the switching via irradiation at 450 nm (2 h) or standing under daylight showed that, while the absorptions peaks trend toward the original spectrum of ***trans*-GaL1Ru**, the photoisomerization is clearly not completely reversible as shown in Figure 5.14c and 5.14d.[43]
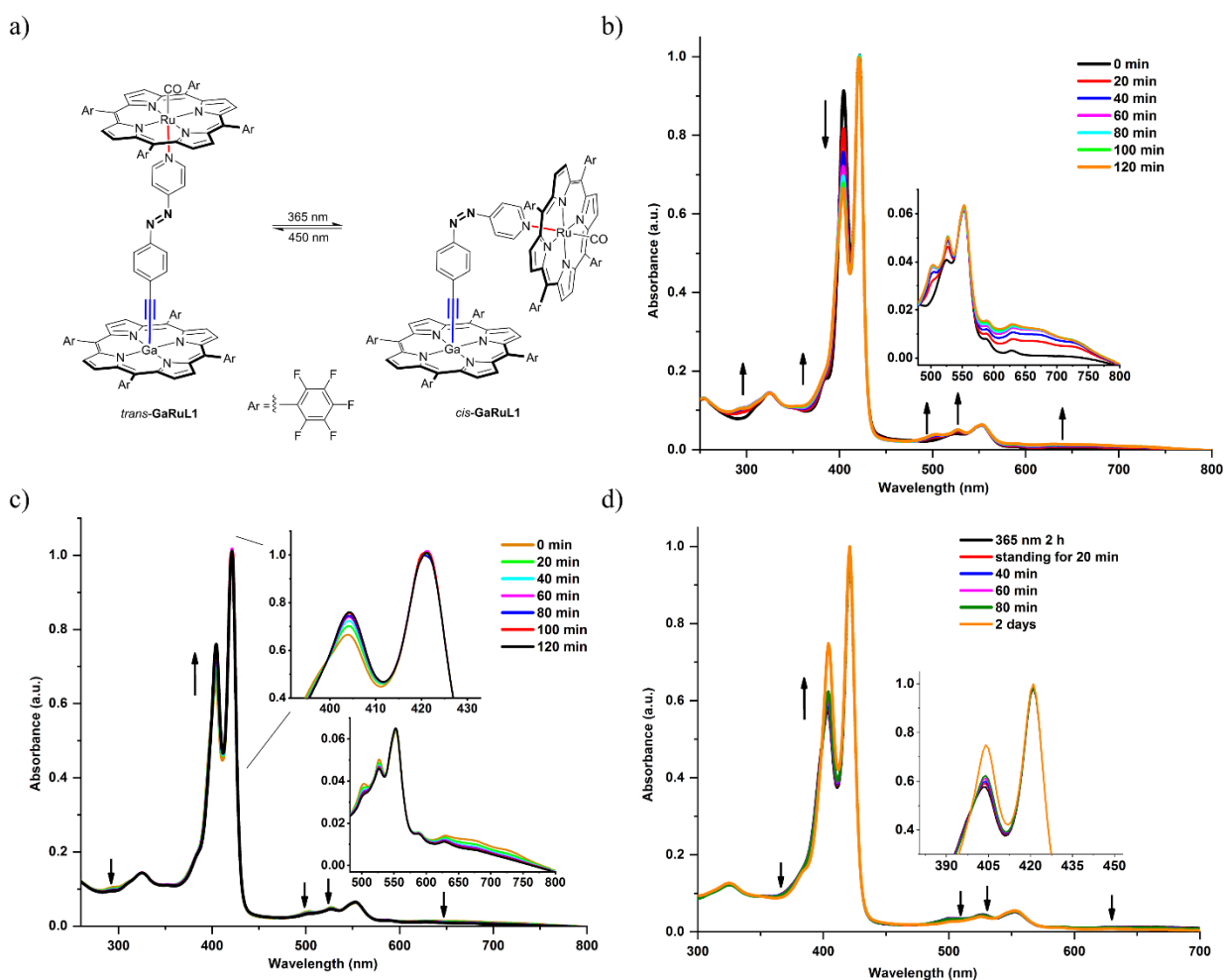
Figure 5.14. a) Schematic isomerization of complex **GaL1Ru**. UV-vis spectral changes of **GaL1Ru** upon irradiation at b) 365 nm and then c) 450 nm; hexanes solution. d) UV-vis spectra changes of **GaL1Ru** upon irradiation at 365 nm for 2 h and then standing under the daylight (hexanes solution).

The irradiation of the model compound **GaL5Ru** allows the decarbonylation process to be documented in the absence of azo switching. Specifically, irradiation of ***trans*-GaL5Ru** in a solution of hexanes results in a dramatic reduction (36%) in the Soret band of Ru-porphyrin, while little change in the Soret band of the Ga-porphyrin is observed. A comparison of the behavior of **GaL1Ru** and **GaL5Ru** upon irradiation (Figure 5.16) highlights differences in the absence of the azo moiety and documents both thermal and photochemical reversibility for **GaL1Ru** consistent with switching:

(a) Upon irradiation, the intensity of the low energy absorptions of **GaL1Ru** (centered at ca. 502 and 525 nm) gradually increases as a function of time, while the absorption for **GaL5Ru** at ca. 525 nm gradually decreases.

(b) Upon irradiation, the Ru-Soret band of **GaL1Ru** shows decreased intensity that is accompanied by broadening of this absorption, while the intensity of Ru-Soret band of **GaL5Ru** decreases without broadening .

(c) After the PSS for **GaL1Ru** has been reached, changes in UV-vis spectra are observed by either allowing the sample to stand (without irradiation) or by irradiation of the sample at 450 nm (Figure 5.14c and 5.14d), and these changes are consistent with *cis-trans* isomerization. Changes to the spectra were not observed for **GaL5Ru** after allowing the sample to stand in the dark without irradiation (Figure 5.15).
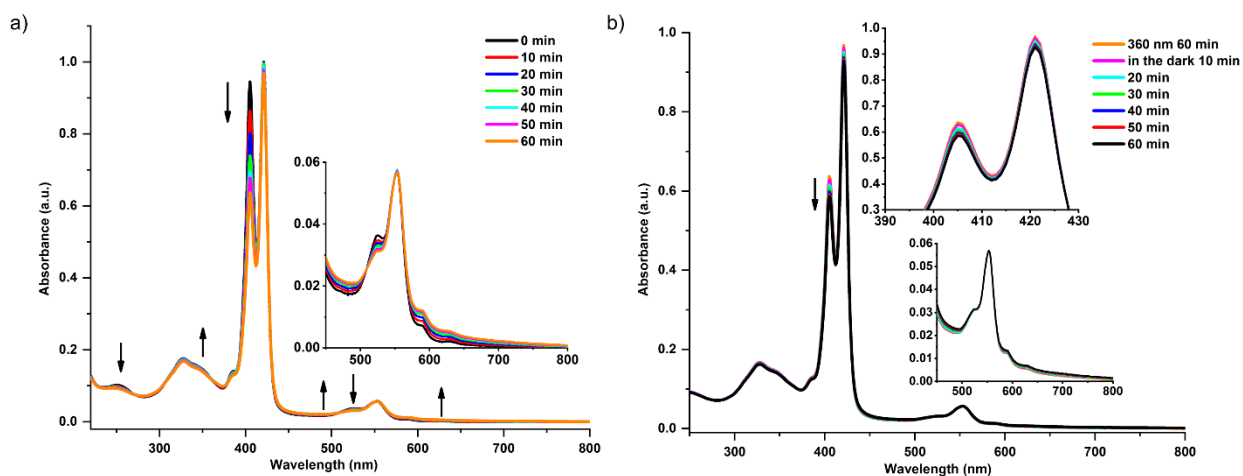
Figure 5.15. UV-vis spectra changes for **GaL5Ru** in hexanes a) upon irradiation at 360 nm and b) after reaching PSS upon standing in the dark.
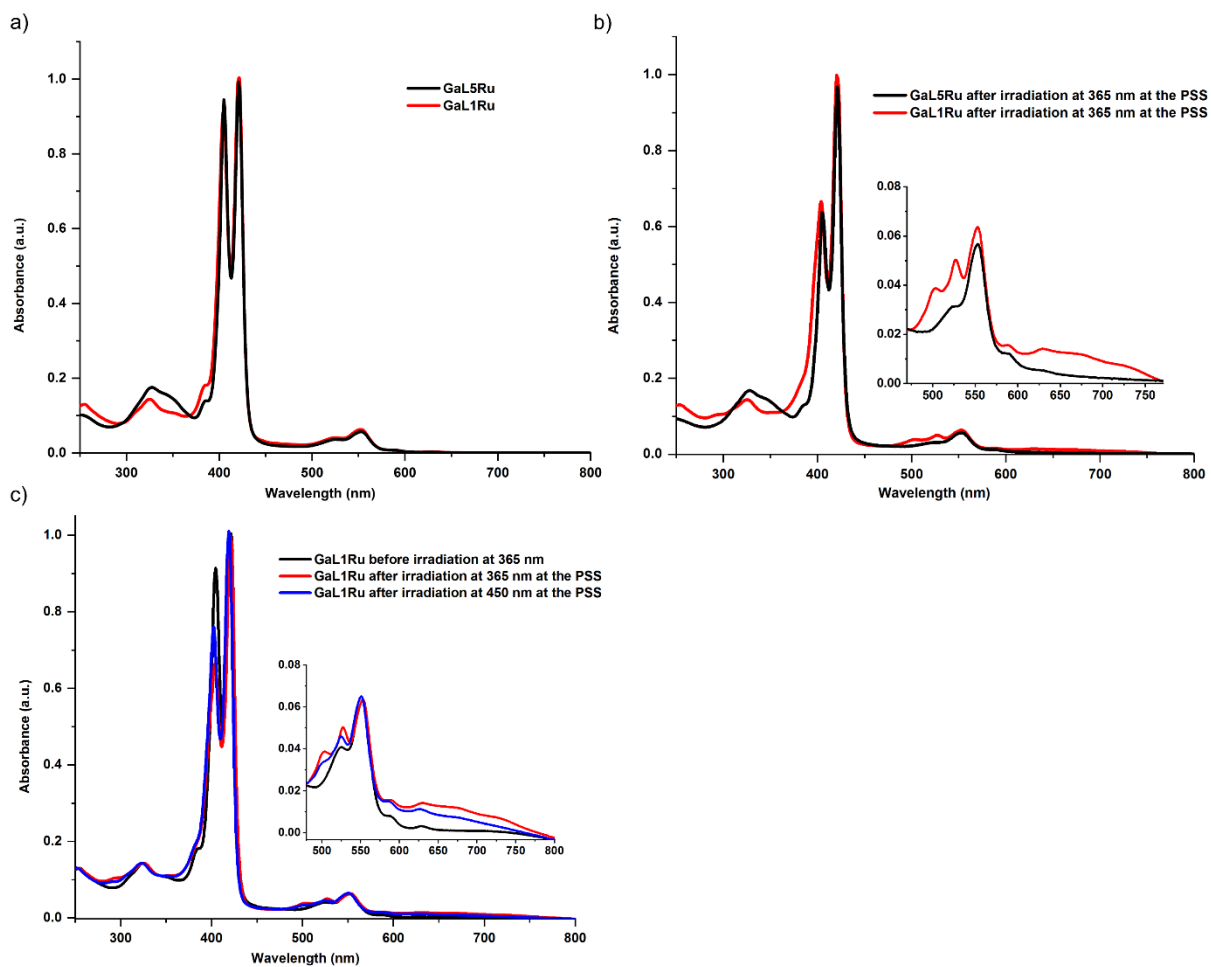
Figure 5.16. a) Comparison of normalized UV-vis spectra of **GaL1Ru** and **GaL5Ru** in hexanes before irradiation. b) Comparison of normalized UV-vis absorption spectra of **GaL1Ru** and **GaL5Ru** in hexanes after irradiation at 365/360 nm at the PSS. c) Comparison of normalized UV-vis absorption spectra of **GaL1Ru** in hexanes before irradiation and after irradiation at 365 and 450 nm at the PSS.

The irreversible spectral changes encountered for **GaL1Ru** and **RuL1** after irradiation suggested the possibility of photochemical decarbonylation of the Ru-porphyrins,[20g, 35b, 35c] which was further explored using Ru(tpfpp)(CO)(pyridine) (**5.13**) as a simplified model to **RuL1**.[44] Complex **5.13** mimics the coordination structure of **RuL1** through incorporation of pyridine in place with the azo-ligand **L1**. Porphyrin **5.13** was irradiated at 360 nm in hexanes, and the photoinduced decarbonylation process was documented by monitoring the Soret band. The intensity was decreased by ca. 15% during the irradiation (ca. 1.5 h), concurrent with the appearance of a broad absorbance centered at ca. 700 nm. Under both thermal and photochemical conditions, the loss of CO was irreversible, and both the loss of intensity of the Soret band and the broad peak at lower energy (700 nm) persisted.

The decarbonylation process thus complicates analysis of photo-switching for systems that contain a Ru-porphyrin (**GaL1Ru, RuL1**, and **RuL4Ru**). In the case of **RuL1** and **RuL4Ru**, decarbonylation appears to dominate, and spectral changes from irradiation are only partially reversible. Looking to the switching process for **GaL1Ru**, irradiation at 365 nm (hexanes) results in 27% reduction of the Soret band, while subsequent irradiation at 450 nm recovers to 44% of the original absorbance, and the broad absorption at 600–800 nm discernibly diminishes. Thus, the photochemical switching of the azo group in **GaL1Ru** is a major contributor to the reversible process, while decarbonylation is a competing process. The system is, however, less than ideal.

5.6 Conclusions

In summary, the synthetic incorporation of azo groups into three bisporphyrin and three porphyrin assemblies via covalent bonding of axial ligands has been developed. All six systems are based on Ga- and/or Ru-metalloporphyrins toward developing switchable systems, based on the "platform approach". The effects of diamagnetic anisotropy (DA) from the metalloporphyrins on the axial ligands has been examined, and the NMR chemical shifts of ligand protons can be effectively modelled using a power-law relationship based on the distance of the protons from the aromatic porphyrin core(s). The developed model shows that, in cases in which the ligand bridges two porphyrins, the effects of DA in the proton shift are additive.

Photophysical studies show that the photoisomerization of the azo moiety is ineffective for complexes bound to Ga-porphyrins (*trans*-**GaL1** and *trans*-**GaL2**). Photoisomerization is also quite limited for those with only Ru-porphyrins as axial ligands (**RuL4R** and **RuL1**). Mixed metal, bisporphyrin **GaL1Ru** undergoes *trans*/*cis*-isomerization upon irradiation, but similar to **RuL4R** and **RuL1**, the presence of the ruthenium carbonyl moiety complicates analysis of the photoisomerization due to irreversible photodecarbonylation. Thus, the formal addition of a Ga-porphyrin to **RuL1** to give **GaL1Ru** provides the most promising, switchable system, albeit the origin of this effect is not currently understood. Expansion of the versatile synthetic protocols developed in this chapter should, thus, be directed to metalloporphyrins with enhanced photostability, in which the troublesome Ru-porphyrin would be replaced by an alternative system, such as, for example, a Zn-porphyrin or a B-subphthalocyanine.

5.7 References

[1]   a) M. Hammerich, R. Herges, *J. Org. Chem.* **2015**, *80*, 11233–11236; b) T. Muraoka, K. Kinbara, T. Aida, *Nature* **2006**, *440*, 512–515.

[2]   a) A. S. Lubbe, W. Szymanski, B. L. Feringa, *Chem. Soc. Rev.* **2017**, *46*, 1052–1079; b) S. Samanta, A. A. Beharry, O. Sadovski, T. M. McCormick, A. Babalhavaeji, V. Tropepe, G. A. Woolley, *J. Am. Chem. Soc.* **2013**, *135*, 9777–9784; c) Q. Shao, B. Xing, *Chem. Soc. Rev.* **2010**, *39*, 2835–2846.

[3]   a) A. Goulet-Hanssens, F. Eisenreich, S. Hecht, *Adv. Mater.* **2020**, *32*, e1905966; b) A. H. Heindl, J. Becker, H. A. Wegner, *Chem. Sci.* **2019**, *10*, 7418–7425.

[4]   a) C. Zong, Y. Zhao, H. Ji, X. Han, J. Xie, J. Wang, Y. Cao, S. Jiang, C. Lu, *Angew. Chem. Int. Ed.* **2016**, *55*, 3931–3935; b) S. Venkataramani, U. Jana, M. Dommaschk, F. D. Sönnichsen, F. Tuczek, R. Herges, *Science* **2011**, *331*, 445–448; c) B. Baisch, D. Raffa, U. Jung, O. M. Magnussen, C. Nicolas, J. Lacour, J. Kubitschke, R. Herges, *J. Am. Chem. Soc.* **2009**, *131*, 442–443.

[5]   a) E. Merino, *Chem. Soc. Rev.* **2011**, *40*, 3835–3853; b) F. Hamon, F. Djedaini-Pilard, F. Barbot, C. Len, *Tetrahedron* **2009**, *65*, 10105–10123.

[6]   M. H. Davey, V. Y. Lee, R. D. Miller, T. J. Marks, *J. Org. Chem.* **1999**, *64*, 4976–4979.

[7]   N. R. Ayyangar, S. N. Naik, K. V. Srinivasan, *Tetrahedron Lett.* **1989**, *30*, 7253–7256.

[8]   C. Zhang, N. Jiao, *Angew. Chem. Int. Ed.* **2010**, *49*, 6174–6177.

[9]   a) C. R. Crecca, A. E. Roitberg, *J. Phys. Chem. A* **2006**, *110*, 8188–8203; b) C. J. Brown, *Acta Crystallogr.* **1966**, *21*, 146–152.

[10]   A. Mostad, C. Rømming, *Acta Chem. Scand.* **1971**, *25*, 3561–3568.

[11]   H. M. Bandara, S. C. Burdette, *Chem. Soc. Rev.* **2012**, *41*, 1809–1825.

[12]   A. Schlimm, R. Low, T. Rusch, F. Rohricht, T. Strunskus, T. Tellkamp, F. Sonnichsen, U. Manthe, O. Magnussen, F. Tuczek, R. Herges, *Angew. Chem. Int. Ed.* **2019**, *58*, 6574–6578.

[13]   T. R. Rusch, M. Hammerich, R. Herges, O. M. Magnussen, *Chem. Commun.* **2019**, *55*, 9511–9514.

[14]   S. Mohnani, D. Bonifazi, *Coord. Chem. Rev.* **2010**, *254*, 2342–2362.

[15]   a) C. B. Kc, F. D'Souza, *Coord. Chem. Rev.* **2016**, *322*, 104–141; b) S. M. Law, D. Chen, S. L. Chan, X. Guan, W. M. Tsui, J. S. Huang, N. Zhu, C. M. Che, *Chem. Eur. J.* **2014**, *20*, 11035–11047.

[16]   J. M. Kamm, C. P. Iverson, W. Y. Lau, M. D. Hopkins, *Langmuir* **2016**, *32*, 487–495.

[17]   V. Walter, Y. Gao, N. Grzegorzek, M. Krempe, F. Hampel, N. Jux, R. R. Tykwinski, *Angew. Chem. Int. Ed.* **2019**, *58*, 494–498.

[18]   a) C. Schutt, G. Heitmann, T. Wendler, B. Krahwinkel, R. Herges, *J. Org. Chem.* **2016**, *81*, 1206–1215; b) M. Dommaschk, C. Schutt, S. Venkataramani, U. Jana, C. Nather, F. D. Sonnichsen, R. Herges, *Dalton Trans.* **2014**, *43*, 17395–17405.

[19]   a) W. Huang, S. K. Lee, Y. M. Sung, F. Peng, B. Yin, M. Ma, B. Chen, S. Liu, S. R. Kirk, D. Kim, J. Song, *Chem. Eur. J.* **2015**, *21*, 15328–15338; b) L. J. Esdaile, P. Jensen, J. C. McMurtrie, D. P. Arnold, *Angew. Chem. Int. Ed.* **2007**, *46*, 2090–2093; c) T. Yamamura, A.

Momotake, T. Arai, *Tetrahedron Lett.* **2004**, *45*, 9219–9223; d) S. Tsuchiya, *J. Am. Chem. Soc.* **1999**, *121*, 48–53; e) H. K. Hombrecher, K. Lüdtke, *Tetrahedron* **1993**, *49*, 9489–9494.

[20]   a) T. Hirose, F. Helmich, E. W. Meijer, *Angew. Chem. Int. Ed.* **2013**, *52*, 304–309; b) S. Dey, S. A. Ikbal, S. P. Rath, *New J. Chem.* **2014**, *38*, 1458–1470; c) J. Otsuki, E. Seki, T. Taguchi, M. Asakawa, K. Miyake, *Chem. Lett.* **2007**, *36*, 740–741; d) O. Tsutsumi, H. Sato, K. Takeda, T. Ogawa, *Thin Solid Films* **2006**, *499*, 219–223; e) J. Otsuki, K. Narutaki, *Bull. Chem. Soc. Jap.* **2004**, *77*, 1537–1544; f) J. Otsuki, K. Harada, K. Araki, *Chem. Lett.* **1999**, *28*, 269–270; g) V. Marvaud, J. P. Launay, *Inorg. Chem.* **1993**, *32*, 1376–1382.

[21]   a) D. R. Reddy, B. G. Maiya, *J. Phys. Chem. A* **2003**, *107*, 6326–6333; b) D. R. Reddy, B. G. Maiya, *Chem. Commun.* **2001**, 117–118.

[22]   S. Yao, Y. Yan, K. L. Wong, K. S. Chan, Z. Shen, *J. Porphyrins Phthalocyanines* **2018**, *22*, 918–924.

[23]   R. Pelagalli, I. Chiarotto, M. Feroci, S. Vecchio, *Green Chem.* **2012**, *14*, 2251–2255.

[24]   R. R. Tykwinski, *Angew. Chem. Int. Ed.* **2003**, *42*, 1566–1568.

[25]   O. Zenkina, M. Altman, G. Leitus, L. J. W. Shimon, R. Cohen, M. E. van der Boom, *Organometallics* **2007**, *26*, 4528–4534.

[26]   L.-X. Liao, F. Stellacci, D. V. McGrath, *J. Am. Chem. Soc.* **2004**, *126*, 2181–2185.

[27]   O. K. Farha, C. D. Malliakas, M. G. Kanatzidis, J. T. Hupp, *J. Am. Chem. Soc.* **2010**, *132*, 950–952.

[28]   I.-Y. Wu, J. T. Lin, J. Luo, S.-S. Sun, C.-S. Li, K. J. Lin, C. Tsai, C.-C. Hsu, J.-L. Lin, *Organometallics* **1997**, *16*, 2038–2048.

[29]   J. S. Lindsey, R. W. Wagner, *J. Org. Chem.* **1989**, *54*, 828–836.

[30]   C. Wang, K. V. Shalyaev, M. Bonchio, T. Carofiglio, J. T. Groves, *Inorg. Chem.* **2006**, *45*, 4769–4782.

[31]   A. R. Waterloo, R. Lippert, N. Jux, R. R. Tykwinski, *J. Coord. Chem.* **2015**, *68*, 3088–3098.

[32]   K. Chichak, N. R. Branda, *Chem. Commun.* **1999**, 523–524.

[33]   a) M. Krempe, R. Lippert, F. Hampel, I. Ivanovic-Burmazovic, N. Jux, R. R. Tykwinski, *Angew. Chem. Int. Ed.* **2016**, *55*, 14802–14806; b) K. Campbell, R. McDonald, N. R. Branda, R. R. Tykwinski, *Org. Lett.* **2001**, *3*, 1045–1048.

[34]   S. Crespi, N. A. Simeth, B. Koinig, *Nat. Rev. Chem.* **2019**, *3*, 133–146.

[35]   a) N. Shafizadeh, S. Boye-Peronne, S. Soorkia, B. K. Cunha de Miranda, G. A. Garcia, L. Nahon, S. Chen, A. de la Lande, L. Poisson, B. Soep, *Phys. Chem. Chem. Phys.* **2018**, *20*, 11730–11739; b) K. Ishii, S.-i. Hoshino, N. Kobayashi, *Inorg. Chem.* **2004**, *43*, 7969–7971; c) M. Hoshino, Y. Kashiwagi, *J. Phys. Chem.* **1990**, *94*, 673–678.

[36]   a) H. Iwamoto, K. Hori, Y. Fukazawa, *Tetrahedron* **2006**, *62*, 2789–2798; b) Y. Uemori, A. Nakatsubo, H. Imai, S. Nakagawa, E. Kyuno, *Inorg. Chem.* **1992**, *31*, 5164–5171; c) R. J. Abraham, S. C. M. Fell, K. M. Smith, *Org. Magn. Reson.* **1977**, *9*, 367–373.

[37]   A. Stanger, *J. Phys. Chem. A* **2019**, *123*, 3922–3927.

[38]   A reasonable definition is required to establish when $\Delta\delta_\infty$ has been achieved. Assuming that the accuracy of the NMR measurements is ± 0.001 ppm, $\Delta\delta_\infty$ is defined by fulfilment of the relationship $\Delta\delta r - \Delta\delta r' \leq 0.001$ ppm, i.e., $\Delta\delta_\infty$ has been achieved if the difference in chemical

shifts at two distances, r and r' cannot be resolved by the NMR measurement.

[39] a) R. A. Al-Balushi, A. Haque, M. Jayapal, M. K. Al-Suti, J. Husband, M. S. Khan, J. M. Skelton, K. C. Molloy, P. R. Raithby, *Inorg. Chem.* **2016**, *55*, 10955–10967; b) N. Masaru, R. Masahiro, W. Masayoshi, S. Kohei, O. Naoya, *Bull. Chem. Soc. Jap.* **1997**, *70*, 737–744.

[40] a) N. Fukui, H. Yorimitsu, A. Osuka, *Chem. Eur. J.* **2016**, *22*, 18476–18483; b) N. Yoshida, T. Ishizuka, A. Osuka, D. H. Jeong, H. S. Cho, D. Kim, Y. Matsuzaki, A. Nogami, K. Tanaka, *Chem. Eur. J.* **2003**, *9*, 58–75.

[41] K. Ghebreyessus, S. M. Cooper, *Organometallics* **2017**, *36*, 3360–3370.

[42] S. J. Carrington, I. Chakraborty, J. R. Alvarado, P. K. Mascharak, *Inorg. Chim. Acta* **2013**, *407*, 121–125.

[43] Thermal reversion was also minimal upon standing at room temperature, although the experiment was not quantified.

[44] Photophysical studies of multiporphyrin arrays incorporating Ru-metalloporphyrins bearing a CO ligand suggested that these systems would be stable under mild irradiation (see ref. 32), while decarbonylation is well known under strong irradiation (refs. 20g, 35b, 35c). In the present case, no attempt was made to identify the product(s) of decarbonylation given the small amounts that were produced in the experiments.

CHAPTER 6 – Summary and Outlook

6.1 Synthesis of oligo-/polyynes on the way to carbyne

The objective of this thesis has been to develop synthetic methods towards pyridyl-endcapped oligo-/polyynes. The successful synthesis of a series of pyridyl-endcapped oligo-/polyynes (**Py**[na]**; n = 2, 4, 6, 8, 10, 12, 16, 24) allows us to study, in depth, the properties of **Py**[na]** as a function of length. The analysis of ^{13}C NMR spectra, UV-vis spectroscopic absorbances, bond length alternation (BLA, using X-ray crystallographic data), and Raman signals provides a better fundamental understanding and more complete prediction of the potential of carbyne.[1] To be more specific, the loss of endgroup effects in the series **Py**[na]** helps define a transition from an oligoyne to a polyyne initiating at ca. n = 20–24. Convergence of experimental values for ^{13}C NMR, UV-vis and Raman spectroscopies, as well as BLA consistently predict that the saturation of properties will be reached by ca. n = 34–37 alkyne units (i.e., the complete disappearance of endgroup effects), which gives estimation of the properties of carbyne.

Synthetic efforts have already reached the limit of the oligoynes passing to polyynes at the longest derivative, with 24 triple bonds. Seemingly, a bit more effort with the synthetic elongation of 10 more triple bonds would reach the saturation length (n = 34–37) to form a true model of carbyne. The effective protection from known endgroups, however, is likely to come to an end since the effect is diminishing as the chain gets longer. In addition to the endgroup strategy, another strategy through the formation of oligoyne rotaxanes has been developed to stabilize oligoynes by using an active metal template (AMT) coupling reaction,[2] in which the copper(I) complex of a phenanthroline macrocycle directs the coupling of two oligoyne precursors through the cavity of the macrocycle.[3] Oligoyne rotaxanes can exhibit enhanced thermal stability due to the protective effect of the threaded macrocycle.[3b] This strategy, however, was only successfully employed to date for relatively short oligoynes ($n \leq 12$).[3] The instability of the terminal oligoynes as precursors encumbered the synthesis of longer oligo-/polyyne rotaxanes under the catalytic conditions that were developed, which required reaction temperatures of 50–60 °C. Additionally, the strategy was limited by the number of macrocycles (one or two) that could be introduced on the oligoyne thread.

It is hypothesized that the formation of a stable terminal oligo-/polyyne precursor by the encapsulation with more than two macrocycles could be a successful strategy to synthesize

polyynes that could mimic "carbyne" rotaxanes ($n \geq 37$; Figure 6.1). The overall strategy is to introduce macrocycles one by one during each of the AMT coupling reactions, and these macrocycles must be held on the oligo-/polyyne axle and not de-thread during or after the deprotection reaction. To be more specific, an AMT reaction introduces a macrocycle onto the oligo-/polyyne thread, followed by using a linker such as an alkyl chain to covalently bind the endgroup and the macrocycle. Repeating the deprotection reaction, the AMT coupling reaction, and the introduction of a linker, in this order, could elongate the oligo-/polyyne chain and finally give a carbyne rotaxane.
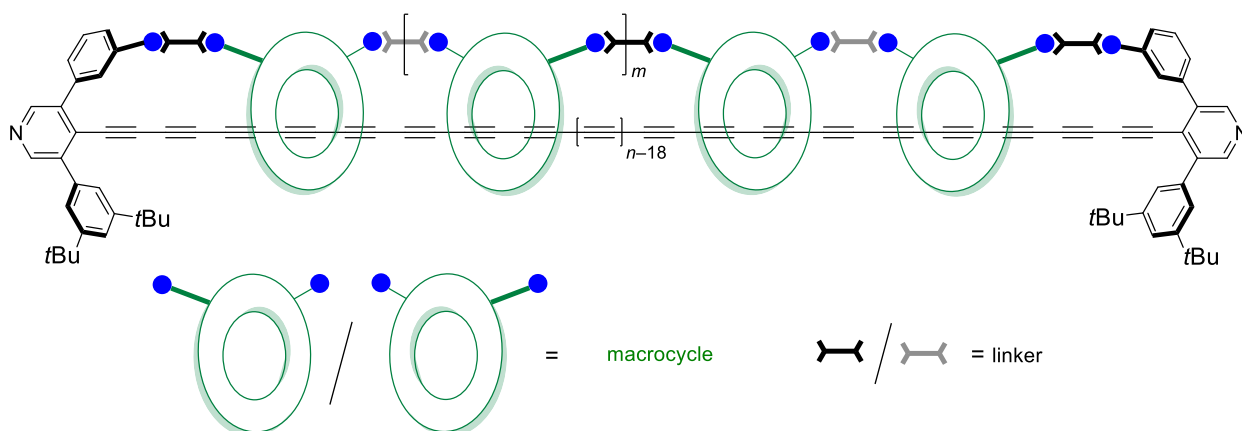
Figure 6.1. Illustration of a carbyne model encapsulated with macrocycles.

6.2 Reactions of oligoynes

Oligoynes can be useful intermediates[4] towards conjugated materials, such as in topochemical polymerization reactions,[5] Diels-Alder reactions,[6] and Huisgen cycloaddition reactions.[6-7] The use of alkynes as precursors to prepare polycyclic compounds, as in the application of alkyne benzannulation reactions to synthesize nanoribbons, is a recent salient example.[8]

In searching for an optimal endgroup, as described in Chapter 2, I found that the CH_2Cl_2 solution of **Py**[2d]**, **Py**[2e]** and **Py**[4d]** decomposed under light and the resulting solutions gave intense red fluorescence. Then, a preliminary photoreaction was conducted for **Py**[2d]** (through the cooperation with Matthew Johnson in our group). The photoreaction of **Py**[2d]** gave cleanly a polycyclic compound through the formation of five- and six-membered rings (Scheme 6.1). This photochemical oxidative cyclization reaction is similar to the Mallory reaction;[9] to my knowledge, however, there is no example using alkyne as precursor in the

Mallory reaction. Therefore, this reaction opens an avenue to make polycyclic compounds by using alkyne precursors.
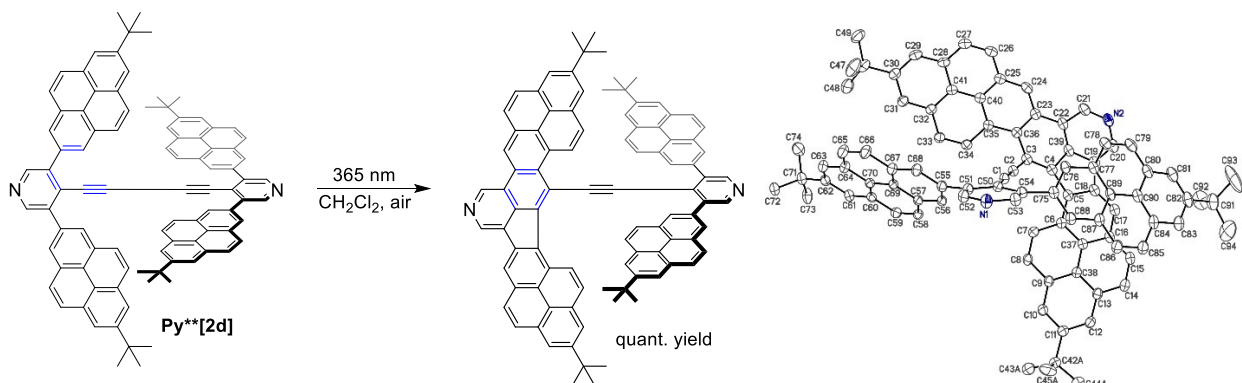
Scheme 6.1. Photocyclization reaction of **Py**[2d]** and the X-ray structure of the polycyclic product.

It is not clear if the extended pi-electron system of the pendent pyrene moiety plays a definitive role. Depending on the importance of the constitution of the pendent aryl substituent, many unusual and unprecedented polycyclic aromatic compounds could be synthesized by using this type of reaction. A few examples to be attempted are presented in Scheme 6.2.
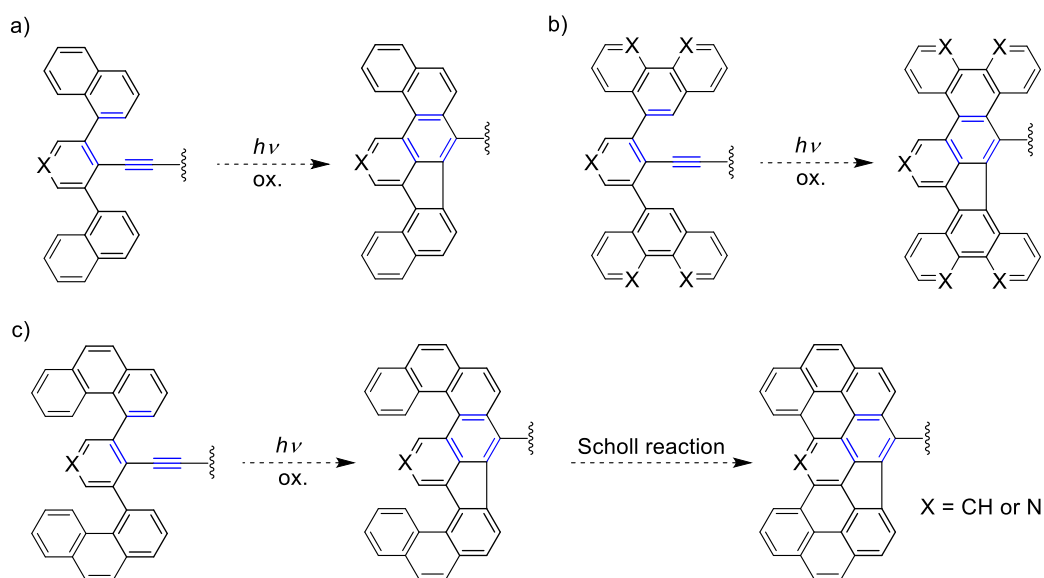
Scheme 6.2. Potential photocyclization reactions.

6.3 Molecular wires

Because of the approximately cylindrical π-electron system of oligoynes and the ability of the

pyridyl group to serve as a ligand, pyridyl-endcapped oligoynes (PEOs) are excellent candidates to serve as molecular wires.[10] The formation of a series of PEOs with the pyridyl anchoring group allows us to incorporate these in STM-break-junction devices. The single-molecule conductance of this series of PEOs is being studied by the team of Dr. González and Dr. Agraït at IMDEA in Madrid, Spain. This series of PEOs provides the opportunity for the examination of single-molecule conductance and, in particular, the determination of the transition from a tunneling to a hopping mechanism in PEOs.[11] Depending on the outcome of the present experiments, molecular design can be adapted to improve performance, given the modular assembly of the terminal pyridyl group.

6.4 Functionalities with azo groups

Many recent advances have revealed the synthetic and structural versatility of pentacene dimers in the investigation of intramolecular singlet fission (iSF).[12] The spacer between two pentacene moieties is the key to control and tune the geometry, distance, and electronic coupling of pentacene dimers, which allows the investigation of specific hypotheses regarding the mechanism of singlet fission.[12d] The introduction of an azo group as a spacer is envisioned as a means to tune and control factors related to iSF via the application of an external stimulus of light and/or heat.

An example of the design is presented in Scheme 6.3. As described in Chapter 5, the reaction of lithium bis(trimethylsilyl)amide (LiHMDS) and *trans*-**L3** gives the acetylide, which can be treated with a pentacene quinone, followed by quenching with MeI. Reductive elimination using $SnCl_2$ would give the ***trans*-azo-pentacene** compound. Selective irradiation of ***trans*-azo-pentacene** and ***cis*-azo-pentacene** at either 365 nm or 450 nm should affect the reversible switching between the *trans*- and *cis*-isomer, respectively. In addition, the molar extinction absorbance of pentacene monomer[13] and azobenzene[14] at 365 nm is ca. 2000 and 20000 $cm^{-1}M^{-1}$, respectively. The weak absorbance of pentacene at 365 nm, as a result, would not be a notable factor to decrease the process of photoisomerization. Upon the isomerization, the distance between two pentacene moieties would be tuned, affecting through space interactions between chromophores. On the other hand, the planarity of the *cis*-isomer would be severely distorted from the co-planar *trans*-isomer, as has been discussed in Chapter 5, which would affect through bond π-delocalization.[15] The changes of distance and planarity in the pentacene dimers would be studied and used to investigate the iSF process. The introduction of the azo group can become a

switch if the efficiency of iSF changes significantly during light/thermal stimulation.
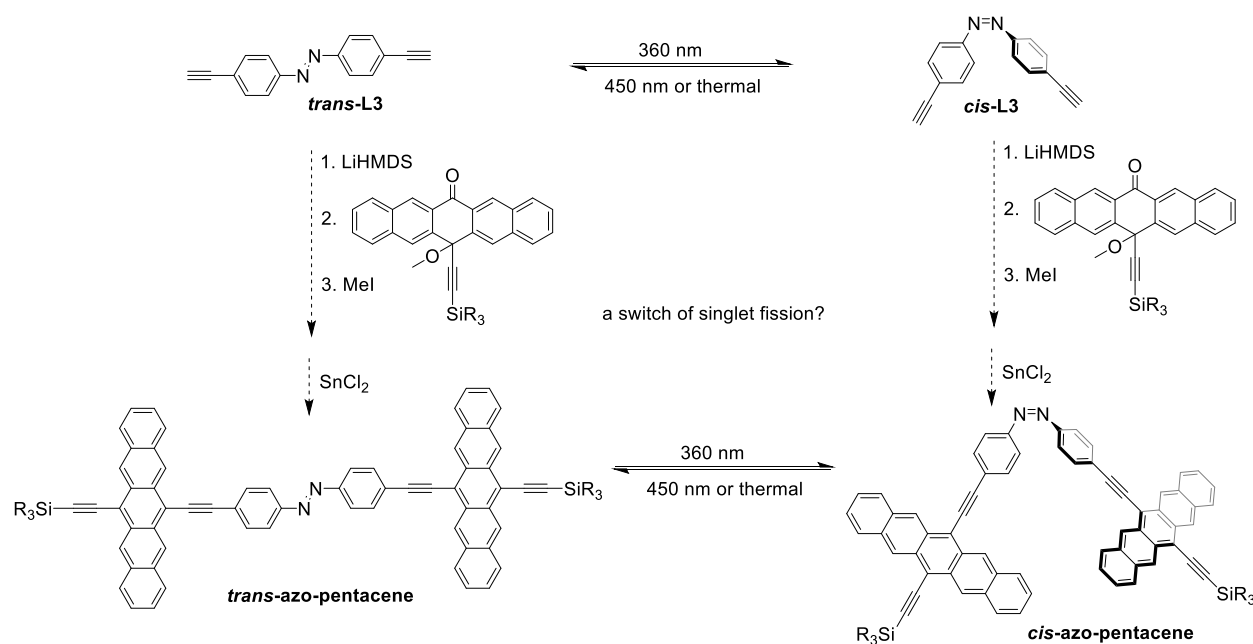
Scheme 6.3. A proposal of the synthesis and photoswitching of azo-pentacene.

6.5 References

[1]   W. A. Chalifoux, R. R. Tykwinski, *Nat. Chem.* **2010**, *2*, 967–971.

[2]   M. Denis, S. M. Goldup, *Nat. Rev. Chem.* **2017**, *1*, 0061.

[3]   a) M. Franz, J. A. Januszewski, F. Hampel, R. R. Tykwinski, *Eur. J. Org. Chem.* **2019**, 3503–3512; b) L. D. Movsisyan, M. Franz, F. Hampel, A. L. Thompson, R. R. Tykwinski, H. L. Anderson, *J. Am. Chem. Soc.* **2016**, *138*, 1366–1376; c) M. Franz, J. A. Januszewski, D. Wendinger, C. Neiss, L. D. Movsisyan, F. Hampel, H. L. Anderson, A. Gorling, R. R. Tykwinski, *Angew. Chem. Int. Ed.* **2015**, *54*, 6645–6649.

[4]   E. T. Chernick, R. R. Tykwinski, *J. Phys. Org. Chem.* **2013**, *26*, 742–749.

[5]   A. Jolly, D. Miao, M. Daigle, J. F. Morin, *Angew. Chem. Int. Ed.* **2020**, *59*, 4624–4633.

[6]   B. Pigulski, N. Gulia, S. Szafert, *Eur. J. Org. Chem.* **2019**, 1420–1445.

[7]   T. Luu, R. McDonald, R. R. Tykwinski, *Org. Lett.* **2006**, *8*, 6035–6038.

[8]   a) W. Yang, R. Bam, V. J. Catalano, W. A. Chalifoux, *Angew. Chem. Int. Ed.* **2018**, *57*, 14773–14777; b) W. Yang, J. H. S. K. Monteiro, A. de Bettencourt-Dias, V. J. Catalano, W. A. Chalifoux, *Angew. Chem. Int. Ed.* **2016**, *55*, 10427–10430.

[9]   a) K. B. Jorgensen, *Molecules* **2010**, *15*, 4334–4358; b) F. B. Mallory, C. S. Wood, J. T. Gordon, *J. Am. Chem. Soc.* **1964**, *86*, 3094–3102.

[10] C. S. Casari, M. Tommasini, R. R. Tykwinski, A. Milani, *Nanoscale* **2016**, *8*, 4414–4435.

[11] X. Zhao, C. Huang, M. Gulcur, A. S. Batsanov, M. Baghernejad, W. Hong, M. R. Bryce, T. Wandlowski, *Chem. Mater.* **2013**, *25*, 4340–4347.

[12]   a) B. S. Basel, R. M. Young, M. D. Krzyaniak, I. Papadopoulos, C. Hetzer, Y. Gao, N. T. La Porte, B. T. Phelan, T. Clark, R. R. Tykwinski, M. R. Wasielewski, D. M. Guldi, *Chem. Sci.* **2019**, *10*, 11130–11140; b) A. Kunzmann, M. Gruber, R. Casillas, R. R. Tykwinski, R. D. Costa, D. M. Guldi, *Nanoscale* **2018**, *10*, 8515–8525; c) C. Hetzer, D. M. Guldi, R. R. Tykwinski, *Chem. Eur. J.* **2018**, *24*, 8245–8257; d) B. S. Basel, J. Zirzlmeier, C. Hetzer, S. R. Reddy, B. T. Phelan, M. D. Krzyaniak, M. K. Volland, P. B. Coto, R. M. Young, T. Clark, M. Thoss, R. R. Tykwinski, M. R. Wasielewski, D. M. Guldi, *Chem* **2018**, *4*, 1092–1111.

[13]   I. Papadopoulos, Y. Gao, C. Hetzer, R. R. Tykwinski, D. M. Guldi, *ChemPhotoChem* **2020**, *4*, 5168–5174.

[14]   Y. Gao, V. Walter, M. J. Ferguson, R. R. Tykwinski, *Chem. Eur. J.* **2020**.

[15]   A. Mostad, C. Rømming, *Acta Chem. Scand.* **1971**, *25*, 3561–3568.

CHAPTER 7 – Experimental Section

7.1 General procedures and methods

Reagents were purchased reagent grade from commercial suppliers and used without further purification. THF, CH_2Cl_2, toluene, and hexanes were distilled from sodium or dried under nitrogen in a commercial solvent purification system (LC Technology Solutions INC). $MgSO_4$ was used as the drying reagent after aqueous work-up. ^1H, ^{13}C, ^{19}F, ^{11}B, and ^{31}P NMR spectra were recorded on a Bruker Advance 300 (^1H: 300 MHz, ^{19}F: 282 MHz, ^{13}C: 75 MHz), an Agilent/Varian Inova three-channel 400 (^1H: 400 MHz, ^{13}C: 100 MHz, ^{19}F: 376 MHz, ^{11}B: 128 MHz, ^{31}P: 162 MHz), an Agilent/Varian Inova four-channel 500 (^1H: 500 MHz, ^{19}F: 470 MHz, ^{11}B: 160 MHz), an Agilent/Varian VNMRS two-channel 500 equipped with a $^{13}C/^1H$ dual cold probe (^1H: 500 MHz, ^{13}C: 125 MHz), or an Agilent VNMRS four-channel 700 equipped with a $^1H(^{15}N/^{13}C)$ triple resonance, Z-gradient cryoprobe (^1H: 700 MHz, ^{13}C: 176 MHz). NMR spectra were referenced to the residual solvent signal (^1H: $CDCl_3$: 7.26 ppm, CD_2Cl_2: 5.30 ppm; ^{13}C: $CDCl_3$: 77.0 ppm, CD_2Cl_2: 54.0 ppm, DMSO-d_6: 40.0 ppm) and recorded at ambient probe temperature. For simplicity, the coupling constants of protons in ^1H spectra have been reported as pseudo first-order when possible, even though they can be higher-order (ABC, ABX, AA'XX', etc.) spin systems.

UV-vis measurements were performed on a Varian Cary 5000 UV-Vis-NIR spectrophotometer or a Cary-400 spectrophotometer at room temperature with quartz cuvettes having 1 cm path length. The cryogenic UV-vis measurements at 80 K were obtained in a cryostat OPTISTAT from Oxford instruments. The wavelength λ is recorded in nm, the molar extinction ε is reported in L mol^{-1} cm^{-1}.

The light source for photoswitching was obtained from "LIGHTNINGCURE Spot Light Source LC8 L9566" equipped with bandpass filters of 360 nm (FWHM = 10 nm), 365 nm (FWHM = 10 nm) and 450 nm (FWHM = 10 nm). The output power was set at the level of 10–20%.

High resolution mass spectra were acquired at the University of Alberta mass spectrometry facility. IR spectra were recorded on a Varian 660-IR spectrometer as solids in ATR mode or on a Thermo Nicolet 8700 FTIR spectrometer and continuum FTIR microscope as a film.

Raman spectra were obtained at the University of Malaga using the RAMII FT-Raman module of a VERTEX 70 FT-IR spectrometer. A continuous–wave Nd–YAG laser working at 1064

nm was employed for excitation, at a laser power in the sample not exceeding 10 mW. Raman scattering radiation was collected in a back–scattering configuration with a standard spectral resolution of 4 cm^{-1}. A total of 2000 scans were averaged for each spectrum.

Differential scanning calorimetry (DSC) measurements were made on a Mettler Toledo DSC or Perkin Elmer Pyris 1 DSC. All DSC measurements were carried out under a flow of nitrogen with a heating rate of 10 °C/min.

Melting points were measured with Thomas-Hoover "uni-melt" apparatus.

X-ray crystallographic analysis was performed using an Atlas SuperNova diffractometer at the Instituted of Organic Chemistry, University of Erlangen-Nürnberg or using a Bruker D8 Duo or a Bruker Platform diffractometer at the Department of Chemistry, University of Alberta.

TLC analyses were carried out on TLC glass plates from Merck KGaA and visualized via UV-light (254/364 nm) or standard coloring reagents. Column chromatography used SiliaFlash® P60 (SiliCycle).

7.2 Pyridyl-endcapped oligoynes (Chapter 2 data)

7.2.1 Synthesis of known compounds
General procedure A:

Bpin(a) (87%)　　**Bpin(b)** (89%)　　**Bpin(c)** (66%)　　**Bpin(f)** (68%)
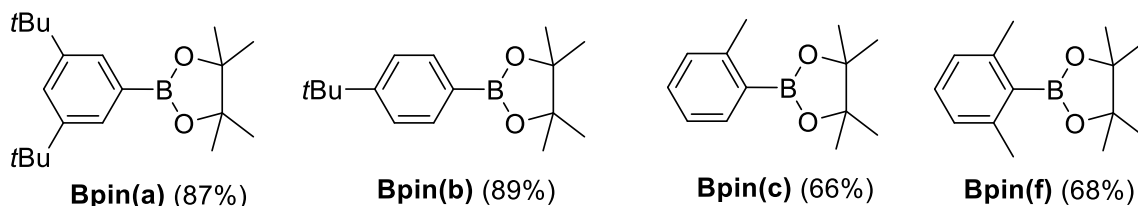
Boronic esters of **Bpin(a)**, **Bpin(b)**, **Bpin(c)**, and **Bpin(f)** were formed by adaptation of a known procedure.[1] A solution of toluene (100 mL; for making **Bpin(a–c)**) or DMF (100 mL; for making **Bpin(f)**) was deoxygenated under a flow of N$_2$ for 20 min. To the solution was the added the Ar-Br (18.6 mmol), bis(pinacolato)diboron (52.4 mmol), potassium acetate (76.5 mmol), and Pd(dppf)Cl$_2$ (1.12 mmol). The mixture was stirred at 110 °C under a N$_2$ atmosphere. TLC analysis was used to monitor the reaction (via the loss of mono substituted intermediate), and it was typically complete in 2–3 days. The reaction mixture was cooled to rt, H$_2$O (80 mL) and ethyl acetate (40 mL) were added, the layers were separated, and the aqueous phase was extracted with ethyl acetate (2 × 40 mL). The organic phases were combined, dried (MgSO$_4$), and filtered. Solvent

removal and purification by column chromatography afforded the desired boronate ester.

R = *t*Bu, **Bpin(d)** (31%)
R = H, **Bpin(e)** (52%)
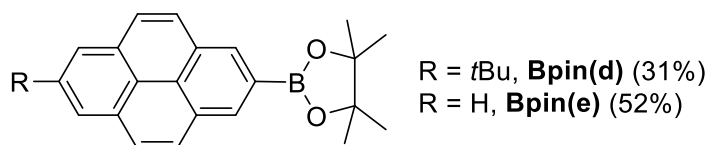
Compound Bpin(d) and **Bpin(e)** were synthesized as described in the literature.[2]

2.1   **2.2** (83%)   **2.3** (79%)
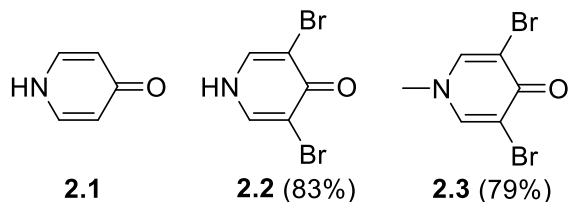
Compound 2.2 was synthesized from compound **2.1** as described in the literature.[3]

Compound 2.3: The methylation of 4-pyridone was carried out by adapting the procedure of Eidamshaus and Reissig.[4] To the solution of compound **2.2**, 3,5-dibromo-4-pyridone (3.0 g, 12 mmol) and K_2CO_3 (3.28 g, 23.7 mmol) in DMF (100 mL) was added methyl iodide (2.52 g, 17.8 mmol). The mixture was stirred at rt for 72 h. NaOH solution (1M, 50 mL) and CH_2Cl_2 (100 mL) were added, the layers were separated, and the aqueous phase was extracted with CH_2Cl_2 (2 × 50 mL). The organic phases were combined, dried ($MgSO_4$), and filtered. Solvent removal and recrystallization from MeOH (20 mL) afforded compound **2.3** (2.5 g, 79%) as a white solid. ^{1}H NMR (500 MHz, CDCl$_3$) δ 7.70 (s, 2H), 3.73 (s, 3H). ^{13}C NMR (125 MHz, CDCl$_3$) δ 167.9, 140.4, 113.3, 44.0. Spectra data were comparable to those reported in the literature.[5]

2.10   **2.11**   **2.12**
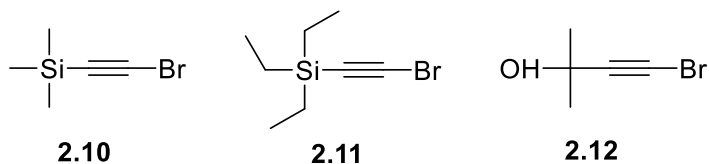
Compound 2.10,[6] **2.11**,[7] and **2.12**[8] were synthesized as described in the literature.

2.13   **2.15**
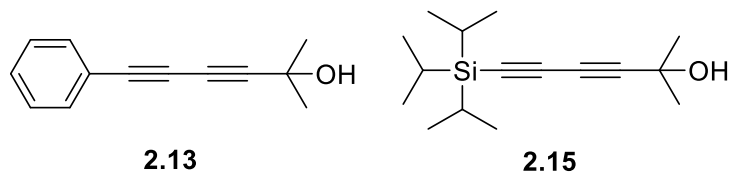
Compound 2.13 and **2.15** were synthesized as described in the literature.[8]

Compound 2.14: To a solution of **2.13**[8] (200 mg, 1.09 mmol) in dry toluene (5 mL) was added TDA-1 (176 mg, 0.544 mmol) and well powdered NaOH

156
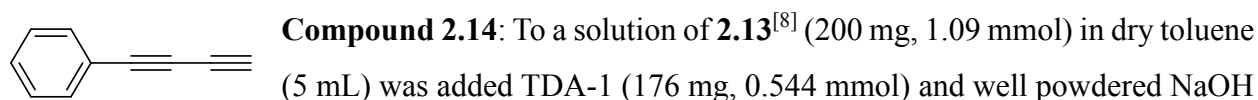
(217 mg, 5.43 mmol). The reaction was stirred at rt for 2 h. H_2O (10 mL) and hexanes (10 mL) were then added, the layers were separated, and the aqueous phase was extracted with hexanes (2 × 10 mL). The organic phases were combined, washed with brine (20 mL), dried ($MgSO_4$), and filtered. Solvent removal and purification by column chromatography (silica gel, hexanes) afforded the titled compound (52 mg, 38%) as a colorless oil. ^{1}H NMR (500 MHz, $CDCl_3$) δ 7.53–7.51 (m, 2H), 7.40–7.37 (m, 1H), 7.34–7.31 (m, 2H), 2.47 (s, 1H). ^{13}C NMR (125 MHz, $CDCl_3$) δ 132.8, 129.5, 128.4, 121.0, 75.3, 73.5, 71.2, 68.1. The data is consistent with that reported.[8]
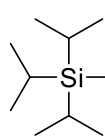
Compound 2.16: To a solution of **2.15**[8] (200 mg, 0.756 mmol) in dry toluene (5 mL) was added TDA-1 (122 mg, 0.377 mmol) and well powdered NaOH (61 mg, 1.5 mmol). The reaction was stirred at rt for 8 h. H_2O (10 mL) and hexanes (10 mL) were then added, the layers were separated, and the aqueous phase was extracted with hexanes (2 × 10 mL). The organic phases were combined, washed with brine (20 mL), dried ($MgSO_4$), and filtered. Solvent removal and purification by column chromatography (silica gel, hexanes) afforded the titled compound (90 mg, 58%) as a colorless oil. ^{1}H NMR (500 MHz, $CDCl_3$) δ 2.07 (s, 1H), 1.09 (brs, 21H). ^{13}C NMR (125 MHz, $CDCl_3$) δ 89.1, 82.0, 68.6, 65.5, 18.5, 11.2. The data is consistent with that reported.[8]
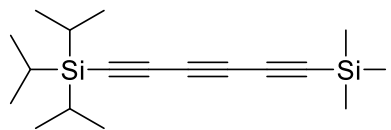
2.17
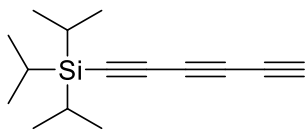
2.18

Compound 2.17[9] and **2.18**[10] were synthesized as described in the literature.

7.2.2 Synthetic protocols
General procedure B:
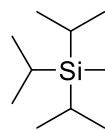
Compound 2.19: To a solution of EtOAc (5 mL) and MeOH (2 mL) was added 1-TIPS-6-TMS-hexa-1,3,5-triyne[9] (**2.17**, 200 mg, 0.661 mmol) and K_2CO_3 (915 mg, 6.62 mmol). The solution was stirred for 30 min at rt. H_2O (10 mL) and EtOAc (5 mL) were then added, the layers were separated, and the aqueous phase was extracted with EtOAc (5 mL). The organic phases were combined, washed with satd aq NH_4Cl (20 mL), dried ($MgSO_4$), and filtered. To this solution was added MeCN (10 mL), *N*-iodosuccinimide (164 mg, 0.729 mmol), and $AgNO_3$ (22.5 mg, 0.132 mmol). The solution

was stirred for 30 min at rt with wrapped in aluminum foil to avoid light. H_2O (20 mL) and hexanes (20 mL) were then added, the layers were separated, and the aqueous phase was extracted with hexanes (2 × 20 mL). The organic phases were combined, washed with brine (20 mL), dried ($MgSO_4$), and filtered. Solvent removal and purification by column chromatography (silica gel, hexanes) afforded **2.19** (200 mg, 85%) as a light-yellow oil. As a neat oil, compound **2.19** begins to decompose under refrigeration at 4 °C in as little as 12 h (i.e., overnight), but can be stored as a solution in hexanes for weeks without noticeable change. R_f = 0.60 (hexanes). IR (cast film) 2944 (s), 2890 (m), 2866 (s), 2173 (w), 2056 (m) cm^{-1}. ^{1}H NMR (500 MHz, $CDCl_3$) δ 1.12–1.10 (m, 21H). ^{13}C NMR (125 MHz, $CDCl_3$) δ 89.1, 84.6, 79.0, 61.6, 59.4, 18.5, 11.3, –0.4. ESI HRMS calcd for $C_{15}H_{21}SiI$ ([M]$^+$) 356.0458, found 356.0454.
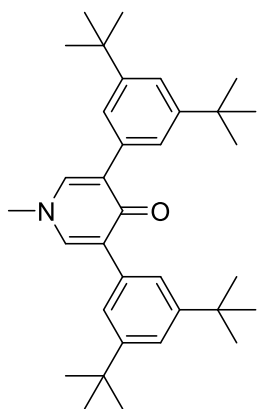
Compound 2.4a: A solution of toluene (120 mL) and EtOH (30 mL) was deoxygenated under a flow of N_2 for 20 min. To the solution was added 2-(3,5-di-*tert*-butylphenyl)-4,4,5,5-tetramethyl-1,3,2-dioxaborolane (**Bpin(a)**, 2.20 g, 6.96 mmol), compound **2.3** (850 mg, 3.18 mmol), Pd(PPh$_3$)$_4$ (220 mg, 0.190 mmol), and Cs_2CO_3 (4.10 g, 12.6 mmol). The mixture was stirred for 3 d at 80 °C under a N_2 atmosphere. The reaction mixture was cooled to rt, H_2O (50 mL) and ethyl acetate (40 mL) were added, the layers were separated, and the aqueous phase was extracted with ethyl acetate (2 × 40 mL). The organic phases were combined, washed with satd aq NH_4Cl (2 × 20 mL), dried ($MgSO_4$), and filtered. Solvent removal and purification by column chromatography (silica gel, EtOAc/CH_2Cl_2 1:10) afforded **2.4a** (1.37 g, 88%) as a white solid. Mp: no visible change ≤ 300 °C. R_f = 0.61 (EtOAc/hexanes 1:2). IR (cast film) 3045 (w), 2962 (s), 2903 (m), 2867 (w), 1643 (s), 1594 (m), 1565 (m) cm^{-1}. ^{1}H NMR (500 MHz, $CDCl_3$) δ 7.44 (d, J = 1.8 Hz, 4H), 7.39 (t, J = 1.8 Hz, 2H), 7.38 (s, 2H), 3.76 (s, 3H), 1.34 (s, 36H). ^{13}C NMR (125 MHz, $CDCl_3$) δ 174.4, 150.4, 138.0, 134.4, 131.8, 123.3, 121.8, 43.9, 34.9, 31.5. ESI HRMS calcd for $C_{34}H_{48}NO$ ([M + H]$^+$) 486.3730, found 486.3723.
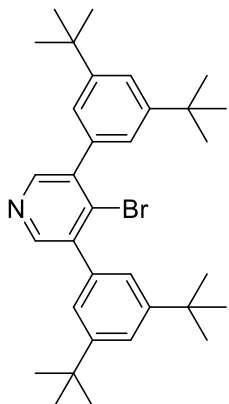
Compound 2.5a: To PBr₃ (4 mL) was added **2.4a** (200 mg, 0.412 mmol). The mixture was stirred for 4 h at 150 °C under a N$_2$ atmosphere. After cooling to rt, the reaction mixture was added dropwise to a NaOH solution (1M, 300 mL) in an ice bath. The mixture was stirred for 5 min. CH$_2$Cl$_2$ (50 mL) was added, the layers were separated, and the aqueous phase was extracted with CH$_2$Cl$_2$ (3 × 50 mL). The organic phases were combined, washed with satd aq NH$_4$Cl (2 × 20 mL), dried (MgSO$_4$) and filtered. Solvent removal and purification by column chromatography (silica gel, EtOAc/hexanes 1:10) afforded **2.5a** (205 mg, 93%) as a white solid. Mp 186–188 °C. R_f = 0.68 (EtOAc/hexanes 1:4). IR (cast film) 3016 (w), 2963 (s), 2904 (m), 2868 (w), 1596 (m), 1542 (w) cm^{-1}. ^{1}H NMR (500 MHz, CDCl$_3$) δ 8.47 (s, 2H), 7.49 (t, J = 1.8 Hz, 2H), 7.32 (d, J = 1.8 Hz, 4H), 1.38 (s, 36H). ^{13}C NMR (125 MHz, CDCl$_3$) δ 150.5, 149.3, 140.0, 137.1, 133.6, 124.1, 122.0, 35.0, 31.5. ESI HRMS calcd for C$_{33}$H$_{45}$N^{79}Br ([M + H]$^+$) 534.2730, found 534.2722.
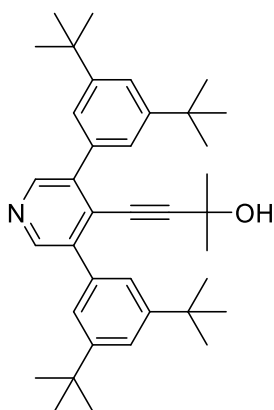
Compound 2.6a: 2-Methylbut-3-yn-2-ol (598 mg, 7.11 mmol) was added to triethylamine (15 mL), and the solution was deoxygenated under a flow of N$_2$ for 20 min. To this solution was added **2.5a** (380 mg, 0.711 mmol), Pd(PPh$_3$)$_4$ (41 mg, 0.035 mmol), and CuI (20.3 mg, 0.107 mmol). The mixture was stirred for 66 h at 80 °C under a N$_2$ atmosphere. The reaction mixture was cooled to rt, H$_2$O (50 mL) and ethyl acetate (30 mL) were added, the layers were separated, and the aqueous phase was extracted with ethyl acetate (2 × 30 mL). The organic phases were combined, washed with satd aq NH$_4$Cl (2 × 20 mL), dried (MgSO$_4$), and filtered. Solvent removal and purification by column chromatography (silica gel, EtOAc/hexanes 1:6) afforded **2.6a** (270 mg, 71%) as a white solid. Mp 207–209 °C. R_f = 0.74 (EtOAc/hexanes 1:2). UV-vis (CH$_2$Cl$_2$) λ_{max} (ε): 306 (7270). IR (cast film) 3336 (br, w), 3037 (w), 2965 (s), 2904 (m), 2869 (m), 2228 (w), 1596 (m), 1568 (w) cm^{-1}. ^{1}H NMR (500 MHz, CDCl$_3$) δ 8.57 (s, 2H), 7.48 (t, J = 1.8 Hz, 2H), 7.35 (d, J = 1.8 Hz, 4H), 1.38 (s, 36H), 1.18 (s, 6H). ^{13}C NMR (125 MHz, CDCl$_3$) δ 150.6, 148.5, 139.9, 136.8, 127.8, 123.5, 122.1, 104.4, 79.6, 65.2, 35.0, 31.6, 30.8. ESI HRMS calcd for C$_{38}$H$_{52}$NO ([M + H]$^+$) 538.4043, found 538.4039. DSC: Mp = 213 °C, decomposition, 366 °C (onset), 401 °C (peak).
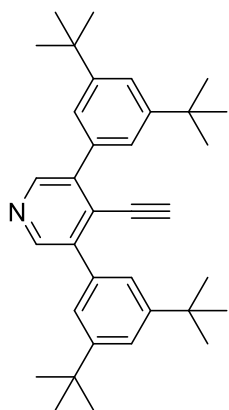
Compound 2.7a: To a solution of **2.6a** (70 mg, 0.13 mmol) in dried toluene (5 mL) was added well-powdered NaOH (52 mg, 1.3 mmol) and TDA-1 (42 mg, 0.13 mmol). The solution was stirred for 4 h at 110 °C. The reaction mixture was cooled to rt, H_2O (20 mL) and ethyl acetate (20 mL) were added, the layers were separated, and the aqueous phase was extracted with ethyl acetate (2 × 20 mL). The organic phases were combined, washed with satd aq NH_4Cl (2 × 20 mL), dried ($MgSO_4$), and filtered. Solvent removal and purification by column chromatography (silica gel, EtOAc/hexanes 1:12) afforded **2.7a** (58 mg, 93%) as a white solid. Mp 196–198 °C. R_f = 0.66 (EtOAc/hexanes 1:4). UV-vis (CH_2Cl_2) λ_{max} (ε): 314 (7350). IR (cast film) 3310 (w), 3276 (w), 2963 (s), 2868 (m), 2093 (w), 1596 (m) cm^{-1}. ^{1}H NMR (500 MHz, CDCl$_3$) δ 8.64 (s, 2H), 7.50–7.48 (m, 6H), 3.19 (s, 1H), 1.38 (s, 36H). ^{13}C NMR (125 MHz, CDCl$_3$) δ 150.4, 148.7, 140.3, 136.0, 126.4, 124.1, 121.9, 87.7, 80.4, 35.1, 31.5. ESI HRMS calcd for $C_{35}H_{46}N$ ($[M + H]^+$) 480.3625, found 480.3624. DSC: Mp = 203 °C, decomposition, 242 °C (onset), 276 °C (peak).
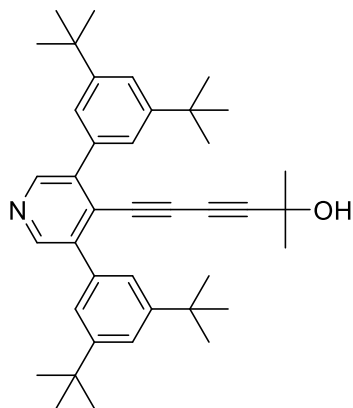
Compound 2.8a: 4-Bromo-2-methyl-3-butyn-2-ol (680 mg, 4.17 mmol) was added to EtOH (15 mL), and the solution was deoxygenated under a flow of N_2 for 20 min. The solution was cooled in an ice bath and **2.7a** (100 mg, 0.208 mmol), CuCl (4.1 mg, 0.041 mmol), hydroxylammonium chloride (2.9 mg, 0.042 mmol), and freshly deoxygenated *n*-propylamine (85 μL) were added. The ice bath was removed after stirring for 10 min. The solution was heated to 80 °C and stirred for 19 h under a N_2 atmosphere. The reaction mixture was cooled to rt, H_2O (20 mL) and ethyl acetate (20 mL) were added, the layers were separated, and the aqueous phase was extracted with ethyl acetate (2 × 20 mL). The organic phases were combined, washed with satd aq NH_4Cl (2 × 20 mL), dried ($MgSO_4$), and filtered. Solvent removal and purification by column chromatography (silica gel, EtOAc/hexanes 1:6) afforded **2.8a** (93 mg, 79%) as a white solid. Mp 240–241 °C. R_f = 0.73 (EtOAc/hexanes 1:2). UV-vis (CH_2Cl_2) λ_{max} (ε): 260 (20000), 312 (9940). IR (cast film) 3236 (br, w), 2964 (s), 2904 (m), 2868 (m), 2232 (w), 2140 (w), 1596 (m) cm^{-1}. ^{1}H NMR (500 MHz, CDCl$_3$) δ 8.65 (s, 2H), 7.50–7.49 (m, 6H), 1.76 (s, 1H), 1.45 (s, 6H), 1.40 (s, 36H). ^{13}C NMR (125 MHz, CDCl$_3$) δ 150.6, 148.5,

140.5, 135.6, 125.9, 124.0, 122.2, 89.2, 83.2, 75.3, 67.1, 65.6, 35.0, 31.5, 30.9. ESI HRMS calcd for $C_{40}H_{52}NO$ ([M + H]$^+$) 562.4043, found 562.4036. DSC: Mp = 243 °C, decomposition, 251 °C (onset), 296 °C (peak).
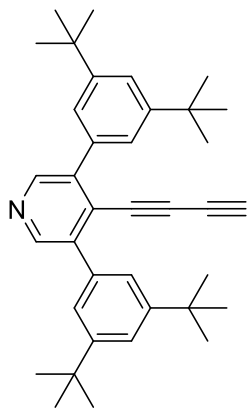
Compound 2.9a: To a solution of **2.8a** (200 mg, 0.356 mmol) in dried toluene (20 mL) was added well-powdered NaOH (142 mg, 3.55 mmol) and TDA-1 (115 mg, 0.356 mmol). The solution was stirred for 2 h at rt, H_2O (30 mL) and ethyl acetate (30 mL) were added, the layers were separated, and the aqueous phase was extracted with ethyl acetate (2 × 20 mL). The organic phases were combined, washed with satd aq NH_4Cl (2 × 20 mL), dried ($MgSO_4$), and filtered. Solvent removal and purification by column chromatography (silica gel, EtOAc/hexanes 1:12) afforded **2.9a** (160 mg, 89%) as a white solid. Mp 170 °C (decomp). R_f = 0.67 (EtOAc/hexanes 1:4). UV-vis (CH_2Cl_2) λ_{max} (ε): 258 (22000), 307 (8340), 318 (sh, 8000). IR (cast film) 3300 (w), 3270 (w), 3135 (br, m), 2964 (s), 2904 (m), 2868 (m), 2214 (m), 2052 (w), 1595 (m), 1566 (w) cm^{-1}. ^{1}H NMR (500 MHz, CDCl$_3$) δ 8.66 (s, 2H), 7.50–7.49 (m, 6H), 2.45 (s, 1H), 1.39 (s, 36H). ^{13}C NMR (125 MHz, CDCl$_3$) δ 150.7, 148.6, 140.8, 135.6, 125.5, 123.9, 122.4, 83.2, 73.7, 71.8, 67.9, 35.0, 31.5. ESI HRMS calcd for $C_{37}H_{46}N$ ([M + H]$^+$) 504.3625, found 504.3620. DSC: decomposition, 176 °C (onset), 184 °C (peak).
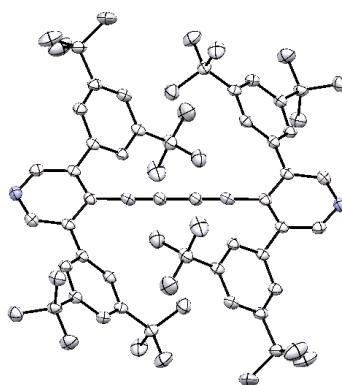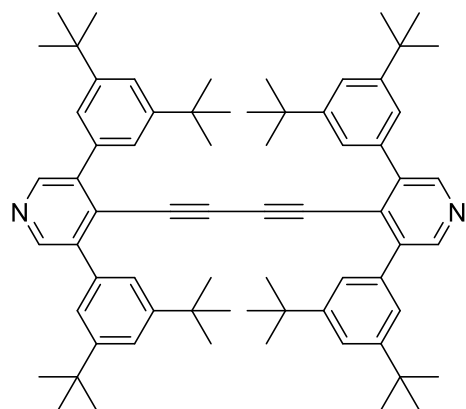
Compound Py[2a]**: To a solution of **2.7a** (100 mg, 0.208 mmol) in pyridine (1 mL) was added Cu(OAc)$_2$ (76 mg, 0.42 mmol), CuCl (4.2 mg, 0.042 mmol), and 4 Å sieves (100 mg). The solution was stirred for 24 h at 100 °C. The reaction mixture was cooled to rt, H_2O (20 mL) and CH_2Cl_2 (20 mL) were added, the layers were separated, and the aqueous phase was extracted with CH_2Cl_2 (2 × 20 mL). The organic phases were combined, washed with satd aq NH_4Cl (2 × 20 mL), dried

(MgSO$_4$), and filtered. Solvent removal and purification by column chromatography (silica gel, EtOAc/hexanes 1:6) afforded **Py**[2a]** (70 mg, 70%) as a white solid. Mp: no visible change ≤ 300 °C. R_f = 0.77 (EtOAc/hexanes 1:2). UV-vis (CH$_2$Cl$_2$) λ_{max} (ε): 324 (21600), 337 (20600), 375 nm (sh, 3460). IR (cast film) 3031 (w), 2960 (s), 2904 (m), 2866 (m), 2140 (w), 1595 (m), 1559 (w) cm^{-1}. ^{1}H NMR (500 MHz, CDCl$_3$) δ 8.60 (s, 4H), 7.39 (s, 12H), 1.26 (s, 72H). ^{13}C NMR (125 MHz, CDCl$_3$) δ 150.6, 148.7, 140.3, 135.5, 125.3, 123.9, 122.1, 83.3, 80.5, 34.9, 31.5. MALDI HRMS (DCTB) calcd for C$_{70}$H$_{89}$N$_2$ ([M + H]$^+$) 957.7020, found 957.7024. DSC: Mp = 360 °C, decomposition, 404 °C (onset), 435 °C (peak).

A crystal of **Py**[2a]** suitable for X-ray crystallographic analysis has been grown at rt by slow evaporation from a CH$_2$Cl$_2$ solution. X-ray data for **Py**[2a]** (C$_{70}$H$_{88}$N$_2$), F_w = 957.42; crystal dimensions 0.31 × 0.26 × 0.05 mm; monoclinic crystal system; space group $P2_1/n$ (No. 14); a = 10.2557(5) Å, b = 29.6077(16) Å, c = 10.8693(5) Å; β = 116.377(3)°; V = 2956.8(3) Å^3; Z = 2; $\rho_{(calcd)}$ = 1.075 g/cm^3; μ = 0.453 mm^{-1}; λ = 1.54178 Å; T = 173 K; $2\theta_{max}$ = 140.57°; total data collected = 17339; R_1 = 0.0673 [4141 observed reflections with $F_o^2 \geq 2\sigma(F_o^2)$]; ωR_2 = 0.1985 for 5627 data, 325 variables, and 0 restraints; largest difference, peak and hole = 0.452 and –0.289 e Å^{-3}. CCDC: 1977437.
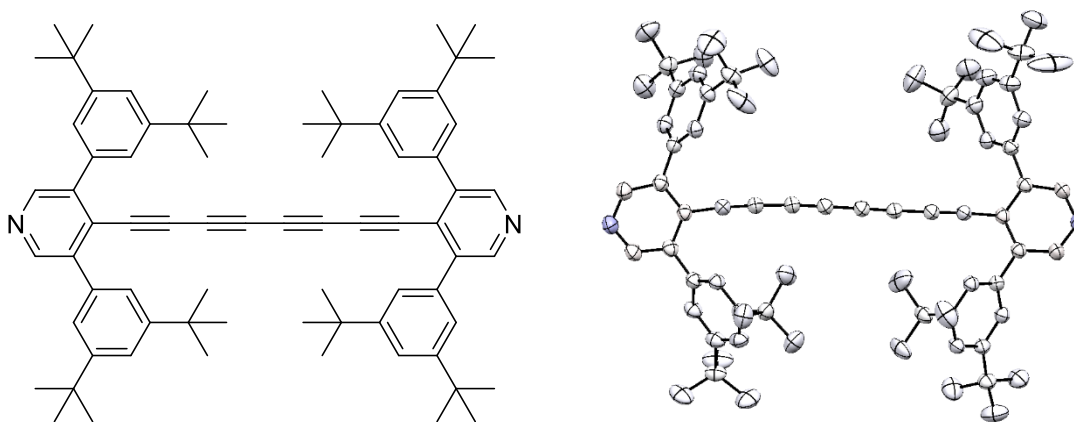
Compound Py**[4a]: To a solution of **2.9a** (50 mg, 0.099 mmol) in pyridine (3 mL) was added Cu(OAc)$_2$ (36.0 mg, 0.198 mmol), CuCl (2.0 mg, 0.020 mmol), and 4 Å sieves (100 mg). The solution was stirred for 4 h at rt, H$_2$O (20 mL) and CH$_2$Cl$_2$ (20 mL) were added, the layers were separated, and the aqueous phase was extracted with CH$_2$Cl$_2$ (2 × 20 mL). The organic phases were combined, washed with satd aq NH$_4$Cl (2 × 20 mL), dried (MgSO$_4$), and filtered. Solvent removal and purification by column chromatography (silica gel, EtOAc/hexanes 1:12) afforded **Py**[4a]**

(42 mg, 84%) as a yellowish to greenish solid. Mp 292–293 °C (decomp). R_f = 0.60 (EtOAc/hexanes 1:4). UV-vis (CH$_2$Cl$_2$) λ_{max} (ε): 298 (42400), 312 (42500), 337 (41900), 360 (31000), 388 (25300), 421 (16900), 448 nm (sh, 1200). IR (cast film) 3031 (w), 2964 (s), 2905 (m), 2868 (m), 2201 (w), 2122 (w), 1596 (m), 1559 (w) cm^{-1}. ^{1}H NMR (500 MHz, CDCl$_3$) δ 8.67 (s, 4H), 7.50–7.46 (m, 12H), 1.38 (s, 72H). ^{13}C NMR (125 MHz, CDCl$_3$) δ 150.9, 148.6, 141.2, 135.4, 124.9, 123.8, 122.5, 83.5, 74.8, 69.0, 64.0, 35.0, 31.5. MALDI HRMS (DCTB) calcd for C$_{74}$H$_{89}$N$_2$ ([M + H]$^+$) 1005.7020, found 1005.7006. DSC: Mp = 298 °C, decomposition, 309 °C (onset), 331 °C (peak).

A crystal of **Py**[4a]** suitable for X-ray crystallographic analysis has been grown at 5 °C, by slow evaporation from a CH$_2$Cl$_2$ solution layered with MeOH. X-ray data for **Py**[4a]** (C$_{74}$H$_{88}$N$_2$•0.5CH$_4$O), F_w = 1021.48; crystal dimensions 0.31 × 0.14 × 0.02 mm; monoclinic crystal system; space group $C2/c$ (No. 15); a = 49.9679(9) Å, b = 12.0092(2) Å, c = 26.1936(5) Å; β = 120.9851(10)°; V = 13475.2(4) Å^3; Z = 8; $\rho_{(calcd)}$ = 1.007 g/cm^3; μ = 0.431 mm^{-1}; λ = 1.54178 Å; T = 173 K; $2\theta_{max}$ = 140.57°; total data collected = 42381; R_1 = 0.0549 [8754 observed reflections with $F_o^2 \geq 2\sigma(F_o^2)$]; ωR_2 = 0.1655 for 12779 data, 756 variables, and 0 restraints; largest difference, peak and hole = 0.288 and –0.220 e Å^{-3}. CCDC: 1977433.
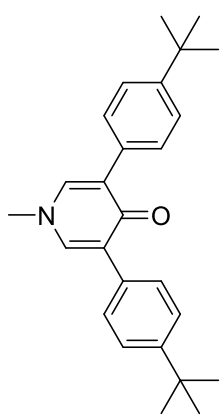
Compound 2.4b: A solution of toluene (100 mL) and EtOH (25 mL) was deoxygenated under a flow of N$_2$ for 20 min. To the solution was added 2-(4-*tert*-butylphenyl)-4,4,5,5-tetramethyl-1,3,2-dioxaborolane (**Bpin(b)**, 3.50 g, 13.5 mmol), compound **2.3** (1.20 g, 4.50 mmol), Pd(PPh$_3$)$_4$ (312 mg, 0.270 mmol), and Cs$_2$CO$_3$ (5.86 g, 18.0 mmol). The mixture was stirred for 62 h at 80 °C under a N$_2$ atmosphere. The reaction mixture was cooled to rt, H$_2$O (50 mL) and ethyl acetate (40 mL) were added, the layers were separated, and the aqueous phase was extracted with ethyl acetate (2 × 40 mL). The organic phases were combined, washed with satd aq NH$_4$Cl (2 × 20 mL), dried (MgSO$_4$), and filtered. Solvent removal and purification by column chromatography (silica gel, EtOAc/CH$_2$Cl$_2$ 1:8) afforded **2.4b** (1.45 g, 86%) as a white solid. Mp: no visible change ≤ 300 °C. R_f = 0.50 (EtOAc/hexanes 1:1). IR (cast film) 3049 (w), 2966 (s), 2867 (w), 1644 (s), 1559 (s) cm^{-1}. ^{1}H NMR (500 MHz, CDCl$_3$) δ 7.60 (d, J = 8.4 Hz, 4H), 7.41 (d, J = 8.4 Hz, 4H), 7.40 (s, 2H), 3.72 (s, 3H), 1.33 (s, 18H). ^{13}C NMR (125 MHz, CDCl$_3$) δ 174.3, 150.4, 137.6, 132.2, 130.3, 128.4, 125.1, 44.0, 34.6, 31.4. ESI

HRMS calcd for $C_{26}H_{32}NO$ ($[M + H]^+$) 374.2478, found 374.2476.
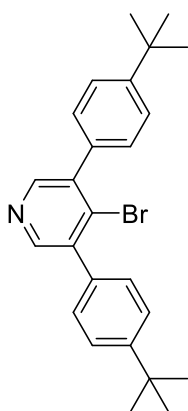
Compound 2.5b: To PBr$_3$ (4 mL) was added **2.4b** (200 mg, 0.535 mmol). The mixture was stirred for 4 h at 150 °C under a N$_2$ atmosphere. After cooling to rt, the reaction mixture was added dropwise to a NaOH solution (1M, 300 mL) in an ice bath. The mixture was stirred for 5 min. CH$_2$Cl$_2$ (50 mL) was added, the layers were separated, and the aqueous phase was extracted with CH$_2$Cl$_2$ (3 × 50 mL). The organic phases were combined, washed with satd aq NH$_4$Cl (2 × 20 mL), dried (MgSO$_4$), and filtered. Solvent removal and purification by column chromatography (silica gel, EtOAc/hexanes 1:10) afforded **2.5b** (192 mg, 85%) as a white solid. Mp 180–181 °C. R_f = 0.57 (EtOAc/hexanes 1:4). IR (cast film) 3046 (w), 3025 (w), 2960 (s), 2903 (m), 2868 (m), 1542 (m), 1508 (m) cm^{-1}. ^{1}H NMR (500 MHz, CDCl$_3$) δ 8.43 (s, 2H), 7.50, 7.41 (ABq, J_{AB} = 8.5 Hz, 8H), 1.39 (s, 18H). ^{13}C NMR (125 MHz, CDCl$_3$) δ 151.3, 149.4, 139.0, 135.0, 133.4, 129.3, 125.2, 34.7, 31.3. ESI HRMS calcd for $C_{25}H_{29}N^{79}Br$ ($[M + H]^+$) 422.1478, found 422.1475.
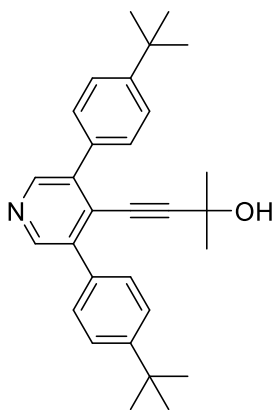
Compound 2.6b: 2-Methylbut-3-yn-2-ol (498 mg, 5.92 mmol) was added to a solution of triethylamine (5 mL) and deoxygenated under a flow of N$_2$ for 20 min. To this solution was added **2.5b** (250 mg, 0.592 mmol), Pd(PPh$_3$)$_4$ (34 mg, 0.030 mmol), and CuI (17 mg, 0.089 mmol). The mixture was stirred for 2 d at 80 °C under a N$_2$ atmosphere. The reaction mixture was cooled to rt, H$_2$O (20 mL) and ethyl acetate (20 mL) were added, the layers were separated, and the aqueous phase was extracted with ethyl acetate (2 × 20 mL). The organic phases were combined, washed with satd aq NH$_4$Cl (2 × 20 mL), dried (MgSO$_4$), and filtered. Solvent removal and purification by column chromatography (silica gel, EtOAc/hexanes 1:6) afforded **2.6b** (182 mg, 72%) as a white solid. Mp 124–126 °C. R_f = 0.56 (EtOAc/hexanes 1:2). IR (cast film) 3223 (br, m), 3032 (m), 2964 (s), 2905 (m), 2868 (m), 2228 (w), 1577 (m), 1508 (m) cm^{-1}. ^{1}H NMR (500 MHz, CDCl$_3$) δ 8.58 (s, 2H), 7.54, 7.48 (ABq, J_{AB} = 8.5 Hz, 8H), 1.37 (s, 18H), 1.30 (s, 6H). ^{13}C NMR (125 MHz, CDCl$_3$) δ 151.3, 148.2, 138.4, 134.3, 129.1, 127.4, 125.0, 104.2, 79.2, 65.4, 34.7, 31.3, 30.3. ESI HRMS calcd for $C_{30}H_{36}NO$ ($[M + H]^+$) 426.2791, found 426.2791.

164
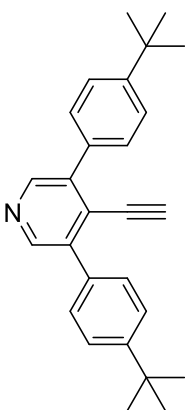
Compound 2.7b: To a solution of **2.6b** (100 mg, 0.235 mmol) in dried toluene (10 mL) was added well-powdered NaOH (94.0 mg, 2.35 mmol) and TDA-1 (76.0 mg, 0.235 mmol). The solution was stirred for 4 h at rt, only a trace amount of product can be observed as monitored by TLC analysis. The solution was then stirred for 4 h at 110 °C until conversion was judged completely by TLC analysis. The reaction mixture was cooled to rt, H_2O (20 mL) and ethyl acetate (20 mL) were added, the layers were separated, and the aqueous phase was extracted with ethyl acetate (2 × 20 mL). The organic phases were combined, washed with satd aq NH_4Cl (2 × 20 mL), dried ($MgSO_4$), and filtered. Solvent removal and purification by column chromatography (silica gel, EtOAc/hexanes 1:12) afforded **2.7b** (82 mg, 95%) as a white solid. Mp 198–199 °C. R_f = 0.52 (EtOAc/hexanes 1:4). IR (cast film) 3290 (s), 3049 (w), 3029 (w), 2960 (s), 2904 (m), 2866 (m), 2110 (w), 1572 (m), 1506 (m) cm^{-1}. ^{1}H NMR (500 MHz, CDCl$_3$) δ 8.58 (s, 2H), 7.57, 7.49 (ABq, J_{AB} = 8.4 Hz, 8H), 3.21 (s, 1H), 1.38 (s, 18H). ^{13}C NMR (125 MHz, CDCl$_3$) δ 151.2, 148.6, 139.1, 134.0, 129.2, 126.3, 125.2, 88.1, 79.7, 34.7, 31.4. ESI HRMS calcd for $C_{27}H_{30}N$ ([M + H]$^+$) 368.2373, found 368.2369. DSC: Mp = 201 °C, decomposition, 210 °C (onset), 254 °C (peak).
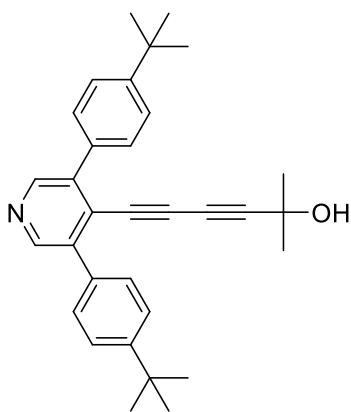
Compound 2.8b: 4-Bromo-2-methyl-3-butyn-2-ol (532 mg, 3.26 mmol) was added to EtOH (10 mL), and the solution was deoxygenated under a flow of N_2 for 20 min. The solution was cooled in an ice bath and **2.7b** (60.0 mg, 0.163 mmol), CuCl (3.2 mg, 0.032 mmol), hydroxylammonium chloride (2.3 mg, 0.033 mmol), and freshly deoxygenated *n*-propylamine (67 μL) were added. The ice bath was removed after stirring for 10 min. The solution was warmed to rt and stirred for 23 h under a N_2 atmosphere. H_2O (20 mL) and ethyl acetate (20 mL) were added, the layers were separated, and the aqueous phase was extracted with ethyl acetate (2 × 20 mL). The organic phases were combined, washed with satd aq NH_4Cl (2 × 20 mL), dried ($MgSO_4$), and filtered. After removing the solvent, the residue was purified by column chromatography (silica gel, EtOAc/hexanes 1:6) to afford the crude product. Recrystallization from CH_2Cl_2/hexanes (0.3 mL/10 mL) gave product **2.8b** (55 mg, 75%) as a white solid. Mp 162–164 °C. R_f = 0.57 (EtOAc/hexanes 1:2). IR (cast film) 3244 (br, m), 3089

(m), 3032 (m), 2966 (s), 2904 (m), 2868 (m), 2231 (w), 2144 (w), 1611 (w), 1576 (m), 1555 (w), 1507 (m) cm^{-1}. ^{1}H NMR (500 MHz, CDCl$_3$) δ 8.59 (s, 2H), 7.55, 7.52 (ABq, J_{AB} = 8.6 Hz, 8H), 1.88 (s, 1H), 1.49 (s, 6H), 1.39 (s, 18H). ^{13}C NMR (125 MHz, CDCl$_3$) δ 151.4, 148.6, 139.5, 133.8, 129.0, 125.9, 125.4, 89.1, 83.1, 75.1, 66.8, 65.7, 34.7, 31.3, 31.0. ESI HRMS calcd for C$_{32}$H$_{36}$NO ([M + H]$^+$) 450.2791, found 450.2795. DSC: Mp = 171 °C, decomposition, 186 °C (onset), 225 °C (peak).
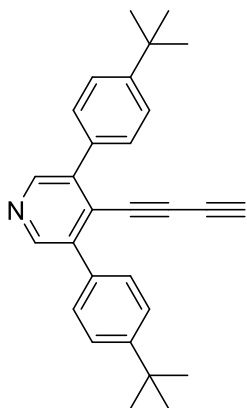
Compound 2.9b: To a solution of **2.8b** (55 mg, 0.12 mmol) in dried toluene (10 mL) was added well-powdered NaOH (49 mg, 1.2 mmol) and TDA-1 (40 mg, 1.2 mmol). The solution was stirred for 1.5 h at rt, H$_2$O (20 mL) and ethyl acetate (20 mL) were added, the layers were separated, and the aqueous phase was extracted with ethyl acetate (2 × 20 mL). The organic phases were combined, washed with satd aq NH$_4$Cl (2 × 20 mL), dried (MgSO$_4$), and filtered. Solvent removal and purification by column chromatography (silica gel, EtOAc/hexanes 1:12) afforded **2.9b** (35 mg, 73%) as a white solid. Mp 187 °C (decomp). R_f = 0.50 (EtOAc/hexanes 1:4). IR (cast film) 3302 (w), 3272 (s), 3031 (m), 2962 (s), 2904 (m), 2867 (m), 2216 (w), 2062 (w), 1571 (m), 1557 (w) cm^{-1}. ^{1}H NMR (500 MHz, CDCl$_3$) δ 8.60 (s, 2H), 7.56, 7.52 (ABq, J_{AB} = 8.4 Hz, 8H), 2.48 (s, 1H), 1.39 (s, 18H). ^{13}C NMR (125 MHz, CDCl$_3$) δ 151.5, 148.6, 139.8, 133.6, 129.0, 125.4, 83.1, 73.8, 71.6, 67.7, 34.7, 31.3 (one signal coincident or not observed). ESI HRMS calcd for C$_{29}$H$_{30}$N ([M + H]$^+$) 392.2373, found 392.2373. DSC: decomposition, 186 °C (onset), 190 °C (peak).
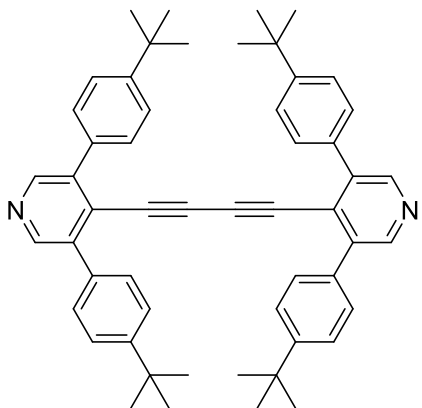
Compound Py**[2b]: To a solution of **2.7b** (100 mg, 0.272 mmol) in pyridine (2 mL) was added Cu(OAc)$_2$ (98.8 mg, 0.544 mmol), CuCl (5.4 mg, 0.055 mmol), and 4 Å sieves (100 mg). The solution was stirred for 20 h at 100 °C. The reaction mixture was cooled to rt, H$_2$O (20 mL) and CH$_2$Cl$_2$ (20 mL) were added, the layers were separated, and the aqueous phase was extracted with CH$_2$Cl$_2$ (2 × 20 mL). The organic phases were combined, washed with satd aq NH$_4$Cl (2 × 20 mL), dried (MgSO$_4$), and filtered. Solvent removal and purification by column chromatography (silica gel, EtOAc/hexanes 1:6) afforded **Py**[2b]** (91 mg, 91%) as a white solid. Mp 278–279 °C. R_f = 0.64

(EtOAc/hexanes 1:2). UV-vis (CH$_2$Cl$_2$) λ_{max} (ε): 328 (sh, 23000), 336 nm (23200). IR (cast film) 3031 (w), 2963 (s), 2904 (m), 2868 (m), 2150 (vw), 1570 (w), 1507 (m) cm^{-1}. ^{1}H NMR (500 MHz, CDCl$_3$) δ 8.58 (s, 4H), 7.48, 7.44 (ABq, J_{AB} = 8.5 Hz, 16H), 1.37 (s, 36H). ^{13}C NMR (125 MHz, CDCl$_3$) δ 151.5, 148.4, 139.2, 133.6, 129.0, 125.8, 125.2, 83.4, 80.8, 34.7, 31.4. ESI HRMS calcd for C$_{54}$H$_{57}$N$_2$ ([M + H]$^+$) 733.4516, found 733.4506. DSC: Mp = 286 °C, decomposition, 341 °C (onset), 356 °C (peak).
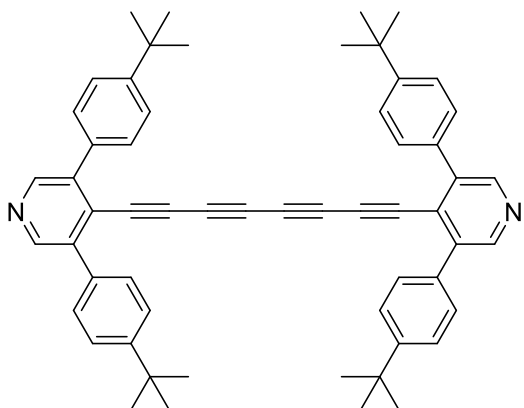
Compound Py**[4b]: To a solution of **2.9b** (50.0 mg, 0.128 mmol) in pyridine (3 mL) was added Cu(OAc)$_2$ (46.0 mg, 0.253 mmol), CuCl (2.5 mg, 0.025 mmol), and 4 Å sieves (100 mg). The solution was stirred for 4 h at rt, H$_2$O (20 mL) and CH$_2$Cl$_2$ (20 mL) were added, the layers were separated, and the aqueous phase was extracted with CH$_2$Cl$_2$ (2 × 20 mL). The organic phases were combined, washed with satd aq NH$_4$Cl (2 × 20 mL), dried (MgSO$_4$), and filtered. Solvent removal and purification by column chromatography (silica gel, EtOAc/hexanes 1:12) afforded **Py**[4b]** (46 mg, 92%) as a yellowish to greenish solid. Mp 242–244 °C (decomp). R_f = 0.36 (EtOAc/hexanes 1:4). UV-vis (CH$_2$Cl$_2$) λ_{max} (ε): 296 (sh, 32300), 307 (30800), 317 (31000), 335 (33800), 359 (25600), 387 (18500), 420 (10400), 445 nm (sh, 537). IR (cast film) 3027 (w), 2965 (s), 2904 (m), 2868 (m), 2199 (w), 2125 (w), 1610 (m), 1570 (m), 1505 (m) cm^{-1}. ^{1}H NMR (500 MHz, CDCl$_3$) δ 8.60 (s, 4H), 7.52, 7.50 (ABq, J_{AB} = 8.7 Hz, 16H), 1.39 (s, 36H). ^{13}C NMR (125 MHz, CDCl$_3$) δ 151.8, 148.6, 140.1, 133.4, 128.9, 125.5, 124.7, 83.2, 74.5, 69.2, 64.2, 34.8, 31.3. ESI HRMS calcd for C$_{58}$H$_{58}$N$_2$ ([M + 2H]$^{2+}$) 391.2295, found 391.2296, calcd for C$_{58}$H$_{57}$N$_2$ ([M + H]$^+$) 781.4516, found 781.4506. DSC: decomposition, 245 °C (onset), 257 °C (peak).
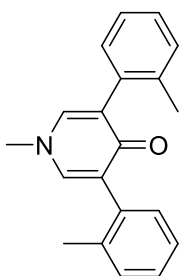
Compound 2.4c: A solution of toluene (100 mL) and EtOH (25 mL) was deoxygenated under a flow of N$_2$ for 20 min. To the solution was added compound **2.3** (1.00 g, 3.75 mmol), 2-(2-methylphenyl)-4,4,5,5-tetramethyl-1,3,2-dioxaborolane (**Bpin(c)**, 2.04 g, 9.35 mmol), Pd(PPh$_3$)$_4$ (260 mg, 0.225 mmol), and Cs$_2$CO$_3$ (4.88 g, 15.0 mmol). The mixture was stirred for 62 h at 80 °C under a N$_2$ atmosphere. The reaction mixture was cooled to rt, H$_2$O (50 mL) and ethyl

acetate (40 mL) were added, the layers were separated, and the aqueous phase was extracted with ethyl acetate (2 × 40 mL). The organic phases were combined, washed with satd aq NH_4Cl (2 × 20 mL), dried ($MgSO_4$), and filtered. Solvent removal and purification by column chromatography (silica gel, $EtOAc/CH_2Cl_2$ 1:5) afforded **2.4c** (900 mg, 83%) as a white solid. Mp 98–100°C. R_f = 0.26 (EtOAc/hexanes 3:1). IR (cast film) 3047 (w), 3016 (w), 2976 (s), 2949 (m), 2925 (w), 1645 (s), 1602 (s), 1555 (s) cm^{-1}. ^{1}H NMR (500 MHz, $CDCl_3$) δ 7.31 (s, 2H), 7.24–7.23 (m, 4H), 7.19–7.18 (m, 4H), 3.72 (s, 3H), 2.28 (s, 6H). ^{13}C NMR (125 MHz, $CDCl_3$) δ 173.6, 138.9, 138.0, 135.2, 131.9, 130.2, 129.9, 127.8, 125.5, 43.7, 20.1. ESI HRMS calcd for $C_{20}H_{20}NO$ ([M + H]$^+$) 290.1539, found 290.1537.
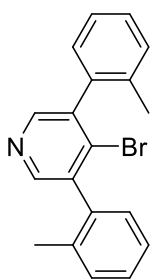
Compound 2.5c: To PBr_3 (6 mL) was added **2.4c** (200 mg, 0.691 mmol). The mixture was stirred for 1 d at 150 °C under a N_2 atmosphere. After cooling to rt, the reaction mixture was added dropwise to a NaOH solution (1M, 450 mL) in an ice bath. The mixture was stirred for 5 min. CH_2Cl_2 (50 mL) was added, the layers were separated, and the aqueous phase was extracted with CH_2Cl_2 (3 × 50 mL). The organic phases were combined, washed with satd aq NH_4Cl (2 × 20 mL), dried ($MgSO_4$), and filtered. Solvent removal and purification by column chromatography (silica gel, EtOAc/hexanes 1:10) afforded **2.5c** (164 mg, 70%) as a white solid. Mp 120–121 °C. R_f = 0.66 (EtOAc/hexanes 1:2). IR (cast film) 3061 (w), 3019 (w), 2975 (w), 2922 (w), 2864 (w), 1549 (s) cm^{-1}. ^{1}H NMR (500 MHz, $CDCl_3$) δ 8.40 (s, 2H), 7.38–7.35 (m, 2H), 7.33–7.29 (m, 4H), 7.21–7.20 (m, 2H), 2.17 (brs, 6H). ^{13}C NMR (125 MHz, $CDCl_3$, rt)* δ 149.3, 139.0, 138.9, 137.59, 137.57, 136.38, 136.36, 135.8, 135.5, 130.11, 130.06, 129.6, 129.4, 128.67, 128.65, 125.9, 125.8, 20.0, 19.8. ^{13}C NMR (100 MHz, DMSO-d_6, 120 °C) δ 148.9, 138.3, 137.3, 135.7, 134.5, 129.8, 129.2, 128.4, 125.6, 19.0. ESI HRMS calcd for $C_{19}H_{17}N^{79}Br$ ([M + H]$^+$) 338.0539, found 338.0537. * The ^{13}C NMR spectrum of **2.5c** at rt shows two sets of signals as a result of two conformers that presumably result from different orientation of the two methyl groups. Upon measuring the sample at 120 °C in DMSO-d_6, the two sets of signals coalesce to one signal.
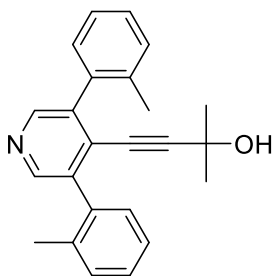
Compound 2.6c: 2-Methylbut-3-yn-2-ol (1.09 g, 13.0 mmol) was added to triethylamine (50 mL), and the solution was deoxygenated under a flow of N_2 for 20 min. To this solution was added **2.5c** (440 mg, 1.30 mmol), $Pd(PPh_3)_4$ (150 mg, 0.130 mmol), and CuI (37.0 mg, 0.194 mmol). After stirring the reaction mixture for 2d at 80 °C under a N_2 atmosphere, another portion of $Pd(PPh_3)_4$ (50 mg, 0.043 mmol) was added and the mixture was stirred for an additional 30 h. The reaction mixture was cooled to rt, H_2O (50 mL) and ethyl acetate (30 mL) were added, the layers were separated, and the aqueous phase was extracted with ethyl acetate (2 × 30 mL). The organic phases were combined, washed with satd aq NH_4Cl (2 × 20 mL), dried ($MgSO_4$), and filtered. Solvent removal and purification by column chromatography (silica gel, EtOAc/hexanes 1:5) afforded **2.6c** (258 mg, 58%) as a white solid. Mp 102–104 °C. $R_f = 0.67$ (EtOAc/hexanes 1:1). IR (cast film) 3230 (br, m), 3062 (w), 3022 (w), 2979 (s), 2927 (m), 2862 (m), 2230 (w), 1568 (m) cm^{-1}. ^{1}H NMR (500 MHz, CD_2Cl_2) δ 8.44 (s, 2H), 7.32–7.21 (m, 8H), 2.20 (s, 6H), 1.52 (s, 1H), 1.06 (s, 6H). ^{13}C NMR (125 MHz, CD_2Cl_2) δ 149.2, 139.0, 137.8, 137.3, 130.4, 130.3 (br), 128.8, 126.1, 104.8, 78.7, 65.5, 30.8, 20.3 (one signal coincident or not observed). ESI HRMS calcd for $C_{24}H_{24}NO$ ([M + H]$^+$) 342.1852, found 342.1849. DSC: Mp = 120 °C, decomposition, 346 °C (onset), 376 °C (peak).
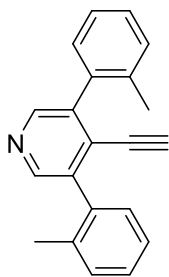
Compound 2.7c: To a solution of **2.6c** (100 mg, 0.293 mmol) in dried toluene (10 mL) was added well-powdered NaOH (117 mg, 2.93 mmol) and TDA-1 (95 mg, 0.29 mmol). The solution was stirred for 15 h at 110 °C. The reaction mixture was cooled to rt, H_2O (20 mL) and ethyl acetate (20 mL) were added, the layers were separated, and the aqueous phase was extracted with ethyl acetate (2 × 20 mL). The organic phases were combined, washed with satd aq NH_4Cl (2 × 20 mL), dried ($MgSO_4$), and filtered. Solvent removal and purification by column chromatography (silica gel, EtOAc/hexanes 1:6) afforded **2.7c** (72 mg, 87%) as a white solid. Mp 107–109 °C. $R_f = 0.63$ (EtOAc/hexanes 1:2). IR (cast film) 3284 (s), 3207 (br, w), 3062 (w), 3024 (m), 2953 (w), 2924 (w), 2863 (w), 2109 (w), 1562 (m) cm^{-1}. ^{1}H NMR (500 MHz, CD_2Cl_2) δ 8.46 (s, 2H), 7.32–7.25 (m, 8H), 3.01 (s, 1H), 2.21 (s, 6H). ^{13}C NMR (125 MHz, $CDCl_3$) δ 149.5, 139.6, 137.5, 137.3, 130.6, 130.3 (br), 128.9, 126.1, 87.4, 79.6, 20.3. ESI HRMS calcd for $C_{21}H_{18}N$ ([M + H]$^+$) 284.1434, found 284.1433. DSC: Mp = 114 °C, decomposition, 222 °C (onset), 273 °C (peak).
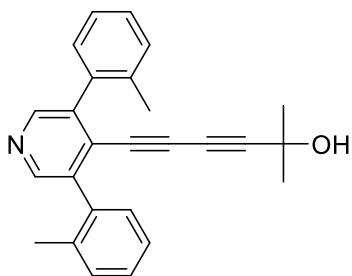
Compound 2.8c: 4-Bromo-2-methyl-3-butyn-2-ol (460 mg, 2.82 mmol) was added to EtOH (20 mL), and the solution was deoxygenated under a flow of N_2 for 20 min. The solution was cooled in an ice bath and **2.7c** (80 mg, 0.282 mmol), CuCl (5.6 mg, 0.057 mmol), hydroxylammonium chloride (3.9 mg, 0.056 mmol), and freshly deoxygenated *n*-propylamine (116 μL) were added. The ice bath was removed after stirring for 10 min. The solution was warmed to rt and stirred for 22 h under a N_2 atmosphere. H_2O (20 mL) and ethyl acetate (20 mL) were added, the layers were separated, and the aqueous phase was extracted with ethyl acetate (2 × 20 mL). The organic phases were combined, washed with satd aq NH_4Cl (2 × 20 mL), dried ($MgSO_4$), and filtered. After removing the solvent, the residue was purified by column chromatography (silica gel, EtOAc/hexanes 1:4) to afford the crude product. Recrystallization from CH_2Cl_2/hexanes (0.3 mL/10 mL) gave product **2.8c** (75 mg, 73%) as a white solid. Mp 196 °C (decomp). R_f = 0.73 (EtOAc/hexanes 1:1). IR (cast film) 3256 (br, s), 3063 (m), 3045 (m), 3022 (m), 2977 (m), 2929 (m), 2866 (m), 2234 (m), 2147 (w), 1570 (m) cm^{-1}. ^1H NMR (500 MHz, CDCl$_3$) δ 8.50 (s, 2H), 7.36–7.28 (m, 6H), 7.25–7.24 (m, 2H), 2.23 (s, 6H), 1.82 (s, 1H), 1.42 (s, 6H). ^{13}C NMR (125 MHz, CDCl$_3$) δ 149.0, 139.5, 136.4, 130.2, 129.9 (br), 128.5, 125.7, 89.1, 82.5, 73.8, 66.4, 65.6, 30.8, 20.0 (two signals coincident or not observed). ESI HRMS calcd for $C_{26}H_{24}NO$ ([M + H]$^+$) 366.1852, found 366.1855. DSC: Mp = 199 °C, decomposition, 206 °C (onset), 226 °C (peak).
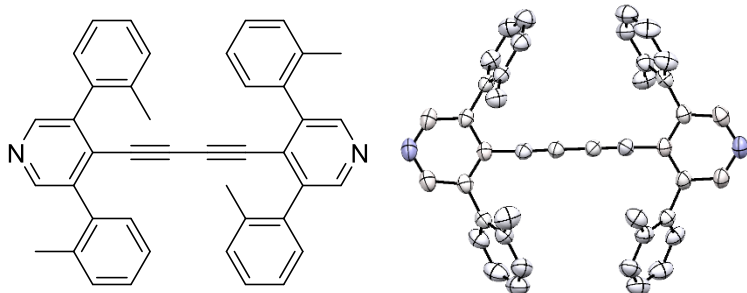
Compound Py[2c]**: To a solution of **2.7c** (80 mg, 0.282 mmol) in pyridine (3 mL) was added Cu(OAc)$_2$ (103 mg, 0.567 mmol), CuCl (5.6 mg, 0.057 mmol), and 4 Å sieves (100 mg). The solution was stirred for 22 h at 100 °C. The reaction mixture was cooled to rt, H_2O (20 mL) and CH_2Cl_2 (20 mL) were added, the layers were separated, and the aqueous phase was extracted with CH_2Cl_2 (2 × 20 mL). The organic phases were combined, washed with satd aq NH_4Cl (2 × 20 mL), dried ($MgSO_4$), and filtered. Solvent removal and purification by column chromatography (silica gel, EtOAc/hexanes 1:4) afforded **Py**[2c]** (66 mg, 83%) as a white solid. Mp 206–208 °C. R_f = 0.73

(EtOAc/hexanes 1:1). UV-vis (CH$_2$Cl$_2$) λ_{max} (ε): 305 (sh, 18200), 321 (21200), 341 nm (sh, 15300). IR (cast film) 3060 (m), 3019 (s), 2954 (m), 2924 (m), 2863 (w), 2159 (w), 1560 (s) cm^{-1}. ^{1}H NMR (500 MHz, CDCl$_3$) δ 8.48 (s, 4H), 7.32 (td, J = 7.5, 1.3 Hz, 4H), 7.25–7.19 (m, 8H), 7.12–7.11 (m, 4H), 2.09 (s, 12H). ^{13}C NMR (125 MHz, CDCl$_3$) δ 148.8, 139.3, 136.3, 136.0, 130.1, 129.8, 128.4, 125.6, 82.1, 79.5, 19.8 (one signal coincident or not observed). ESI HRMS calcd for C$_{42}$H$_{33}$N$_2$ ([M + H]$^+$) 565.2638, found 565.2637. DSC: Mp = 212 °C, decomposition, 335 °C (onset), 358 °C (peak).

A crystal of **Py**[2c]** suitable for X-ray crystallographic analysis has been grown at rt, by slow evaporation from a CH$_2$Cl$_2$ solution layered with MeOH. X-ray data for **Py**[2c]** (C$_{42}$H$_{32}$N$_2$•CH$_3$OH), F_w = 596.74; crystal dimensions 0.30 × 0.12 × 0.08 mm; monoclinic crystal system; space group $P2_1/c$ (No. 14); a = 12.5087(14) Å, b = 7.6185(9) Å, c = 35.652(4) Å; β = 98.9368(18)°; V = 3356.3(7) Å^3; Z = 4; $\rho_{(calcd)}$ = 1.181 g/cm^3; μ = 0.070 mm^{-1}; λ = 0.71073 Å; T = 193 K; $2\theta_{max}$ = 51.50°; total data collected = 22981; R_1 = 0.0567 [3585 observed reflections with $F_o^2 \geq 2\sigma(F_o^2)$]; ωR_2 = 0.1815 for 6382 data, 486 variables, and 135 restraints; largest difference, peak and hole = 0.359 and –0.282 e Å^{-3}. The disordered 2-methylphenyl group was restrained to have approximately the same geometry as the ordered one by use of the *SHELXL* **SAME** instruction. Further, a rigid-bond restraint was applied to improve the quality of the anisotropic displacement parameters by use of the *SHELXL* **RIGU** instruction. CCDC: 1977432.
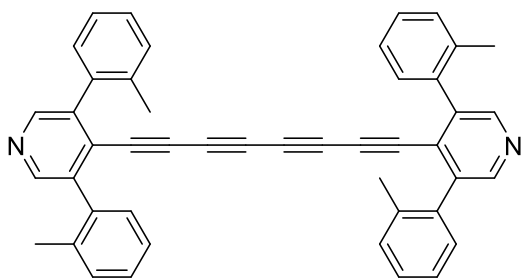
Compound Py**[4c]: To a solution of **2.8c** (50 mg, 0.137 mmol) in dried toluene (5 mL) was added well-powdered NaOH (55 mg, 1.4 mmol) and TDA-1 (44 mg, 0.14 mmol). The solution was stirred for 1 h at rt, H$_2$O (20 mL) and ethyl acetate (20 mL) were added, the layers were separated, and the aqueous phase was extracted with ethyl acetate (2 × 20 mL). The organic phases were combined, washed with satd aq NH$_4$Cl (2 × 20 mL), dried (MgSO$_4$), and filtered. Solvent was removed, and pyridine (3 mL) was added immediately to the crude product. To this solution was added Cu(OAc)$_2$ (50 mg, 0.28 mmol), CuCl (2.7 mg, 0.027 mmol), and 4 Å sieves (100 mg). The solution was stirred for 4 h at rt, H$_2$O (20 mL) and CH$_2$Cl$_2$ (20 mL) were added, the layers were separated, and the aqueous phase was extracted with CH$_2$Cl$_2$ (2 × 20 mL). The organic phases were combined, washed with satd aq

NH$_4$Cl (2 × 20 mL), dried (MgSO$_4$), and filtered. Solvent removal and purification by column chromatography (silica gel, EtOAc/hexanes 1:4) afforded **Py**[4c]** (29 mg, 69%) as a yellowish to greenish solid. Mp 241 °C (decomp). R_f = 0.77 (EtOAc/hexanes 1:1). UV-vis (CH$_2$Cl$_2$) λ_{max} (ε): 261 (45600), 280 (51200), 294 (69200), 302 (sh, 66700), 316 (sh, 55000), 327 (44300), 352 (26400), 379 (26400), 411 (17000), 436 nm (sh, 1150). IR (cast film) 3061 (m), 3019 (m), 2952 (m), 2924 (m), 2857 (w), 2202 (m), 1561 (m) cm^{-1}. ^{1}H NMR (500 MHz, CD$_2$Cl$_2$) δ 8.48 (s, 4H), 7.34–7.29 (m, 8H), 7.25 (td, J = 7.2, 1.4 Hz, 4H), 7.21–7.19 (m, 4H), 2.17 (s, 12H). ^{13}C NMR (125 MHz, CDCl$_3$) δ 149.0, 140.0, 136.3, 135.9, 130.3, 129.7 (br), 128.8, 125.8, 82.5, 73.5, 69.1, 63.7, 19.9 (one signal coincident or not observed). ESI HRMS calcd for C$_{46}$H$_{33}$N$_2$ ([M + H]$^+$) 613.2638, found 613.2643. DSC: decomposition, 241 °C (onset), 246 °C (peak).
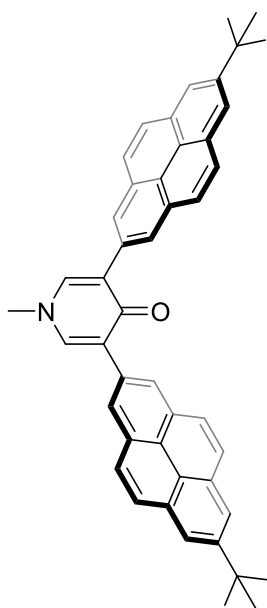
Compound 2.4d: A solution of toluene (120 mL) and EtOH (30 mL) was deoxygenated under a flow of N$_2$ for 20 min. To the solution was added compound **2.3** (750 mg, 2.81 mmol), 2-[7-(*tert*-butyl)pyren-2-yl]-4,4,5,5-tetramethyl-1,3,2-dioxaborolane (**Bpin(d)**, 2.7 g, 7.0 mmol), Pd(PPh$_3$)$_4$ (195 mg, 0.169 mmol), and Cs$_2$CO$_3$ (3.66 g, 11.2 mmol). The mixture was stirred for 109 h at 80 °C under a N$_2$ atmosphere. The reaction mixture was cooled to rt, EtOH was removed *in vacuo*. The residue was poured into MeOH/H$_2$O (250 mL/50 mL), and the precipitate was collected on a filter paper, washed with MeOH (50 mL). The precipitate was dissolved in CH$_2$Cl$_2$ (20 mL), the solution was filtered through a plug of silica gel and eluted with ethyl acetate. Solvent removal afforded **2.4d** (1.31 g, 75%) as a white solid. Mp: no visible change ≤ 300 °C. R_f = 0.28 (EtOAc/hexanes 1:1). IR (cast film) 3035 (w), 2962 (m), 1640 (m), 1603 (w), 1557 (s) cm^{-1}. ^{1}H NMR (500 MHz, CDCl$_3$) δ 8.55 (s, 4H), 8.22 (s, 4H), 8.08, 8.04 (ABq, J_{AB} = 9.0 Hz, 8H), 7.71 (s, 2H), 3.84 (s, 3H), 1.60 (s, 18H). ^{13}C NMR (125 MHz, CDCl$_3$) δ 174.6, 149.0, 138.9, 132.4, 131.1, 130.9, 127.6, 127.5, 125.2, 124.1, 122.8, 122.2, 44.2, 35.3, 32.0 (one signal coincident or not observed). ESI HRMS calcd for C$_{46}$H$_{40}$NO ([M + H]$^+$) 622.3104, found 622.3104, calcd for C$_{46}$H$_{40}$NONa ([M + Na]$^+$) 644.2924, found 644.2922.
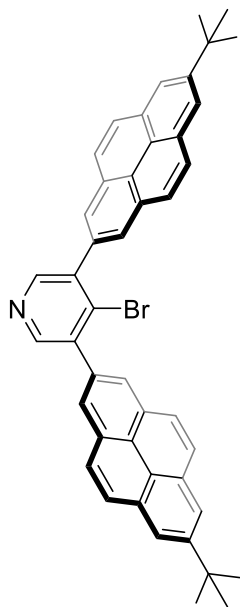
Compound 2.5d: PBr₃ (5 mL) and **2.4d** (100 mg, 0.161 mmol) was sealed in a microwave vial (30 mL). The mixture was stirred for 5 h at 170 °C. After cooling to rt, the reaction mixture was added dropwise to a NaOH solution (1M, 400 mL) in an ice bath. The mixture was stirred for 5 min. CH_2Cl_2 (100 mL) was added, the layers were separated, and the aqueous phase was extracted with CH_2Cl_2 (3 × 30 mL). The organic phases were combined, washed with satd aq NH_4Cl (2 × 40 mL), dried ($MgSO_4$), and filtered. Solvent removal and purification by column chromatography (silica gel, EtOAc/hexanes 1:6) afforded **2.5d** (55 mg, 51%) as a white solid. Mp: no visible change ≤ 300 °C. R_f = 0.53 (EtOAc/hexanes 1:2). IR (cast film) 3041 (w), 2962 (s), 2904 (w), 2868 (w), 1605 (m), 1542 (w) cm⁻¹. ¹H NMR (500 MHz, $CDCl_3$) δ 8.76 (s, 2H), 8.29 (s, 4H), 8.27 (s, 4H), 8.14, 8.12 (ABq, J_{AB} = 9.1 Hz, 8H), 1.61 (s, 18H). ¹³C NMR (176 MHz, $CDCl_3$) δ 150.1, 149.5, 139.7, 135.1, 134.3, 131.1, 130.9, 128.3, 127.2, 125.7, 124.2, 122.69, 122.66, 35.3, 31.9. ESI HRMS calcd for $C_{45}H_{37}N^{79}Br$ ([M + H]⁺) 670.2104, found 670.2115.
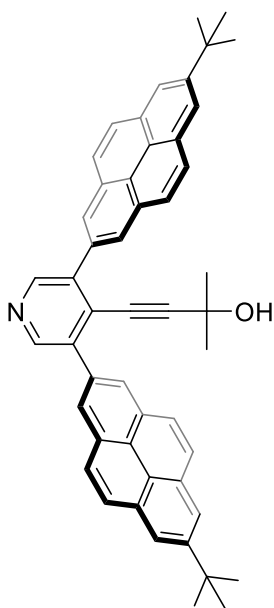
Compound 2.6d: 2-Methylbut-3-yn-2-ol (125 mg, 1.49 mmol) was added to a solution of triethylamine (20 mL) and deoxygenated under a flow of N_2 for 30 min. To this solution was added **2.5d** (100 mg, 0.149 mmol), $Pd(PPh_3)_4$ (17.2 mg, 0.0149 mmol), and CuI (4.3 mg, 0.075 mmol). The mixture was stirred for 48 h at 80 °C under a N_2 atmosphere. The reaction mixture was cooled to rt, H_2O (30 mL) and CH_2Cl_2 (30 mL) were added, the layers were separated, and the aqueous phase was extracted with CH_2Cl_2 (2 × 30 mL). The organic phases were combined, washed with satd aq NH_4Cl (2 × 20 mL), dried ($MgSO_4$), and filtered. Solvent removal and purification by column chromatography (silica gel, EtOAc/CH_2Cl_2/hexanes 1:2:10) afforded **2.6d** (75 mg, 75%) as a white solid. Mp 190–192 °C. R_f = 0.55 (EtOAc/hexanes 1:1). IR (cast film) 3563 (br, w), 3261 (br, w), 3041 (m), 2964 (s), 2903 (m), 2868 (m), 2220 (w), 1605 (m), 1564 (w) cm⁻¹. ¹H NMR (500 MHz, $CDCl_3$) δ 8.96 (s, 2H), 8.48 (s, 4H), 8.27 (d, 4H), 8.13 (s, 8H), 1.61 (s, 18H), 1.07 (s, 6H). ¹³C NMR (125 MHz, $CDCl_3$) δ 149.5, 149.3, 139.0, 134.3, 131.1, 130.8, 128.4, 128.3,

173

127.1, 125.8, 124.2, 122.8, 122.6, 104.3, 79.4, 65.3, 35.3, 32.0, 30.5. ESI HRMS calcd for $C_{50}H_{44}NO$ ([M + H]$^+$) 674.3417, found 674.3421.
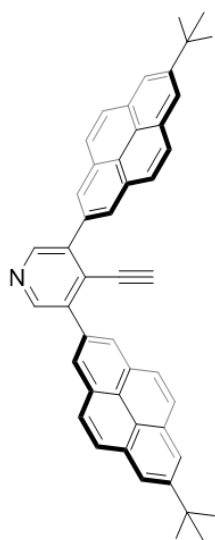
Compound 2.7d: To a solution of **2.6d** (50 mg, 0.074 mmol) in dried toluene (5 mL) was added well-powdered NaOH (30 mg, 0.75 mmol) and TDA-1 (24 mg, 0.074 mmol). The solution was stirred for 14 h at 110 °C. The reaction mixture was cooled to rt, toluene (4 mL) was removed *in vacuo*. The residue was poured into MeOH/H$_2$O (10 mL/1 mL), and the precipitate was collected on a filter paper, washed with MeOH (10 mL) to afford **2.7d** (43 mg, 94%) as a white solid without further purification. Mp 290 °C (decomp). R_f = 0.47 (EtOAc/hexanes 1:2). IR (cast film) 3293 (w), 3171 (br, m), 3041 (m), 2963 (s), 2904 (m), 2869 (m), 2097 (m), 1604 (m), 1564 (m) cm^{-1}. ^{1}H NMR (500 MHz, CDCl$_3$) δ 8.93 (s, 2H), 8.45 (s, 4H), 8.26 (s, 4H), 8.13 (s, 8H), 3.03 (s, 1H), 1.61 (s, 18H). ^{13}C NMR (125 MHz, CDCl$_3$) δ 149.5, 149.46, 139.9, 134.2, 131.1, 130.9, 128.2, 127.7, 127.2, 125.7, 124.3, 122.7, 122.6, 88.0, 79.9, 35.3, 32.0. ESI HRMS calcd for $C_{47}H_{38}N$ ([M + H]$^+$) 616.2999, found 616.3002.
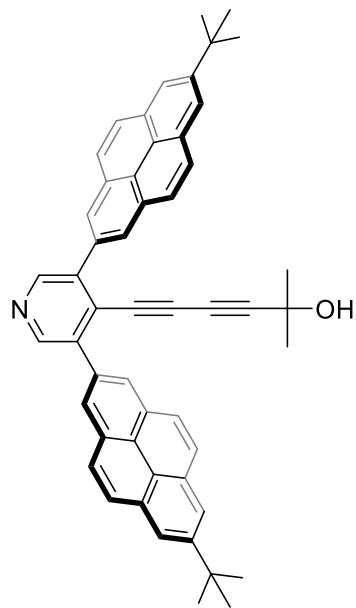
Compound 2.8d: 4-Bromo-2-methyl-3-butyn-2-ol (264 mg, 1.62 mmol) was added to EtOH (50 mL), and the solution was deoxygenated under a flow of N$_2$ for 30 min. The solution was cooled in an ice bath and **2.7d** (100 mg, 0.162 mmol), CuCl (3.2 mg, 0.032 mmol), hydroxylammonium chloride (2.3 mg, 0.033 mmol), and freshly deoxygenated *n*-propylamine (135 μL) were added. The ice bath was removed after stirring for 10 min. The solution was heated to 80 °C and stirred for 24 h under a N$_2$ atmosphere. The reaction mixture was cooled to rt, H$_2$O (20 mL) and CH$_2$Cl$_2$ (50 mL) were added, the layers were separated, and the aqueous phase was extracted with CH$_2$Cl$_2$ (2 × 30 mL). The organic phases were combined, washed with satd aq NH$_4$Cl (2 × 20 mL), dried (MgSO$_4$),

and filtered. After removing the solvent, the residue was purified by column chromatography (silica gel, EtOAc/CH$_2$Cl$_2$/hexanes 1:2:5) to afford the crude product. Recrystallization from CH$_2$Cl$_2$/MeOH (1 mL/10 mL) gave product **2.8d** (71 mg, 63%) as a yellowish solid. Mp 246 °C

(decomp). R_f = 0.55 (EtOAc/hexanes 1:1). IR (cast film) 3219 (br, w), 3042 (m), 2964 (s), 2904 (m), 2869 (m), 2231 (w), 2144 (w), 1606 (m), 1565 (w) cm^{-1}. ^{1}H NMR (500 MHz, CDCl$_3$) δ 8.94 (s, 2H), 8.44 (s, 4H), 8.27 (s, 4H), 8.16, 8.13 (ABq, J_{AB} = 8.9 Hz, 8H), 1.65 (s, 1H), 1.61 (s, 18H), 1.26 (s, 6H). ^{13}C NMR (176 MHz, CDCl$_3$) δ 149.54, 149.45, 140.2, 134.0, 131.2, 131.0, 128.2, 127.4, 127.3, 125.6, 124.4, 122.7, 122.6, 89.3, 83.2, 75.1, 66.3, 65.4, 35.3, 32.0, 30.6. ESI HRMS calcd for C$_{52}$H$_{44}$NO ([M + H]$^+$) 698.3417, found 698.3415.
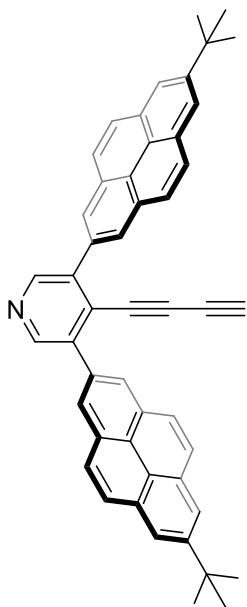
Compound 2.9d: To a solution of **2.8d** (30 mg, 0.043 mmol) in dried toluene (10 mL) was added well-powdered NaOH (17.2 mg, 0.430 mmol) and TDA-1 (13.9 mg, 0.0430 mmol). The solution was stirred for 2 h at rt, no product was observed by checking with TLC. The solution was heated to 110 °C and stirred for 1. The reaction mixture was cooled to rt, H$_2$O (20 mL) and CH$_2$Cl$_2$ (20 mL) were added, the layers were separated, and the aqueous phase was extracted with CH$_2$Cl$_2$ (2 × 20 mL). The organic phases were combined, washed with satd aq NH$_4$Cl (2 × 20 mL), dried (MgSO$_4$), and filtered. Solvent removal and purification by column chromatography (silica gel, EtOAc/CH$_2$Cl$_2$/hexanes 1:2:10) afforded **2.9d** (16 mg, 58%) as a white solid. Mp 180 °C (decomp). R_f = 0.44 (EtOAc/hexanes 1:2). IR (cast film) 3282 (m), 3042 (s), 2963 (s), 2903 (m), 2868 (m), 2202 (w), 2060 (w), 1605 (m), 1564 (w) cm^{-1}. ^{1}H NMR (500 MHz, CDCl$_3$) δ 8.96 (s, 2H), 8.45 (s, 4H), 8.27 (s, 4H), 8.16, 8.13 (ABq, J_{AB} = 9.0 Hz, 8H), 2.20 (s, 1H), 1.61 (s, 18H). ^{13}C NMR (176 MHz, CDCl$_3$) δ 149.5, 149.4, 140.5, 133.7, 131.1, 131.0, 128.2, 127.3, 126.9, 125.6, 124.3, 122.7, 122.6, 83.1, 73.9, 71.6, 67.1, 35.3, 31.9. ESI HRMS calcd for C$_{49}$H$_{38}$N ([M + H]$^+$) 640.2999, found 640.2997.
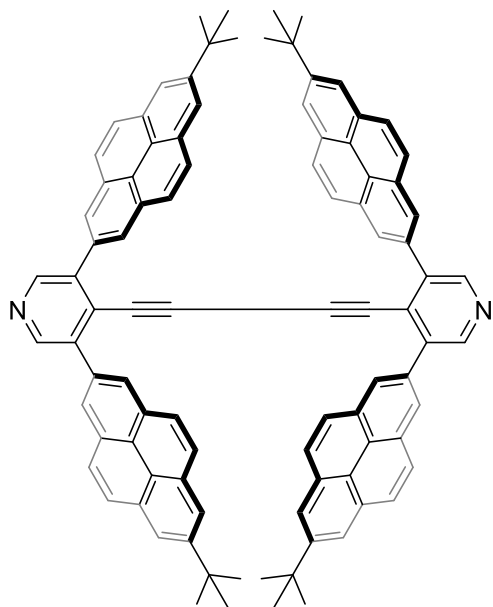
Compound Py**[2d]: To a solution of **2.7d** (35 mg, 0.057 mmol) in pyridine (3 mL) was added Cu(OAc)$_2$ (20.6 mg, 0.113 mmol) and CuCl (1.1 mg, 0.011 mmol). The solution was stirred for 2.5 h at 100 °C. The reaction mixture was cooled to rt, pyridine (2.5 mL) was removed *in vacuo*. The residue was poured into MeOH/H$_2$O (10 mL/1 mL), and the precipitate was collected on a filter paper, washed with MeOH (10 mL) to afford **Py**[2d]** (33 mg, 95%) as a yellowish solid without further purification. Mp: no visible change ≤ 300 °C. R_f = 0.55 (EtOAc/hexanes 1:1). UV-vis (CH$_2$Cl$_2$) λ_{max} (ε): 277 (174000), 314 (sh, 63300), 328 (113000), 344 (158000), 391 nm (sh, 6780). IR (cast film) 3038 (m), 2961 (s), 2903 (m), 2869 (m), 2140 (vw), 1600 (m), 1559 (m) cm^{-1}. ^{1}H NMR (500 MHz, CDCl$_3$) δ 8.79 (s, 4H), 8.20 (s, 8H), 8.17 (s, 8H), 7.75, 7.67 (ABq, J_{AB} = 8.9 Hz, 16H), 1.61 (s, 36H). ^{13}C NMR (125 MHz, CDCl$_3$) δ 149.5, 149.4, 139.8, 133.5, 131.1, 130.8, 128.0, 127.0, 126.6, 125.4, 124.1, 122.6, 122.5, 82.6, 80.2, 35.3, 32.0. ESI HRMS calcd for C$_{94}$H$_{73}$N$_2$ ([M + H]$^+$) 1229.5768, found 1229.5755, calcd for C$_{94}$H$_{72}$N$_2$Na ([M + Na]$^+$) 1251.5588, found 1251.5602. DSC: decomposition, 356 °C (onset), 374 °C (peak).
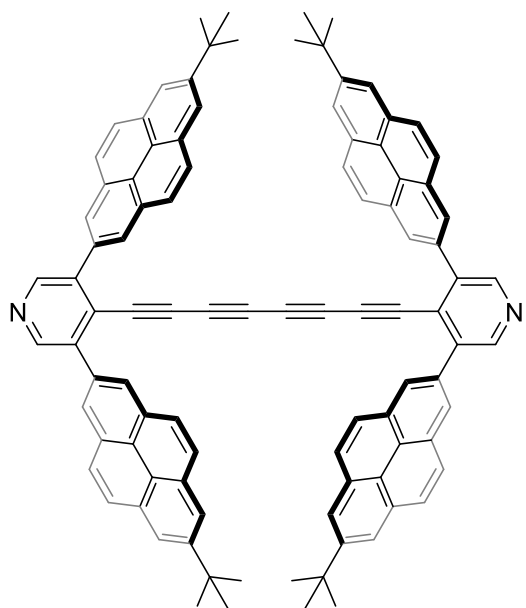
Compound Py**[4d]: To a solution of **2.9d** (28 mg, 0.044 mmol) in pyridine (3 mL) was added Cu(OAc)$_2$ (16 mg, 0.088 mmol) and CuCl (0.9 mg, 0.009 mmol). The solution was stirred for 20 h at rt, H$_2$O (20 mL) was added, and the precipitate was collected on a filter paper, washed with MeOH (30 mL) to afford **Py**[4d]** (26 mg, 93%) as a yellowish to brownish solid. Mp 250 °C (decomp). R_f = 0.33 (EtOAc/hexanes 1:1). UV-vis (CH$_2$Cl$_2$) λ_{max} (ε): 270 (206000), 311 (79800), 327 (106000), 342 (141000), 360 (sh, 46000), 388 (24700), 423 (11800), 452 nm (sh, 3000). IR (cast film) 3042 (w), 2962 (s), 2905 (w), 2869 (w), 2197 (vw), 2117

(vw), 1605 (m), 1560 (w) cm^{-1}. ^{1}H NMR (500 MHz, CDCl$_3$) δ 8.91 (s, 4H), 8.32 (s, 8H), 8.22 (s, 8H), 8.04 (s, 16H), 1.59 (s, 36H). ^{13}C NMR (176 MHz, CDCl$_3$) δ 149.5, 149.4, 133.4, 131.1, 131.0, 128.3, 128.1, 127.2, 125.4, 124.3, 122.6, 83.2, 74.4, 69.0, 63.5, 35.3, 32.0 (two signals coincident or not observed). ESI HRMS calcd for C$_{98}$H$_{73}$N$_2$ ([M + H]$^+$) 1277.5768, found 1277.5776. DSC: decomposition, 224 °C (onset), 254 °C (peak).
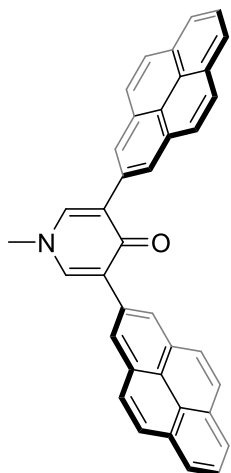
Compound 2.4e: A solution of toluene (100 mL) and EtOH (25 mL) was deoxygenated under a flow of N$_2$ for 20 min. To the solution was added compound **2.3** (300 mg, 1.12 mmol), 2-pyren-2-yl-4,4,5,5-tetramethyl-1,3,2-dioxaborolane (**Bpin(e)**, 922 mg, 2.81 mmol), Pd(PPh$_3$)$_4$ (78 mg, 0.068 mmol), and Cs$_2$CO$_3$ (1.46 g, 4.48 mmol). The mixture was stirred for 90 h at 80 °C under a N$_2$ atmosphere. The reaction mixture was cooled to rt, H$_2$O (50 mL) and CHCl$_3$ (50 mL) were added, the layers were separated, and the aqueous phase was extracted with CHCl$_3$ (6 × 200 mL). The organic phases were combined, washed with satd aq NH$_4$Cl (3 × 50 mL), dried (MgSO$_4$), and filtered. The solvent was reduced *in vacuo* to 80 mL and EtOH (100 mL) was added. The precipitate was collected on a filter paper and washed with EtOH (50 mL) to afford **2.4e** (395 mg, 69%) as a white solid without further purification. Mp: no visible change ≤ 300 °C. R_f = 0.19 (EtOAc/hexanes 1:1). IR (cast film) 3041 (w), 2943 (w), 1643 (s), 1601 (m), 1551 (s) cm^{-1}. ^{1}H NMR (500 MHz, CDCl$_3$) δ 8.60 (s, 4H), 8.18 (d, J = 7.6 Hz, 4H), 8.12, 8.08 (ABq, J_{AB} = 9.0 Hz, 8H), 8.00 (t, J = 7.6 Hz, 2H), 7.79 (s, 2H), 3.93 (s, 3H). ^{13}C NMR (125 MHz, CDCl$_3$) δ 174.6, 138.9, 132.8, 131.24, 131.15, 131.1, 127.7, 127.4, 125.9, 125.4, 124.9, 124.6, 124.2, 44.3. ESI HRMS calcd for C$_{38}$H$_{24}$NO ([M + H]$^+$) 510.1852, found 510.1858.
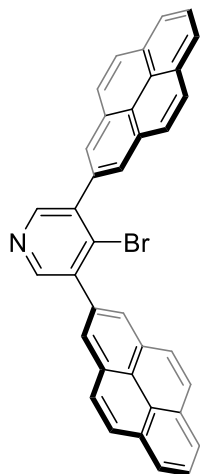
Compound 2.5e: To PBr$_3$ (6 mL) was added **2.4e** (200 mg, 0.393 mmol). The mixture was stirred for 20 h at 150 °C under a N$_2$ atmosphere. After cooling to rt, the reaction mixture was added dropwise to a NaOH solution (1M, 450 mL) in an ice bath. The mixture was stirred for 5 min. CHCl$_3$ (100 mL) was added, the layers were separated, and the aqueous phase was extracted with CHCl$_3$ (3 × 200 mL). The organic phases were combined, washed with satd aq NH$_4$Cl (2 × 40 mL), dried (MgSO$_4$), and filtered. Solvent removal and purification by column chromatography (silica gel, EtOAc/hexanes 1:5) afforded **2.5e** (130 mg,

177

59%) as a white solid. Mp 262 °C (decomp). R_f = 0.63 (EtOAc/hexanes 1:1). IR (cast film) 3036 (m), 2954 (w), 2923 (w), 2852 (w), 1601 (m), 1543 (w) cm^{-1}. ^{1}H NMR (500 MHz, CDCl$_3$) δ 8.77 (s, 2H), 8.34 (s, 4H), 8.25 (d, J = 7.6 Hz, 4H), 8.17 (s, 8H), 8.06 (t, J = 7.6 Hz, 2H). ^{13}C NMR (125 MHz, CDCl$_3$) δ 150.2, 139.6, 135.5, 134.3, 131.3, 131.1, 128.2, 127.3, 126.3, 125.9, 125.4, 124.5, 124.3. ESI HRMS calcd for C$_{37}$H$_{21}$N^{79}Br ([M + H]$^+$) 558.0852, found 558.0849.
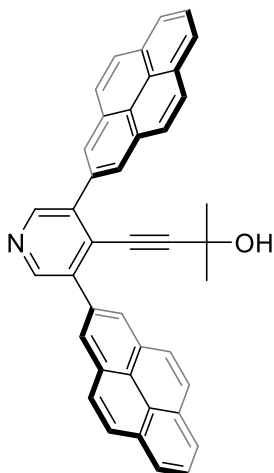
Compound 2.6e: 2-Methylbut-3-yn-2-ol (196 mg, 2.33 mmol) was added to a solution of THF (25 mL) and triethylamine (25 mL) and deoxygenated under a flow of N$_2$ for 20 min. To this solution was added **2.5e** (130 mg, 0.233 mmol), Pd(PPh$_3$)$_4$ (27 mg, 0.023 mmol), and CuI (6.7 mg, 0.035 mmol). The mixture was stirred for 67 h at 80 °C under a N$_2$ atmosphere. The reaction mixture was cooled to rt, H$_2$O (30 mL) and CHCl$_3$ (30 mL) were added, the layers were separated, and the aqueous phase was extracted with CHCl$_3$ (2 × 30 mL). The organic phases were combined, washed with satd aq NH$_4$Cl (2 × 20 mL), dried (MgSO$_4$), and filtered. Solvent removal and purification by column chromatography (silica gel, EtOAc/CHCl$_3$/hexanes 1:2:5) afforded **2.6e** (85 mg, 65%) as a white solid. Mp: no visible change ≤ 300 °C. R_f = 0.43 (EtOAc/hexanes 1:1). IR (cast film) 3262 (br, m), 3040 (m), 2981 (m), 2927 (w), 2235 (w), 1601 (m), 1572 (w) cm^{-1}. ^{1}H NMR (500 MHz, CDCl$_3$) δ 8.97 (s, 2H), 8.52 (s, 4H), 8.24 (d, J = 7.6 Hz, 4H), 8.16 (s, 8H), 8.06 (t, J = 7.6 Hz, 2H), 1.33 (s, 1H), 1.10 (s, 6H). ^{13}C NMR (125 MHz, CDCl$_3$) δ 149.4, 138.9, 134.7, 131.3, 131.0, 128.4, 128.1, 127.3, 126.3, 126.0, 125.3, 124.5, 124.3, 84.9, 79.3, 65.4, 30.5. ESI HRMS calcd for C$_{42}$H$_{28}$NO ([M + H]$^+$) 562.2165, found 562.2161.
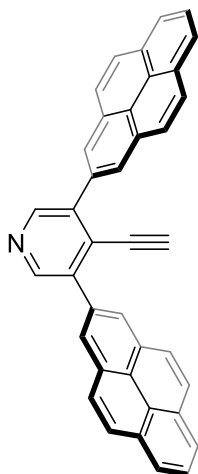
Compound 2.7e: To a solution of **2.6e** (90 mg, 0.16 mmol) in dried toluene (20 mL) was added well-powdered NaOH (64 mg, 1.6 mmol) and TDA-1 (52 mg, 0.16 mmol). The solution was stirred for 18 h at 110 °C. The reaction mixture was cooled to rt, EtOH (30 mL) was added. The precipitate was collected on a filter paper and washed with EtOH (30 mL) to afford **2.7e** (60 mg, 74%) as a white solid without further purification. Mp: no visible change ≤ 300 °C. R_f = 0.57 (EtOAc/hexanes 1:1). IR (cast film) 3289 (w), 3163 (br, m), 3036 (m), 2090 (m), 1647 (br, m), 1601 (m), 1566 (m) cm^{-1}. ^{1}H NMR (500 MHz, CDCl$_3$) δ 8.94 (s, 2H), 8.49 (s, 4H), 8.24 (d, J = 7.6 Hz, 4H), 8.17, 8.16 (ABq, J_{AB} = 9.1 Hz,

8H), 8.05 (t, $J = 7.6$ Hz, 2H), 3.04 (s, 1H). A useful ^{13}C NMR spectrum could not be obtained due to instability of the sample. ESI HRMS calcd for $C_{39}H_{22}N$ ([M + H]$^+$) 504.1747, found 504.1743.
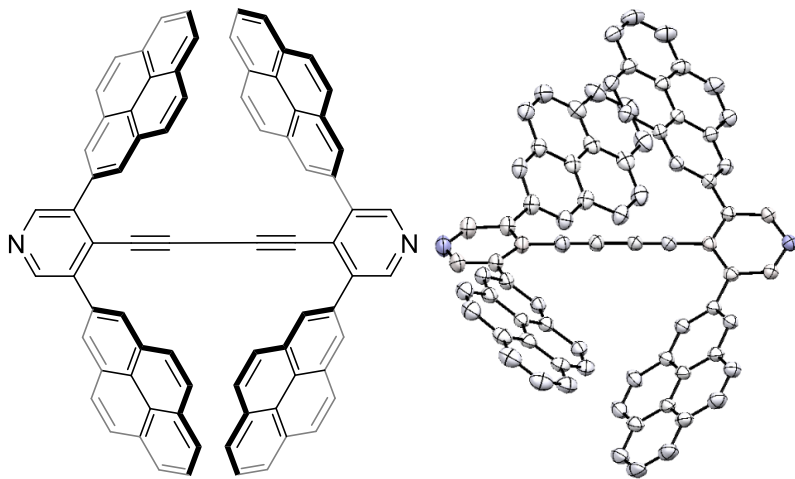
Compound Py**[2e]: To a solution of **2.7e** (20 mg, 0.040 mmol) in pyridine (5 mL) was added Cu(OAc)$_2$ (14.4 mg, 0.0793 mmol) and CuCl (0.8 mg, 0.008 mmol). The solution was stirred for 17 h at 100 °C. The reaction mixture was cooled to rt, H$_2$O (2 mL) and MeOH (20 mL) were added. The precipitate was collected on a filter paper and washed with MeOH (30 mL) to afford **Py**[2e]** (16 mg, 80%) as a yellowish solid without further purification. Mp: no visible change $\leq$ 300 °C. $R_f = 0.30$ (EtOAc/hexanes 1:1). UV-vis (CH$_2$Cl$_2$) λ_{max} (ε): 275 (137000), 313 (sh, 50100), 326 (92300), 342 (130000), 388 nm (sh, 4950). IR (cast film) 3038 (m), 2022 (m), 1599 (m) cm^{-1}. ^{1}H NMR (500 MHz, CDCl$_3$) δ 8.82 (s, 4H), 8.22 (s, 8H), 8.15 (d, $J = 7.6$ Hz, 8H), 8.02 (t, $J = 7.6$ Hz, 4H), 7.71, 7.64 (ABq, $J_{AB} = 9.0$ Hz, 16H). ^{13}C NMR (125 MHz, CDCl$_3$) δ 149.5, 139.7, 133.8, 131.2, 131.0, 127.8, 127.1, 126.5, 126.3, 125.5, 125.3, 124.3, 124.2, 82.7, 80.1. ESI HRMS calcd for $C_{78}H_{41}N_2$ ([M + H]$^+$) 1005.3264, found 1005.3276. DSC: decomposition, 363 °C (onset), 366 °C (peak).

A crystal of **Py**[2e]** suitable for X-ray crystallographic analysis has been grown at rt by slow evaporation from a CH$_2$Cl$_2$ solution. X-ray data for **Py**[2e]** ($C_{78}H_{40}N_2 \cdot CH_2Cl_2$), $F_w = 1005.12$; crystal dimensions $0.19 \times 0.10 \times 0.08$ mm; monoclinic crystal system; space group $P2_1/n$ (No. 14); $a = 21.2706(4)$ Å, $b = 11.5896(2)$ Å, $c = 25.5654(5)$ Å; $\beta = 109.2870(10)°$; $V = 5948.61(19)$ Å^3; $Z = 4$; $\rho_{(calcd)} = 1.217$ g/cm^3; $\mu = 1.342$ mm^{-1}; $\lambda = 1.54178$ Å; $T = 173$ K; $2\theta_{max} = 148.32°$; total data collected = 82183; $R_1 = 0.0563$ [8767 observed reflections with $F_o^2 \geq 2\sigma(F_o^2)$]; $\omega R_2 = 0.1743$ for 11812 data, 721 variables, and 0 restraints; largest difference, peak and hole = 0.323 and −0.309 e Å^{-3}. Attempts to refine peaks of residual electron density as disordered or partial-occupancy solvent dichloromethane were unsuccessful. The data were corrected for

disordered electron density through use of the SQUEEZE procedure as implemented in *PLATON*.[11] A total solvent-accessible void volume of 655 Å^3 with a total electron count of 169e$^-$ (consistent with four molecules of solvent dichloromethane) was found in the unit cell. CCDC: 1977434.
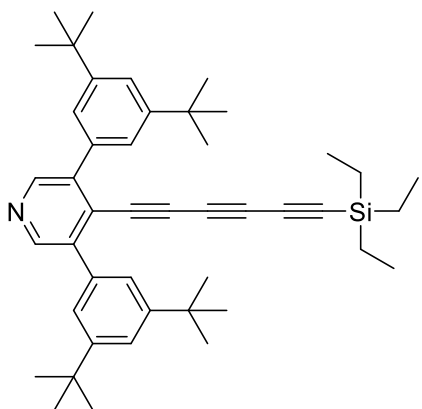
Compound Py**[3a]Si: Compound **2.9a** (110 mg, 0.218 mmol) was added to a solution of CH_2Cl_2 (10 mL) and EtOH (10 mL), and the solution was deoxygenated under a flow of N_2 for 30 min. The solution was cooled in an ice bath and CuCl (4.3 mg, 0.043 mmol) and hydroxylammonium chloride (3.0 mg, 0.043 mmol) were added. Separately, compound **2.11**, (239.3 mg, 1.092 mmol) was added to EtOH (10 mL), and the solution was deoxygenated under a flow of N_2 for 30 min. The second solution was transferred to the solution containing compound **2.9a** through a syringe, and freshly deoxygenated *n*-propylamine (180 L) was added. The solution was allowed to warm to rt and stirred for 21 h under a N_2 atmosphere. H_2O (20 mL) and CH_2Cl_2 (20 mL) were then added, the layers were separated, and the aqueous phase was extracted with CH_2Cl_2 (2 × 20 mL). The organic phases were combined, washed with satd aq NH_4Cl (20 mL), dried ($MgSO_4$), and filtered. Solvent removal and purification by column chromatography (silica gel, EtOAc/hexanes 1:10 to 1:5) afforded **Py**[3a]Si** (121 mg, 86%) as a light-yellow solid. Mp 82–86 °C. R_f = 0.70 (EtOAc/hexanes 1:4). UV-vis (CH_2Cl_2) λ_{max} (ε): 257 (sh, 54400), 271 (sh, 37200), 300 (sh, 12700), 313 (14300), 335 (18500), 360 (15100), 398 nm (2340). IR (cast film) 3030 (vw), 2962 (s), 2906 (m), 2876 (m), 2164 (vw), 2073 (w), 1596 (m), 1560 (w) cm^{-1}. ^{1}H NMR (500 MHz, CDCl$_3$) δ 8.65 (s, 2H), 7.50 (t, J = 1.7 Hz, 2H), 7.46 (d, J = 1.8 Hz, 4H), 1.39 (s, 36H), 0.97 (t, J = 7.9 Hz, 9H), 0.61 (q, J = 7.9 Hz, 6H). ^{13}C NMR (176 MHz, CDCl$_3$) δ 150.8, 148.5, 141.0, 135.5, 125.5, 123.8, 122.4, 89.0, 88.7, 83.8, 73.3, 69.6, 60.5, 35.0, 31.5, 7.2, 4.0. ESI HRMS calcd for C$_{45}$H$_{60}$NSi ([M + H]$^+$) 642.4490, found 642.4489.
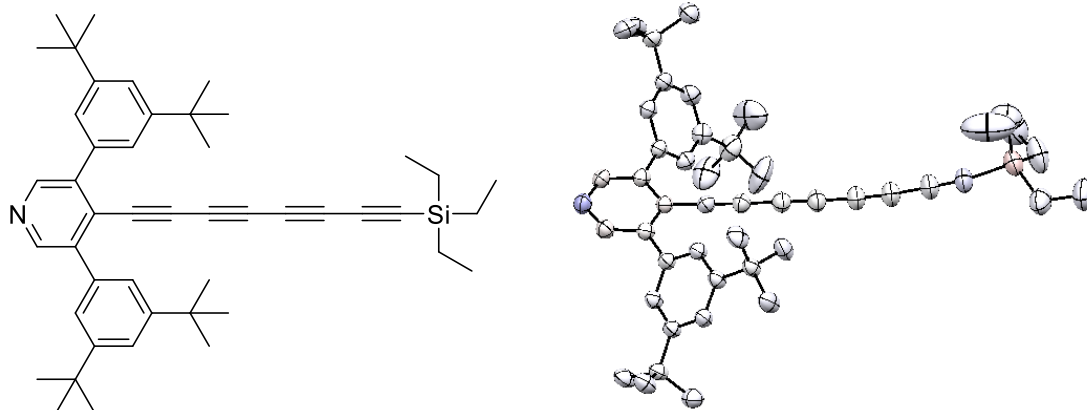
Compound Py**[4a]Si: Compound **2.11** (375.5 mg, 1.713 mmol) was added to CH_2Cl_2 (10 mL), and the solution was deoxygenated under a flow of N_2 for 30 min. Separately, to a solution of compound **Py**[3a]Si** (110 mg, 0.171 mmol) in THF (10 mL) and H_2O (2 mL) was added CsF (65 mg, 0.428 mmol). The solution was stirred at rt, and the reaction was monitored by TLC analysis until deemed complete; ca. 20 min. H_2O (10 mL) and CH_2Cl_2 (20 mL) were then added, the layers were separated, and the aqueous phase was extracted with CH_2Cl_2 (2 × 10 mL). The organic phases were combined, washed with brine (20 mL), dried ($MgSO_4$), and filtered. The resulted solution was deoxygenated under a flow of N_2 for 30 min. The solution was cooled in an ice bath and CuCl (3.4 mg, 0.034 mmol) and hydroxylammonium chloride (2.4 mg, 0.034 mmol) were added. To this solution was transferred the solution containing **2.11** through a syringe, and freshly deoxygenated *n*-propylamine (171 μL) was added. The solution was allowed to warm to rt and stirred for 19 h under a N_2 atmosphere. H_2O (20 mL) and CH_2Cl_2 (20 mL) were then added, the layers were separated, and the aqueous phase was extracted with CH_2Cl_2 (2 × 20 mL). The organic phases were combined, washed with satd aq NH_4Cl (20 mL), dried ($MgSO_4$), and filtered. Solvent removal and purification by column chromatography (silica gel, EtOAc/hexanes 1:10 to 1:5) afforded **Py**[4a]Si** (82 mg, 72%) as a yellow-green solid. Mp 178–180 °C (decomp). $R_f =$ 0.70 (EtOAc/hexanes 1:4). UV-vis (CH_2Cl_2) λ_{max} (ε): 261 (sh, 65100), 274 (56000), 287 (49800), 300 (42200), 313 (sh, 22400), 321 (sh, 18100), 343 (17700), 369 (19400), 398 (12100), 430 nm (617). IR (cast film) 3030 (vw), 2961 (s), 2907 (m), 2875 (m), 2193 (vw), 2128 (w), 2058 (w), 1596 (m), 1560 (w) cm^{-1}. ^1H NMR (500 MHz, $CDCl_3$) δ 8.66 (s, 2H), 7.50 (t, $J = 1.7$ Hz, 2H), 7.46 (d, $J = 1.8$ Hz, 4H), 1.39 (s, 36H), 0.99 (t, $J = 7.9$ Hz, 9H), 0.64 (q, $J = 7.9$ Hz, 6H). ^{13}C NMR (176 MHz, $CDCl_3$) δ 150.9, 148.5, 141.3, 135.4, 125.1, 123.8, 122.5, 88.7, 88.1, 83.6, 73.1, 69.6,

65.3, 61.1, 60.9, 35.0, 31.5, 7.3, 4.0. ESI HRMS calcd for $C_{47}H_{60}NSi$ ($[M + H]^+$) 646.4490, found 646.4490.

A crystal of **Py**[4a]Si** suitable for X-ray crystallographic analysis has been grown at rt, by slow evaporation from a CH_2Cl_2 solution layered with MeOH. X-ray data for **Py**[4a]Si** ($C_{47}H_{59}NSi$), F_w = 666.04; crystal dimensions 0.18 × 0.14 × 0.06 mm; triclinic crystal system; space group P-1 (No. 2); a = 9.6728(3) Å, b = 11.8168(4) Å, c = 19.9359(6) Å; α = 73.000(2)°; β = 79.516(2)°; γ = 79.695(3)°; V = 2123.53(12) Å^3; Z = 2; $\rho_{(calcd)}$ = 1.042 g/cm^3; μ = 0.698 mm^{-1}; λ = 1.54178 Å; T = 173 K; $2\theta_{max}$ = 148.20°; total data collected = 61939; R_1 = 0.0701 [6010 observed reflections with $F_o^2 \geq 2\sigma(F_o^2)$]; ωR_2 = 0.2101 for 8259 data, 540 variables, and 36 restraints; largest difference, peak and hole = 0.345 and –0.425 e Å^{-3}.
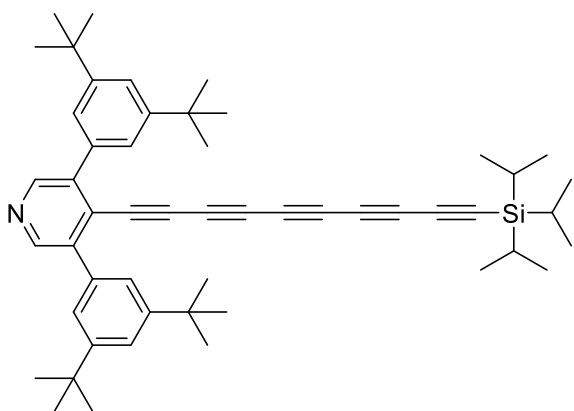
Compound Py**[5a]Si: Triyne **2.19** (ca. 0.842 mmol) was generated according to **General Procedure B** from 1-TIPS-6-TMS-hexa-1,3,5-triyne (**2.17**, 300 mg, 0.991 mmol) and added immediately to triethylamine (30 mL). The resulting solution was deoxygenated under a flow of N_2 for 30 min. To this solution was added compound **2.9a** (100 mg, 0.199 mmol), Pd(PPh$_3$)$_4$ (23.0 mg, 0.0199 mmol), and CuI (5.7 mg, 0.030 mmol). This solution was stirred for 21 h at rt and wrapped in aluminum foil to avoid light. H_2O (20 mL) and CH_2Cl_2 (20 mL) were then added, the layers were separated, and the aqueous phase was extracted with CH_2Cl_2 (2 × 20 mL). The organic phases were combined, washed with brine (20 mL), dried (MgSO$_4$), and filtered. Solvent removal and purification by column chromatography (silica gel, EtOAc/hexanes 1:80 to 1:50) afforded **Py**[5a]Si** (70 mg, 48%) as a yellow-brown solid. Mp 102–106 °C (decomp). R_f = 0.70 (EtOAc/hexanes 1:4). UV-vis (CH_2Cl_2) λ_{max} (ε): 264 (81900), 274 (84800), 284 (74800), 300 (67900), 314 (67300), 329 (56700), 345 (sh, 23400), 370 (16700), 399 (13900), 433 (7850), 468 nm (404). IR (cast film) 3032 (vw), 2963 (s), 2904 (m), 2867 (s), 2187 (w), 2116 (vw), 2091 (w), 2045 (w), 1596 (m), 1560 (w) cm^{-1}. ^{1}H NMR (500 MHz, CDCl$_3$) δ 8.67 (s, 2H), 7.51 (t, J = 1.7 Hz, 2H), 7.46 (d, J = 1.8 Hz, 4H), 1.39 (s, 36H), 1.10–1.07 (m, 21H). ^{13}C NMR (125 MHz, CDCl$_3$) δ 150.9, 148.6, 141.4, 135.4, 124.9, 123.8, 122.5, 89.4, 87.6, 83.4, 73.6, 69.6, 65.8, 64.2, 61.7,

61.09, 60.98, 35.0, 31.5, 18.5, 11.3. MALDI HRMS (DCTB) calcd for $C_{52}H_{66}NSi$ ([M + H]$^+$) 732.4959, found 732.4955.
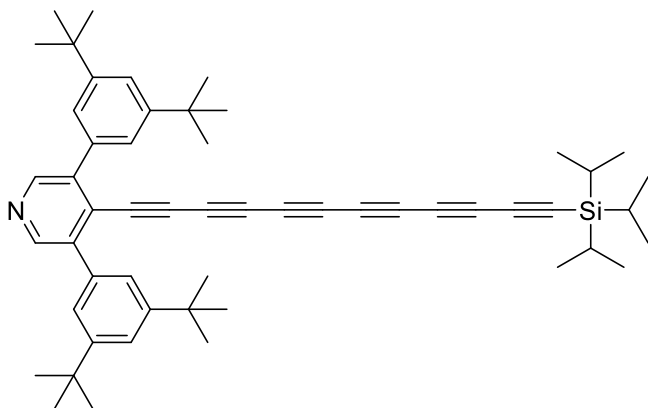
Compound Py**[6a]Si: Triyne **2.19** (ca. 0.795 mmol) was generated according to **General Procedure B** from 1-TIPS-6-TMS-hexa-1,3,5-triyne (**2.17**, 283 mg, 0.935 mmol) and added immediately to triethylamine (10 mL). To compound **Py**[3a]Si** (120 mg, 0.187 mmol) in THF (10 mL) and H_2O (2 mL) was added CsF (71 mg, 0.47 mmol). The solution was stirred at rt, and the reaction was monitored by TLC analysis until deemed complete; ca. 20 min. H_2O (10 mL) and CH_2Cl_2 (20 mL) were then added, the layers were separated, and the aqueous phase was extracted with CH_2Cl_2 (2 × 10 mL). The organic phases were combined, washed with brine (20 mL), dried (MgSO$_4$), and filtered. To the resulting solution was added triethylamine (20 mL), and the CH_2Cl_2 of the solution was removed through rotary evaporation. To the resulting solution was added freshly prepared solution of **2.19** (as described above), and the solution was deoxygenated under a flow of N_2 for 30 min. Pd(PPh$_3$)$_4$ (22 mg, 0.019 mmol) and CuI (5.3 mg, 0.028 mmol) were added. The solution was stirred for 21 h at rt and wrapped in aluminum foil to avoid light. H_2O (20 mL) and CH_2Cl_2 (20 mL) were added, the layers separated, and the aqueous phase extracted with CH_2Cl_2 (2 × 20 mL). The organic phases were combined, washed with brine (20 mL), dried (MgSO$_4$), and filtered. Solvent removal and purification by column chromatography (silica gel, EtOAc/hexanes 1:80 to 1:50) afforded **Py**[6a]Si** (91 mg, 65%) as a yellowish solid. Mp 176–180 °C (decomp). R_f = 0.70 (EtOAc/hexanes 1:4). UV-vis (CH$_2$Cl$_2$) λ_{max} (ε): 257 (sh, 54300), 271 (sh, 73300), 278 (sh, 82700), 286 (sh, 93700), 292 (98100), 306 (116000), 321 (100000), 341 (89300), 351 (sh, 73500), 366 (sh, 25800), 394 (13800), 426 (11200), 464 nm (5880). IR (cast film) 3030 (vw), 2963 (s), 2903 (m), 2867 (s), 2188 (vw), 2159 (w), 2058 (vw), 2038 (vw), 1596 (m), 1559 (w) cm^{-1}. ^{1}H NMR (500 MHz, CDCl$_3$) δ 8.67 (s, 2H), 7.51 (t, J = 1.7 Hz, 2H), 7.46 (d, J = 1.8 Hz, 4H), 1.39 (s, 36H), 1.10–1.07 (m, 21H). ^{13}C NMR (125 MHz, CDCl$_3$) δ 150.9, 148.6, 141.4, 135.3, 124.7, 123.8, 122.6, 89.3, 87.6, 83.3, 73.7, 69.5, 65.8, 64.4, 63.6, 62.0, 61.9, 61.2, 61.1, 35.0, 31.5, 18.5, 11.3. ESI HRMS calcd for $C_{54}H_{66}NSi$ ([M

+ H]$^+$) 756.4959, found 756.4965.
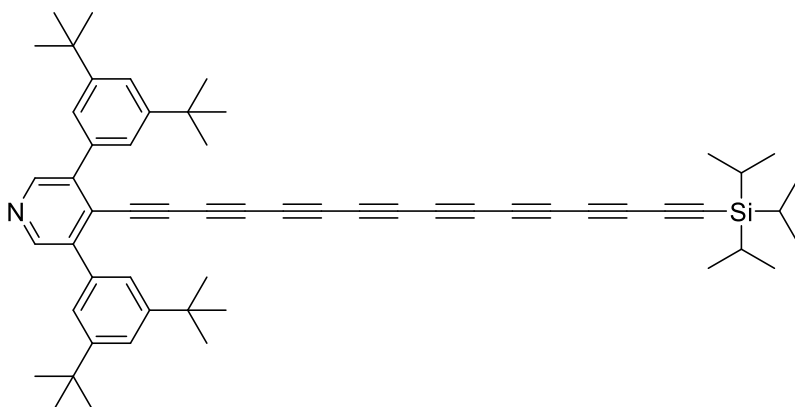
Compound Py**[8a]Si: Triyne **2.19** (ca. 0.289 mmol) was generated according to **General Procedure B** from 1-TIPS-6-TMS-hexa-1,3,5-triyne (**2.17**, 103 mg, 0.340 mmol) and added immediately to THF (10 mL). To compound **Py**[5a]Si** (50 mg, 0.068 mmol) in THF (10 mL) and H_2O (2 mL) was added CsF (25.9 mg, 0.171 mmol). The solution was stirred at rt, and the reaction was monitored by TLC analysis until deemed complete; ca. 30 min. H_2O (10 mL) and CH_2Cl_2 (10 mL) were then added, the layers were separated, and the aqueous phase was extracted with CH_2Cl_2 (2 × 10 mL). The organic phases were combined, washed with brine (20 mL), dried (MgSO$_4$), and filtered. To this resulting solution was added freshly prepared solution of **2.19** (as described above) in THF (10 mL), and the solution was deoxygenated under a flow of N$_2$ for 30 min. To this solution was added Pd(PPh$_3$)$_4$ (7.9 mg, 0.0068 mmol), CuI (2.0 mg, 0.011 mmol), and freshly deoxygenated diisopropylethylamine (120 μL). The solution was stirred for 16 h at rt and wrapped in aluminum foil to avoid light. H_2O (20 mL) was then added, the layers were separated, and the aqueous phase was extracted with CH_2Cl_2 (2 × 20 mL). The organic phases were combined, washed with brine (20 mL), dried (MgSO$_4$), and filtered. Solvent removal, purification by column chromatography (silica gel, EtOAc/hexanes 1:80 to 1:50), and recrystallization from CH_2Cl_2/MeOH (0.5 mL/10 mL) afforded **Py**[8a]Si** (22 mg, 40%) as an orange solid. Mp 148–150 °C (decomp). R_f = 0.70 (EtOAc/hexanes 1:4). UV-vis (CH_2Cl_2) λ_{max} (ε): 258 (37900), 271 (sh, 37300), 283 (sh, 46700), 295 (sh, 67500), 310 (114000), 328 (195000), 350 (230000), 361 (sh, 160000), 379 (130000), 398 (sh, 29100), 405 (sh, 17600), 432 (7630), 468 (5880), 511 nm (2620). IR (cast film) 3033 (vw), 2963 (s), 2904 (m), 2867 (s), 2188 (w), 2166 (w), 2111 (m), 2054 (vw), 2008 (w), 1596 (m), 1560 (w) cm^{-1}. ^{1}H NMR (500 MHz, CDCl$_3$) δ 8.67 (s, 2H), 7.51 (t, J = 1.8 Hz, 2H), 7.45 (d, J = 1.8 Hz, 4H), 1.39 (s, 36H), 1.10–1.07 (m, 21H). ^{13}C NMR (125 MHz, CDCl$_3$) δ 151.0, 148.6, 141.5, 135.3, 124.6, 123.8, 122.6, 89.3, 87.9, 83.1, 74.1, 69.3, 65.6, 64.3, 63.9, 63.8, 63.4, 62.5, 62.4, 62.3, 62.1, 61.6, 61.1, 35.0, 31.5, 18.5, 11.3. MALDI

HRMS (DCTB) calcd for $C_{58}H_{66}NSi$ ([M + H]$^+$) 804.4959, found 804.4941.
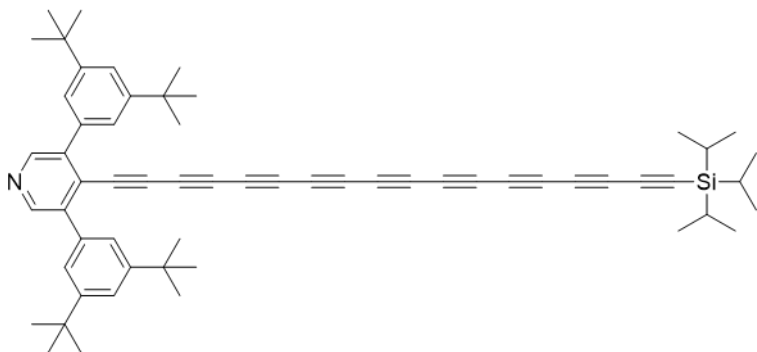
Compound Py**[9a]Si**: Triyne **2.19** (ca. 0.281 mmol) was generated according to **General Procedure B** from 1-TIPS-6-TMS-hexa-1,3,5-triyne (**2.17**, 100 mg, 0.330 mmol) and added immediately to THF (10 mL). To compound **Py****[6a]Si** (50 mg, 0.066 mmol) in THF (35 mL) and H_2O (7 mL) was added CsF (25.1 mg, 0.165 mmol). The solution was stirred at rt, and the reaction was monitored by TLC analysis until deemed complete; ca. 20 min. H_2O (20 mL) and CH_2Cl_2 (40 mL) were then added, the layers were separated, and the aqueous phase was extracted with CH_2Cl_2 (2 × 30 mL). The organic phases were combined, washed with brine (20 mL), dried (MgSO$_4$), and filtered. To this resulting solution was added freshly prepared solution of **2.19** (as described above) in THF (10 mL), and the solution was deoxygenated under a flow of N_2 for 30 min. To this solution was added Pd(PPh$_3$)$_4$ (7.6 mg, 0.0066 mmol), CuI (1.9 mg, 0.010 mmol), and freshly deoxygenated diisopropylethylamine (116 µL). The solution was stirred for 17 h at rt and wrapped in aluminum foil to avoid light. H_2O (30 mL) was then added, the layers were separated, and the aqueous phase was extracted with CH_2Cl_2 (2 × 20 mL). The organic phases were combined, washed with brine (20 mL), dried (MgSO$_4$), and filtered. Solvent removal, purification by column chromatography (silica gel, EtOAc/hexanes 1:80 to 1:50), and recrystallization from CH_2Cl_2/MeOH (0.5 mL/10 mL) afforded **Py****[9a]Si** (20 mg, 36%) as an orange solid. Mp 158–162 °C (decomp). R_f = 0.70 (EtOAc/hexanes 1:4). UV-vis (CH_2Cl_2) λ_{max} (ε): 259 (37800), 271 (34600), 281 (sh, 33100), 295 (sh, 44600), 307 (sh, 68900), 325 (124000), 344 (205000), 368 (255000), 378 (sh, 169000), 396 (111000), 413 (sh, 23400), 421 (sh, 14300), 446 (6340), 484 (4430), 511 (sh, 1060), 529 nm (1870). IR (cast film) 3030 (vw), 2963 (s), 2903 (m), 2867 (m), 2185 (w), 2150 (vw), 2090 (m), 2025 (vw), 1988 (w), 1596 (w), 1559 (w) cm^{-1}. ^{1}H NMR (700 MHz, CDCl$_3$) δ 8.67 (s, 2H), 7.51 (t, J = 1.8 Hz, 2H), 7.45 (d, J = 1.8 Hz, 4H), 1.39 (s, 36H), 1.10–1.08 (m, 21H). ^{13}C NMR (125 MHz, CDCl$_3$) δ 151.0, 148.6, 141.5, 135.3, 124.6, 123.8, 122.6, 89.2, 88.0, 83.1, 74.2, 69.3, 65.6, 64.3, 63.8, 63.7, 63.4, 62.8, 62.6, 62.3, 62.1, 61.7, 61.1, 35.0, 31.5, 18.5, 11.3 (two signals coincident or not observed). ESI HRMS calcd for

C$_{60}$H$_{66}$NSi ([M + H]$^+$) 828.4959, found 828.4950.
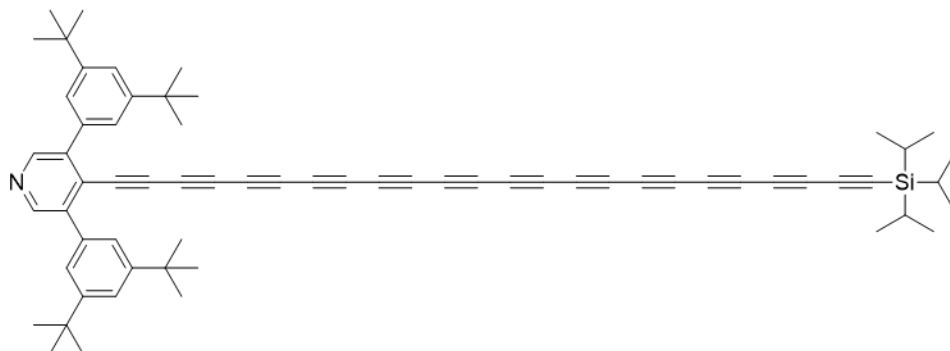
Compound Py**[12a]Si: Triyne **2.19** (ca. 0.118 mmol) was generated according to **General Procedure B** from 1-TIPS-6-TMS-hexa-1,3,5-triyne (**2.17**, 42.0 mg, 0.139 mmol) and added immediately to THF (10 mL). To compound **Py**[9a]Si** (23 mg, 0.028 mmol) in THF (20 mL) and H$_2$O (4 mL) was added CsF (8.4 mg, 0.055 mmol). The solution was stirred at rt, and the reaction was monitored by TLC analysis until deemed complete; ca. 10 min. H$_2$O (20 mL) and CH$_2$Cl$_2$ (40 mL) were then added, the layers were separated, and the aqueous phase was extracted with CH$_2$Cl$_2$ (2 × 30 mL). The organic phases were combined, washed with brine (20 mL), dried (MgSO$_4$), and filtered. To this resulting solution was added freshly prepared solution of **2.19** (as described above) in THF (10 mL), and the solution was deoxygenated under a flow of N$_2$ for 30 min. To this solution was added Pd(PPh$_3$)$_4$ (3.2 mg, 0.0028 mmol), CuI (0.8 mg, 0.004 mmol), and freshly deoxygenated diisopropylethylamine (50 μL). The solution was stirred for 20 h at rt and wrapped in aluminum foil to avoid light. H$_2$O (30 mL) was then added, the layers were separated, and the aqueous phase was extracted with CH$_2$Cl$_2$ (2 × 20 mL). The organic phases were combined, washed with brine (20 mL), dried (MgSO$_4$), and filtered. Solvent removal, purification by column chromatography (silica gel, EtOAc/hexanes 1:80 to 1:50), and recrystallization from CH$_2$Cl$_2$/MeOH (0.5 mL/10 mL) afforded **Py**[12a]Si** (6 mg, 24%) as an orange solid. Mp 152 °C (decomp). R_f = 0.70 (EtOAc/hexanes 1:4). UV-vis (CH$_2$Cl$_2$) λ_{max} (ε): 257 (56000), 269 (58600), 280 (52700), 292 (45300), 304 (sh, 40600), 314 (sh, 49300), 323 (sh, 62500), 339 (115000), 358 (220000), 381 (347000), 410 (390000), 435 (61700), 458 (sh, 11100), 478 (5410), 490 (sh, 4310), 518 (2810), 564 nm (643). IR (cast film) 3028 (vw), 2963 (s), 2905 (m), 2867 (s), 2183 (w), 2150 (m), 2102 (w), 2069 (w), 2034 (s), 1949 (w), 1595 (m), 1559 (w) cm^{-1}. ^{1}H NMR (500 MHz, CDCl$_3$) δ 8.67 (s, 2H), 7.51 (t, J = 1.8 Hz, 2H), 7.45 (d, J = 1.8 Hz, 4H), 1.39 (s, 36H), 1.10–1.08 (m, 21H). ^{13}C NMR (125 MHz, CDCl$_3$) δ 151.0, 148.6, 141.5, 135.3, 124.5, 123.8,

122.6, 89.2, 88.1, 83.0, 74.3, 69.2, 65.5, 64.1, 63.8, 63.7, 63.60, 63.57, 63.5, 63.20, 63.15, 63.0, 62.9, 62.8, 62.6, 62.3, 62.0. 61.9, 61.0, 35.0, 31.5, 18.5, 11.3 (two signals coincident or not observed). MALDI HRMS (DCTB) calcd for $C_{66}H_{66}NSi$ ([M + H]$^+$) 900.4959, found 900.4947.

triclinic

monoclinic
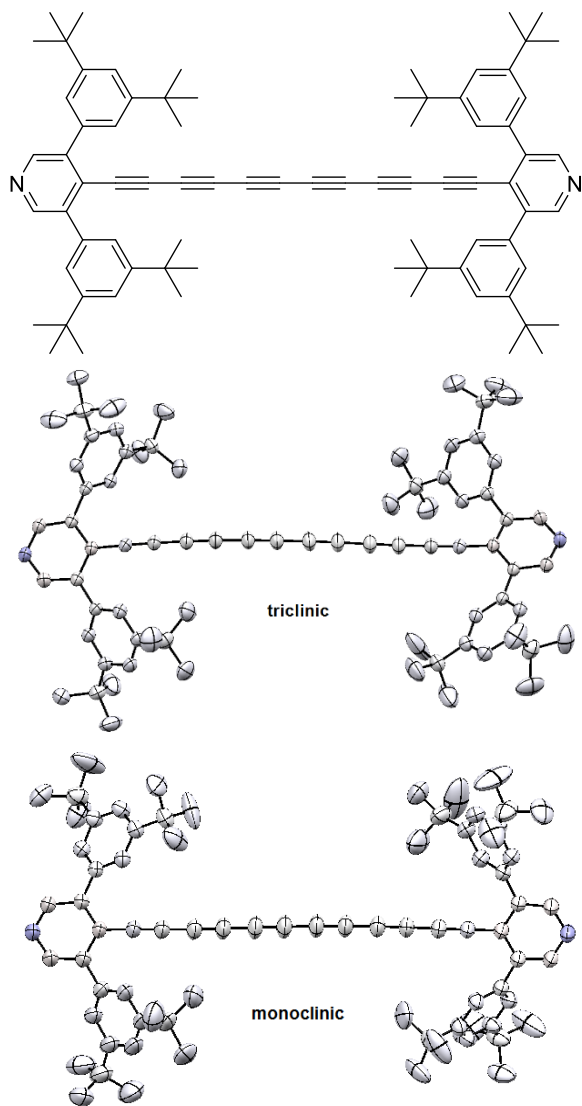
Compound Py**[6a]: To compound **Py**[3a]Si** (20 mg, 0.031 mmol) in THF (10 mL) and H_2O (2 mL) was added CsF (11.8 mg, 0.0777 mmol). The solution was stirred at rt, and the reaction was monitored by TLC analysis until deemed complete; ca. 20 min. H_2O (10 mL) and $CHCl_3$ (20 mL) were added, the layers were separated, and the aqueous phase was extracted with $CHCl_3$ (2 × 5 mL). The organic phases were combined, washed with brine (20 mL), dried ($MgSO_4$), and filtered. To the resulting solution was added a solution of CuCl (0.6 mg, 0.006 mmol) and TMEDA (7.2 mg, 0.062 mmol) in $CHCl_3$ (2 mL). The solution was stirred for 3.5 h at rt. H_2O (10 mL) was then added, the layers were separated, and the aqueous phase was extracted with CH_2Cl_2 (2 × 10 mL). The organic phases were combined, washed with brine (20 mL), dried ($MgSO_4$), and filtered. Solvent removal and purification by column chromatography (silica gel, EtOAc/CH_2Cl_2/hexanes 1:5:10), and recrystallization from CH_2Cl_2/MeOH (0.5 mL/10

mL) afforded **Py**[6a]** (14 mg, 85%) as a yellow-brown solid. Mp 178–182 °C (decomp). R_f = 0.63 (EtOAc/hexanes 1:4). UV-vis (CH_2Cl_2) λ_{max} (ε): 257 (74000), 272 (82100), 282 (84400), 298 (80600), 315 (88300), 336 (97600), 355 (115000), 374 (85400), 404 (26200), 437 (19200), 477 nm (9460). IR (cast film) 3032 (vw), 2964 (s), 2904 (m), 2868 (m), 2156 (m), 2051 (w), 1596 (m), 1559 (w) cm^{-1}. ^{1}H NMR (500 MHz, CDCl$_3$) δ 8.67 (s, 4H), 7.50 (t, J = 1.6 Hz, 4H), 7.45 (d, J = 1.7 Hz, 8H), 1.38 (s, 72H). ^{13}C NMR (125 MHz, CDCl$_3$) δ 150.9, 148.6, 141.4, 135.3, 124.7, 123.8,

122.6, 83.2, 74.2, 69.3, 65.4, 63.7, 62.1, 35.0, 31.5. MALDI HRMS (DCTB) calcd for $C_{78}H_{89}N_2$ ([M + H]$^+$) 1053.7020, found 1053.7017. DSC: decomposition, 278 °C (onset), 286 °C (peak).

A crystal of **Py**[6a]** (triclinic crystal system) suitable for X-ray crystallographic analysis has been grown at rt, by slow vapour diffusion of a THF solution into MeOH. X-ray data for **Py**[6a]** [$C_{78}H_{88}N_2 \cdot 2.5(C_4H_8O) \cdot 2(CH_3OH)$], $F_w = 1297.84$; crystal dimensions $0.18 \times 0.08 \times 0.06$ mm; triclinic crystal system; space group P-1 (No. 2); $a = 14.6184(8)$ Å, $b = 16.3315(9)$ Å, $c = 19.0495(10)$ Å; $\alpha = 76.343(4)°$; $\beta = 85.524(5)°$; $\gamma = 69.437(4)°$; $V = 4137.7(4)$ Å^3; $Z = 2$; $\rho_{(calcd)} = 1.042$ g/cm^3; $\mu = 0.478$ mm^{-1}; $\lambda = 1.54178$ Å; $T = 173$ K; $2\theta_{max} = 148.45°$; total data collected = 55669; $R_1 = 0.0633$ [8794 observed reflections with $F_o^2 \geq 2\sigma(F_o^2)$]; $\omega R_2 = 0.1901$ for 15543 data, 776 variables, and 16 restraints; largest difference, peak and hole = 0.445 and -0.280 e Å^{-3}. Attempts to refine peaks of residual electron density as disordered or partial-occupancy solvent tetrahydrofuran atoms and methanol atoms were unsuccessful. The data were corrected for disordered electron density through use of the SQUEEZE procedure as implemented in *PLATON*.[11] A total solvent-accessible void volume of 1221 Å^3 with a total electron count of 251 e$^-$ (consistent with four molecules of solvent tetrahydrofuran and five molecules of solvent methanol) was found in the unit cell. The bond lengths of C25–C30A and C25–C30B were restrained to be similar by the *SHELXL* command **SADI**. The bond lengths of C30A–C31A, C30A–C32A, C30A–C33A, C30B–C31B, C30B–C32B and C30B–C33B were restrained to be similar by the *SHELXL* command **SADI**. CCDC: 1977438.

A crystal of **Py**[6a]** (monoclinic crystal system) suitable for X-ray crystallographic analysis has been grown at rt, by slow evaporation of a THF solution layered with hexanes. X-ray data for **Py**[6a]** ($C_{78}H_{88}N_2 \cdot C_6H_{14}$), $F_w = 1139.67$; crystal dimensions $0.33 \times 0.17 \times 0.09$ mm; monoclinic crystal system; space group $P2_1/c$ (No. 14); $a = 14.5726(3)$ Å, $b = 19.9165(4)$ Å, $c = 30.7237(5)$ Å; $\beta = 99.0458(11)°$; $V = 8806.2(3)$ Å^3; $Z = 4$; $\rho_{(calcd)} = 0.860$ g/cm^3; $\mu = 0.362$ mm^{-1}; $\lambda = 1.54178$ Å; $T = 193$ K; $2\theta_{max} = 136.89°$; total data collected = 48768; $R_1 = 0.0790$ [10469 observed reflections with $F_o^2 \geq 2\sigma(F_o^2)$]; $\omega R_2 = 0.2746$ for 16152 data, 829 variables, and 256 restraints; largest difference, peak and hole = 0.343 and -0.218 e Å^{-3}. Attempts to refine peaks of residual electron density as disordered or partial-occupancy solvent hexanes carbon atoms were unsuccessful. The data were corrected for disordered electron density through use of the SQUEEZE procedure as implemented in *PLATON*.[11] A total solvent-accessible void volume of

2761 Å^3 with a total electron count of 211 e$^-$ (consistent with four molecules of solvent hexanes, or one molecule per formula unit of the polyyne molecule) was found in the unit cell. The C–C distances of the disordered *tert*-butyl groups were restrained to be approximately the same by use of the *SHELXL* **SADI** instruction. Likewise, the anisotropic displacement parameters of the disordered *tert*-butyl groups were restrained by the "rigid-bond-restraint" **RIGU**. CCDC: 1977436.
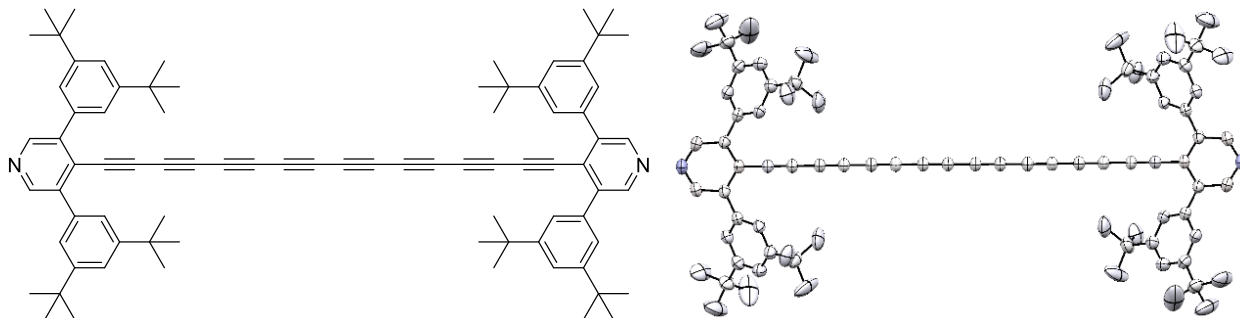
Compound Py**[8a]: To compound **Py**[4a]Si** (30 mg, 0.045 mmol) in THF (10 mL) and H$_2$O (2 mL) was added CsF (17.1 mg, 0.113 mmol). The solution was stirred at rt, and the reaction was monitored by TLC analysis until deemed complete; ca. 30 min. H$_2$O (10 mL) and CHCl$_3$ (20 mL) were added, the layers were separated, and the aqueous phase was extracted with CHCl$_3$ (2 × 5 mL). The organic phases were combined, washed with brine (20 mL), dried (MgSO$_4$), and filtered. To the resulting solution was added a solution of CuCl (2.2 mg, 0.022 mmol) and TMEDA (10.5 mg, 0.0903 mmol) in CHCl$_3$ (2 mL). The solution was stirred for 3 h at rt. H$_2$O (10 mL) was then added, the layers were separated, and the aqueous phase was extracted with CH$_2$Cl$_2$ (2 × 10 mL). The organic phases were combined, washed with brine (20 mL), dried (MgSO$_4$), and filtered. Solvent removal and purification by column chromatography (silica gel, EtOAc/CH$_2$Cl$_2$/hexanes 1:5:10), and recrystallization from CH$_2$Cl$_2$/MeOH (2 mL/10 mL) afforded **Py**[8a]** (17 mg, 69%) as an orange solid. Mp 162–166 °C (decomp). R_f = 0.63 (EtOAc/hexanes 1:4). UV-vis (CH$_2$Cl$_2$) λ_{max} (ε): 254 (56500), 274 (sh, 49600), 287 (52200), 303 (67200), 317 (91300), 334 (128000), 355 (159000), 370 (169000), 391 (140000), 411 (sh, 56000), 439 (14000), 476 (9430), 520 nm (3970). IR (cast film) 3035 (vw), 2962 (s), 2929 (m), 2869 (m), 2187 (vw), 2156 (vw), 2107 (w), 1595 (m) cm^{-1}. ^{1}H NMR (700 MHz, CDCl$_3$) δ 8.67 (s, 4H), 7.51 (t, *J* = 1.6 Hz, 4H), 7.45 (d, *J* = 1.7 Hz, 8H), 1.39 (s, 72H). ^{13}C NMR (125 MHz, CDCl$_3$) δ 151.0, 148.5, 141.5, 135.3, 124.6, 123.8, 122.6, 83.1, 74.3, 69.3, 65.5, 64.1, 63.5, 63.0, 61.9, 35.0, 31.5. MALDI HRMS (DCTB) calcd for C$_{82}$H$_{89}$N$_2$ ([M + H]$^+$) 1101.7020, found 1101.7013. ESI HRMS calcd for C$_{82}$H$_{90}$N$_2$ ([M + 2H]$^{2+}$) 551.3547,

found 551.3572. DSC: decomposition, 171 °C (onset), 187 °C (peak).

A crystal of **Py**[8a]** suitable for X-ray crystallographic analysis has been grown at rt, by slow vapour diffusion of a THF solution into MeOH. X-ray data for **Py**[8a]** ($C_{82}H_{88}N_2 \cdot 2C_4H_8O$), F_w = 1245.75; crystal dimensions 0.17 × 0.13 × 0.05 mm; monoclinic crystal system; space group $C2/_m$ (No. 12); a = 21.5287(7) Å, b = 18.1889(6) Å, c = 11.5387(4) Å; β = 114.046(2)°; V = 4126.3(2) Å^3; Z = 2; $\rho_{(calcd)}$ = 1.003 g/cm^3; μ = 0.442 mm^{-1}; λ = 1.54178 Å; T = 173 K; $2\theta_{max}$ = 136.86°; total data collected = 11008; R_1 = 0.0533 [2857 observed reflections with $F_o^2 \geq 2\sigma(F_o^2)$]; ωR_2 = 0.1801 for 3888 data, 249 variables, and 70 restraints; largest difference, peak and hole = 0.347 and −0.170 e Å^{-3}. Attempts to refine peaks of residual electron density as disordered or partial-occupancy solvent tetrahydrofuran oxygen or carbon atoms were unsuccessful. The data were corrected for disordered electron density through use of the SQUEEZE procedure as implemented in *PLATON*.[11] A total solvent-accessible void volume of 994 Å^3 with a total electron count of 220 e$^-$ (consistent with ~four molecules of solvent tetrahydrofuran, or two molecules per formula unit of the octayne molecule) was found in the unit cell. The C–C distances of the disordered *tert*-butyl group (carbon atoms C23, C27A to C34B) were restrained to be approximately the same by use of the *SHELXL* **SADI** instruction. Likewise, the rigid bond restraint was applied to the aforementioned *tert*-butyl group by use of the *SHELXL* **RIGU** instruction. Finally, C27A and C27B were refined with equivalent anisotropic displacement parameters. CCDC: 1977435.
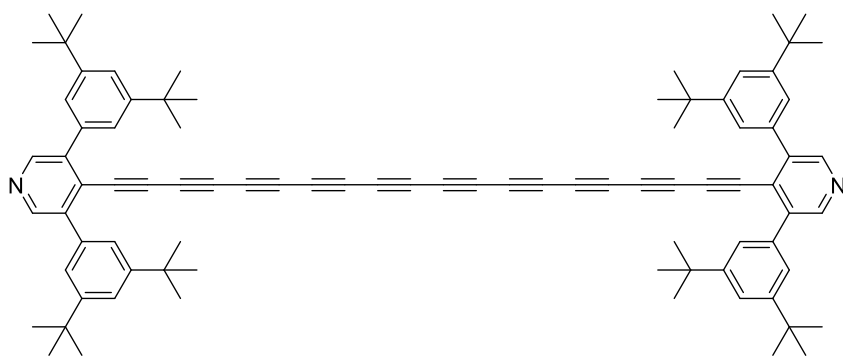
Compound Py**[10a]: To compound **Py**[5a]Si** (17 mg, 0.023 mmol) in THF (15 mL) and H$_2$O (3 mL) was added CsF (8.8 mg, 0.058 mmol). The solution was stirred at rt, and the reaction was monitored by TLC analysis until deemed complete; ca. 30 min. H$_2$O (30 mL) and CH$_2$Cl$_2$ (30 mL) were added, the layers were separated, and the aqueous phase was extracted with CH$_2$Cl$_2$ (2 × 20 mL). The organic phases were combined, washed with brine (2 × 10 mL), dried (MgSO$_4$), and filtered. To the resulting solution was added 6,6'-dimethyl-2,2'-bipyridine (DMBP, 8.6 mg,

0.047 mmol) and a solution of CuCl (4.6 mg, 0.047 mmol) and 4,4'-di-*t*-butyl-2,2'-bipyridine (dtBBP, 9.3 mg, 0.035 mmol) in CH_2Cl_2 (5 mL). The solution was stirred for 4 h at rt. H_2O (30 mL) was then added, the layers were separated, and the aqueous phase was extracted with CH_2Cl_2 (2 × 10 mL). The organic phases were combined, washed with brine (20 mL), dried (MgSO$_4$), and filtered. Solvent removal and purification by column chromatography (silica gel, EtOAc/CH$_2$Cl$_2$/hexanes 1:5:10), and recrystallization from CH$_2$Cl$_2$/MeOH (0.5 mL/10 mL) afforded **Py**[10a]** (8.5 mg, 64%) as an orange solid (**Py**[9a]** was present as a byproduct in ca. 2%, based on MS analysis). Mp 156–160 °C (decomp). R_f = 0.63 (EtOAc/hexanes 1:4). UV-vis (CH$_2$Cl$_2$) λ_{max} (ε): 254 (60700), 265 (sh, 53400), 276 (sh, 45300), 307 (sh, 51500), 321 (sh, 74000), 339 (sh, 113000), 363 (172000), 383 (sh, 200000), 389 (206000), 401 (193000), 419 (120000), 434 (sh, 38000), 463 (8550), 470 (7200), 502 (4920), 550 nm (1910). IR (cast film) 3029 (vw), 2963 (s), 2905 (m), 2868 (w), 2173 (w), 2132 (vw), 2064 (m), 2019 (vw), 1967 (w), 1596 (m) cm^{-1}. ^{1}H NMR (500 MHz, CDCl$_3$) δ 8.67 (s, 4H), 7.51 (t, J = 1.8 Hz, 4H), 7.45 (d, J = 1.8 Hz, 8H), 1.39 (s, 72H). ^{13}C NMR (125 MHz, CDCl$_3$) δ 151.0, 148.6, 141.5, 135.3, 124.5, 123.8, 122.6, 83.0, 74.3, 69.2, 65.5, 64.1, 63.6, 63.4, 63.3, 62.9, 61.9, 35.0, 31.5. ESI HRMS calcd for C$_{86}$H$_{90}$N$_2$ ([M + 2H]$^{2+}$) 575.3547, found 575.3551. DSC: decomposition, 172 °C (onset), 183 °C (peak).
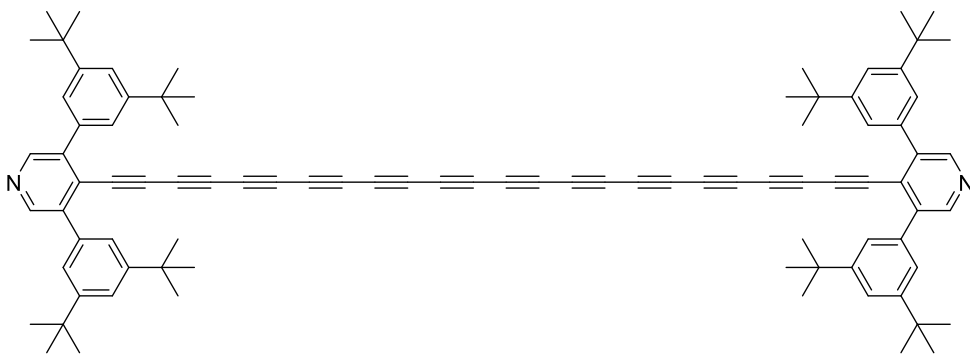
Compound Py**[12a]: To compound **Py**[6a]Si** (20 mg, 0.026 mmol) in THF (15 mL) and H_2O (3 mL) was added CsF (10 mg, 0.066 mmol). The solution was stirred at rt, and the reaction was monitored by TLC analysis until deemed complete; ca. 20 min. H_2O (20 mL) and CH_2Cl_2 (20 mL) were added, the layers were separated, and the aqueous phase was extracted with CH_2Cl_2 (2 × 20 mL). The organic phases were combined, washed with brine (2 × 10 mL), dried (MgSO$_4$), and filtered. Ethyl acetate (10 mL) was added to the solution, and the resulting solution was filtered through a short plug of silica. To the resulting solution was added a solution of CuCl (5.2 mg, 0.053 mmol) and 4,4'-di-*t*-butyl-2,2'-bipyridine (dtBBP, 10.6 mg, 0.0395 mmol) in CH_2Cl_2 (5 mL).

The solution was stirred for 3 h at rt. H_2O (30 mL) was then added, the layers were separated, and the aqueous phase was extracted with CH_2Cl_2 (2 × 10 mL). The organic phases were combined, washed with brine (20 mL), dried (MgSO$_4$), and filtered. Solvent removal and purification by column chromatography (silica gel, EtOAc/CH_2Cl_2/hexanes 1:5:10), and recrystallization from CH_2Cl_2/MeOH (5 mL/20 mL) afforded **Py**[12a]** (11 mg, 70%) as an orange solid (that also contained a trace of **Py**[11a]** based on MS analysis). Mp 198–202 °C (decomp). R_f = 0.63 (EtOAc/hexanes 1:4). UV-vis (CH_2Cl_2) λ_{max} (ε): 258 (59200), 272 (sh, 53300), 284 (sh, 45800), 298 (41700), 311 (sh, 44100), 329 (sh, 65600), 346 (102000), 363 (167000), 389 (247000), 418 (275000), 442 (sh, 86600), 452 (sh, 34700), 481 (6440), 492 (sh, 4930), 523 (2990), 571 nm (879). IR (cast film) 3038 (w), 2966 (s), 2926 (s), 2862 (m), 2188 (w), 2149 (w), 2035 (s), 1595 (w) cm^{-1}. ^{1}H NMR (400 MHz, CDCl$_3$) δ 8.67 (s, 4H), 7.51 (t, J = 1.7 Hz, 4H), 7.45 (d, J = 1.7 Hz, 8H), 1.39 (s, 72H). ^{13}C NMR (125 MHz, CDCl$_3$) δ 151.0, 148.6, 141.5, 135.3, 124.5, 123.8, 122.6, 83.0, 74.4, 69.2, 65.4, 64.1, 63.5, 63.4, 63.34, 63.31, 63.0, 61.9, 35.0, 31.5 (one signal coincident or not observed). ESI HRMS calcd for $C_{90}H_{90}N_2$ ([M + 2H]$^{2+}$) 599.3547, found 599.3548. DSC: decomposition, 204 °C (onset), 214 °C (peak).
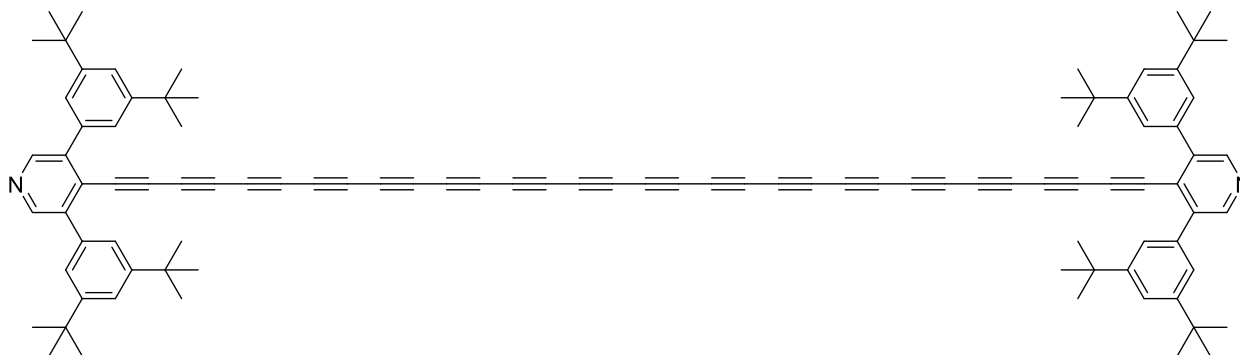
Compound Py**[16a]: To compound **Py**[8a]Si** (11 mg, 0.014 mmol) in THF (20 mL) and H_2O (4 mL) was added CsF (3.1 mg, 0.020 mmol). The solution was stirred at rt, and the reaction was monitored by TLC analysis until deemed complete; ca. 30 min. H_2O (30 mL) and CH_2Cl_2 (40 mL) were added, the layers were separated, and the aqueous phase was extracted with CH_2Cl_2 (2 × 30 mL). The organic phases were combined, washed with brine (2 × 20 mL), dried (MgSO$_4$), and filtered. To the resulting solution was added 6,6'-dimethyl-2,2'-bipyridine (DMBP, 5 mg, 0.027 mmol) and a solution of CuCl (2.7 mg, 0.027 mmol) and 4,4'-di-t-butyl-2,2'-bipyridine (dtBBP, 5.5 mg, 0.021 mmol) in CH_2Cl_2 (5 mL). The solution was stirred for 15 h at rt. H_2O (30 mL) was then added, the layers were separated, and the aqueous phase was extracted with CH_2Cl_2 (2 × 10

mL). The organic phases were combined, washed with brine (20 mL), dried (MgSO₄), and filtered. Solvent removal and purification by column chromatography (silica gel, EtOAc/CH$_2$Cl$_2$/hexanes 1:5:10), and recrystallization from CH$_2$Cl$_2$/MeOH (5 mL/20 mL) afforded **Py**[16a]** (5 mg, 57%) as an orange solid (**Py**[15a]** was present as a byproduct in ca. 3–5%, based on MS analysis). Mp 134–138 °C (decomp). R_f = 0.63 (EtOAc/hexanes 1:4). UV-vis (CH$_2$Cl$_2$) λ_{max} (ε): 255 (74100), 271 (sh, 66400), 284 (sh, 60500), 300 (62400), 314 (70400), 330 (76300), 349 (95500), 366 (153000), 388 (282000), 414 (476000), 446 (487000), 490 (sh, 13900), 523 (sh, 4440), 546 (2650), 563 (sh, 1720), 593 nm (505). IR (cast film) 2957 (s), 2922 (s), 2854 (s), 2099 (w), 1987 (w), 1729 (w), 1594 (w) cm^{-1}. ^{1}H NMR (500 MHz, CDCl$_3$) δ 8.67 (s, 4H), 7.51 (t, J = 1.8 Hz, 4H), 7.45 (d, J = 1.8 Hz, 8H), 1.38 (s, 72H). ^{13}C NMR (125 MHz, CDCl$_3$) δ 151.0, 148.6, 141.5, 135.3, 124.5, 123.8, 122.6, 83.0, 74.4, 69.2, 65.4, 64.0, 63.5, 63.41, 63.38, 63.37, 63.32, 63.29, 63.27, 63.0, 62.0, 35.0, 31.5 (two signals coincident or not observed). MALDI HRMS (DCTB) calcd for C$_{98}$H$_{89}$N$_2$ ([M + H]$^+$) 1293.7020, found 1293.7004. DSC: decomposition, 145 °C (onset), 158 °C (peak).
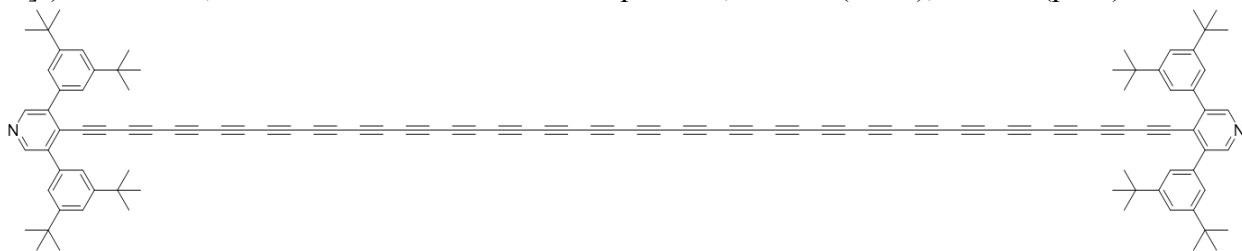
Compound Py**[24a]: To compound **Py**[12a]Si** (3.5 mg, 0.0024 mmol) in THF (25 mL) and H$_2$O (5 mL) was added CsF (1.2 mg, 0.0078 mmol). The solution was stirred at rt, and the reaction was monitored by TLC analysis until deemed complete; ca. 45 min. H$_2$O (10 mL) and CH$_2$Cl$_2$ (30 mL) were added, the layers were separated, and the aqueous phase was extracted with CH$_2$Cl$_2$ (3 × 10 mL). The organic phases were combined, washed with brine (20 mL), dried (MgSO₄), and filtered. The solution was cooled in an ice bath to 0 °C, and a solution of CuCl (0.39 mg, 0.0039 mmol) and TMEDA (1.8 mg, 0.015 mmol) in CH$_2$Cl$_2$ (2 mL) was added. The solution was allowed to warm to rt and stirred for 12 h. H$_2$O (30 mL) was then added, the layers were separated, and the aqueous phase was extracted with CH$_2$Cl$_2$ (2 × 10 mL). The organic phases were combined, washed with brine (20 mL), dried (MgSO₄), and filtered. Solvent removal and purification by column chromatography (silica gel, EtOAc/hexanes 1:20 to EtOAc/CH$_2$Cl$_2$ 1:20) afforded **Py**[24a]** (0.8 mg, 28%) as a dark red solid. **Py**[24a]** slowly decomposed as a solid at room temperature over a period of hours (monitored by the UV-vis changes in spectra). When **Py**[24a]**

was stored in a solution of EtOAc/CH$_2$Cl$_2$ at 5 °C, this solution discolored over three days and precipitated as a dark solid. R_f = 0.60 (EtOAc/CH$_2$Cl$_2$ 1:20). UV-vis (CH$_2$Cl$_2$) λ_{max}: 328 (sh), 340 (sh), 356 (sh), 370 (sh), 388, 411, 439, 473 nm. ^{1}H NMR (500 MHz, CDCl$_3$) δ 8.67 (s, 4H), 7.51 (t, J = 1.7 Hz, 4H), 7.45 (d, J = 1.8 Hz, 8H), 1.38 (s, 72H). MALDI HRMS (DCTB) calcd for C$_{113}$^{13}CH$_{89}$N$_2$ ([M + H]$^+$) 1486.7020, found 1486.7046.

7.3 ^{13}C labelling oligoynes (Chapter 3 data)
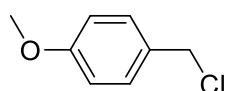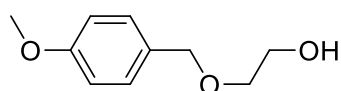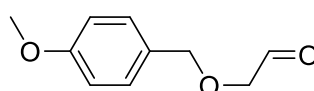
3.1 (74%)   **3.2** (77%)   **3.3** (51%)

Compound **3.1**,[12] **3.2**,[13] and **3.3**[14] were synthesized as described in the literature.
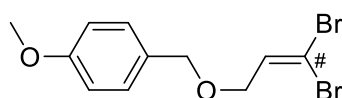
Compound 3.4: Compound **3.4** was formed by adaption of a known procedure reported in the literature.[13] A solution of PPh$_3$ (1.6 g, 6.1 mmol) in CH$_2$Cl$_2$ (10 mL) was added to a solution of ^{13}CBr$_4$ (1.0 g, 3.0 mmol) in CH$_2$Cl$_2$ (15 mL) over 1 min. After the solution was stirred for 10 min at rt, this solution was cooled to −78 °C under a N$_2$ atmosphere. To this solution was added **3.3** (0.60 g, 3.3 mmol) dissolved in CH$_2$Cl$_2$ (10 mL) over 10 min. This mixture was stirred for 5 h and allowed to warm to rt while stirring. Satd aq NaHCO$_3$ (30 mL) solution was added, the layers were separated, and the aqueous phase was extracted with CH$_2$Cl$_2$ (2 × 30 mL). The organic phases were combined, washed with satd aq NH$_4$Cl (2 × 20 mL), dried (MgSO$_4$), and filtered. Solvent removal and purification by column chromatography (silica gel, CH$_2$Cl$_2$/hexanes 1:3) afforded Compound **3.4** (560 mg, 55%) as a slightly yellow oil. ^{1}H NMR (500 MHz, CDCl$_3$) δ 7.27 (d, J = 8.6 Hz, 2H), 6.89 (d, J = 8.7 Hz, 2H), 6.63 (td, J_{HH} = 6.1 Hz, $^2J_{CH}$ = 0.6 Hz, 1H), 4.03 (dd, $^3J_{CH}$ = 7.7, J_{HH} = 6.1 Hz, 1H), 4.45 (s, 2H), 3.81 (s, 3H). ^{13}C NMR (125 MHz, CDCl$_3$) δ 159.4, 135.6 (d, $^1J_{CC}$ = 84.7 Hz), 129.6, 129.5, 113.9, 91.4 (labeled carbon), 72.3, 69.5 (d, $^2J_{CC}$ = 1.8 Hz), 55.3.
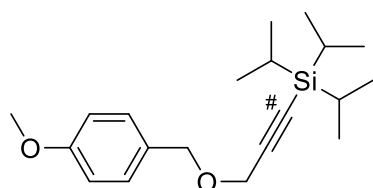
Compound 3.5: The synthesis of compound **3.5** (372 mg, 72%) with 20% enriched ^{13}C at the indicated position has been previously reported.[13] Following this procedure using 100% labeled **3.4**, compound **3.5** (400 mg, 64%) was obtained as a colorless oil. ^{1}H NMR (500 MHz, CDCl$_3$) δ 7.29 (d, J = 8.8 Hz, 2H), 6.88 (d, J = 8.7 Hz, 2H), 4.57 (s, 2H), 4.18

(d, $^3J_{CH}$ = 3.7 Hz, 2H), 3.81 (s, 3H), 1.10 (m, 21H). ^{13}C NMR (125 MHz, CDCl$_3$) δ 159.4, 129.9, 129.6, 113.8, 103.4 (d, $^1J_{CC}$ = 131.4 Hz), 87.8 (labeled carbon), 70.6, 57.4 (d, $^2J_{CC}$ = 8.4 Hz), 55.3, 18.6, 11.2 (d, $^2J_{CC}$ = 4.5 Hz).
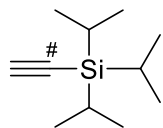
Compound 3.6: The synthesis of compound **3.6** (167 mg, 82%) with 20% enriched ^{13}C at the indicated position has been described in the literature.[13] Following this procedure using 100% labeled **3.5** (390 mg, 1.17 mmol), compound **3.6** (134 mg, 63%) was obtained as a colorless oil. ^{1}H NMR (500 MHz, CDCl$_3$) δ 2.35 (d, $^2J_{CH}$ = 41.7 Hz, 1H), 1.11–1.07 (m, 21H). ^{13}C NMR (125 MHz, CDCl$_3$) δ 97.4 (d, $^1J_{CC}$ = 130.5 Hz), 86.2 (labeled carbon), 18.5 (d, $^3J_{CC}$ = 1.0 Hz), 11.0 (d, $^2J_{CC}$ = 4.5 Hz).
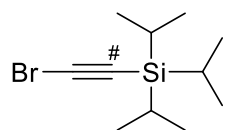
Compound 3.7: The synthesis of compound **3.7** (1.16 g, 99%) without ^{13}C labelling at the indicated position has been described in the literature.[15] Following this procedure using 100% labeled **3.6** (130 mg, 0.709), compound **3.7** (160 mg, 86%) was obtained as a colorless oil. ^{1}H NMR (500 MHz, CDCl$_3$) δ 1.09–1.07 (m, 21H). ^{13}C NMR (100.5 MHz, CDCl$_3$) δ 83.5 (labeled carbon), 61.7 (d, $^1J_{CC}$ = 141.1 Hz), 18.5, 11.3 (d, $^2J_{CC}$ = 4.6 Hz).
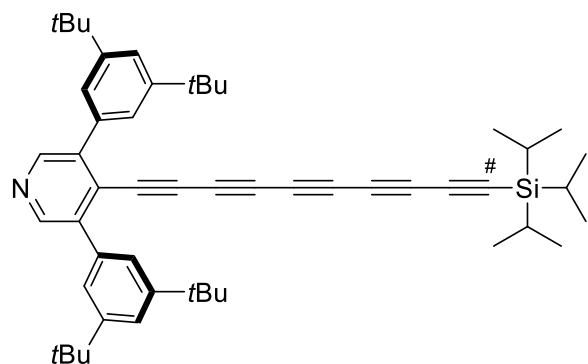
Py**[5a]Si$^#$: To compound **Py**[4a]Si** (30 mg, 0.045 mmol) in THF (5 mL) and H$_2$O (1 mL) was added CsF (17 mg, 0.11 mmol). The solution was stirred at rt, and the reaction was monitored by TLC analysis until deemed complete; ca. 30 min. H$_2$O (10 mL) and CH$_2$Cl$_2$ (10 mL) were then added, the layers were separated, and the aqueous phase was extracted with CH$_2$Cl$_2$ (2 × 5 mL). The organic phases were combined, washed with brine (20 mL), dried (MgSO$_4$), and filtered. To the resulting solution was added compound **3.7** (60 mg, 0.23 mmol) in THF (10 mL), and the solution was deoxygenated under a flow of N$_2$ for 30 min. Pd(PPh$_3$)$_4$ (5.2 mg, 0.0045 mmol), CuI (1.3 mg, 0.0068 mmol), and freshly deoxygenated diisopropylethylamine (79 μL, 0.45 mmol) were added. The solution was stirred for 17 h at rt. H$_2$O (20 mL) and CH$_2$Cl$_2$ (20 mL) were added, the layers separated, and the aqueous phase extracted with CH$_2$Cl$_2$ (2 × 20 mL). The organic phases were combined, washed with brine (20 mL), dried (MgSO$_4$), and filtered. Solvent removal and purification by column chromatography (silica gel,

EtOAc/hexanes 1:50 to 1:20) afforded **Py**[5a]Si#** (6 mg, 18%) as a yellow-brown solid. ^{1}H NMR (700 MHz, CDCl$_3$) δ 8.66 (s, 2H), 7.51 (t, J = 1.8 Hz, 2H), 7.46 (d, J = 1.8 Hz, 4H), 1.39 (s, 36H), 1.10–1.06 (m, 21H). ^{13}C NMR (125 MHz, CDCl$_3$) δ 150.9, 148.6, 141.4, 135.4, 124.9, 123.8, 122.5, 89.4 (ABq, $^1J_{CC}$ = 145.6 Hz), 87.6 (labeled carbon), 83.4, 73.5, 69.6, 65.8 ($^5J_{CC}$ = 3.5 Hz), 64.2 ($^3J_{CC}$ = 12.3 Hz), 61.7 ($^4J_{CC}$ = 5.5 Hz), 61.09 ($^2J_{CC}$ = 15.5 Hz), 60.98 ($^6J_{CC}$ = 2.4 Hz), 35.0, 31.5, 18.5, 11.3 ($^2J_{CC}$ = 4.2 Hz). MALDI HRMS (DCTB) calcd for C$_{51}$^{13}C H$_{66}$NSi ([M + H]$^+$) 733.4993, found 733.4991.
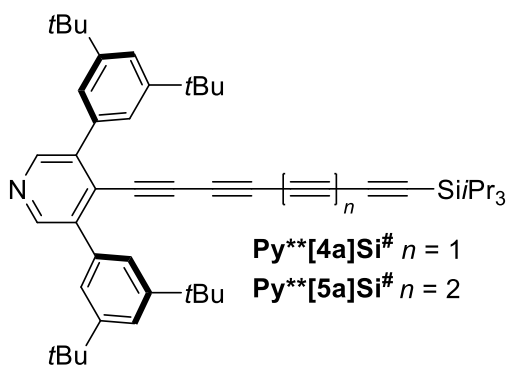
Py**[4a]Si# n = 1
Py**[5a]Si# n = 2

Py**[5a]Si# and **Py**[4a]Si#**: An alternative method (Cadiot-Chodkiewicz coupling reaction) gave a mixture of compound **Py**[5a]Si#** and **Py**[4a]Si#**. Compound **3.7** (98.4 mg, 0.375 mmol) was added to EtOH (10 mL), and the solution was deoxygenated under a flow of N$_2$ for 30 min. Separately, to a solution of compound **Py**[4a]Si** (50 mg, 0.075 mmol) in THF (6 mL) and H$_2$O (1.2 mL) was added CsF (28.5 mg, 0.188 mmol). The solution was stirred at rt, and the reaction was monitored by TLC analysis until deemed complete; ca. 30 min. H$_2$O (10 mL) and CH$_2$Cl$_2$ (10 mL) were then added, the layers were separated, and the aqueous phase was extracted with CH$_2$Cl$_2$ (2 × 5 mL). The organic phases were combined, washed with brine (20 mL), dried (MgSO$_4$), and filtered. The resulting solution was deoxygenated under a flow of N$_2$ for 30 min. The solution was cooled in an ice bath and CuCl (1.5 mg, 0.015 mmol) and hydroxylammonium chloride (1.0 mg, 0.014 mmol) were added. To this solution was transferred the solution containing **3.7** through a syringe, and freshly deoxygenated n-propylamine (63 uL, 0.75 mmol) was added. The resulting solution was allowed to warm to rt and stirred for 45 h under a N$_2$ atmosphere. H$_2$O (20 mL) and CH$_2$Cl$_2$ (20 mL) were then added, the layers were separated, and the aqueous phase was extracted with CH$_2$Cl$_2$ (2 × 20 mL). The organic phases were combined, washed with satd aq NH$_4$Cl (20 mL), dried (MgSO$_4$), and filtered. Solvent removal and purification by column chromatography (silica gel, EtOAc/hexanes 1:80 to 1:50) afforded **Py**[5a]Si#** and **Py**[4a]Si#** as an inseparable mixture (6.4 mg, 12%, **Py**[4a]Si#** is 20% relative to **Py**[5a]Si#**, based on

mass spectrometric analysis and ^{1}H NMR spectroscopic analysis). MALDI HRMS (DCTB) calcd for C$_{51}^{13}$CH$_{66}$NSi ([M + H]$^+$) 733.4993, found 733.4996; calcd for C$_{49}^{13}$CH$_{66}$NSi ([M + H]$^+$) 709.4993, found 709.4992

*t*Bu

*t*Bu

*t*Bu

*t*Bu

N

N

# #

Py**[10a]$^{\#\#}$

*t*Bu

*t*Bu

*t*Bu

*t*Bu

*t*Bu

*t*Bu

*t*Bu

*t*Bu

N

N

#

Py**[9a]$^{\#}$

*t*Bu

*t*Bu

*t*Bu

*t*Bu
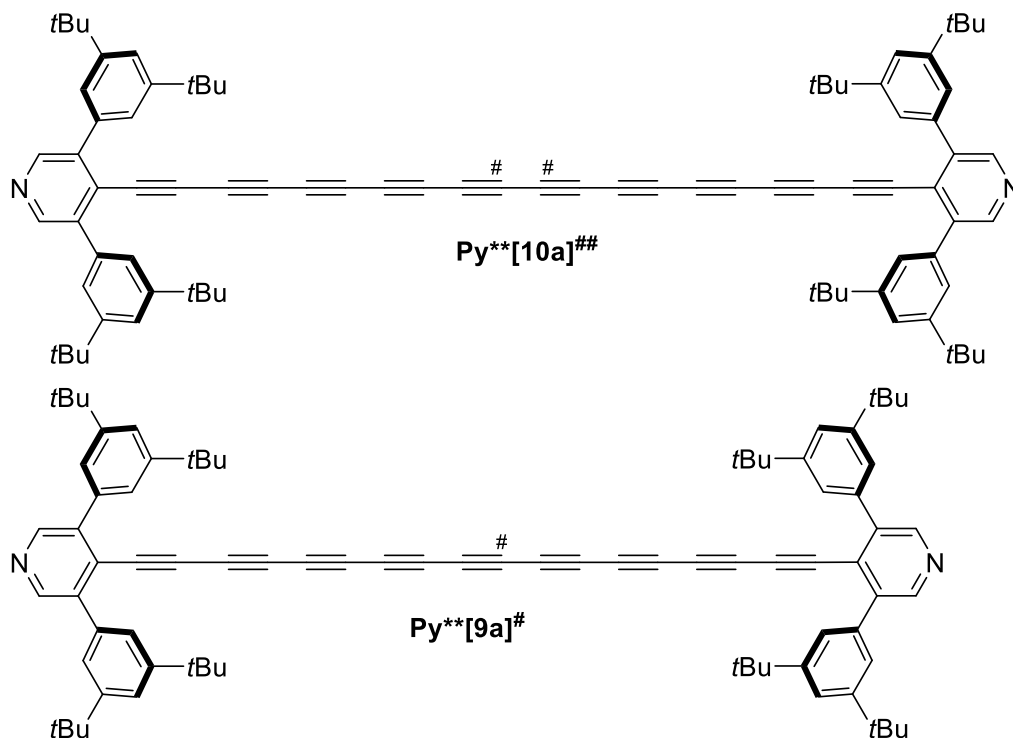
Py**[10a]$^{\#\#}$ and **Py*[9a]$^{\#}$**: To compound **Py**[5a]Si$^{\#}$** (5.5 mg, 0.0075 mmol) in THF (2.5 mL) and H$_2$O (0.5 mL) was added CsF (2.9 mg, 0.019 mmol). The solution was stirred at rt, and the reaction was monitored by TLC analysis until deemed complete; ca. 20 min. H$_2$O (10 mL) and CH$_2$Cl$_2$ (10 mL) were added, the layers were separated, and the aqueous phase was extracted with CH$_2$Cl$_2$ (2 × 5 mL). The organic phases were combined, washed with brine (20 mL), dried (MgSO$_4$), and filtered. To the resulting solution was added a solution of CuCl (0.4 mg, 0.004 mmol) and TMEDA (1.0 mg, 0.009 mmol) in CH$_2$Cl$_2$ (2 mL). The resulting solution was stirred for 2 h at rt. H$_2$O (10 mL) was then added, the layers were separated, and the aqueous phase was extracted with CH$_2$Cl$_2$ (2 × 10 mL). The organic phases were combined, washed with brine (20 mL), dried (MgSO$_4$), and filtered. Solvent removal and purification by column chromatography (silica gel, EtOAc/hexanes 1:5), and recrystallization from CH$_2$Cl$_2$/MeOH (0.5 mL/5 mL) afforded **Py**[10a]$^{\#\#}$** and **Py**[9a]$^{\#}$** as a mixture (2 mg, 47%, **Py**[9a]$^{\#}$** is 5% relative to **Py**[10a]$^{\#\#}$**,

based on mass spectrometric analysis). ^{1}H NMR (400 MHz, CDCl$_3$) δ 8.67 (s, 4H), 7.51 (t, J = 1.7 Hz, 4H), 7.45 (d, J = 1.8 Hz, 8H), 1.39 (s, 72H). ^{13}C NMR (125 MHz, CDCl$_3$) δ 151.0, 148.6, 141.5, 135.3, 124.5, 123.8, 122.6, 83.0, 74.3, 69.2, 65.5, 63.6 (labeled carbon of **Py**[10a]**[##]), 63.5 (labeled carbon of **Py**[9a]**[#]), 62.9, 61.9, 35.0, 31.5 (three signals could not be resolved due to second-order coupling). ESI HRMS calcd for C$_{84}$[13]C$_2$H$_{90}$N$_2$ ([M + 2H]$^{2+}$) 576.3580, found 576.3578; calcd for C$_{83}$[13]CH$_{90}$N$_2$ ([M + 2H]$^{2+}$) 563.8563, found 563.8545.

7.4 Platinum complexes with oligoynes (Chapter 4 data)
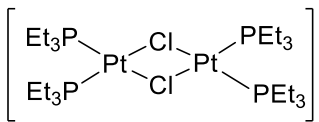
Pt$_2$(PEt$_3$)$_4$Cl$_2$(BF$_4$)$_2$ (4.1): The titled compound **4.1** (88 mg, 80%) was synthesized as described in the literature.[16] Mp 280–281 ºC (decomp). IR (ATR) 2973 (m), 2938 (m), 2882 (w), 1634 (w), 1454 (m), 1419 (m), 1386 (vw) cm^{-1}; ^{1}H NMR (400 MHz, CD$_2$Cl$_2$) δ 2.03 (dq, $^2J_{\text{H-P}}$ = 9.5 Hz, $^3J_{\text{H-H}}$ = 7.6 Hz, 24H), 1.25 (dt, $^3J_{\text{H-P}}$ = 18.6 Hz, $^3J_{\text{H-H}}$ = 7.6 Hz, 36H); ^{13}C NMR (101 MHz, CD$_2$Cl$_2$) δ 17.2–16.1 (m), 8.6; ^{31}P NMR (162 MHz, CD$_2$Cl$_2$) δ 19.7 ($^1J_{\text{P-Pt}}$ = 3584.8 Hz); ^{11}B NMR (128 MHz, CD$_2$Cl$_2$) δ −1.18; ^{19}F NMR (376 MHz, CD$_2$Cl$_2$) δ −152.6, −152.7; ESI HRMS calcd for C$_{24}$H$_{60}$P$_4$[195]Pt$_2$[35]Cl$_3$ [M − (BF$_4$)$_2$ + Cl]$^+$ 967.2001, found 967.2003; calcd for C$_{12}$H$_{30}$P$_2$[195]Pt[35]Cl [½M − BF$_4$]$^+$ 466.1154, found 466.1154.
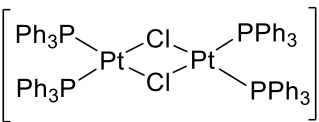
Pt$_2$(PPh$_3$)$_4$Cl$_2$(BF$_4$)$_2$ (4.2): The synthesis of the titled compound **4.2** was adapted from a known procedure.[16] A suspension of *cis*-PtCl$_2$(PPh$_3$)$_2$ (100 mg, 0.127 mmol) and Me$_3$OBF$_4$ (37.4 mg, 0.253 mmol) in CH$_2$Cl$_2$ (10 mL) was stirred at 45 ºC for 23 h. After cooling to rt, the solvent was removed in *vacuo* and the residue was dissolved in MeCN (10 mL). The resulting solution was filtered and concentrated, EtOH (5 mL) was added the solution slowly. A white solid was precipitated after standing this solution at 5 ºC. The white solid was filtered, collected, and recrystallized from CH$_2$Cl$_2$/hexane (1 mL/20 mL) affording **4.2** (90 mg, 85%) as a white solid. Mp 270–273 ºC (decomp). IR (CH$_2$Cl$_2$, cast) 3080 (w), 3064 (w), 3042 (w), 1481 (m), 1437 (s), cm^{-1}; ^{1}H NMR (400 MHz, CD$_2$Cl$_2$) δ 7.47–7.43 (m, 12H), 7.40–7.35 (m, 24H), 7.31–7.27 (m, 24H); ^{13}C NMR (126 MHz, CD$_2$Cl$_2$) δ 135.0 (t, $J_{\text{C-P}}$ = 4.9 Hz), 133.3, 129.6 (t, $J_{\text{C-P}}$ = 5.9 Hz), one signal coincident or not observed; ^{31}P NMR (162 MHz, CD$_2$Cl$_2$) δ 14.2 ($^1J_{\text{P-Pt}}$ = 3846.0 Hz); ^{11}B NMR (128 MHz, CD$_2$Cl$_2$) δ −0.7; ^{19}F NMR (376 MHz, CD$_2$Cl$_2$) δ −152.19, −152.24; ESI

HRMS calcd for $C_{36}H_{30}P_2{}^{195}Pt{}^{35}Cl$ [½M − BF$_4$]$^+$ 754.1154, found 754.1156; calcd for $C_{72}H_{60}F_4P_4{}^{11}B{}^{195}Pt_2{}^{35}Cl_2$ [M − BF$_4$]$^+$ 1595.2342, found 1595.2342.
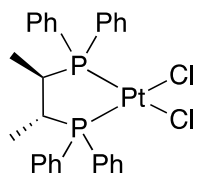
(R,R)-ChiraphosPtCl₂ (4.3): The titled compound **4.3** (275 mg, 78%) was synthesized as described in the literature.[17]
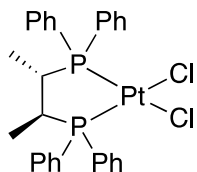
(R,R)-ChiraphosPtCl₂ (4.4): The titled compound **4.4** (289 mg, 82%) was synthesized as described in the literature.[17]
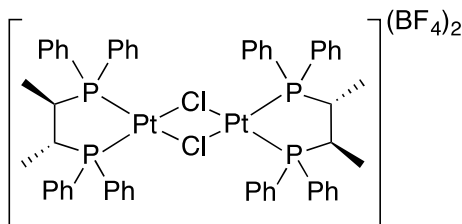
Compound 4.5: The synthesis of the titled compound **4.5** was adapted from a known procedure.[16] Under N$_2$, an oven dried Schlenk flask was charged with **4.3** (250 mg, 0.361 mmol) and dry CH$_2$Cl$_2$ (25 mL). Me$_3$OBF$_4$ (160 mg, 1.08 mmol) was added to the Schlenk flask. The resulting solution was stirred at rt for 72 h. Dry Et$_2$O (25 mL) was then added, and the resultant mixture was filtered under N$_2$ into a clean, oven dried Schlenk flask. Dry hexanes (50 mL) were carefully layered onto the filtered solution and the slow diffusion of hexanes into the Et$_2$O/CH$_2$Cl$_2$ solution at rt resulted in the formation of **4.5** as large colorless crystals (187 mg, 70%). UV-vis (CH$_2$Cl$_2$) λ_{max} (ε) 224 (60400), 269 (34000), 310 nm (7400); $[\alpha]_D^{20}$ −82.2° (c = 0.3380 CH$_2$Cl$_2$); Circular Dichroism (CH$_2$Cl$_2$) λ_{max} ($\Delta\varepsilon$), 244 (107.8), 265 (−12.1), 284 (22.7), 310 nm (−8.0); IR (CH$_2$Cl$_2$, cast), 3059 (m), 2976 (m), 2936 (m), 1437 (s) cm^{-1}; ^{1}H NMR (700 MHz, CD$_2$Cl$_2$) δ 7.81–7.78 (m, 4H), 7.75–7.69 (m, 8H), 7.65–7.61 (m, 8H), 7.59–7.56 (m, 4H), 7.53–7.49 (m, 8H), 7.48–7.43 (m, 8H), 2.60–2.54 (m, 4H), 1.08–1.00 (m, 12H); ^{13}C NMR (126 MHz, CD$_2$Cl$_2$) δ 136.5 (t, J_{C-P} = 5.7 Hz), 135.2, 134.3, 132.8 (t, J_{C-P} = 4.8 Hz), 130.4 (t, J_{C-P} = 5.8 Hz), 122.8 (dd, $^1J_{C-P}$ = 69.0 Hz, J_{C-P} = 3.0 Hz), 121.2 (dd, $^1J_{C-P}$ = 67.2 Hz, J_{C-P} = 3.7 Hz), 36.9–35.7 (m), 13.4–12.5 (m), one signal coincident or not observed; ^{31}P NMR (202 MHz, CD$_2$Cl$_2$) δ 44.7 ($^1J_{P-Pt}$ = 3697 Hz); ^{11}B NMR (160

MHz, CD$_2$Cl$_2$) δ –1.0; ^{19}F NMR (469 MHz, CD$_2$Cl$_2$) δ –152.7, –152.8; ESI HRMS calcd for C$_{56}$H$_{56}$^{11}B^{35}Cl$_2$F$_4$P$_4$^{195}Pt$_2$ [M – ^{11}BF$_4$]$^+$ 1399.2026, found 1399.2038; calcd for C$_{56}$H$_{56}$^{35}Cl$_3$P$_4$^{195}Pt$_2$ [M – (^{11}BF$_4$)$_2$ + ^{35}Cl]$^+$ 1347.1672, found 1347.1678; DSC: decomposition 221 °C (onset), 230 °C (peak).
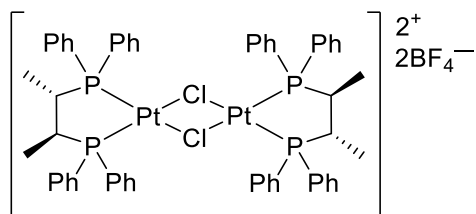
Compound 4.6: The synthesis of the titled compound **4.6** was adapted from a known procedure.[16] Under N$_2$, an oven dried Schlenk flask was charged with **4.4** (250 mg, 0.361 mmol) and dry CH$_2$Cl$_2$ (25 mL). Me$_3$OBF$_4$ (160 mg, 1.08 mmol) was added to the Schlenk flask. The resulting solution was stirred at rt for 72 h. Dry Et$_2$O (25 mL) was then added, and the resultant mixture was filtered under N$_2$ into a clean, oven dried Schlenk flask. Dry hexanes (50 mL) were carefully layered onto the filtered solution and the slow diffusion of hexanes into the Et$_2$O/CH$_2$Cl$_2$ solution at rt resulted in the formation of **4.6** as large colorless crystals (189 mg, 71%). UV-vis (CH$_2$Cl$_2$) λ$_{max}$ (ε) 225 (60100), 269 (34200), 310 nm (7400); [α]$_D^{20}$ +81.7° (c = 0.3900 CH$_2$Cl$_2$); Circular Dichroism (CH$_2$Cl$_2$) λ$_{max}$ (Δε), 244 (–119.0), 265 (13.6), 284 (–24.6), 307 nm (9.0); IR (CH$_2$Cl$_2$, cast), 3061 (m), 2978 (m), 2936 (m), 1819 (m), 1437 (s) cm^{-1}; ^{1}H NMR (700 MHz, CD$_2$Cl$_2$) δ 7.82–7.77 (m, 4H), 7.75–7.68 (m, 8H), 7.66–7.60 (m, 8H), 7.59–7.55 (m, 4H), 7.54–7.49 (m, 8H), 7.49–7.42 (m, 8H), 2.60–2.54 (m, 4H), 1.09–0.99 (m, 12H); ^{13}C NMR (126 MHz, CD$_2$Cl$_2$) δ 136.5 (t, J_{C-P} = 5.7 Hz), 135.2, 134.3, 132.8 (t, J_{C-P} = 4.9 Hz), 130.4 (t, J_{C-P} = 5.7 Hz), 122.8 (dd, $^1J_{C-P}$ = 69.6 Hz, J_{C-P} = 2.3 Hz), 121.2 (dd, $^1J_{C-P}$ = 67.1 Hz, J_{C-P} = 3.6 Hz), 36.7–35.9 (m), 13.3–12.7 (m), one signal coincident or not observed; ^{31}P NMR (202 MHz, CD$_2$Cl$_2$) δ 44.7 ($^1J_{P-Pt}$ = 3696 Hz); ^{11}B NMR (160 MHz, CD$_2$Cl$_2$) δ –1.0; ^{19}F NMR (469 MHz, CD$_2$Cl$_2$) δ –152.7, –152.8; ESI HRMS calcd for C$_{56}$H$_{56}$^{11}B^{35}Cl$_2$F$_4$P$_4$^{195}Pt$_2$ [M – ^{11}BF$_4$]$^+$ 1399.2026, found 1399.2040; calcd for C$_{56}$H$_{56}$^{35}Cl$_3$P$_4$^{195}Pt$_2$ [M – (^{11}BF$_4$)$_2$ + ^{35}Cl]$^+$ 1347.1672, found 1347.1685; DSC: decomposition 218 °C (onset), 227 °C (peak).
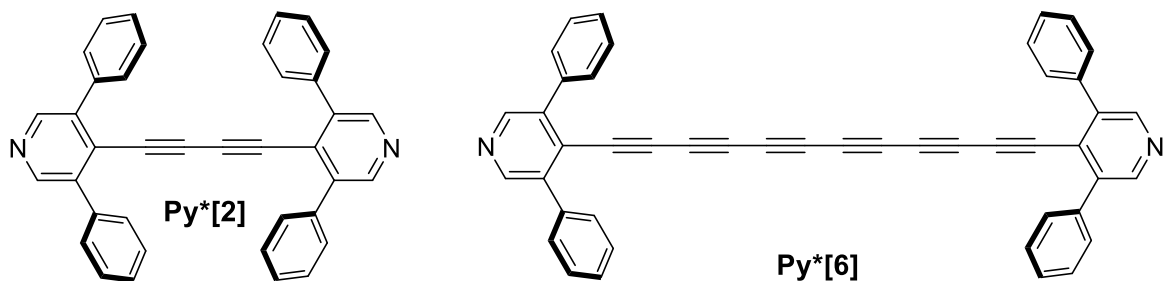
Py*[2] and **Py*[6]** were synthesized as described in the literature.[18]
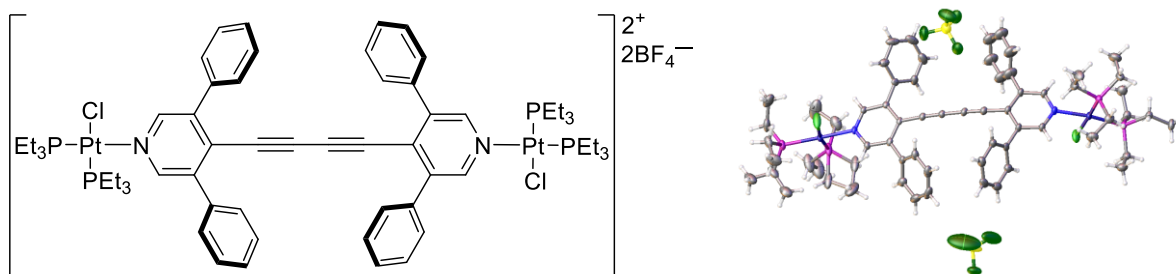
Compound (Et)-Py*[2]Pt: A vial was charged with compound **Py*[2]** (10.0 mg, 0.0197 mmol) and dry CH_2Cl_2 (1 mL). A separate vial was charged with **4.1** (21.8 mg, 0.0197 mmol) and dry CH_2Cl_2 (2 mL). To a flask filled with N_2 was transferred the solution containing **Py*[2]** and the solution containing **4.1**, respectively. The mixture was stirred for 26 h at rt under a N_2 atmosphere. The solvent was removed in *vacuo*, the residue was dissolved in CH_2Cl_2 (0.5 mL), and ethyl acetate (10 mL) was carefully layered onto the CH_2Cl_2 layer. After standing this solution at 0 ºC overnight, the product **(Et)-Py*[2]Pt** was precipitated, filtered, and collected as a light yellow-brown solid (20 mg, 63%). Mp 188 °C; UV-vis (CH_2Cl_2) λ_{max} (ε) 351 (25700), 373 (sh, 23700), 393 nm (sh, 16700); IR (CH_2Cl_2, cast), 3062 (w), 2972 (m), 2938 (m), 2880 (w), 2215 (vw), 2145 (w), 1591 (m), 1455 (m), 1418 (s) cm^{-1}; ^1H NMR (400 MHz, CD_2Cl_2) δ 8.51 (d, $^4J_{H\text{-}P}$ = 3.0 Hz, 4H), 7.61–7.57 (m, 4H), 7.54–7.49 (m, 16H), 2.11 (dq, $^2J_{H\text{-}P}$ = 9.9 Hz, $^3J_{H\text{-}H}$ = 7.6 Hz, 12H), 1.86 (dq, $^2J_{H\text{-}P}$ = 9.2 Hz, $^3J_{H\text{-}H}$ = 7.6 Hz, 12H), 1.25 (dt, $^3J_{H\text{-}P}$ = 18.0 Hz, $^3J_{H\text{-}H}$ = 7.6 Hz, 18H), 1.20 (dt, $^3J_{H\text{-}P}$ = 17.9 Hz, $^3J_{H\text{-}H}$ = 7.6 Hz, 18H); ^{13}C NMR (176 MHz, CD_2Cl_2) δ 149.3, 144.0 (d, $J_{C\text{-}P}$ = 3.1 Hz), 134.3, 130.6, 129.7, 129.5, 86.4, 81.2, 16.6 (d, $^1J_{C\text{-}P}$ = 31.3 Hz), 16.4 (d, $^1J_{C\text{-}P}$ = 33.1 Hz), 8.9 (d, $^2J_{C\text{-}P}$ = 3.7 Hz), 8.6 (d, $^2J_{C\text{-}P}$ = 3.1 Hz), one signal coincident or not observed; ^{31}P NMR (202 MHz, CD_2Cl_2) δ 7.1 (d, $^1J_{P\text{-}Pt}$ = 3437.0 Hz, $^2J_{P\text{-}P}$ = 19.3 Hz), 3.7 (d, $^1J_{P\text{-}Pt}$ = 3100.2 Hz, $^2J_{P\text{-}P}$ = 19.4 Hz);

^{11}B NMR (128 MHz, CD$_2$Cl$_2$) δ −1.2; ^{19}F NMR (376 MHz, CD$_2$Cl$_2$) δ −152.87, −152.93; ESI HRMS calcd for C$_{50}$H$_{54}$N$_2$P$_2$^{35}Cl^{195}Pt [M − Pt(PEt$_3$)$_2$Cl − (BF$_4$)$_2$]$^+$ 974.3093, found 974.3062; calcd for C$_{62}$H$_{84}$N$_2$P$_4$^{35}Cl$_2$^{195}Pt$_2$ [M − (^{11}BF$_4$)$_2$]$^{2+}$ 720.2123, found 720.2115; calcd for C$_{12}$H$_{30}$P$_2$^{35}Cl ^{195}Pt [M − Pt (PEt$_3$)$_2$Cl − **Py*[2]** − (BF$_4$)$_2$]$^+$ 466.1154, found 466.1142.

A crystal of **(Et)-Py*[2]Pt** suitable for X-ray crystallographic analysis has been grown at rt, by slow diffusion of a CH$_2$Cl$_2$ solution of **(Et)-Py*[2]Pt** layered with hexane. X-ray crystallographic data for **(Et)-Py*[2]Pt** (C$_{64}$H$_{87}$B$_2$Cl$_6$F$_8$N$_2$P$_4$Pt$_2$): F_w = 1784.73; triclinic crystal system; space group P–1 (No.2); a = 11.2872(3) Å, b = 14.7811(4) Å, c = 23.2603(5) Å; α = 74.4593(19)°, β = 79.3665(19)°, γ = 88.288(2)°; V = 3673.85(15) Å^3; Z = 2; $\rho_{(calcd)}$ = 1.613 g/cm^3; μ = 4.168 mm^{-1}; λ = 0.71073 Å; T = 153 K; $2\theta_{max}$ = 58.04°; total data collected = 56557; R_1 = 0.0335 [16389 independent reflections with $I \geq 2\sigma(I)$]; ωR_2 = 0.0770 for 16389 data, 756 variables, and 30 restraints; largest difference, peak and hole = 2.40 and −0.198 e Å^{-3}.
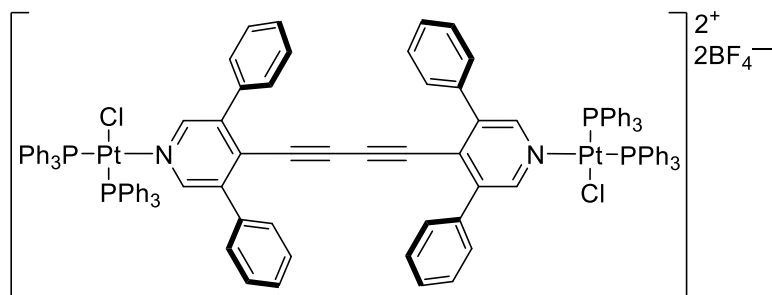
Compound (Ph)-Py*[2]Pt: A vial was charged with **Py*[2]** (10.0 mg, 0.0197 mmol) and dry CH$_2$Cl$_2$ (4 mL). A separate vial was charged with **4.2** (33.1 mg, 0.0197 mmol) and dry CH$_2$Cl$_2$ (4 mL). To a flask filled with N$_2$ was transferred the solution containing **Py*[2]** and the solution containing **4.2**, respectively. The mixture was stirred for 15 h at rt under a N$_2$ atmosphere. The solvent was removed in *vacuo*, the residue was dissolved in CH$_2$Cl$_2$ (2 mL), and ethyl acetate (10 mL) was carefully layered onto the CH$_2$Cl$_2$ layer. After standing this solution at rt overnight, the product **(Ph)-Py*[2]Pt** was precipitated, filtered, and collected as a colorless solid (42 mg, 97%). Mp 244–246 °C; UV-vis (CH$_2$Cl$_2$) λ_{max} (ε) 262 (80300), 353 (30200), 372 (29800), 393 nm (21400); IR (CH$_2$Cl$_2$, cast), 3056 (br, m), 2138 (vw), 1590 (m), 1574 (w), 1482 (m), 1437 (s), 1418 (m) cm^{-1}; ^{1}H NMR (400 MHz, CD$_2$Cl$_2$) δ 8.39 (d, $^4J_{H-P}$ = 3.4 Hz, 4H), 7.59–7.56 (m, 4H), 7.50–7.39 (m, 44H), 7.31–7.29 (m, 8H), 7.27–7.22 (m, 24H); ^{13}C NMR (176 MHz, CD$_2$Cl$_2$) δ 149.3, 143.4 (d, J_{C-P} = 3.2 Hz), 135.5 (d, J_{C-P} = 10.2 Hz), 134.3 (d, J_{C-P} = 11.0 Hz), 134.2, 133.0 (d, J_{C-P} = 2.3 Hz), 132.4 (d, J_{C-P} = 2.6 Hz), 130.4, 129.8 (d, J_{C-P} = 11.5 Hz), 129.5 (d, J_{C-P} = 25.3 Hz), 129.0 (d, J_{C-P} = 11.6 Hz), 127.8 (d, $^1J_{C-P}$ = 66.4 Hz), 126.9 (d, $^1J_{C-P}$ = 64.1 Hz), 86.1, 80.7, two signals are

coincident or not observed; ^{31}P NMR (162 MHz, CD$_2$Cl$_2$) δ 15.4 (d, $^1J_{\text{P-Pt}}$ = 3649.8 Hz, $^2J_{\text{P-P}}$ = 18.6 Hz), 3.7 (d, $^1J_{\text{P-Pt}}$ = 3268.4 Hz, $^2J_{\text{P-P}}$ = 18.7 Hz); ^{11}B NMR (128 MHz, CD$_2$Cl$_2$) δ −1.1; ^{19}F NMR (376 MHz, CD$_2$Cl$_2$) δ −153.15, −153.20; ESI HRMS calcd for C$_{74}$H$_{54}$N$_2$P$_2$^{35}Cl^{195}Pt [M − Pt(PPh$_3$)$_2$Cl − (^{11}BF$_4$)$_2$]$^+$ 1262.3093, found 1262.3093; calcd for C$_{110}$H$_{84}$N$_2$P$_4$^{35}Cl$_2$^{195}Pt$_2$ [M − (^{11}BF$_4$)$_2$]$^{2+}$ 1008.2123, found 1008.2115; calcd for C$_{36}$H$_{30}$P$_2$^{195}Pt^{35}Cl [M − Py*[2] − Pt(PPh$_3$)$_2$Cl − (^{11}BF$_4$)$_2$]$^+$ 754.1154, found 754.1152.
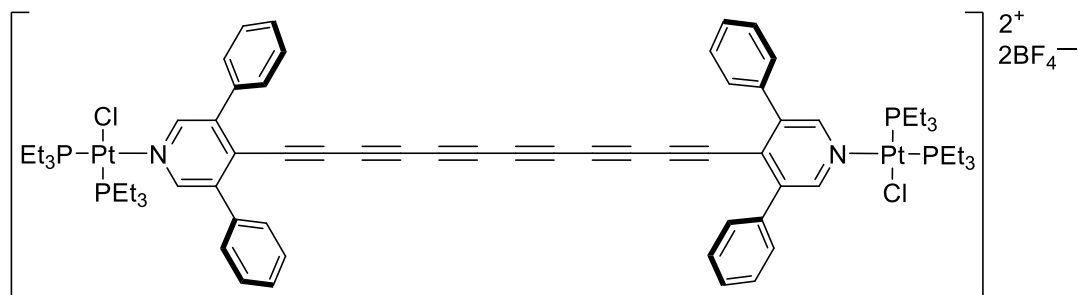
Compound (Et)-Py*[6]Pt: A vial was charged with **Py*[6]** (15.0 mg, 0.0248 mmol) and dry CH$_2$Cl$_2$ (2 mL). A separate vial was charged with **4.1** (27.5 mg, 0.0248 mmol) and dry CH$_2$Cl$_2$ (3 mL). To a flask filled with N$_2$ was transferred the solution containing **Py*[6]** and the solution containing **4.1**, respectively. The mixture was stirred for 8 h at rt under a N$_2$ atmosphere. The solvent was removed in *vacuo*, the residue was dissolved in CH$_2$Cl$_2$ (1.5 mL), and toluene (10 mL) was carefully layered onto the CH$_2$Cl$_2$ layer. After standing this solution at rt overnight, the product **(Et)-Py*[6]Pt** was precipitated, filtered, and collected as a dark brown solid (39 mg, 92%). Mp 180 °C (decomposition); UV-vis (CH$_2$Cl$_2$) λ$_{\text{max}}$ (ε) 256 (73900), 274 (sh, 73400), 287 (82000), 302 (71700), 317 (65200), 337 (85400), 360 (131000), 384 (103000), 409 (42700), 444 (30400), 484 nm (15000); IR (CH$_2$Cl$_2$, cast), 3061 (w), 2971 (w), 2939 (w), 2881 (w), 2156 (w), 2049 (w), 1591 (m), 1458 (m), 1429 (m), 1418 (m) cm^{-1}; ^{1}H NMR (700 MHz, CD$_2$Cl$_2$) δ 8.52 (d, $^4J_{\text{H-P}}$ = 3.0 Hz, 4H), 7.60–7.58 (m, 20H), 2.11 (dq, $^2J_{\text{H-P}}$ = 9.9 Hz, $^3J_{\text{H-H}}$ = 7.6 Hz, 12H), 1.86 (dq, $^2J_{\text{H-P}}$ = 9.1 Hz, $^3J_{\text{H-H}}$ = 7.6 Hz, 12H), 1.25 (dt, $^3J_{\text{H-P}}$ = 18.0 Hz, $^3J_{\text{H-H}}$ = 7.6 Hz, 18H), 1.20 (dt, $^3J_{\text{H-P}}$ = 17.9 Hz, $^3J_{\text{H-H}}$ = 7.6 Hz, 18H); ^{13}C NMR (176 MHz, CD$_2$Cl$_2$) δ 149.4, 144.8 (d, $J_{\text{C-P}}$ = 2.8 Hz), 134.3, 130.8, 130.2, 129.73, 129.68, 87.6, 72.3, 72.0, 67.1, 64.5, 61.8, 16.6 (d, $^1J_{\text{C-P}}$ = 28.9 Hz), 16.4 (d, $^1J_{\text{C-P}}$ = 30.7 Hz), 8.9 (d, $^2J_{\text{C-P}}$ = 3.7 Hz), 8.6 (d, $^2J_{\text{C-P}}$ = 3.2 Hz); ^{31}P NMR (202 MHz, CD$_2$Cl$_2$) δ 7.1 (d, $^1J_{\text{P-Pt}}$ = 3426.0 Hz, $^2J_{\text{P-P}}$ = 19.5 Hz), 3.8 (d, $^1J_{\text{P-Pt}}$ = 3096.5 Hz, $^2J_{\text{P-P}}$ = 19.4 Hz); ^{11}B NMR (128 MHz, CD$_2$Cl$_2$) δ −1.2; ^{19}F NMR (376 MHz, CD$_2$Cl$_2$) δ −152.96, −153.01; ESI HRMS calcd for

$C_{58}H_{54}N_2P_2{}^{35}Cl^{195}Pt$ [M − Pt(PEt$_3$)$_2$Cl − (^{11}BF$_4$)$_2$]$^+$ 1070.3093, found 1070.3102; calcd for $C_{24}H_{60}P_4{}^{35}Cl_3{}^{195}Pt_2$ [M − C$_{46}$H$_{24}$N$_2$ − (^{11}BF$_4$)$_2$ + ^{35}Cl]$^+$ 967.2001, found 967.2002; calcd for $C_{70}H_{84}N_2P_4{}^{35}Cl_2{}^{195}Pt_2$ [M − (^{11}BF$_4$)$_2$]$^{2+}$ 768.2123, found 768.2113.
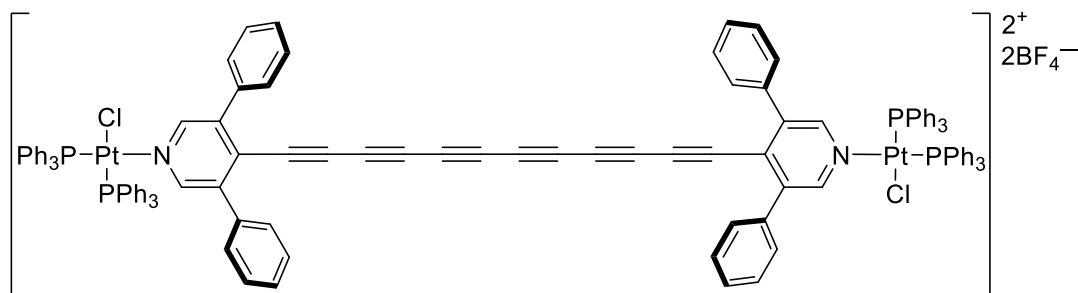
Compound (Ph)-Py*[6]Pt: A vial was charged with **Py*[6]** (15.0 mg, 0.0248 mmol) and dry CH$_2$Cl$_2$ (2 mL). A separate vial was charged with **4.2** (41.8 mg, 0.0248 mmol) and dry CH$_2$Cl$_2$ (3 mL). To a flask filled with N$_2$ was transferred the solution containing **Py*[6]** and the solution containing **4.2**, respectively. The mixture was stirred for 28 h at rt under a N$_2$ atmosphere. The solvent was removed in *vacuo,* the residue was dissolved in CH$_2$Cl$_2$ (1 mL) and ethyl acetate (10 mL) was carefully layered onto the CH$_2$Cl$_2$ layer. After standing this solution at rt overnight, the product **(Ph)-Py*[6]Pt** was precipitated, filtered, and collected as a yellow-brown solid (40 mg, 70%). Mp 180 °C (decomposition); UV-vis (CH$_2$Cl$_2$) λ_{max} (ε) 272 (103000), 276 (sh, 103000), 285 (102000), 302 (83600), 317 (73800), 337 (92900), 361 (141000), 385 (111000), 410 (48900), 444 (34000), 485 nm (16500); IR (CH$_2$Cl$_2$, cast), 3059 (br, m), 2156 (vw), 2048 (w), 1591 (m), 1575 (w), 1482 (m), 1437 (s) cm^{-1}; ^{1}H NMR (400 MHz, CD$_2$Cl$_2$) δ 8.42 (d, $^4J_{\text{H-P}}$ = 3.4 Hz, 4H), 7.58–7.56 (m, 12H), 7.51–7.40 (m, 44H), 7.29–7.24 (m, 24H); ^{13}C NMR (176 MHz, CD$_2$Cl$_2$) δ 149.3, 144.2 (d, $J_{\text{C-P}}$ = 3.2 Hz), 135.5 (d, $J_{\text{C-P}}$ = 10.1 Hz), 134.3 (d, $J_{\text{C-P}}$ = 11.0 Hz), 134.2, 133.1 (d, $J_{\text{C-P}}$ = 2.0 Hz), 132.4 (d, $J_{\text{C-P}}$ = 2.5 Hz), 130.6, 129.9 (part of a 'd' pattern), 129.8 (d, $J_{\text{C-P}}$ = 11.6 Hz), 129.6 (d, $J_{\text{C-P}}$ = 6.4 Hz), 129.5 (part of a 'd' pattern), 129.0 (d, $J_{\text{C-P}}$ = 11.6 Hz), 127.8 (d, $^1J_{\text{C-P}}$ = 66.4 Hz), 126.9 (d, $^1J_{\text{C-P}}$ = 64.2 Hz), 87.4, 72.2, 71.7, 67.1, 64.4, 61.7; ^{31}P NMR (162 MHz, CD$_2$Cl$_2$) δ 15.5 (d, $^1J_{\text{P-Pt}}$ = 3663.2 Hz, $^2J_{\text{P-P}}$ = 18.7 Hz), 3.7 (d, $^1J_{\text{P-Pt}}$ = 3269.7 Hz, $^2J_{\text{P-P}}$ = 18.7 Hz); ^{11}B NMR (128 MHz, CD$_2$Cl$_2$) δ −1.1; ^{19}F NMR (376 MHz, CD$_2$Cl$_2$) δ −153.18, −153.23; ESI HRMS calcd for $C_{82}H_{54}N_2P_2{}^{35}Cl^{195}Pt$ [M − Pt(PPh$_3$)$_2$Cl − (^{11}BF$_4$)$_2$]$^+$ 1358.3093, found 1358.3087; calcd for $C_{118}H_{84}N_2P_4{}^{35}Cl_2{}^{195}Pt_2$ [M − (^{11}BF$_4$)$_2$]$^{2+}$ 1056.2123, found 1056.2127; $C_{36}H_{30}P_2{}^{195}Pt^{35}Cl$ [M − C$_{46}$H$_{24}$N$_2$ − Pt(PPh$_3$)$_2$Cl − (^{11}BF$_4$)$_2$]$^+$ 754.1154, found 754.1153.
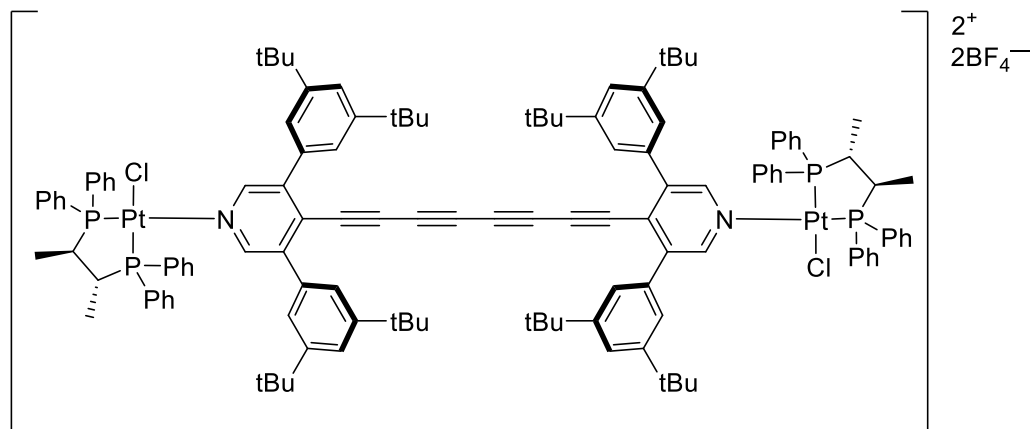
(R,R,R,R)-Py**[4a]Pt: A vial was charged with **Py**[4a]** (7.5 mg, 0.0075 mmol) and dry CH_2Cl_2 (2 mL). A separate vial was charged with **4.5** (11.1 mg, 0.00746 mmol) and dry CH_2Cl_2 (2 mL). To a flask filled with N_2 was transferred the solution containing **Py**[4a]** and the solution containing **4.5**, respectively. The mixture was stirred for 8 h at rt under a N_2 atmosphere. The solvent was removed in *vacuo*, the residue was dissolved in CH_2Cl_2 (0.5 mL), ethyl acetate (5 mL) was carefully layered onto the CH_2Cl_2 layer, and hexanes (10 mL) was carefully layered onto the ethyl acetate layer. After standing this solution at rt for several hours, the product **(R,R,R,R)-Py**[4a]Pt** was precipitated, filtered, washed with a mixed solution of EtOAc/hexanes (10 mL/10mL), and collected as a yellow solid (16 mg, 86%). UV-vis (CH_2Cl_2) λ_{max} (ε): 267 (sh, 90600), 275 (86700), 286 (sh, 80200), 307 (sh, 58200), 326 (sh, 43000), 349 (43900), 373 (45700), 405 (36000), 441 (27200), 472 (sh, 1830). ^{1}H NMR (700 MHz, CDCl$_3$) δ 8.01 (d, $^4J_{H\text{-}P}$ = 3.0 Hz, 4H), 7.97–7.94 (m, 8H), 7.85–7.82 (m, 4H), 7.72–7.70 (m, 2H), 7.67–7.58 (m, 16H), 7.48 (t, J = 1.7 Hz, 4H), 7.47–7.44 (m, 4H), 7.37 (td, J = 7.8, 2.8 Hz, 4H), 7.30–7.28 (m, 2H), 7.02 (d, J = 1.7 Hz, 8H), 3.20–3.15 (m, 2H), 2.36–2.31 (m, 2H), 1.31 (s, 72H), 1.24 (dd, J = 15.7, 6.7 Hz, 6H), 1.15 (dd, J = 15.1, 6.8 Hz, 6H); ^{13}C NMR (126 MHz, CDCl$_3$) δ 151.4, 147.9, 144.5 (d, $J_{C\text{-}P}$ = 2.6 Hz), 136.3 (d, $J_{C\text{-}P}$ = 11.6 Hz), 135.5 (d, $J_{C\text{-}P}$ = 11.1 Hz), 134.3 (d, $J_{C\text{-}P}$ = 1.3 Hz), 133.4 (d, $J_{C\text{-}P}$ = 9.1 Hz), 133.2 (d, $J_{C\text{-}P}$ = 2.4 Hz), 132.9, 132.7 (d, $J_{C\text{-}P}$ = 2.5 Hz), 132.5 (d, $J_{C\text{-}P}$ = 3.1 Hz), 131.7 (d, $J_{C\text{-}P}$ = 9.6 Hz), 129.8 (d, $J_{C\text{-}P}$ = 14.0 Hz), 129.8 (d, $J_{C\text{-}P}$ = 8.3 Hz), 129.4 (d, $J_{C\text{-}P}$ = 11.3 Hz), 129.3 (d, $J_{C\text{-}P}$ = 12.0 Hz), 128.3, 124.4 (d, $^1J_{C\text{-}P}$ = 64.8 Hz), 123.7, 123.3, 122.8 (d, $^1J_{C\text{-}P}$ = 63.5 Hz), 122.7 (d, $^1J_{C\text{-}P}$ = 61.8 Hz), 121.3 (d, $^1J_{C\text{-}P}$ = 58.6 Hz), 86.7, 73.2, 70.8, 64.4, 38.6–38.4 (m), 35.4–34.9 (m), 35.0, 31.4, 13.3 (dd, $^2J_{C\text{-}P}$ = 19.5 Hz, $^3J_{C\text{-}P}$ = 3.4 Hz), 13.1 (dd, $^2J_{C\text{-}P}$ = 17.5 Hz, $^3J_{C\text{-}P}$ = 4.8 Hz); ^{31}P NMR (162 MHz, CDCl$_3$) δ 43.9 (brs, $^1J_{P\text{-}Pt}$ = 3407.6 Hz), 34.6 (brs, $^1J_{P\text{-}Pt}$ = 3190.2 Hz); ^{11}B

NMR (128 MHz, CDCl$_3$) δ −0.9; ^{19}F NMR (376 MHz, CDCl$_3$) δ −153.16, −153.21; ESI HRMS calcd for C$_{130}$H$_{144}$N$_2$P$_4$^{35}Cl$_2$^{195}Pt$_2$ [M − (^{11}BF$_4$)$_2$]$^{2+}$ 1158.4471, found 1158.4462.
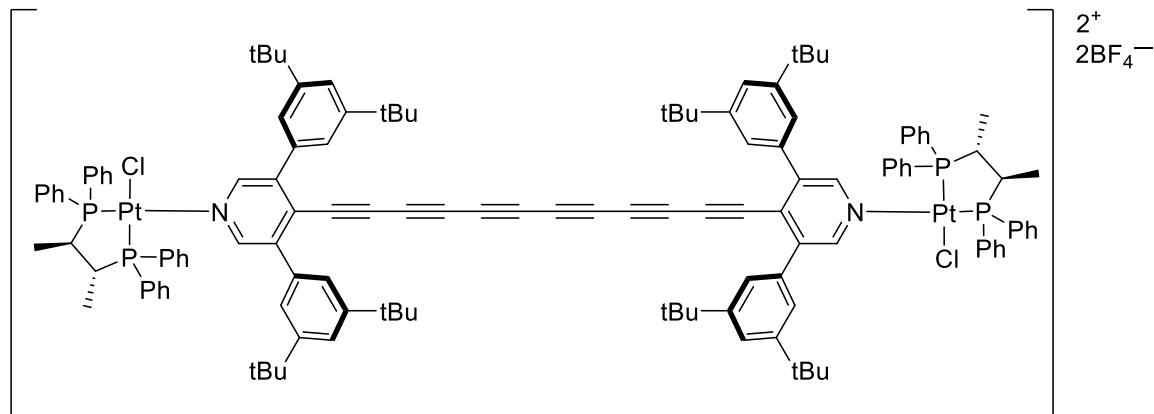
(R,R,R,R)-Py**[6a]Pt: A vial was charged with **Py**[6a]** (8.0 mg, 0.0076 mmol) and dry CH$_2$Cl$_2$ (2 mL). A separate vial was charged with **4.5** (11.3 mg, 0.00760 mmol) and dry CH$_2$Cl$_2$ (3 mL). To a flask filled with N$_2$ was transferred the solution containing **Py**[6a]** and the solution containing **4.5**, respectively. The mixture was stirred for 12 h at rt under a N$_2$ atmosphere. The solvent was removed in *vacuo*, the residue was redissolved in CH$_2$Cl$_2$ (0.5 mL), ethyl acetate (5 mL) was carefully layered onto the CH$_2$Cl$_2$ layer, and hexanes (10 mL) was carefully layered onto the ethyl acetate layer. After standing this solution at rt for several hours, the product **(R,R,R,R)-Py**[6a]Pt** was precipitated, filtered, washed with a mixed solution of EtOAc/hexanes (10 mL/10mL), and collected as a yellow solid (17.7 mg, 92%). UV-vis (CH$_2$Cl$_2$) λ$_{max}$ (ε): 258 (101000), 275 (89100), 291 (86000), 319 (69700), 338 (69100), 364 (85700), 384 (73800), 411 (44700), 446 (27800), 487 nm (14000). ^{1}H NMR (500 MHz, CDCl$_3$) δ 8.02 (d, $^4J_{H-P}$ = 3.1 Hz, 4H), 7.97–7.93 (m, 8H), 7.86–7.81 (m, 4H), 7.73–7.70 (m, 2H), 7.68–7.58 (m, 16H), 7.49 (t, J = 1.7 Hz, 4H), 7.47–7.43 (m, 4H), 7.37 (td, J = 7.7, 2.9 Hz, 4H), 7.31–7.28 (m, 2H), 7.03 (d, J = 1.7 Hz, 8H), 3.19–3.13 (m, 2H), 2.38–2.31 (m, 2H), 1.32 (s, 72H), 1.24 (dd, J = 15.7, 6.7 Hz, 6H), 1.15 (dd, J = 15.1, 6.8 Hz, 6H); ^{13}C NMR (126 MHz, CDCl$_3$) δ 151.5, 147.9, 144.7 (d, J_{C-P} = 2.8 Hz), 136.3 (d, J_{C-P} = 11.3 Hz), 135.5 (d, J_{C-P} = 10.9 Hz), 134.3 (d, J_{C-P} = 1.7 Hz), 133.4 (d, J_{C-P} = 9.1 Hz), 133.2 (d, J_{C-P} = 2.2 Hz), 132.9, 132.7 (d, J_{C-P} = 2.1 Hz), 132.5 (d, J_{C-P} = 2.1 Hz), 131.6 (d, J_{C-P} = 9.4 Hz), 129.8 (d, J_{C-P} = 13.9 Hz), 129.8 (d, J_{C-P} = 8.2 Hz), 129.4 (d, J_{C-P} = 11.3 Hz), 129.3 (d, J_{C-P} = 12.0 Hz), 128.2, 124.3 (d, $^1J_{C-P}$ = 65.0 Hz), 123.7, 123.3, 122.8 (d, $^1J_{C-P}$ = 63.3 Hz), 122.7

(d, $^1J_{C-P}$ = 61.7 Hz), 121.2 (d, $^1J_{C-P}$ = 58.1 Hz), 86.7, 72.0, 71.5, 66.6, 63.9, 61.5, 38.6 (dd, $^1J_{C-P}$ = 41.7 Hz, $^2J_{C-P}$ = 9.4 Hz), 35.1 (dd, $^1J_{C-P}$ = 52.4 Hz, $^2J_{C-P}$ = 11.4 Hz), 35.0, 31.4, 13.3 (dd, $^2J_{C-P}$ = 18.4 Hz, $^3J_{C-P}$ = 3.3 Hz), 13.1 (dd, $^2J_{C-P}$ = 18.0 Hz, $^3J_{C-P}$ = 3.6 Hz); ^{31}P NMR (162 MHz, CDCl$_3$) δ 43.9 (brs, $^1J_{P-Pt}$ = 3428.2 Hz), 34.7 (brs, $^1J_{P-Pt}$ = 3178.0 Hz); ^{11}B NMR (128 MHz, CDCl$_3$) δ –0.9; ^{19}F NMR (376 MHz, CDCl$_3$) δ –153.27, –153.32; ESI HRMS calcd for C$_{134}$H$_{144}$N$_2$P$_4$^{35}Cl$_2$^{195}Pt$_2$ [M – (^{11}BF$_4$)$_2$]$^{2+}$ 1182.4471, found 1182.4470.
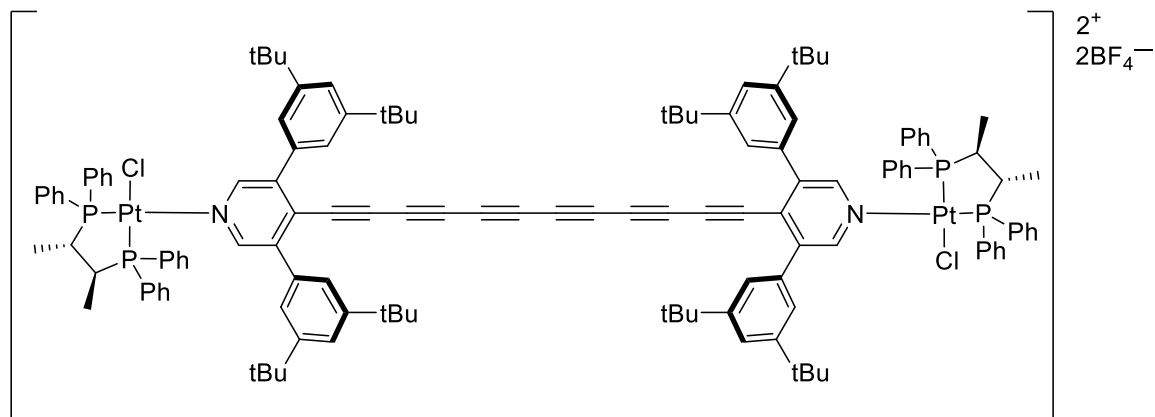
(*S,S,S,S*)-Py**[6a]Pt: A vial was charged with **Py**[6a]** (10.0 mg, 0.00949 mmol) and dry CH$_2$Cl$_2$ (2 mL). A separate vial was charged with **4.6** (14.1 mg, 0.00948 mmol) and dry CH$_2$Cl$_2$ (3 mL). To a flask filled with N$_2$ was transferred the solution containing **Py**[6a]** and the solution containing **4.6**, respectively. The mixture was stirred for 12 h at rt under a N$_2$ atmosphere. The solvent was removed in *vacuo*, the residue was redissolved in CH$_2$Cl$_2$ (0.5 mL), ethyl acetate (5 mL) was carefully layered onto the CH$_2$Cl$_2$ layer, and hexanes (10 mL) was carefully layered onto the ethyl acetate layer. After standing this solution at rt for several hours, the product **(*S,S,S,S*)-Py**[6a]Pt** was precipitated, filtered, washed with a mixed solution of EtOAc/hexanes (10 mL/10mL), and collected as a yellow solid (18 mg, 75%). UV-vis (CH$_2$Cl$_2$) λ$_{max}$ (ε): 260 (103000), 277 (93800), 292 (96300), 319 (80300), 338 (80200), 364 (10200), 384 (87900), 411 (52700), 446 (32000), 487 nm (15600). ^{1}H NMR (500 MHz, CDCl$_3$) δ 8.02 (d, $^4J_{H-P}$ = 3.0 Hz, 4H), 7.97–7.93 (m, 8H), 7.86–7.81 (m, 4H), 7.73–7.70 (m, 2H), 7.68–7.58 (m, 16H), 7.49 (t, J = 1.6 Hz, 4H), 7.47–7.43 (m, 4H), 7.38 (td, J = 7.5, 2.7 Hz, 4H), 7.31–7.28 (m, 2H), 7.03 (d, J = 1.7 Hz, 8H), 3.19–3.12 (m, 2H), 2.38–2.31 (m, 2H), 1.32 (s, 72H), 1.24 (dd, J = 15.9, 6.8 Hz, 6H), 1.15 (dd, J = 15.1, 6.8 Hz, 6H); ^{13}C NMR (126 MHz, CDCl$_3$) δ 151.5, 147.9, 144.7 (d, J_{C-P} = 2.9 Hz), 136.3 (d, J_{C-P} = 11.3 Hz), 135.5 (d, J_{C-P} = 11.0 Hz), 134.3 (d, J_{C-P} = 2.1 Hz), 133.4 (d, J_{C-P} = 9.0 Hz),

133.2 (d, J_{C-P} = 1.8 Hz), 132.9, 132.7 (d, J_{C-P} = 2.3 Hz), 132.5 (d, J_{C-P} = 2.1 Hz), 131.7 (d, J_{C-P} = 9.2 Hz), 129.8 (d, J_{C-P} = 15.7 Hz), 129.8 (d, J_{C-P} = 6.9 Hz), 129.4 (d, J_{C-P} = 11.4 Hz), 129.3 (d, J_{C-P} = 12.1 Hz), 128.2, 124.4 (d, $^1J_{C-P}$ = 64.9 Hz), 123.7, 123.3, 122.8 (d, $^1J_{C-P}$ = 63.3 Hz), 122.7 (d, $^1J_{C-P}$ = 61.6 Hz), 121.3 (d, $^1J_{C-P}$ = 57.9 Hz), 86.7, 72.0, 71.5, 66.6, 63.9, 61.5, 38.6 (dd, $^1J_{C-P}$ = 42.0 Hz, $^2J_{C-P}$ = 9.4 Hz), 35.4–34.9 (m), 35.0, 31.4, 13.3 (dd, $^2J_{C-P}$ = 17.7 Hz, $^3J_{C-P}$ = 3.6 Hz), 13.1 (dd, $^2J_{C-P}$ = 17.0 Hz, $^3J_{C-P}$ = 4.3 Hz); ^{31}P NMR (162 MHz, CDCl$_3$) δ 44.0 (d, $^1J_{P-Pt}$ = 3416.8 Hz, $^2J_{P-P}$ = 16.0 Hz), 34.7 (d, $^1J_{P-Pt}$ = 3197.0 Hz, $^2J_{P-P}$ = 16.1 Hz); ^{11}B NMR (128 MHz, CDCl$_3$) δ –0.9; ^{19}F NMR (376 MHz, CDCl$_3$) δ –153.26, –153.32.
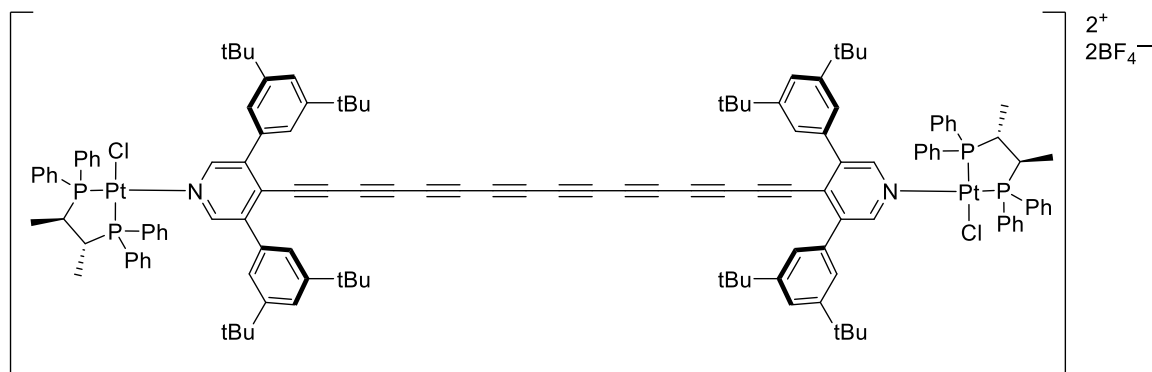
(**R,R,R,R**)-**Py**[8a]Pt:** A vial was charged with **Py**[8a]** (8.5 mg, 0.0077 mmol) and dry CH$_2$Cl$_2$ (2 mL). A separate vial was charged with **4.5** (11.5 mg, 0.00773 mmol) and dry CH$_2$Cl$_2$ (3 mL). To a flask filled with N$_2$ was transferred the solution containing **Py**[8a]** and the solution containing **4.5**, respectively. The mixture was stirred for 14 h at rt under a N$_2$ atmosphere. The solvent was removed in *vacuo*, the residue was redissolved in CH$_2$Cl$_2$ (0.5 mL), ethyl acetate (5 mL) was carefully layered onto the CH$_2$Cl$_2$ layer, and hexanes (10 mL) was carefully layered onto the ethyl acetate layer. After standing this solution at rt for several hours, the product (**R,R,R,R**)-**Py**[8a]Pt** was precipitated, filtered, washed with a mixed solution of EtOAc/hexanes (10 mL/10mL), and collected as a brown solid (17 mg, 85%). UV-vis (CH$_2$Cl$_2$) λ_{max} (ε): 267 (sh, 86700), 275 (sh, 80500), 291 (73000), 307 (74600), 323 (83800), 339 (93100), 359 (110000), 374 (102000), 398 (108000), 414 (83800), 443 (26700), 480 (16300), 524 nm (7530). ^{1}H NMR (500 MHz, CDCl$_3$) δ 8.02 (d, $^4J_{H-P}$ = 3.1 Hz, 4H), 7.97–7.93 (m, 8H), 7.86–7.82 (m, 4H), 7.73–7.70 (m, 2H), 7.68–7.58 (m, 16H), 7.50 (t, J = 1.7 Hz, 4H), 7.47–7.43 (m, 4H), 7.38 (td, J = 7.7, 2.9 Hz, 4H), 7.31–7.28 (m, 2H), 7.03 (d, J = 1.7 Hz, 8H), 3.19–3.12 (m, 2H), 2.40–2.30 (m, 2H), 1.32 (s, 72H), 1.24 (dd, J = 15.7, 6.5 Hz, 6H), 1.15 (dd, J = 15.1, 6.9 Hz, 6H); ^{13}C NMR (126 MHz, CDCl$_3$) δ 151.5,

147.9, 144.8 (d, J_{C-P} = 2.9 Hz), 136.3 (d, J_{C-P} = 11.0 Hz), 135.5 (d, J_{C-P} = 11.0 Hz), 134.3 (d, J_{C-P} = 2.0 Hz), 133.4 (d, J_{C-P} = 9.0 Hz), 133.2 (d, J_{C-P} = 2.4 Hz), 132.9, 132.7 (d, J_{C-P} = 2.0 Hz), 132.5 (brs), 131.7 (d, J_{C-P} = 9.5 Hz), 129.8 (d, J_{C-P} = 16.5 Hz), 129.8 (d, J_{C-P} = 5.7 Hz), 129.4 (d, J_{C-P} = 11.4 Hz), 129.3 (d, J_{C-P} = 12.0 Hz), 128.2, 124.4 (d, $^{1}J_{C-P}$ = 64.8 Hz), 123.7, 123.3, 122.8 (d, $^{1}J_{C-P}$ = 63.6 Hz), 122.7 (d, $^{1}J_{C-P}$ = 61.5 Hz), 121.3 (d, $^{1}J_{C-P}$ = 58.5 Hz), 86.7, 71.7, 71.6, 66.9, 64.8, 63.7, 62.6, 60.9, 35.0, 31.4, 13.3 (dd, $^{2}J_{C-P}$ = 17.8 Hz, $^{3}J_{C-P}$ = 4.2 Hz), 13.1 (dd, $^{2}J_{C-P}$ = 16.7 Hz, $^{3}J_{C-P}$ = 4.7 Hz), two signals are not observed due to signal-to-noise; ^{31}P NMR (162 MHz, CDCl$_3$) δ 43.9 (brs, $^{1}J_{P-Pt}$ = 3419.6 Hz), 34.7 (brs, $^{1}J_{P-Pt}$ = 3181.7 Hz); ^{11}B NMR (128 MHz, CDCl$_3$) δ −0.9; ^{19}F NMR (376 MHz, CDCl$_3$) δ −153.27, −153.32.

7.5 Azo-porphyrin compounds (Chapter 5 data)

7.5.1 General procedures

General methods for photoswitching. A solution of the desired compound was prepared in a suitable concentration (ca. 0.003–0.008 mM for complexes and 0.06 mM for free ligands), and the solution was sealed in a cuvette with a Teflon cap. The solution was irradiated under a specific wavelength as specified in the individual spectra. After every irradiation period, a UV-vis spectrum was recorded until it was deemed that the solution had reached PSS.

The choice of solvent for UV-vis spectra. Quantitative UV-vis measurements of **GaL1**, **GaL2**, **GaL1Ru**, **RuL1**, **RuL4Ru**, **GaL3Ga**, and **GaL5Ru** were done in solutions of CH$_2$Cl$_2$, which is the only common solvent for which all derivatives are soluble. For photoswitching measurements, however, CH$_2$Cl$_2$ is not an acceptable choice, because derivatives bearing Ga-porphyrins are not sufficiently stable over the timeframe of the irradiation experiments (decomposition was observed for Ga-porphyrins under photo-irradiation in CH$_2$Cl$_2$ after only a couple hours). For the irradiation experiments for complexes bearing Ga-porphyrins, hexanes was employed as it provides good solubility, stability, and an obvious response upon irradiation. As **RuL1** and **RuL4Ru** are insoluble in hexanes, toluene was chosen as an alternative, apolar solvent for photophysical analyses of these derivatives.

Titration procedures. Solutions of **5.12** in toluene (2.21 mg in 250 mL) and *trans*-**L1** in toluene

(3.27 mg in 5 mL) were prepared separately. The solution of *trans*-**L1** was irradiated at 360 nm and the photoreaction was monitored by UV-vis analysis at the absorption of 450 nm until it was clear that the PSS had been reached to give a mixture of *trans*-/*cis*-**L1**; ca. 7 h. A portion of the resulting solution of *trans*-/*cis*-**L1** (ca. 61 μL, 0.1 equiv) was added to the solution of **5.12** in toluene. The resulting solution was stirred for 2 min and then a spectrum recorded using UV-vis spectroscopy. The procedure was then repeated with another aliquot of ligand solution. Solutions of **5.12** in toluene (1.01 mg in 100 mL) and *trans*-**L1** in toluene (1.35 mg in 5 mL) were prepared separately. A portion of *trans*-**L1** (ca. 68 μL, 0.1 equiv) was added to the solution of **5.12** in toluene. The resulting solution was stirred for 2 min and then a spectrum recorded using UV-vis spectroscopy. The procedure was then repeated with another aliquot of ligand solution.

7.5.2 Synthesis of known compounds
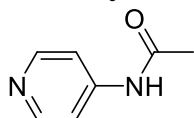
Compound 5.1: The formation of compound **5.1** was adapted of a reported procedure.[19] To isopropenyl acetate (30 g, 0.30 mol) was added 4-aminopyridine (5.6 g, 0.060 mol). The mixture was stirred for 5 h at 85 °C. The reaction mixture was cooled to rt. Solvent removal and purification by column chromatography (silica gel, MeOH/CH$_2$Cl$_2$ 1:20 to 1:10) afforded **5.1** (7 g, 86%) as a white solid.
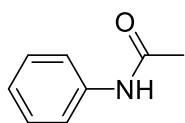
Compound 5.4: The formation of compound **5.4** was adapted from a reported procedure.[19] To isopropenyl acetate (8.4 g, 0.084 mol) was added aniline (5.4 g, 0.058 mol). The mixture was stirred for 5 h at 85 °C. The reaction mixture was cooled to rt. Solvent removal and recrystallization from CH$_2$Cl$_2$/hexanes (2/20 mL) afforded **5.4** (6.45 g, 83%) as a white solid.

5.5 (32%)   **5.6** (95%)
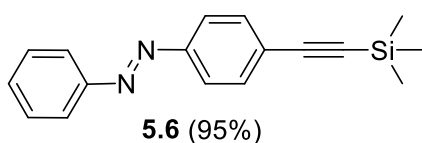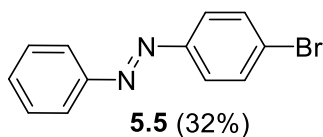
Compound 5.5 was synthesized as described in the literature.[20]

Compound 5.6 was synthesized by the adaption from a known procedure in the literature.[21] Compound **5.5** (870 mg, 3.33 mmol) was added to a degassed solution of trimethyl acetylene (655 mg, 6.67 mmol) in triethylamine (20 mL). PdCl$_2$(PPh$_3$)$_2$ (116 mg, 0.165 mmol) and CuI (63 mg, 0.331 mmol) were added, and the mixture was stirred for 20 h at 45 °C. The reaction mixture was cooled to rt, and ethyl acetate (20 mL) and satd aq NH$_4$Cl (20 mL) were then added. The layers

were separated, and the organic phase was washed with satd aq NH$_4$Cl (2 × 20 mL), dried (MgSO$_4$), and filtered. Solvent removal and purification by column chromatography (silica gel, hexanes/CH$_2$Cl$_2$ 10:1) afforded **5.6** (880 mg, 95%) as an orange solid.

5.7 (44%)   **5.8** (46%)   *trans*-**L3** (97%)
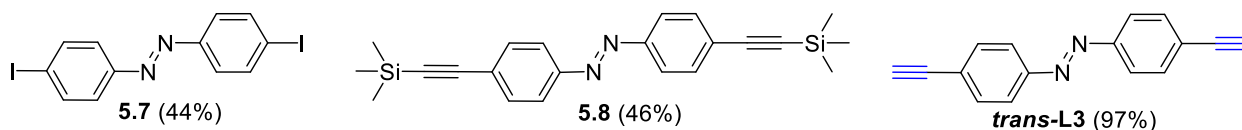
Compound 5.7,[22] **5.8,**[23] and ***trans*-L3**[23] were synthesized as described in the literature.
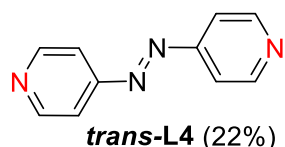
trans-**L4** (22%)

Compound *trans*-L4 was synthesized as described in the literature.[24]

5.9   **5.10** (75%)
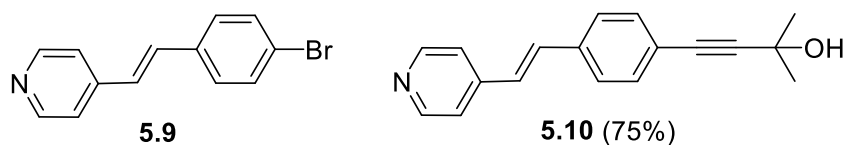
Compound 5.9 and **5.10** were synthesized as described in the literature.[25]

Ga(tpfpp)Cl (**5.11**)   Ru(tpfpp)(CO)(MeCN) (**5.12**)   Ru(tpfpp)(CO)(pyridine) (**5.13**)
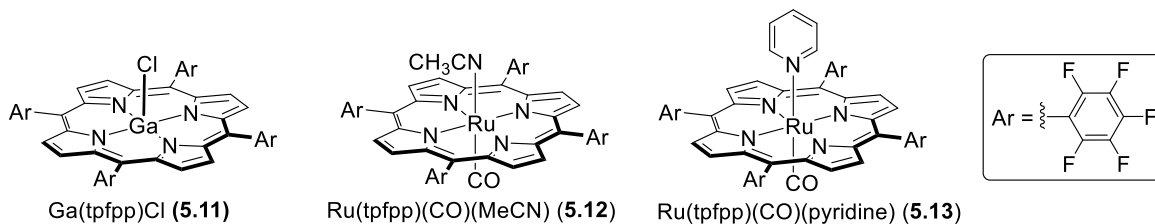
Ga(tpfpp)Cl (**5.11**) was synthesized as described in the literature.[26] Ru(tpfpp)(CO)(MeCN) (**5.12**) was formed by stirring Ru(tpfpp)(CO)[27] in a solution of MeCN by adaption from a procedure reported in the literature.[28] Ru(tpfpp)(CO)(pyridine) (**5.13**) was formed from **5.12** via reaction with pyridine through adaption of the procedure reported in the literature.[29]

7.5.3 Synthetic protocols
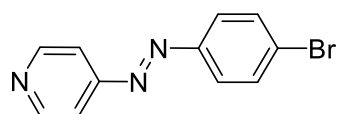
Compound 5.2: The formation of **5.2** was accomplished as descried in the literature.[20] To a solution of **5.1** (1.36 g, 10.0 mmol) in xylene (30 mL) were added NaOH (1.6 g, 40 mmol), K$_2$CO$_3$ (1.38 g, 10.0 mmol), and tris[2-(2-methoxyethoxy)ethyl]amine (TDA-1) (129 mg, 0.400 mmol). The mixture was stirred for 1 h at 100 °C and 1-bromo-4-nitrobenzene (2.02 g, 10.0 mmol) was then

211

added. The reaction mixture was stirred for 16 h at 130 °C. The contents were filtered hot through a fritted funnel and the resulting solid washed with ethyl acetate (50 mL). The filtrate was collected, cooled to rt, and satd aq NH_4Cl (50 mL) was added. The layers were separated, and the organic phase was washed with saturated aq. NH_4Cl (2 × 50 mL), dried ($MgSO_4$), and filtered. Solvent removal and purification by column chromatography (silica gel, hexanes/EtOAc 4:1) afforded **5.2** (0.84 g, 32%) as an orange solid. Mp 143–144 °C. R_f = 0.52 (hexanes/ EtOAc 1:1). UV/Vis (CH_2Cl_2) λ_{max} (ε) 236 (9720), 324 (21000), 450 nm (484). IR (ATR) 1578 (m), 1476 (m), 1401 (m), 1064 (m), 835 (s) cm^{-1}. ^1H NMR (300 MHz, $CDCl_3$) δ 8.80 (d, J = 6.2 Hz, 2H), 7.83 (d, J = 8.8 Hz, 2H), 7.69 (d, J = 6.2 Hz, 2H), 7.67 (d, J = 8.8 Hz, 2H). ^{13}C NMR (75 MHz, $CDCl_3$) δ 156.7, 151.3, 150.8, 132.4, 127.0, 124.7, 116.1. APPI HRMS (CH_2Cl_2) m/z calcd. for $C_{11}H_9{}^{79}BrN_3$ ([M + H]$^+$) 261.9974, found 261.9977.
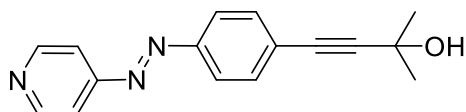
Compound 5.3: Compound **5.2** (1.0 g, 3.8 mmol) was added to a degassed solution of 2-methyl-3-butyn-2-ol (0.48 g, 0.56 mL, 5.7 mmol) in diethylamine (20 mL). $PdCl_2(PPh_3)_2$ (133 mg, 0.190 mmol) and CuI (72 mg, 0.38 mmol) were added and the mixture was stirred for 24 h at 45 °C. The reaction mixture was cooled to rt, ethyl acetate (20 mL) and satd aq NH_4Cl (20 mL) were added. The layers were separated, and the organic phase was washed with satd aq NH_4Cl (2 × 20 mL), dried ($MgSO_4$), and filtered. Solvent removal and purification by column chromatography (silica gel, hexanes/EtOAc 3:1) afforded **5.3** (494 mg, 49%) as an orange solid. Mp 111–114 °C. R_f = 0.35 (hexanes/ EtOAc 1:1). UV/Vis (CH_2Cl_2) λ_{max} (ε) 229 (13000), 344 (15100), 459 nm (452). IR (ATR) 3141 (m), 2090 (w), 1585 (m), 1405 (s), 848 (s) cm^{-1}. ^1H NMR (300 MHz, $CDCl_3$) δ 8.79 (d, J = 6.1 Hz, 2H), 7.89 (d, J = 8.6 Hz, 2H), 7.68 (d, J = 6.1 Hz, 2H), 7.55 (d, J = 8.6 Hz, 2H), 2.46 (s, 1H), 1.63 (s, 6H). ^{13}C NMR (75 MHz, $CDCl_3$) δ 157.0, 151.4, 151.3, 132.6, 127.0, 123.4, 116.2, 97.2, 81.6, 65.6, 31.4. APPI HRMS (CH_2Cl_2) m/z calcd. for $C_{16}H_{16}N_3O$ ([M + H]$^+$) 266.1288, found 266.1289.
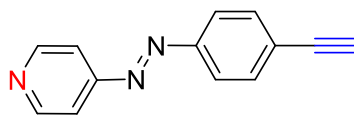
Compound *trans*-L1: To a solution of **5.3** (200 mg, 0.750 mmol) in toluene (40 mL) was added NaOH (60 mg, 1.5 mmol). The mixture was stirred for 16 h at 110 °C. The reaction mixture was cooled to rt, satd aq NH_4Cl (50 mL) was added. The layers were separated, and the aqueous phase was extracted

with ethyl acetate (2 × 50 mL), the solution was dried (MgSO$_4$), and filtered. Solvent removal and purification by column chromatography (silica gel, hexanes/EtOAc 4:1) afforded *trans*-L1 (133 mg, 85%) as an orange solid. Mp 193 °C (decomp). R_f = 0.52 (hexanes/ EtOAc 1:1). UV/Vis (CH$_2$Cl$_2$) λ_{max} (ε) 237 (9630), 333 (22000), 450 nm (593). IR (ATR) 3141 (m), 2090 (w), 1585 (m), 1405 (s), 848 (s) cm^{-1}. ^{1}H NMR (500 MHz, CDCl$_3$) δ 8.82 (d, J = 6.2 Hz, 2H), 7.93 (d, J = 8.5 Hz, 2H), 7.71 (d, J = 6.2 Hz, 2H), 7.66 (d, J = 8.5 Hz, 2H), 3.28 (s, 1H). ^{1}H NMR (500 MHz, C$_6$D$_6$) δ 8.63 (d, J = 6.1 Hz, 2H), 7.68 (d, J = 8.5 Hz, 2H), 7.38 (d, J = 6.1 Hz, 2H), 7.37 (d, J = 8.5 Hz, 2H), 2.79 (s, 1H). ^{13}C NMR (75 MHz, CDCl$_3$) δ 157.0, 151.7, 151.3, 133.1, 126.2, 123.4, 116.3, 82.9, 80.4. ^{1}H–^{13}C HSQC (500 MHz, CDCl$_3$) δ 8.62 ↔ 151.3; δ 7.93 ↔ 123.4; δ 7.71 ↔ 116.3; δ 7.66 ↔ 133.1; δ 3.28 ↔ 80.4. ^{1}H–^{13}C HMBC (500 MHz, CDCl$_3$) δ 8.62 ↔ 157.0, 151.3, 116.3; δ 7.93 ↔ 151.7, 123.4; δ 7.71 ↔ 157.0, 151.3, 116.3; δ 7.66 ↔ 151.7, 133.1, 123.4, 82.9; δ 3.28 ↔ 133.1, 126.2, 82.9, 80.4. APPI HRMS (CH$_2$Cl$_2$) *m/z* calcd. for C$_{13}$H$_{10}$N$_3$ ([M + H]$^+$) 208.0869, found 208.0875.
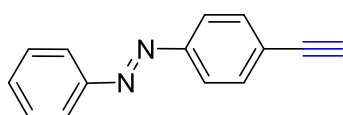
Compound *trans*-L2: To a solution of **5.6** (400 mg, 1.44 mmol) in CH$_2$Cl$_2$/MeOH (5 mL/30 mL) was added Na$_2$CO$_3$ (248 mg, 1.80 mmol). The mixture was stirred for 30 min at rt. CH$_2$Cl$_2$ (20 mL) and satd aq NH$_4$Cl (20 mL) were added. The layers were separated, and the aqueous phase was extracted with CH$_2$Cl$_2$ (2 × 10 mL), the solution was dried (MgSO$_4$), and filtered. Solvent removal and purification by column chromatography (silica gel, hexanes/CH$_2$Cl$_2$ 10:1) afforded *trans*-L2 (290 mg, 98%) as an orange solid. A mixture of *trans*- and *cis*-L2 in C$_6$D$_6$ under daylight can be observed as shown in the ^{1}H NMR spectrum (Figure S32). Mp 80 °C. R_f = 0.30 (CH$_2$Cl$_2$/hexanes 1:4). UV/vis (CH$_2$Cl$_2$) λ_{max} (ε) 235 (12600), 334 (24400), 451 nm (968). IR (ATR) 3275 (m), 2920 (w), 1585 (w), 1480 (w), 850 (s) cm^{-1}. ^{1}H NMR (300 MHz, CDCl$_3$) δ 7.93–7.86 (m, 4H), 7.63 (d, J = 8.5 Hz, 2H), 7.55–7.47 (m, 3H), 3.22 (s, 1H). ^{1}H NMR (500 MHz, C$_6$D$_6$) δ 7.96 (dd, J = 8.4, 1.3 Hz, 2H), 7.78 (d, J = 8.7 Hz, 2H), 7.40 (d, J = 8.6 Hz, 2H), 7.16–7.13 (m, 2H), 7.09–7.06 (m, 1H), 2.78 (s, 1H). ^{13}C NMR (75 MHz, CDCl$_3$) δ 152.5, 152.1, 133.0, 131.3, 129.1, 124.6, 123.0, 122.8, 83.3, 79.5. ^{13}C NMR (176 MHz, C$_6$D$_6$) δ 153.1, 152.6, 133.2, 131.4, 129.3, 125.2, 123.4, 123.3, 83.5, 79.9. ^{1}H–^{1}H COSY (500 MHz, C$_6$D$_6$) δ 7.96 ↔ 7.09–7.06; δ 7.16–7.13 ↔ 7.09–7.06; δ 7.96 ↔ 7.16–7.13; δ 7.78 ↔ 7.40. ^{1}H–^{13}C HMBC (700 MHz, C$_6$D$_6$) δ 7.96 ↔ 153.1, 131.4, 123.4, 123.3; δ 7.96 ↔ 152.6, 125.2; δ 7.40 ↔ 152.6, 133.2, 83.5; δ 7.16–7.13 ↔ 153.1, 152.6,

133.2, 131.4, 129.3; δ 7.09–7.06 ↔ 123.4, 123.3; δ 2.78 ↔ 133.2, 125.2. APPI HRMS (CH$_2$Cl$_2$) *m/z* calcd. for C$_{14}$H$_{10}$N$_2$ ([M + H]$^+$) 206.0839, found 206.0838.
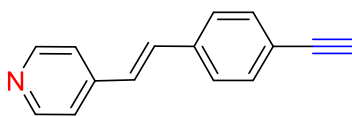
Compound *trans*-L5: The synthesis of ***trans*-L5** was adapted from a known procedure.[25] To a solution of **5.10** (300 mg, 1.14 mmol) in toluene (20 mL) was added well powdered NaOH (91 mg, 2.3 mmol) and tris[2-(2-methoxyethoxy)ethyl]amine (TDA-1, 368 mg, 1.14 mmol). The mixture was stirred for 16 h at 110 °C. The reaction mixture was cooled to rt, and CH$_2$Cl$_2$ (50 mL) and satd aq NH$_4$Cl (20 mL) were added. The layers were separated, the aqueous phase was extracted with CH$_2$Cl$_2$ (2 × 10 mL), and the solution was dried (MgSO$_4$) and filtered. Solvent removal and recrystallization from CH$_2$Cl$_2$/hexanes (ca. 3 mL/20 mL) afforded ***trans*-L5** (200 mg, 85%) as a yellow solid. Mp 200 °C (lit. 205–206 °C).[25] ^{1}H NMR (500 MHz, CDCl$_3$) δ 8.59 (d, *J* = 4.6 Hz, 2H), 7.51 (ABq, *J* = 8.7 Hz, 2H), 7.49 (ABq, *J* = 8.7 Hz, 2H), 7.36 (d, *J* = 5.9 Hz, 2H), 7.27 (d, *J* = 16.3 Hz, 1H), 7.03 (d, *J* = 16.3 Hz, 1H), 3.16 (s, 1H). ^{13}C NMR (126 MHz, CDCl$_3$) δ 150.3, 144.2, 136.5, 132.6, 132.2, 127.1, 126.8, 122.3, 120.9, 83.4, 78.5. ESI HRMS *m/z* calcd. for C$_{15}$H$_{12}$N ([M + H]$^+$) 206.0964, found 206.0961.
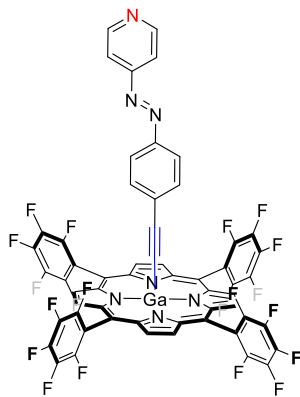
Ga[tpfpp][(C≡C)(Ph)(N=N)(py)] (GaL1): *Using nBuLi.* To a solution of ***trans*-L1** (50 mg, 0.24 mmol) in THF (10 mL) was added *n*BuLi (77 μL, 0.19 mmol, 2.5 M in hexanes) over 2 min at −78 °C under a N$_2$ atmosphere. The mixture was stirred for 50 min at −78 °C, then the cooling bath was removed, the solution was allowed to stir for 10 min. To the resulted mixture was added compound **5.11** (52 mg, 0.048 mmol) in toluene (5 mL) via a syringe under a N$_2$ atmosphere. After stirring for 30 min at −78 °C, the cooling bath was removed. The reaction mixture was allowed to heat to 50 °C and stirred for 40 h. Solvent removal and purification by size exclusion column chromatography (bio-beads SX-3 support, toluene) resulted an unidentified pink porphyrin and recovered ***trans*-L1** (the mass was not recorded).

Using LiHMDS. To a solution of ***trans*-L1** (40 mg, 0.19 mmol) in THF (12 mL) was added lithium bis(trimethylsilyl)amide (116 μL, 0.12 mmol, 1 M in methyl *tert*-butyl ether) over 2 min at −78 °C under a N$_2$ atmosphere. The mixture was stirred for 2 h at −78 °C. To the acetylide mixture was added compound **5.11** (41.6 mg, 0.0390 mmol) in THF (5 mL) via a syringe under a

N$_2$ atmosphere. After stirring for 30 min at −78 °C, the cooling bath was removed. The reaction mixture was allowed to warm to rt and stirred for 18 h. Solvent removal and purification by size exclusion column chromatography (bio-beads SX-3 support, toluene) afforded **GaL1** (41 mg, 85%) as a dark red solid. Mp: no visible change ≤ 300 °C. UV/vis (CH$_2$Cl$_2$) λ_{max} (ε) 328 (48700), 401 (sh, 58400), 422 (498000), 509 (4290), 552 (22800), 588 nm (3790). IR (ATR) 1489 (s), 1343 (w), 985 (s), 938 (s), 759 (s) cm^{-1}. ^{1}H NMR (300 MHz, C$_6$D$_6$) δ 8.94 (s, 8H), 8.38 (d, J = 6.2 Hz, 2H), 6.99 (d, J = 6.2 Hz, 2H), 6.72 (d, J = 8.7 Hz, 2H), 5.40 (d, J = 8.7 Hz, 2H). ^{13}C {^{1}H, ^{19}F} NMR (100 MHz, C$_6$D$_6$) δ 156.8, 151.3, 150.2, 149.3, 147.0, 146.5, 142.6, 142.5, 138.0, 137.8, 132.3, 131.5, 126.8, 122.2, 115.9, 115.6, 104.3, 96.3. ^{19}F NMR (282 MHz, C$_6$D$_6$) δ −134.8 to −134.9 (m, 4F), −136.1 to −136.2 (m, 4F), −148.3 (app t, J = 22 Hz, 4F), −159.2 (ddd, J = 24, 22, 8 Hz, 4F), −159.9 (ddd, J = 27, 19, 9 Hz, 4F). ^{1}H–^{13}C HSQC (700 MHz, C$_6$D$_6$) δ 8.94 ↔ 132.3; δ 8.38 ↔ 151.3; δ 6.99 ↔ 115.9; δ 6.72 ↔ 122.2; δ 5.40 ↔ 131.5. ^{19}F–^{13}C HSQC (376 MHz, C$_6$D$_6$) δ −134.8 to −134.9 ↔ 147.0; δ −136.1 to −136.2 ↔ 146.5; δ −148.3 ↔ 142.5; δ −159.2 ↔ 138.0; δ −159.9 ↔ 137.8. ^{1}H–^{13}C HMBC (700 MHz, C$_6$D$_6$) δ 8.94 ↔ 149.3, 147.0, 132.3, 104.3; δ 8.38 ↔ 115.9; δ 6.99 ↔ 156.8, 151.3, 115.6; δ 6.72 ↔ 150.2, 126.8, 122.2; δ 5.40 ↔ 150.2, 131.5, 122.2, 96.3. APPI HRMS (toluene) *m/z* calcd. for C$_{57}$H$_{16}$F$_{20}$^{69}GaN$_7$ (M$^+$) 1247.0420, found 1247.0402.
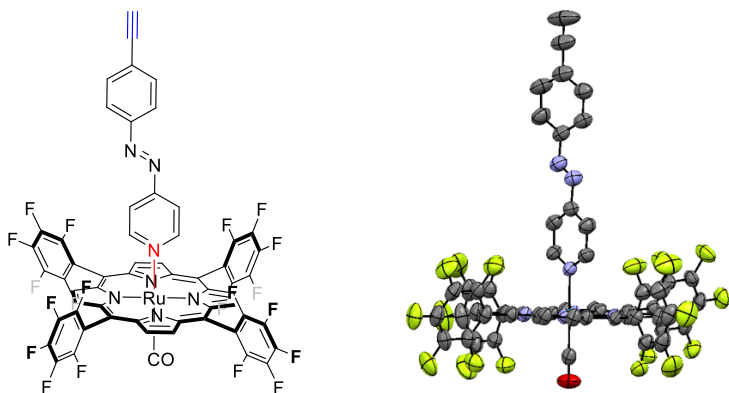
Ru[tpfpp][(C≡C)(Ph)(N=N)(py)][CO] (RuL1): To a solution of *trans*-**L1** (18 mg, 0.087 mmol) in CH$_2$Cl$_2$ (10 mL) was added compound **5.12** (50 mg, 0.044 mmol). The mixture was stirred at rt for 1 h. Solvent removal and purification by column chromatography (silica gel, hexanes/CH$_2$Cl$_2$ 4:1) afforded **RuL1** (55 mg, 96%) as a violet solid. Mp: no visible change ≤ 300 °C. R_f = 0.36 (hexanes/CH$_2$Cl$_2$ 2:1). UV/vis (CH$_2$Cl$_2$) λ_{max} (ε) 325 (39200), 344 (sh, 36300), 386 (42700), 405 (333000), 526 (16500), 555 nm (sh, 6610). IR (ATR) 3308 (w), 1978 (m), 1519 (s), 1493 (s), 990 (s), 945 (s), 850 (s) cm^{-1}. ^{1}H NMR (500 MHz, CDCl$_3$) δ 8.65 (s, 8H), 7.35 (d, J = 9.0 Hz, 2H),

7.31 (d, J = 9.0 Hz, 2H), 5.60 (d, J = 7.0 Hz, 2H), 3.15 (s, 1H), 1.59 (d, J = 7.0 Hz, 2H). ^{1}H NMR (500 MHz, C$_6$D$_6$) δ 8.65 (s, 8H), 7.05 (d, J = 8.8 Hz, 2H), 6.95 (d, J = 8.9 Hz, 2H), 5.01 (d, J = 7.0 Hz, 2H), 2.69 (s, 1H), 1.74 (d, J = 7.0 Hz, 2H). ^{13}C NMR {^{1}H, ^{19}F} (100 MHz, CDCl$_3$) δ 176.8, 154.4, 151.0, 146.4, 146.2, 145.3, 143.7, 142.03, 141.99 137.6, 137.4, 132.8, 132.2, 126.6, 123.0, 116.0, 114.4, 105.0, 82.6, 80.7 (an unexplained, extra signal is observed). ^{19}F NMR (376 MHz, CDCl$_3$) δ −136.2 (dd, J = 24, 7 Hz, 4F), −137.9 (dd, J = 24, 8 Hz, 4F), −152.3 (app t, J = 21 Hz, 4F), −161.4 to −161.6 (m, 4F), −162.2 to −162.3 (m, 4F). ^{1}H–^{13}C HSQC (500 MHz, CDCl$_3$) δ 8.65 ↔ 132.2; δ 7.35 ↔ 132.8; δ 7.31 ↔ 123.0; δ 5.60 ↔ 114.4; δ 1.59 ↔ 145.3. ^{1}H–^{13}C HMBC (500 MHz, C$_6$D$_6$) δ 8.65 ↔ 145.1, 144.4, 132.9, 132.7, 105.7; δ 7.05 ↔ 151.1, 132.9, 82.8; δ 6.95 ↔ 126.8, 123.2; δ 5.01 ↔ 154.4, 145.1, 114.6; δ 2.69 ↔ 132.9, 126.8, 82.8; δ 1.74 ↔ 154.4, 145.1, 114.6. APPI HRMS (toluene/MeCN) *m/z* calcd. for C$_{59}$H$_{20}$F$_{20}$^{102}RuN$_8$ ([M − CO + MeCN]$^+$) 1322.0545, found 1322.0543; calcd. for C$_{57}$H$_{17}$F$_{20}$^{102}RuN$_7$ ([M − CO]$^+$) 1298.0307, found 1298.0326; calcd. for C$_{45}$H$_8$F$_{20}$^{102}RuON$_4$ ([M − **L1**]$^+$) 1101.9429, found 1101.9418.

A crystal of **RuL1** suitable for X-ray crystallographic analysis has been grown at rt, by slow diffusion of a CH$_2$Cl$_2$ solution into hexanes. X-ray data for **RuL1** (C$_{58}$H$_{17}$F$_{20}$N$_7$ORu•0.5C$_5$H$_{12}$•0.5CH$_2$Cl$_2$), F_w = 1394.40; crystal dimensions 0.18 × 0.11 × 0.03 mm; monoclinic crystal system; space group $P2_1/n$ (No. 14); a = 13.4569(4) Å, b = 23.2285(7) Å, c = 18.0831(5) Å; $β$ = 96.390(2)°; V = 5617.4(3) Å^3; Z = 4; $ρ_{(calcd)}$ = 1.649 g/cm^3; $μ$ = 3.757 mm$^{−1}$; $λ$ = 1.54178 Å; T = 193 K; $2θ_{max}$ = 140.64°; total data collected = 34217; R_1 = 0.0549 [6146 observed reflections with $F_o^2 ≥ 2σ(F_o^2)$]; ωR_2 = 0.1564 for 10655 data, 811 variables, and 0 restraints; largest difference, peak and hole = 0.555 and −0.856 e Å$^{−3}$. CCDC 1999060.
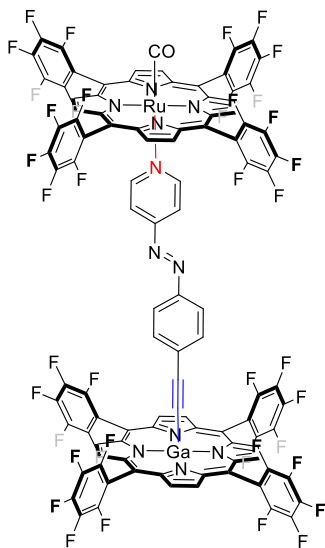
Ga[tpfpp]|[(C≡C)(Ph)(N=N)(py)]-Ru[tpfpp][CO] (GaL1Ru). To a solution of **GaL1** (30 mg, 0.024 mmol) in toluene (7 mL) was added compound **5.12** (41 mg, 0.036 mmol) in toluene (7 mL) under a N_2 atmosphere via a syringe. The mixture was stirred at 50 °C for 20 h. Solvent removal and purification by size exclusion column chromatography (bio-beads SX-3 support, toluene) afforded **GaL1Ru** (25 mg, 44%) as a dark red solid. Mp: no visible change ≤ 300 °C. UV/vis (CH_2Cl_2) λ_{max} (ε) 326 (59300), 385 (sh, 73300), 405 (398000), 422 (505000), 527 (18900), 552 (27600), 588 (3520), 631 nm (827). IR (ATR) 2362 (m), 2335 (m), 1975 (m), 1516 (s), 1492 (s), 989 (s), 943 (s) cm^{-1}. ^{1}H NMR (500 MHz, C_6D_6) δ 8.86 (s, 8H), 8.54 (s, 8H), 6.00 (d, J = 9.1 Hz, 2H), 5.09 (d, J = 9.2 Hz, 2H), 4.62 (d, J = 7.3 Hz, 2H), 1.49 (d, J = 7.3 Hz, 2H). ^{13}C NMR {^{1}H, ^{19}F} (125 MHz, C_6D_6) δ 176.6, 154.2, 149.3, 147.9 (br), 147.5 (br), 145.9 (br), 145.5 (br), 144.6, 144.3, 143.5, 143.2, 141.5 (br), 141.1 (br), 138.8 (br), 136.8 (br), 132.5, 132.2, 131.2, 121.8, 116.2 (br), 115.5 (br), 114.3, 105.5, 104.2, 96.0, 76.3 (two signals coincident or not observed). ^{19}F NMR (469 MHz, C_6D_6) δ −136.8 (dd, J = 24, 6 Hz, 4F), −137.0 (dd, J = 24, 7 Hz, 4F), −137.9 (dd, J = 25, 6 Hz, 4F), −139.1 (dd, J = 25, 7 Hz, 4F), −149.9 (app t, J = 22 Hz, 4F), −151.4 (app t, J = 22 Hz, 4F), −161.0 (app td, J = 23, 8 Hz, 4F), −161.5 (app td, J = 23, 8 Hz, 8F), −162.7 (app td, J = 23, 8 Hz, 4F). ^{1}H–^{1}H COSY (400 MHz, C_6D_6) δ 6.00 ↔ 5.09; δ 5.09 ↔ 6.00; δ 4.62 ↔ 1.49; δ 1.42 ↔ 6.49. ^{19}F–^{19}F COSY (376 MHz, C_6D_6) δ −136.8 ↔ −137.9, −161.0, −161.5; δ −137.0 ↔ −139.1, −161.5, −162.7; δ −137.9 ↔ −136.8, −161.0, −161.5; δ −139.1 ↔ −137.0, −161.0, −161.5, −162.7; δ −149.9 ↔ −161.0, −161.5; δ −151.4 ↔ −161.5, −162.7. ^{1}H–^{13}C HSQC (700 MHz, C_6D_6) δ 8.86 ↔ 132.2; δ 8.54 ↔ 132.5; δ 6.00 ↔ 121.8; δ 5.09 ↔ 131.2; δ 4.62 ↔ 114.3; δ 1.49 ↔ 144.6. ^{19}F–^{13}C HSQC (376 MHz, C_6D_6) δ −136.8 ↔ 145.9 (br); δ −137.0 ↔ 145.5 (br); δ −137.9 ↔ 145.5 (br); δ −149.9 ↔ 141.5 (br); δ −151.4 ↔ 141.1 (br); δ −161.0, −161.5, −162.7 ↔ 136.8 (br). ^{1}H–^{13}C HMBC (700 MHz, C_6D_6) δ 8.86 ↔ 154.2, 149.3, 138.8 (br), 132.2, 104.2; δ 8.54 ↔ 144.3, 132.5, 105.5; δ 6.00 ↔ 121.8; δ 5.09 ↔ 149.3, 131.2, 96.0; δ 4.62 ↔ 154.2, 144.6, 114.3; δ 1.49 ↔ 154.2, 144.6, 114.3. APPI HRMS (toluene/MeCN) *m/z* calcd. for $C_{57}H_{16}F_{20}{}^{69}GaN_7$ ([M − Ru(tpfpp)(CO)+H]$^+$) 1248.0476, found 1248.0493; calcd. for $C_{45}H_8F_{20}{}^{102}RuON_4$ ([Ru(tpfpp)(CO)]$^+$) 1101.9429, found 1101.9452.
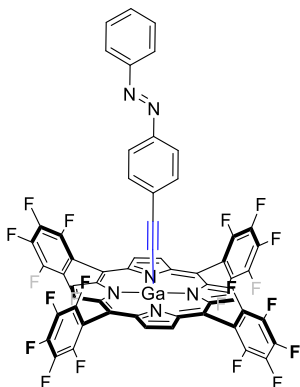
Ga[tpfpp][(C≡C)(N=N)(Ph)₂] (GaL2). To a solution of *trans*-L2 (56 mg, 0.27 mmol) in THF (4 mL) was added *n*BuLi (84 μL, 0.21 mmol, 2.5 M in hexanes) over 2 min at –78 °C under a N_2 atmosphere. The mixture was stirred for 10 min at –78 °C. After removing the cooling bath, the reaction mixture was stirred for another 10 min. The acetylide mixture was added to a solution of compound **5.11** (58 mg, 0.054 mmol) in toluene (10 mL) at rt under a N_2 atmosphere via a syringe. The reaction mixture was stirred at 50 °C for 20 h. Solvent removal and purification by size exclusion column chromatography (bio-beads SX-3 support, toluene) afforded **GaL2** as a dark red solid (63 mg, 93%). Mp: no visible change ≤ 300 °C. UV/vis (CH_2Cl_2) λ_{max} (ε) 329 (50700), 401 (51800), 422 (528000), 513 (2960), 553 (22200), 588 nm (2580). IR (ATR) 1514 (sh, m), 1487 (s), 1342 (w), 987 (s), 939 (s), 759 (s) cm^{-1}; ¹H NMR (700 MHz, C_6D_6) δ 8.94 (s, 8H), 7.57 (d, J = 7.7 Hz, 2H), 6.94 (app t, J = 7.8 Hz, 2H), 6.90–6.88 (m, 1H), 6.82 (d, J = 8.9 Hz, 2H), 5.43 (d, J = 8.8 Hz, 2H). ¹³C NMR {¹H, ¹⁹F} (100 MHz, C_6D_6) δ 152.9, 150.6, 149.3, 147.0, 146.5, 142.57, 142.52, 138.0, 137.7, 132.2, 131.5, 130.6, 128.9, 125.5, 122.9, 121.8, 115.7, 104.3, 96.6. ¹⁹F NMR (282 MHz, C_6D_6) δ –133.8 to –133.9 (m, 4F), –122.0 to –122.1 (m, 4F), –134.3 (app t, J = 22 Hz, 4F), –145.0 to –145.2 (m, 4F), –145.8 to –146.0 (m, 4F). ¹H–¹³C HSQC (700 MHz, C_6D_6) δ 8.94 ↔ 132.2; δ 7.57 ↔ 122.9; δ 6.94 ↔ 128.9; δ 6.90–6.88 ↔ 130.6; δ 6.82 ↔ 121.8; δ 5.43 ↔ 131.5. ¹⁹F–¹³C HSQC (376 MHz, C_6D_6) δ –133.8 to –133.9 ↔ 147.0; δ –122.0 to –122.1 ↔ 146.5; δ –134.3 ↔ 142.57, 142.52; δ –145.0 to –145.2 ↔ 138.0; δ –145.8 to –146.0 ↔ 137.7. ¹H–¹³C HMBC (700 MHz, C_6D_6) δ 8.94 ↔ 149.3, 132.2, 104.3; δ 7.57 ↔ 130.6, 122.9; δ 6.94 ↔ 152.9, 128.9; δ 6.90–6.88 ↔ 122.9; δ 6.82 ↔ 150.6, 125.5, 121.8; δ 5.43 ↔ 150.6, 131.5, 96.6. APPI HRMS (toluene) *m/z* calcd. for $C_{58}H_{17}F_{20}{}^{69}GaN_6$ (M⁺) 1246.0446, found 1246.0439.
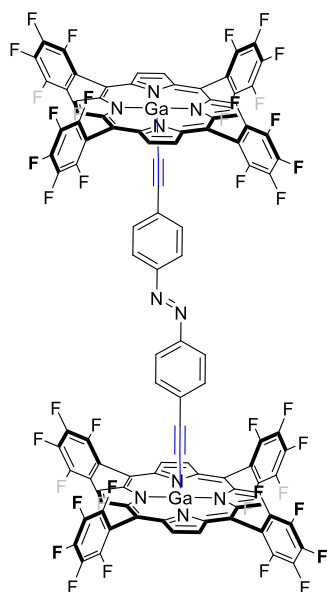
Ga$_2$[tpfpp]$_2$[(C≡C)$_2$(N=N)(Ph)$_2$] (GaL3Ga). To a solution of *trans-**L3*** (5.3 mg, 0.023 mmol) in THF (5 mL) was added lithium bis(trimethylsilyl)amide (51 μL, 0.051 mmol, 1 M in hexane) over 2 min at −78 °C under a N$_2$ atmosphere. The mixture was stirred for 2 h at −78 °C. To compound **5.11** (55 mg, 0.051 mmol) in THF (10 mL) was added the acetylide mixture via a cannula under a N$_2$ atmosphere. After stirring for 30 min at −78 °C, the cooling bath was removed, and the reaction mixture was stirred at rt for 30 h. Solvent removal and purification by size exclusion column chromatography (bio-beads SX-3 support, toluene) afforded **GaL3Ga** (2 mg, 4%) as a red solid. UV/vis (THF) 329, 402 (sh), 422, 514, 554, 586, 624 nm; UV/vis (CH$_2$Cl$_2$) 328 (51000), 401 (sh, 90500), 421 (626000), 509 (3860), 553 (28000), 589 (3280), 629 (663). ^{1}H NMR (500 MHz, C$_6$D$_6$) δ 8.86 (s, 16H), 6.37 (d, J = 9.0 Hz, 4H), 5.20 (d, J = 9.1 Hz, 4H). ^{13}C NMR {^{1}H, ^{19}F} (100 MHz, CD$_2$Cl$_2$) δ 150.7, 149.6, 147.4, 146.8, 143.1, 138.4, 138.3, 133.0, 131.5, 125.5, 121.9, 115.7, 104.4, 96.4 (one signal coincident or not observed). ^{19}F NMR (376 MHz, C$_6$D$_6$) δ −136.3 to −136.4 (m, 8F), −137.9 to −138.0 (m, 8F), −150.2 (app t, J = 22 Hz, 8F), −161.0 (app td, J = 23, 8 Hz, 8F), −161.8 (app td, J = 23, 8 Hz, 8F). MALDI HRMS (DCTB, DCM) m/z calcd. for C$_{104}$H$_{24}$F$_{40}$^{69}Ga$_2$N$_{10}$ (M$^+$) 2310.0053, found 2310.0063.
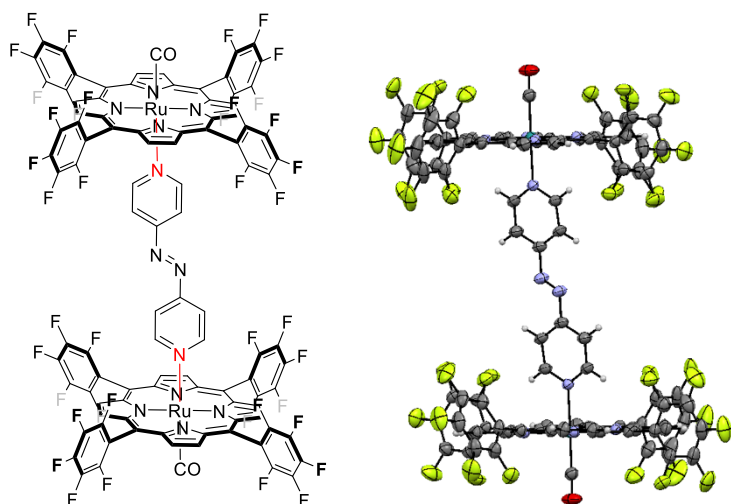
Ru$_2$[tpfpp]$_2$[(N=N)(py)$_2$][CO]$_2$ (RuL4Ru). To a solution of *trans-**L4*** (2.2 mg, 0.012 mmol) in CH$_2$Cl$_2$ (10 mL) was added compound **5.12** (30 mg, 0.026 mmol). The mixture was stirred at rt for 1 h. Solvent removal and purification by column chromatography (silica gel, hexanes/CH$_2$Cl$_2$

4:1) afforded **RuL4Ru** (28 mg, 97%) as a violet solid. Mp: no visible change $\leq$ 300 °C. R_f = 0.30 (hexanes/CH$_2$Cl$_2$ 2:1). UV/vis (CH$_2$Cl$_2$) λ_{max} (ε) 312 (59800), 317 (60100), 385 (82000), 404 (684000), 526 (34700), 555 nm (sh, 14200). IR (cast film) 1978 (s), 1520 (sh, s), 1492 (s), 990 (s), 946 (s) cm^{-1}. ^{1}H NMR (500 MHz, CDCl$_3$) δ 8.52 (s, 16H), 5.03 (d, J = 7.4 Hz, 4H), 1.32 (d, J = 7.3 Hz, 4H). ^{13}C NMR {^{1}H, ^{19}F} (100 MHz, CDCl$_3$) δ 176.9, 152.9, 146.22, 146.18, 145.4, 143.6, 142.0, 137.6, 137.3, 132.1, 115.8, 113.9, 105.0. ^{19}F NMR (469 MHz, CDCl$_3$) δ 136.3 (dd, J = 24, 8 Hz, 8F), −138.4 (dd, J = 24, 7 Hz, 8F), −152.2 (app t, J = 21 Hz, 8F), −161.5 (app td, J = 24, 9 Hz, 8F), −162.4 (app td, J = 24, 9 Hz, 8F). APPI HRMS (toluene/MeCN) *m/z* calcd. for C$_{45}$H$_8$F$_{20}$^{102}RuON$_4$ ([Ru(tpfpp)(CO)]$^+$) 1101.9429, found 1101.9409.

A crystal of **RuL4Ru** suitable for X-ray crystallographic analysis has been grown at rt, by slow evaporation from ethyl acetate solution. X-ray data for **RuL4Ru** (C$_{100}$H$_{24}$F$_{40}$N$_{12}$O$_2$Ru$_2$•2(C$_6$H$_{14}$)•2(C$_6$H$_{12}$)), F_w = 2728.10; crystal dimensions 0.70 × 0.15 × 0.14 mm; monoclinic crystal system; space group *P2$_1$/c* (No. 14); a = 11.0325(5) Å, b = 21.0303(10) Å, c = 24.8542(11) Å; β = 102.4969(6)°; V = 5630.0(4) Å^3; Z = 2; $\rho_{(calcd)}$ = 1.609 g/cm^3; μ = 0.395 mm^{-1}; λ = 0.71073 Å; T = 173 K; $2\theta_{max}$ = 55.15°; total data collected = 49439; R_1 = 0.0485 [10403 observed reflections with $F_o^2 \geq 2\sigma(F_o^2)$]; ωR_2 = 0.1428 for 12970 data, 794 variables, and 26 restraints; largest difference, peak and hole = 1.499 and −0.634 e Å^{-3}. The C–C bond distances within the disordered solvent methylcyclopentane molecule were constrained to a target distance of 1.52(2) Å during refinement. The 1,3-C···C distances within each C–C–C bond angle of within the disordered solvent methylcyclopentane molecule were constrained to a target distance of 2.52(2) Å during refinement. CCDC 1999059.
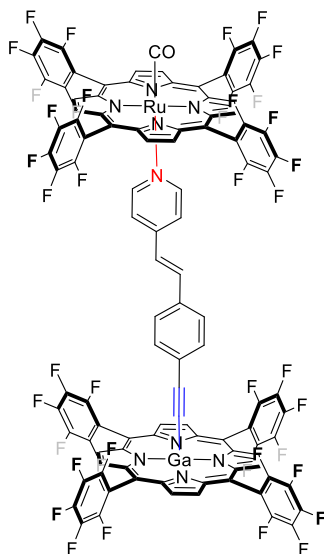
Ga[tpfpp][(C≡C)(Ph)(C=C)(py)]-Ru[tpfpp][CO] (GaL5Ru). To a solution of *trans*-L5 (57 mg, 0.28 mmol) in THF (10 mL) was added lithium bis(trimethylsilyl)amide (350 μL, 0.233 mmol, 0.665 M in THF) over 2 min at −78 °C under a N_2 atmosphere. The mixture was stirred for 30 min at −78 °C and 30 min at rt. To the acetylide mixture was added compound **5.11** (50 mg, 0.046 mmol) in THF (10 mL) via a syringe under a N_2 atmosphere. The reaction mixture was stirred at −78 °C, and the mixture was allowed to warm to rt and stirred for 17 h. Solvent removal and purification by size exclusion column chromatography (bio-beads SX-3 support, toluene) afforded a **GaL5** as a crude product, which was carried on directly without further purification. To a solution of the **GaL5** (22 mg, 0.018 mmol) in toluene (10 mL) was added compound **5.12** (24 mg, 0.021 mmol) in toluene (10 mL) under a N_2 atmosphere via a syringe. The mixture was stirred at 50 °C for 20 h. Solvent removal and purification by size exclusion column chromatography (bio-beads SX-3 support, toluene) afforded **GaL5Ru** (27 mg, 55% based on **5.12**) as a dark red solid. Mp: no visible change ≤ 300 °C. UV/vis (CH_2Cl_2) λ_{max} (ε) 329 (80500), 386 (sh, 61900), 406 (426000), 422 (478000), 528 (16900), 552 (25500), 587 (sh, 1620). IR (cast film) 1975 (s), 1651 (m), 1613 (m), 14517 (s), 1491 (s), 990 (s), 944 (s) cm^{-1}. ^{1}H NMR (500 MHz, C_6D_6) δ 8.85 (s, 8H), 8.55 (s, 8H), 5.44 (d, J = 8.6 Hz, 2H), 5.15 (d, J = 8.6 Hz, 2H), 4.74 (d, J = 16.3 Hz, 1H), 4.35 (d, J = 16.2 Hz, 1H), 4.08 (d, J = 6.7 Hz, 2H), 1.33 (d, J = 6.9 Hz, 2H). ^{13}C NMR {^{1}H, ^{19}F} (101 MHz, C_6D_6) δ 149.3, 146.5 (br), 146.0, 144.3, 143.4, 143.0, 142.6 (br), 142.1 (br), 137.9 (br), 137.7 (br), 133.4, 132.9, 132.5, 132.2, 130.8, 125.4, 123.3, 122.3, 118.6, 116.3 (br), 115.6 (br), 115.5, 105.5, 104.2 (two signals coincident or not observed). ^{19}F NMR (376 MHz, C_6D_6) δ −136.6 (dd, J = 24, 7 Hz, 4F), −136.8 (dd, J = 24, 8 Hz, 4F), −137.8 (dd, J = 24, 7 Hz, 4F), −139.3 (dd, J = 25, 8 Hz, 4F), −150.1 (app t, J = 22 Hz, 4F), −151.5 (app t, J = 22 Hz, 4F), −161.2 (app td, J = 23, 8 Hz, 4F), −161.4 to −161.6 (m, 8F), −162.8 (app td, J = 24, 8 Hz, 4F). MALDI HRMS (DCTB) *m/z* calcd. for $C_{103}H_{26}F_{40}{}^{69}GaN_9{}^{102}Ru$ ([M − (CO)]$^+$) 2318.9966, found 2318.9969; calcd. for $C_{120}H_{44}F_{40}{}^{69}GaN_{11}{}^{102}Ru$ ([M − (CO) + DCTB]$^+$) 2569.1436, found 2569.1484.

7.6 Spectra Appendix

7.6.1 Spectra of Chapter 2
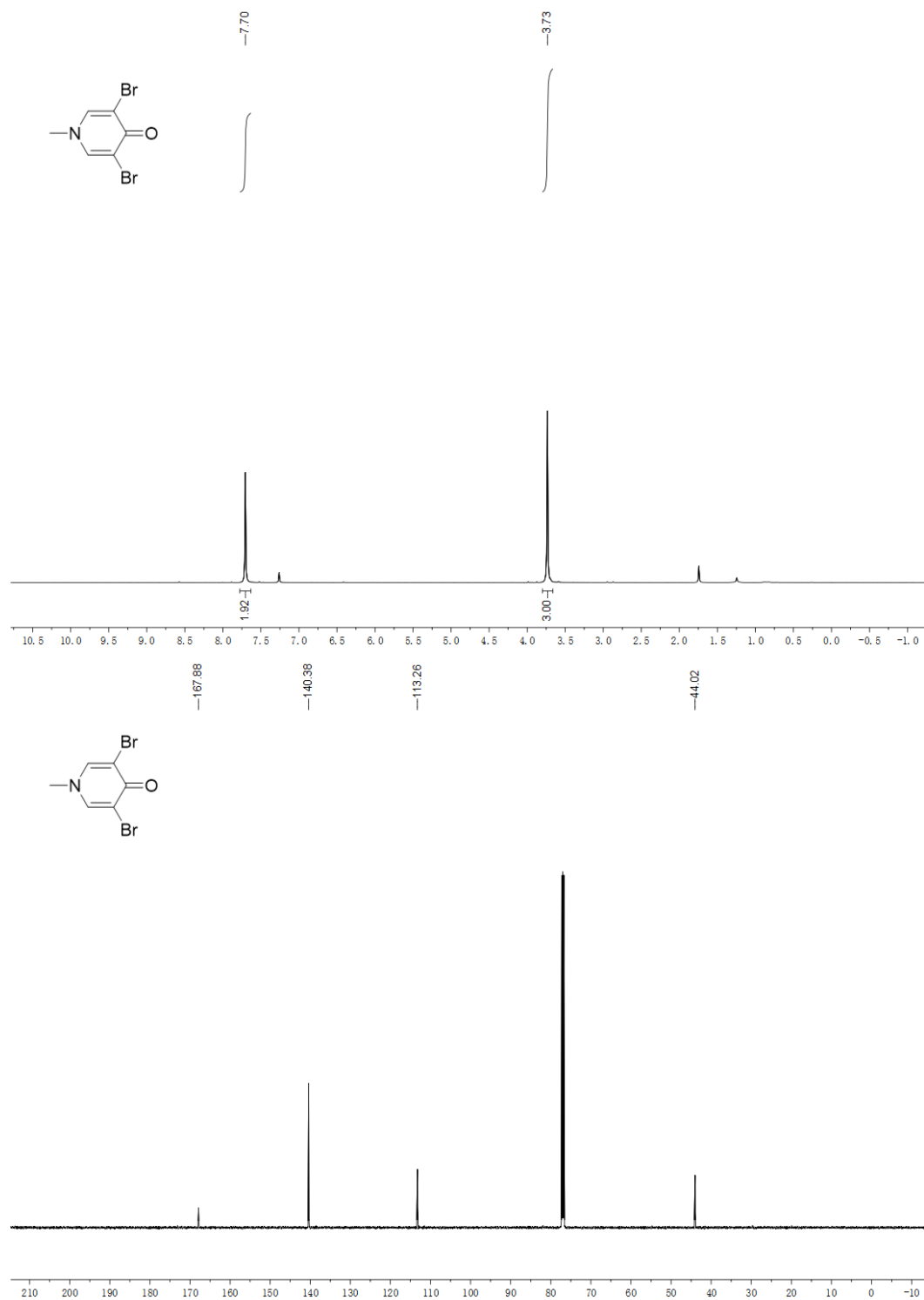
Figure 7.1. ^{1}H NMR and ^{13}C NMR spectra of compound **2.3** in CDCl$_3$.
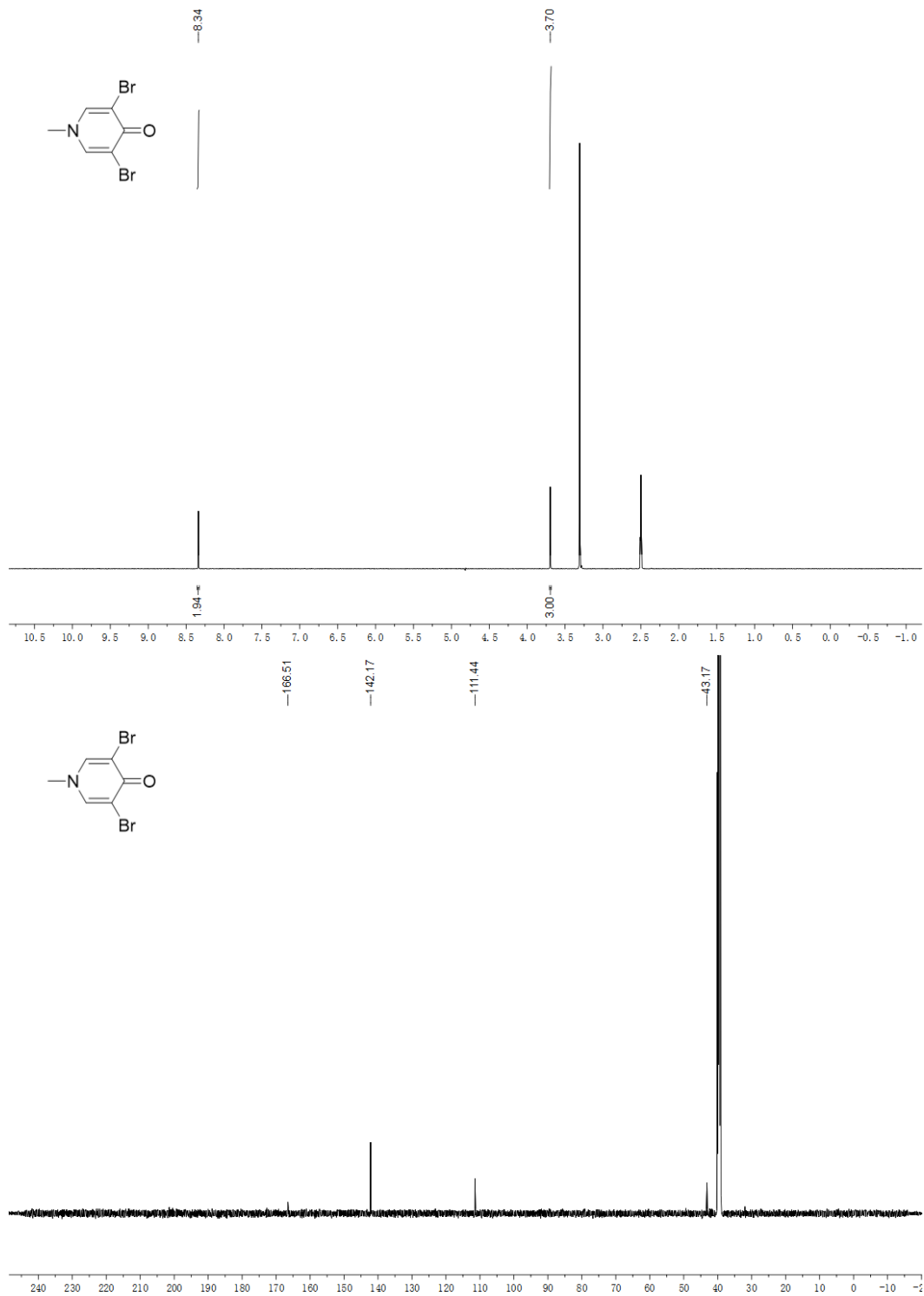
Figure 7.2. ^{1}H NMR and ^{13}C NMR spectra of compound **2.3** in DMSO-d6.
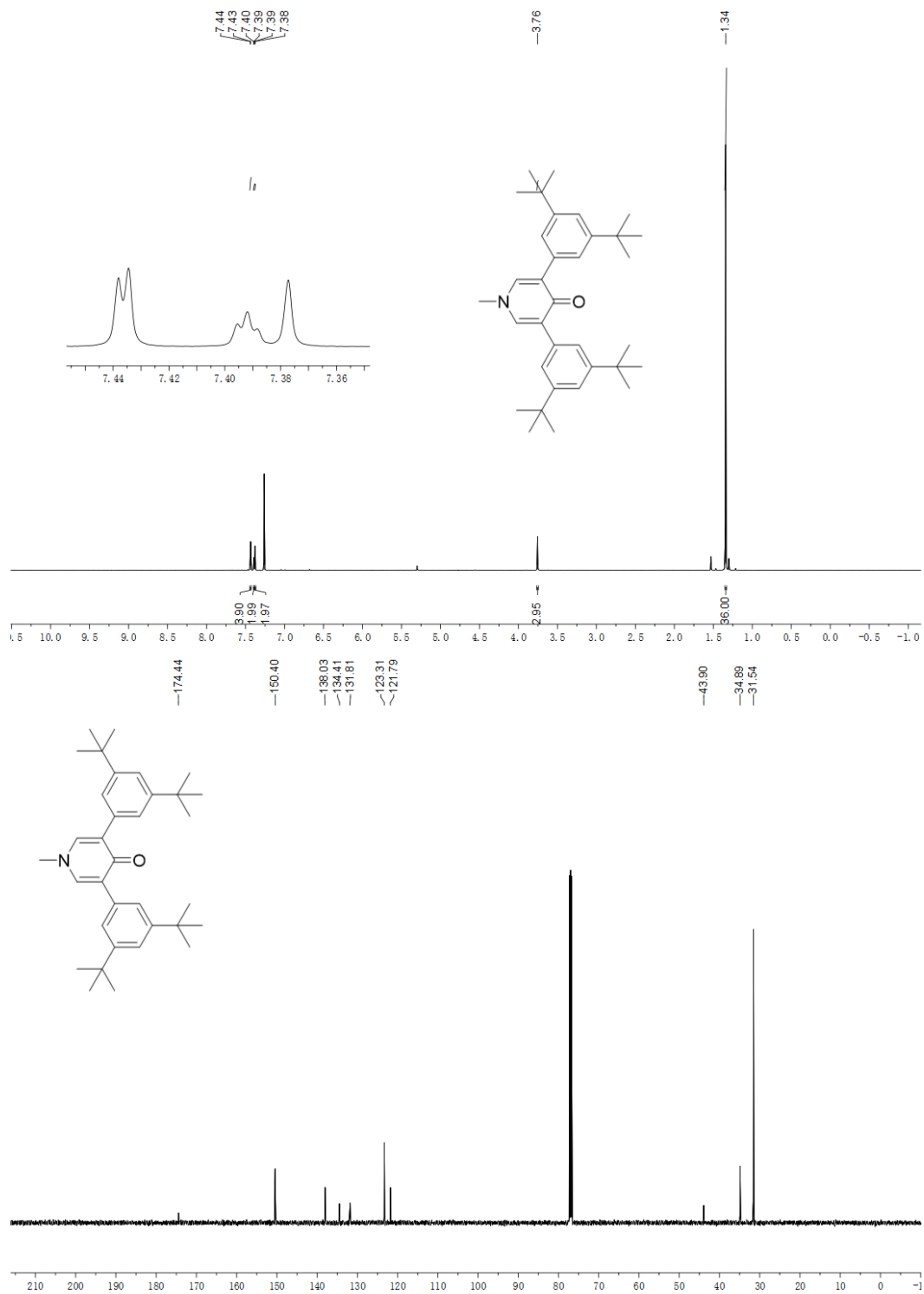
Figure 7.3. ^{1}H NMR and ^{13}C NMR spectra of compound **2.4a** in CDCl$_3$.
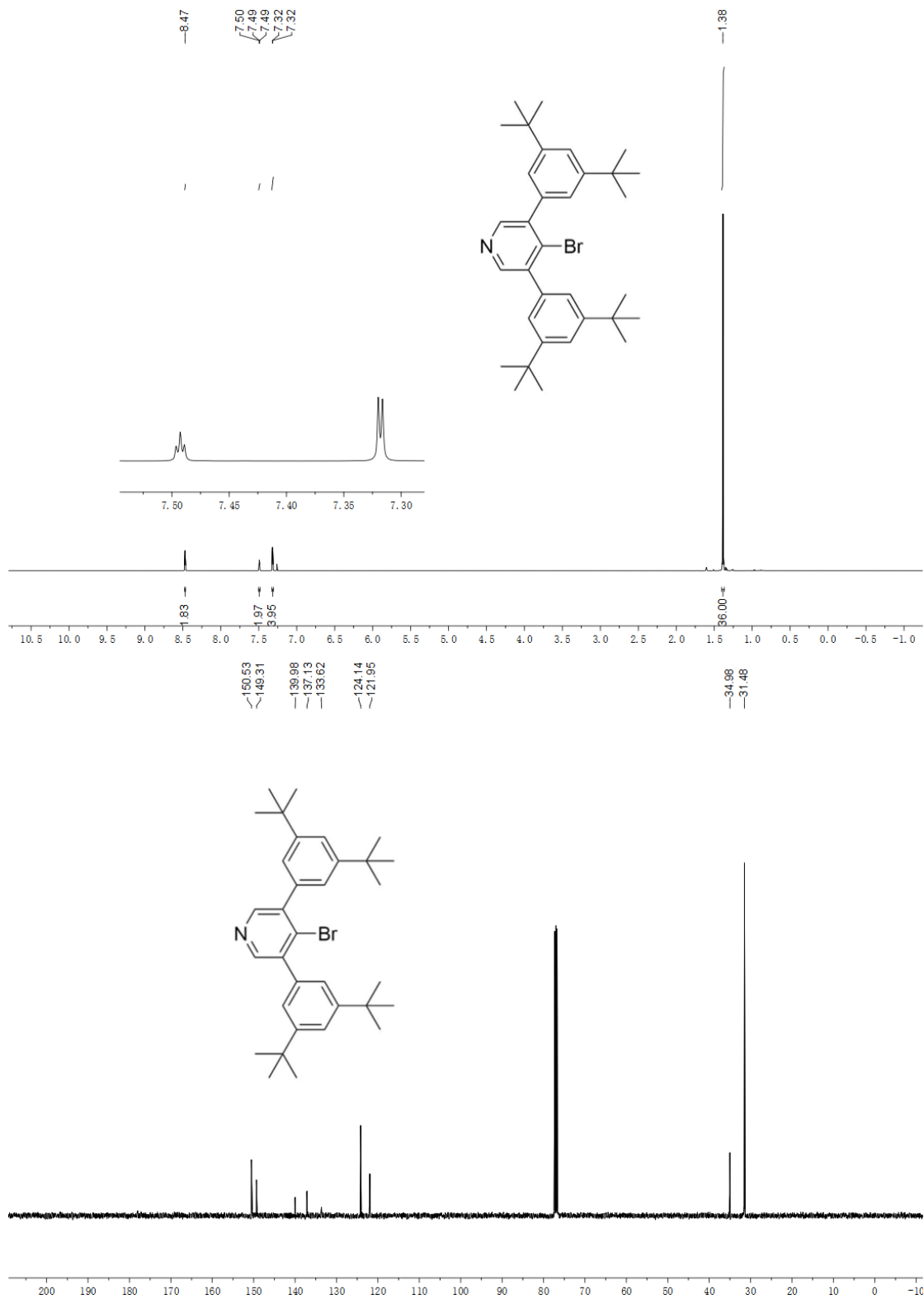
Figure 7.4. ^{1}H NMR and ^{13}C NMR spectra of compound **2.5a** in CDCl$_3$.

225
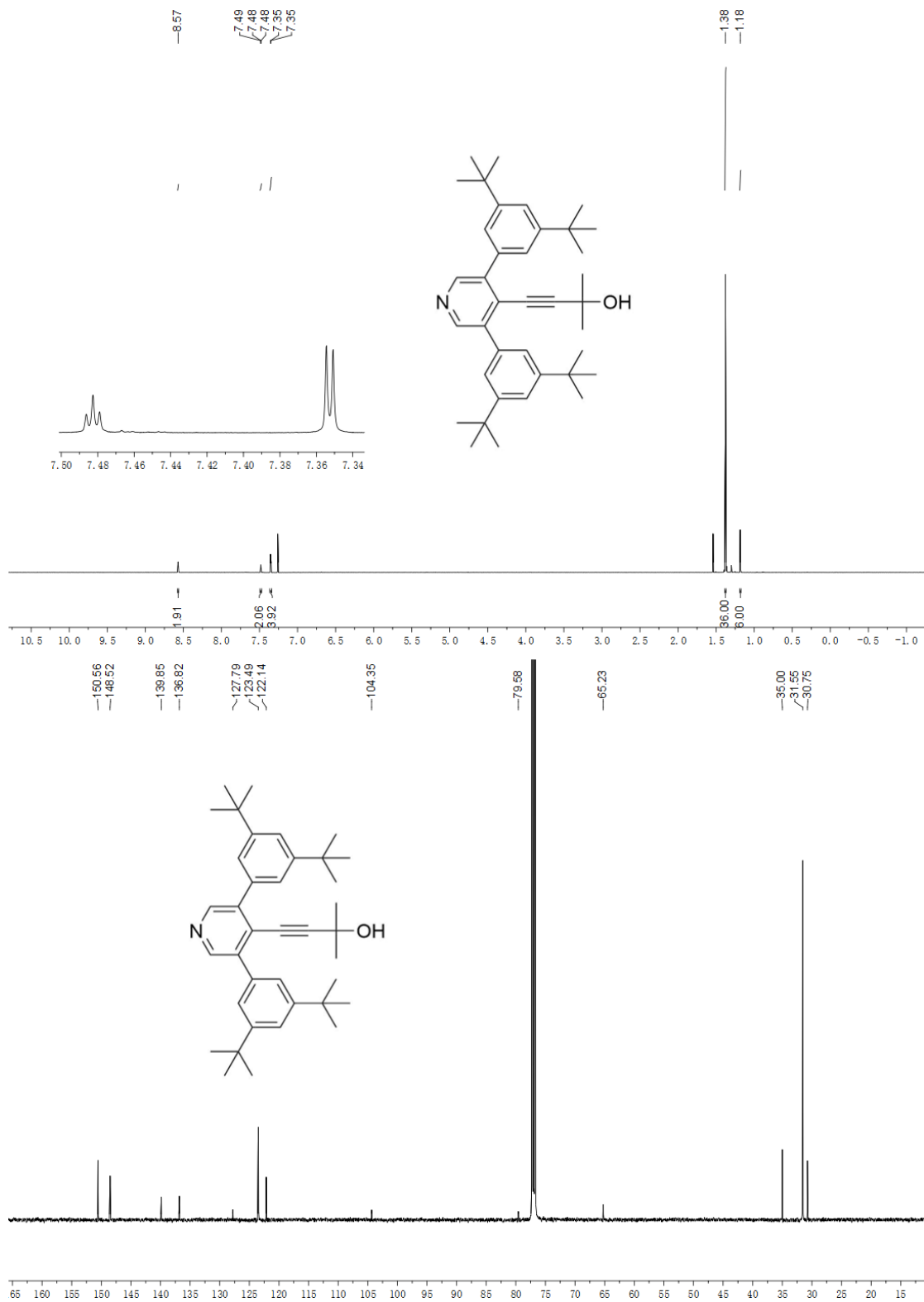
Figure 7.5. ^{1}H NMR and ^{13}C NMR spectra of compound **2.6a** in CDCl$_3$.
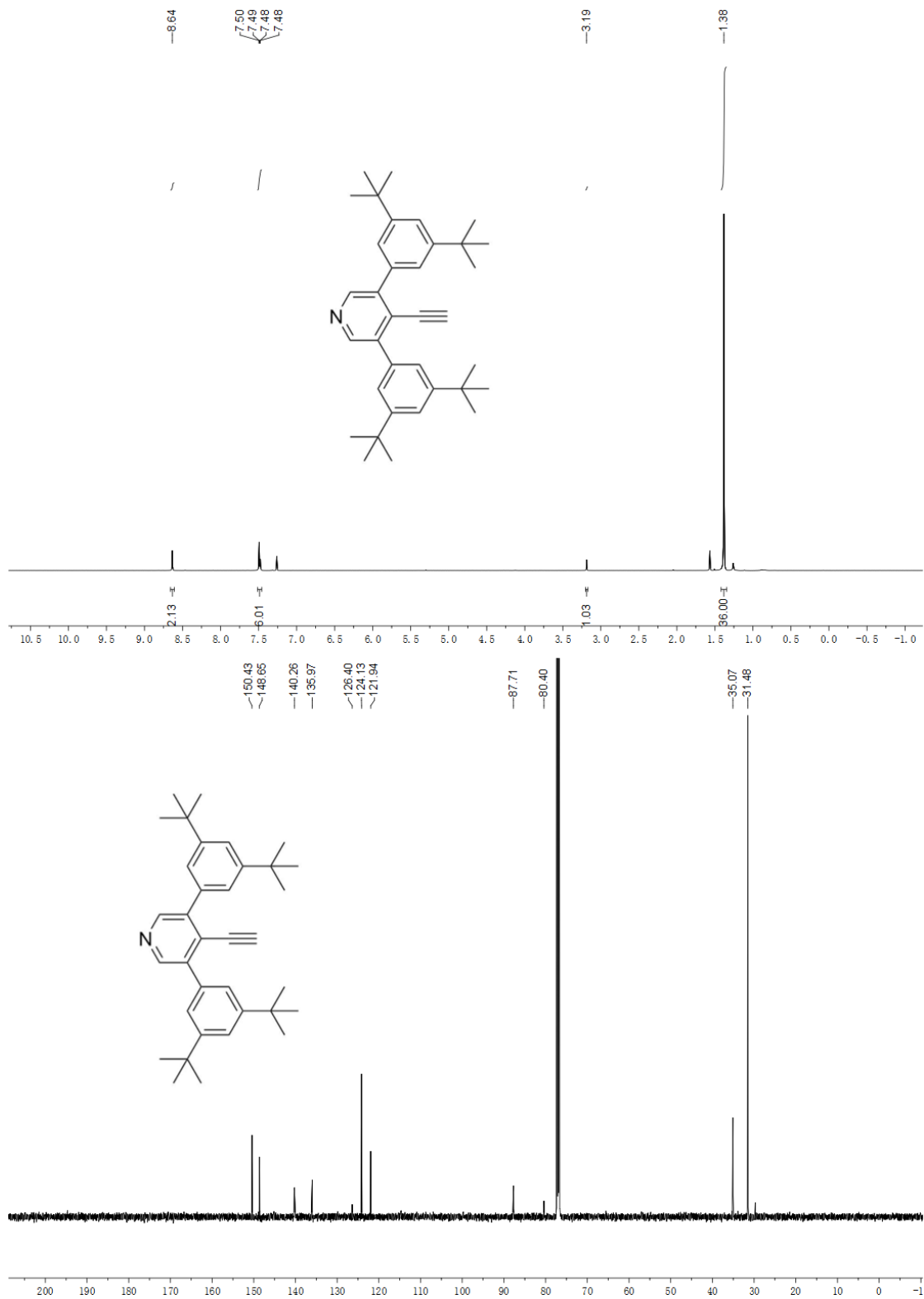
Figure 7.6. ^{1}H NMR and ^{13}C NMR spectra of compound **2.7a** in CDCl$_3$.
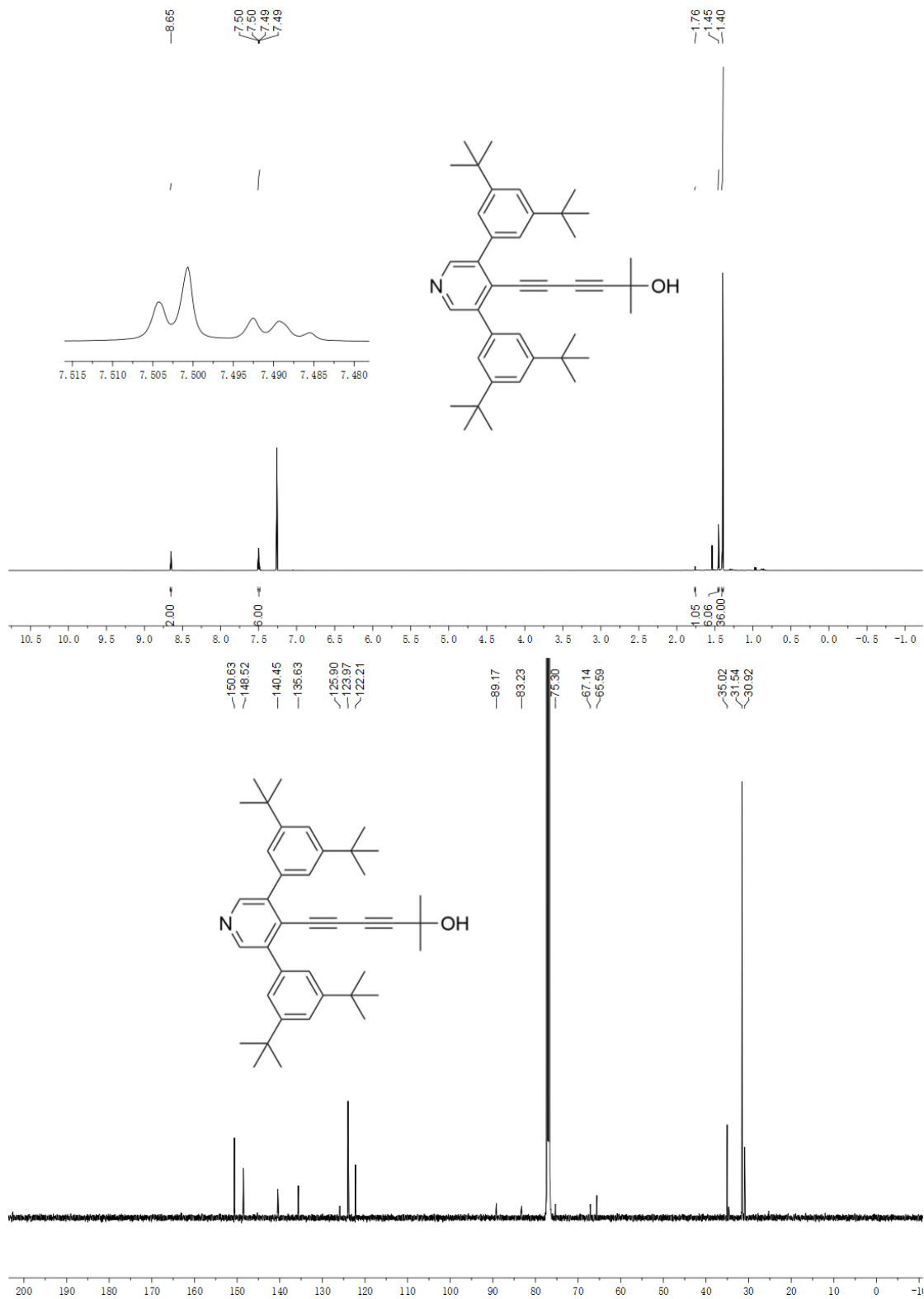
Figure 7.7. ^{1}H NMR and ^{13}C NMR spectra of compound **2.8a** in CDCl$_3$.
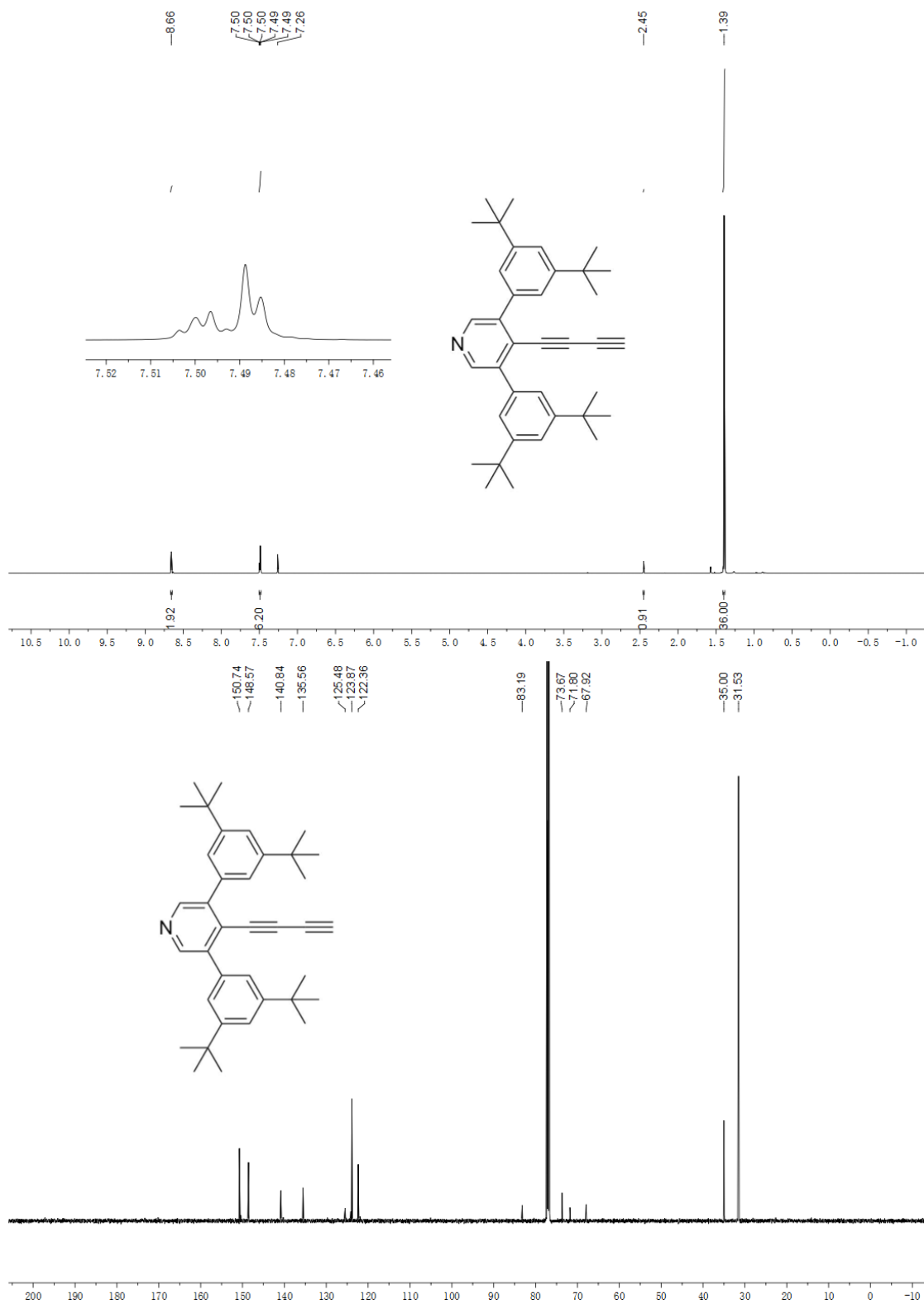
Figure 7.8. ^{1}H NMR and ^{13}C NMR spectra of compound **2.9a** in CDCl$_3$.
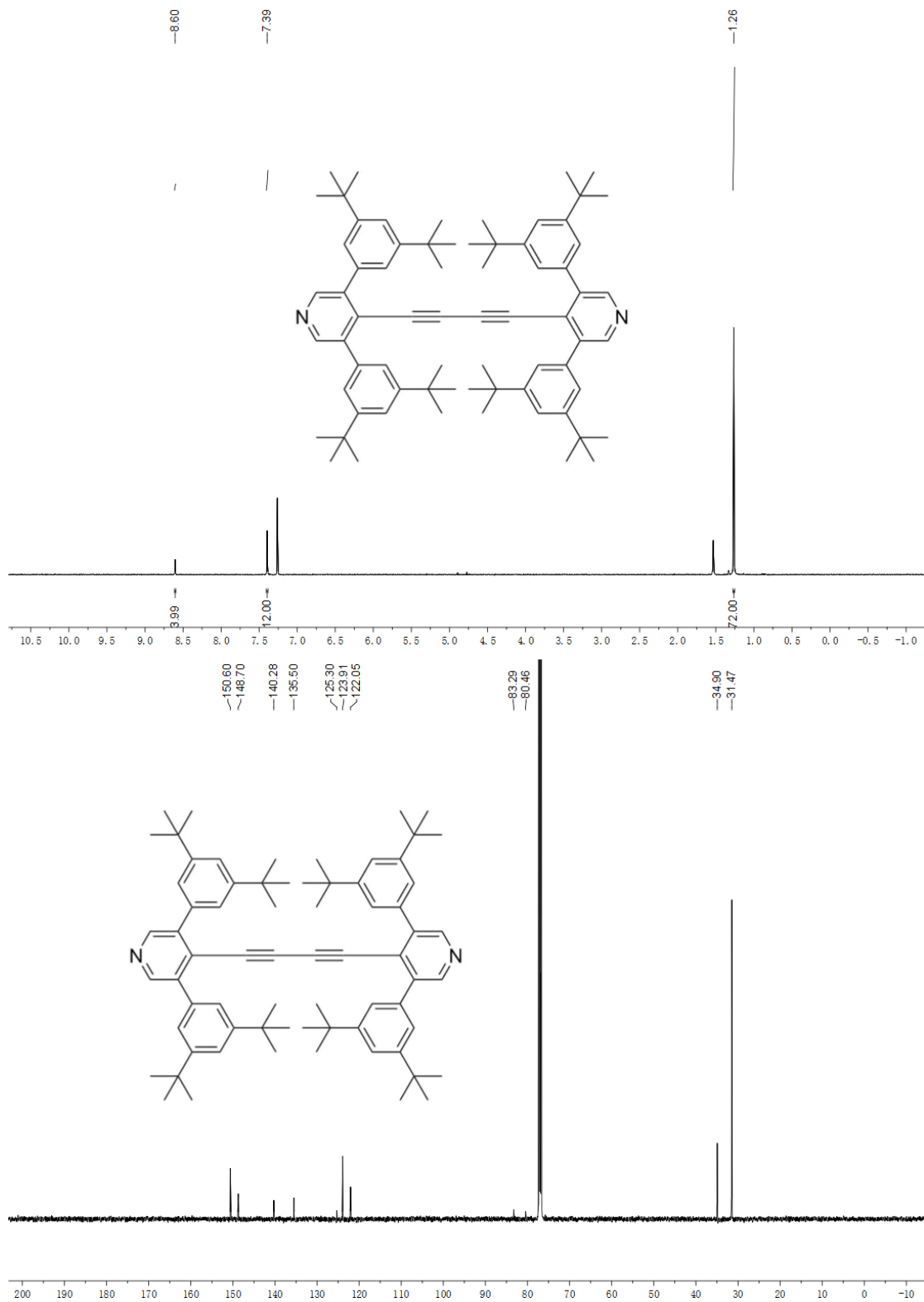
Figure 7.9. ^{1}H NMR and ^{13}C NMR spectra of compound **Py**[2a]** in CDCl$_3$.
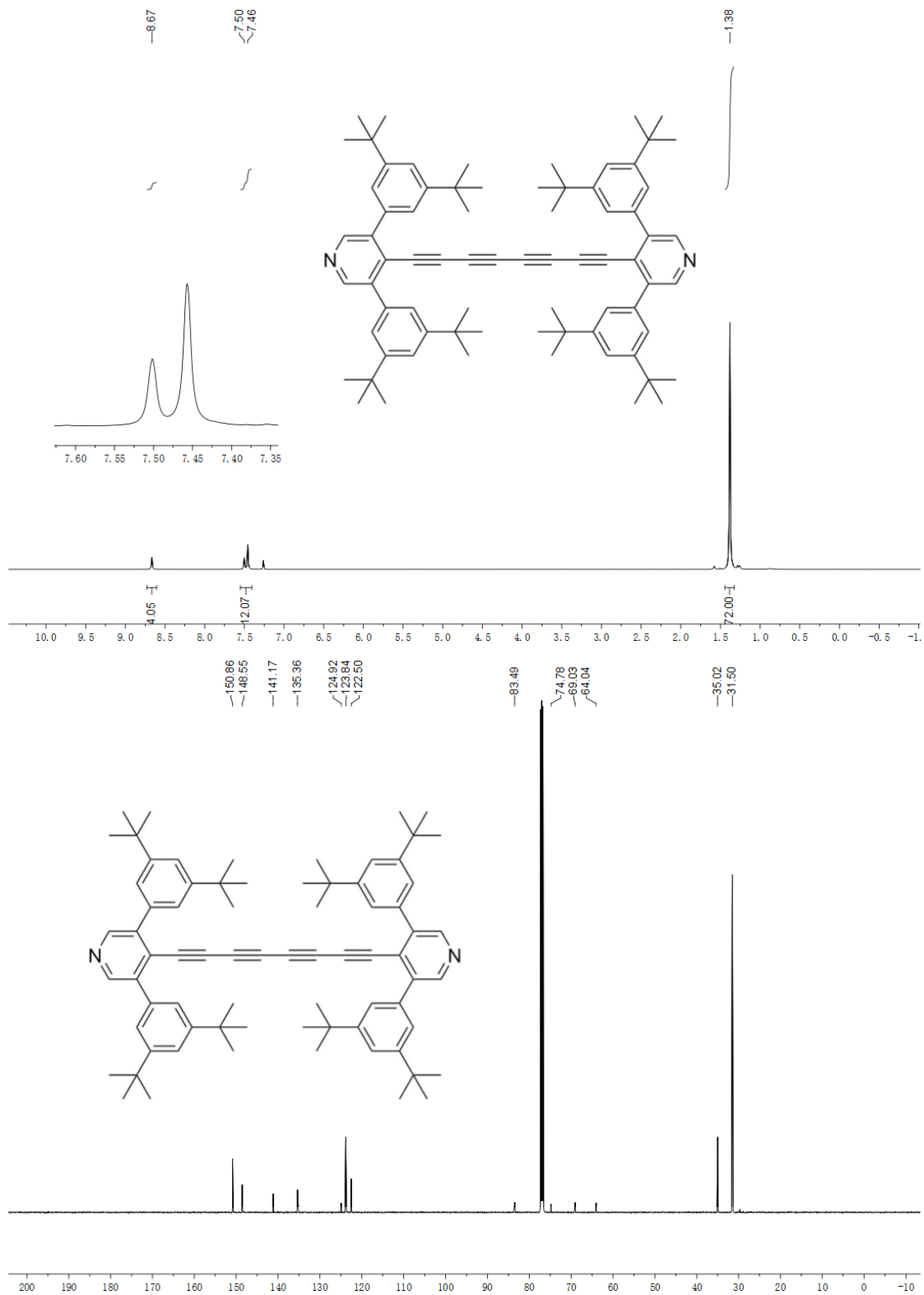
Figure 7.10. ^{1}H NMR and ^{13}C NMR spectra of compound **Py**[4a]** in CDCl₃.
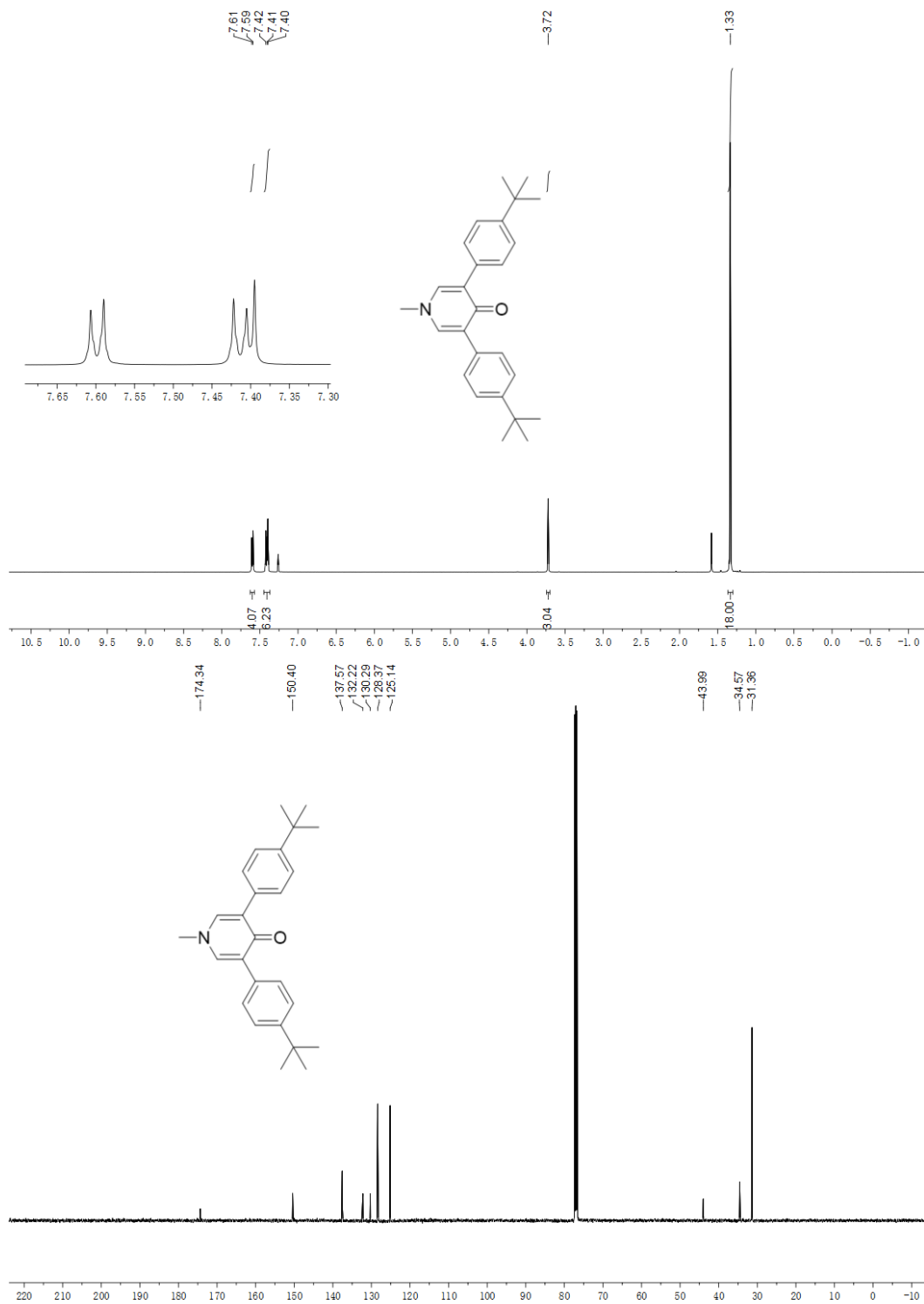
Figure 7.11. ^{1}H NMR and ^{13}C NMR spectra of compound **2.4b** in CDCl$_3$.
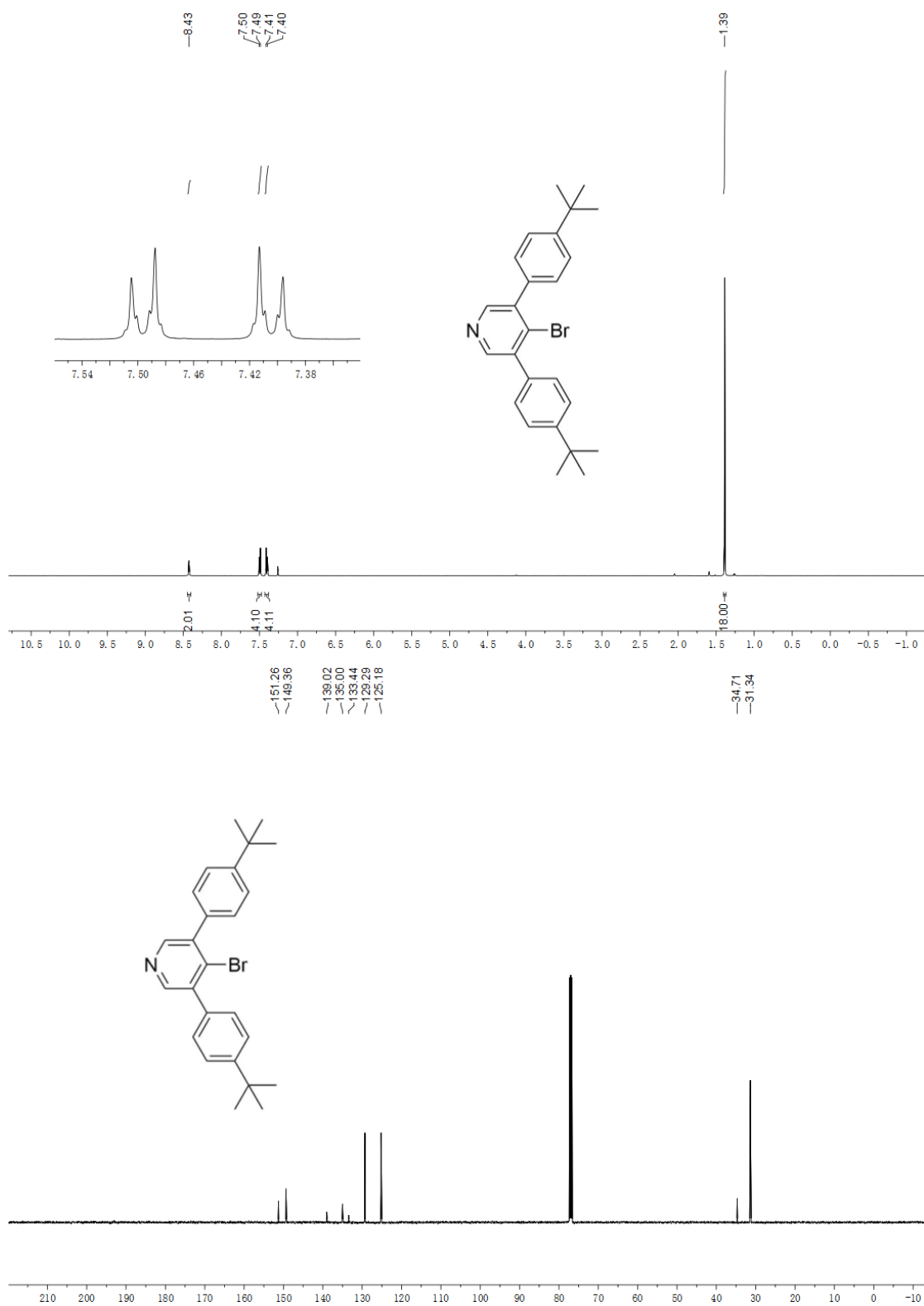
Figure 7.12. ^{1}H NMR and ^{13}C NMR spectra of compound **2.5b** in CDCl$_3$.
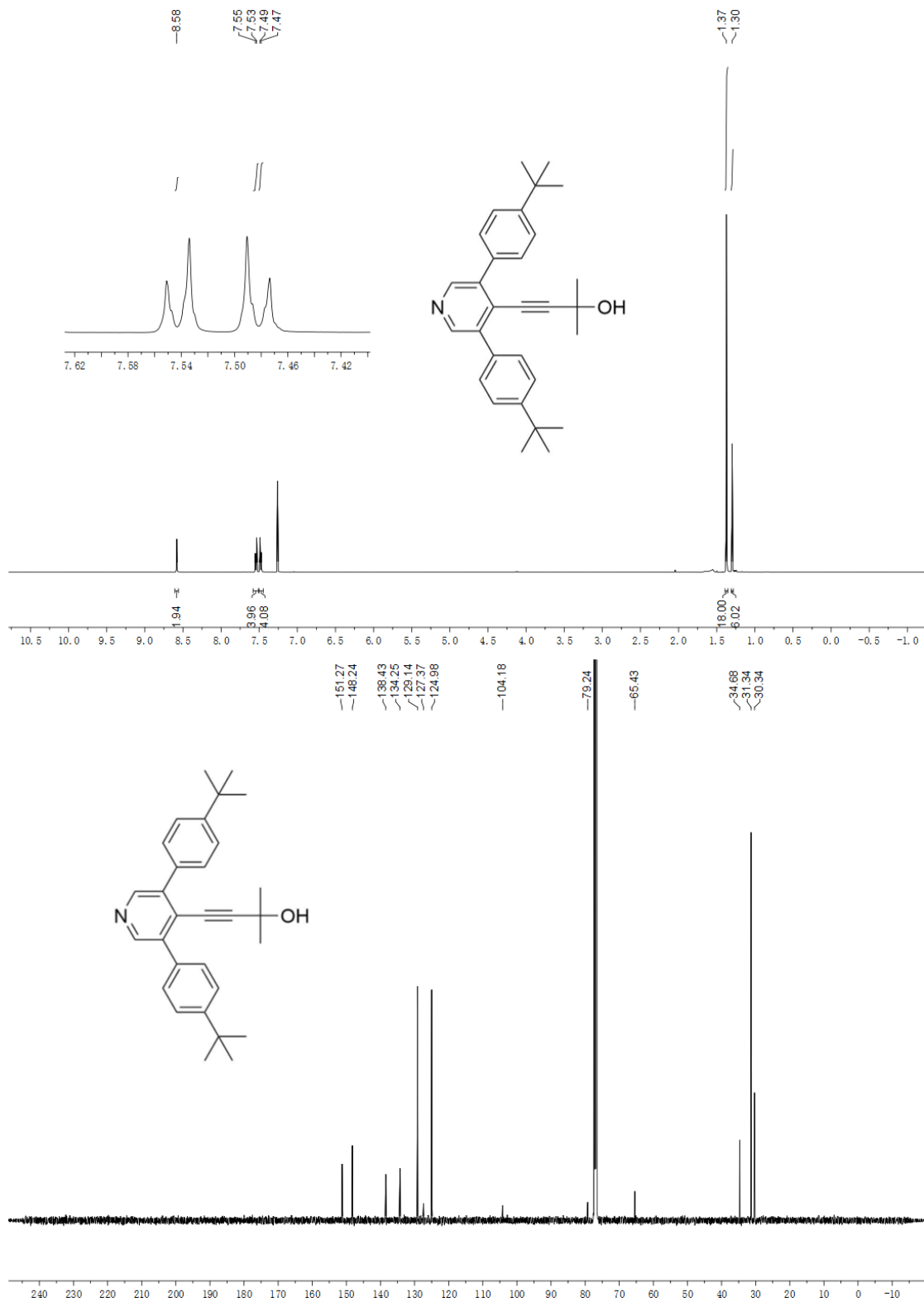
Figure 7.13. ^{1}H NMR and ^{13}C NMR spectra of compound **2.6b** in CDCl$_3$.
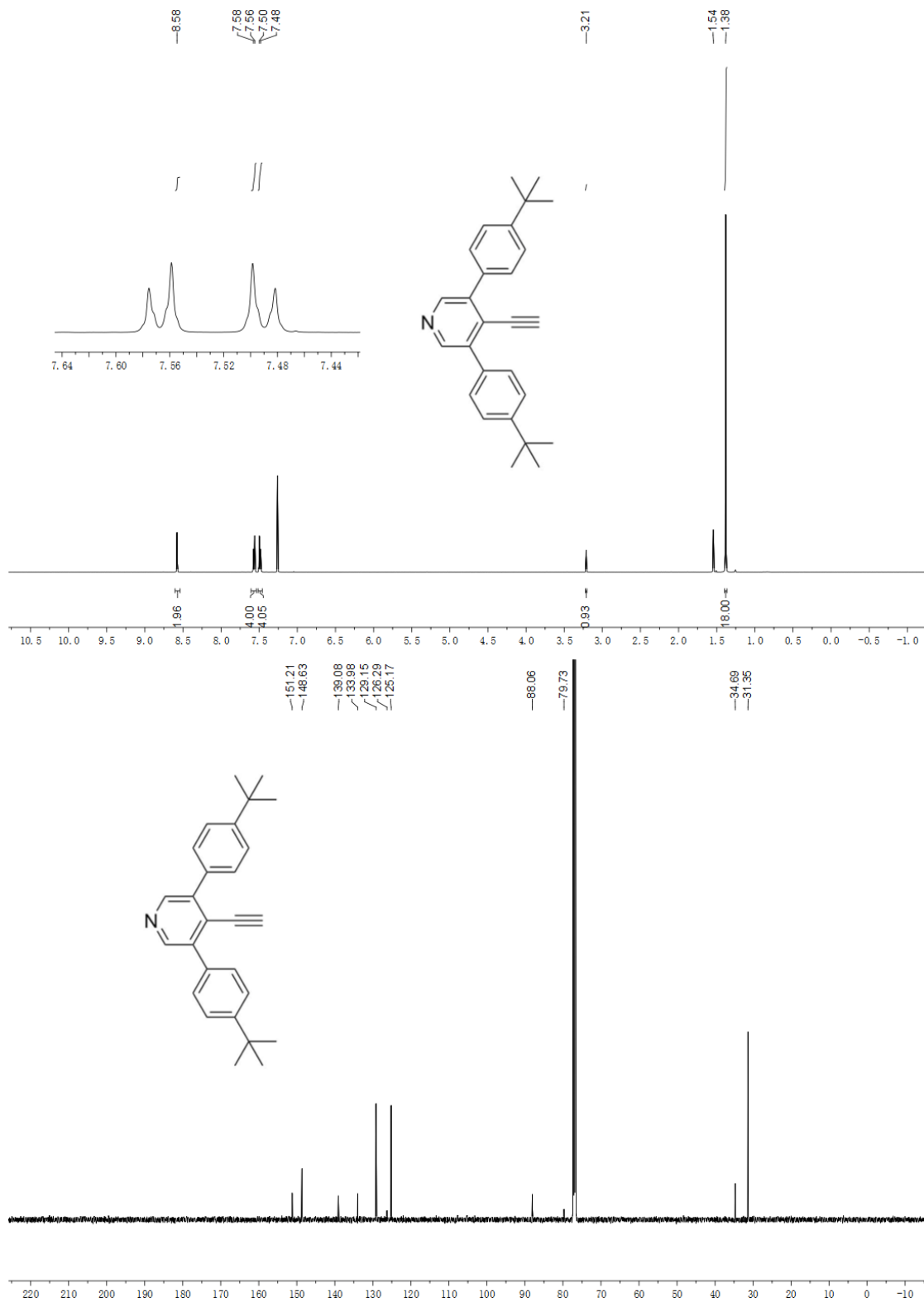
Figure 7.14. ^{1}H NMR and ^{13}C NMR spectra of compound **2.7b** in CDCl$_3$.
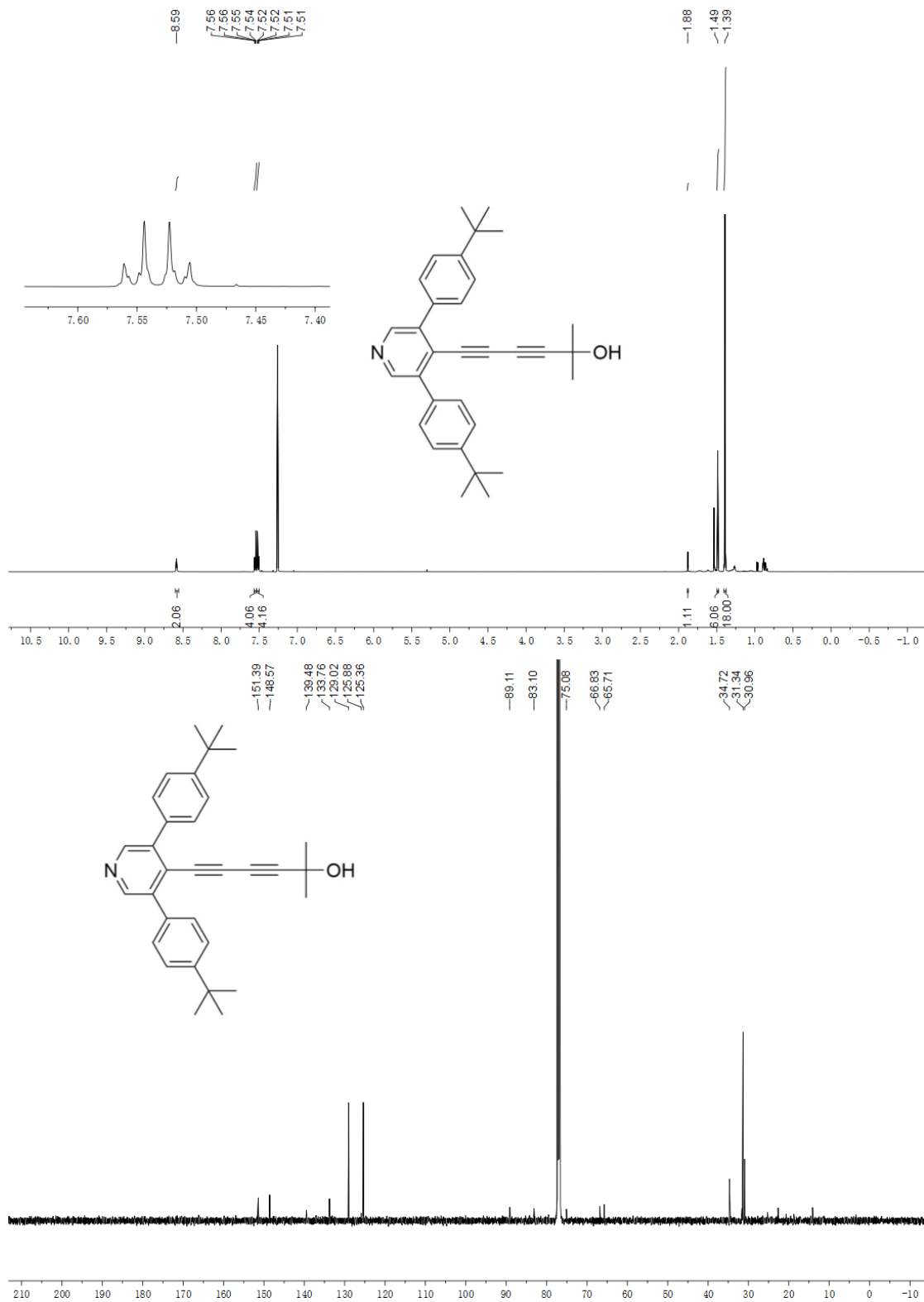
Figure 7.15. ¹H NMR and ¹³C NMR spectra of compound **2.8b** in CDCl₃.
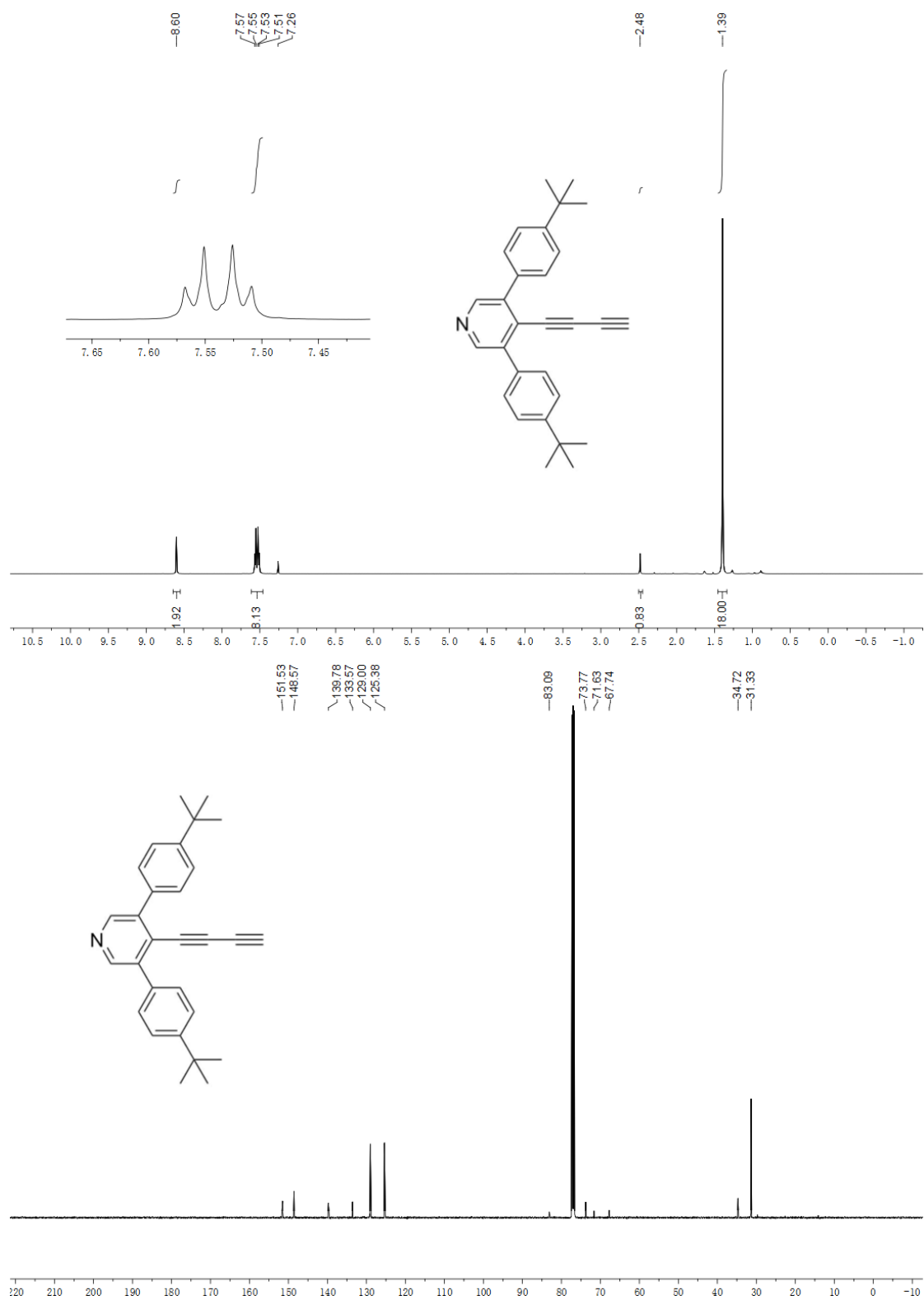
Figure 7.16. ¹H NMR and ¹³C NMR spectra of compound **2.9b** in CDCl₃.
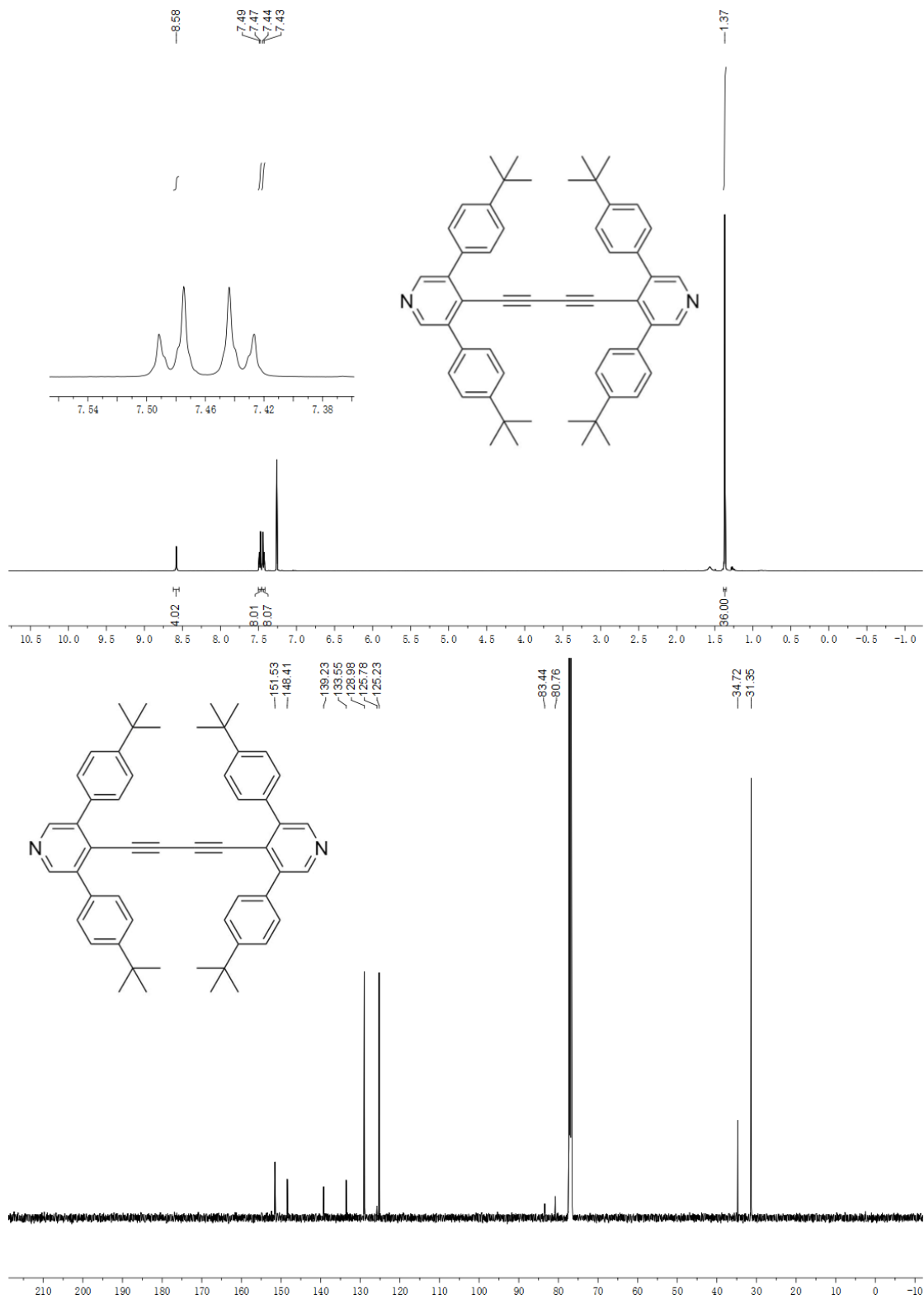
Figure 7.17. ^{1}H NMR and ^{13}C NMR spectra of compound **Py**[2b]** in CDCl$_3$.
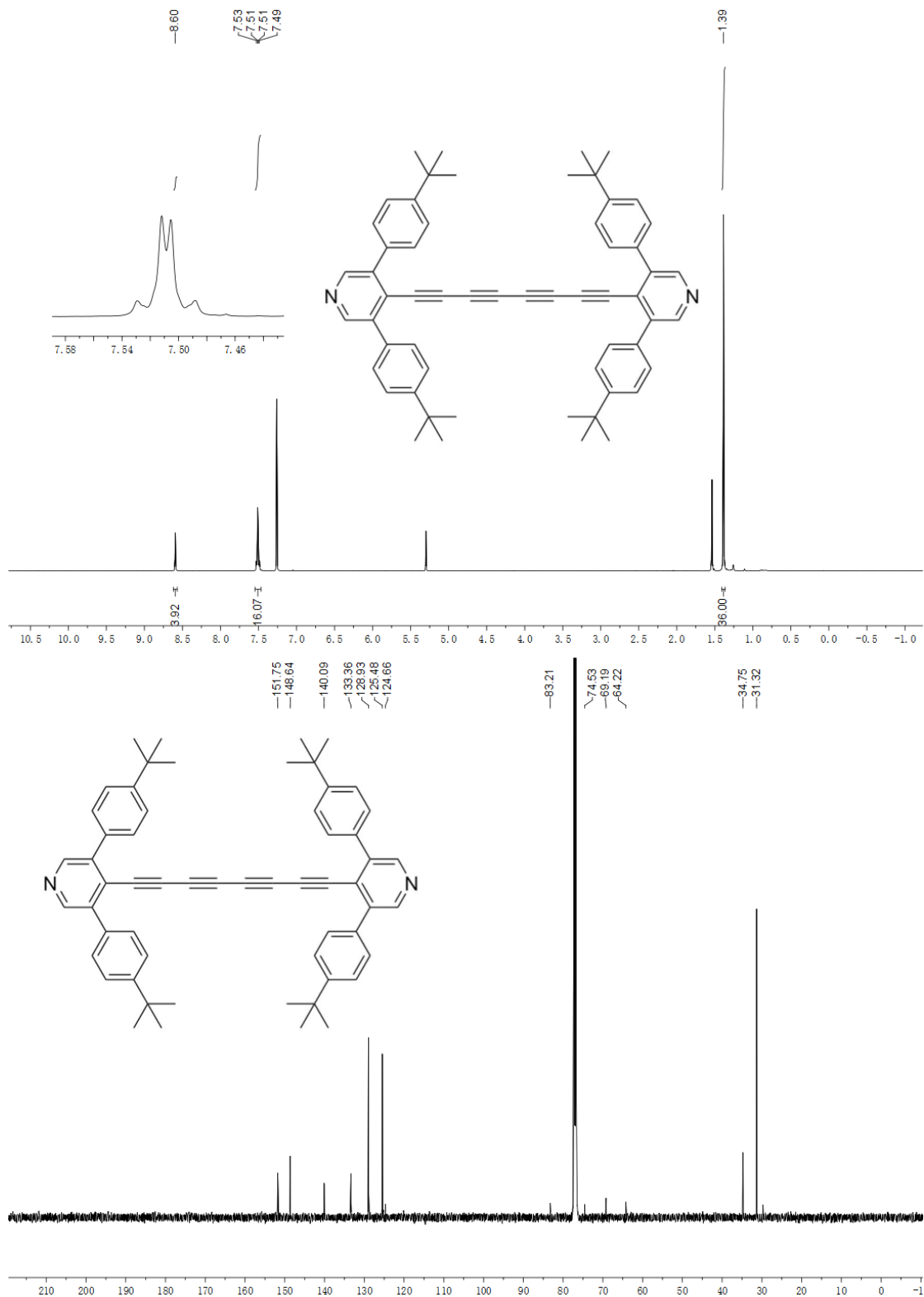
Figure 7.18. ¹H NMR and ¹³C NMR spectra of compound **Py**[4b]** in CDCl₃.
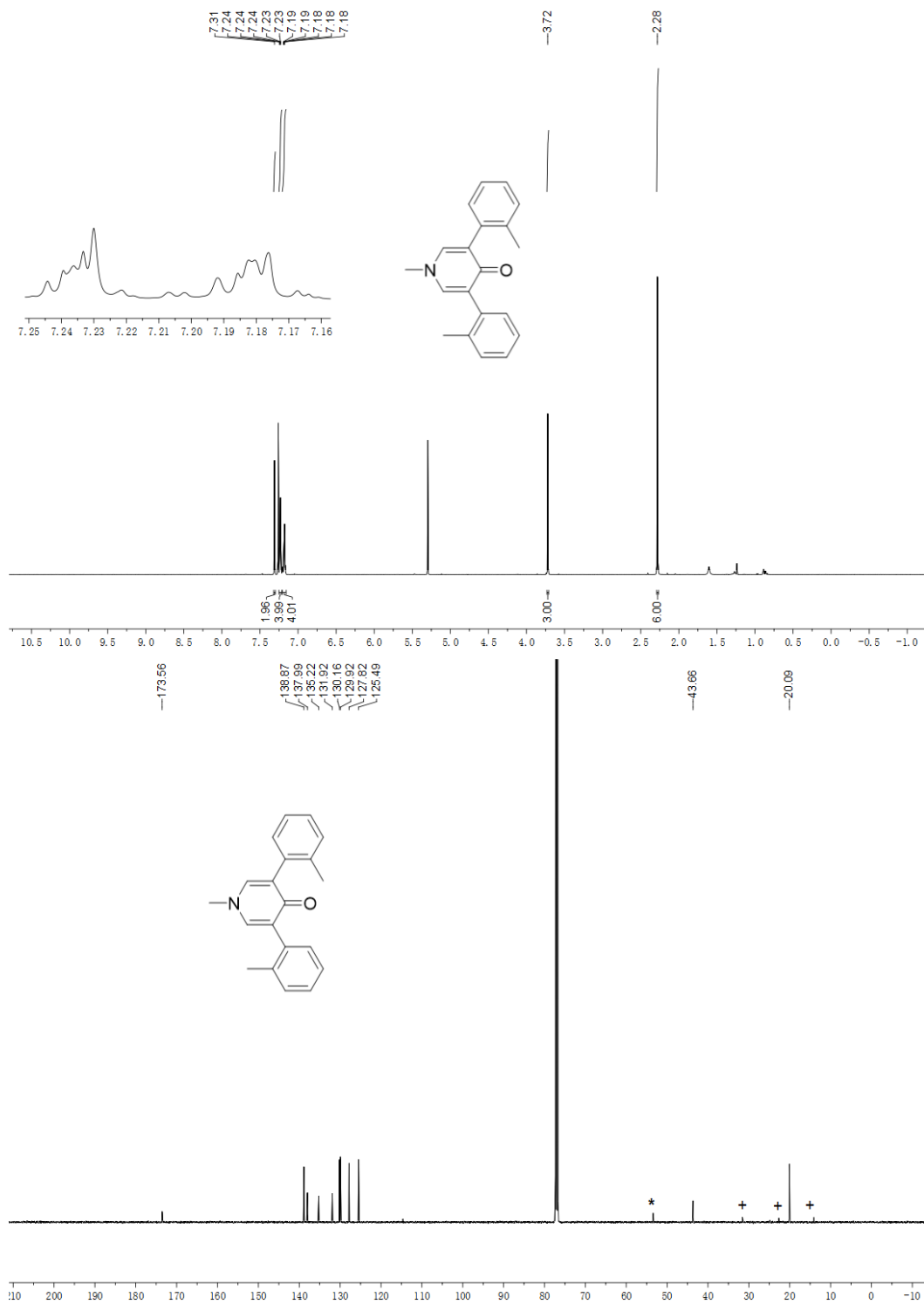
Figure 7.19. ^{1}H NMR and ^{13}C NMR spectra of compound **2.4c** in CDCl$_3$ (* indicates signals of CH$_2$Cl$_2$ and $^+$ hexanes).
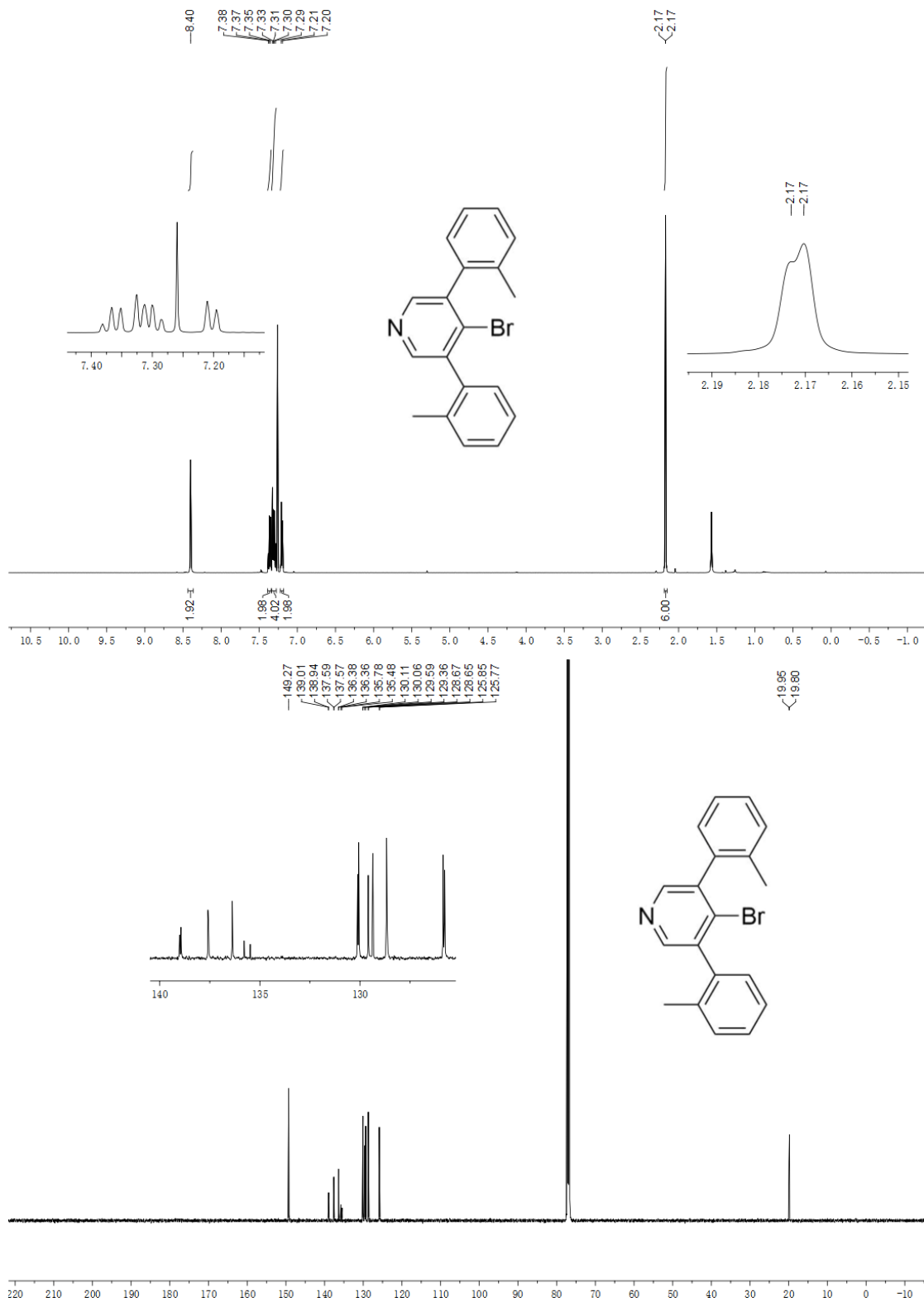
Figure 7.20. ^{1}H NMR and ^{13}C NMR spectra of compound **2.5c** in CDCl$_3$.
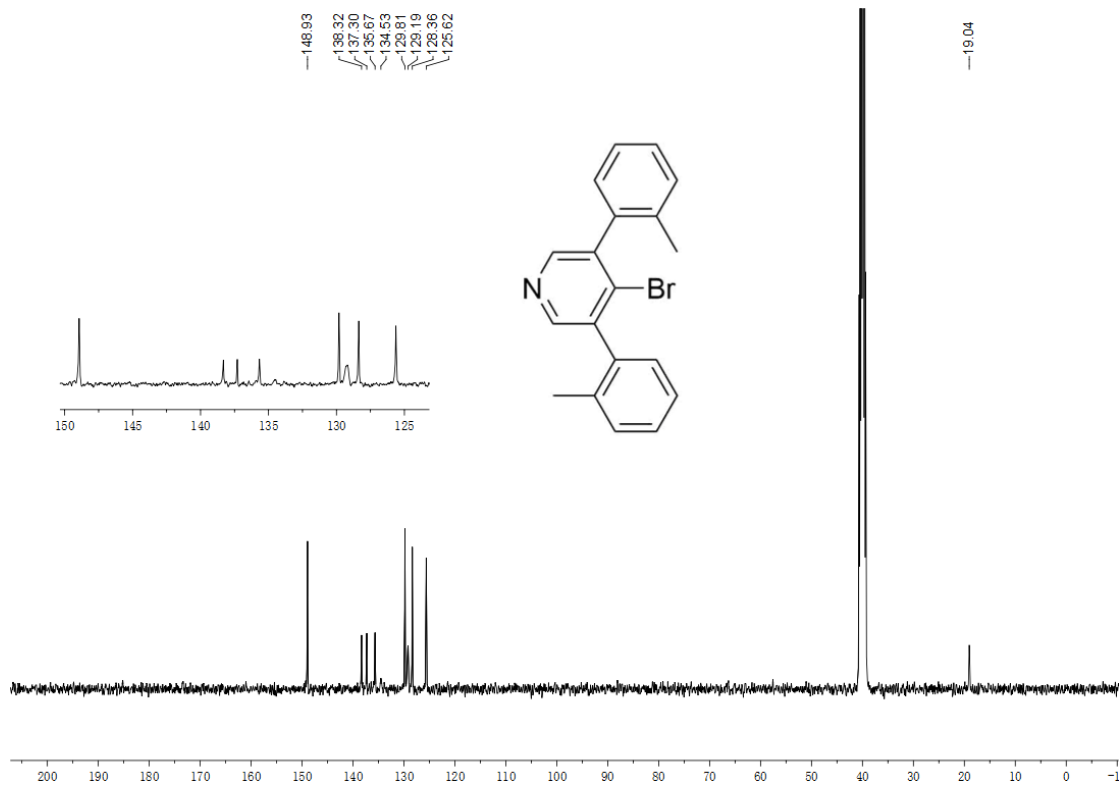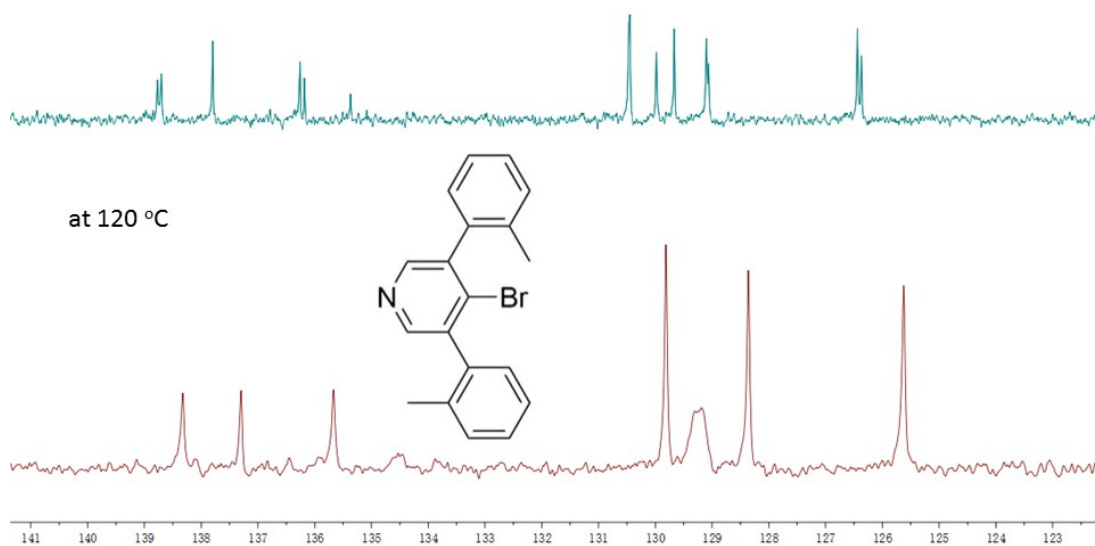
Figure 7.21. ^{13}C NMR spectrum of compound **2.5c** in DMSO-d_6 at 120 °C and the comparison of ^{13}C NMR spectra of compound **2.5c** in DMSO-d_6 at rt and 120 °C.
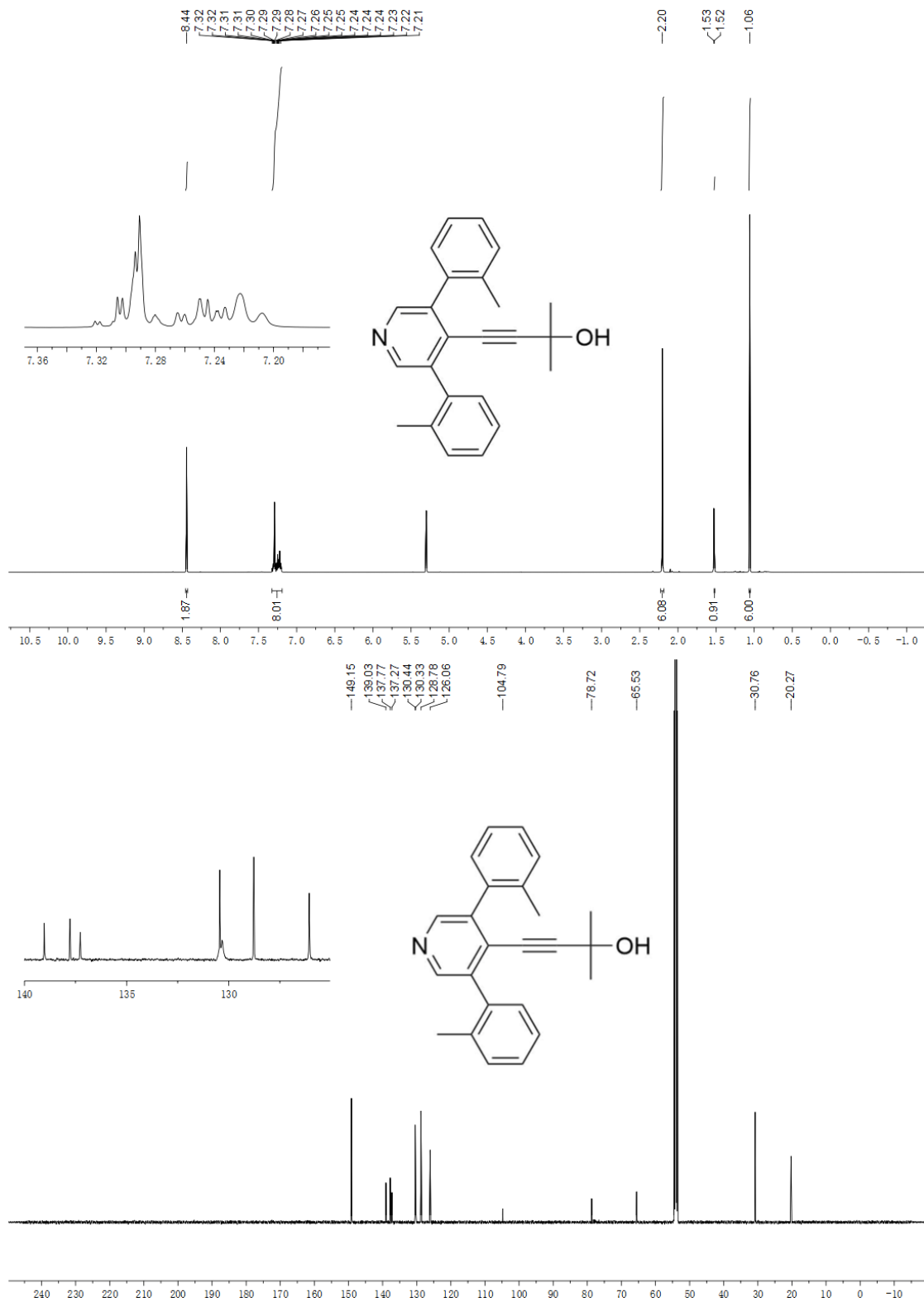
Figure 7.22. ^{1}H NMR and ^{13}C NMR spectra of compound **2.6c** in CD_2Cl_2.

243
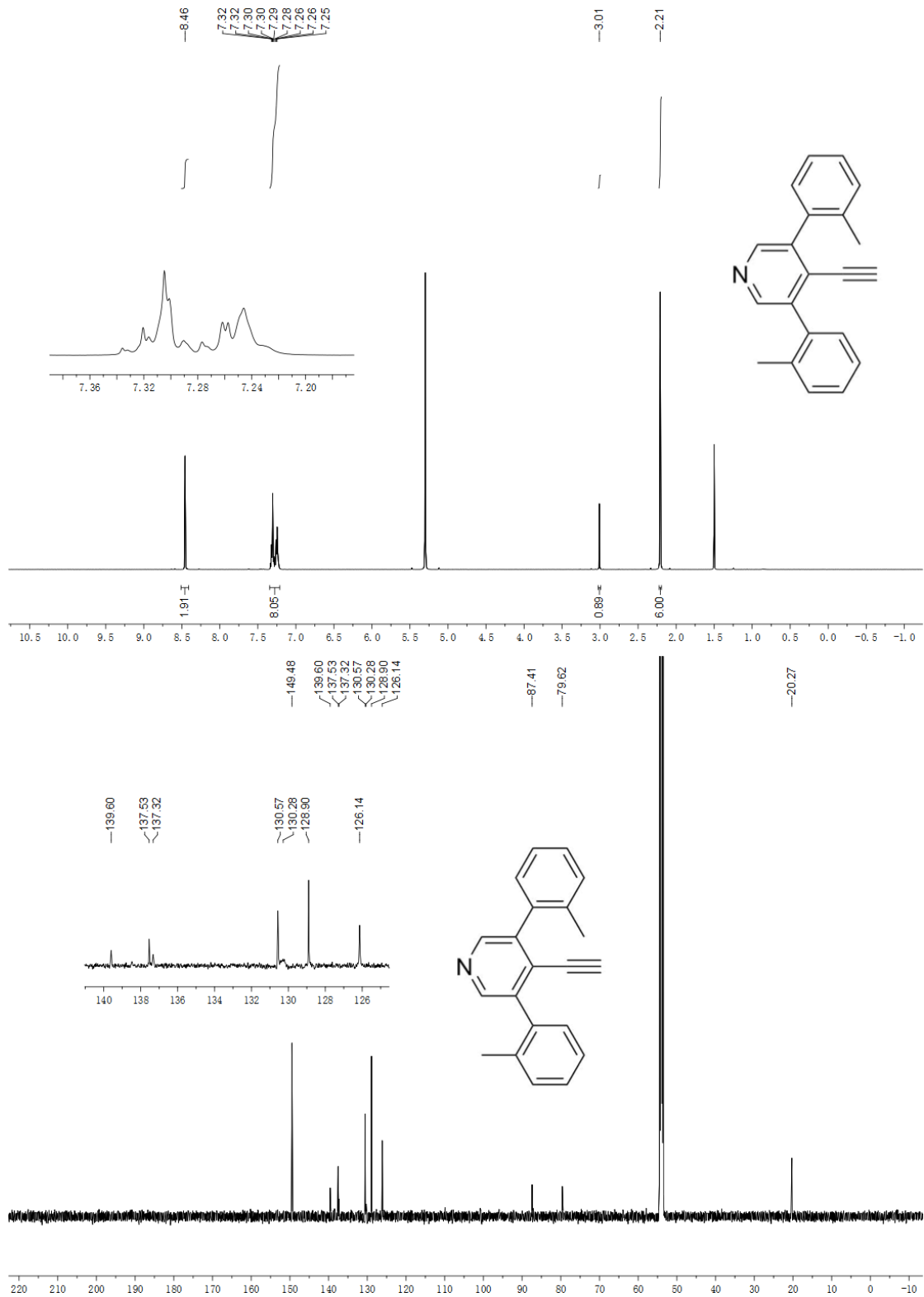
Figure 7.23. ^{1}H NMR and ^{13}C NMR spectra of compound **2.6c** in CD$_2$Cl$_2$.
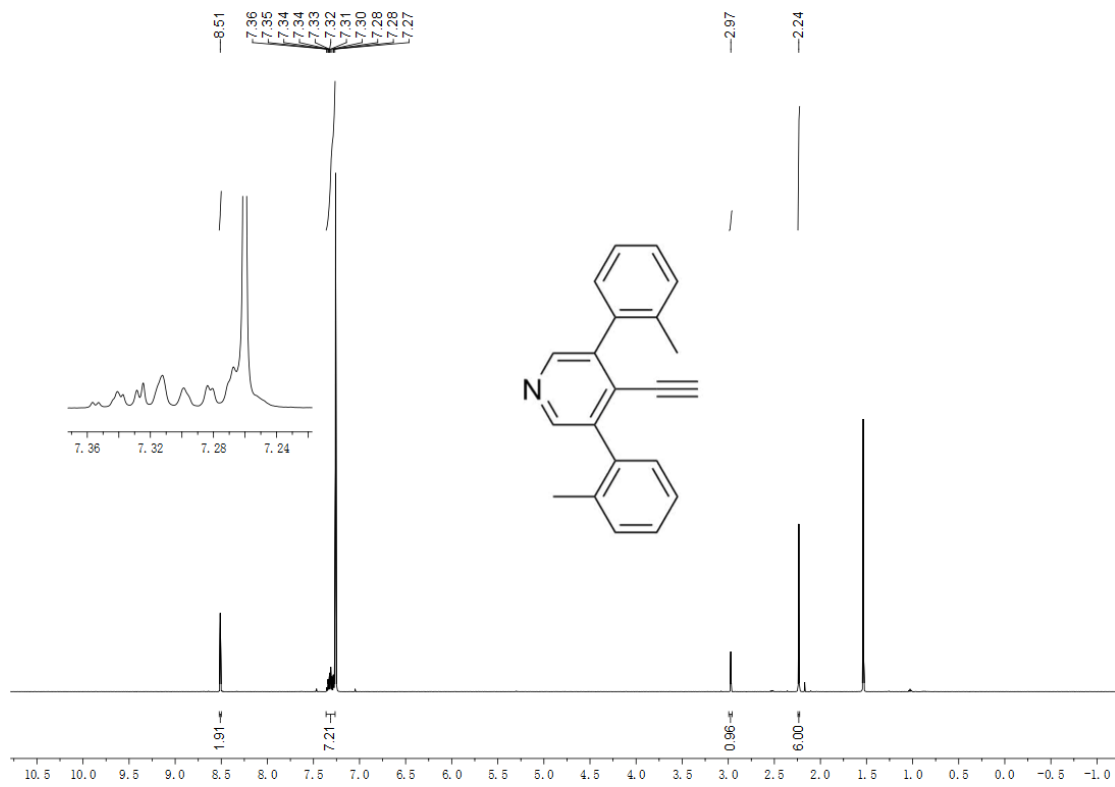
Figure 7.24. ^{1}H NMR spectrum of compound **2.7c** in CDCl$_3$.
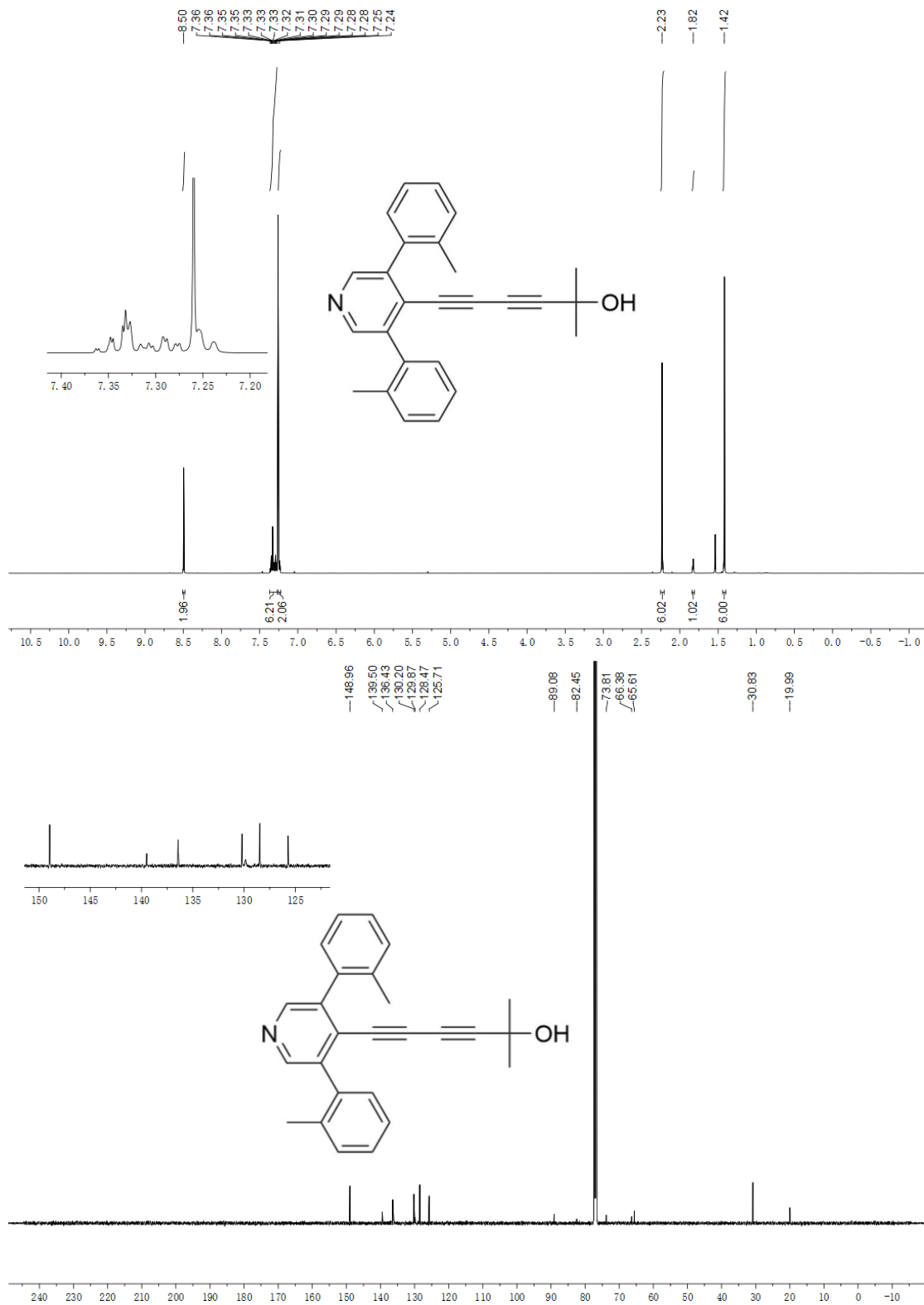
Figure 7.25. ^{1}H NMR and ^{13}C NMR spectra of compound **2.8c** in CDCl$_3$.
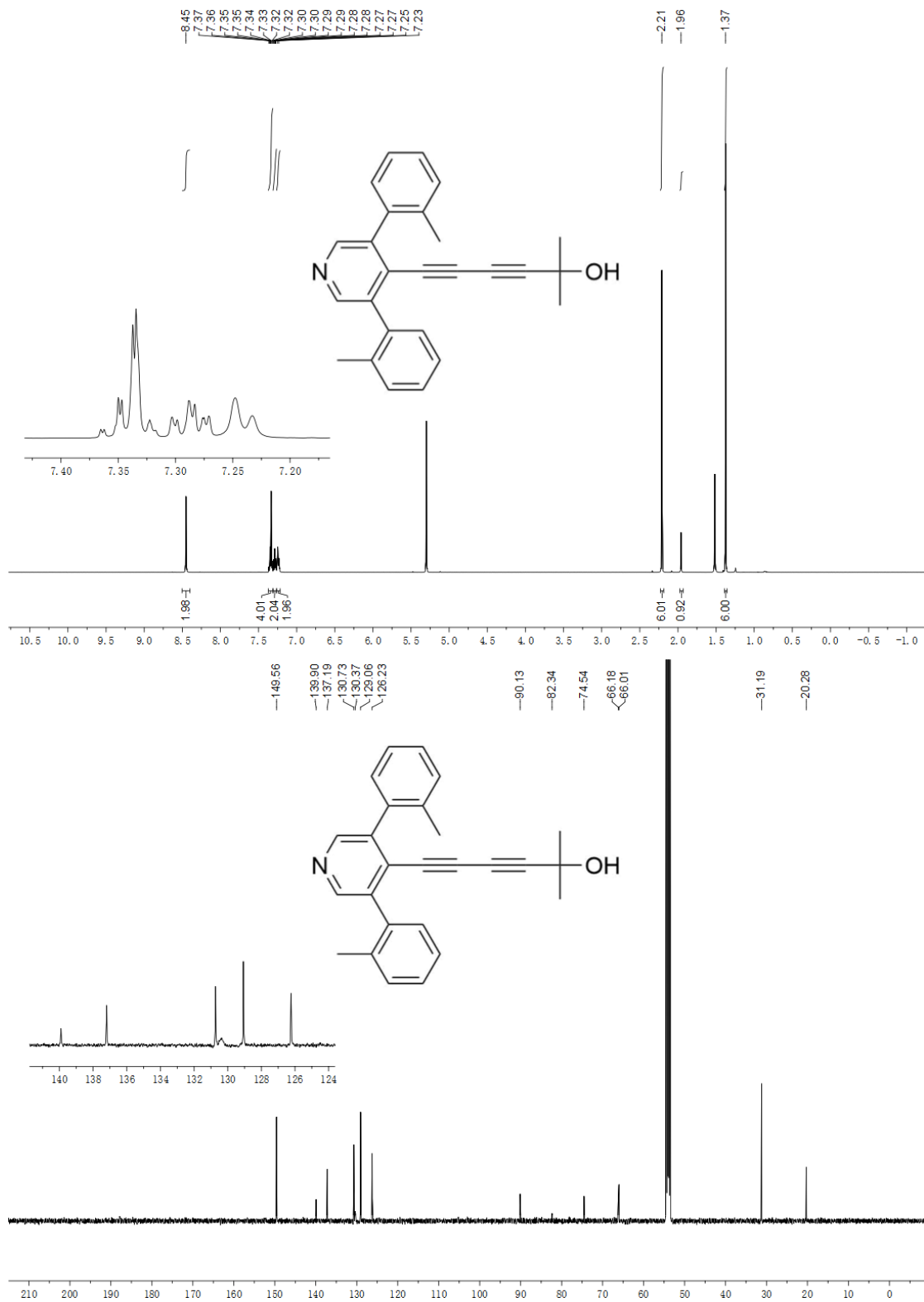
Figure 7.26. ^{1}H NMR and ^{13}C NMR spectra of compound **2.8c** in CD$_2$Cl$_2$.
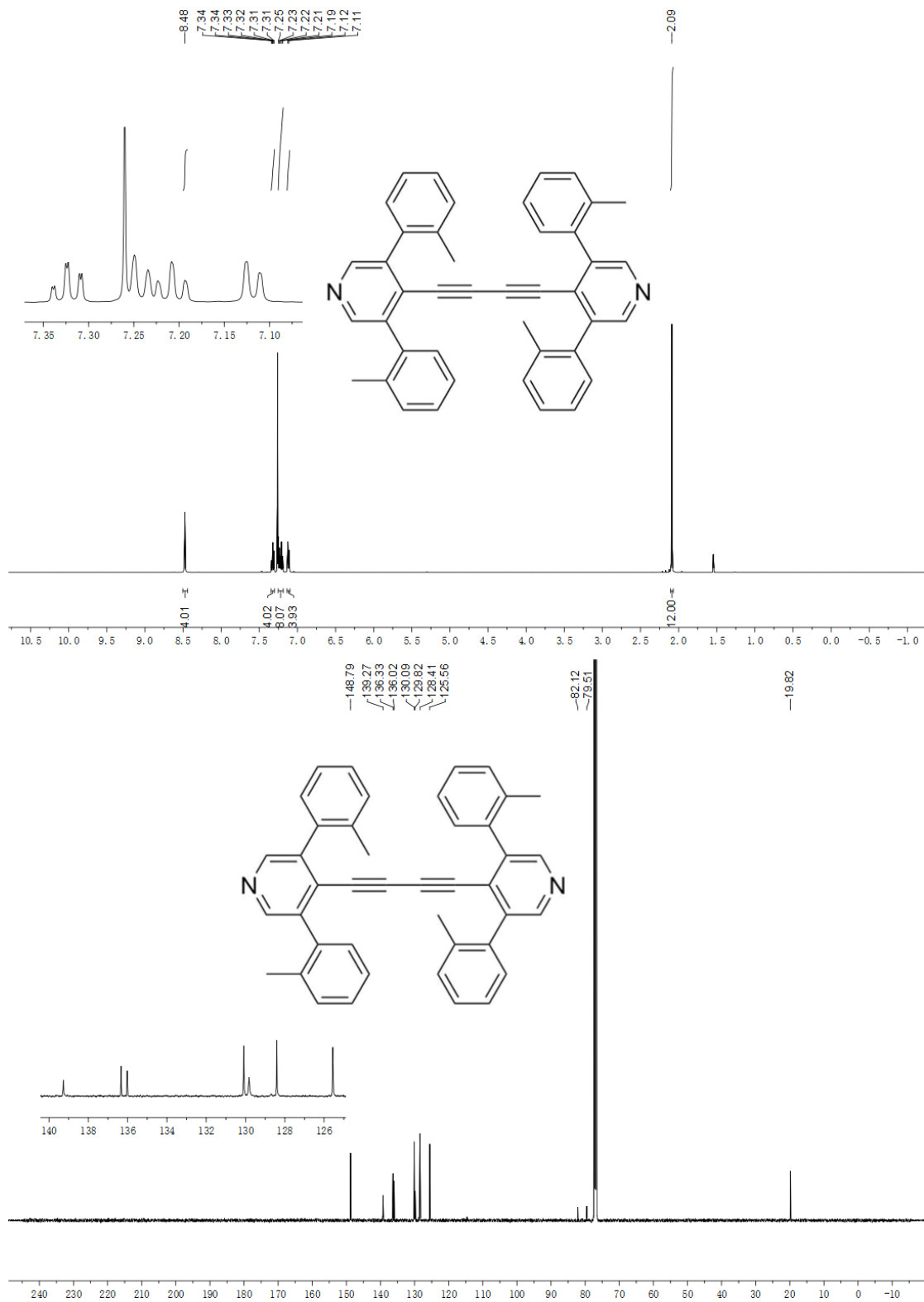
Figure 7.27. ^{1}H NMR and ^{13}C NMR spectra of compound **Py**[2c]** in CDCl₃.
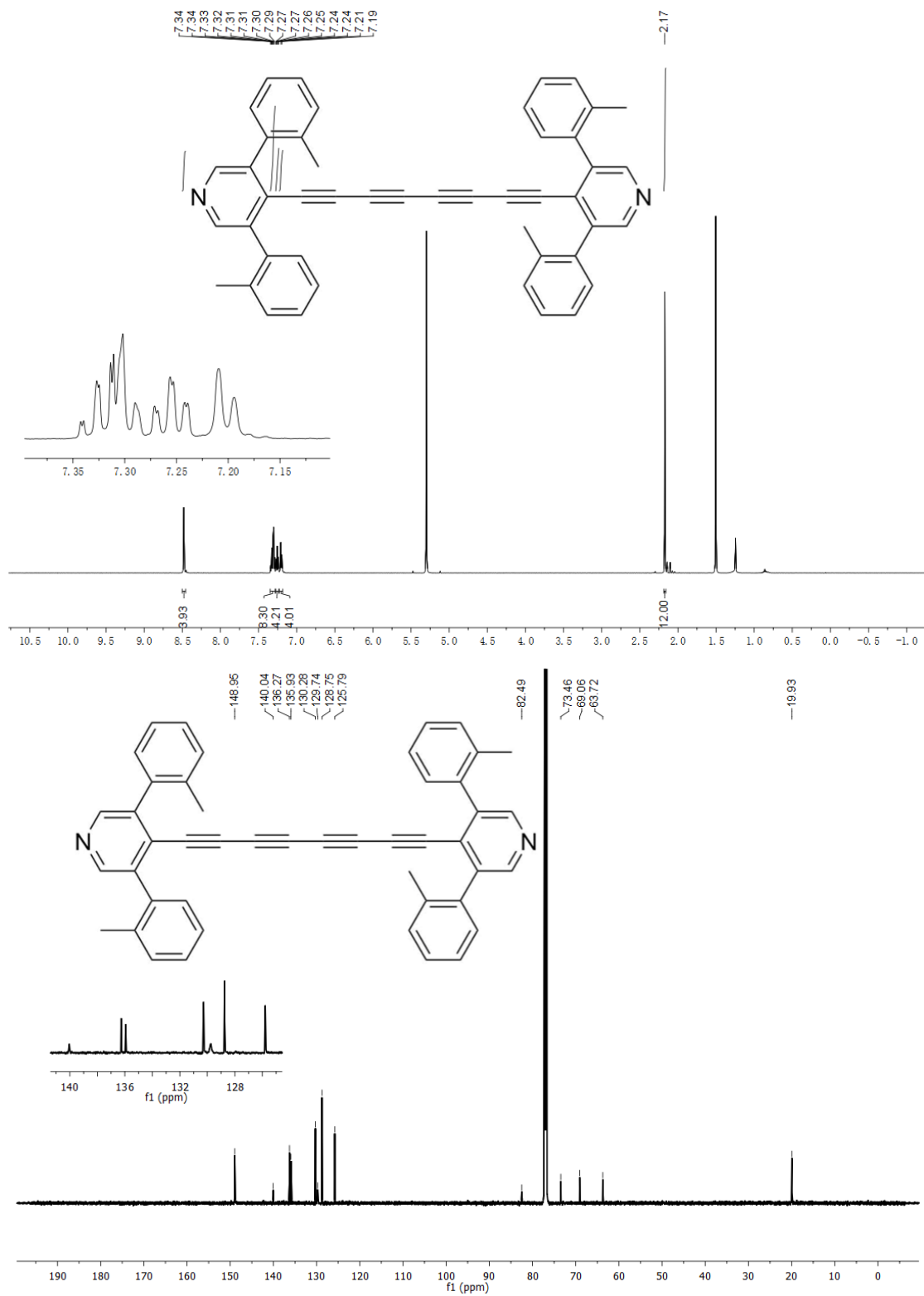
Figure 7.28. ^{1}H NMR spectrum of compound **Py**[4c]** in CD$_2$Cl$_2$ and ^{13}C NMR spectrum in CDCl$_3$.

249
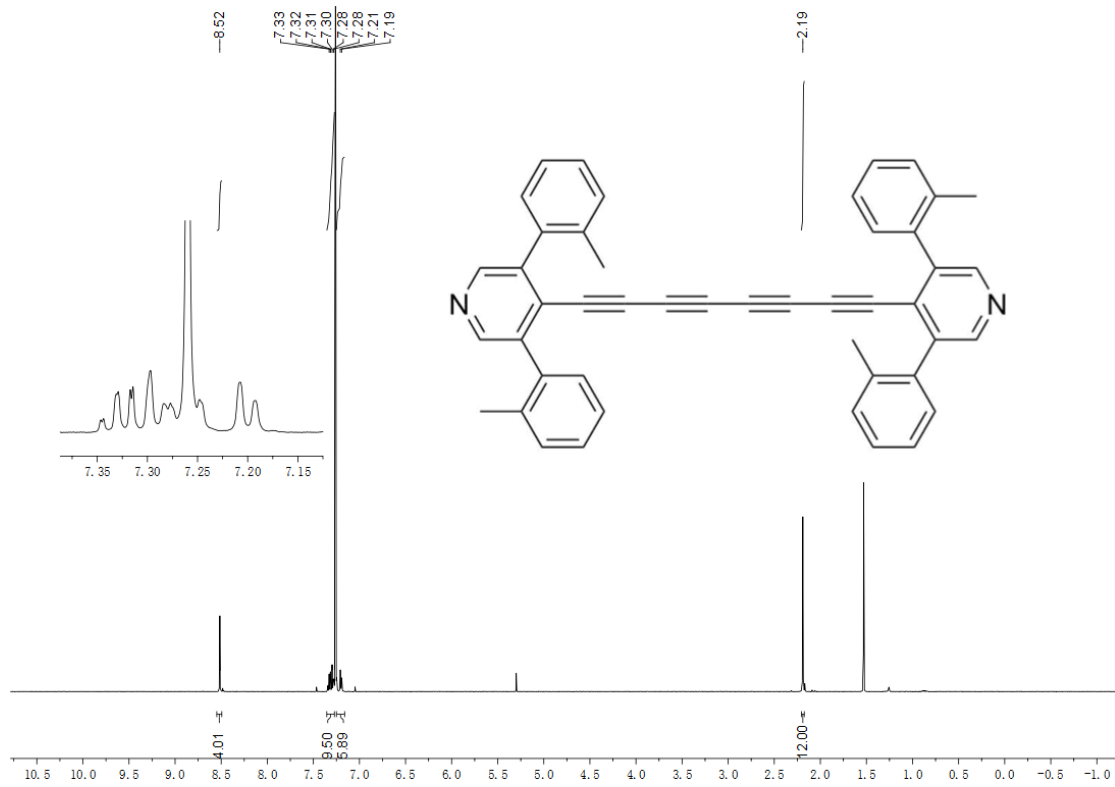
Figure 7.29. ^{1}H NMR spectrum of compound **Py**[4c]** in CDCl$_3$.
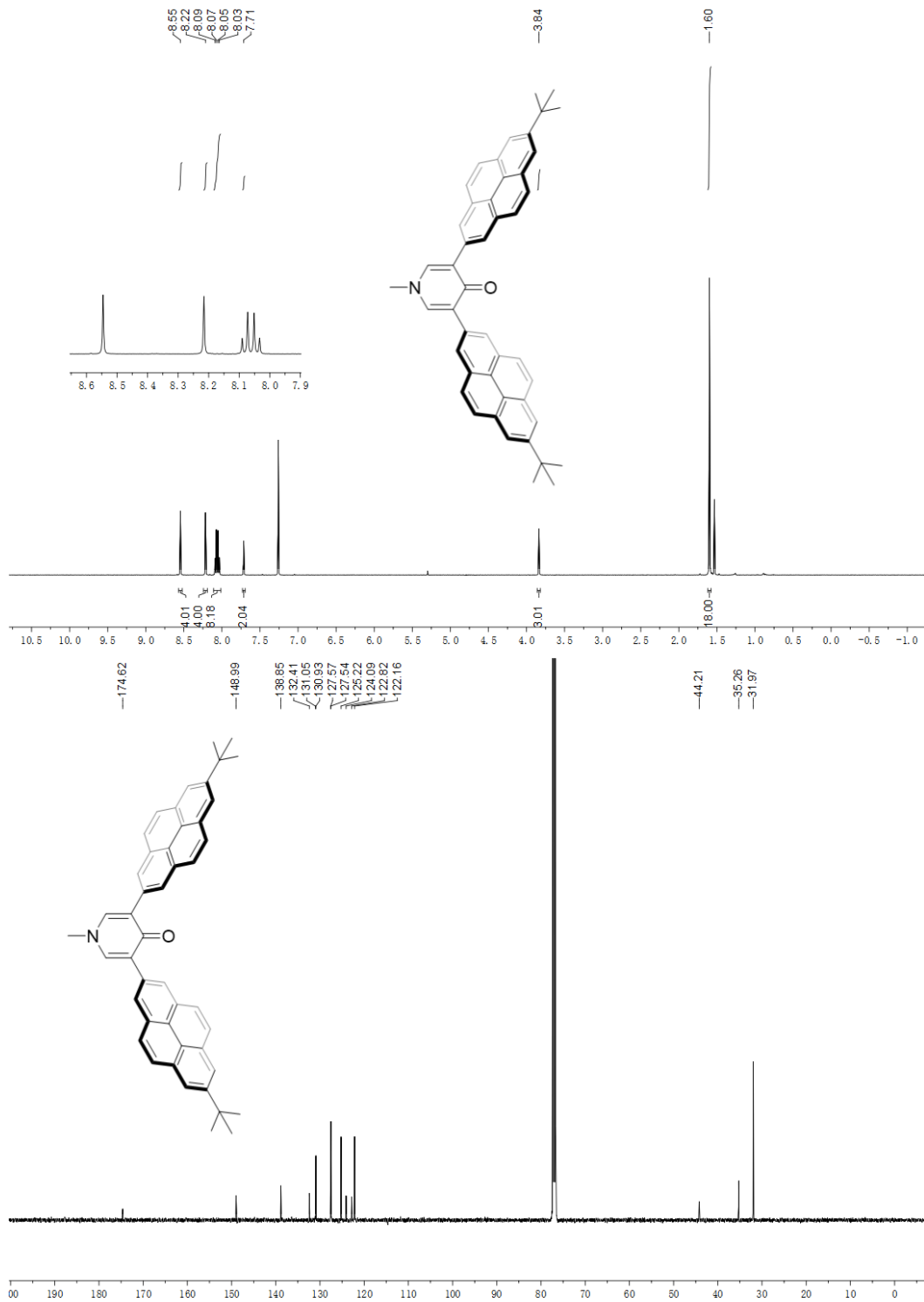
Figure 7.30. ^{1}H NMR and ^{13}C NMR spectra of compound **2.4d** in CDCl$_3$.
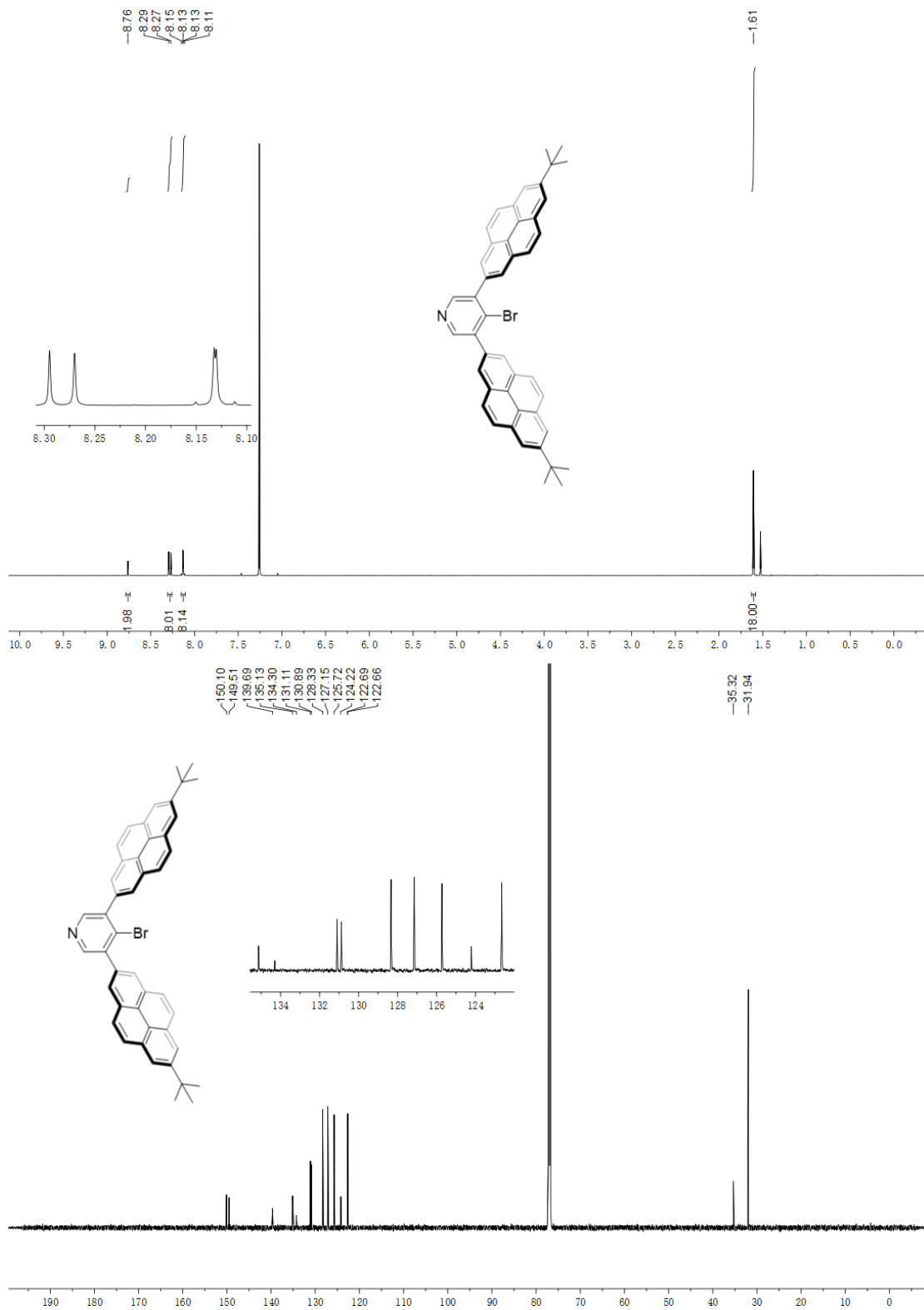
Figure 7.31. ^{1}H NMR and ^{13}C NMR spectra of compound **2.5d** in CDCl$_3$.
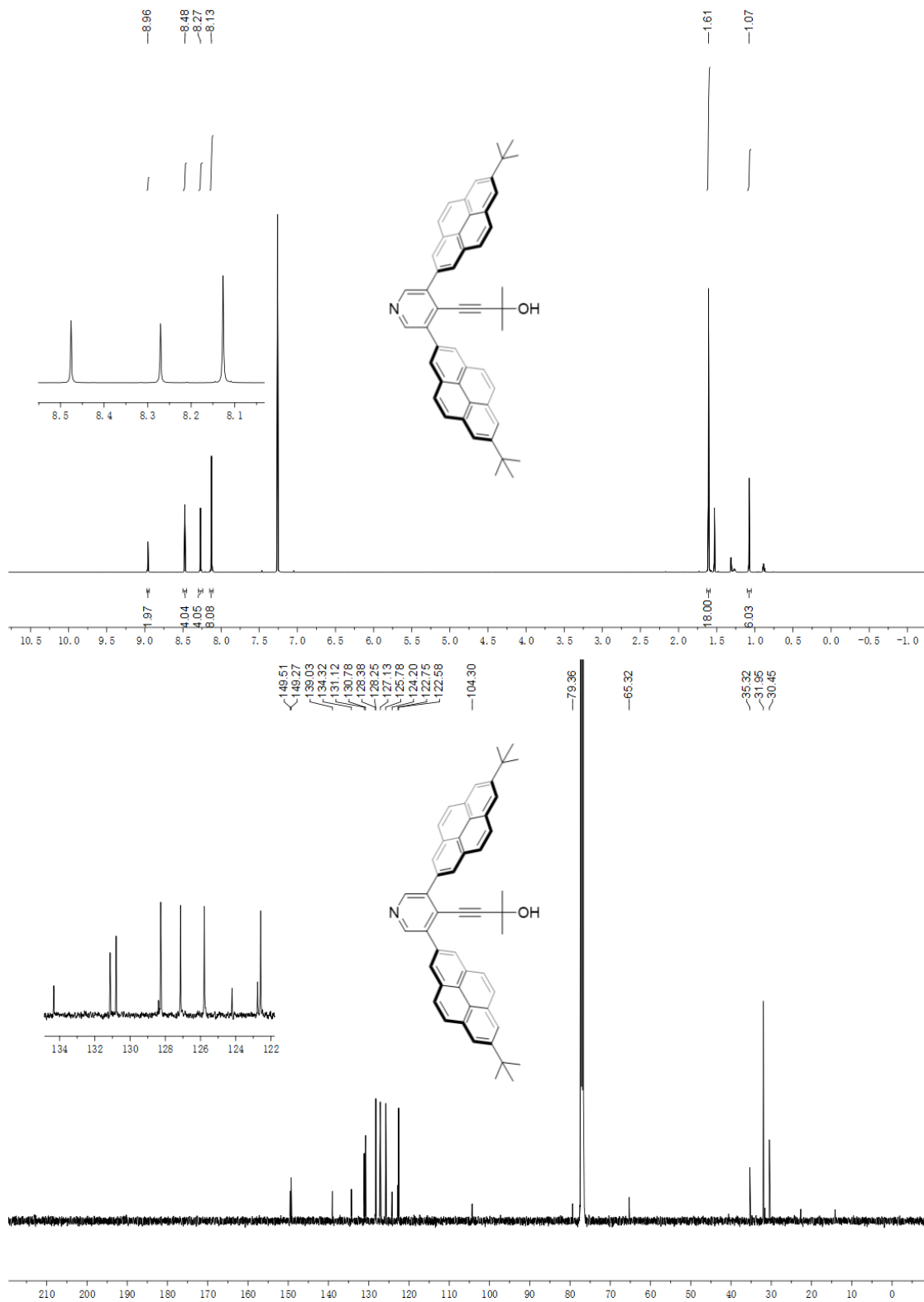
Figure 7.32. ¹H NMR and ¹³C NMR spectra of compound **2.6d** in CDCl₃.
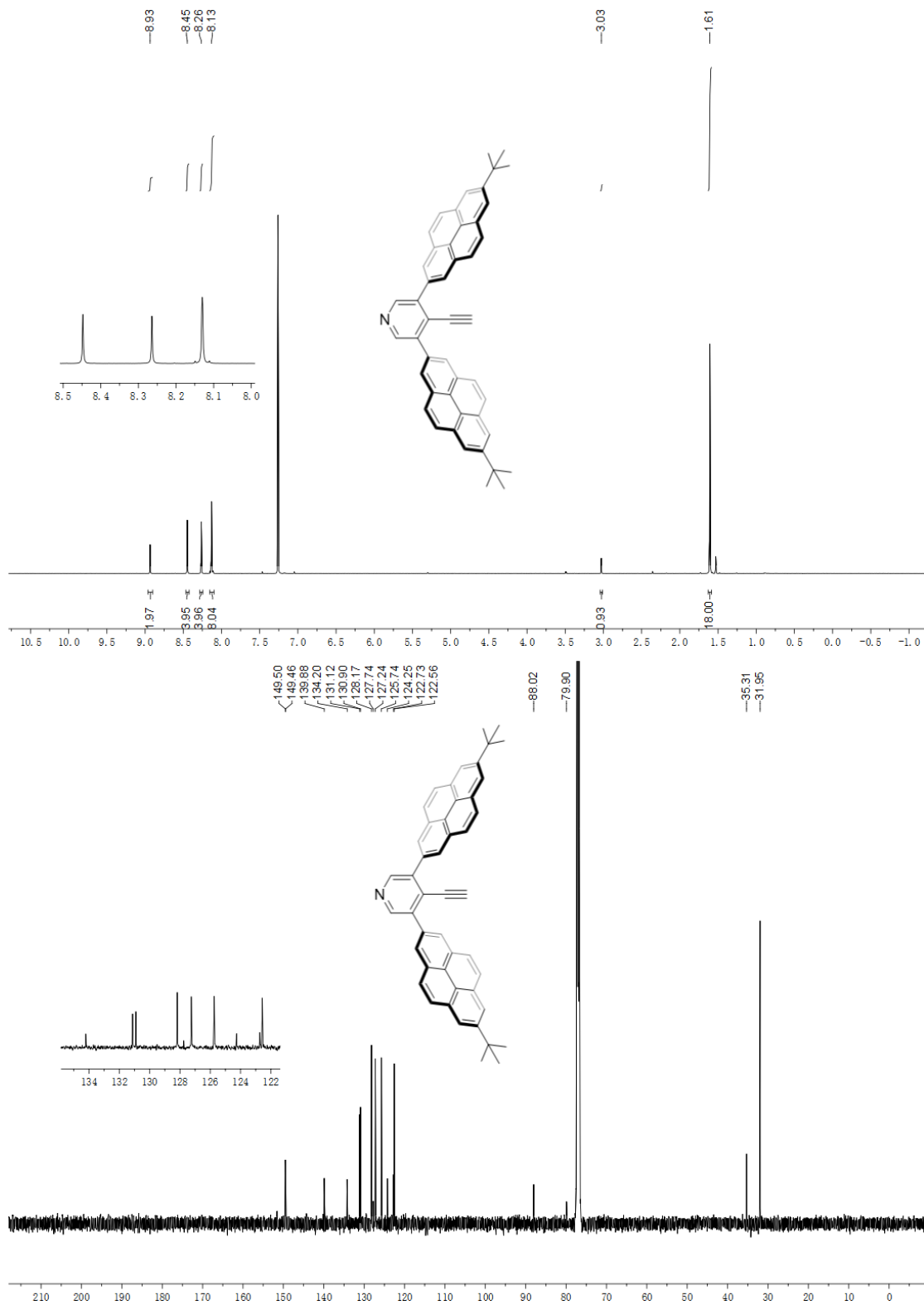
Figure 7.33. ^{1}H NMR and ^{13}C NMR spectra of compound **2.7d** in CDCl$_3$.

254
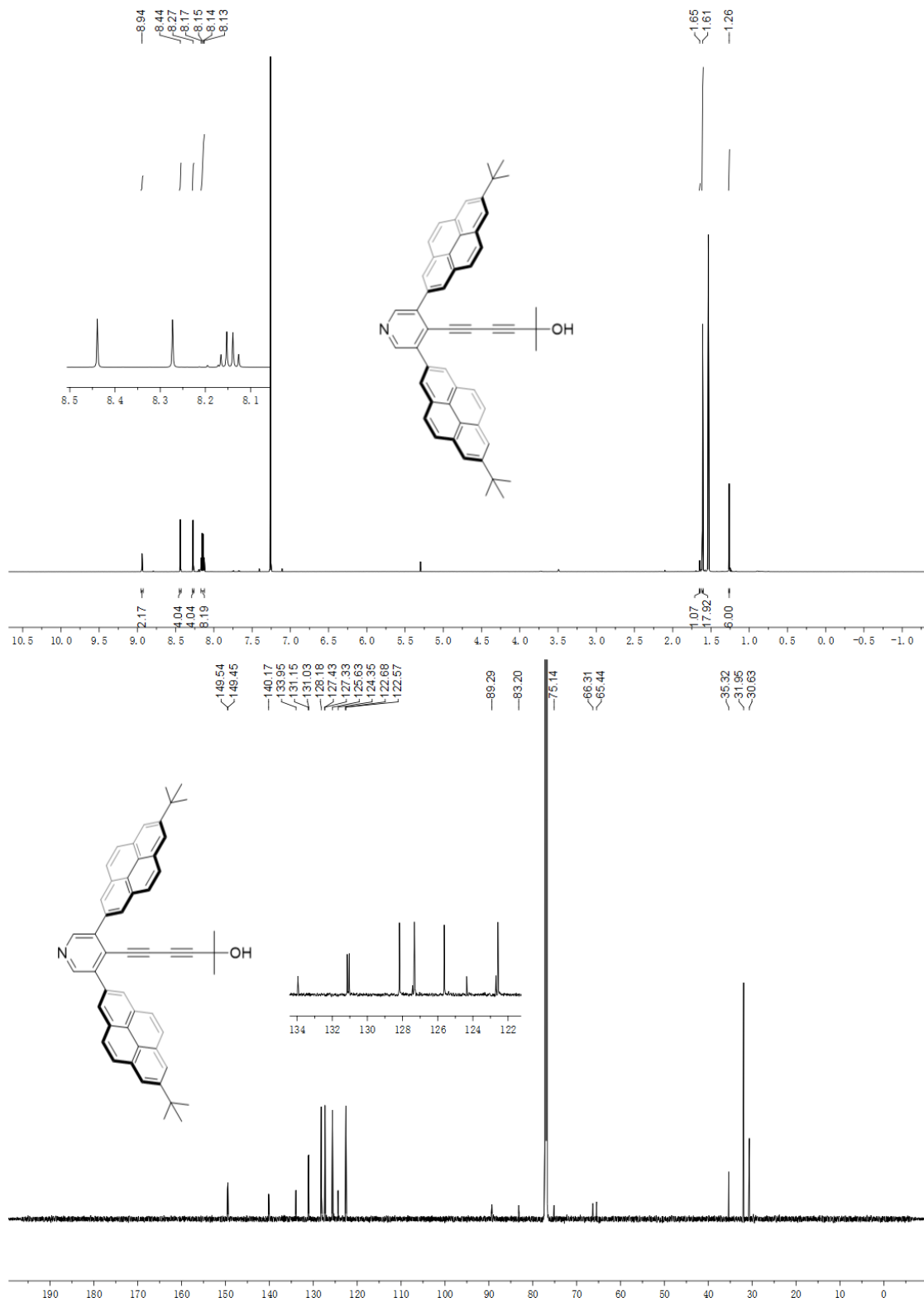
Figure 7.34. ^{1}H NMR and ^{13}C NMR spectra of compound **2.8d** in CDCl$_3$.
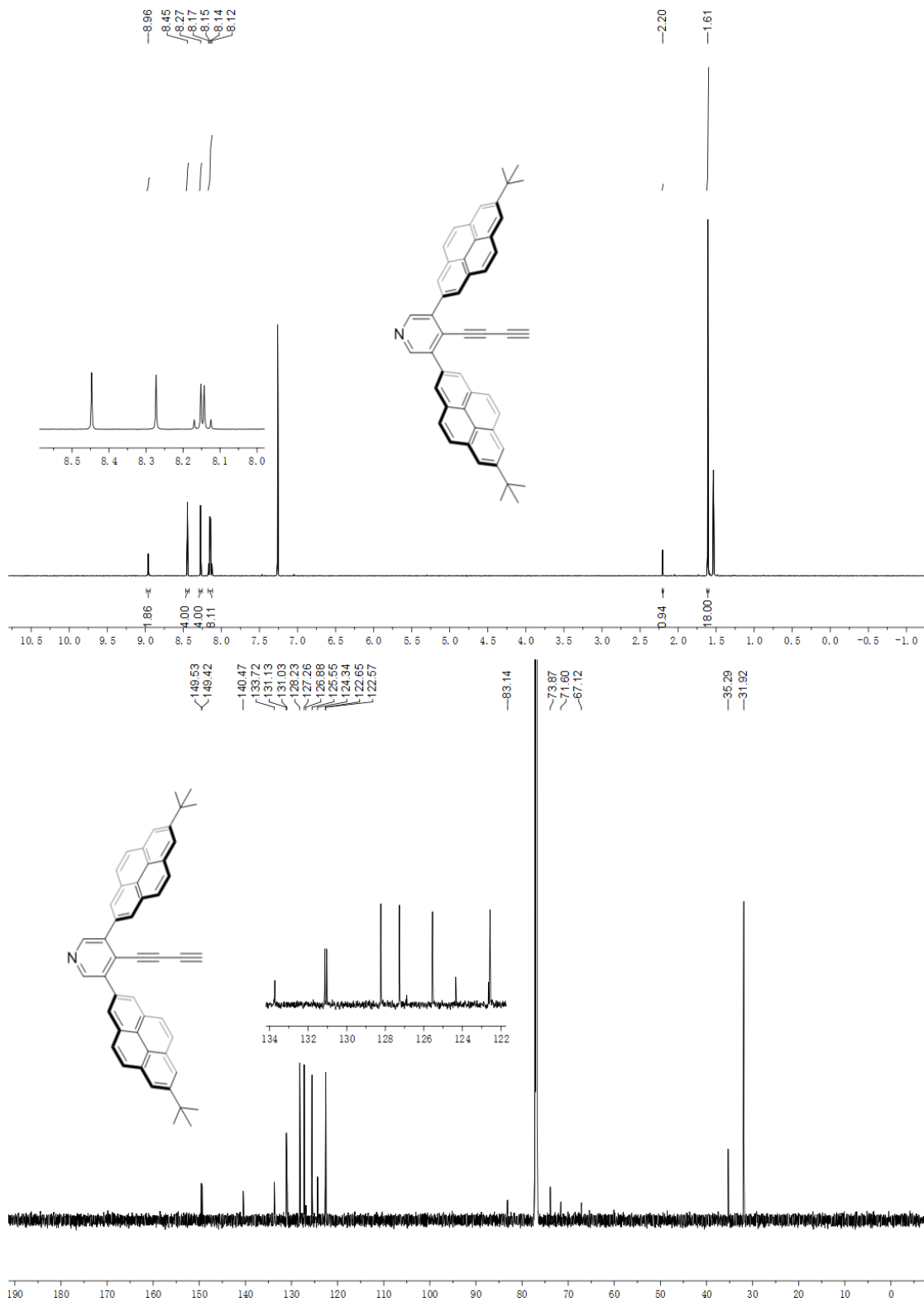
Figure 7.35. ^{1}H NMR and ^{13}C NMR spectra of compound **2.9d** in CDCl$_3$.
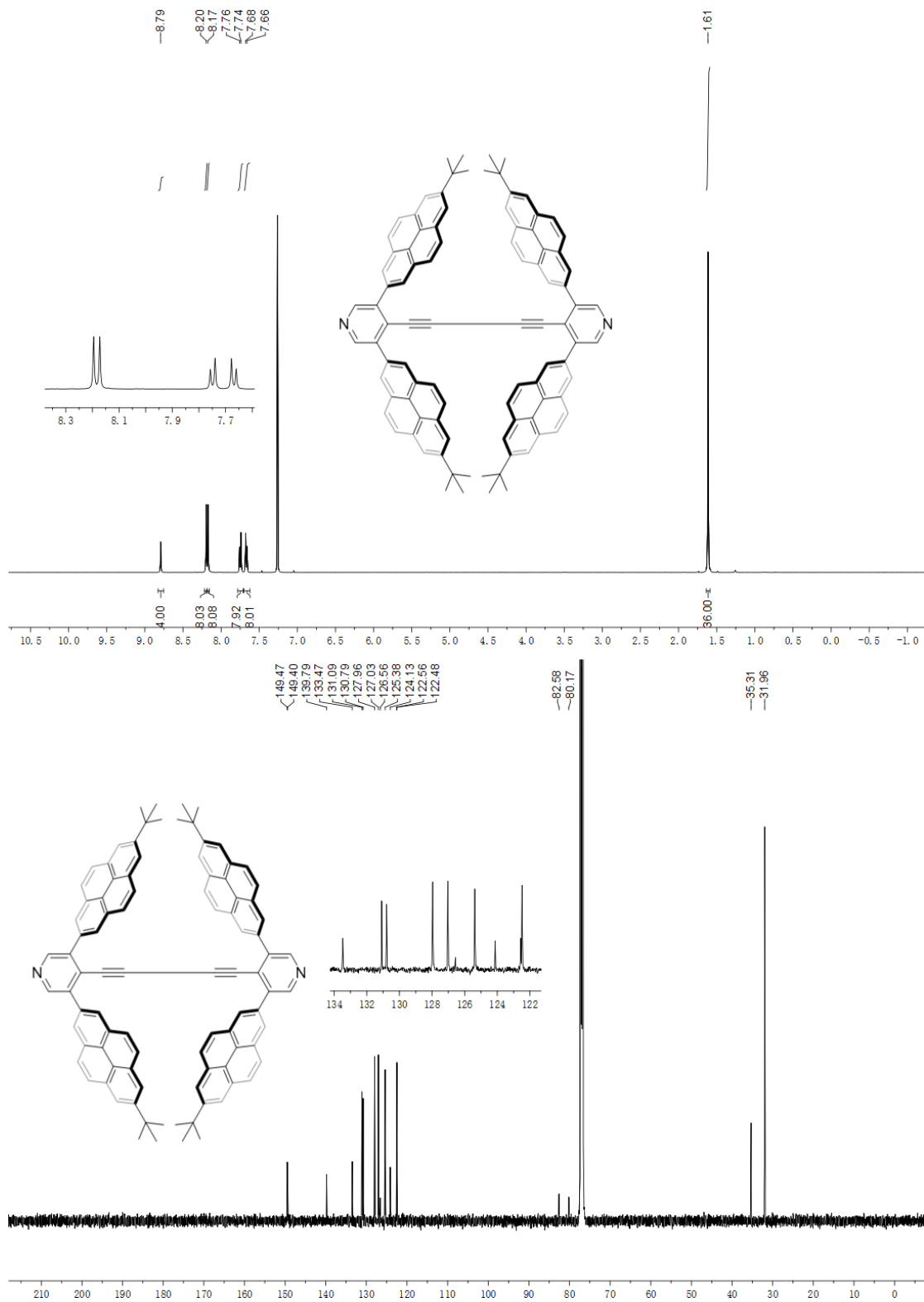
Figure 7.36. ^{1}H NMR and ^{13}C NMR spectra of compound **Py**[2d]** in CDCl$_3$.
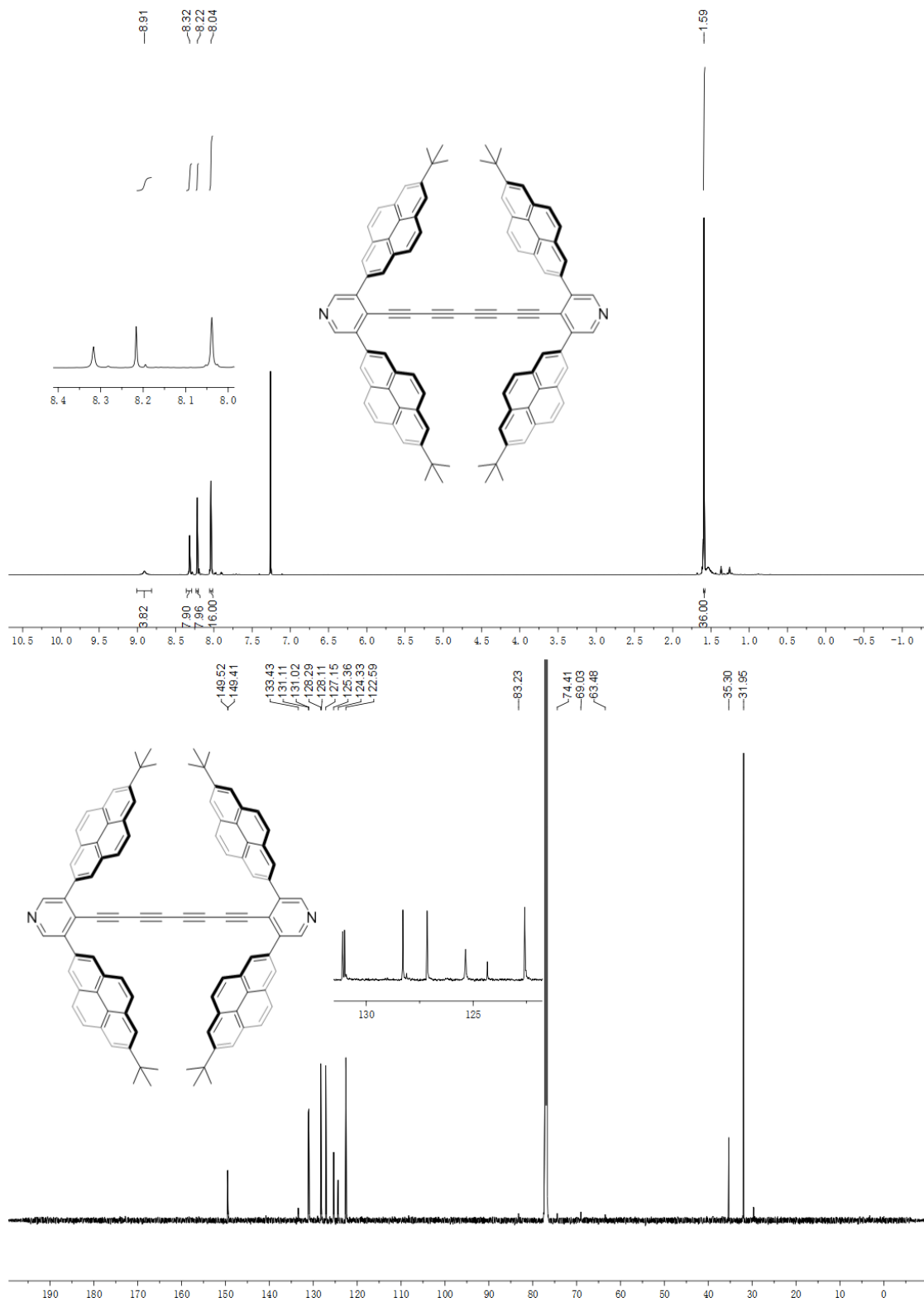
Figure 7.37. ^{1}H NMR and ^{13}C NMR spectra of compound **Py**[4d]** in CDCl$_3$.
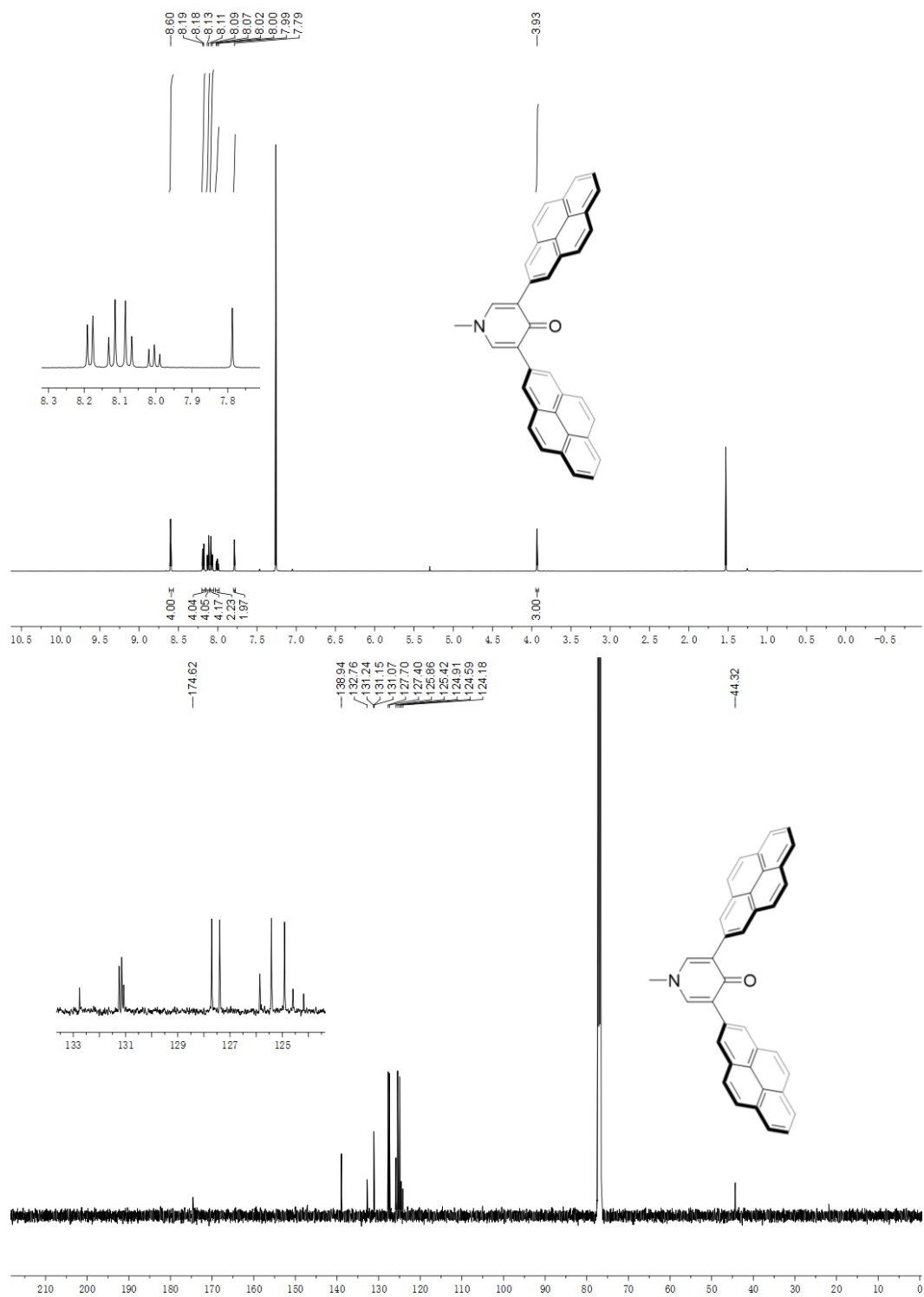
Figure 7.38. ^{1}H NMR and ^{13}C NMR spectra of compound **2.4e** in CDCl$_3$.
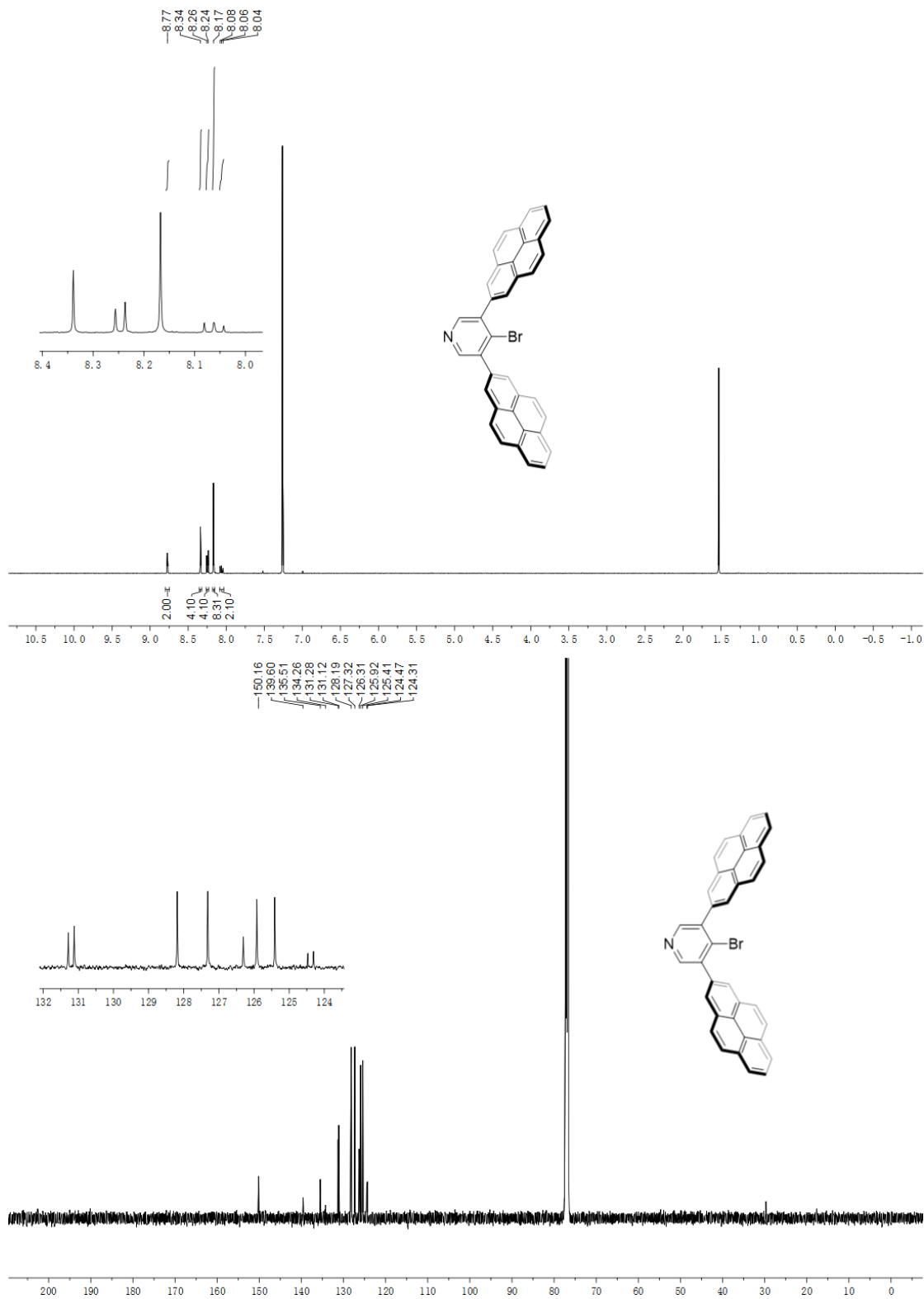
Figure 7.39. ^{1}H NMR and ^{13}C NMR spectra of compound **2.5e** in CDCl$_3$.
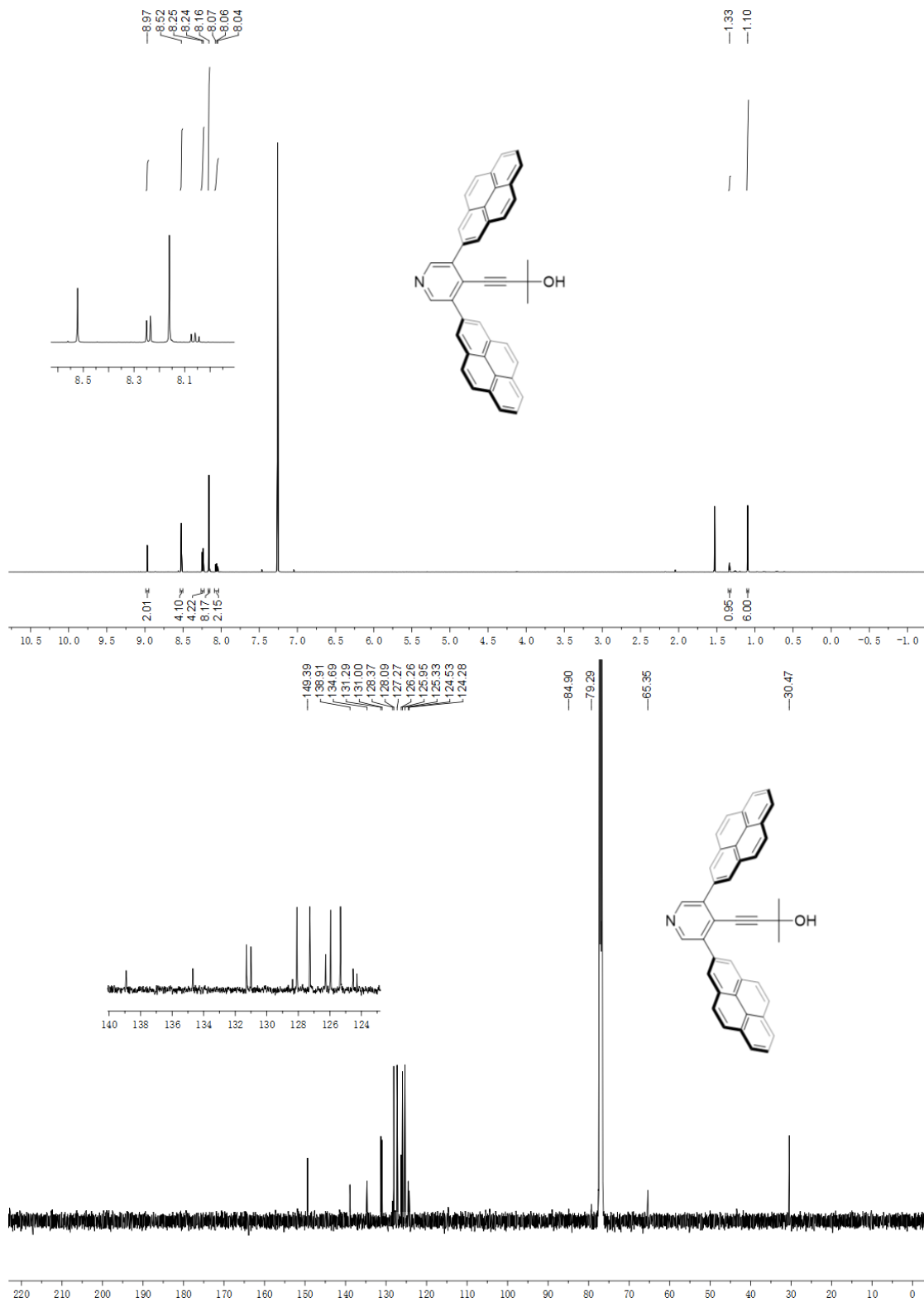
Figure 7.40. [^1]H NMR and [^13]C NMR spectra of compound **2.6e** in CDCl₃.
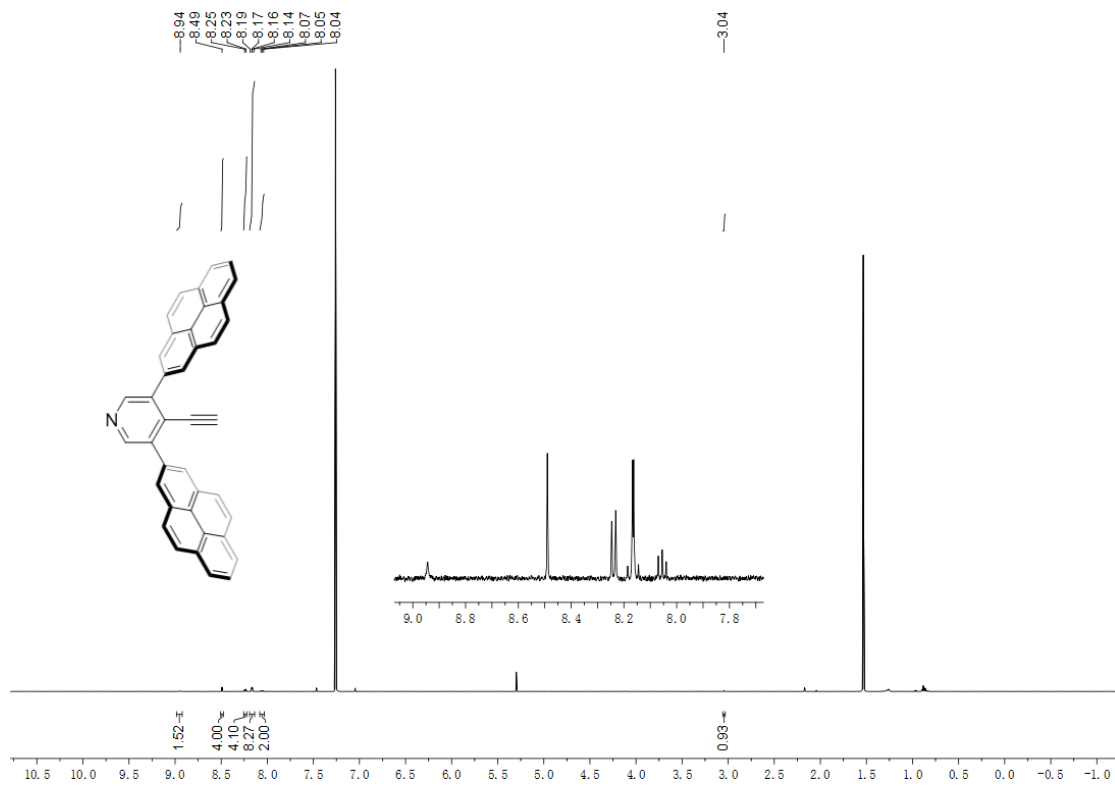
Figure 7.41. ^{1}H NMR spectrum of compound **2.7e** in CDCl$_3$.
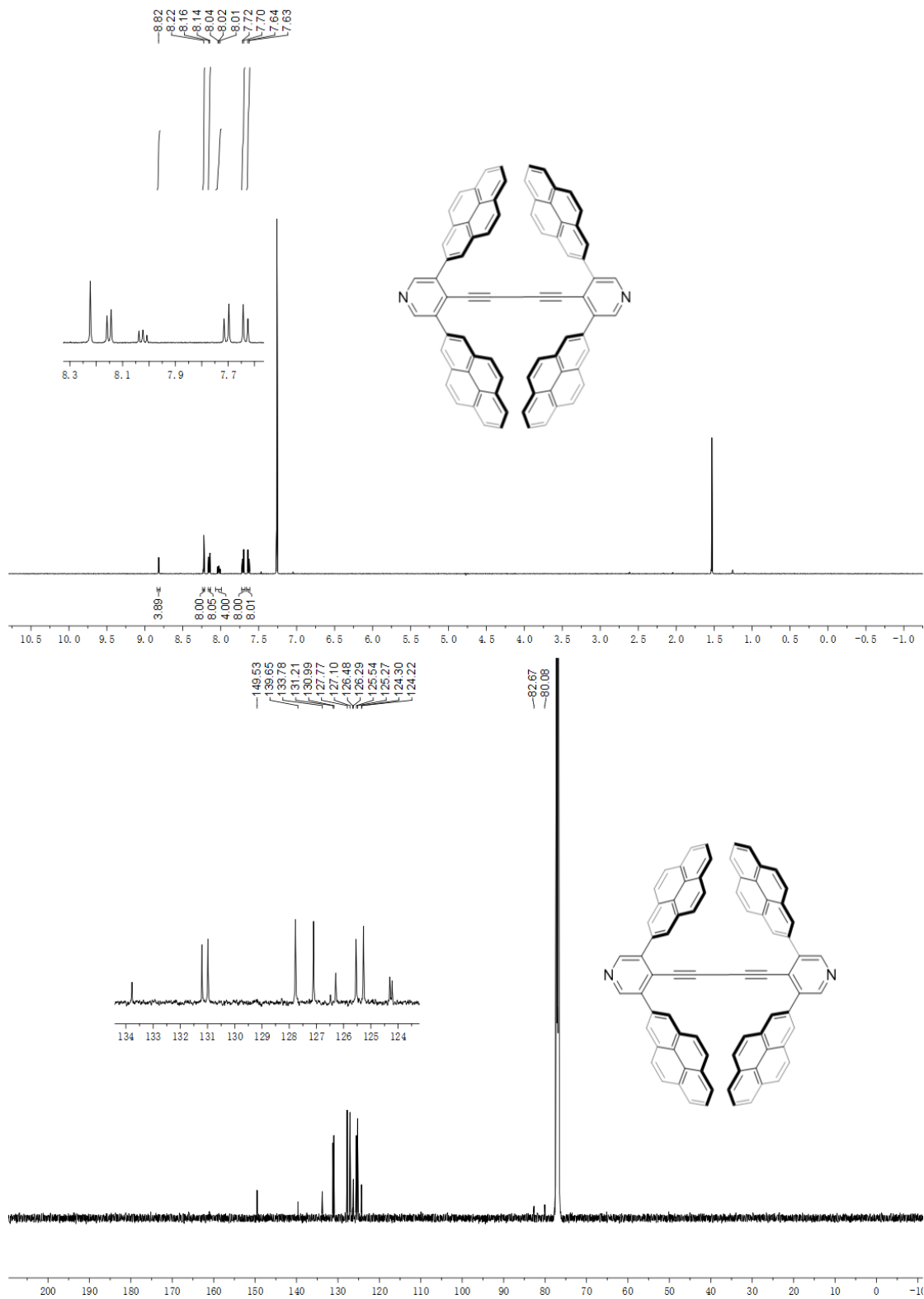
Figure 7.42. ^{1}H NMR and ^{13}C NMR spectra of compound **Py**[2e]** in CDCl$_3$.

Figure 7.43. ^{1}H NMR and ^{13}C NMR spectra of compound **2.19** in CDCl$_3$.
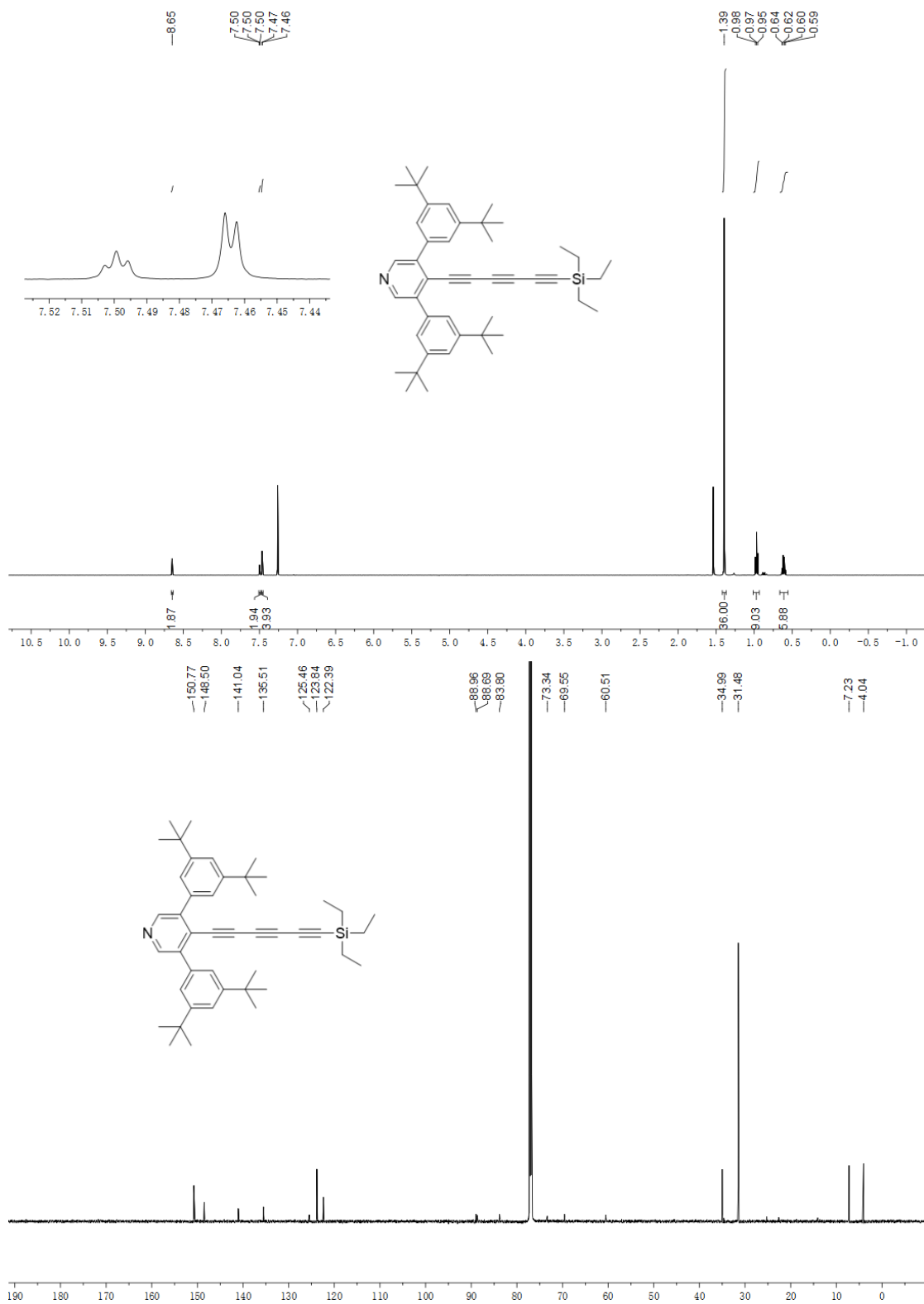
Figure 7.44. ^{1}H NMR and ^{13}C NMR spectra of compound **Py**[3a]Si** in CDCl$_3$.
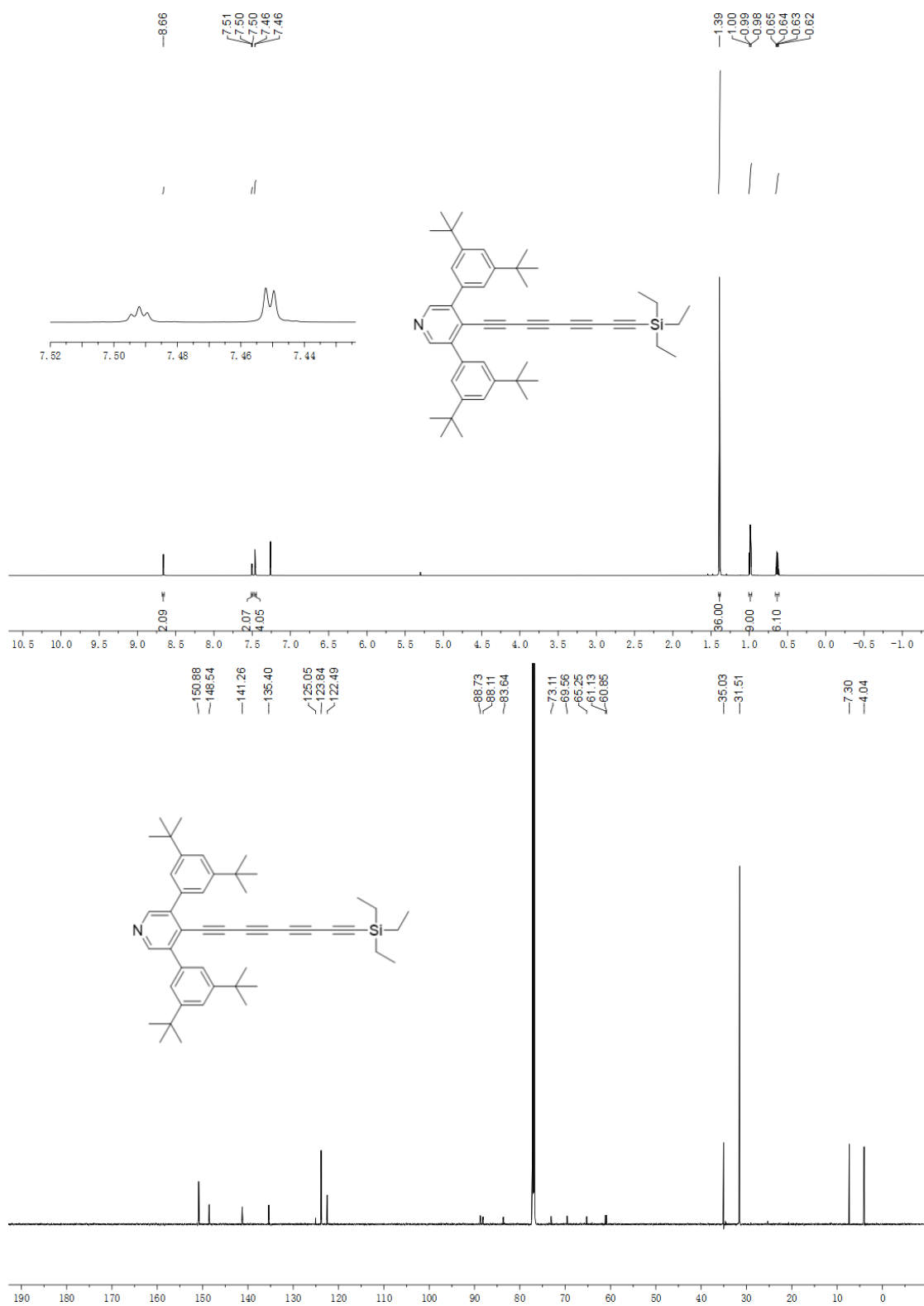
Figure 7.45. ^{1}H NMR and ^{13}C NMR spectra of compound **Py**[4a]Si** in CDCl$_3$.
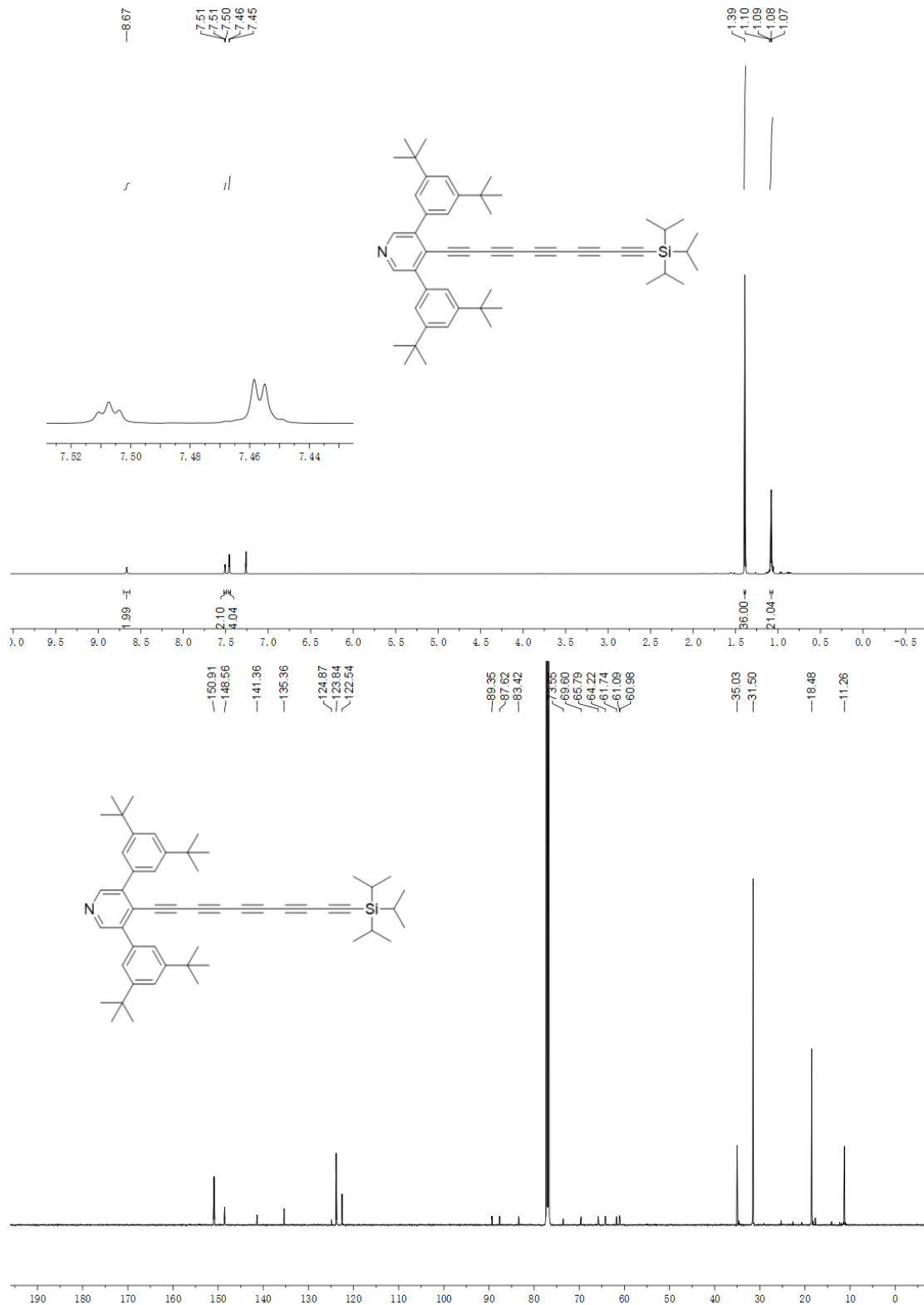
Figure 7.46. ^{1}H NMR and ^{13}C NMR spectra of compound **Py**[5a]Si** in CDCl$_3$.
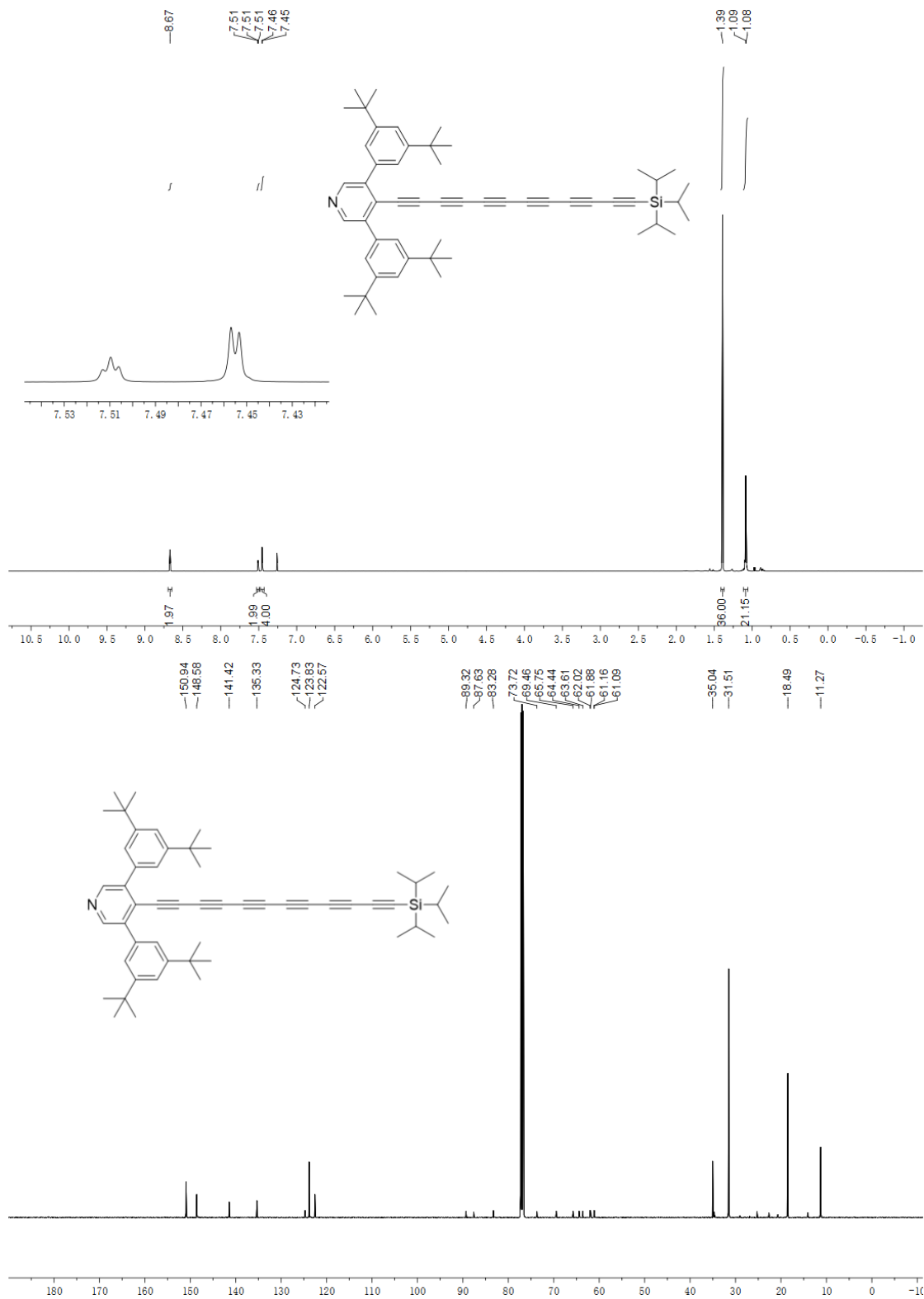
Figure 7.47. ^{1}H NMR and ^{13}C NMR spectra of compound **Py**[6a]Si** in CDCl$_3$.
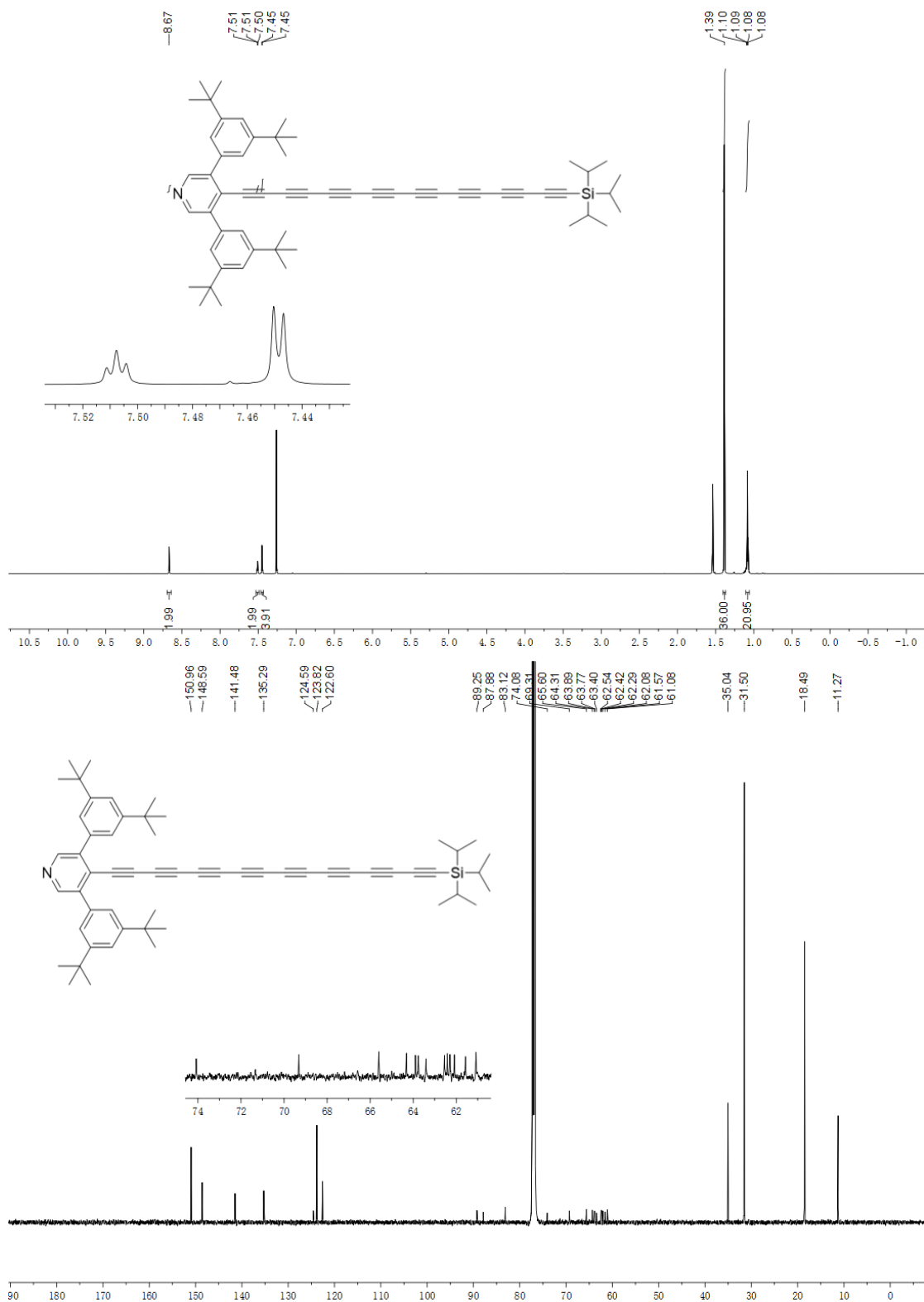
Figure 7.48. ^{1}H NMR and ^{13}C NMR spectra of compound **Py**[8a]Si** in CDCl$_3$.
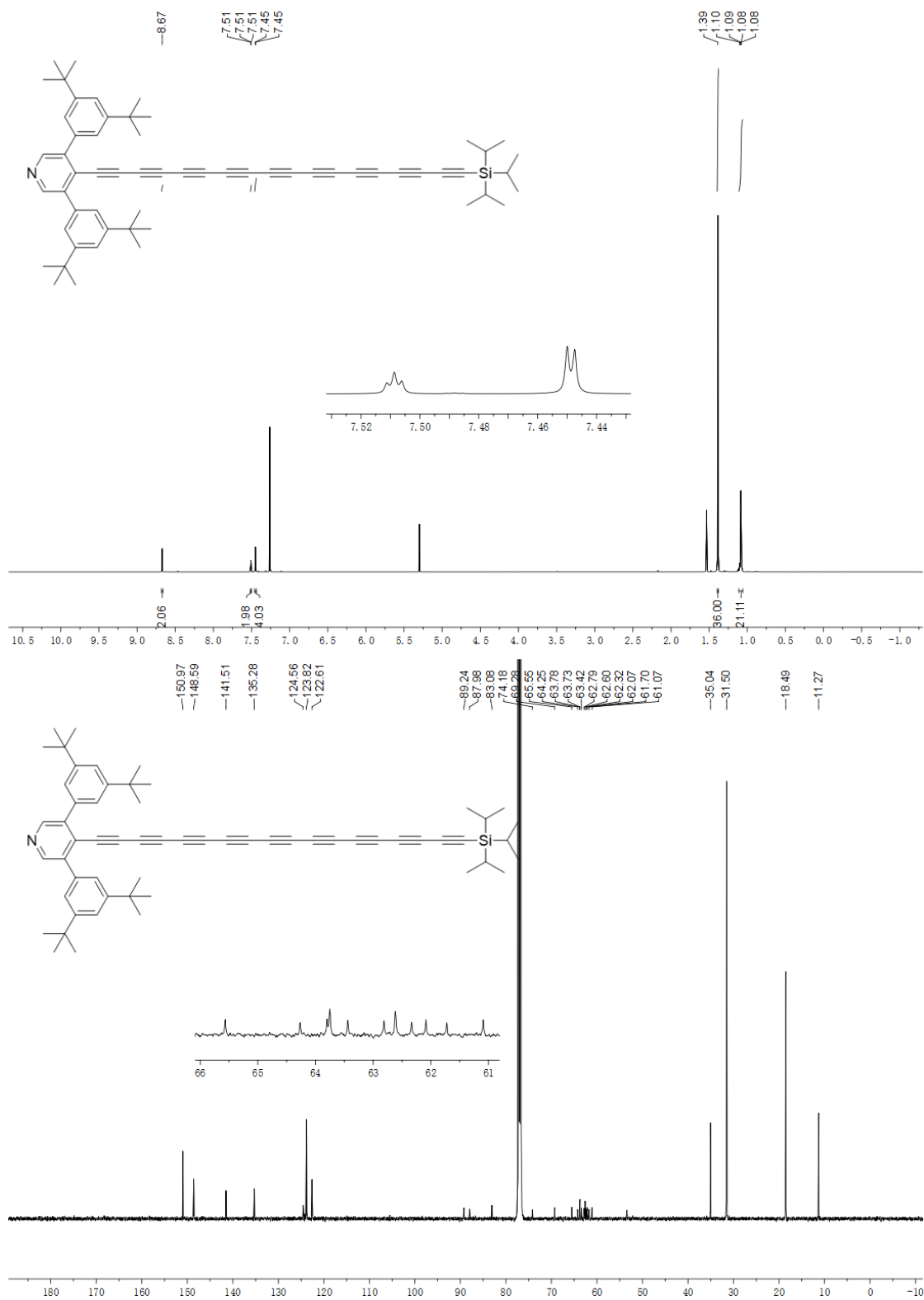
Figure 7.49. ^{1}H NMR and ^{13}C NMR spectra of compound **Py**[9a]Si** in CDCl$_3$.

270
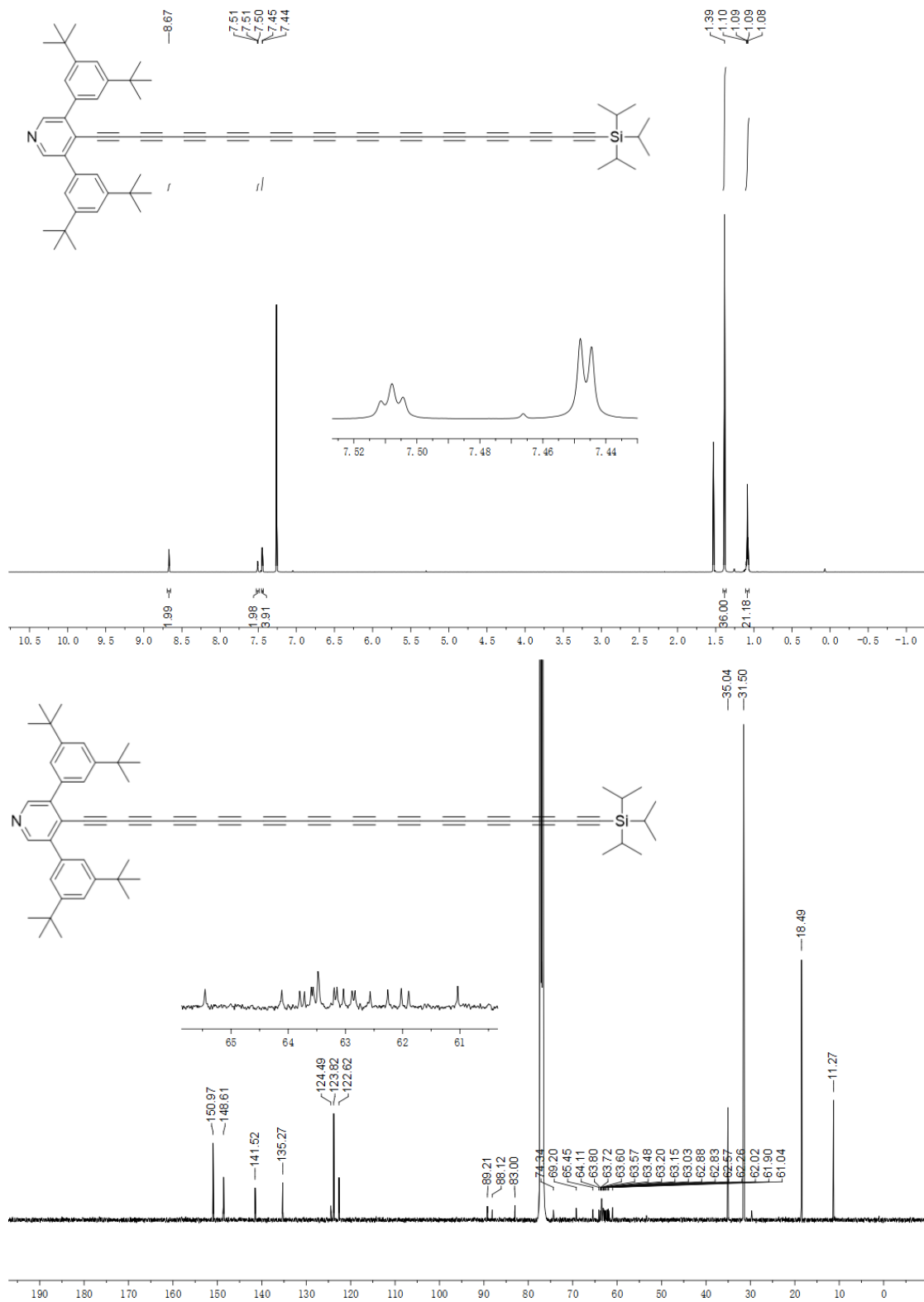
Figure 7.50. ^{1}H NMR and ^{13}C NMR spectra of compound **Py**[12a]Si** in CDCl$_3$.
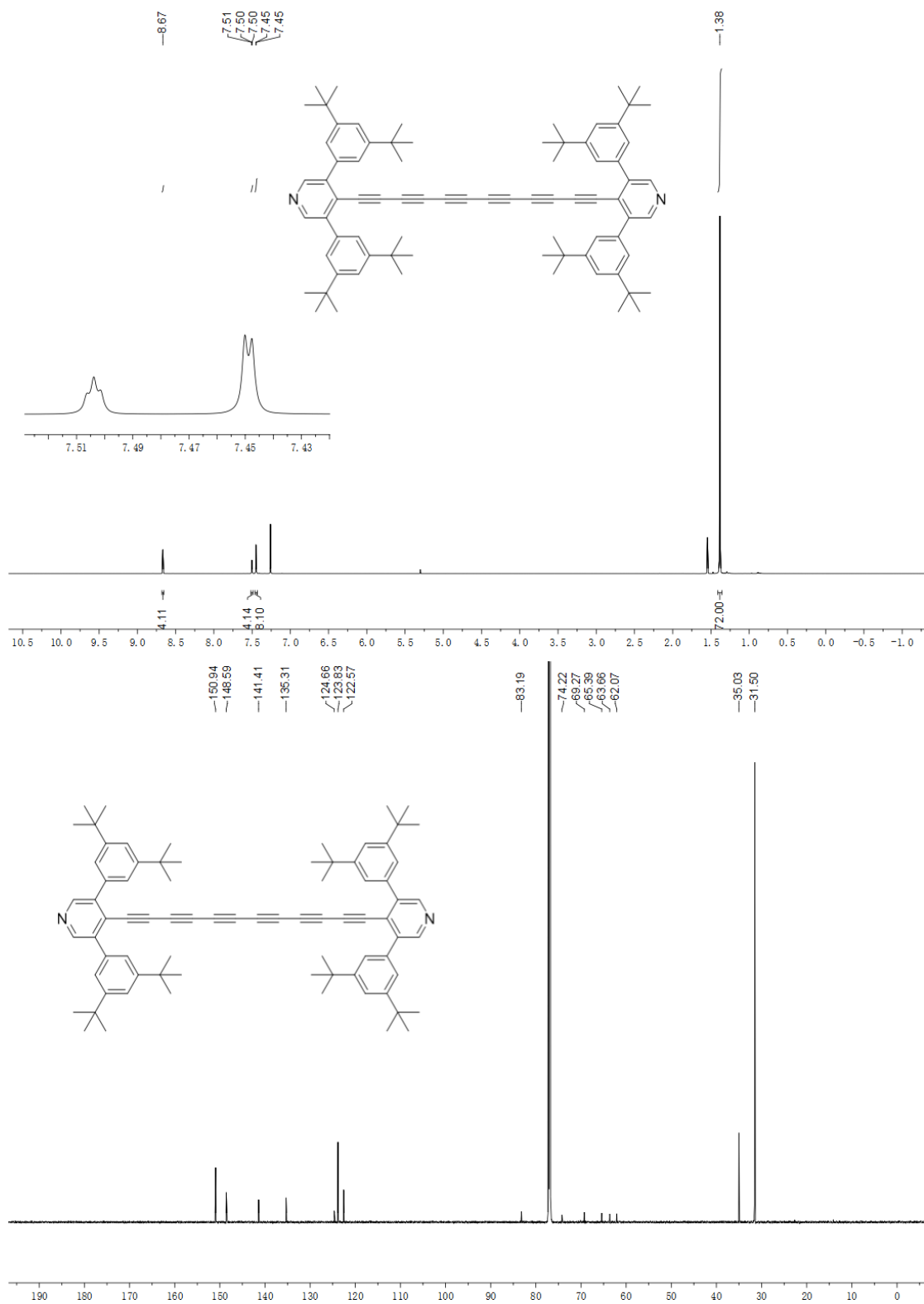
Figure 7.51. ^{1}H NMR and ^{13}C NMR spectra of compound **Py**[6a]** in CDCl₃.
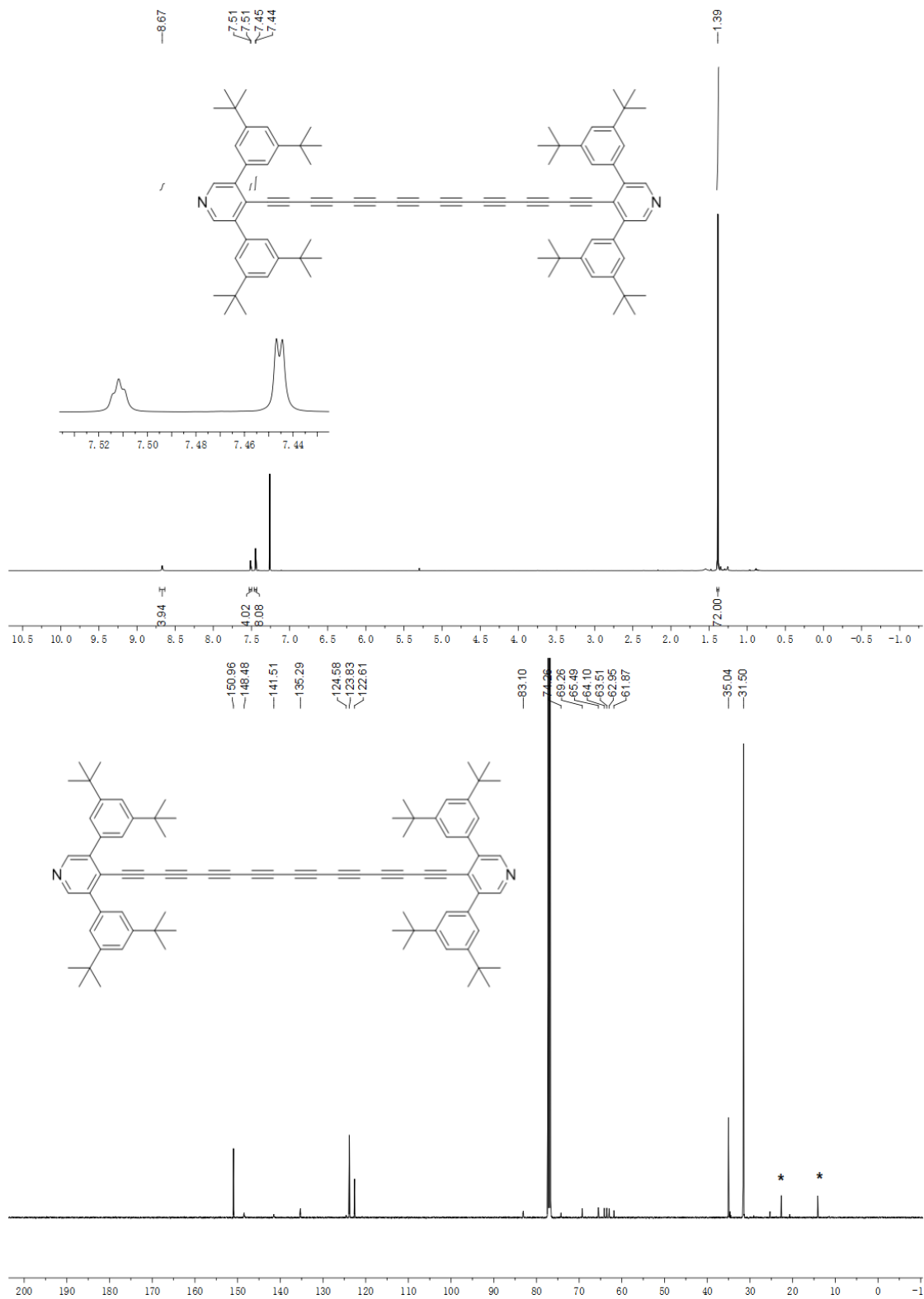
Figure 7.52. ^{1}H NMR and ^{13}C NMR spectra of compound **Py******[8a]** in CDCl$_3$ (* indicates hexanes).
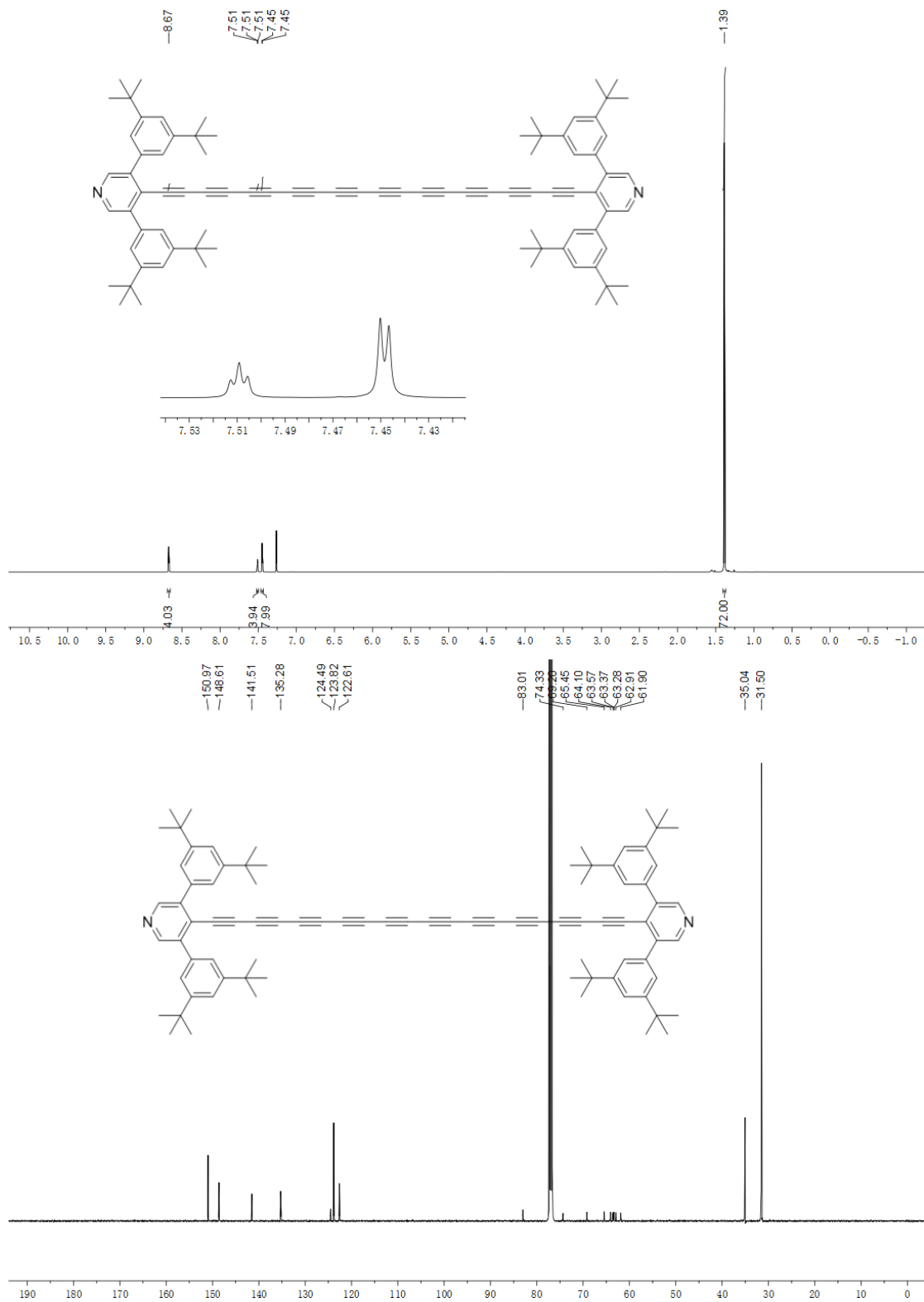
Figure 7.53. ^{1}H NMR and ^{13}C NMR spectra of compound **Py**[10a]** in CDCl$_3$.
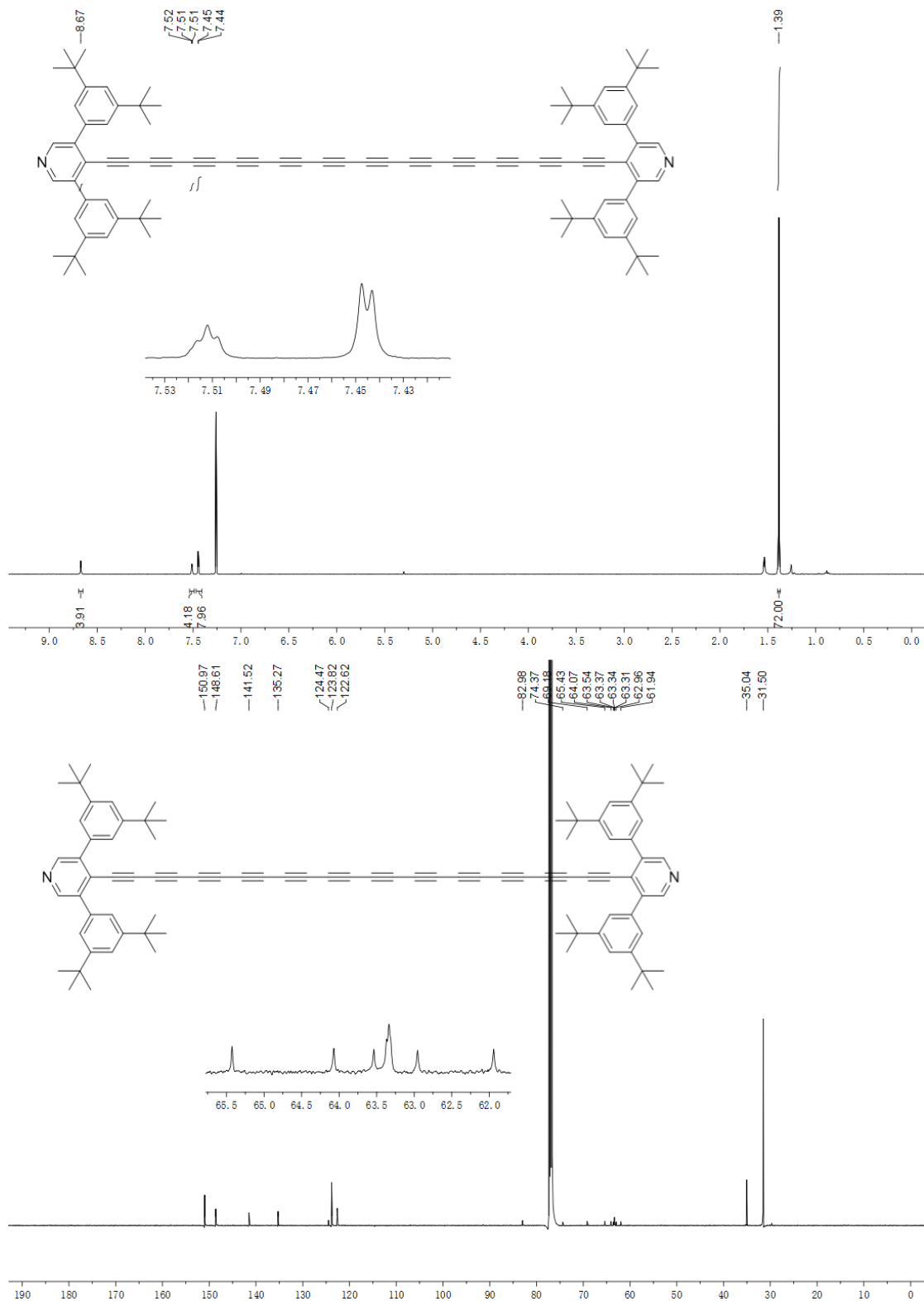
Figure 7.54. ^{1}H NMR and ^{13}C NMR spectra of compound **Py****[12a] in CDCl$_3$.
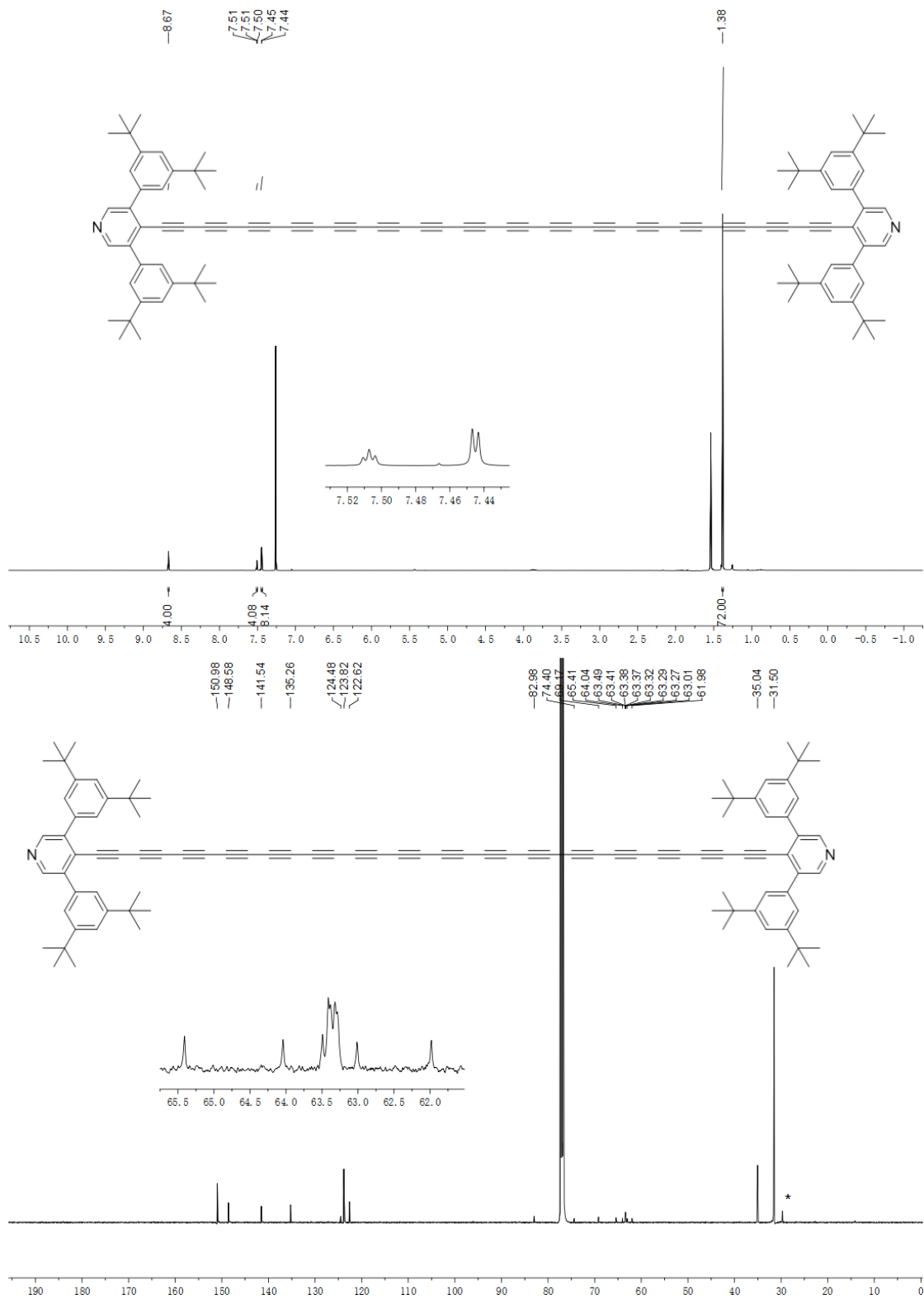
Figure 7.55. ¹H NMR and ¹³C NMR spectra of compound **Py**[16a]** in CDCl₃ (* indicates H grease).
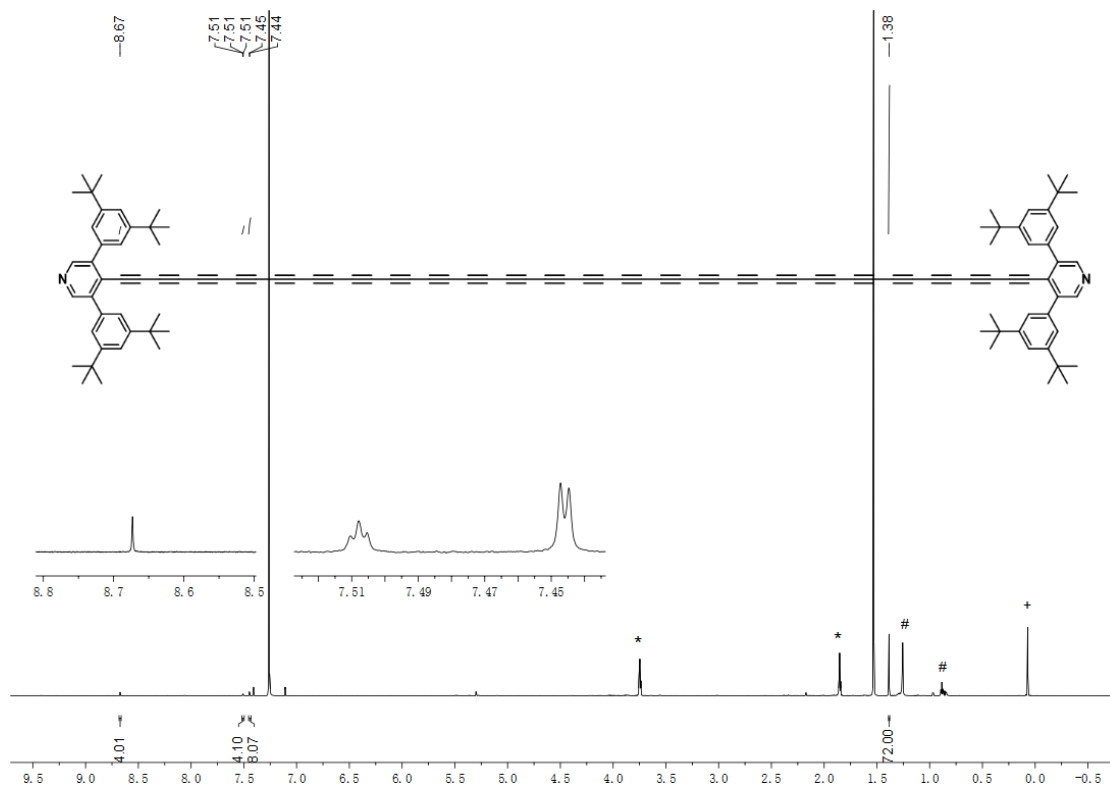
Figure 7.56. ^{1}H NMR spectrum of compound **Py****[24a] in CDCl$_3$ (* indicates THF, # hexanes, and + silicone grease).

7.6.2 Spectra of Chapter 3
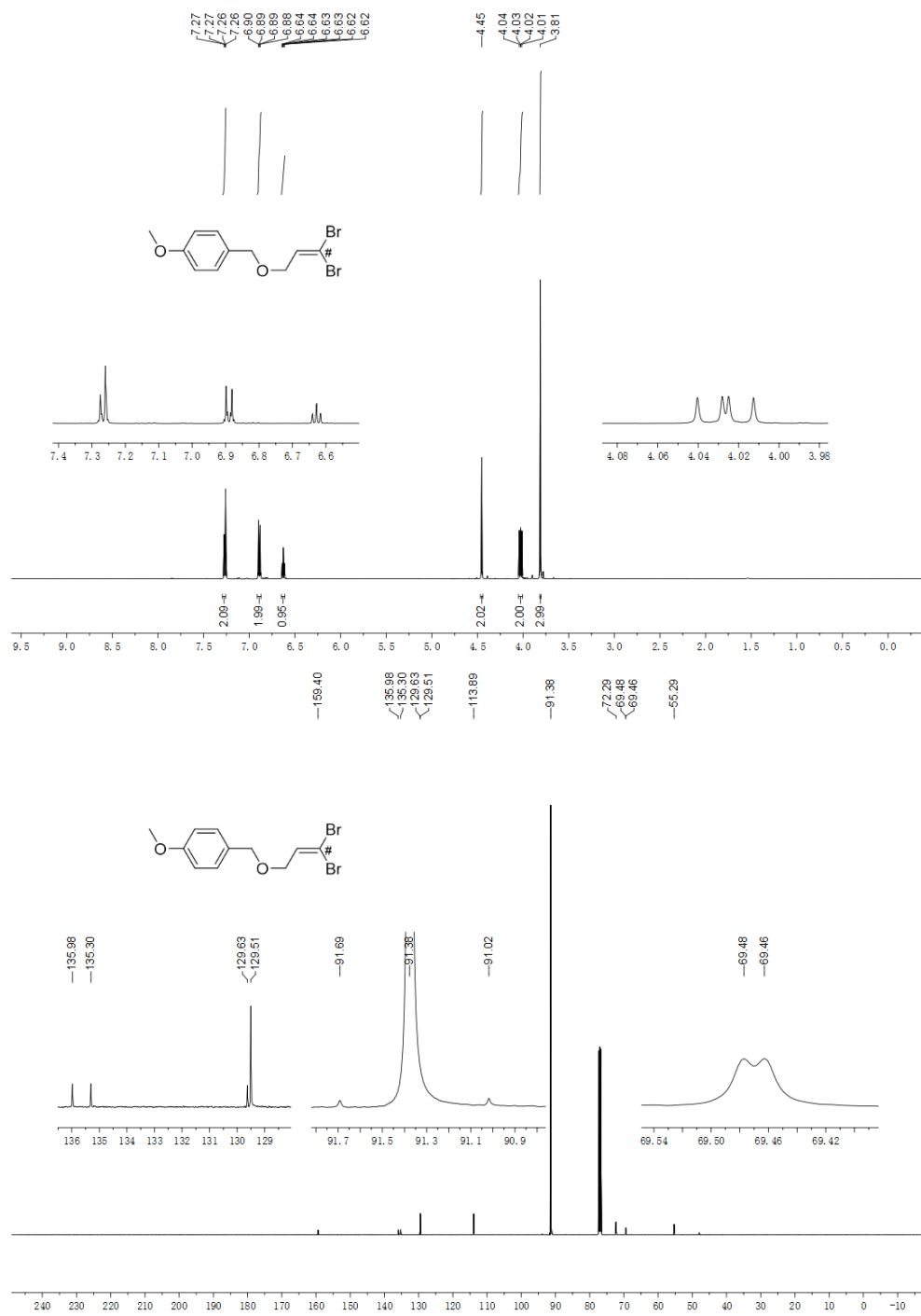
Figure 7. 57. ^{1}H NMR and ^{13}C NMR spectra of compound **3.4** in CDCl$_3$.
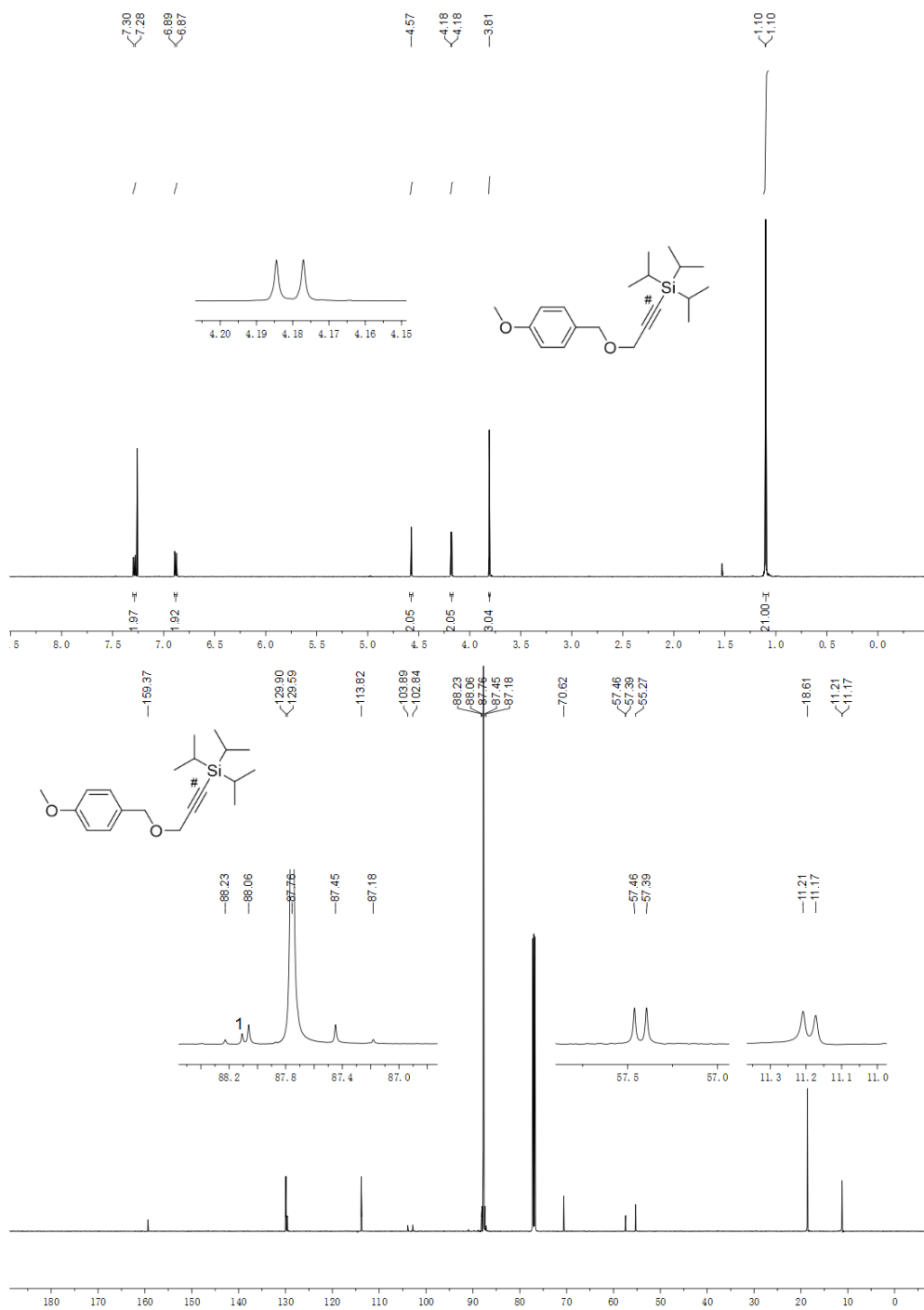
Figure 7.58. ^{1}H NMR and ^{13}C NMR spectra of compound **3.5** in CDCl$_3$ (^{1}denotes an unknown signal).
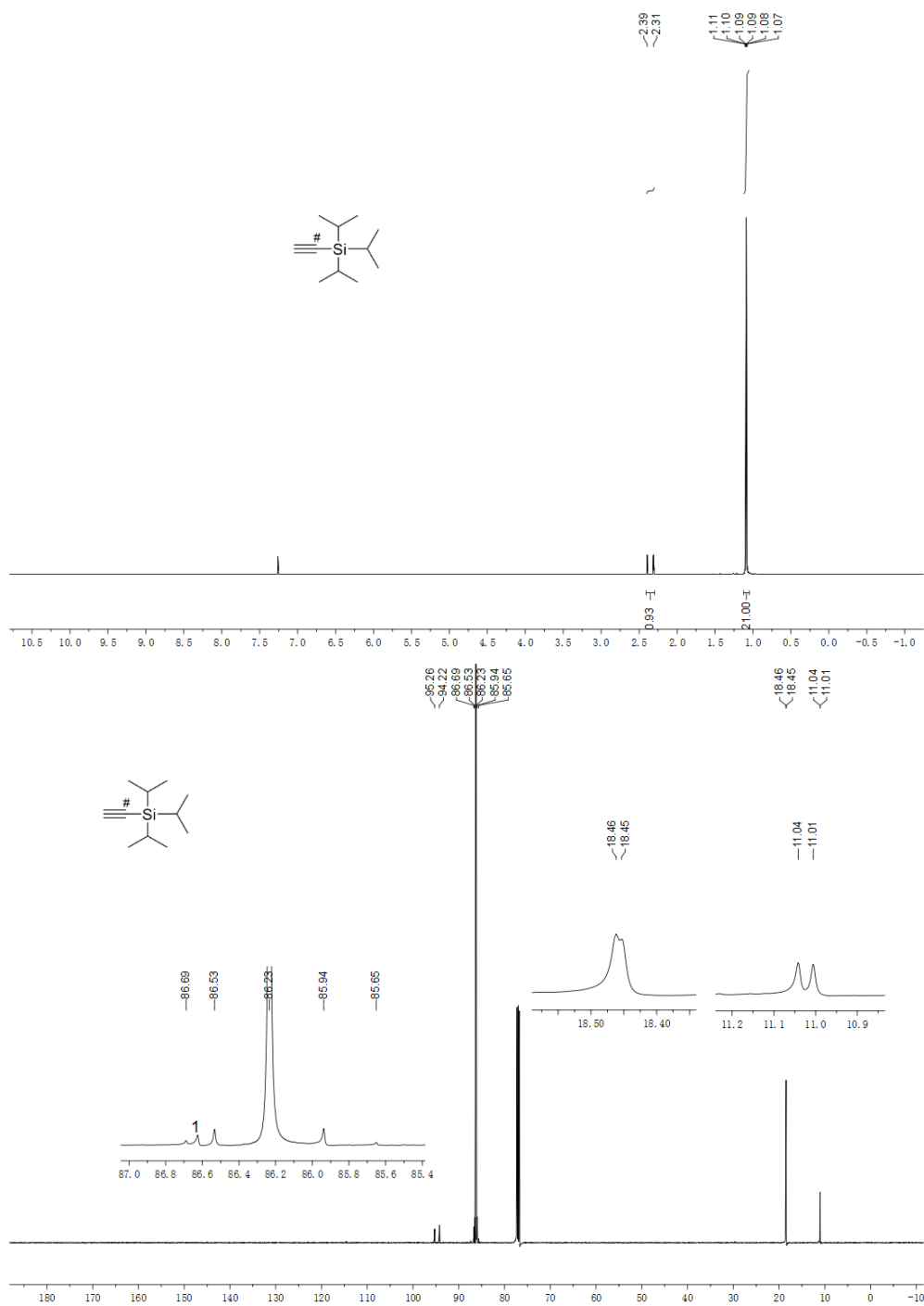
Figure 7.59. ^{1}H NMR and ^{13}C NMR spectra of compound **3.6** in CDCl$_3$ (^{1}denotes an unknown signal).
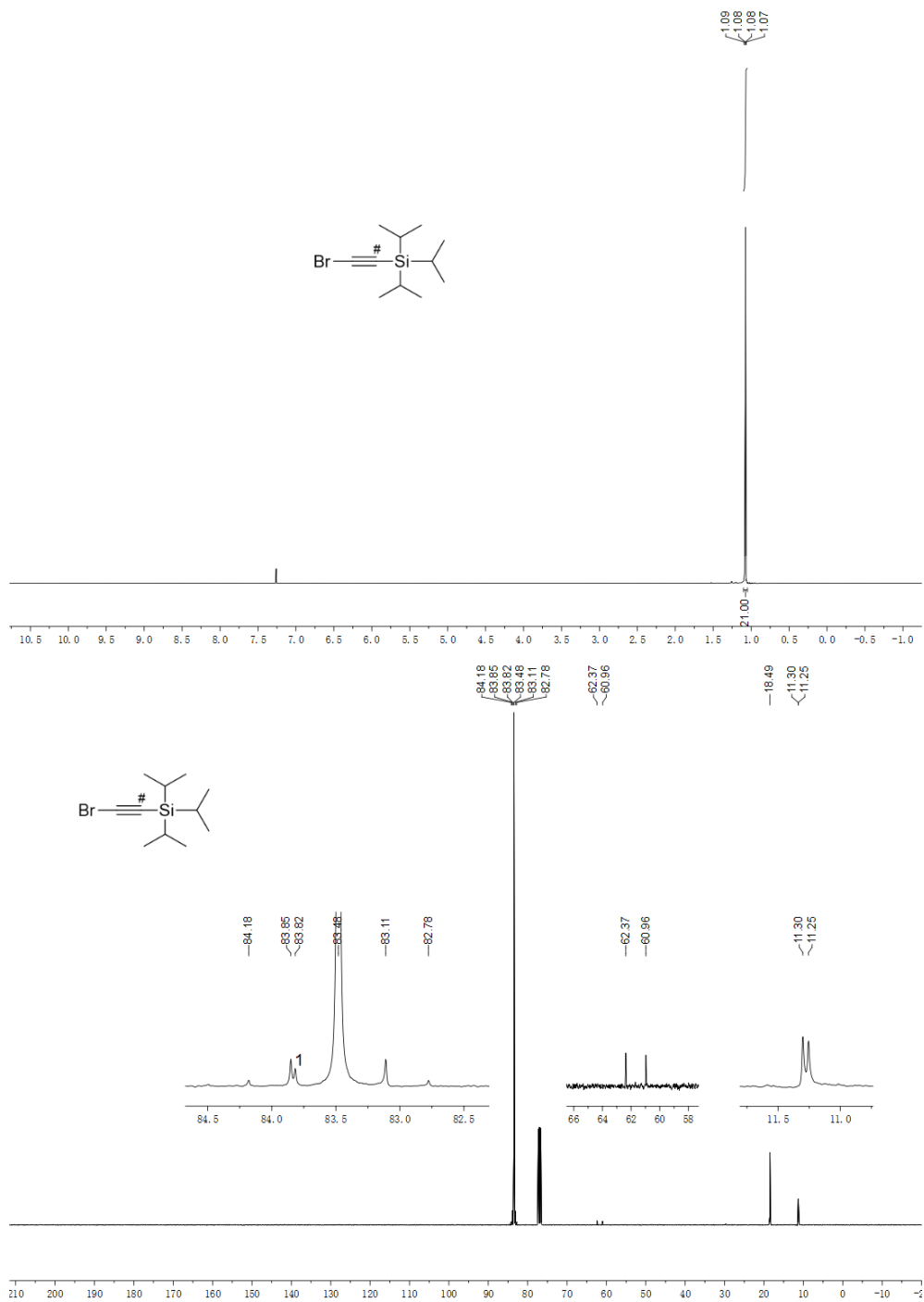
Figure 7.60. ^{1}H NMR and ^{13}C NMR spectra of compound **3.7** in CDCl$_3$ (^{1}denotes an unknown signal).
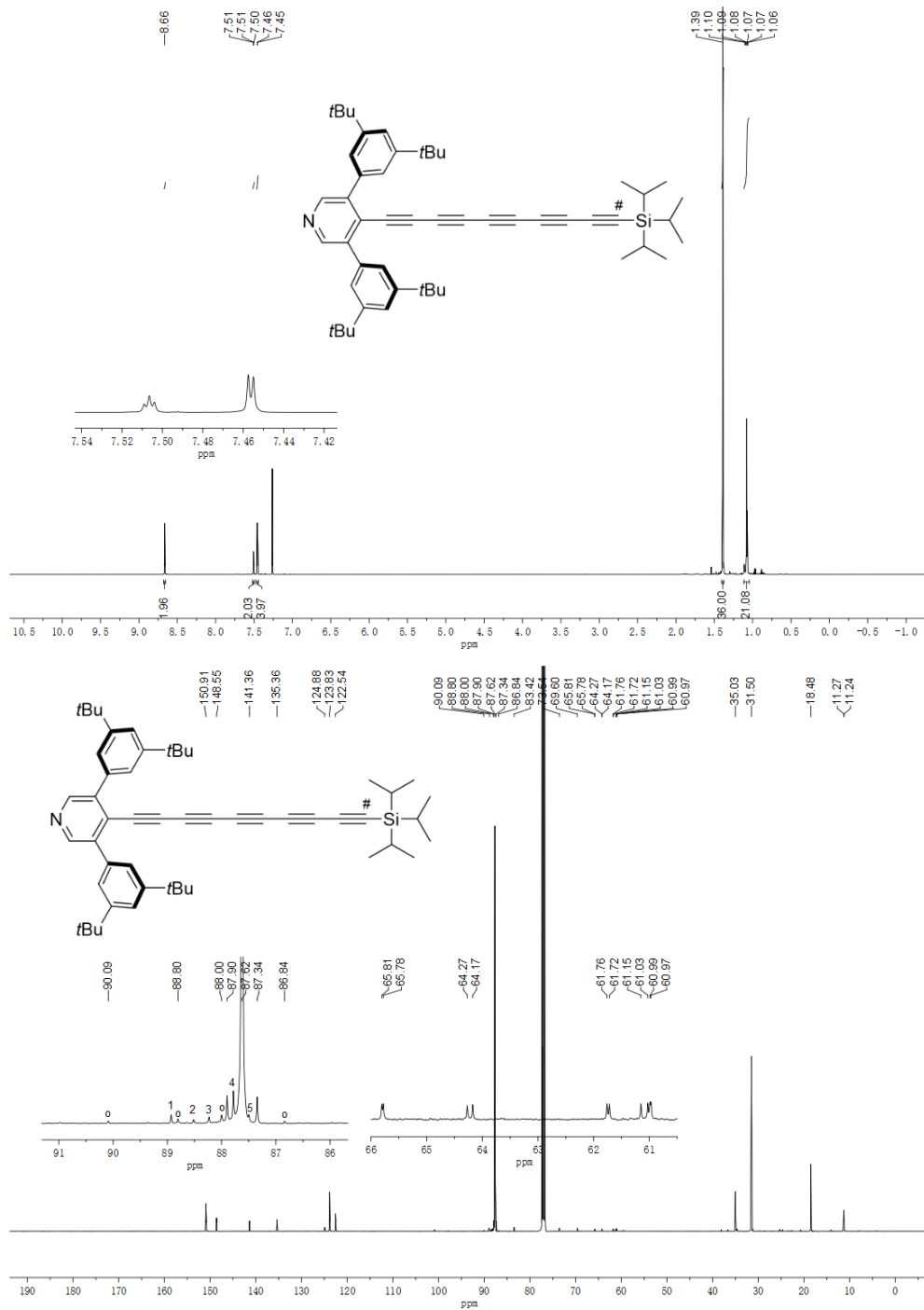
Figure 7.61. ^{1}H NMR and ^{13}C NMR spectra of compound **Py**[5a]Si$^\#$** in CDCl$_3$ (°denotes parts of ABq, $^{1-5}$denote unknown signals).
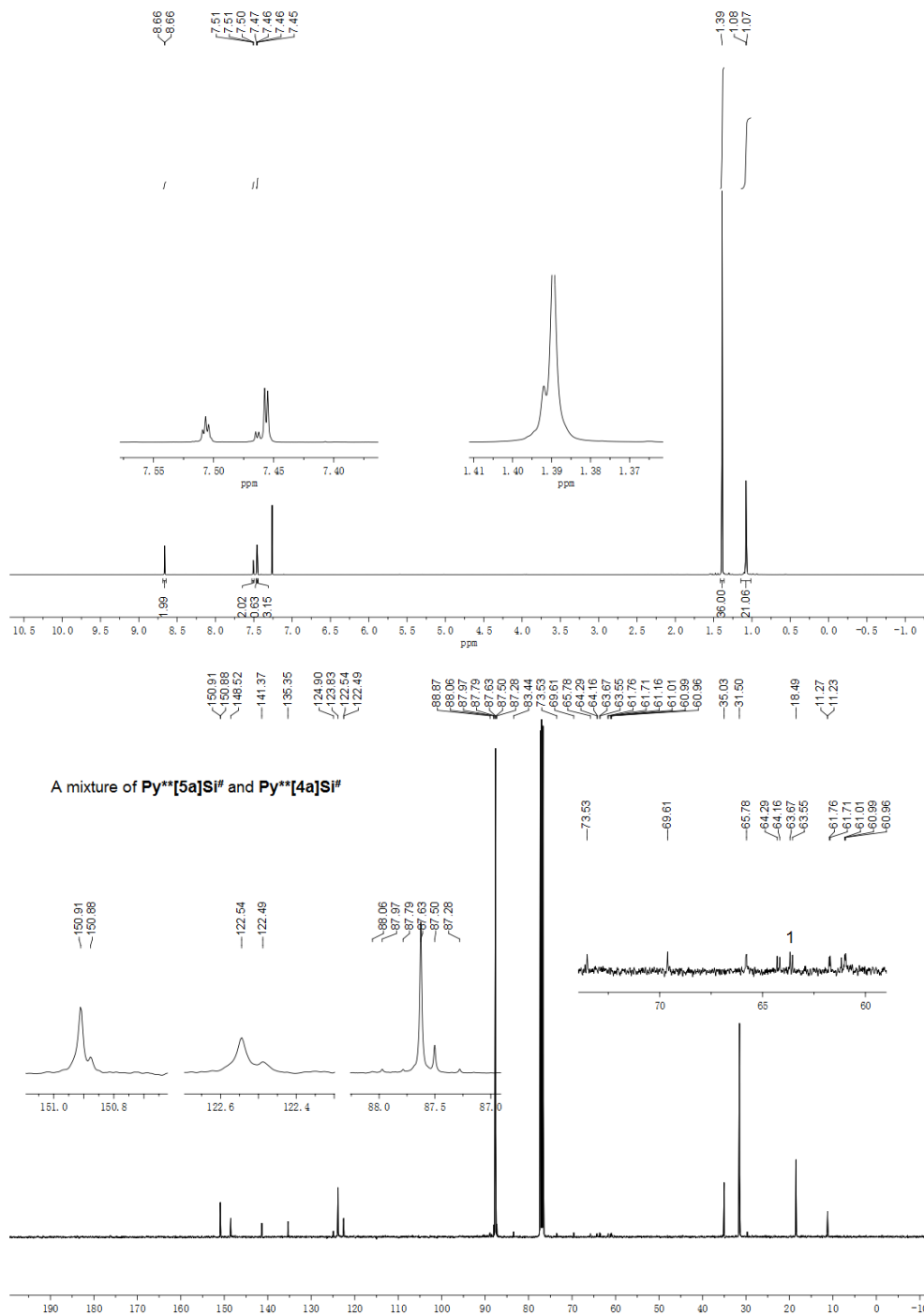
Figure 7.62. ^{1}H NMR and ^{13}C NMR spectra of a mixture of compound **Py**[5a]Si$^#$** and **Py**[4a]Si$^#$** in CDCl$_3$.^{1}Denotes unknown signals.
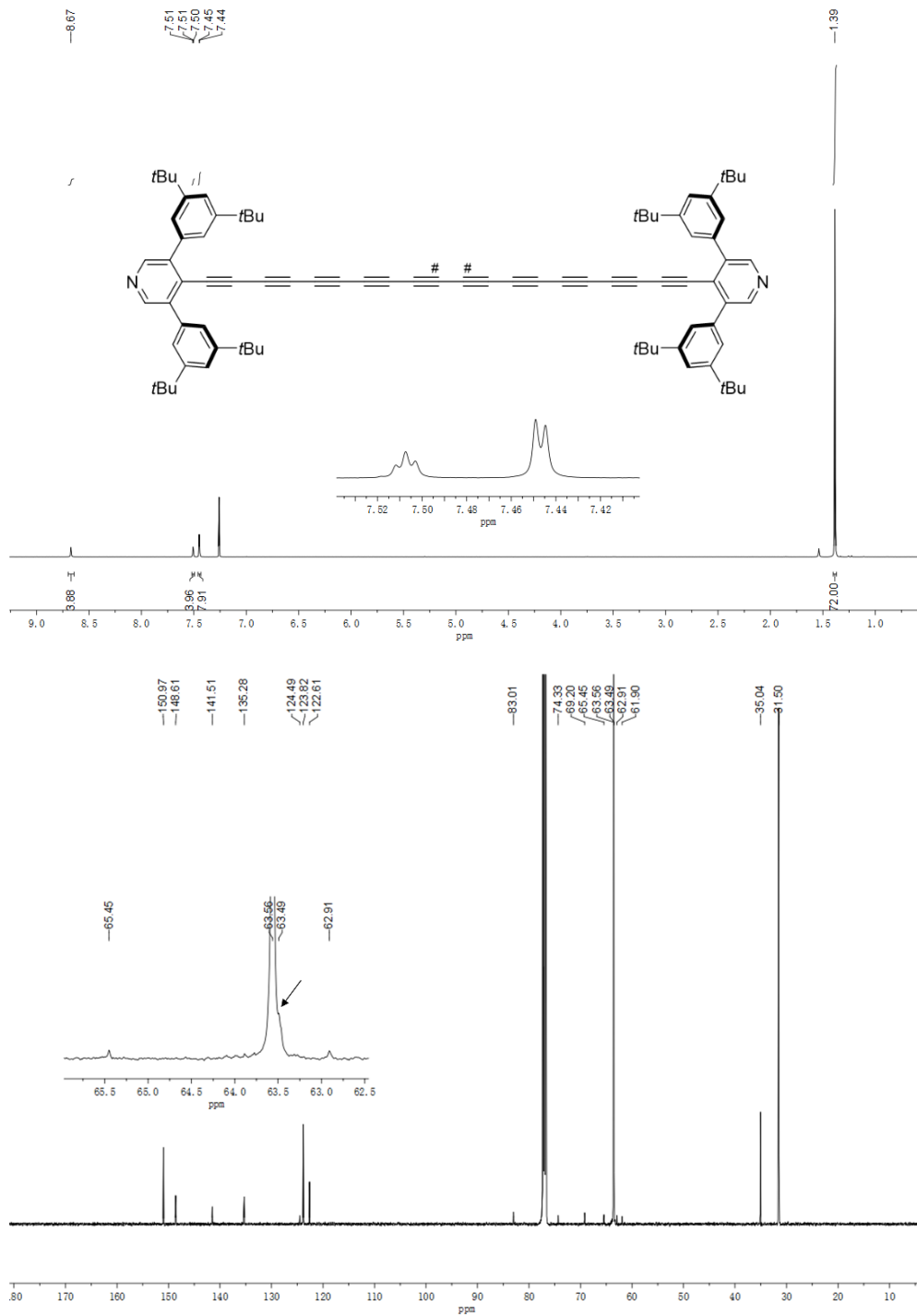
Figure 7.63. ^{1}H NMR and ^{13}C NMR spectra of a mixture of compound **Py******[10a]**$^{##}$ and **Py******[9a]**$^#$ in CDCl$_3$ (the arrow denotes the labeled carbon of **Py******[9a]**$^#$).

7.6.3 Spectra of Chapter 4
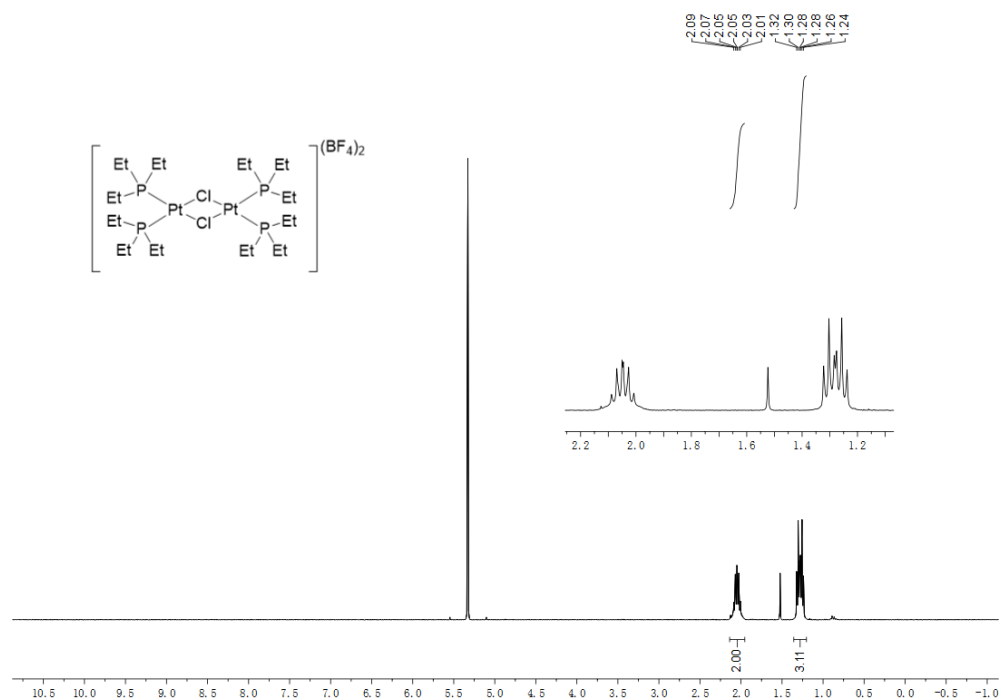
Figure 7.64. ^{1}H NMR spectrum of **4.1** in CD$_2$Cl$_2$.
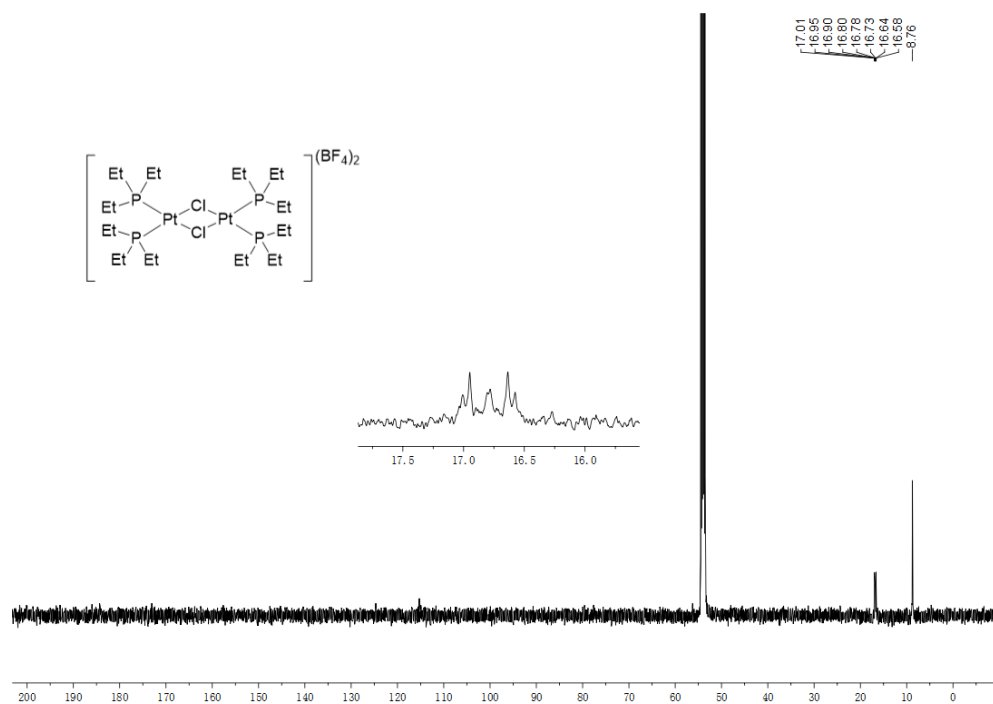
Figure 7.65. ^{13}C NMR spectrum of **4.1** in CD$_2$Cl$_2$.
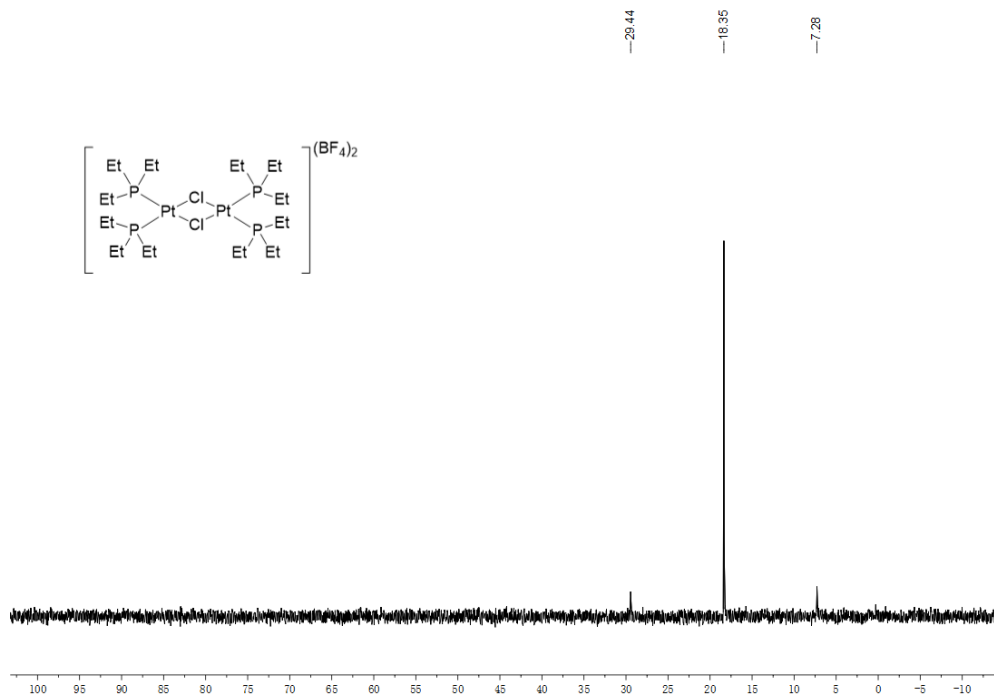
Figure 7.66. ^{31}P NMR spectrum of **4.1** in CD$_2$Cl$_2$.
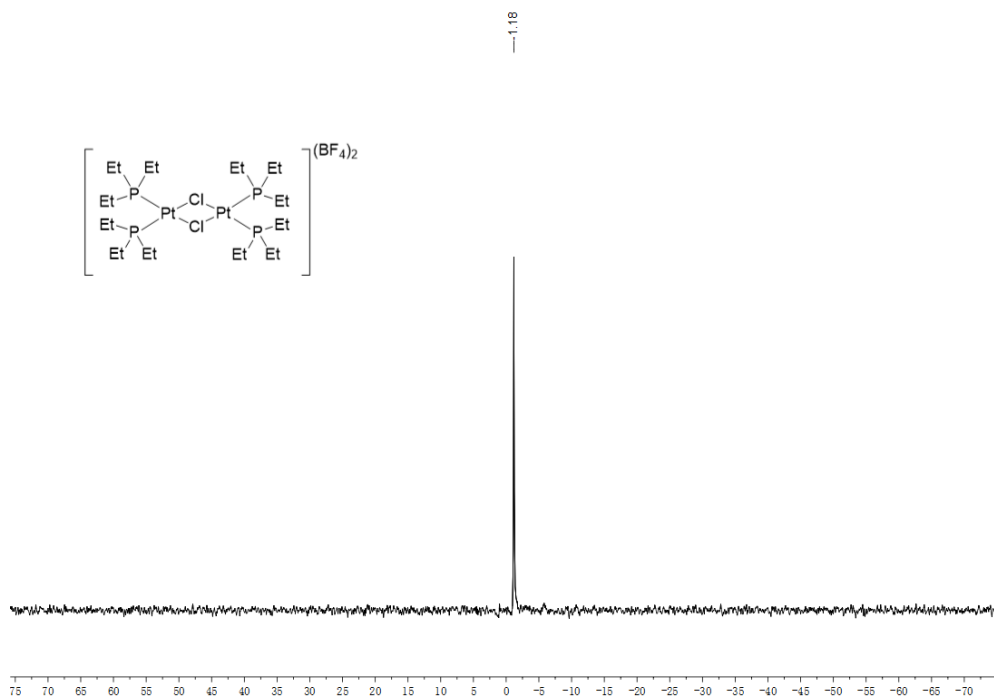
Figure 7.67. ^{11}B NMR spectrum of **4.1** in CD$_2$Cl$_2$.
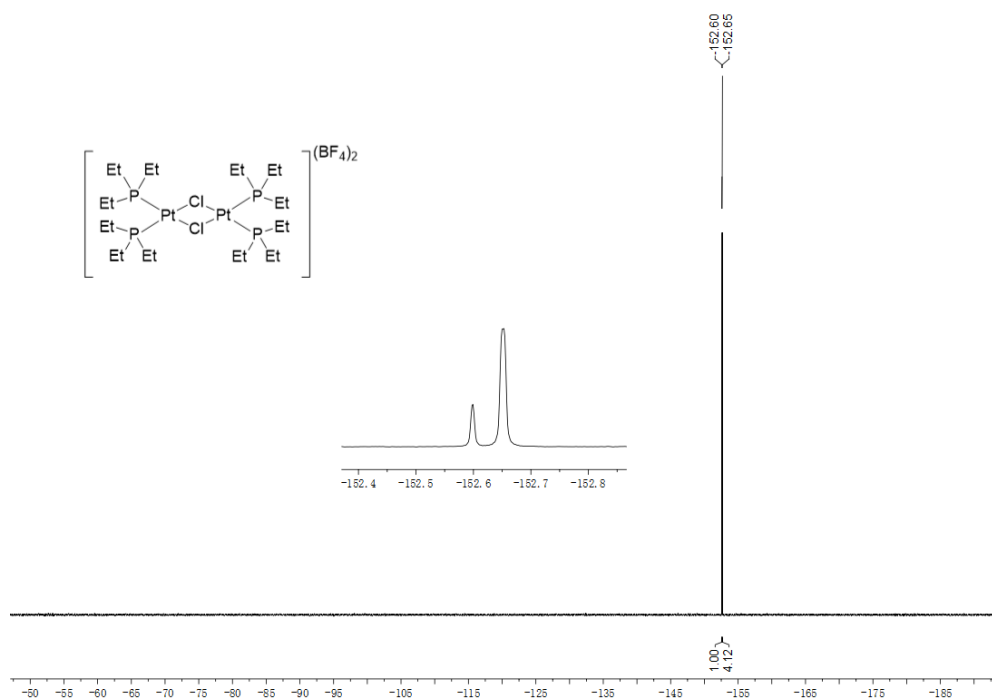
Figure 7.68. ^{19}F NMR spectrum of **4.1** in CD$_2$Cl$_2$.
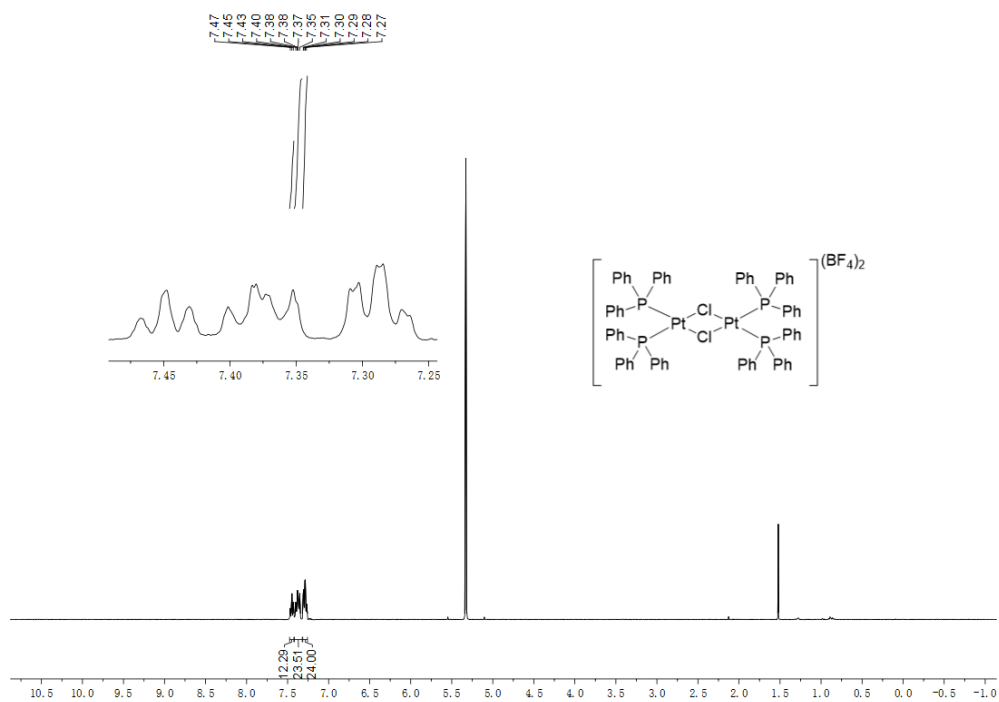
Figure 7.69. ^{1}H NMR spectrum of **4.2** in CD$_2$Cl$_2$.

287
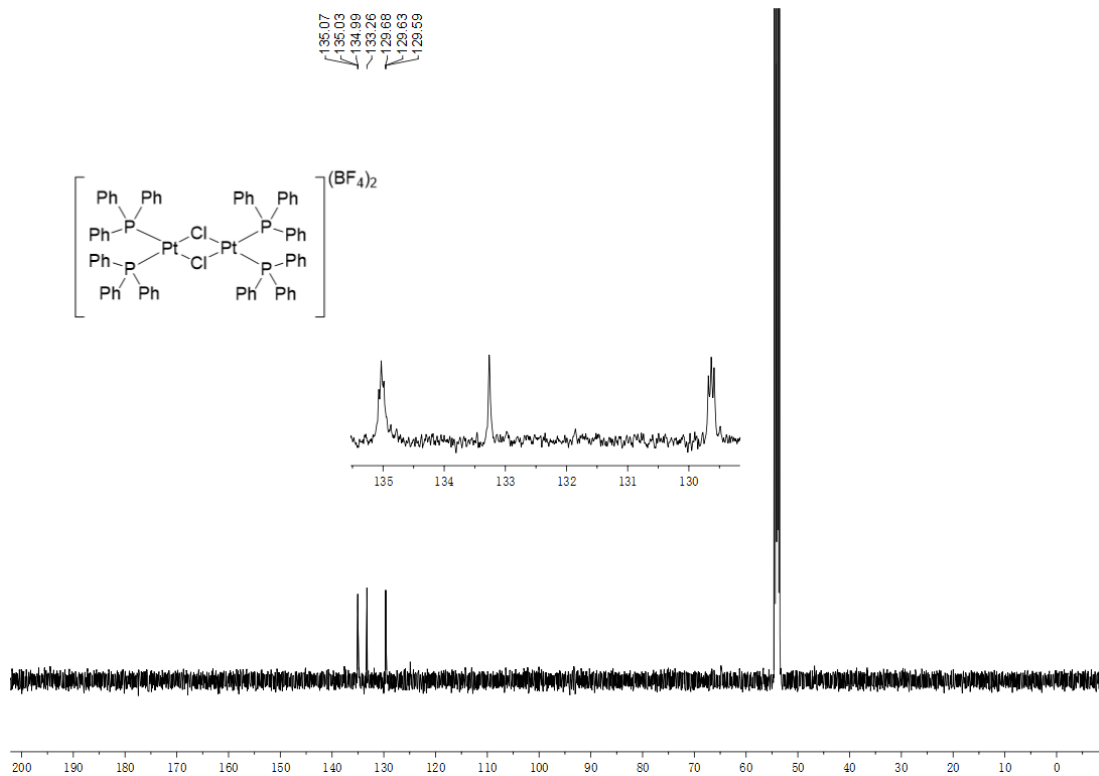
Figure 7.70. ^{13}C NMR spectrum of **4.2** in CD$_2$Cl$_2$.
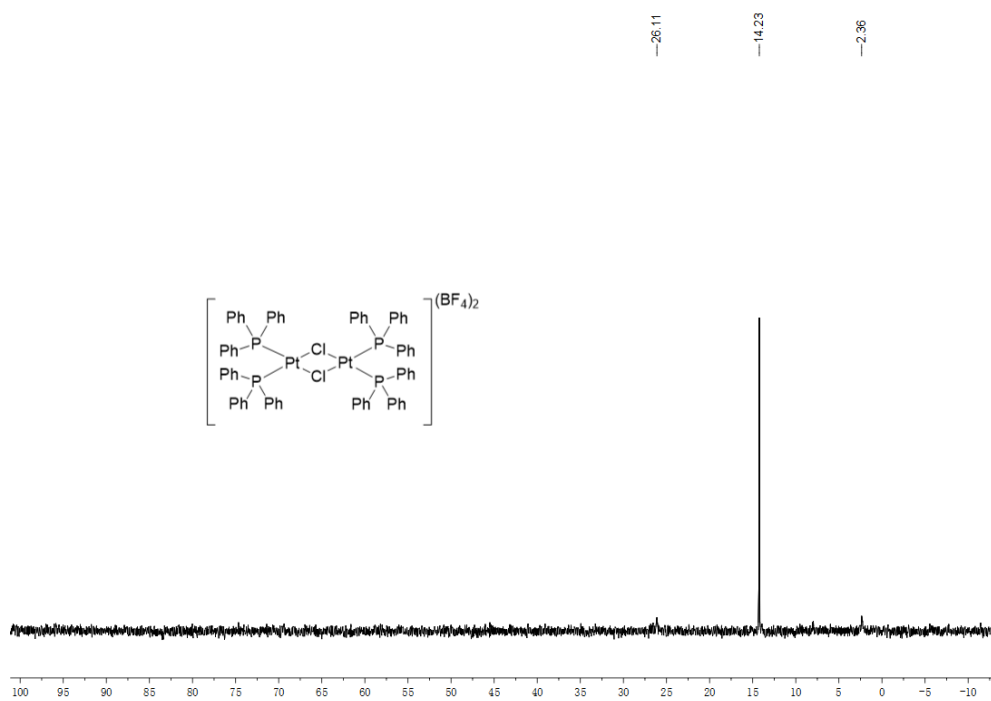
Figure 7.71. ^{31}P NMR spectrum of **4.2** in CD$_2$Cl$_2$.
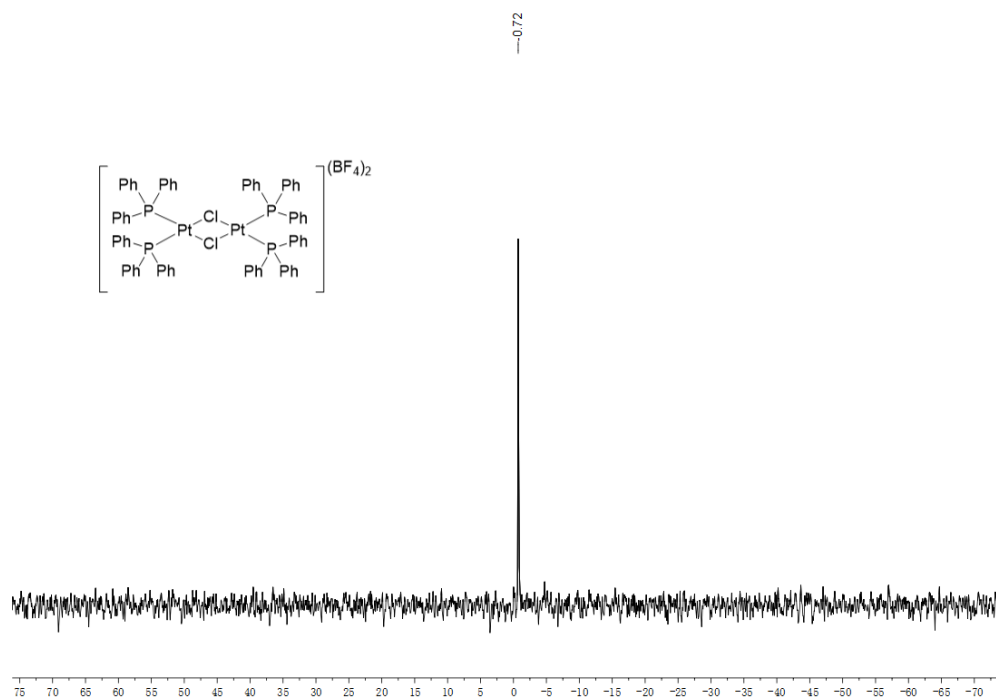
Figure 7.72. ^{11}B NMR spectrum of **4.2** in CD$_2$Cl$_2$.
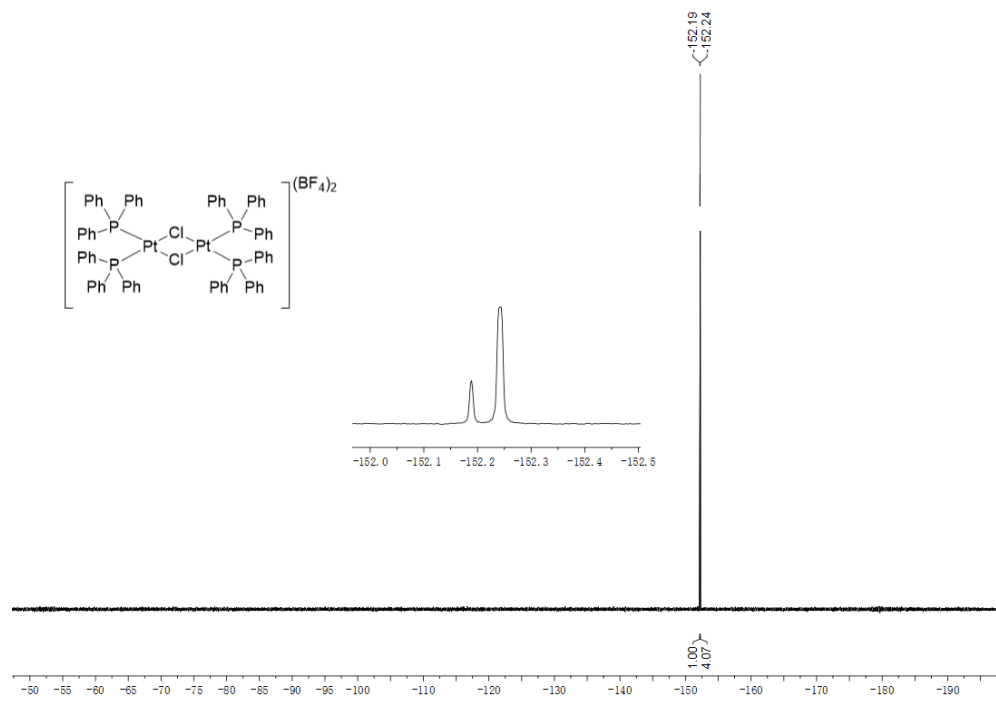
Figure 7.73. ^{19}F NMR spectrum of **4.2** in CD$_2$Cl$_2$.
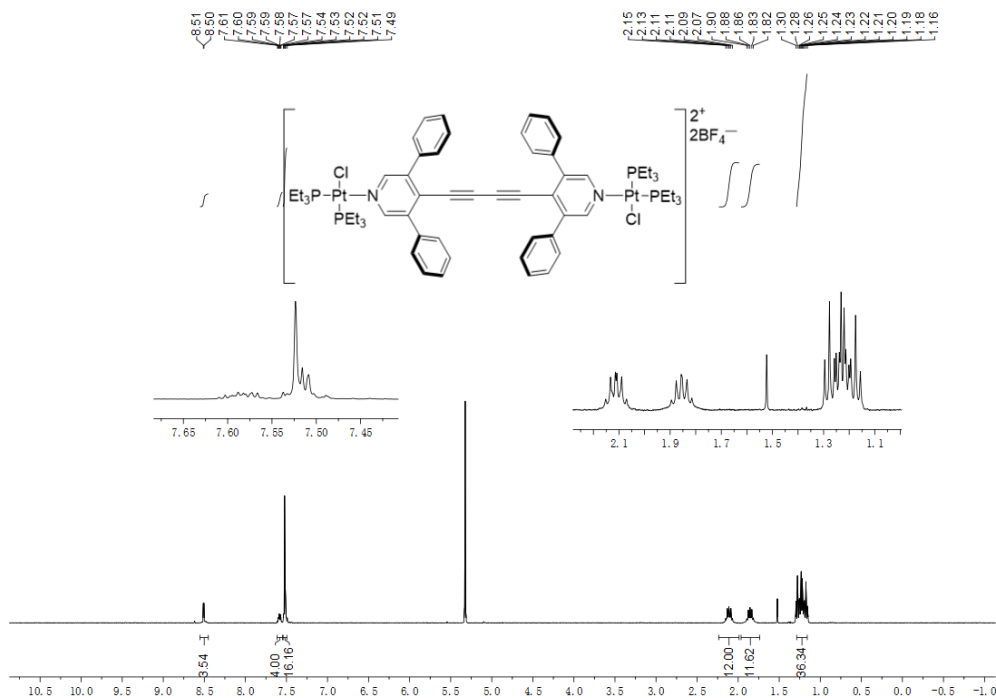
Figure 7.74. ^{1}H NMR spectrum of **(Et)-Py*[2]Pt** in CD_2Cl_2.
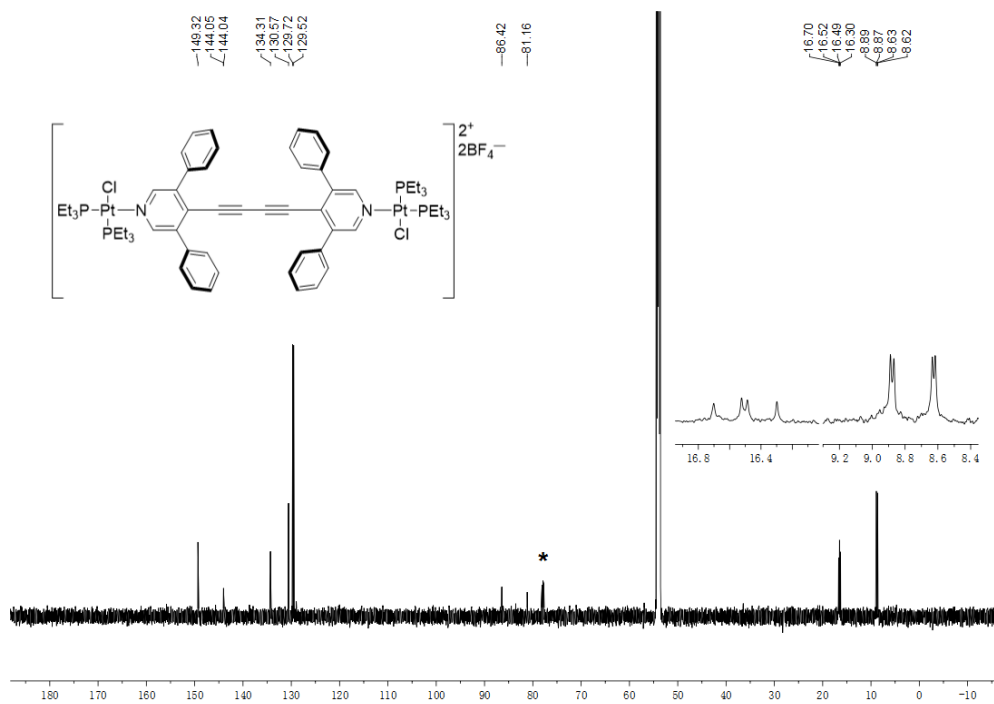
Figure 7.75. ^{13}C NMR spectrum of **(Et)-Py*[2]Pt** in CD_2Cl_2, *indicates $CHCl_3$ contamination.
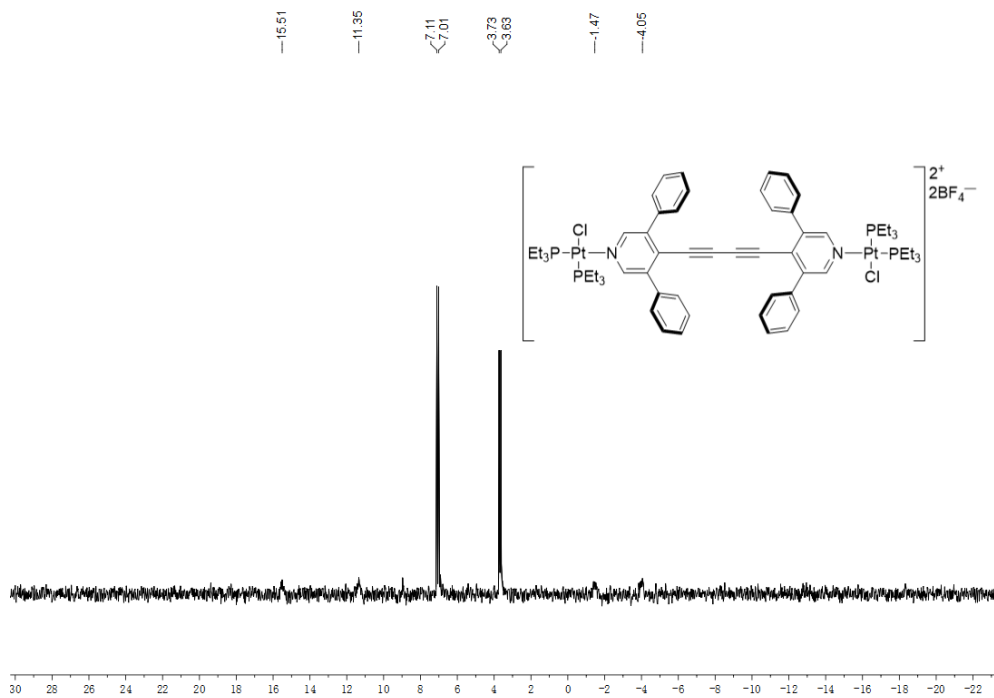
Figure 7.76. ^{31}P NMR spectrum of **(Et)-Py*[2]Pt** in CD$_2$Cl$_2$.
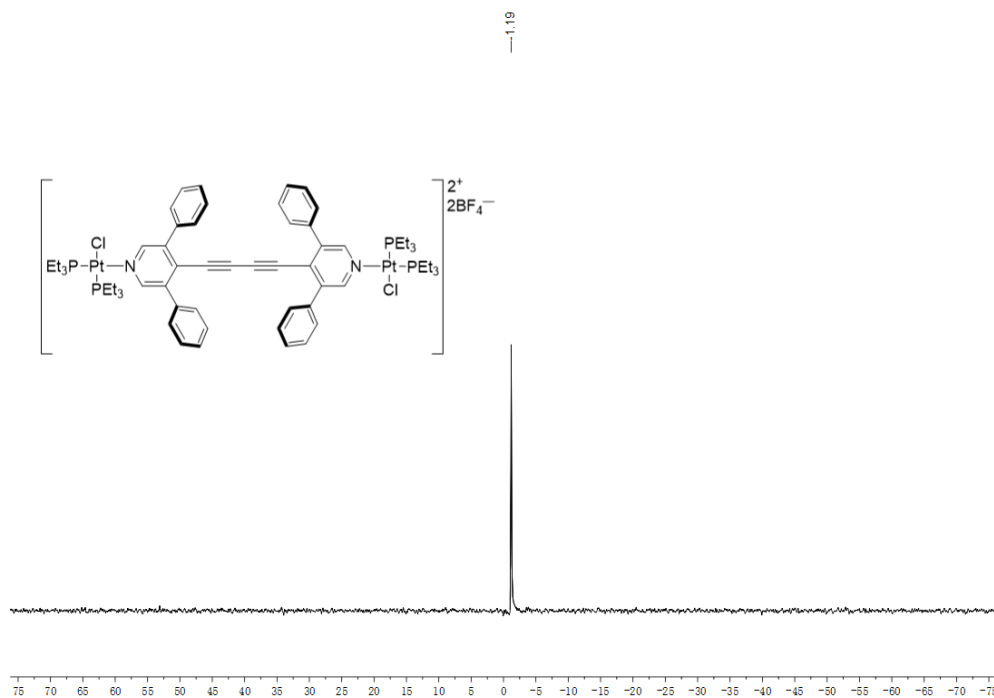
Figure 7.77. ^{11}B NMR spectrum of **(Et)-Py*[2]Pt** in CD$_2$Cl$_2$.
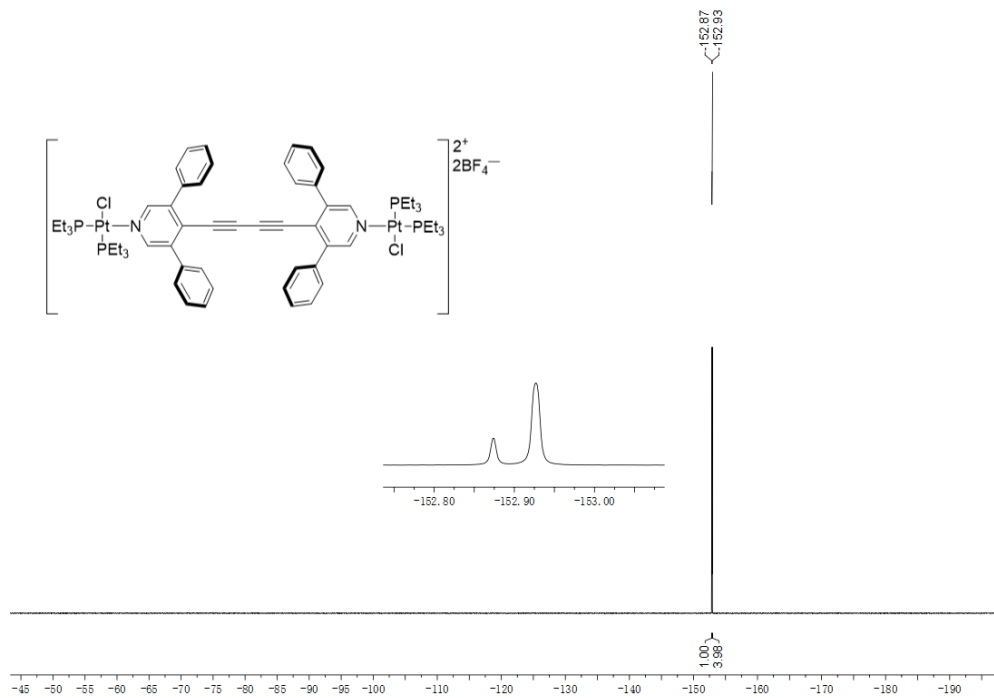
Figure 7.78. ^{19}F NMR spectrum of **(Et)-Py*[2]Pt** in CD$_2$Cl$_2$.
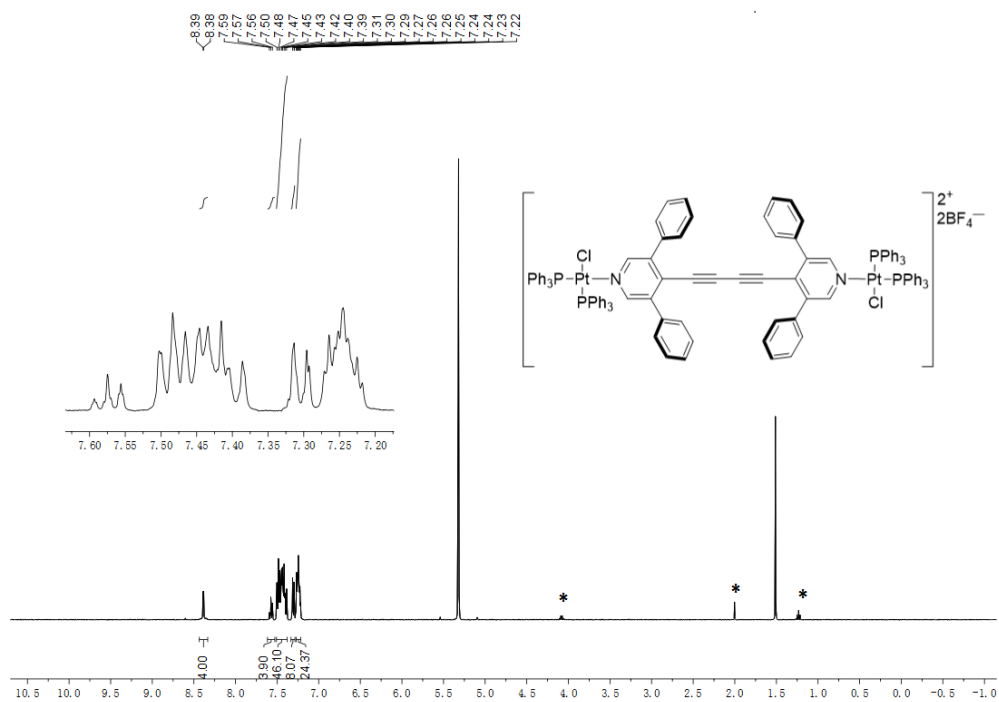
Figure 7.79. ^{1}H NMR spectrum of **(Ph)-Py*[2]Pt** in CD$_2$Cl$_2$, *indicates EtOAc contamination.
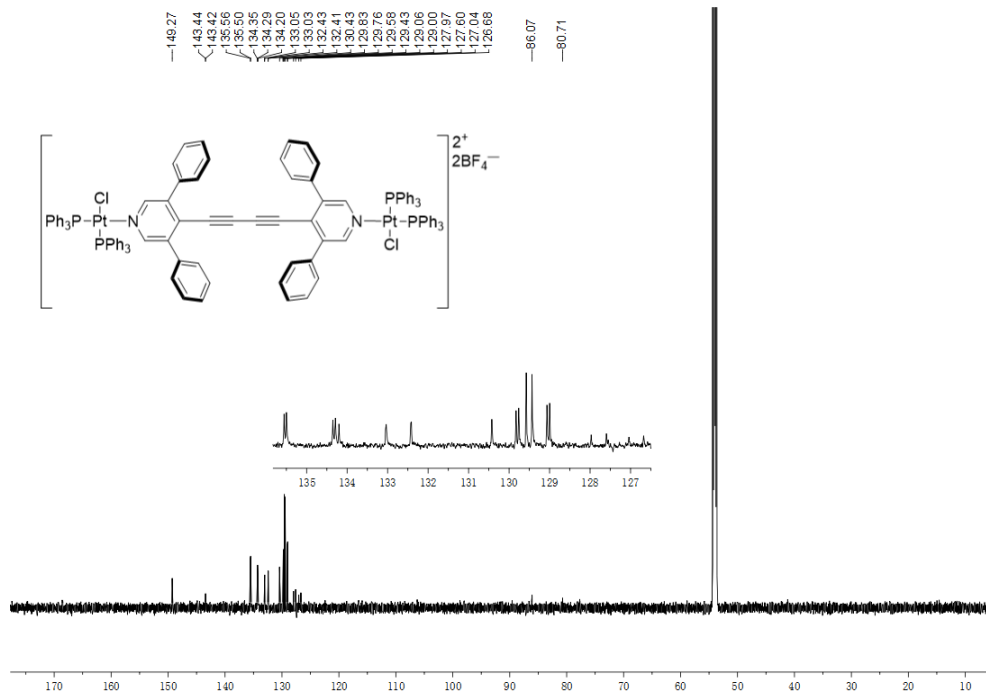
Figure 7.80. ^{13}C NMR spectrum of **(Ph)-Py*[2]Pt** in CD$_2$Cl$_2$.
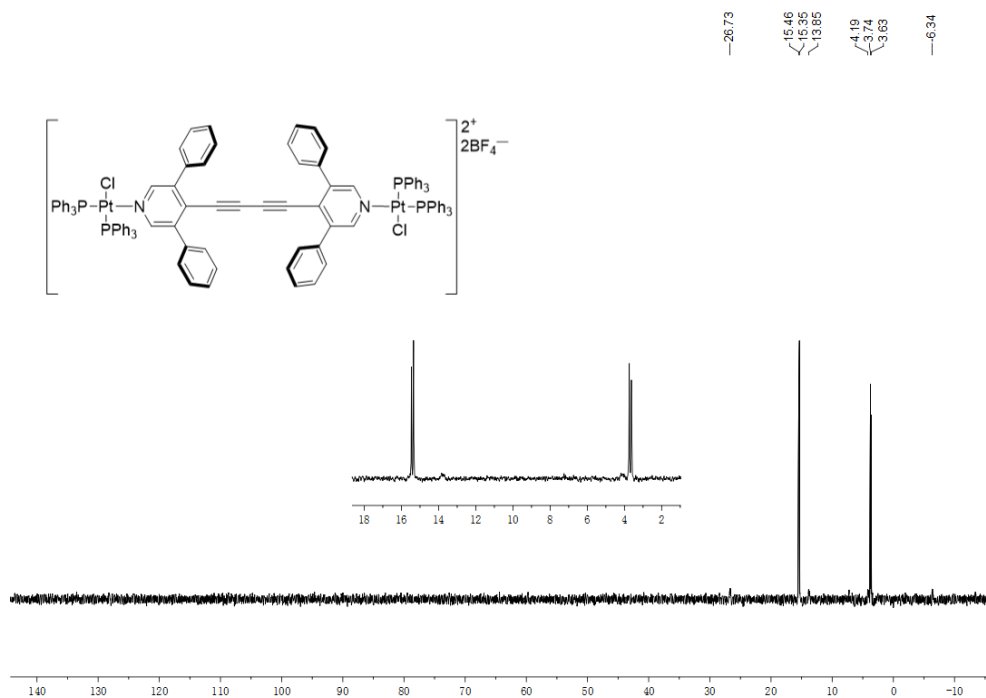
Figure 7.81. ^{31}P NMR spectrum of **(Ph)-Py*[2]Pt** in CD$_2$Cl$_2$.
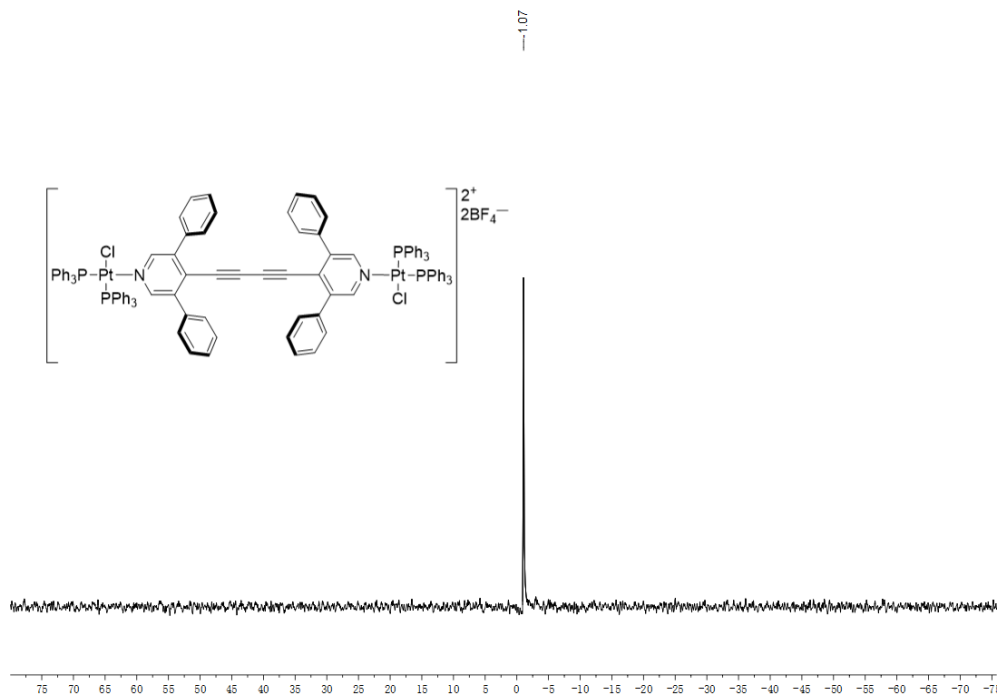
Figure 7.82. ^{11}B NMR spectrum of **(Ph)-Py*[2]Pt** in CD$_2$Cl$_2$.
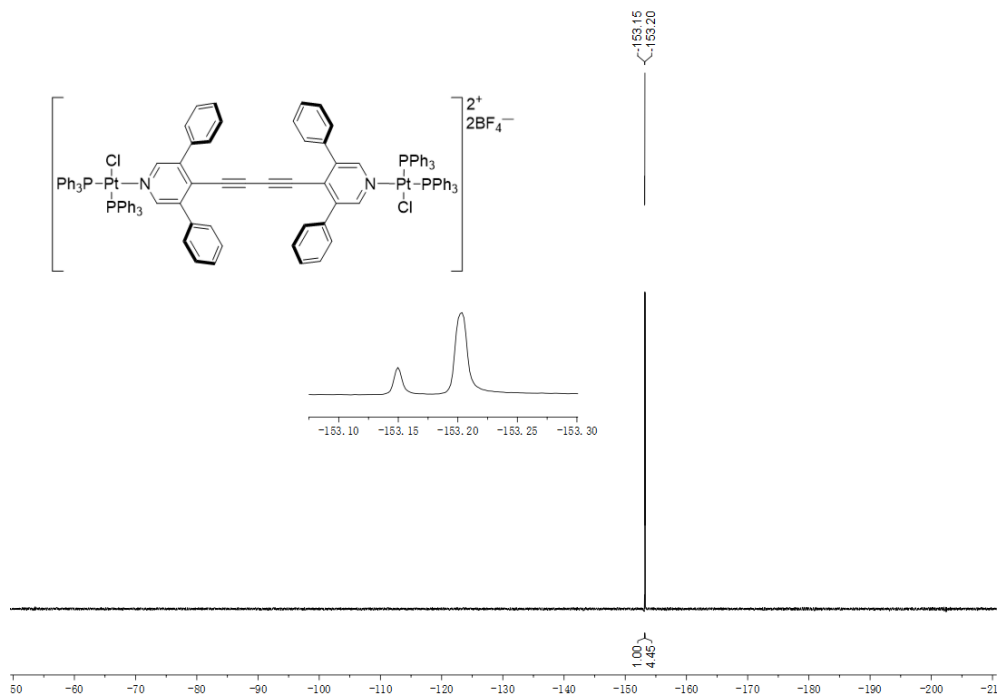
Figure 7.83. ^{19}F NMR spectrum of **(Ph)-Py*[2]Pt** in CD$_2$Cl$_2$.
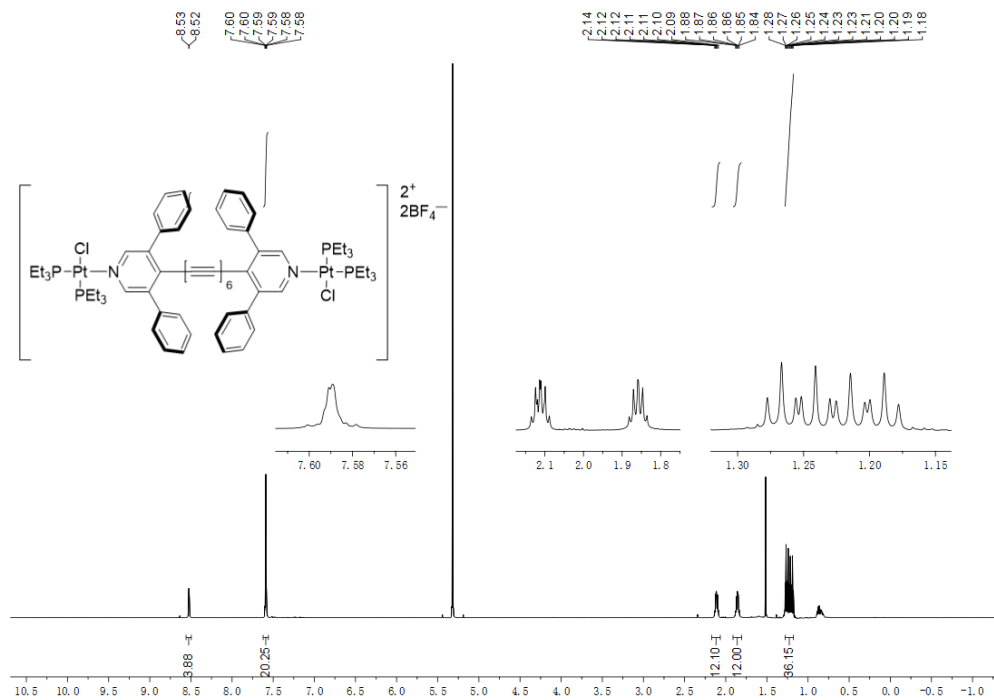
Figure 7.84. ^{1}H NMR spectrum of **(Et)-Py*[6]Pt** in CD$_2$Cl$_2$.
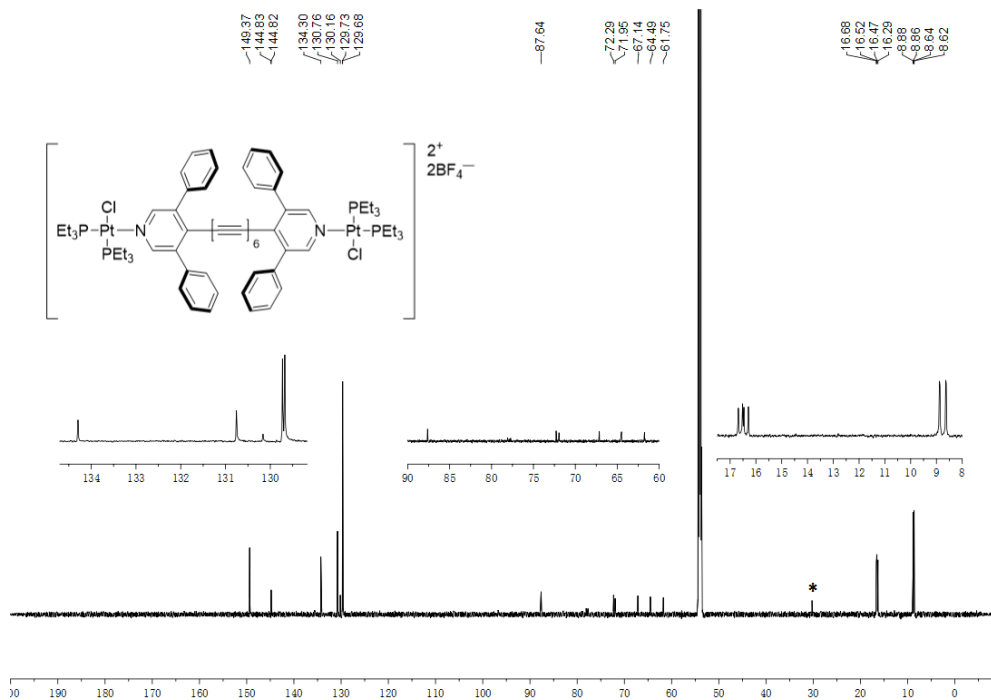
Figure 7.85. ^{13}C NMR spectrum of **(Et)-Py*[6]Pt** in CD$_2$Cl$_2$, *indicates H grease contamination.
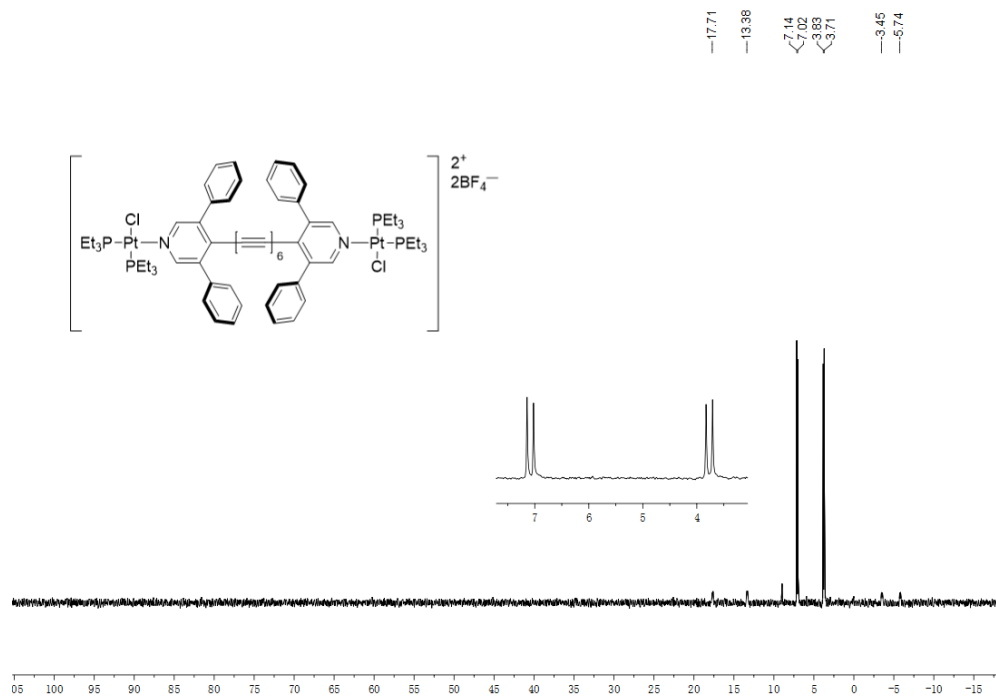
Figure 7.86. ^{31}P NMR spectrum of **(Et)-Py*[6]Pt** in CD$_2$Cl$_2$.
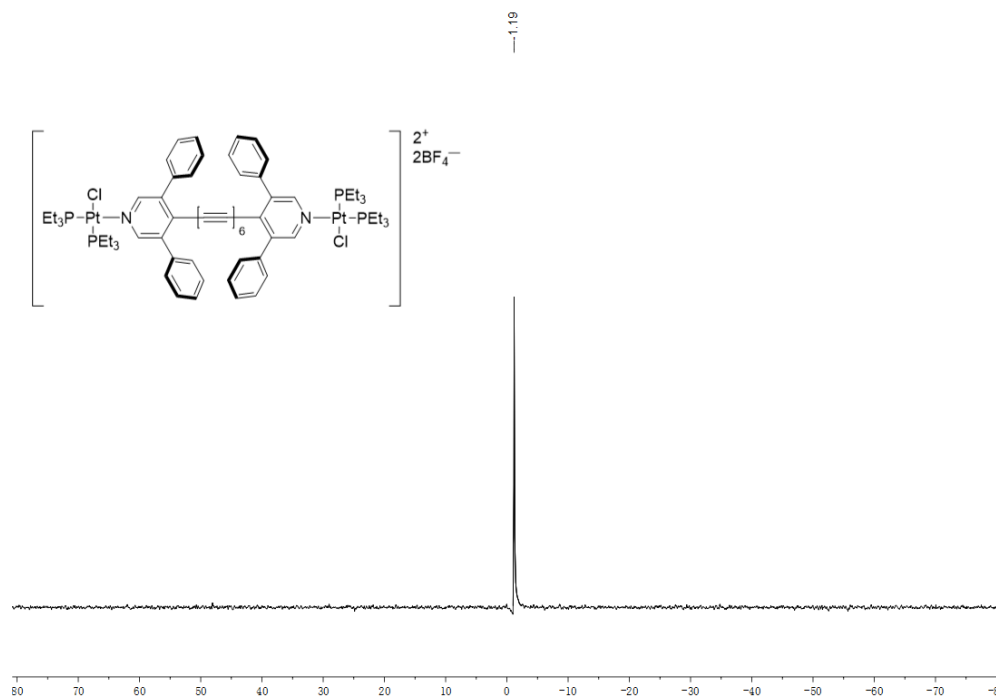
Figure 7.87. ^{11}B NMR spectrum of **(Et)-Py*[6]Pt** in CD$_2$Cl$_2$.
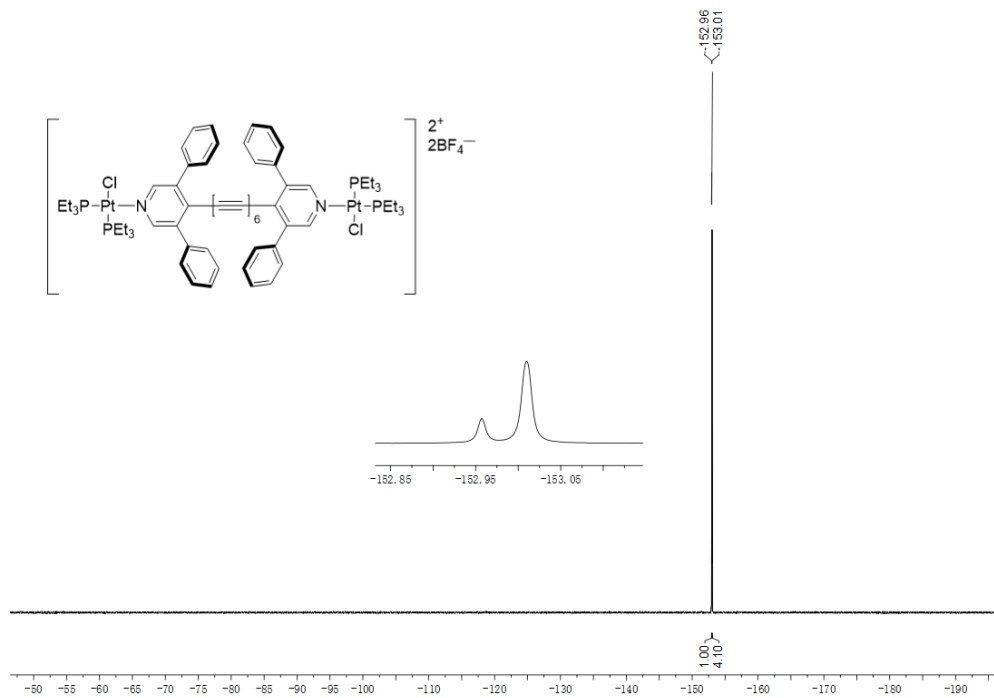
Figure 7.88. ^{19}F NMR spectrum of **(Et)-Py*[6]Pt** in CD$_2$Cl$_2$.
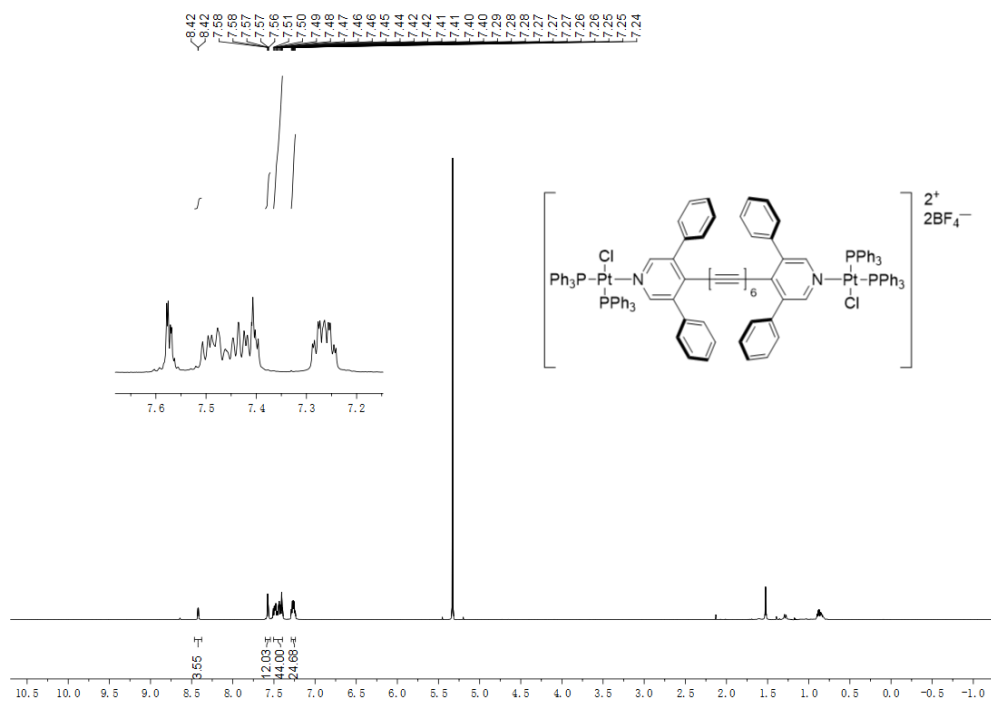
Figure 7. 89. ^{1}H NMR spectrum of **(Ph)-Py*[6]Pt** in CD$_2$Cl$_2$.
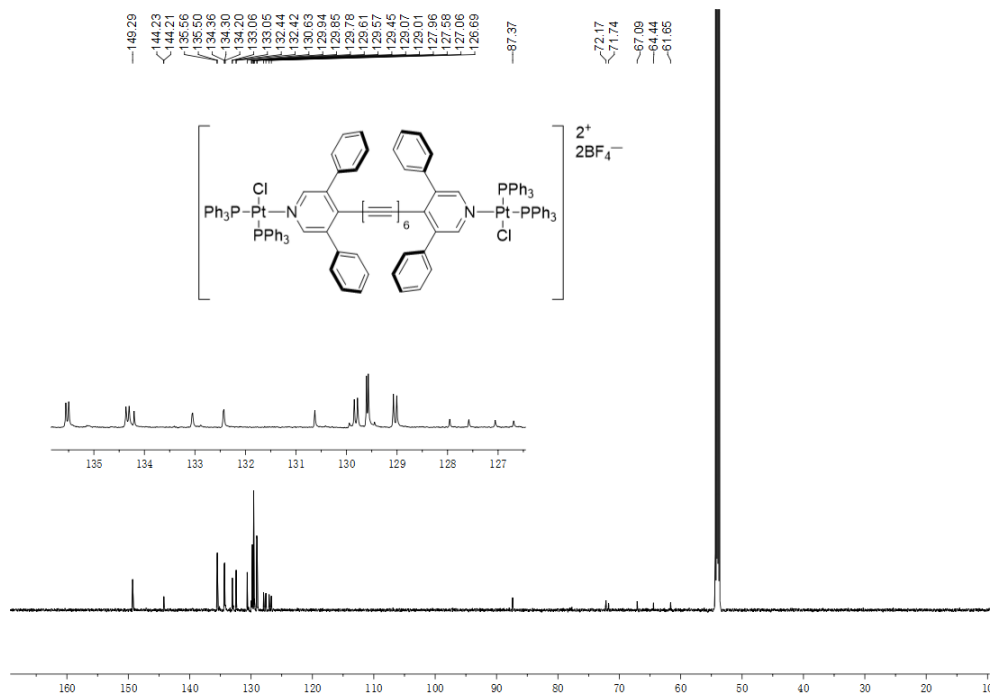
Figure 7.90. ^{13}C NMR spectrum of **(Ph)-Py*[6]Pt** in CD$_2$Cl$_2$.
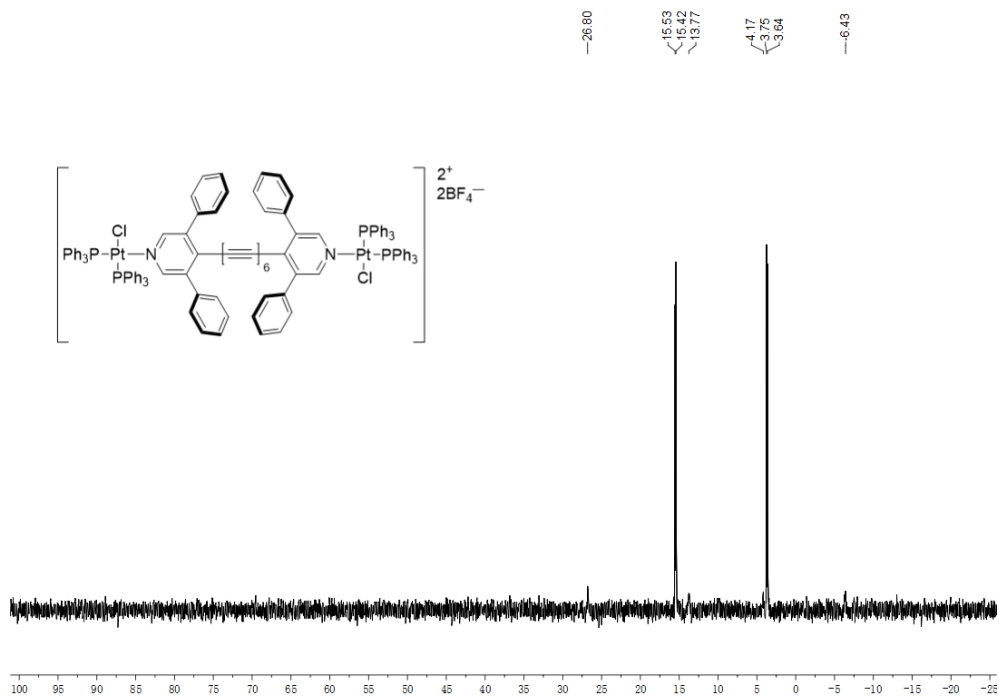
Figure 7.91. ^{31}P NMR spectrum of **(Ph)-Py*[6]Pt** in CD$_2$Cl$_2$.
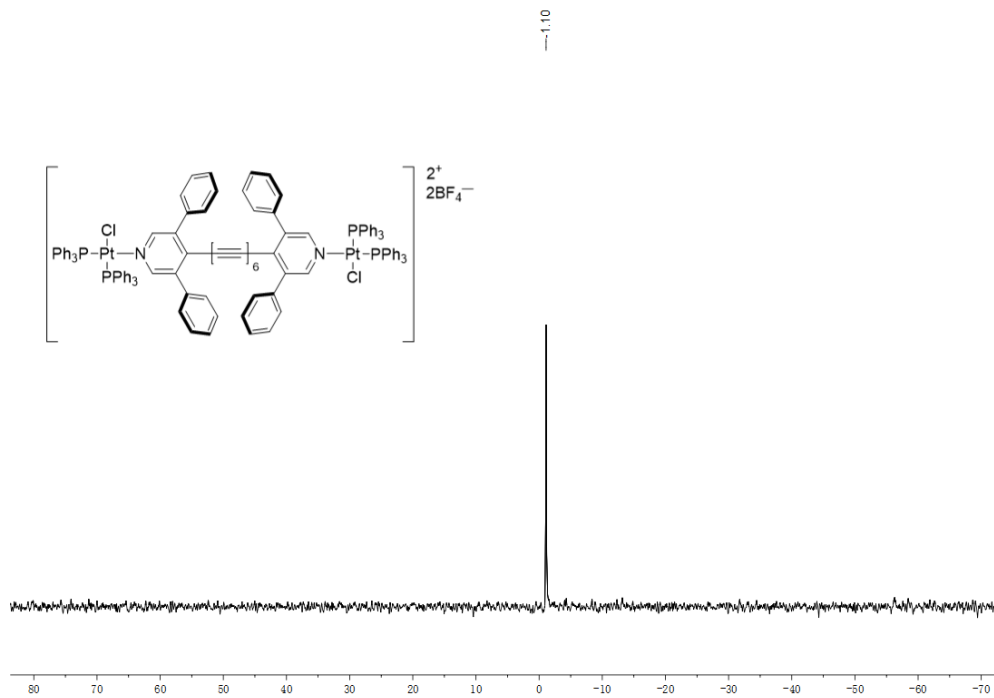
Figure 7.92. ^{11}B NMR spectrum of **(Ph)-Py*[6]Pt** in CD$_2$Cl$_2$.
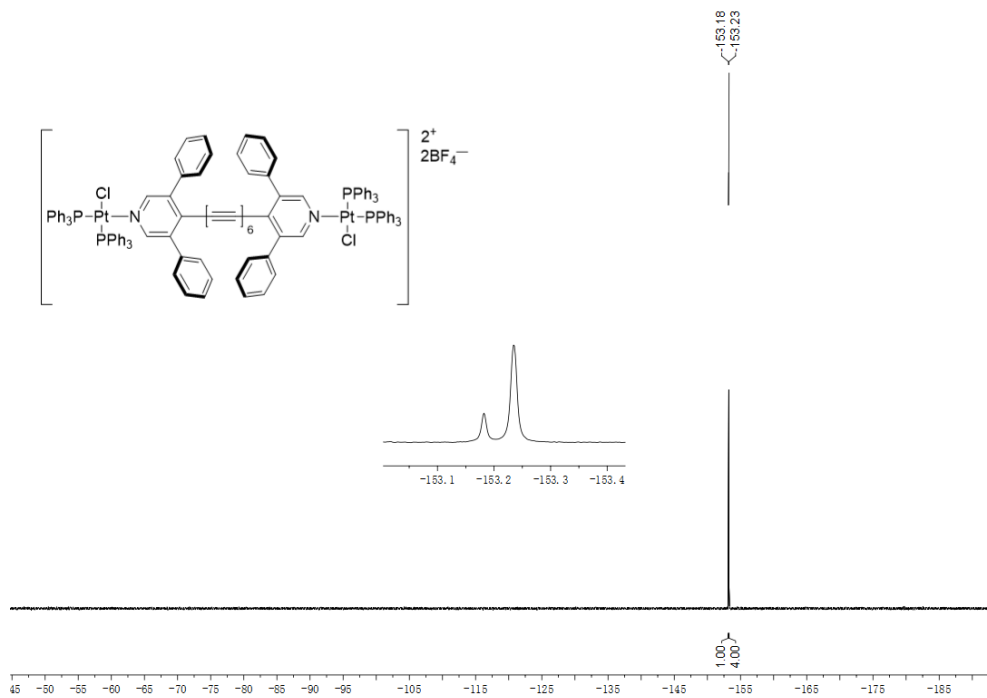
Figure 7.93. ^{19}F NMR spectrum of **(Ph)-Py*[6]Pt** in CD$_2$Cl$_2$.
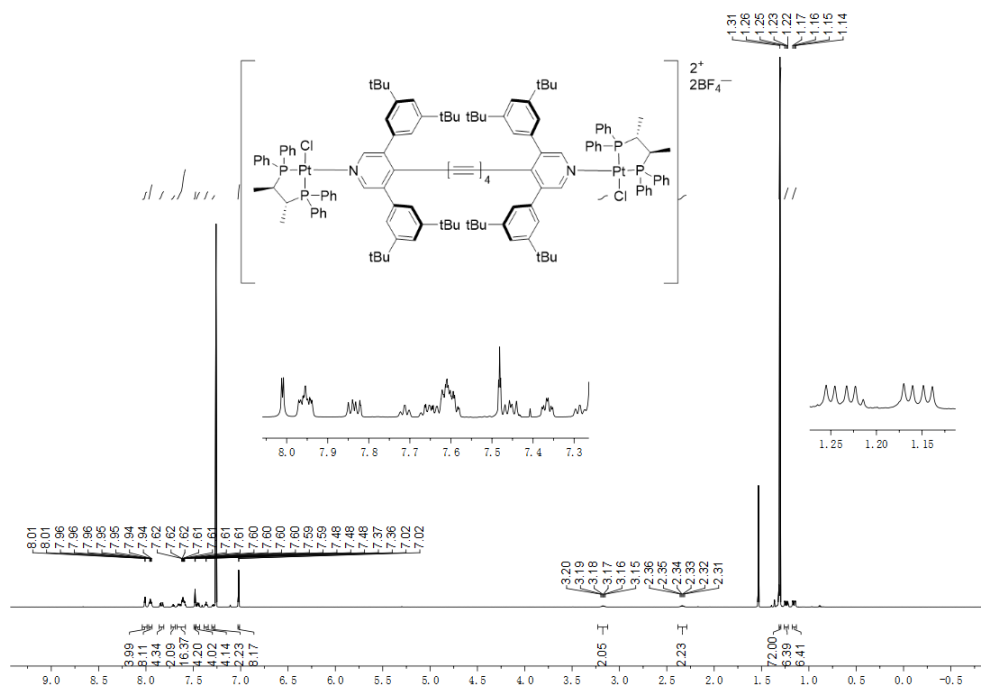
Figure 7.94. ^{1}H NMR spectrum of **(R,R,R,R)-Py**[4a]Pt** in CDCl$_3$.
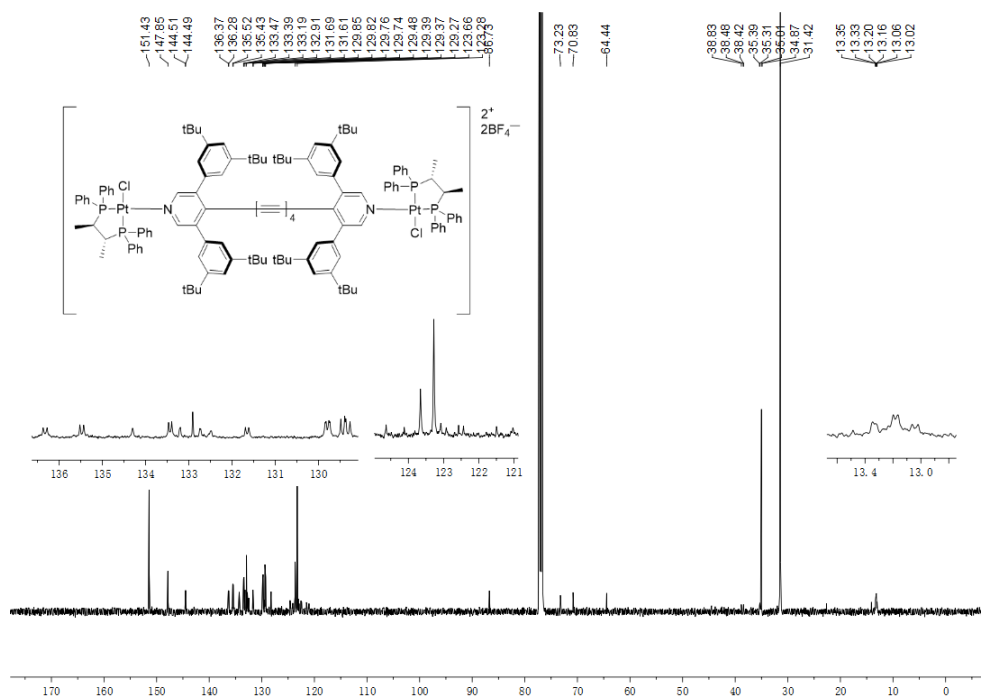
Figure 7.95. ^{13}C NMR spectrum of **(R,R,R,R)-Py**[4a]Pt** in CDCl$_3$.
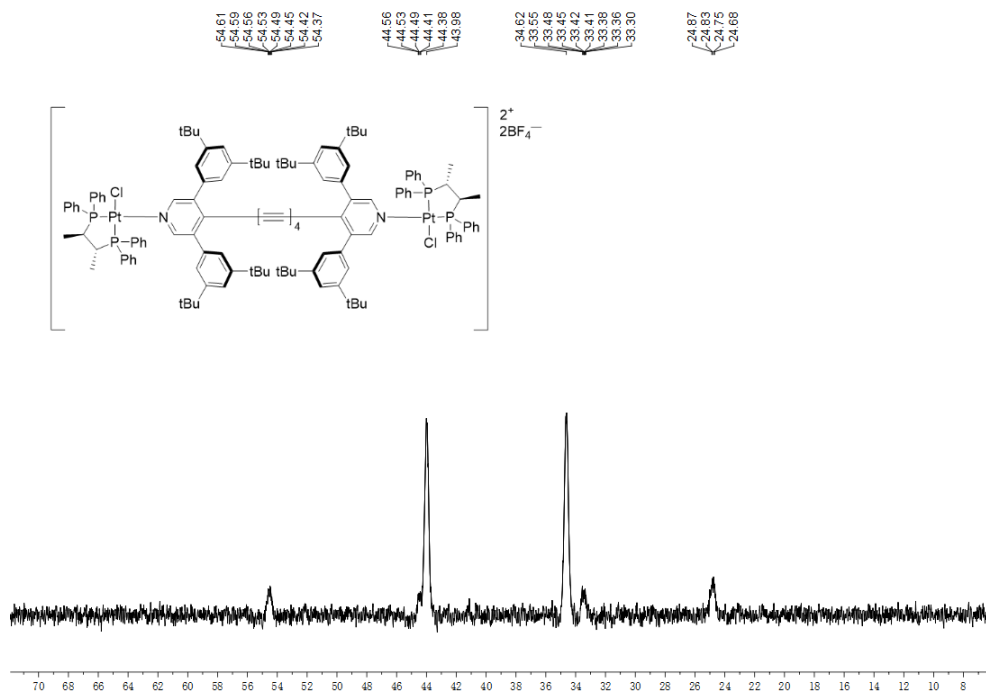
Figure 7.96. ^{31}P NMR spectrum of (***R,R,R,R***)-**Py**[4a]Pt** in CDCl$_3$.
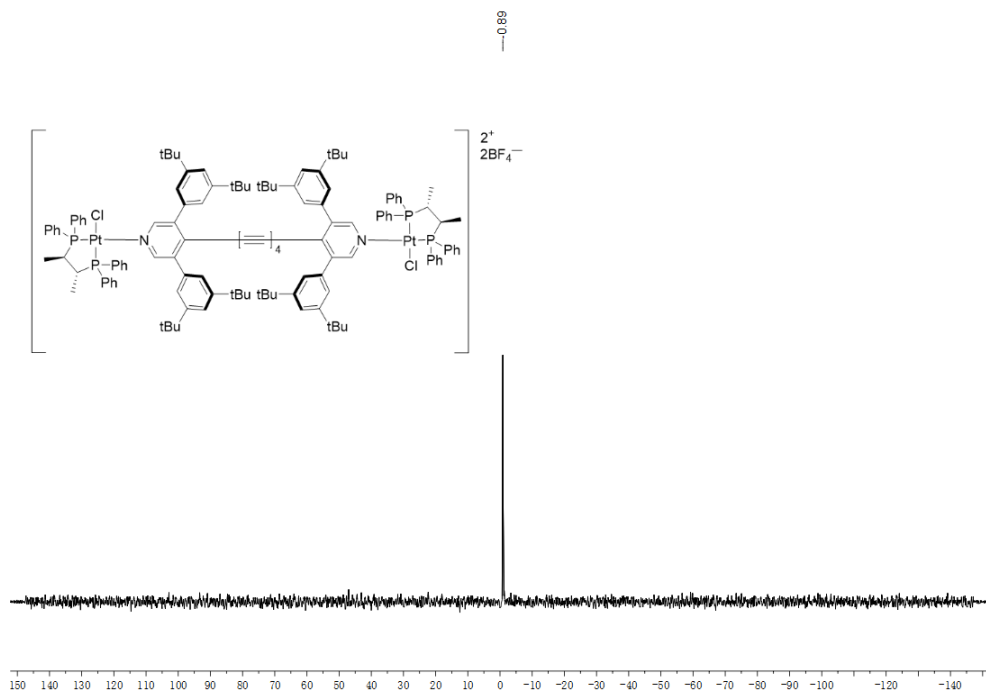
Figure 7.97. ^{11}B NMR spectrum of (***R,R,R,R***)-**Py**[4a]Pt** in CDCl$_3$.
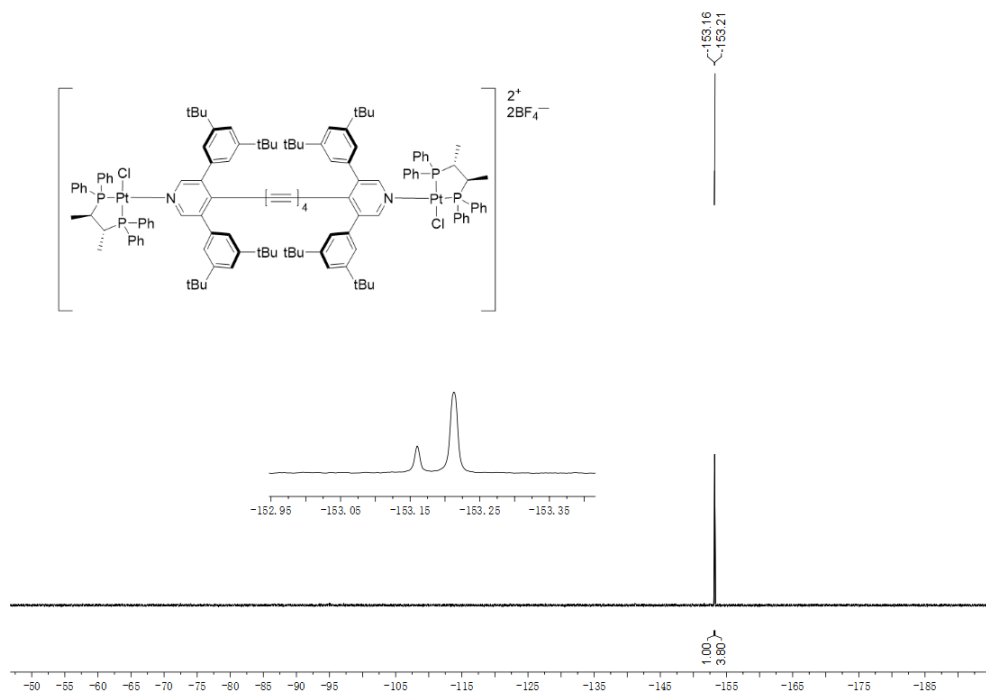
Figure 7.98. ^{19}F NMR spectrum of **(R,R,R,R)-Py**[4a]Pt** in CDCl₃.
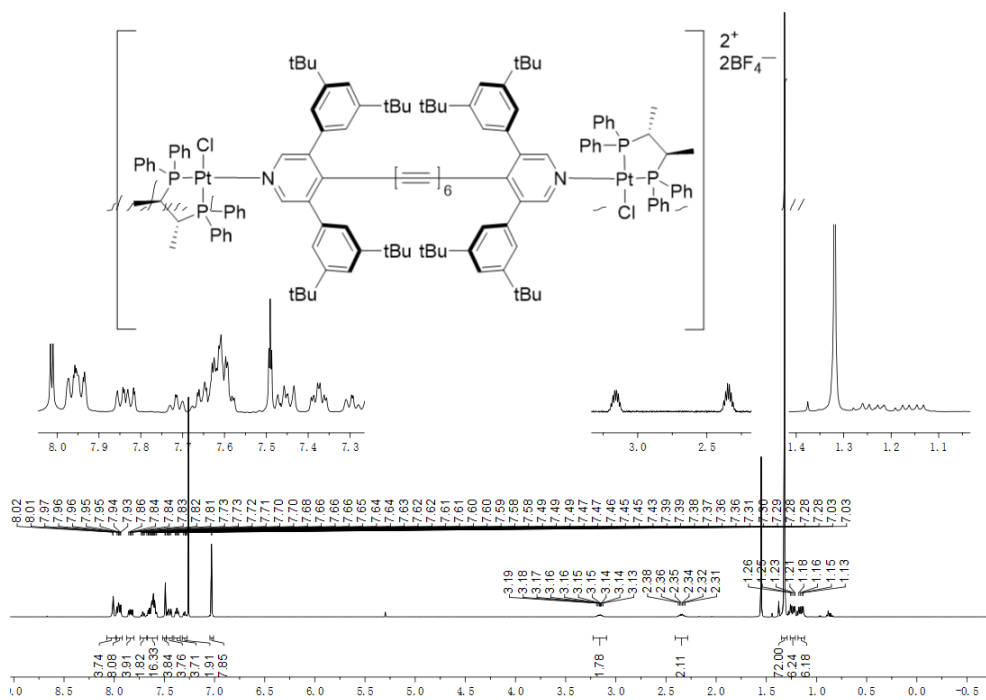
Figure 7.99. ^{1}H NMR spectrum of **(R,R,R,R)-Py**[6a]Pt** in CDCl₃.

Figure 7.100. ^{13}C NMR spectrum of **(*R,R,R,R*)-Py**[6a]Pt** in CDCl$_3$.

Figure 7.101. ^{31}P NMR spectrum of **(*R,R,R,R*)-Py**[6a]Pt** in CDCl$_3$.
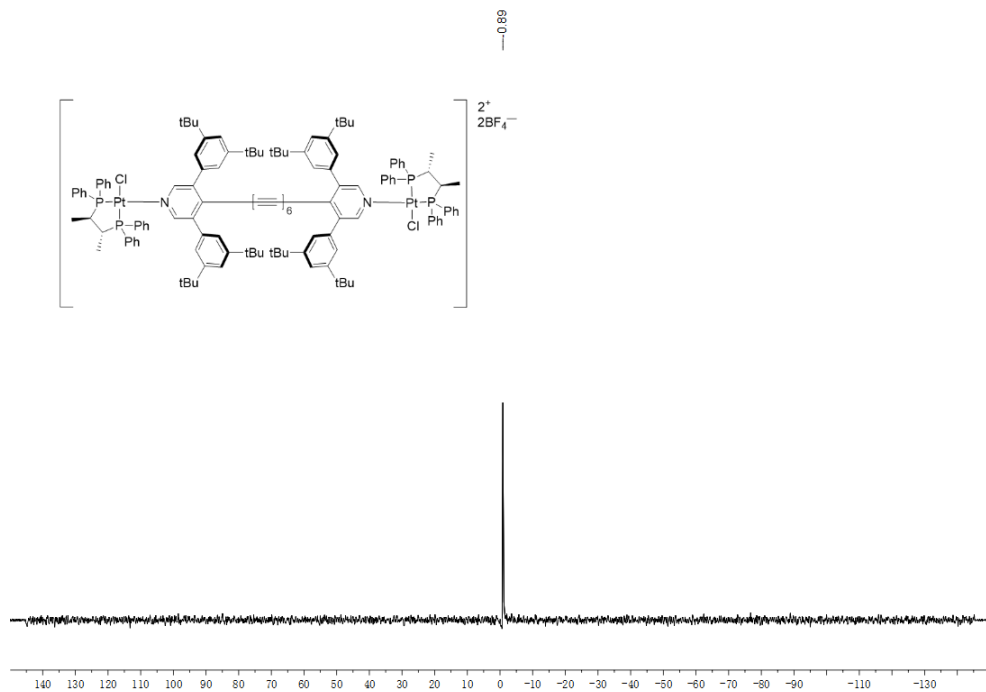
Figure 7.102. ^{11}B NMR spectrum of **(*R,R,R,R*)-Py**[6a]Pt** in CDCl₃.
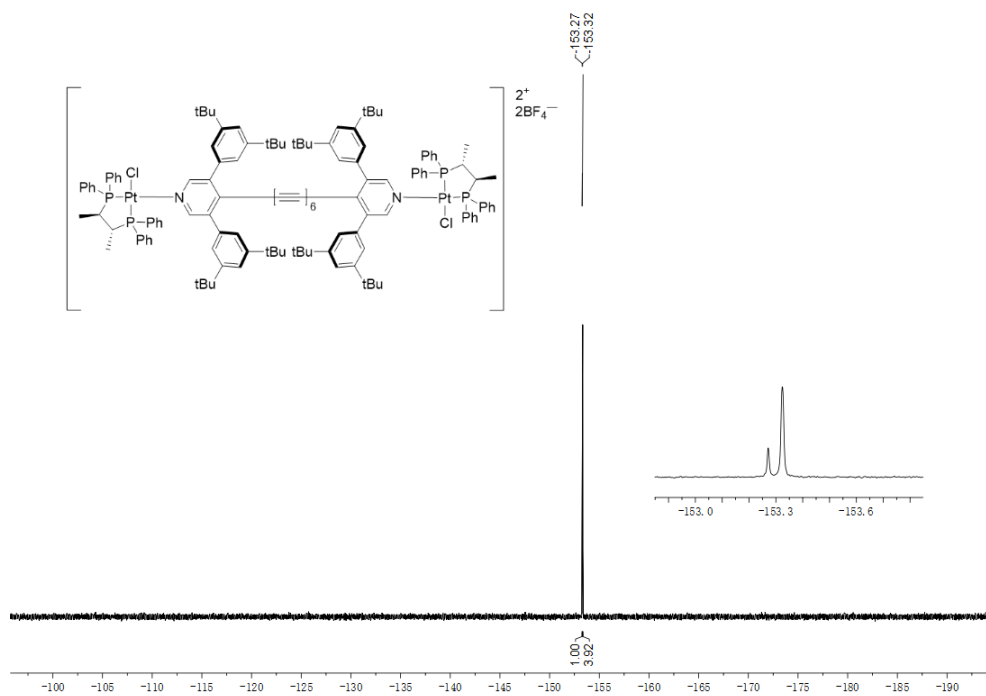
Figure 7.103. ^{19}F NMR spectrum of **(*R,R,R,R*)-Py**[6a]Pt** in CDCl₃.
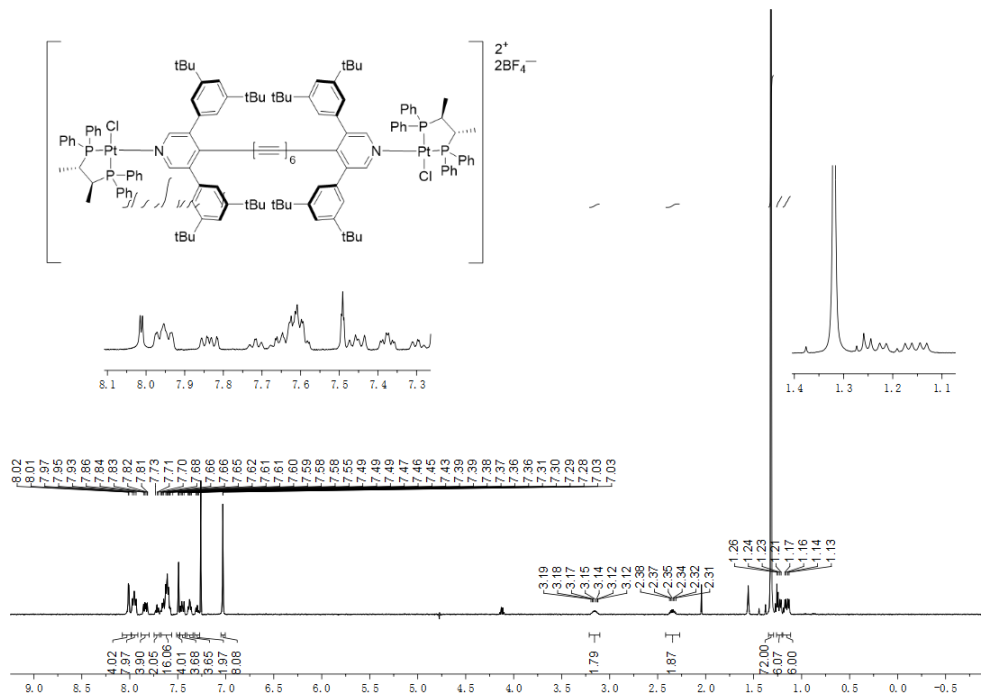
Figure 7.104. ^{1}H NMR spectrum of **(S,S,S,S)-Py**[6a]Pt** in CDCl$_3$.
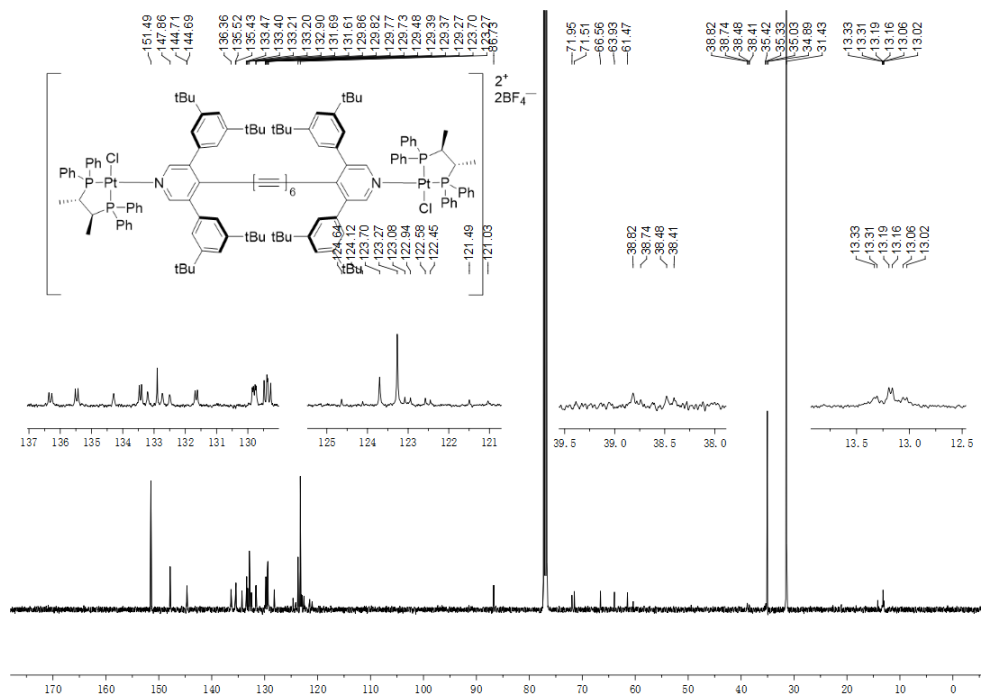
Figure 7.105. ^{13}C NMR spectrum of **(S,S,S,S)-Py**[6a]Pt** in CDCl$_3$.
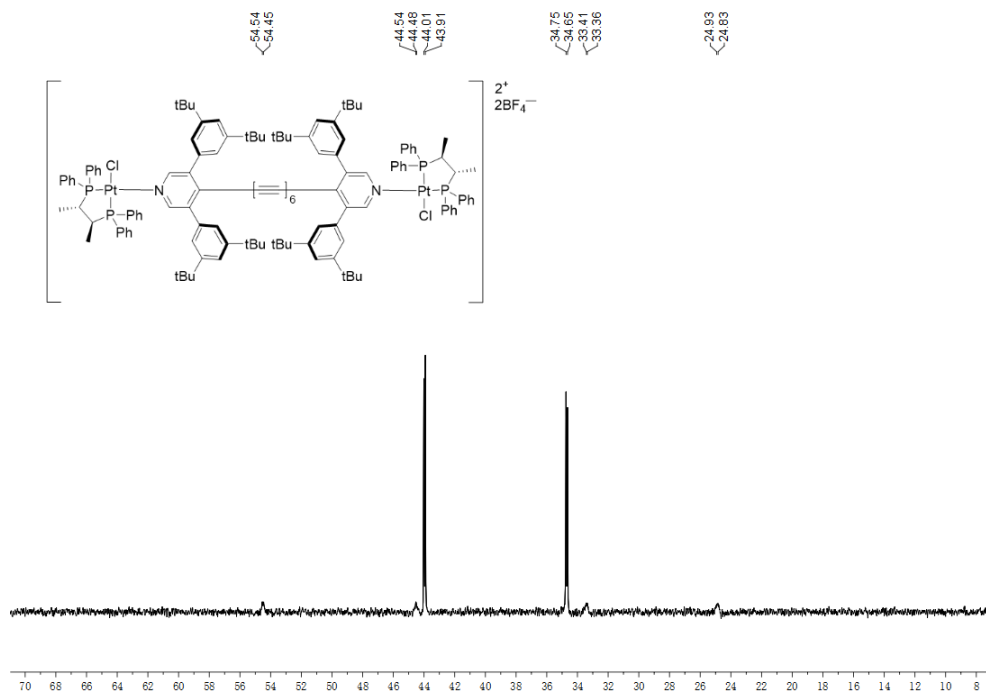
Figure 7.106. ^{31}P NMR spectrum of **(*S*,*S*,*S*,*S*)-Py**[6a]Pt** in CDCl$_3$.
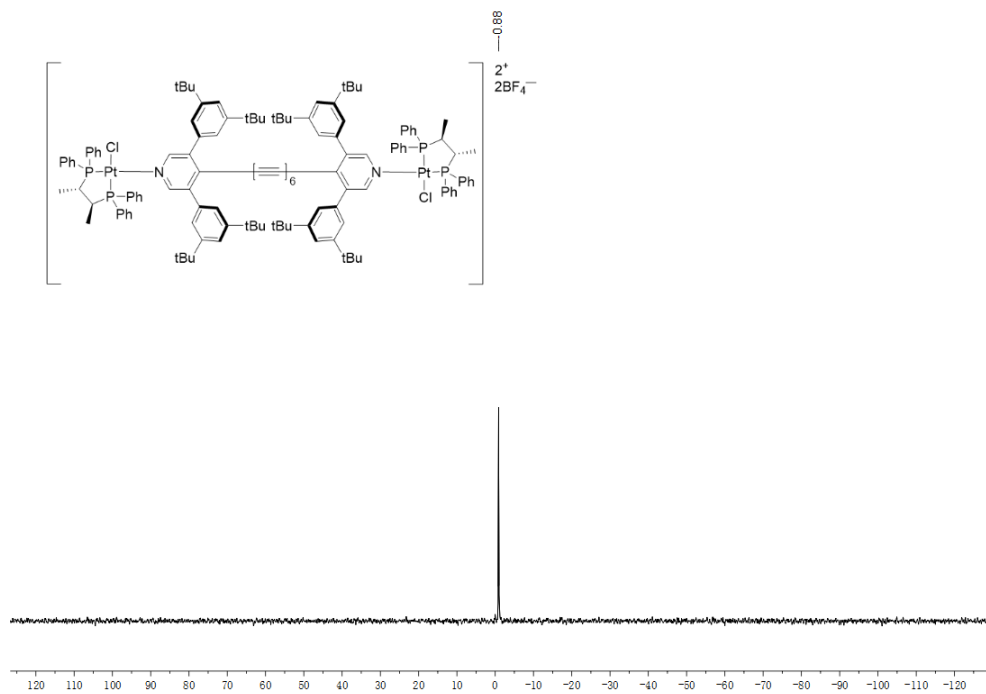
Figure 7.107. ^{11}B NMR spectrum of **(*S*,*S*,*S*,*S*)-Py**[6a]Pt** in CDCl$_3$.
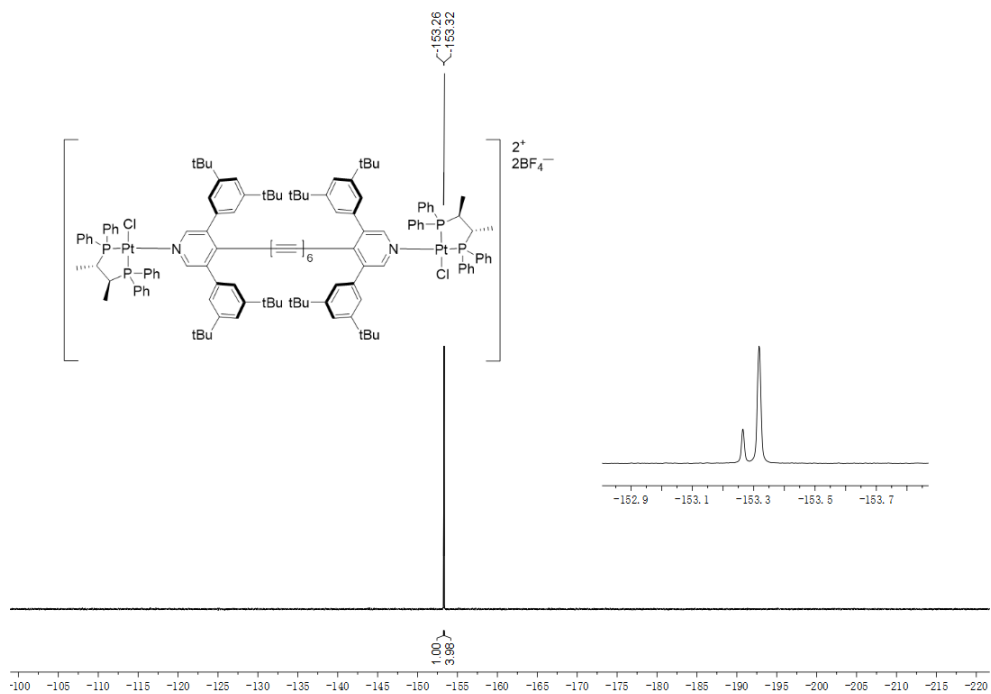
Figure 7.108. ^{19}F NMR spectrum of **(S,S,S,S)-Py**[6a]Pt** in CDCl$_3$.
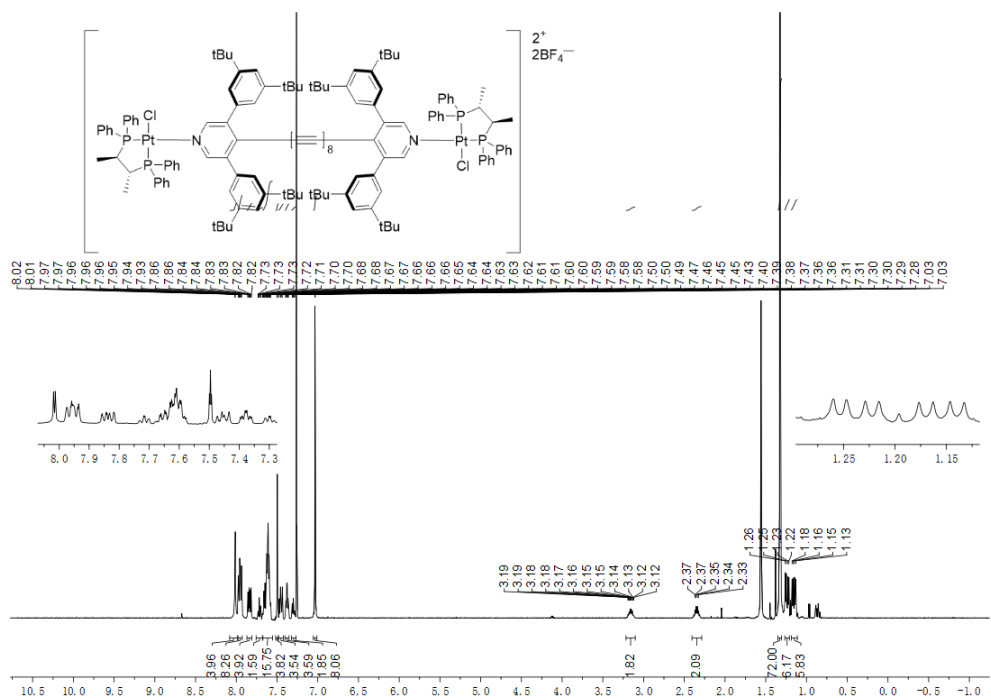
Figure 7.109. ^{1}H NMR spectrum of **(R,R,R,R)-Py**[8a]Pt** in CDCl$_3$.
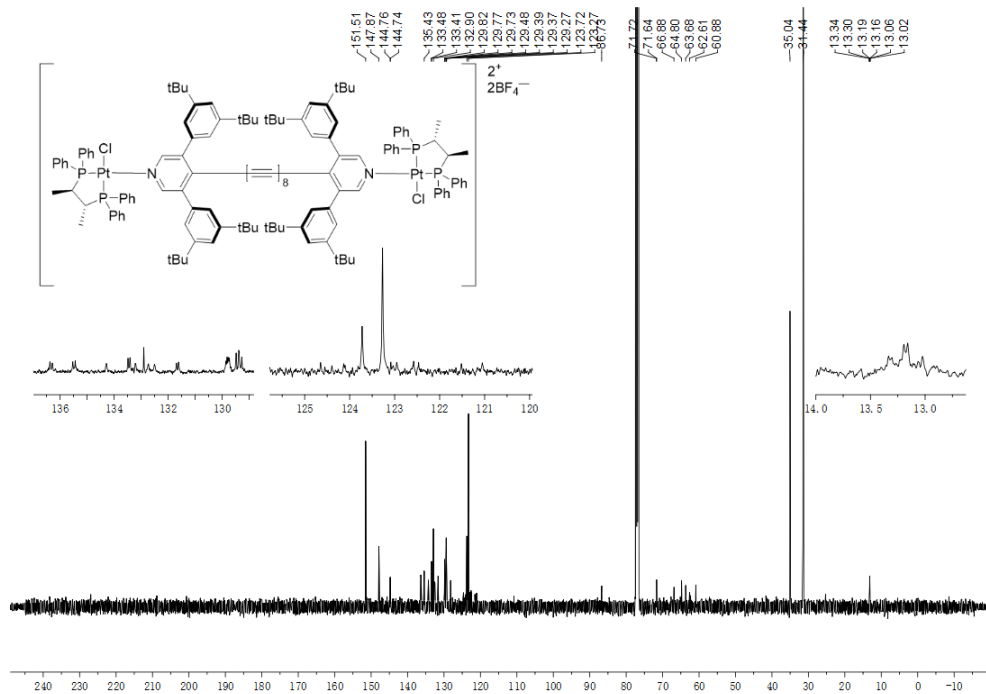
Figure 7.110. ^{13}C NMR spectrum of (***R,R,R,R***)-**Py**[8a]Pt** in CDCl$_3$.
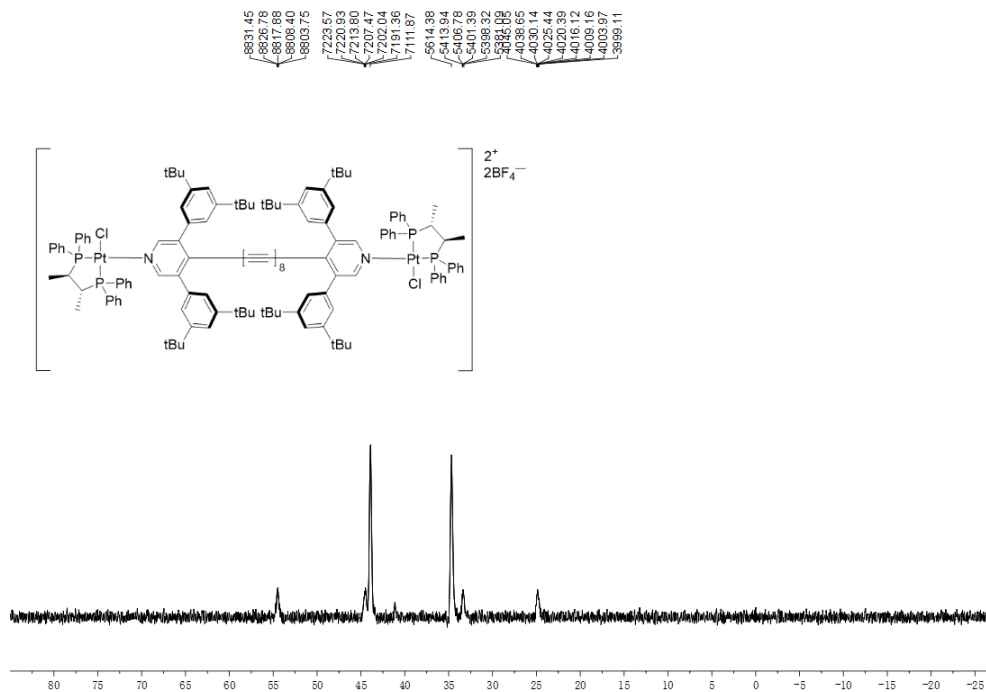
Figure 7.111. ^{31}P NMR spectrum of (***R,R,R,R***)-**Py**[8a]Pt** in CDCl$_3$.
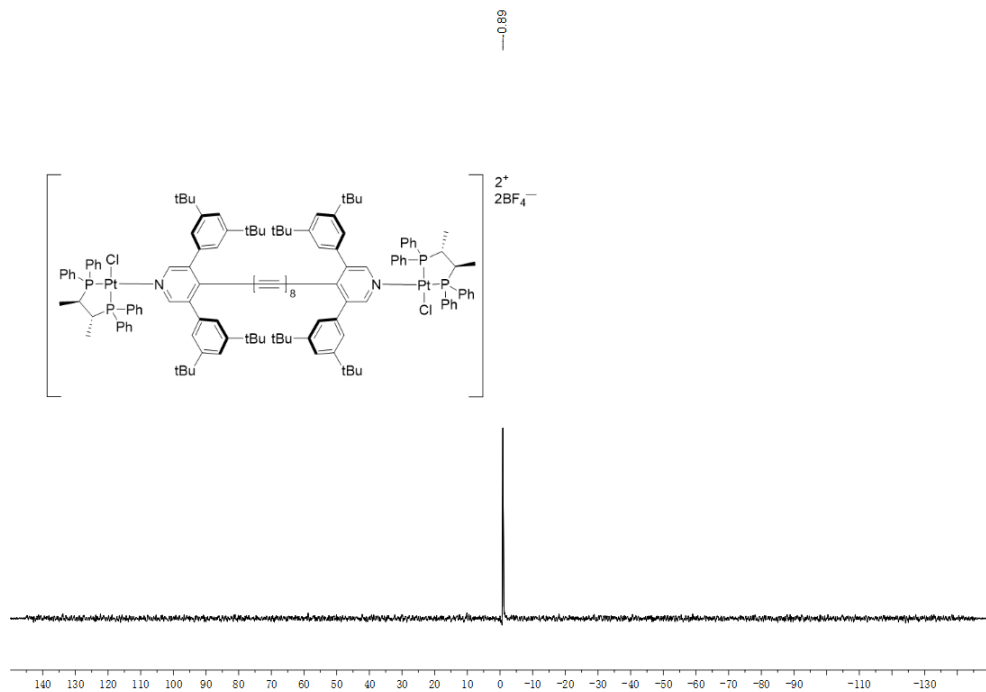
Figure 7.112. ^{11}B NMR spectrum of (**R,R,R,R**)-**Py**[8a]Pt** in CDCl₃.
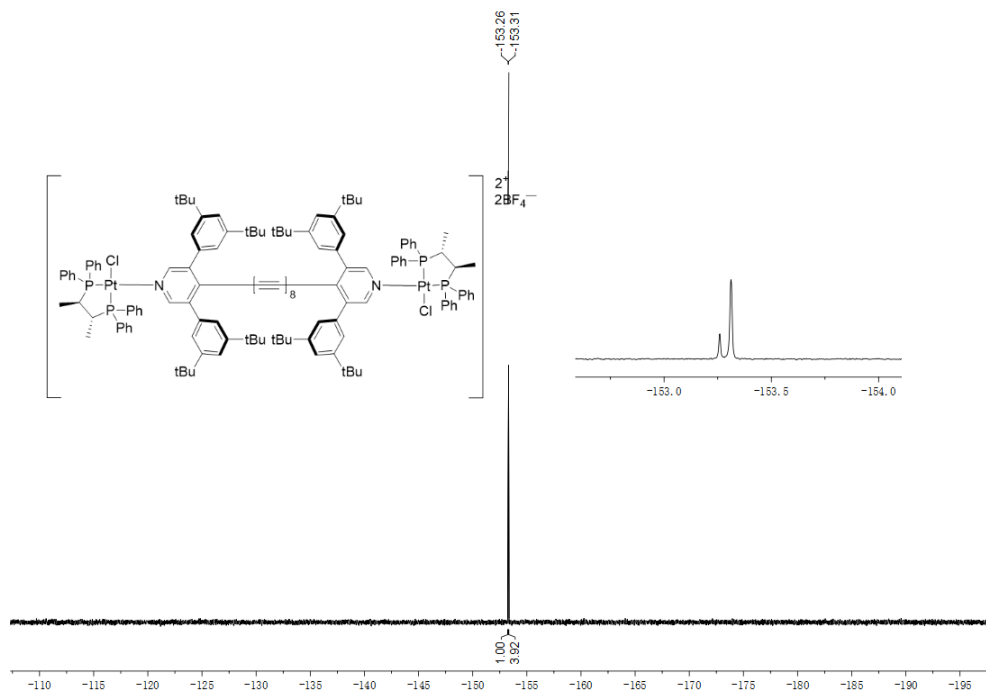
Figure 7.113. ^{19}F NMR spectrum of (**R,R,R,R**)-**Py**[8a]Pt** in CDCl₃.

7.6.4 Spectra of Chapter 5
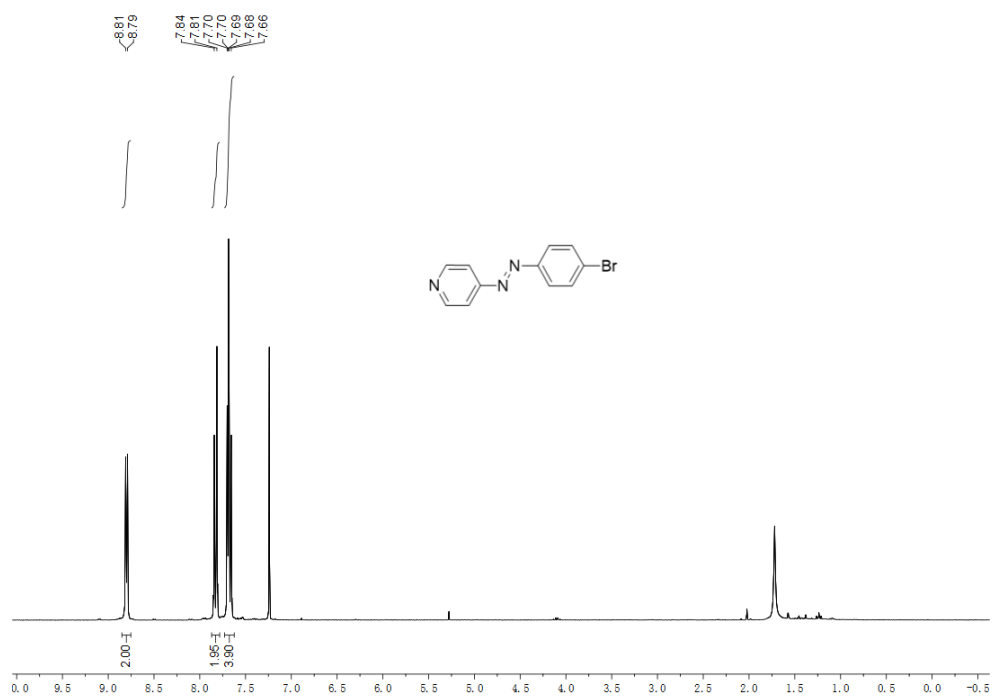
Figure 7.114. ^{1}H NMR spectrum of **5.2** in CDCl$_3$.
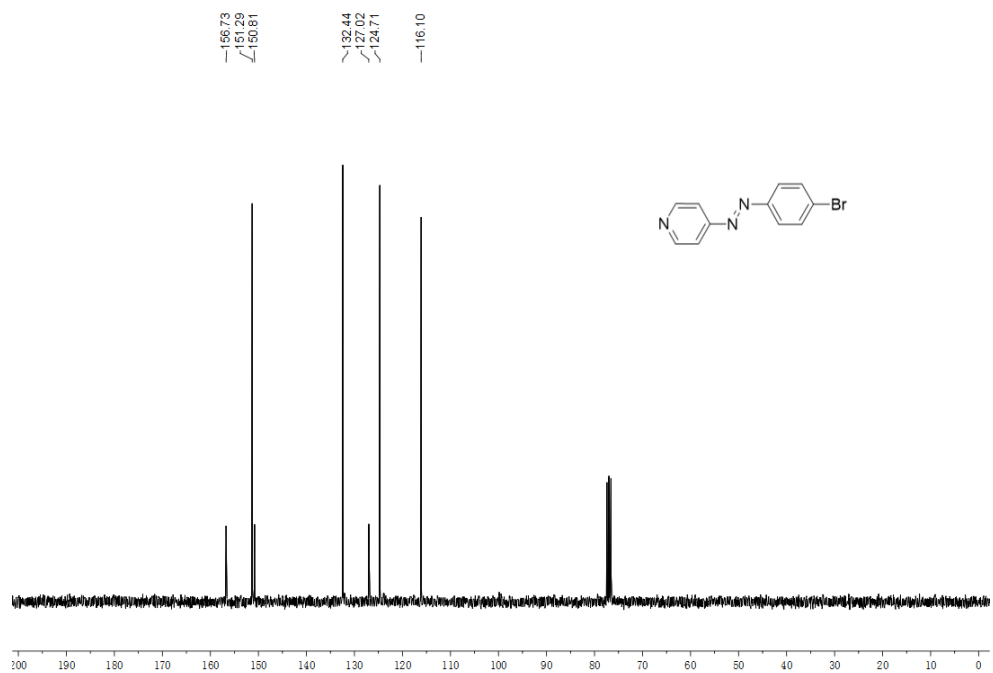
Figure 7.115. ^{13}C NMR spectrum of **5.2** in CDCl$_3$.
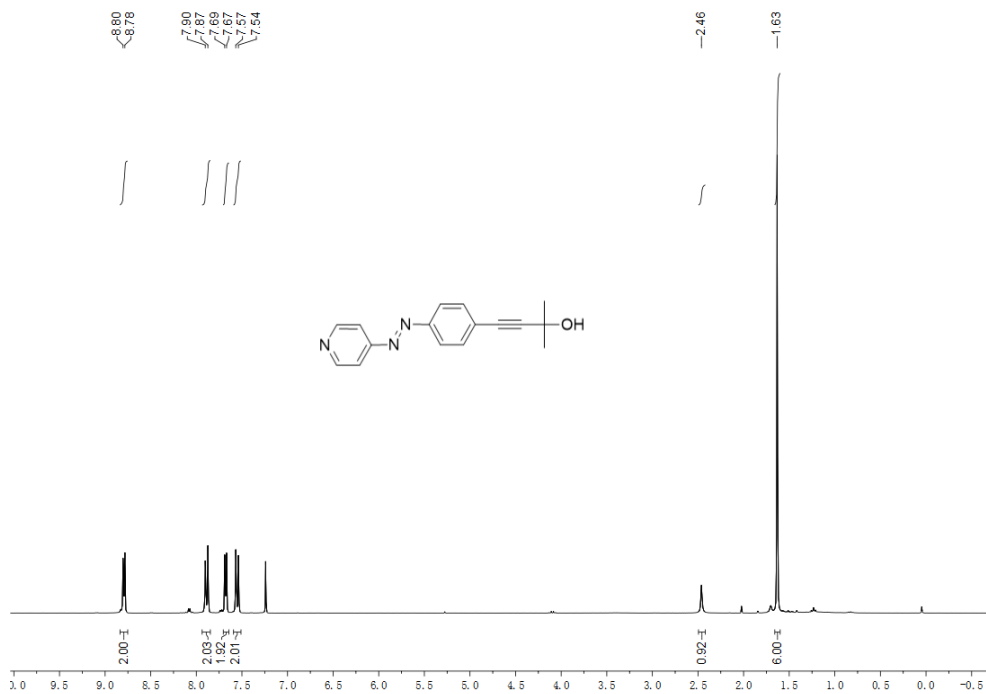
Figure 7.116. ^{1}H NMR spectrum of **5.3** in CDCl$_3$.
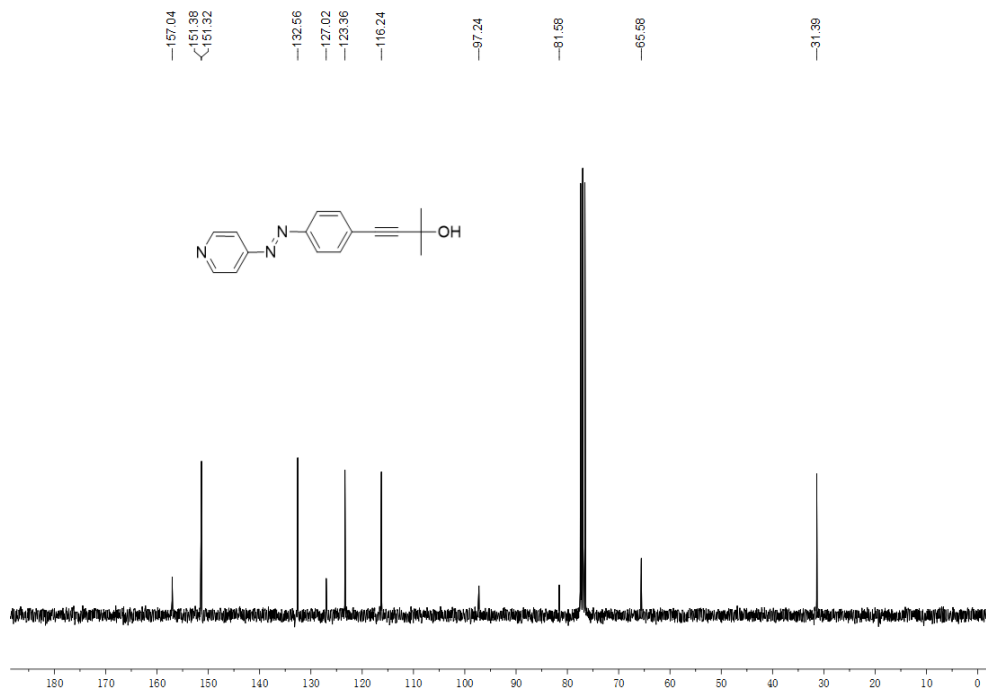
Figure 7.117. ^{13}C NMR spectrum of **5.3** in CDCl$_3$.
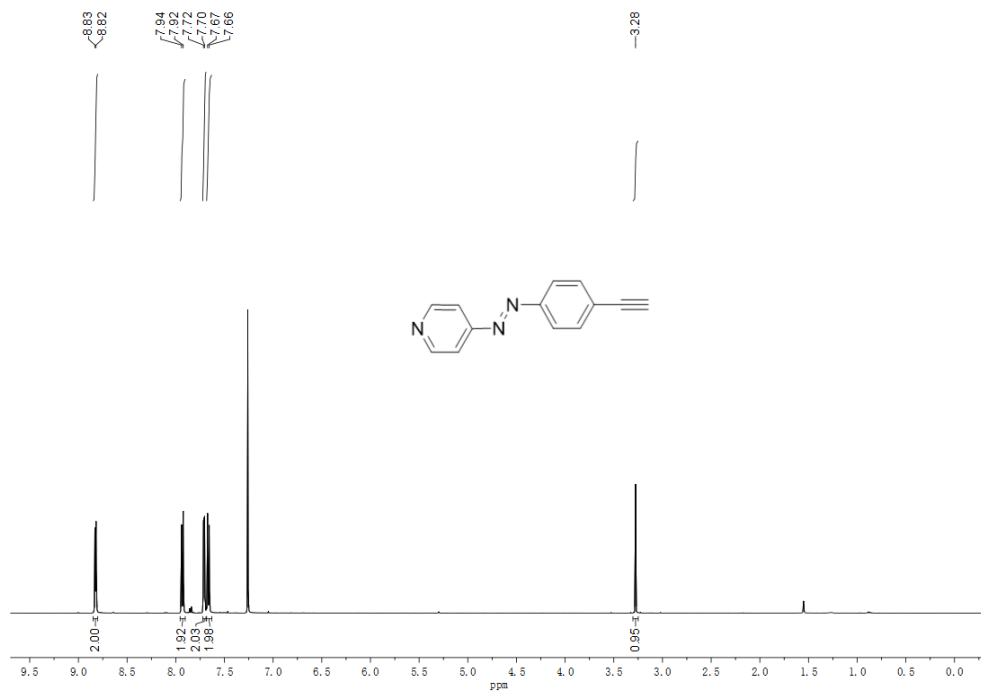
Figure 7.118. ^{1}H NMR spectrum of *trans*-**L1** in CDCl$_3$.
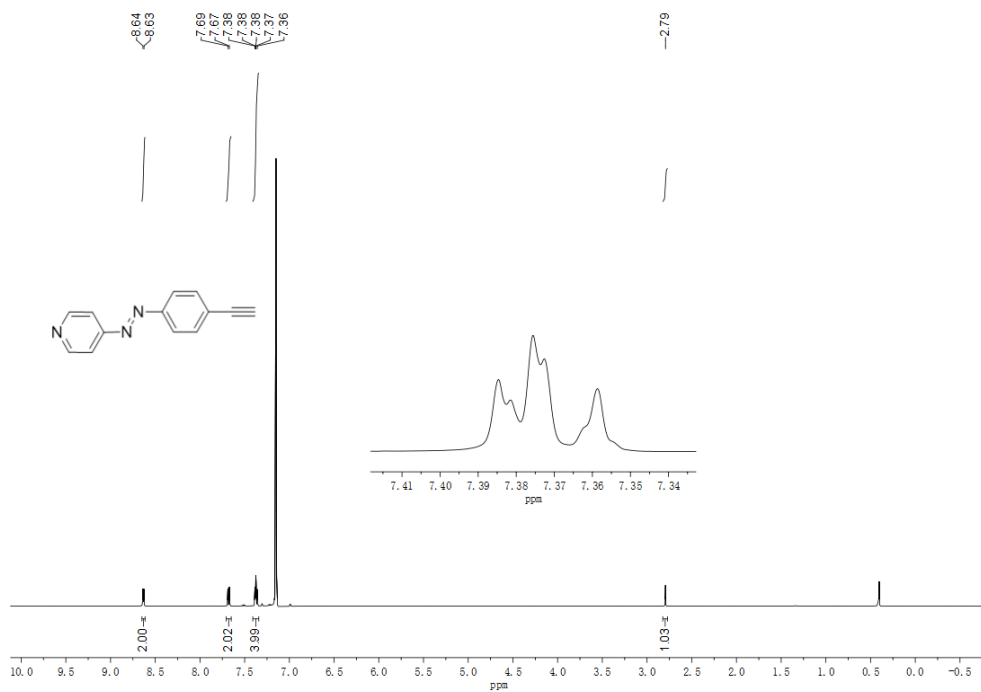
Figure 7.119. ^{1}H NMR spectrum of *trans*-**L1** in C$_6$D$_6$ shielding from light.
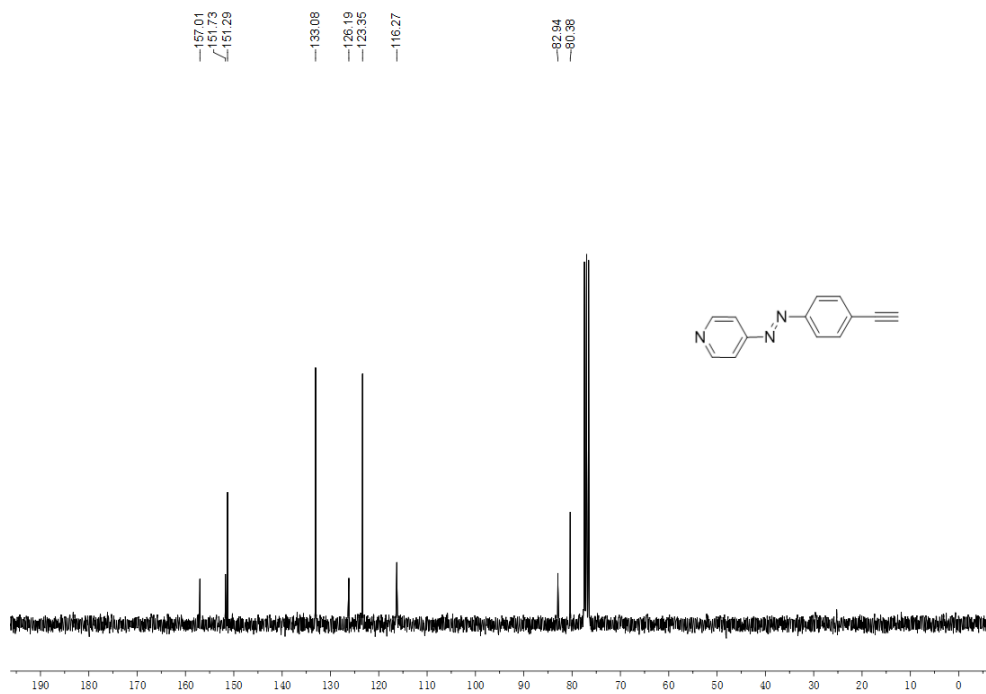
Figure 7.120. ^{13}C NMR spectrum of *trans*-**L1** in CDCl$_3$.
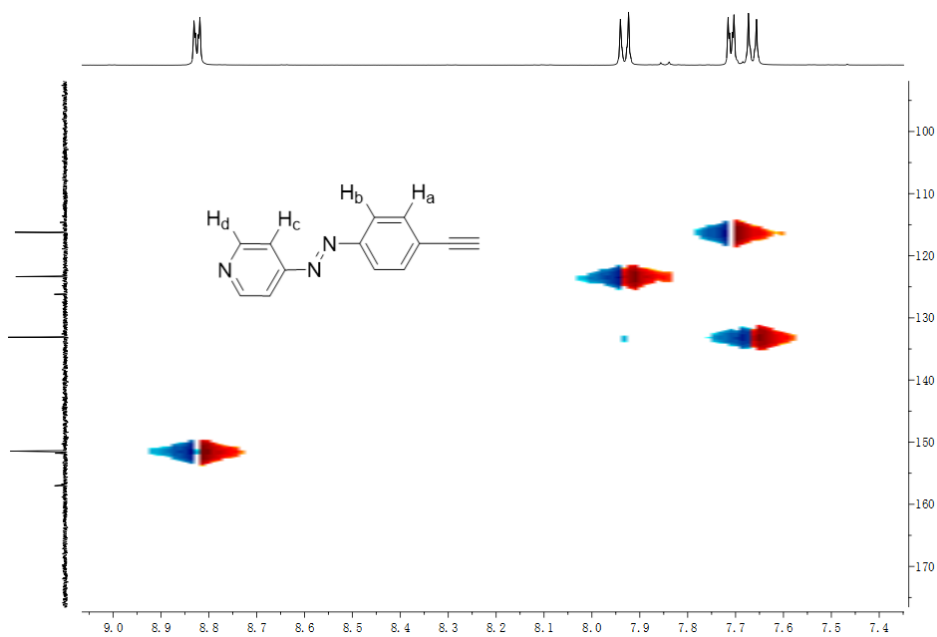
Figure 7.121. ^{1}H–^{13}C HSQC spectrum of *trans*-**L1** in CDCl$_3$.
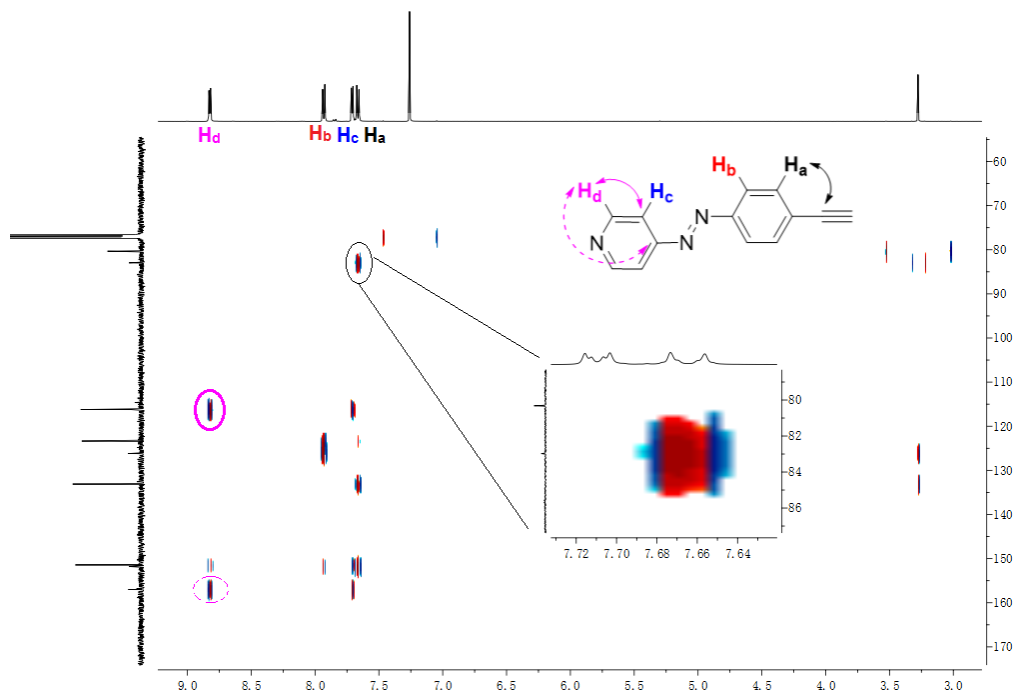
Figure 7.122. ^{1}H–^{13}C HMBC spectrum of **trans-L1** in CDCl$_3$.
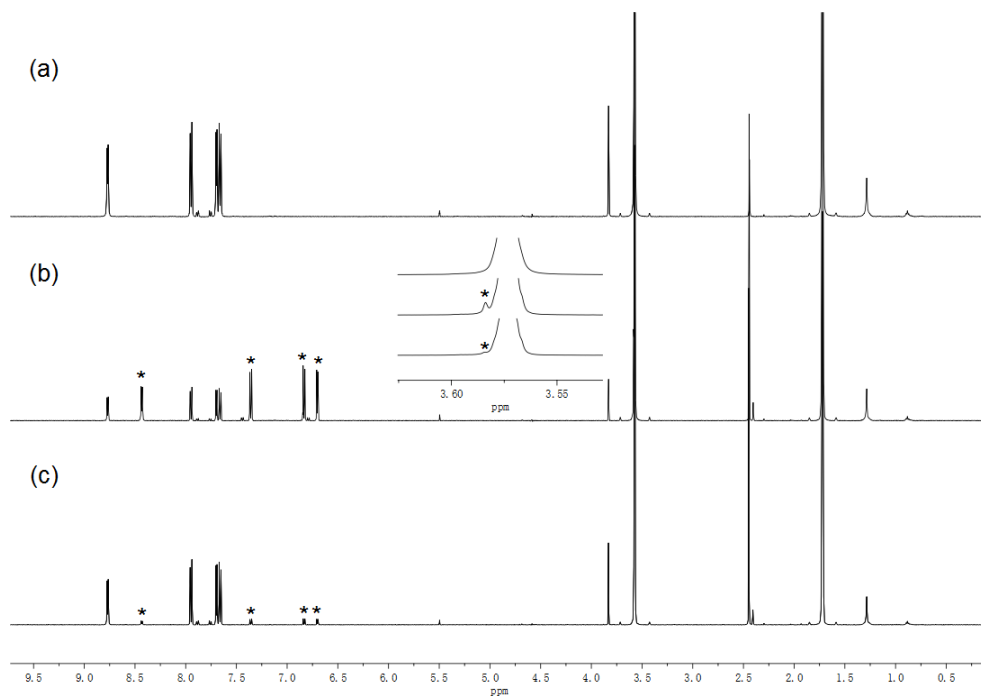
Figure 7.123. ^{1}H NMR spectra of **L1** in THF-d$_6$ (a) **trans-L1**; (b) irradiation at 365 nm for 6 h, at the PSS with 63% **cis-L1**, *indicates **cis-L1**; and (c) irradiation at 450 nm for 4 h, at the PSS with 92% **trans-L1**, *indicates **cis-L1**.

314
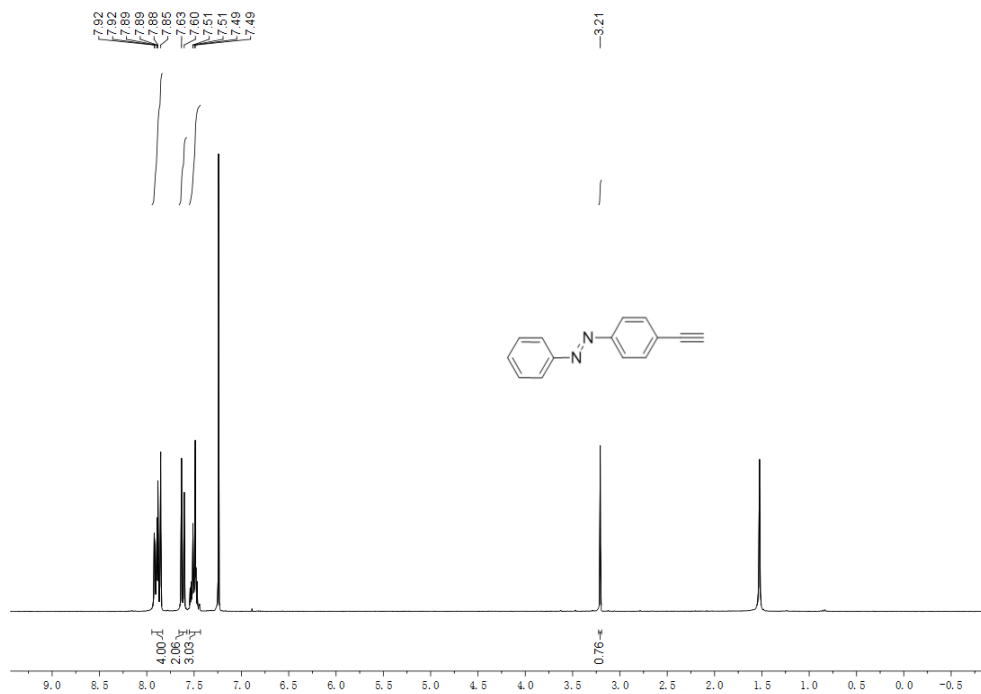
Figure 7.124. ^{1}H NMR spectrum of *trans*-**L2** in CDCl$_3$.
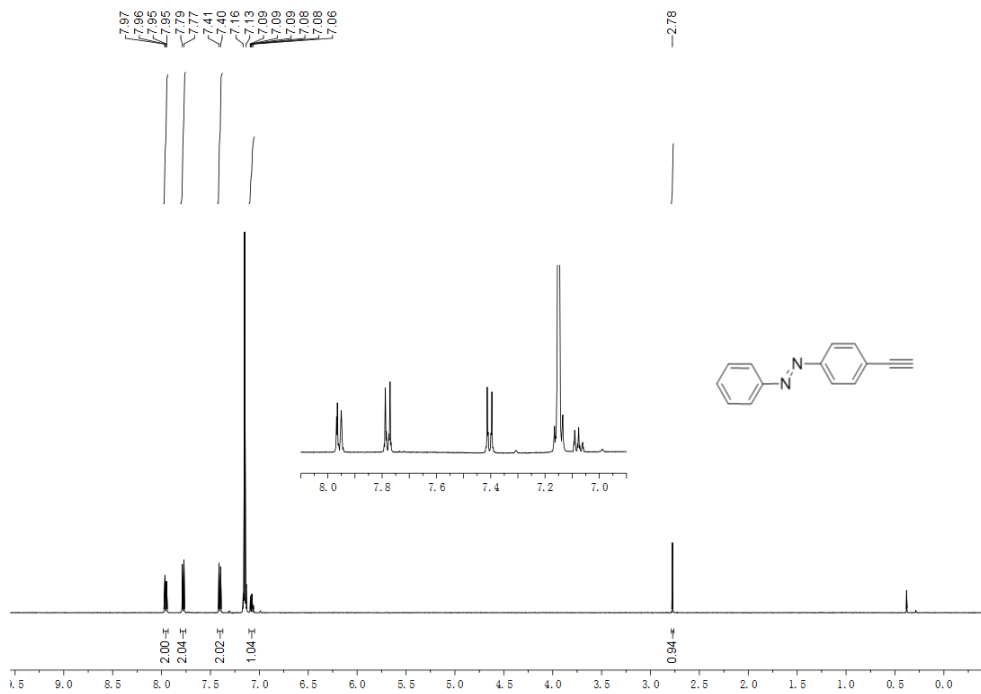
Figure 7.125. ^{1}H NMR spectrum of *trans*-**L2** in C$_6$D$_6$ shielding from light (two protons are coincident with C$_6$D$_6$).
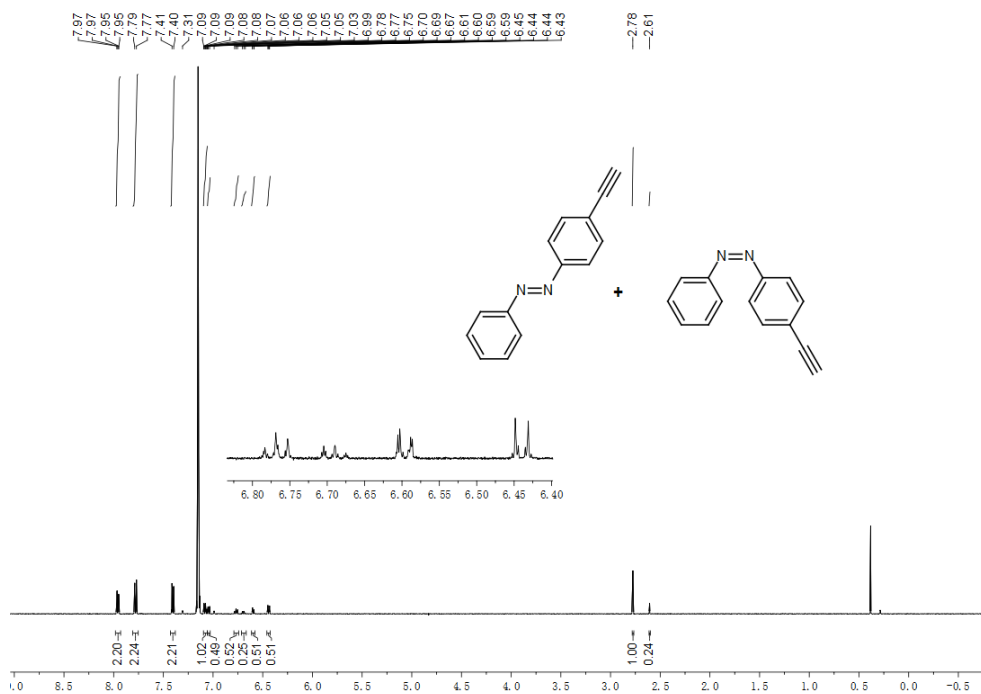
Figure 7.126. ¹H NMR spectrum of *trans*-L2 in C₆D₆ without shielding from daylight (two protons from the *trans* isomer are coincident with C₆D₆).
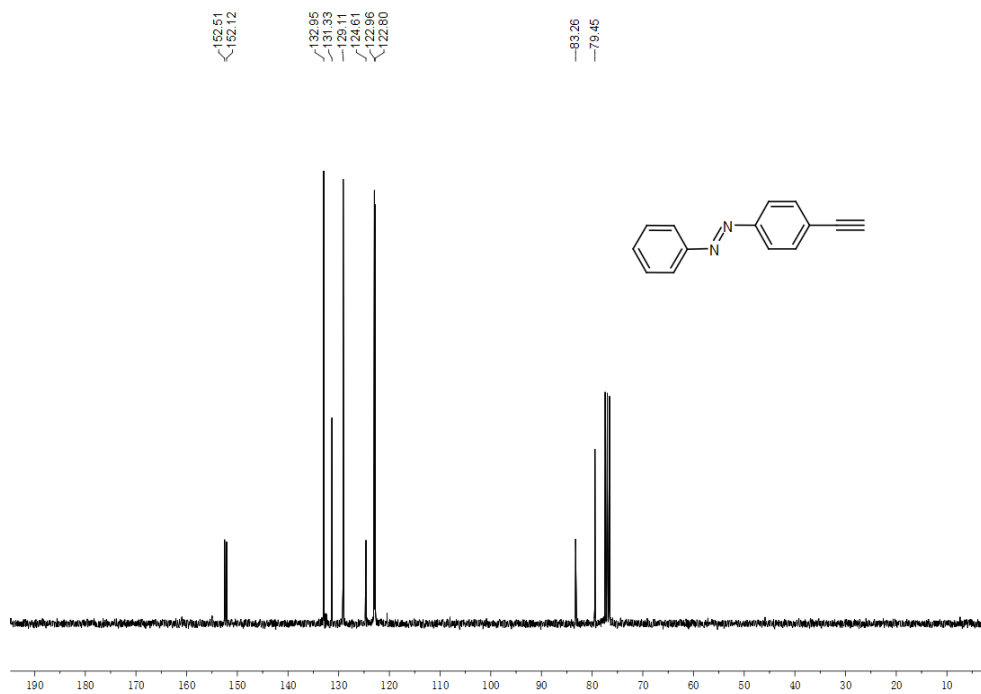
Figure 7.127. ¹³C NMR spectrum of *trans*-L2 in CDCl₃.
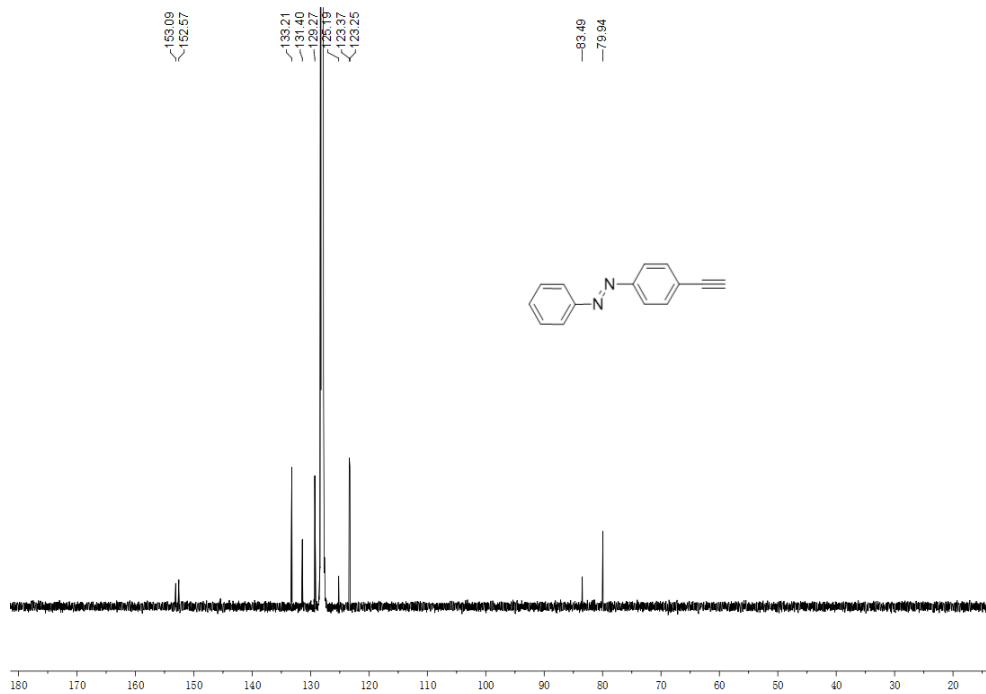
Figure 7.128. ^{13}C NMR spectrum of *trans*-L2 in C$_6$D$_6$.
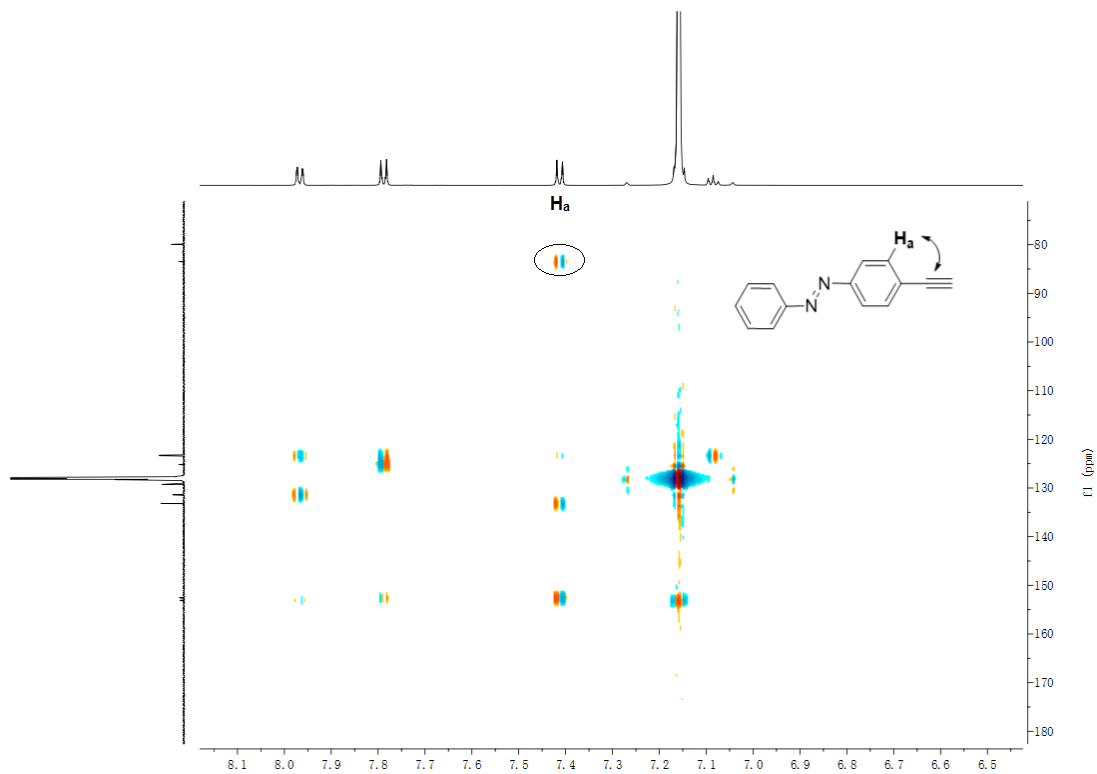
Figure 7.129. ^{1}H–^{13}C HMBC spectrum of *trans*-L2 in C$_6$D$_6$.
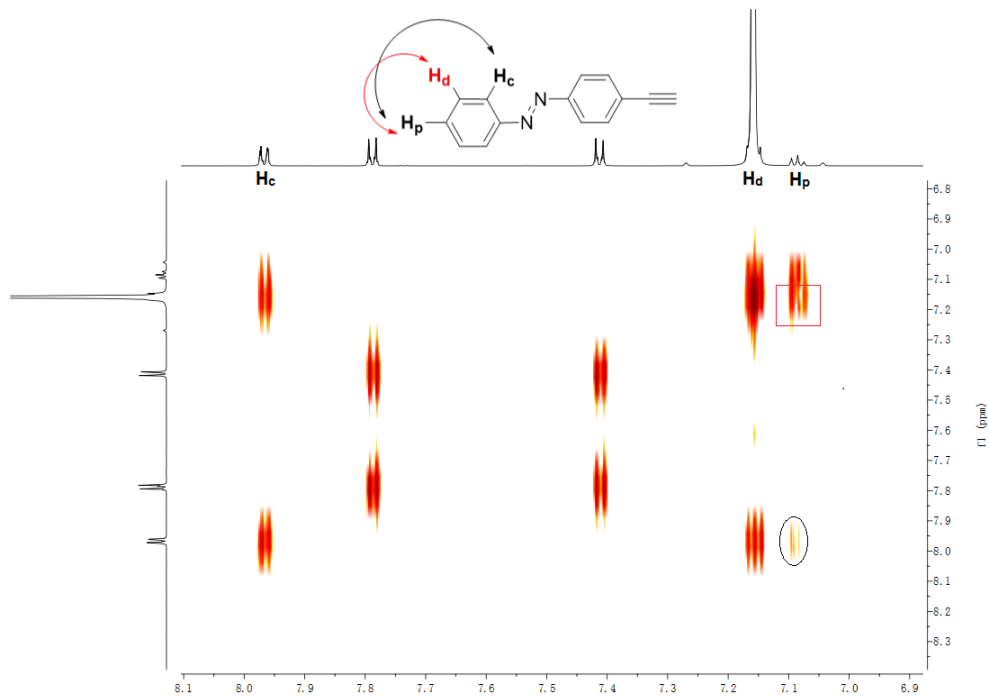
Figure 7.130. ^1H–^1H COSY spectrum of ***trans*-L2** in C_6D_6.
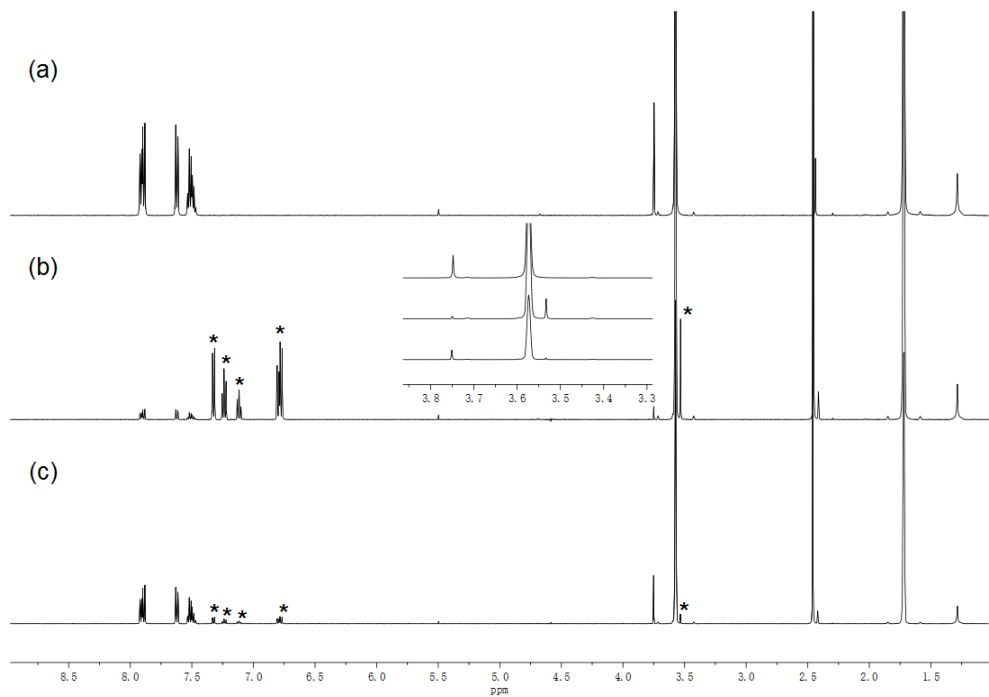
Figure 7.131. ^1H NMR spectra of **L2** in THF-d_6 (a) ***trans*-L2**; (b) irradiation at 365 nm for 4 h, at PSS with 90% ***cis*-L2**, *indicates ***cis*-L2**; and (c) irradiation at 450 nm for 4 h, at PSS with 85% ***trans*-L2**, *indicates ***cis*-L2**.
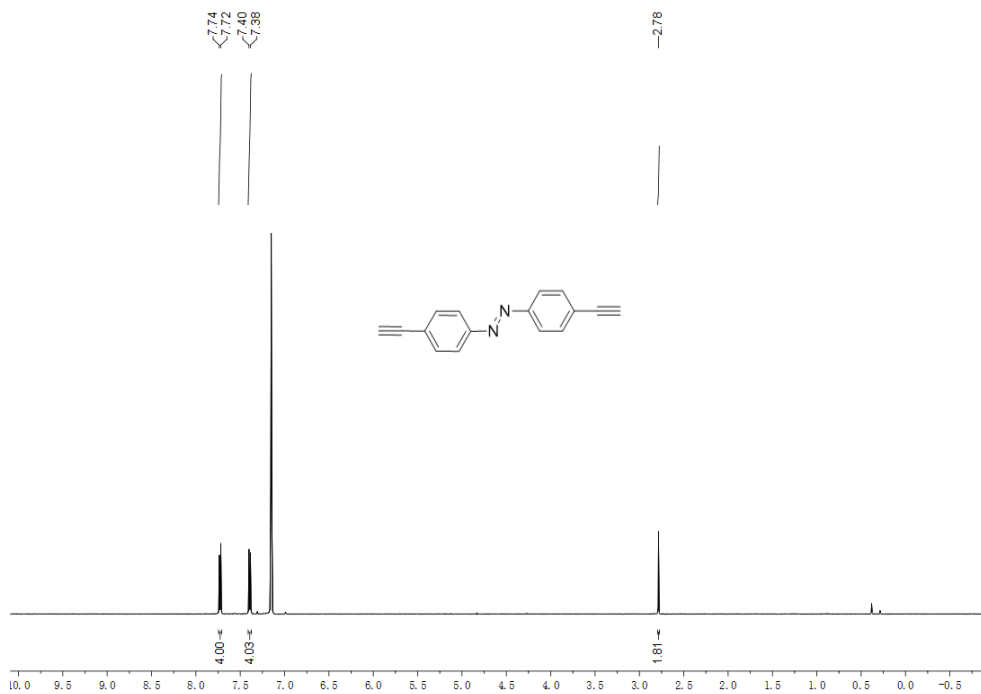
Figure 7.132. ^{1}H NMR spectrum of *trans*-**L3** in C$_6$D$_6$.
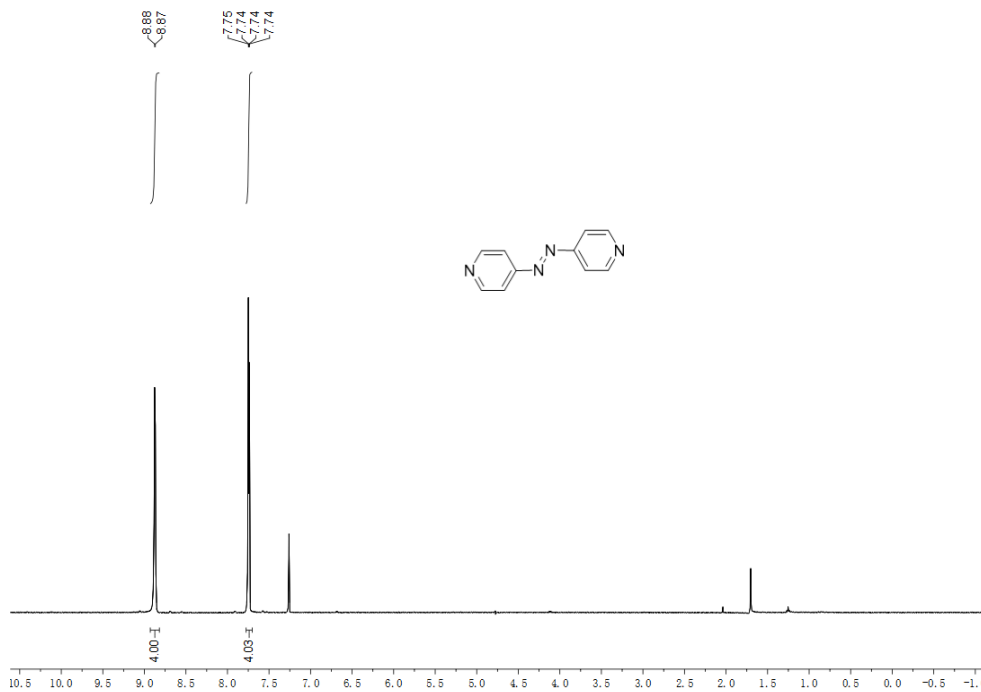
Figure 7.133. ^{1}H NMR spectrum of *trans*-**L4** in CDCl$_3$.

319
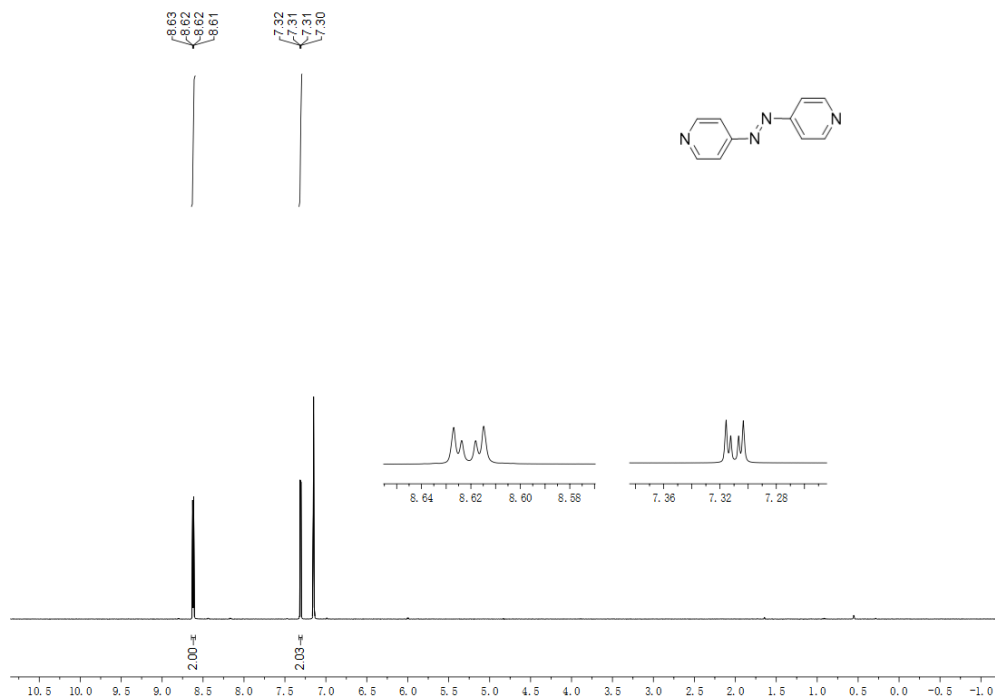
Figure 7.134. ^{1}H NMR spectrum of *trans*-L4 in C₆D₆.
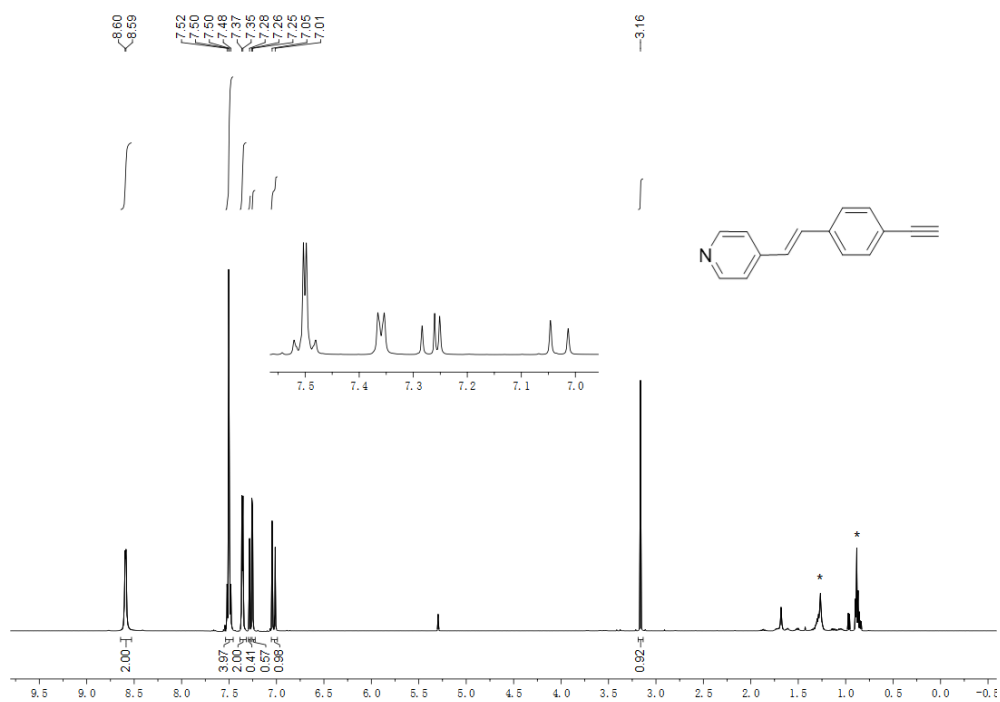
Figure 7.135. ^{1}H NMR spectrum of *trans*-L5 in CDCl₃ (*indicates residual hexanes solvent).
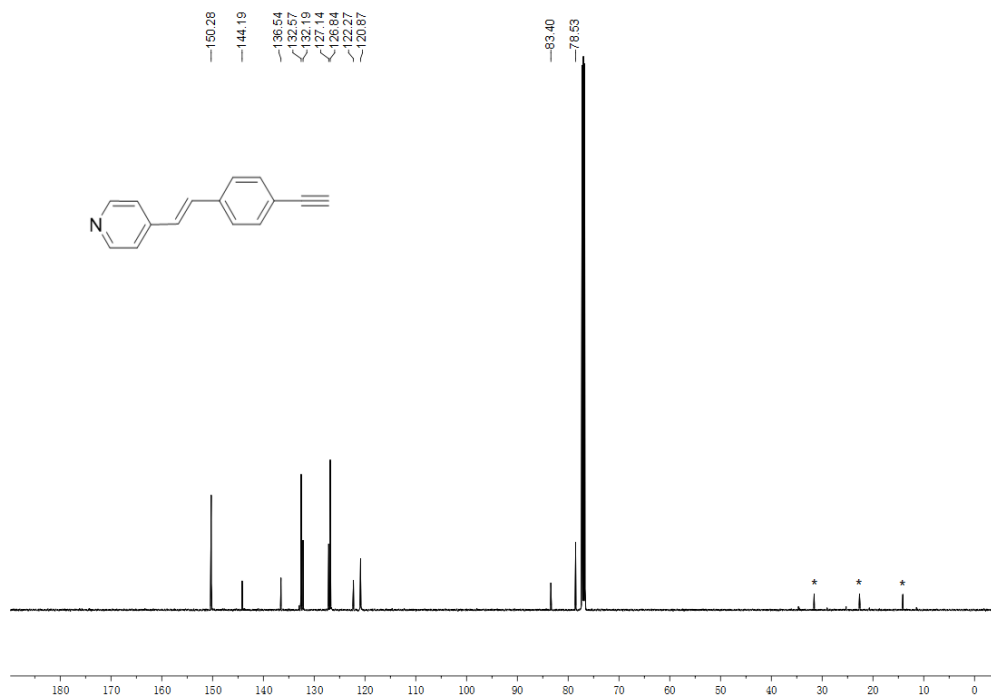
Figure 7.136. ^{13}C NMR spectrum of *trans*-**L5** in CDCl$_3$ (*indicates residual hexanes solvent).
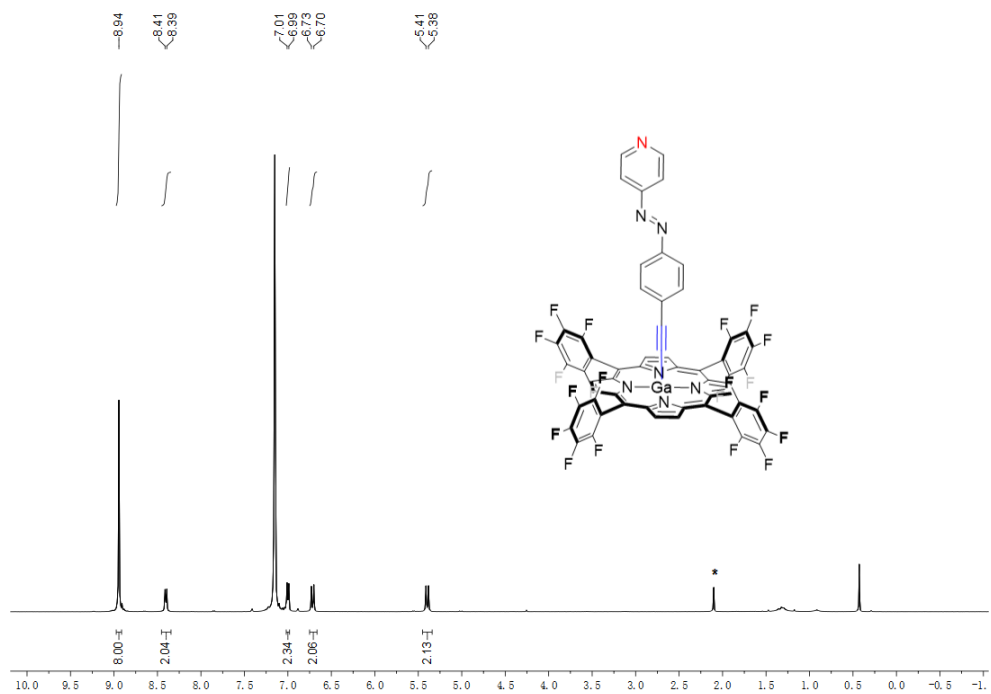
Figure 7.137. ^{1}H NMR spectrum of **GaL1** in C$_6$D$_6$ (*indicates toluene).
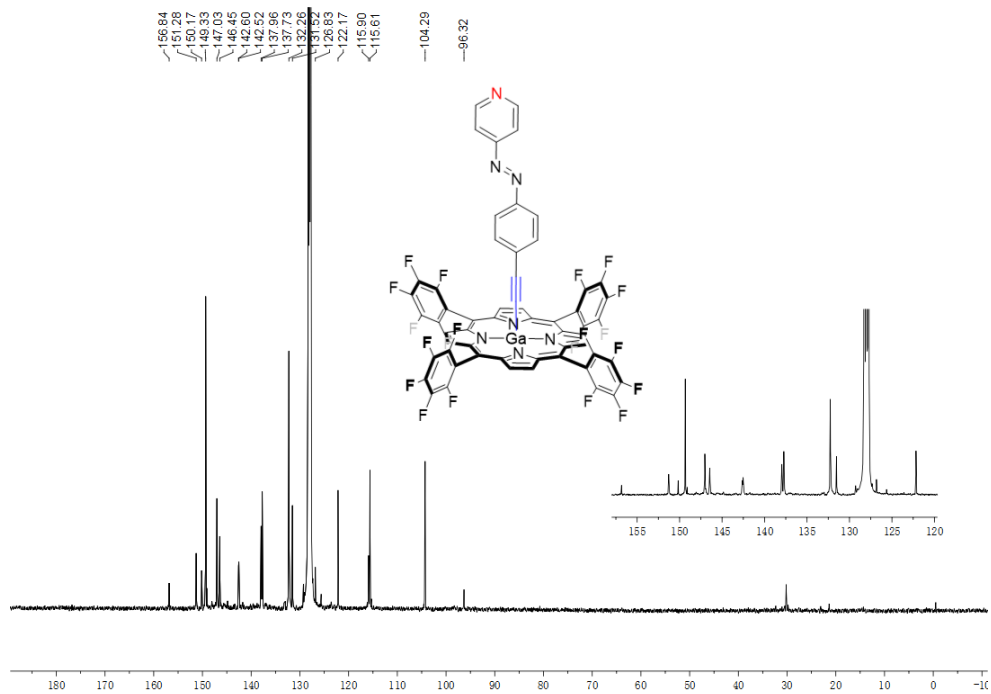
Figure 7.138. ^{13}C NMR spectrum of **GaL1** in C$_6$D$_6$.
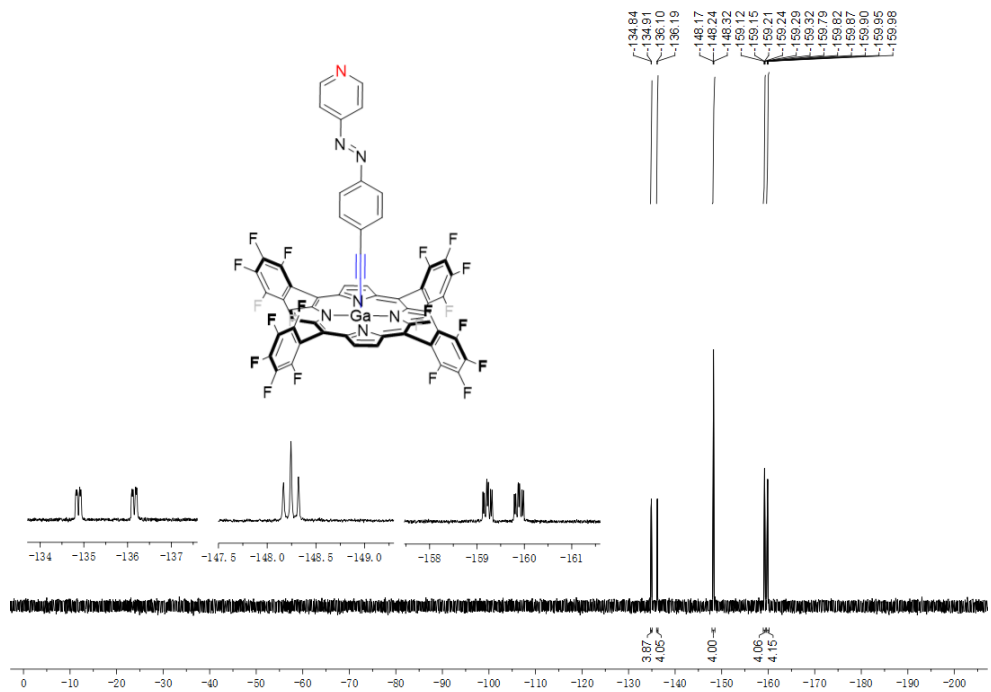
Figure 7.139. ^{19}F NMR spectrum of **GaL1** in C$_6$D$_6$.
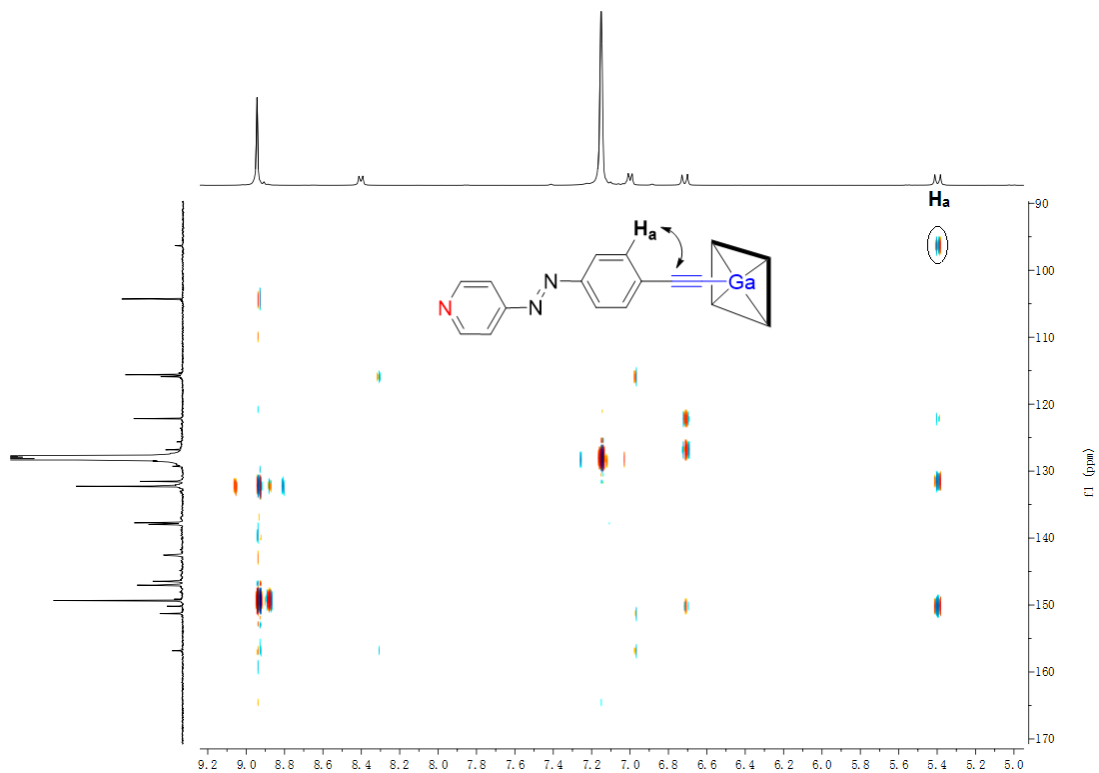
Figure 7.140. ^{1}H–^{13}C HMBC spectrum of **GaL1** in C_6D_6.
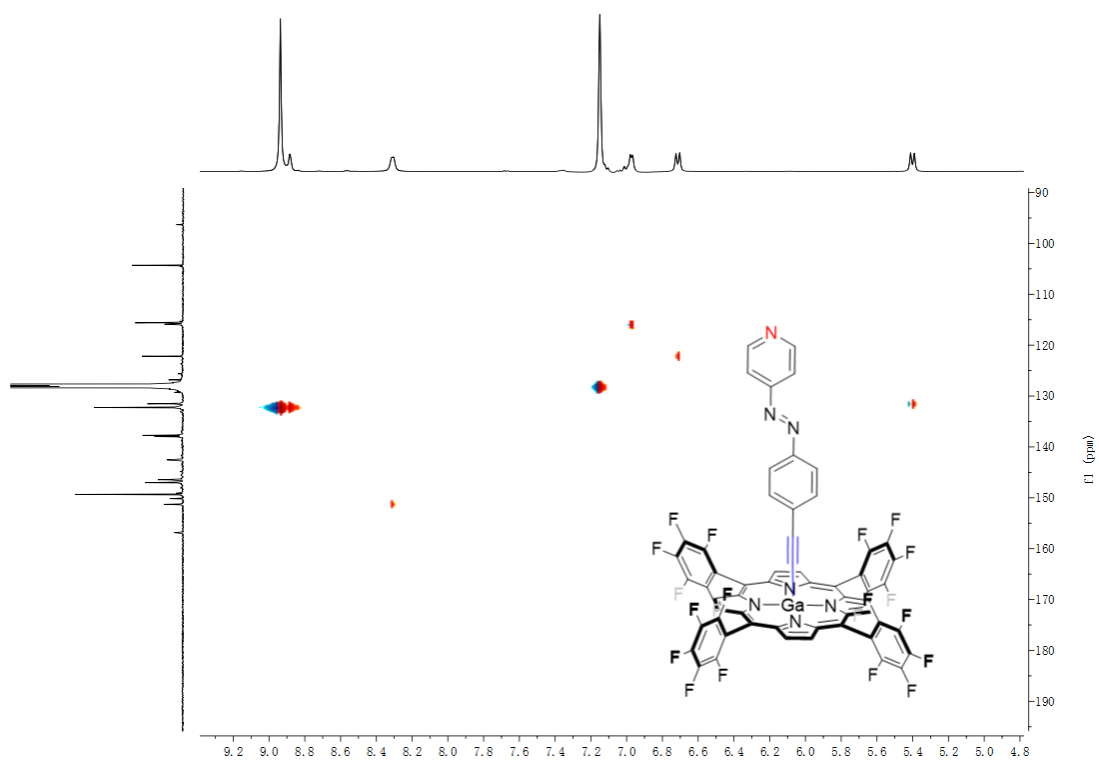
Figure 7.141. ^{1}H–^{13}C HSQC spectrum of **GaL1** in C_6D_6.
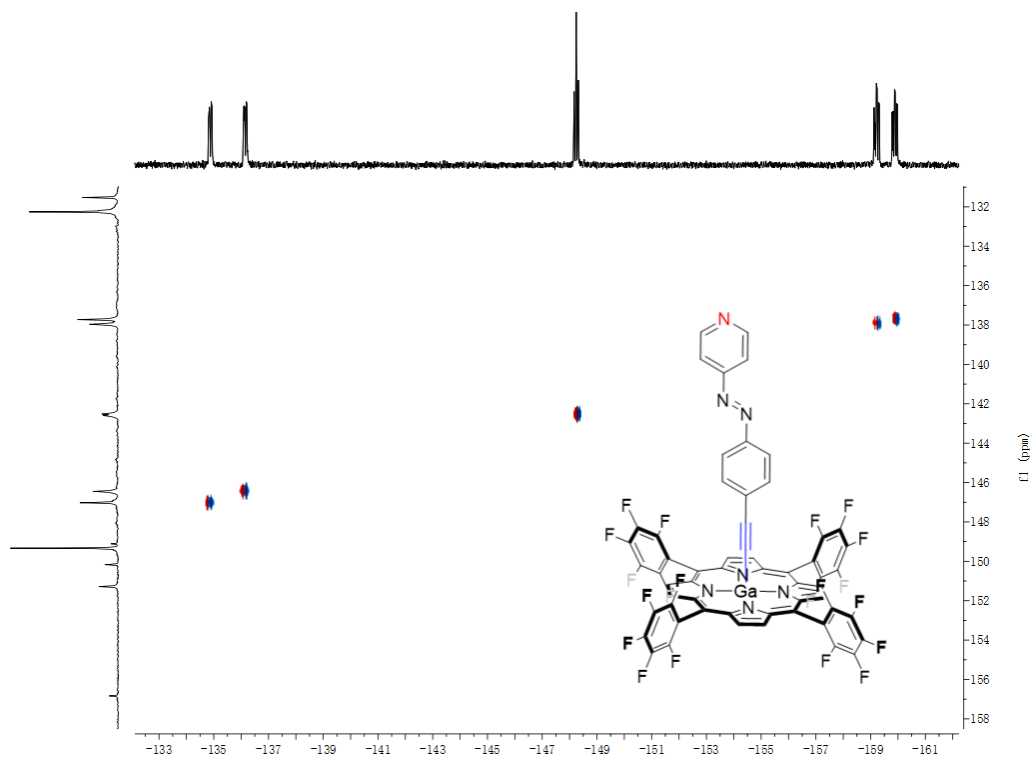
Figure 7.142. $^{19}F-^{13}C$ HSQC spectrum of **GaL1** in C_6D_6.
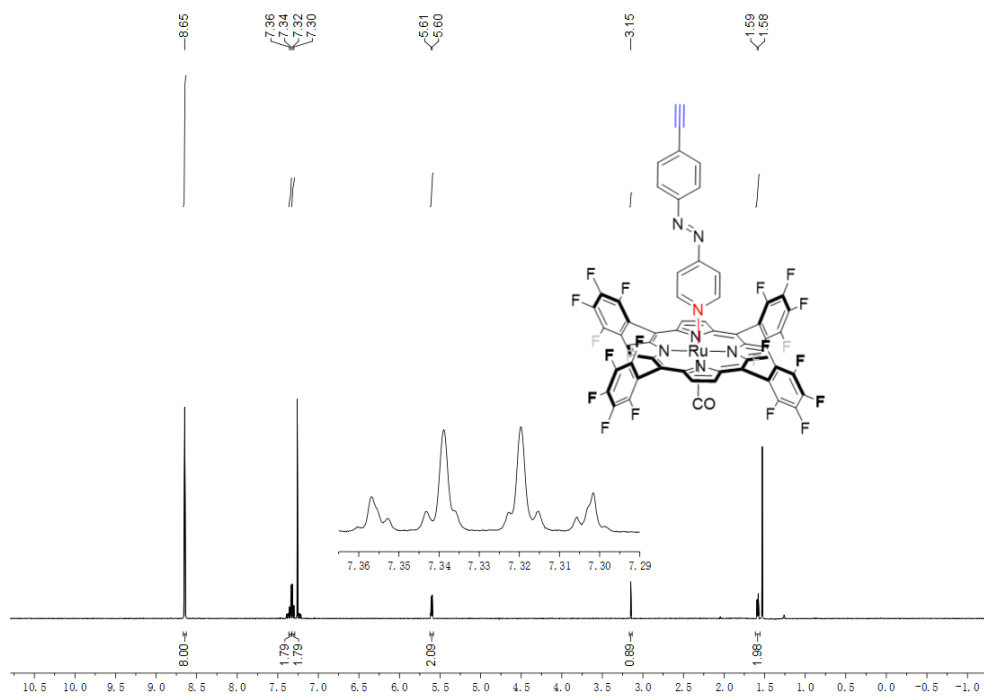
Figure 7.143. ^1H NMR spectrum of **RuL1** in $CDCl_3$.
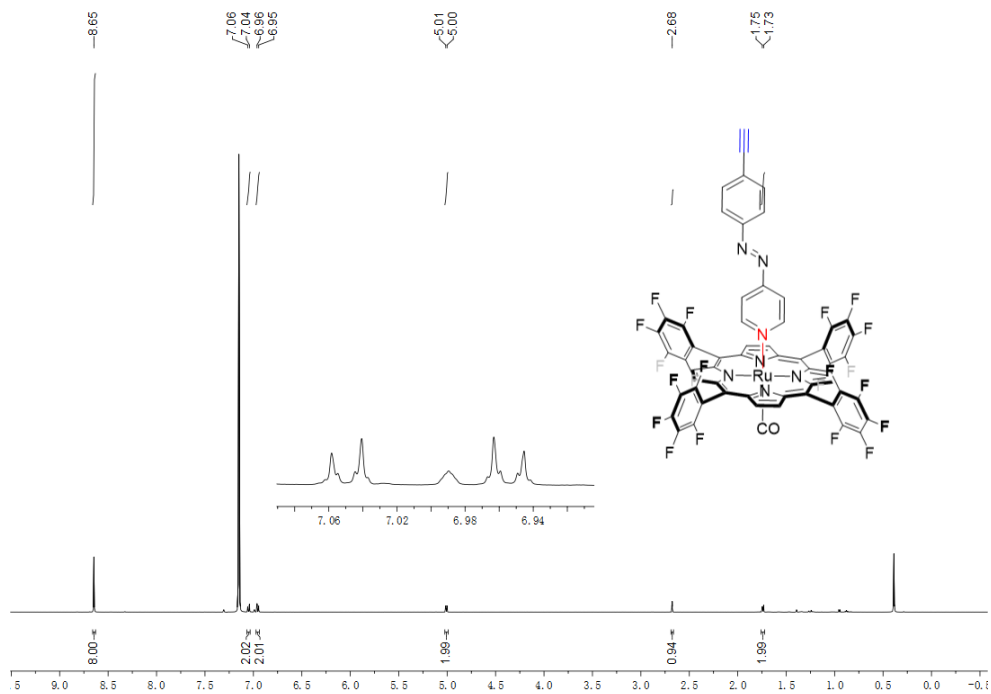
Figure 7.144. ^{1}H NMR spectrum of **RuL1** in C$_6$D$_6$.
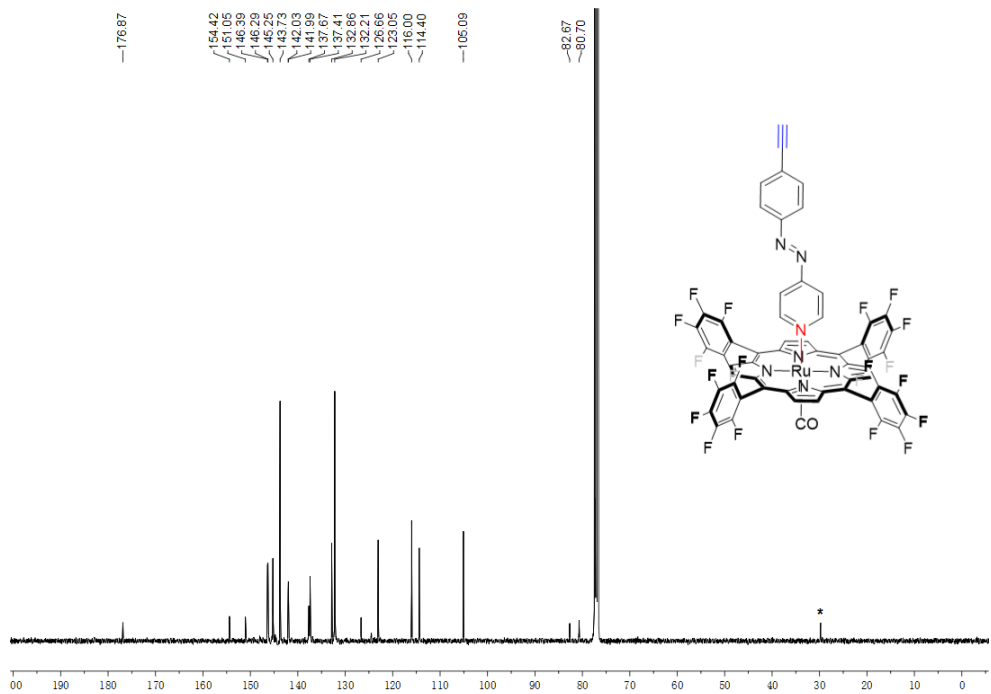
Figure 7.145. ^{13}C NMR spectrum of **RuL1** in CDCl$_3$ (*indicates H grease).
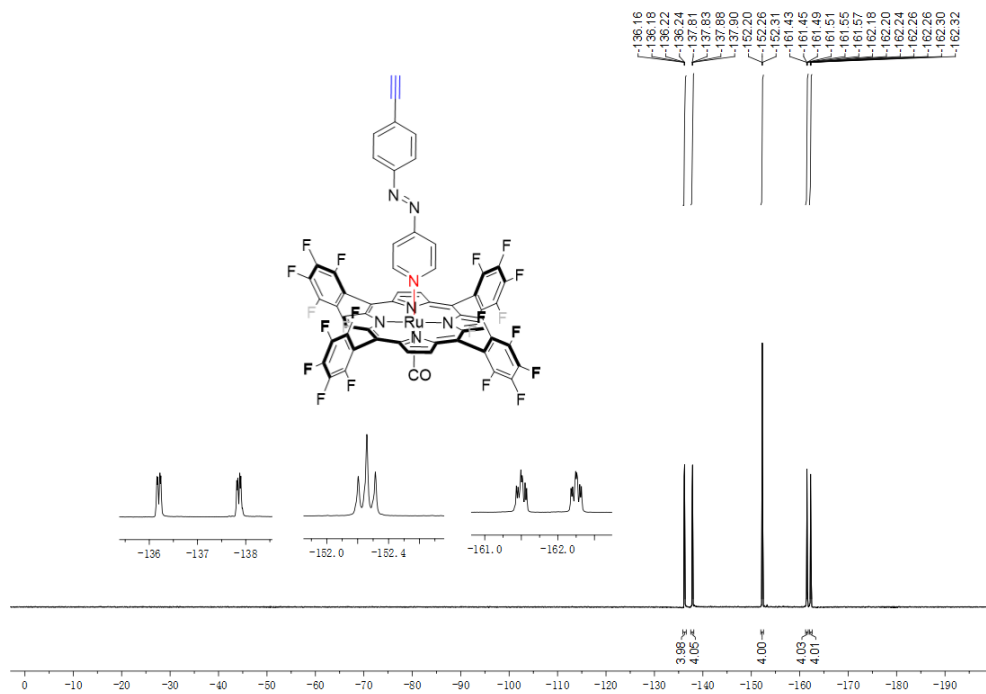
Figure 7.146. ^{19}F NMR spectrum of **RuL1** in CDCl$_3$.
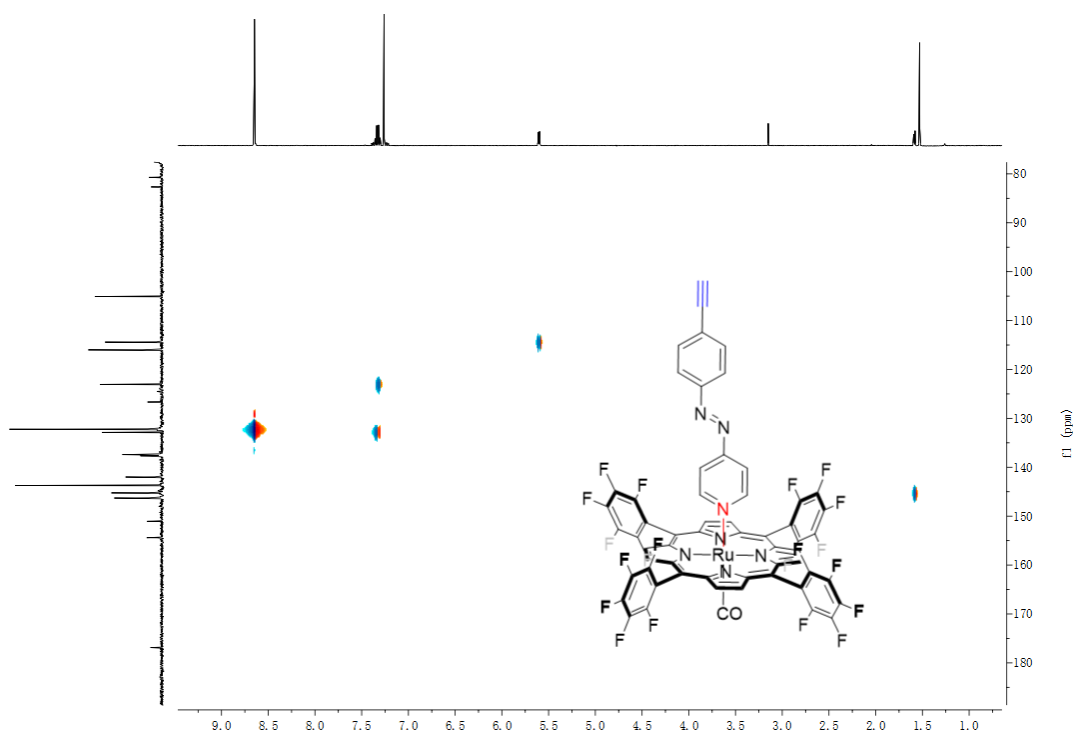
Figure 7.147. ^{1}H–^{13}C HSQC spectrum of **RuL1** in CDCl$_3$.
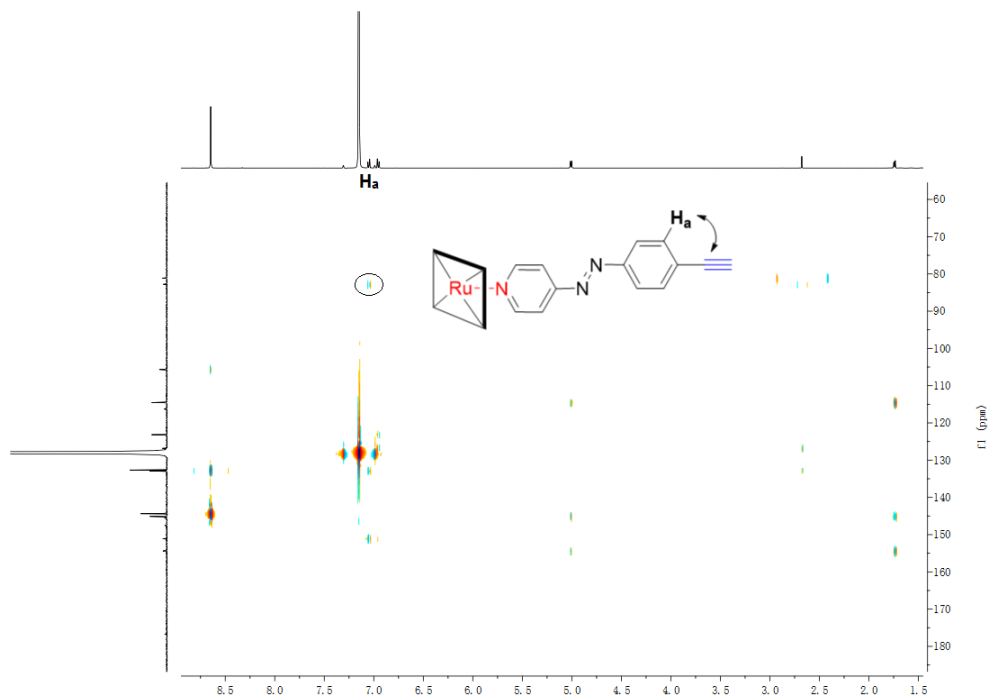
Figure 7.148. ^{1}H–^{13}C HMBC spectrum of **RuL1** in C$_6$D$_6$.
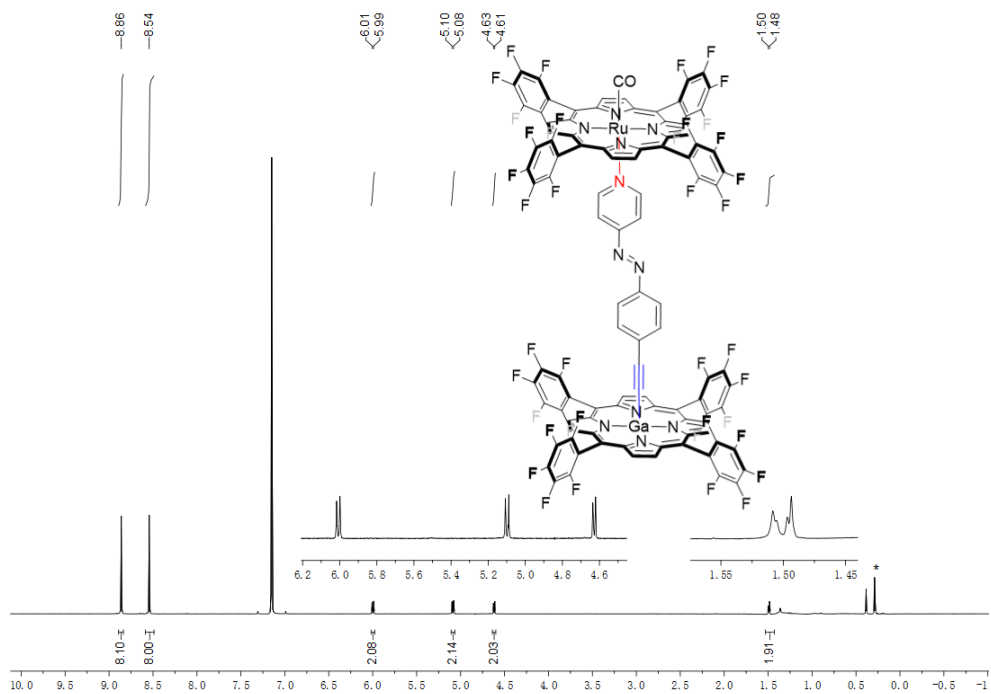
Figure 7.149. ^{1}H NMR spectrum of **GaL1Ru** in C$_6$D$_6$ (*indicates silicone grease).
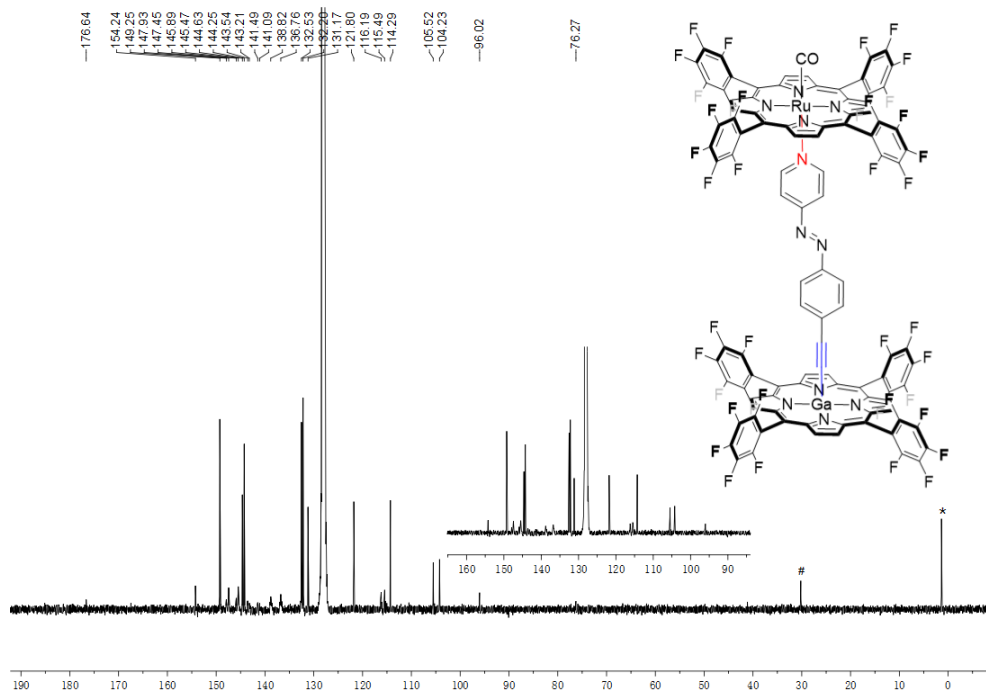
Figure 7.150. ^{13}C NMR spectrum of **GaL1Ru** in C$_6$D$_6$ ($^{\#}$indicates H grease and *silicone grease).
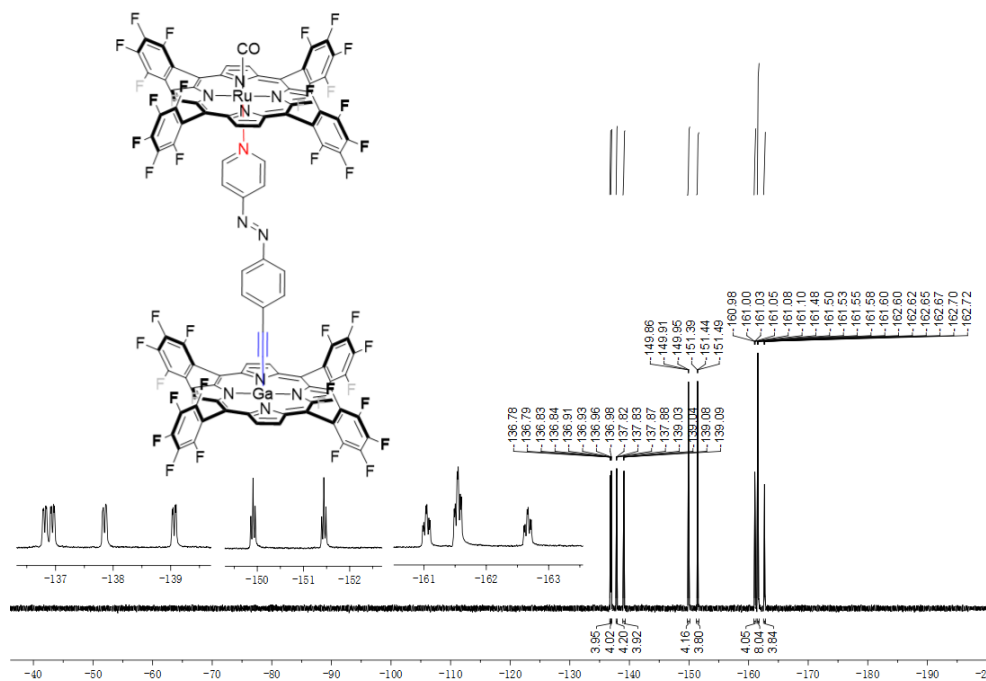
Figure 7.151. ^{19}F NMR spectrum of **GaL1Ru** in C$_6$D$_6$.
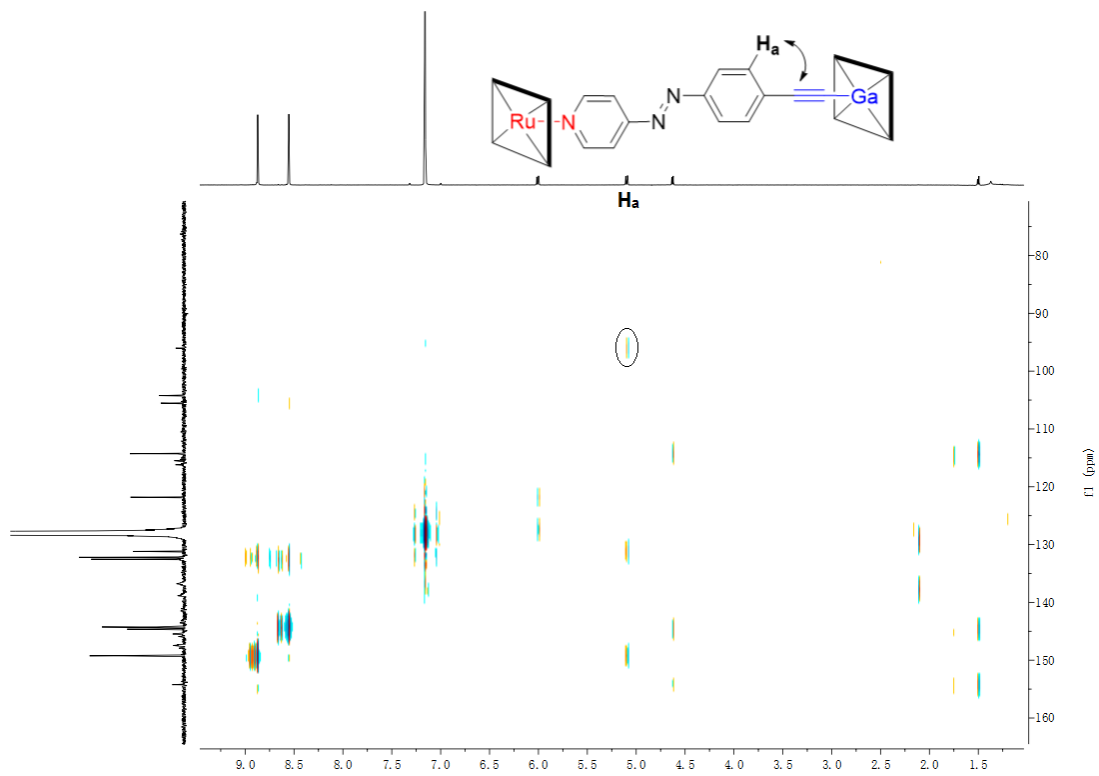
Figure 7.152. HMBC spectrum of **GaL1Ru** in C_6D_6.
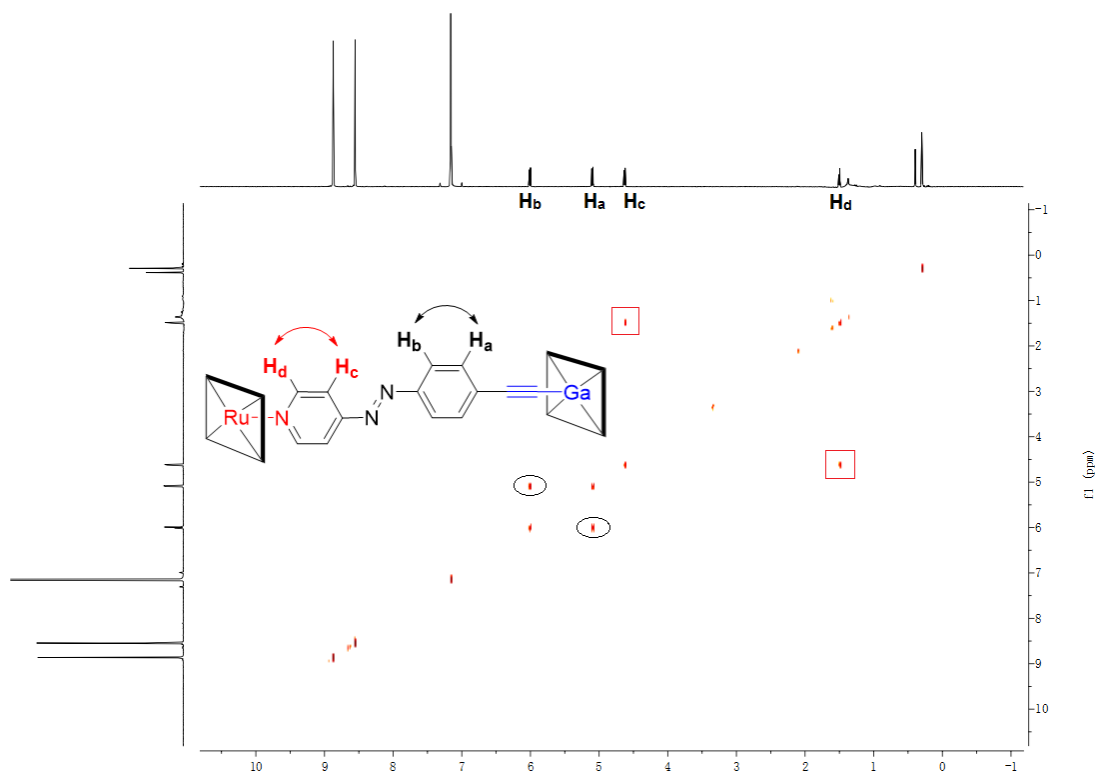
Figure 7.153. ^{1}H–^{1}H COSY spectrum of **GaL1Ru** in C_6D_6.

329
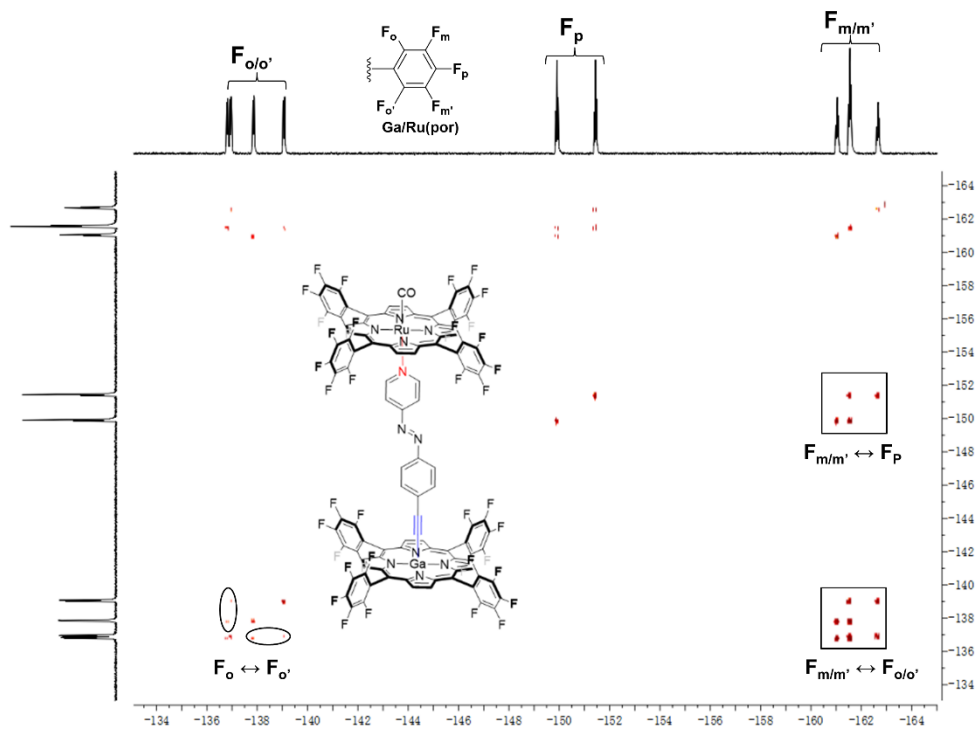
Figure 7.154. $^{19}F-^{19}F$ COSY spectrum of **GaL1Ru** in C_6D_6.
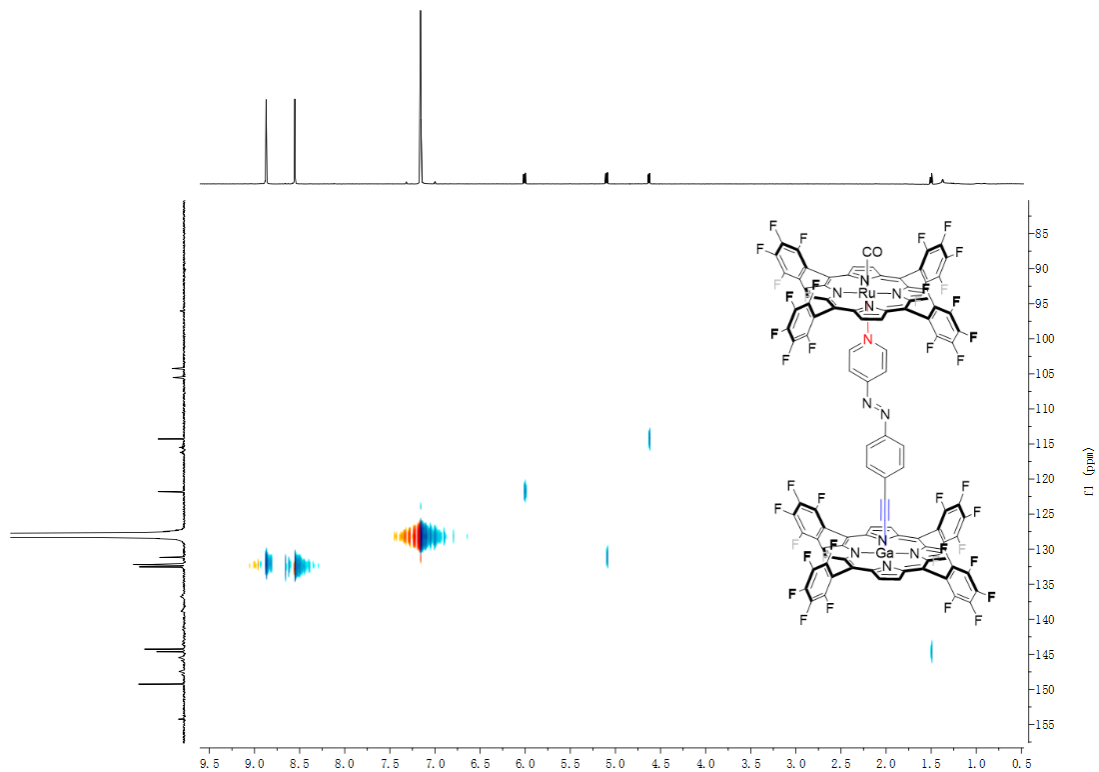
Figure 7.155. $^1H-^{13}C$ HSQC spectrum of **GaL1Ru** in C_6D_6.
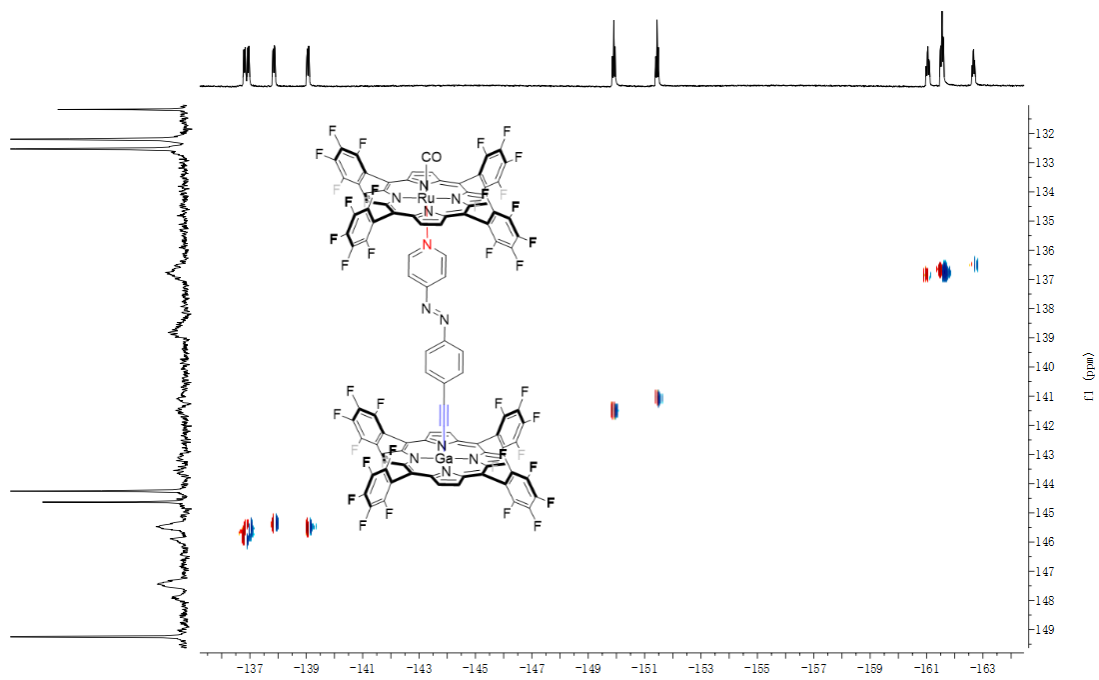
Figure 7.156. $^{19}F-^{13}C$ HSQC spectrum of **GaL1Ru** in C_6D_6.
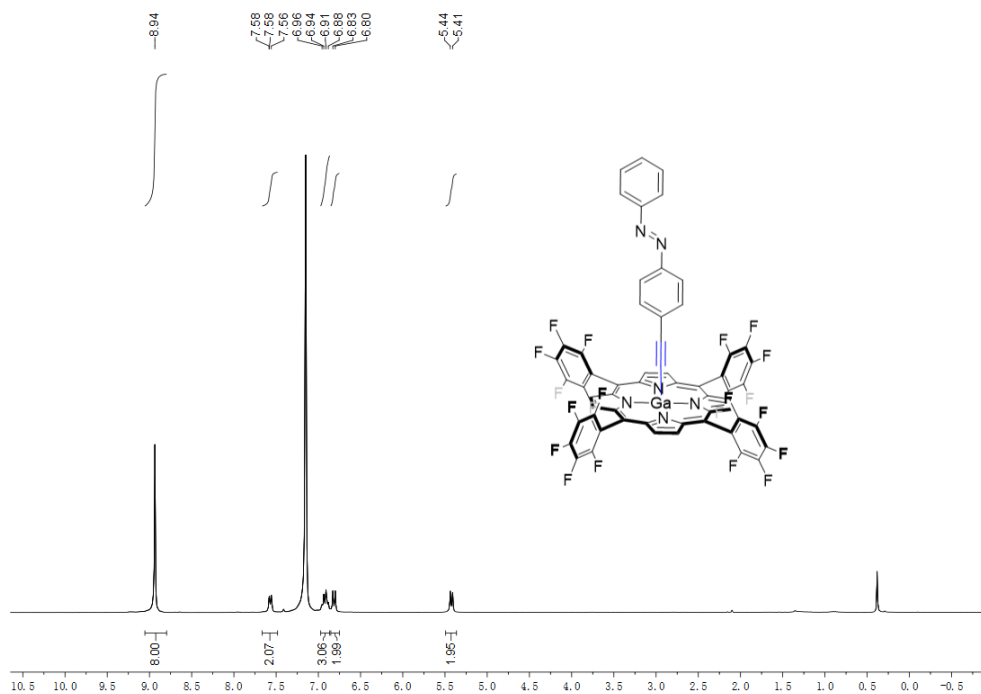
Figure 7.157. ^1H NMR (300 M) spectrum of **GaL2** in C_6D_6.
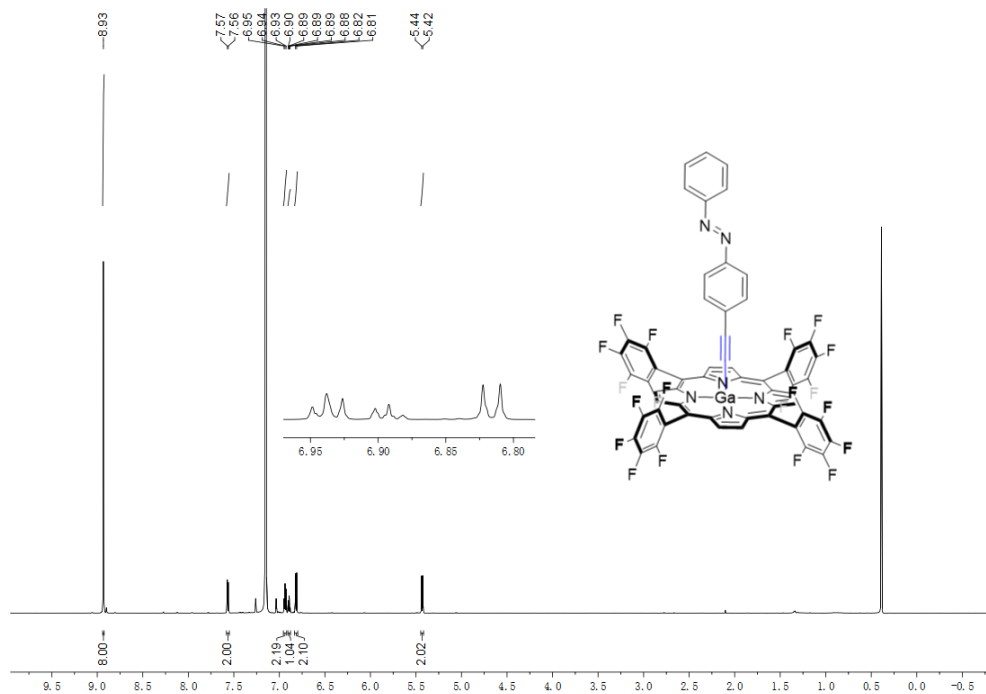
Figure 7.158. ^{1}H NMR (700 M) spectrum of **GaL2** in C_6D_6.
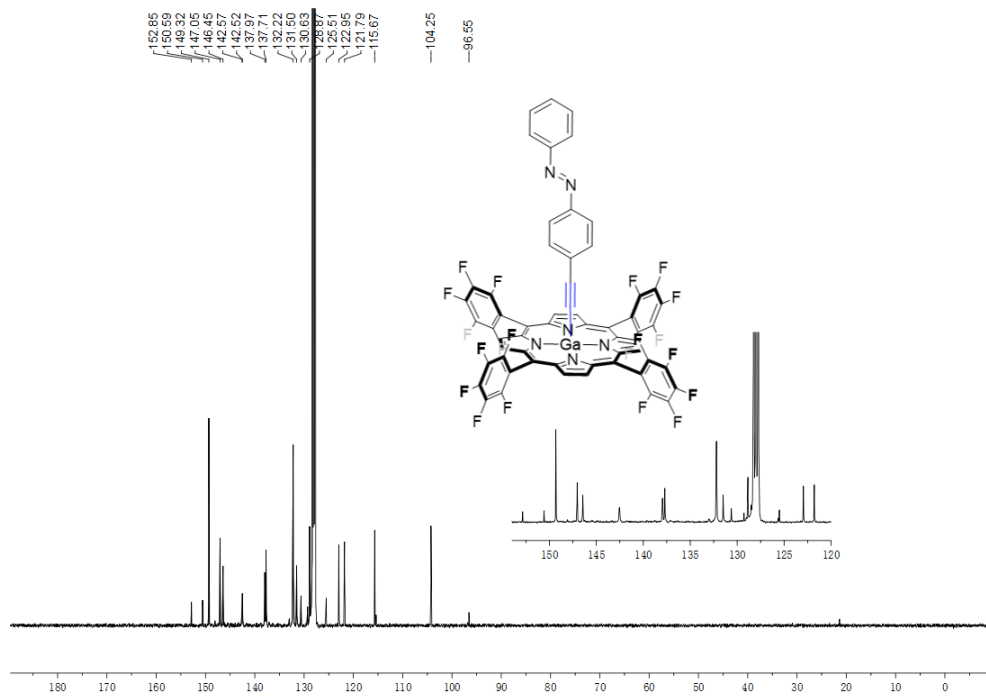
Figure 7.159. ^{13}C NMR spectrum of **GaL2** in C_6D_6.
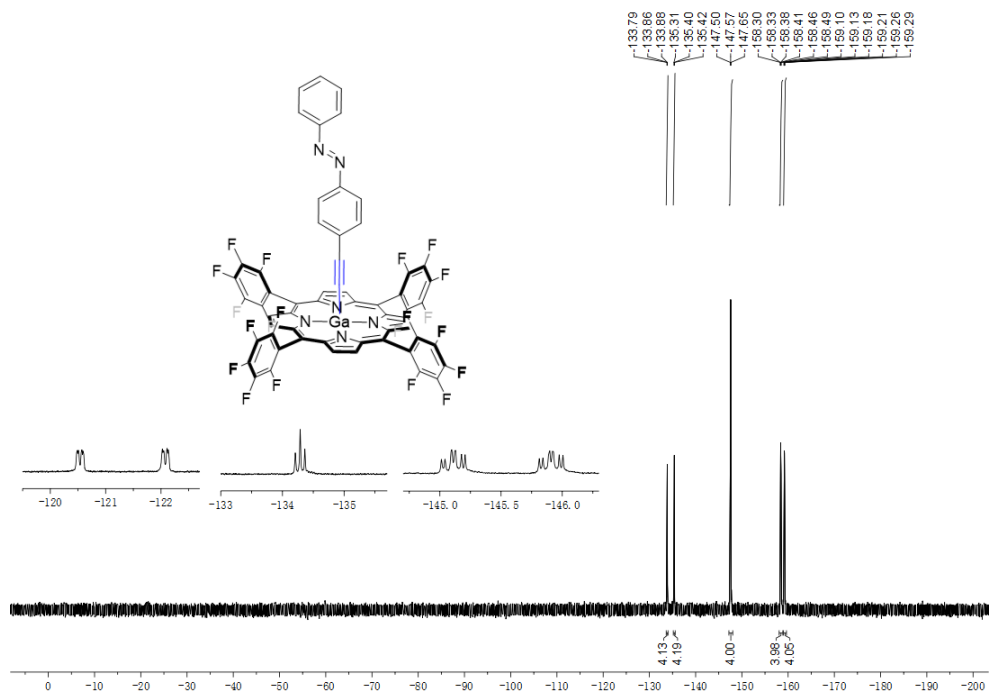
Figure 7.160. ^{19}F NMR spectrum of **GaL2** in C_6D_6.
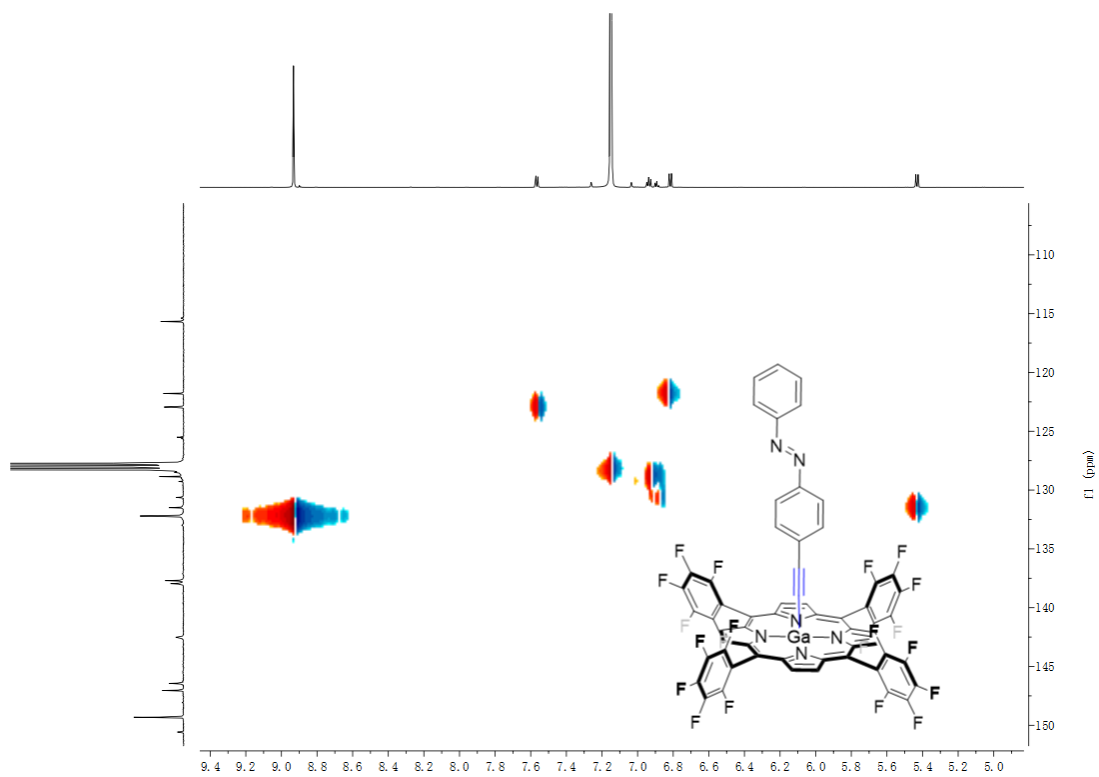
Figure 7.161. ^{1}H–^{13}C HSQC spectrum of **GaL2** in C_6D_6.
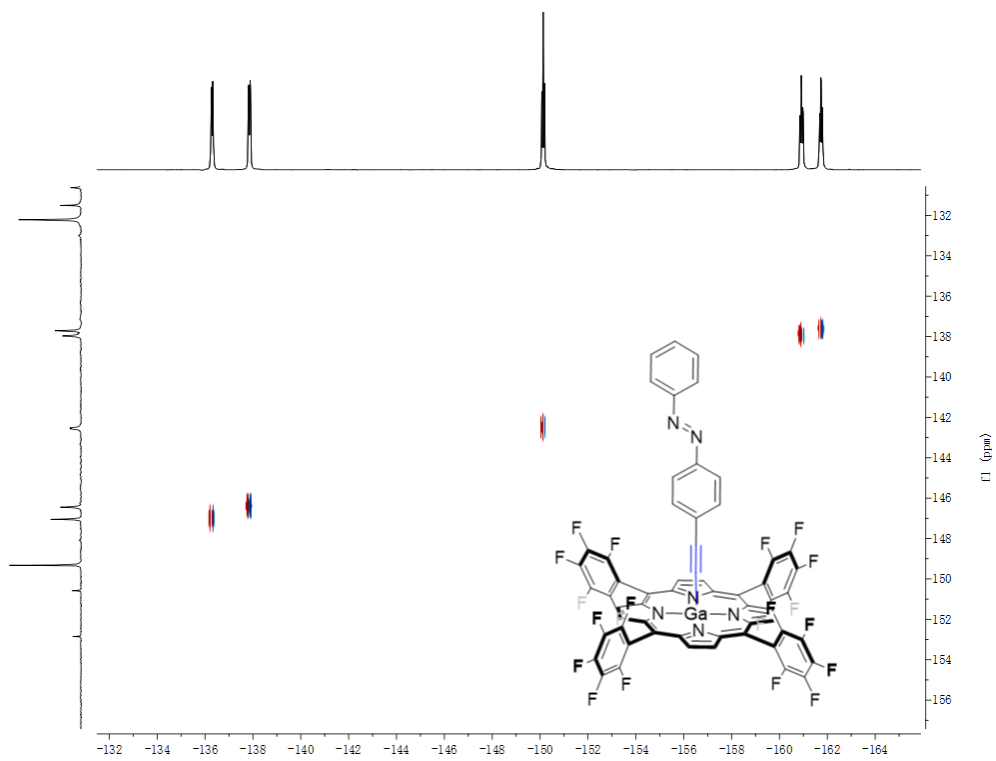
Figure 7.162. ^{19}F–^{13}C HSQC spectrum of **GaL2** in C_6D_6.
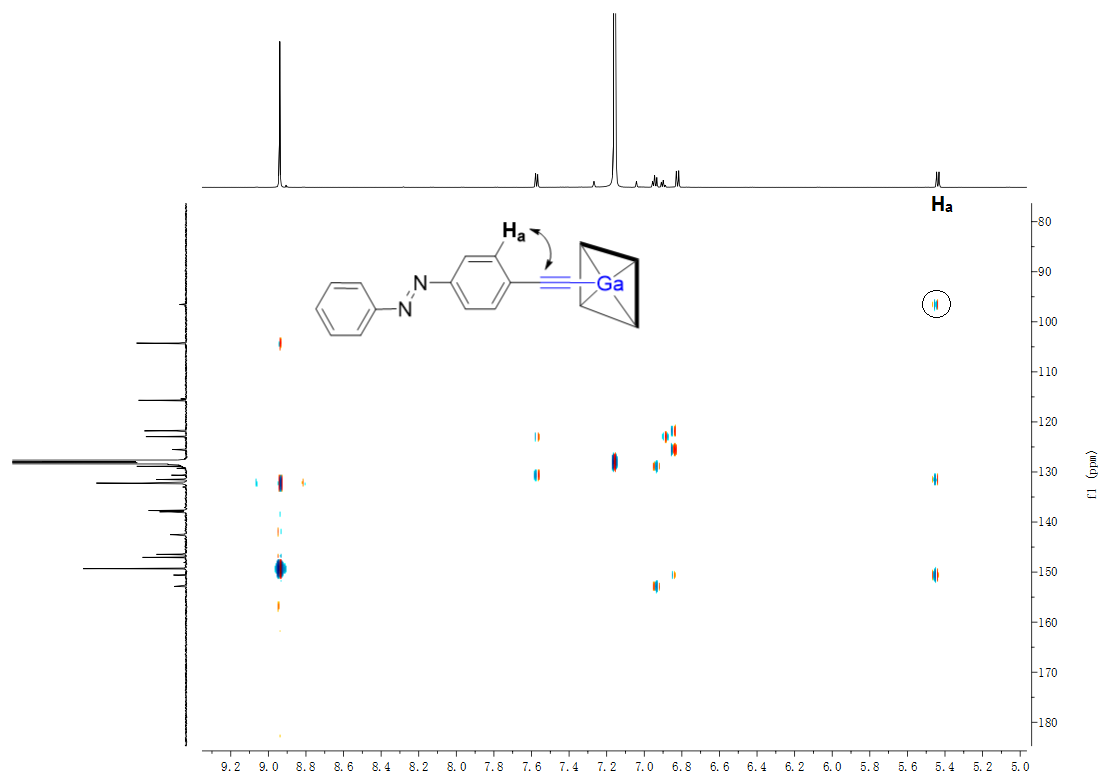
Figure 7.163. ^{1}H–^{13}C HMBC spectrum of **GaL2** in C_6D_6.
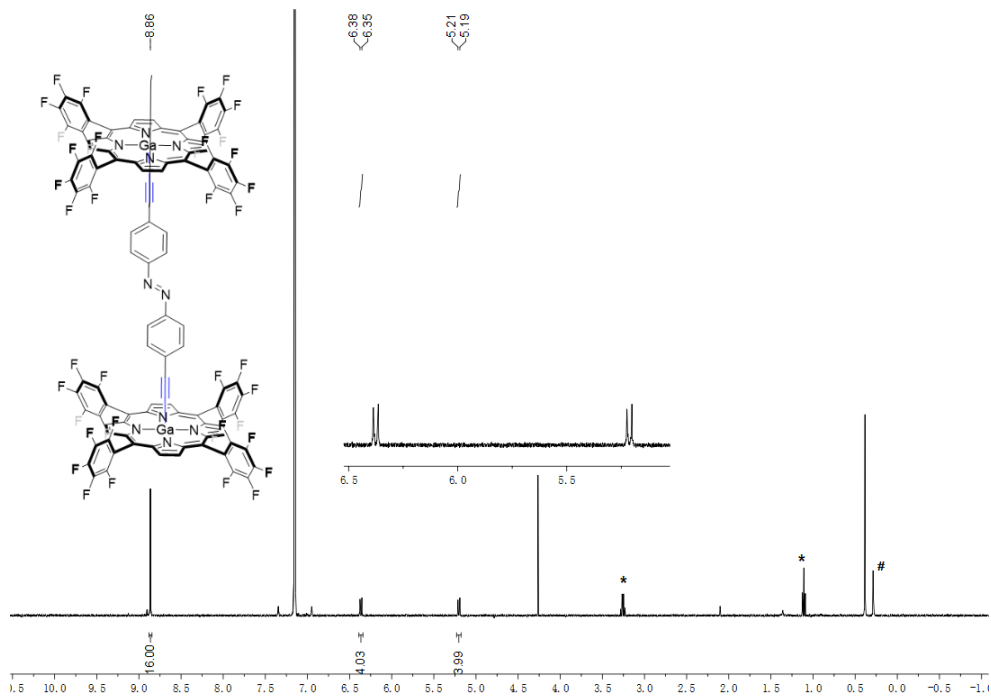
Figure 7.164. ^{1}H NMR spectrum of **GaL3Ga** in C_6D_6 (*indicates diethyl ether and $^\#$silicone grease).
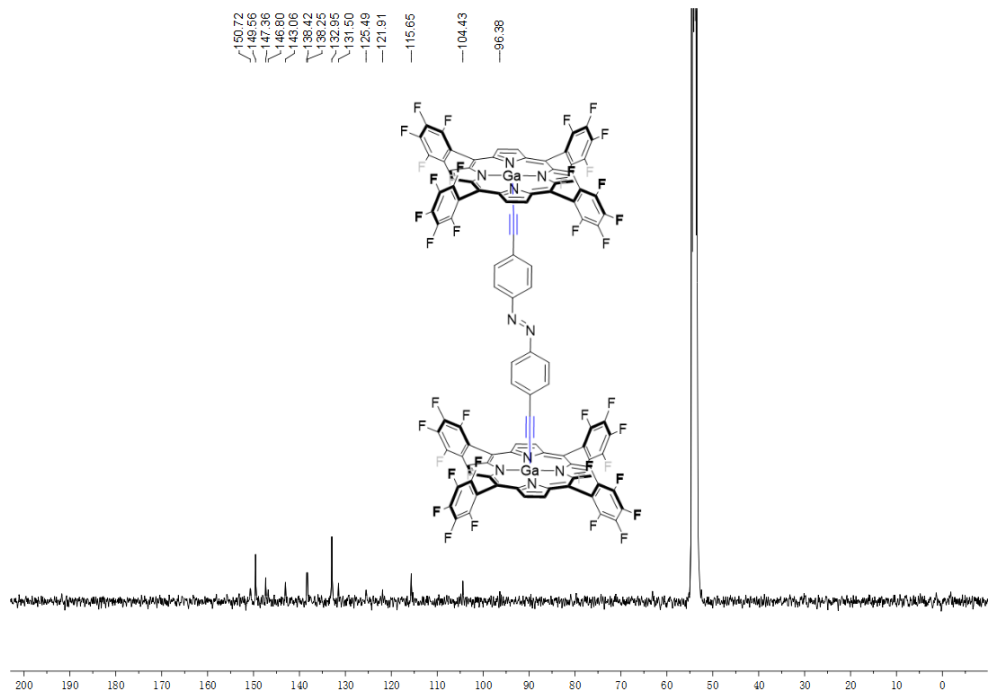
Figure 7.165. ^{13}C NMR spectrum of **GaL3Ga** in CD_2Cl_2.
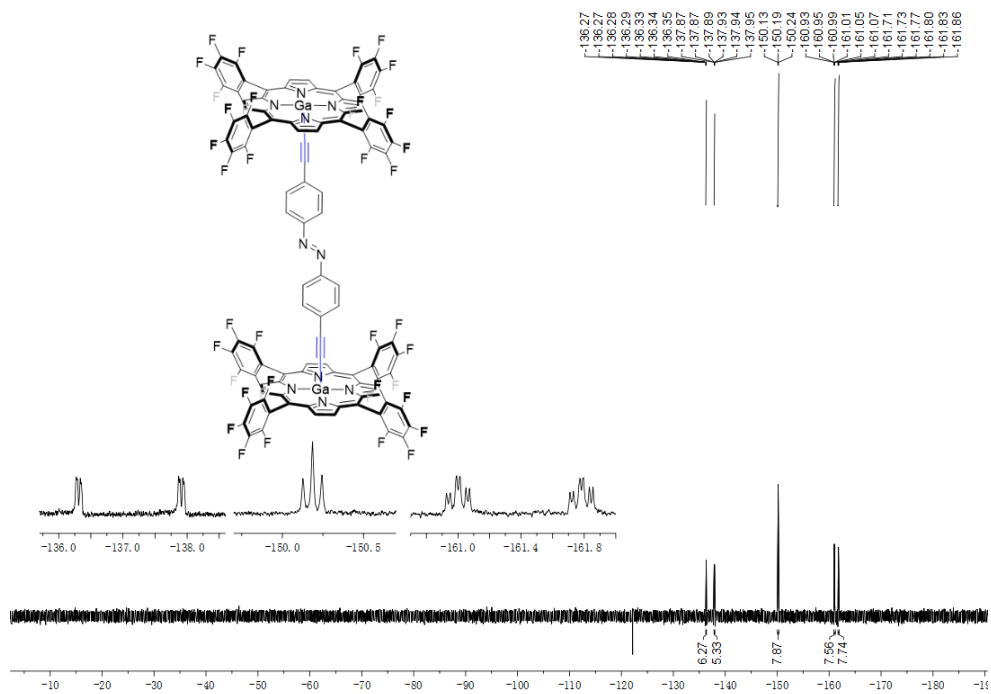
Figure 7.166. ^{19}F NMR spectrum of **GaL3Ga** in C$_6$D$_6$.
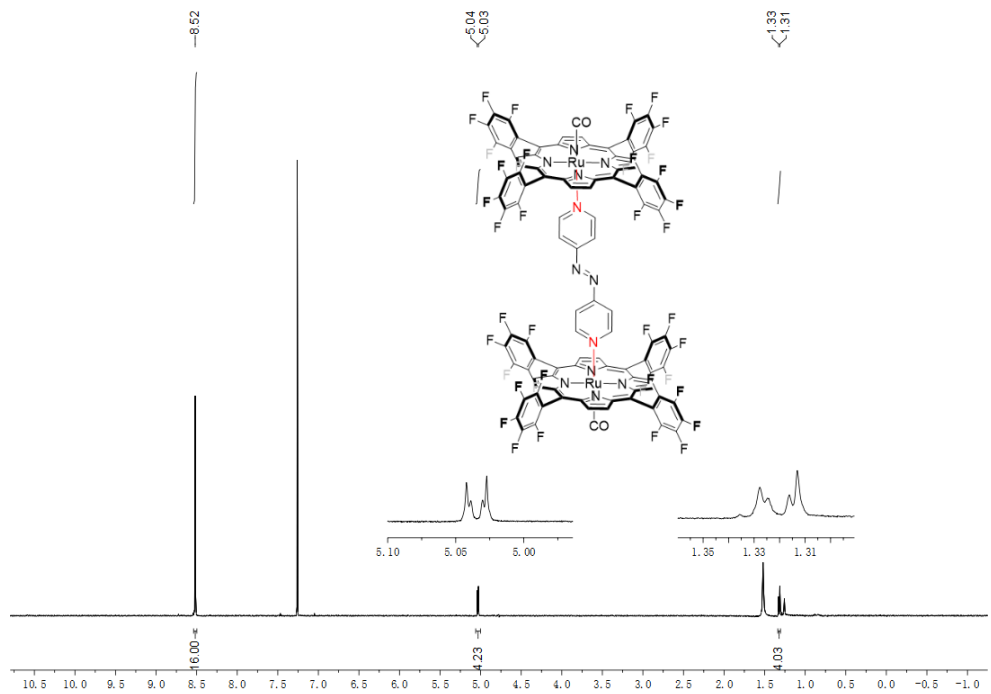
Figure 7.167. ^{1}H NMR spectrum of **RuL4Ru** in CDCl$_3$.
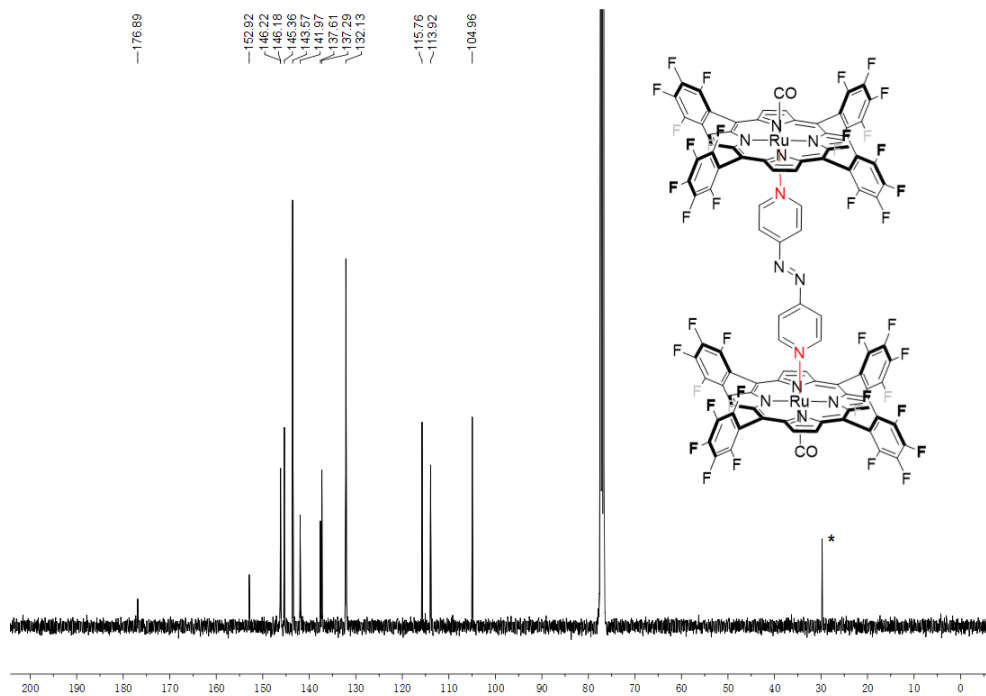
Figure 7.168. ^{13}C NMR spectrum of **RuL4Ru** in CDCl$_3$ (*indicates silicone grease).
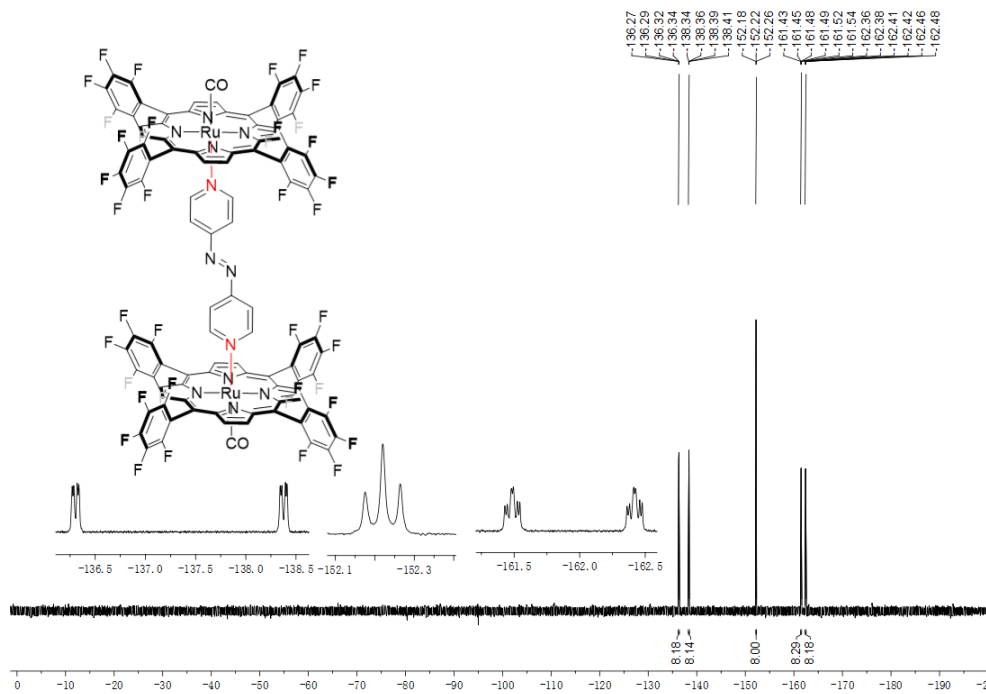
Figure 7.169. ^{19}F NMR spectrum of **RuL4Ru** in CDCl$_3$.
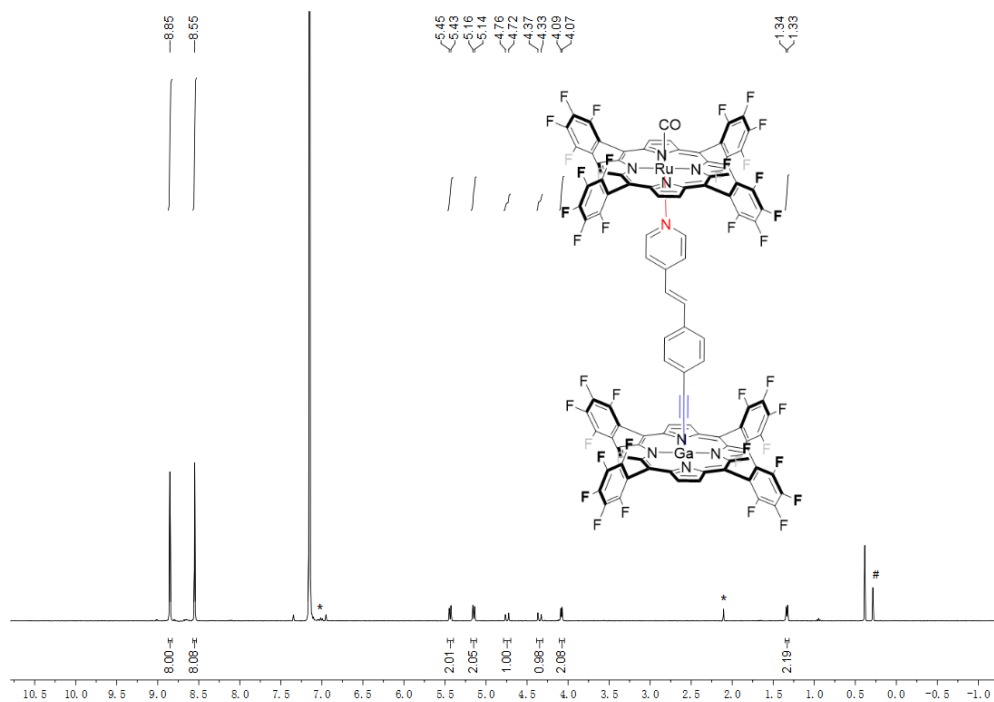
Figure 7.170. ^{1}H NMR spectrum of **GaL5Ru** in C$_6$D$_6$ (*indicates residual toluene solvent; #indicates silicone grease).
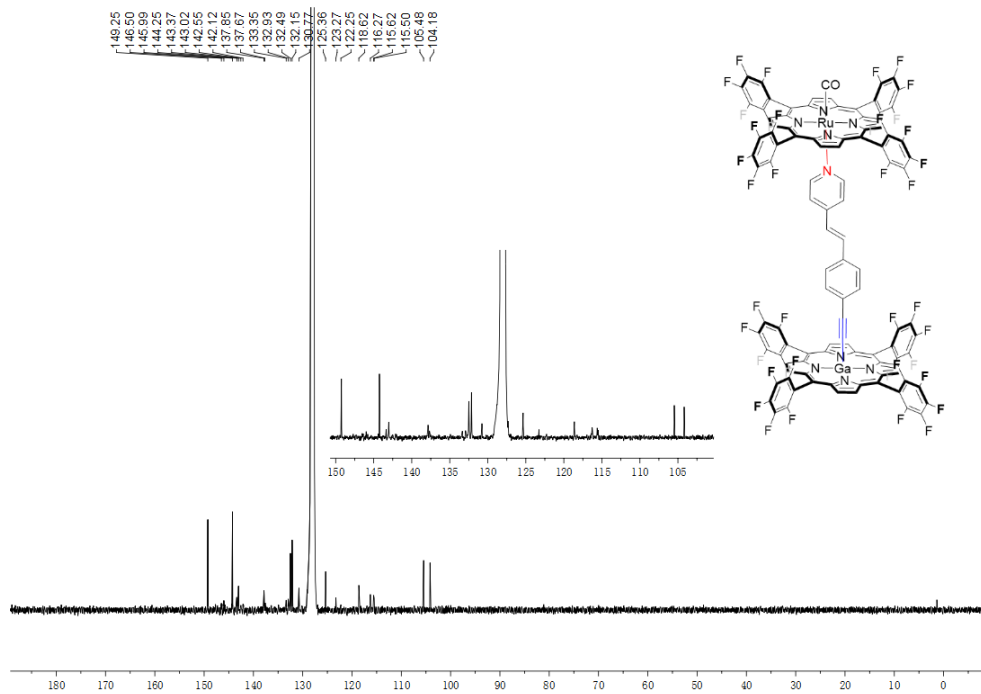
Figure 7.171. ^{13}C NMR spectrum of **GaL5Ru** in C$_6$D$_6$.

338
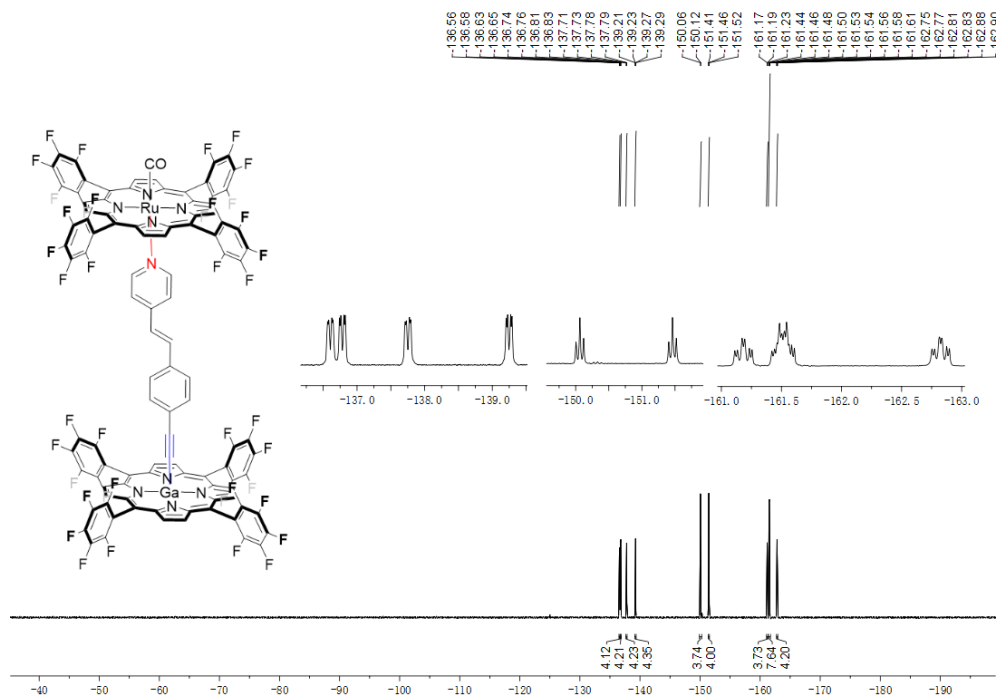
Figure 7.172. ^{19}F NMR spectrum of **GaL5Ru** in C_6D_6.

7.7 References

[1]   J. Ranta, T. Kumpulainen, H. Lemmetyinen, A. Efimov, *J. Org. Chem.* **2010**, *75*, 5178–5194.

[2]   a) D. N. Coventry, A. S. Batsanov, A. E. Goeta, J. A. Howard, T. B. Marder, R. N. Perutz, *Chem. Commun.* **2005**, 2172–2174; b) A. G. Crawford, Z. Liu, I. A. Mkhalid, M. H. Thibault, N. Schwarz, G. Alcaraz, A. Steffen, J. C. Collings, A. S. Batsanov, J. A. Howard, T. B. Marder, *Chem. Eur. J.* **2012**, *18*, 5022–5035.

[3]   a) A. C. Spivey, T. Fekner, S. E. Spey, *J. Org. Chem.* **2000**, *65*, 3154–3159; b) O. S. Tee, M. Paventi, *Can. J. Chem.* **1983**, *61*, 2556–2562; c) L. Robke, T. Rodrigues, P. Schröder, D. J. Foley, G. J. L. Bernardes, L. Laraia, H. Waldmann, *Tetrahedron* **2018**, *74*, 4531–4537.

[4]   C. Eidamshaus, H.-U. Reissig, *Eur. J. Org. Chem.* **2011**, 6056–6069.

[5]   X. Yi, J. Chen, X. Xu, Y. Ma, *Synth. Commun.* **2017**, *47*, 872–877.

[6]   C. D. Campbell, R. L. Greenaway, O. T. Holton, P. R. Walker, H. A. Chapman, C. A. Russell, G. Carr, A. L. Thomson, E. A. Anderson, *Chem. Eur. J.* **2015**, *21*, 12627–12639.

[7]   X. Nie, G. Wang, *J. Org. Chem.* **2006**, *71*, 4734–4741.

[8]   M. Turlington, Y. Du, S. G. Ostrum, V. Santosh, K. Wren, T. Lin, M. Sabat, L. Pu, *J. Am. Chem. Soc.* **2011**, *133*, 11780–11794.

[9]   S. Eisler, N. Chahal, R. McDonald, R. R. Tykwinski, *Chem. Eur. J.* **2003**, *9*, 2542–2550.

[10]   W. A. Chalifoux, R. R. Tykwinski, *Nat. Chem.* **2010**, *2*, 967–971.

[11]   A. L. Spek, *Acta Crystallogr. C* **2015**, *71*, 9–18.

[12]   K. Usami, E. Yamaguchi, N. Tada, A. Itoh, *Org. Lett.* **2018**, *20*, 5714–5717.

[13]   J. P. Brand, J. Charpentier, J. Waser, *Angew. Chem. Int. Ed.* **2009**, *48*, 9346–9349.

[14]   S. B. Kamptmann, R. Brückner, *Eur. J. Org. Chem.* **2013**, 6584–6600.

[15]   R. Frei, J. Waser, *J. Am. Chem. Soc.* **2013**, *135*, 9620–9623.

[16]   a) C. Eaborn, N. Farrell, J. L. Murphy, A. Pidcock, *J. Chem. Soc., Dalton Trans.* **1976**, 58–67; b) P. M. Treichel, K. P. Wagner, W. J. Knebel, *Inorg. Chim. Acta* **1972**, *6*, 674–676.

[17]   F. Morandini, G. Consiglio, O. Piccolo, *Inorg. Chim. Acta* **1982**, *57*, 15–19.

[18]   M. Krempe, R. Lippert, F. Hampel, I. Ivanovic-Burmazovic, N. Jux, R. R. Tykwinski, *Angew. Chem. Int. Ed.* **2016**, *55*, 14802–14806.

[19]   R. Pelagalli, I. Chiarotto, M. Feroci, S. Vecchio, *Green Chem.* **2012**, *14*, 2251–2255.

[20]   N. R. Ayyangar, S. N. Naik, K. V. Srinivasan, *Tetrahedron Lett.* **1989**, *30*, 7253–7256.

[21]   M. E. Moustafa, P. D. Boyle, R. J. Puddephatt, *Can. J. Chem.* **2014**, *92*, 706–715.

[22]   J. Strueben, P. J. Gates, A. Staubitz, *J. Org. Chem.* **2014**, *79*, 1719–1728.

[23]   L.-X. Liao, F. Stellacci, D. V. McGrath, *J. Am. Chem. Soc.* **2004**, *126*, 2181–2185.

[24]   O. K. Farha, C. D. Malliakas, M. G. Kanatzidis, J. T. Hupp, *J. Am. Chem. Soc.* **2010**, *132*, 950–952.

[25]   I.-Y. Wu, J. T. Lin, J. Luo, S.-S. Sun, C.-S. Li, K. J. Lin, C. Tsai, C.-C. Hsu, J.-L. Lin, *Organometallics* **1997**, *16*, 2038–2048.

[26]   J. S. Lindsey, R. W. Wagner, *J. Org. Chem.* **1989**, *54*, 828–836.

[27]   C. Wang, K. V. Shalyaev, M. Bonchio, T. Carofiglio, J. T. Groves, *Inorg. Chem.* **2006**, *45*, 4769–4782.

[28] V. Walter, Y. Gao, N. Grzegorzek, M. Krempe, F. Hampel, N. Jux, R. R. Tykwinski, *Angew. Chem. Int. Ed.* **2019**, *58*, 494–498.

[29] A. R. Waterloo, R. Lippert, N. Jux, R. R. Tykwinski, *J. Coord. Chem.* **2015**, *68*, 3088–3098.

Bibliography

Chapter 1

[1]   a) X. Y. Wang, X. L. Yao, K. Mullen, *Sci. China Chem.* **2019**, *62*, 1099–1144; b) Y. Segawa, D. R. Levine, K. Itami, *Acc. Chem. Res.* **2019**, *52*, 2760–2767.

[2]   H. W. Kroto, J. R. Heath, S. C. Obrien, R. F. Curl, R. E. Smalley, *Nature* **1985**, *318*, 162–163.

[3]   K. S. Novoselov, A. K. Geim, S. V. Morozov, D. Jiang, Y. Zhang, S. V. Dubonos, I. V. Grigorieva, A. A. Firsov, *Science* **2004**, *306*, 666–669.

[4]   a) R. H. Baughman, A. A. Zakhidov, W. A. de Heer, *Science* **2002**, *297*, 787–792; b) Y. N. Xia, P. D. Yang, Y. G. Sun, Y. Y. Wu, B. Mayers, B. Gates, Y. D. Yin, F. Kim, Y. Q. Yan, *Adv. Mater.* **2003**, *15*, 353–389.

[5]   a) C. S. Huang, Y. J. Li, N. Wang, Y. R. Xue, Z. C. Zuo, H. B. Liu, Y. L. Li, *Chem. Rev.* **2018**, *118*, 7744–7803; b) X. Gao, H. B. Liu, D. Wang, J. Zhang, *Chem. Soc. Rev.* **2019**, *48*, 908–936.

[6]   A. Hirsch, *Nat. Mater.* **2010**, *9*, 868–871.

[7]   J. M. Cai, P. Ruffieux, R. Jaafar, M. Bieri, T. Braun, S. Blankenburg, M. Muoth, A. P. Seitsonen, M. Saleh, X. L. Feng, K. Mullen, R. Fasel, *Nature* **2010**, *466*, 470–473.

[8]   E. R. Darzi, R. Jasti, *Chem. Soc. Rev.* **2015**, *44*, 6401–6410.

[9]   M. D. Kilde, A. H. Murray, C. L. Andersen, F. E. Storm, K. Schmidt, A. Kadziola, K. V. Mikkelsen, F. Hampel, O. Hammerich, R. R. Tykwinski, M. B. Nielsen, *Nat. Commun.* **2019**, *10*, 3714.

[10]   A. Narita, X. Feng, Y. Hernandez, S. A. Jensen, M. Bonn, H. Yang, I. A. Verzhbitskiy, C. Casiraghi, M. R. Hansen, A. H. Koch, G. Fytas, O. Ivasenko, B. Li, K. S. Mali, T. Balandina, S. Mahesh, S. De Feyter, K. Mullen, *Nat. Chem.* **2014**, *6*, 126–132.

[11]   R. Jasti, J. Bhattacharjee, J. B. Neaton, C. R. Bertozzi, *J. Am. Chem. Soc.* **2008**, *130*, 17646–17647.

[12]   H. Omachi, T. Nakayama, E. Takahashi, Y. Segawa, K. Itami, *Nat. Chem.* **2013**, *5*, 572–576.

[13]   S. Yang, M. Kertesz, *J. Phys. Chem. A* **2006**, *110*, 9771–9774.

[14]   J. A. Januszewski, R. R. Tykwinski, *Chem. Soc. Rev.* **2014**, *43*, 3184–3203.

[15]   R. Hoffmann, *Angew. Chem. Int. Ed. Engl.* **1987**, *26*, 846–878.

[16]   C. S. Casari, A. Milani, *Mrs Commun.* **2018**, *8*, 207–219.

[17]   a) B. Pan, J. Xiao, J. Li, P. Liu, C. Wang, G. Yang, *Sci. Adv.* **2015**, *1*, e1500857; b) P. Tarakeshwar, P. R. Buseck, H. W. Kroto, *J. Phys. Chem. Lett.* **2016**, *7*, 1675−1681.

[18]   M. Liu, V. I. Artyukhov, H. Lee, F. Xu, B. I. Yakobson, *ACS Nano* **2013**, *7*, 10075–10082.

[19]   L. P. Kobets, I. S. Deev, *Compos. Sci. Technol.* **1998**, *57*, 1571−1580.

[20]   P. B. Sorokin, H. Lee, L. Y. Antipina, A. K. Singh, B. I. Yakobson, *Nano Lett.* **2011**, *11*, 2660–2665.

[21]   A. Malhotra, M. Maldovan, *Nanotechnology* **2019**, *30*, 372002.

[22]   Y. Zhang, H. L. Zhang, J. H. Wu, X. T. Wang, *Scr. Mater.* **2011**, *65*, 1097–1100.

[23] M. Wang, S. Lin, *Sci. Rep.* **2015**, *5*, 18122.

[24] a) C. Wang, A. S. Batsanov, M. R. Bryce, S. Martín, R. J. Nichols, S. J. Higgins, V. M. García-Suárez, C. J. Lambert, *J. Am. Chem. Soc.* **2009**, *131*, 15647–15654; b) P. Moreno-Garcia, M. Gulcur, D. Z. Manrique, T. Pope, W. J. Hong, V. Kaliginedi, C. C. Huang, A. S. Batsanov, M. R. Bryce, C. Lambert, T. Wandlowski, *J. Am. Chem. Soc.* **2013**, *135*, 12228–12240.

[25] C. S. Casari, M. Tommasini, R. R. Tykwinski, A. Milani, *Nanoscale* **2016**, *8*, 4414–4435.

[26] D. M. Guldi, H. Nishihara, L. Venkataraman, *Chem. Soc. Rev.* **2015**, *44*, 842–844.

[27] a) D. C. Milan, M. Krempe, A. K. Ismael, L. D. Movsisyan, M. Franz, I. Grace, R. J. Brooke, W. Schwarzacher, S. J. Higgins, H. L. Anderson, C. J. Lambert, R. R. Tykwinski, R. J. Nichols, *Nanoscale* **2017**, *9*, 355–361; b) P. Moreno-Garcia, M. Gulcur, D. Z. Manrique, T. Pope, W. J. Hong, V. Kaliginedi, C. C. Huang, A. S. Batsanov, M. R. Bryce, C. Lambert, T. Wandlowski, *J. Am. Chem. Soc.* **2013**, *135*, 12228–12240.

[28] a) X. Zhao, C. Huang, M. Gulcur, A. S. Batsanov, M. Baghernejad, W. Hong, M. R. Bryce, T. Wandlowski, *Chem. Mater.* **2013**, *25*, 4340–4347; b) A. Shah, B. Adhikari, S. Martic, A. Munir, S. Shahzad, K. Ahmad, H. B. Kraatz, *Chem. Soc. Rev.* **2015**, *44*, 1015–1027.

[29] E. Leary, A. La Rosa, M. T. Gonzalez, G. Rubio-Bollinger, N. Agrait, N. Martin, *Chem. Soc. Rev.* **2015**, *44*, 920–942.

[30] C. Glaser, *Ber. Dtsch. Chem. Ges.* **1869**, 422–424.

[31] G. Eglinton, A. R. Galbraith, *Chem. Ind. (London)* **1956**, 737–738.

[32] A. S. Hay, *J. Org. Chem.* **1962**, *27*, 3320–3321.

[33] a) J. H. Li, Y. Liang, Y. X. Xie, *J. Org. Chem.* **2005**, *70*, 4393–4396; b) A. Toledo, I. Funes-Ardoiz, F. Maseras, A. C. Albeniz, *Acs Catal.* **2018**, *8*, 7495–7506.

[34] A. Sagadevan, V. P. Charpe, K. C. Hwang, *Catal. Sci. Technol.* **2016**, *6*, 7688–7692.

[35] a) P. Siemsen, R. C. Livingston, F. Diederich, *Angew. Chem. Int. Ed.* **2000**, *39*, 2632–2657; b) A. Studer, M. Maji, *Synthesis* **2009**, 2467–2470; c) M. S. Maji, T. Pfeifer, A. Studer, *Angew. Chem. Int. Ed.* **2008**, *47*, 9547–9550.

[36] a) E. H. Smith, J. Whittall, *Organometallics* **1994**, *13*, 5169–5172; b) S. Oae, Y. Inubushi, M. Yoshihara, *Phosphorus Sulfur* **1995**, *103*, 101–110.

[37] a) K. West, C. Wang, A. S. Batsanov, M. R. Bryce, *J. Org. Chem.* **2006**, *71*, 8541–8544; b) C. Wang, A. S. Batsanov, K. West, M. R. Bryce, *Org. Lett.* **2008**, *10*, 3069–3072; c) K. West, L. N. Hayward, A. S. Batsanov, M. R. Bryce, *Eur. J. Org. Chem.* **2008**, 5093–5098.

[38] a) J. Anthony, A. M. Boldi, Y. Rubin, M. Hobi, V. Gramlich, C. B. Knobler, P. Seiler, F. Diederich, *Helv. Chim. Acta* **1995**, *78*, 13–45; b) R. Eastmond, T. R. Johnson, D. R. M. Walton, *J. Organomet. Chem.* **1973**, *50*, 87–92.

[39] W. A. Chalifoux, R. McDonald, M. J. Ferguson, R. R. Tykwinski, *Angew. Chem. Int. Ed.* **2009**, *48*, 7915–7919.

[40] W. A. Chalifoux, M. J. Ferguson, R. McDonald, F. Melin, L. Echegoyen, R. R. Tykwinski, *J. Phys. Org. Chem.* **2012**, *25*, 69–76.

[41] T. N. Hoheisel, H. Frauenrath, *Org. Lett.* **2008**, *10*, 4525–4528.

[42] W. A. Chalifoux, R. R. Tykwinski, *Nat. Chem.* **2010**, *2*, 967–971.

[43] M. Krempe, R. Lippert, F. Hampel, I. Ivanovic-Burmazovic, N. Jux, R. R. Tykwinski, *Angew. Chem. Int. Ed.* **2016**, *55*, 14802–14806.

[44] J. Kendall, R. McDonald, M. J. Ferguson, R. R. Tykwinski, *Org. Lett.* **2008**, *10*, 2163–2166.

[45] T. R. Johnson, D. R. M. Walton, *Tetrahedron* **1972**, *28*, 5221–5236.

[46] T. Gibtner, F. Hampel, J. P. Gisselbrecht, A. Hirsch, *Chem. Eur. J.* **2002**, *8*, 408–432.

[47] R. Eastmond, D. R. M. Walton, T. R. Johnson, *Tetrahedron* **1972**, *28*, 4601–4616.

[48] a) Q. L. Zheng, J. C. Bohling, T. B. Peters, A. C. Frisch, F. Hampel, J. A. Gladysz, *Chem. Eur. J.* **2006**, *12*, 6486–6505; b) Q. L. Zheng, J. A. Gladysz, *J. Am. Chem. Soc.* **2005**, *127*, 10508–10509.

[49] W. Mohr, J. Stahl, F. Hampel, J. A. Gladysz, *Chem. Eur. J.* **2003**, *9*, 3324–3340.

[50] R. Dembinski, T. Bartik, B. Bartik, M. Jaeger, J. A. Gladysz, *J. Am. Chem. Soc.* **2000**, *122*, 810–822.

[51] K. Nakamura, T. Fujimoto, S. Takara, K.-i. Sugiura, H. Miyasaka, T. Ishii, M. Yamashita, Y. Sakata, *Chem. Lett.* **2003**, *32*, 694–695.

[52] K. Schlögl, W. Steyrer, *J. Organomet. Chem.* **1966**, *6*, 399–411.

[53] E. Jones, H. Lee, M. Whiting, *J. Chem. Soc.* **1960**, 3483–3489.

[54] a) M. Franz, J. A. Januszewski, F. Hampel, R. R. Tykwinski, *Eur. J. Org. Chem.* **2019**, 3503–3512; b) H. Amini, Z. Baranova, N. Weisbach, S. Gauthier, N. Bhuvanesh, J. H. Reibenspies, J. A. Gladysz, *Chem. Eur. J.* **2019**, *25*, 15896–15914; c) L. D. Movsisyan, M. Franz, F. Hampel, A. L. Thompson, R. R. Tykwinski, H. L. Anderson, *J. Am. Chem. Soc.* **2016**, *138*, 1366–1376; d) M. Franz, J. A. Januszewski, D. Wendinger, C. Neiss, L. D. Movsisyan, F. Hampel, H. L. Anderson, A. Gorling, R. R. Tykwinski, *Angew. Chem. Int. Ed.* **2015**, *54*, 6645–6649.

[55] a) D. Chakraborty, S. Nandi, D. Mullangi, S. Haldar, C. P. Vinod, R. Vaidhyanathan, *ACS Appl. Mater. Interfaces* **2019**, *11*, 15670–15679; b) L. Su, J. Dong, L. Liu, M. Sun, R. Qiu, Y. Zhou, S. F. Yin, *J. Am. Chem. Soc.* **2016**, *138*, 12348–12351; c) M. K. Holganza, L. Trigoura, S. Elfarra, Y. Seo, J. Oiler, Y. Xing, *Tetrahedron Lett.* **2019**, *60*, 1179–1181.

[56] F. Bohlmann, H. Schönowsky, E. Inhoffen, G. Grau, *Chem. Ber.* **1964**, *97*, 794–800.

[57] W. Chodkiewicz, P. Cadiot, *C. R. Hebd. Seances Acad. Sci.* **1955**, *241*, 1055–1057.

[58] a) B. Pigulski, N. Gulia, S. Szafert, *Chem. Eur. J.* **2015**, *21*, 17769–17778; b) N. Gulia, B. Pigulski, S. Szafert, *Organometallics* **2015**, *34*, 673–682; c) C. Klinger, O. Vostirowsky, A. Hirsch, *Eur. J. Org. Chem.* **2006**, 1508–1524; d) R. C. DeCicco, A. Black, L. Li, N. S. Goroff, *Eur. J. Org. Chem.* **2012**, 4699–4704.

[59] R. Eastmond, D. R. M. Walton, *Tetrahedron* **1972**, *28*, 4591–4599.

[60] E. Métay, Q. Hu, E.-i. Negishi, *Org. Lett.* **2006**, *8*, 5773–5776.

[61] H. H. Peng, Y. M. Xi, N. Ronaghi, B. L. Dong, N. G. Akhmedov, X. D. Shi, *J. Am. Chem. Soc.* **2014**, *136*, 13174–13177.

[62] W. Y. Yin, C. He, M. Chen, H. Zhang, A. W. Lei, *Org. Lett.* **2009**, *11*, 709–712.

[63] A. Sagadevan, P. C. Lyu, K. C. Hwang, *Green Chem.* **2016**, *18*, 4526–4530.

[64] A. B. Antonova, M. I. Bruce, B. G. Ellis, M. Gaudio, P. A. Humphrey, M. Jevric, G. Melino, B. K. Nicholson, G. J. Perkins, B. W. Skelton, B. Stapleton, A. H. White, N. N. Zaitseva,

Chem. Commun. **2004**, 960–961.

[65] K. Gao, N. S. Goroff, *J. Am. Chem. Soc.* **2000**, *122*, 9320–9321.

[66] M. I. Bruce, N. N. Zaitseva, B. K. Nicholson, B. W. Skelton, A. H. White, *J. Organomet. Chem.* **2008**, *693*, 2887–2897.

[67] a) S. Eisler, R. R. Tykwinski, *J. Am. Chem. Soc.* **2000**, *122*, 10736–10737; b) E. Jahnke, R. R. Tykwinski, *Chem. Commun.* **2010**, *46*, 3235–3249.

[68] a) F. Diederich, Y. Rubin, C. B. Knobler, R. L. Whetten, K. E. Schriver, K. N. Houk, Y. Li, *Science* **1989**, *245*, 1088–1090; b) Y. Rubin, F. Diederich, *J. Am. Chem. Soc.* **1989**, *111*, 6870–6871; c) Y. Rubin, C. B. Knobler, F. Diederich, *J. Am. Chem. Soc.* **1990**, *112*, 1607–1617; d) S. W. Mcelvany, M. M. Ross, N. S. Goroff, F. Diederich, *Science* **1993**, *259*, 1594–1596; e) Y. Tobe, T. Fujii, K. Naemura, *J. Org. Chem.* **1994**, *59*, 1236–1237; f) Y. Tobe, T. Fujii, H. Matsumoto, K. Naemura, Y. Achiba, T. Wakabayashi, *J. Am. Chem. Soc.* **1996**, *118*, 2758–2759; g) Y. Tobe, R. Umeda, N. Iwasa, M. Sonoda, *Chem. Eur. J.* **2003**, *9*, 5549–5559; h) D. R. Kohn, P. Gawel, Y. Y. Xiong, K. E. Christensen, H. L. Anderson, *J. Org. Chem.* **2018**, *83*, 2077–2086.

[69] a) J. Zhao, Y. Zhang, Y. Fang, Z. Fan, G. Ma, Y. Liu, X. Zhao, *Chem. Phys. Lett.* **2017**, *682*, 96–100; b) J. H. Park, W. C. Mitchel, H. E. Smith, L. Grazulis, K. G. Eyink, *Carbon* **2010**, *48*, 1670–1673; c) M. Tsuji, T. Tsuji, S. Kuboyama, S.-H. Yoon, Y. Korai, T. Tsujimoto, K. Kubo, A. Mori, I. Mochida, *Chem. Phys. Lett.* **2002**, *355*, 101–108.

[70] a) G. Schermann, T. Grösser, F. Hampel, A. Hirsch, *Chem. Eur. J.* **1997**, *3*, 1105–1112; b) T. Grösser, A. Hirsch, *Angew. Chem. Int. Ed. Engl.* **1993**, *32*, 1340–1342.

[71] a) K. Kaiser, L. M. Scriven, F. Schulz, P. Gawel, L. Gross, H. L. Anderson, *Science* **2019**, *365*, 1299–1301; b) N. Pavlicek, P. Gawel, D. R. Kohn, Z. Majzik, Y. Y. Xiong, G. Meyer, H. L. Anderson, L. Gross, *Nat. Chem.* **2018**, *10*, 853–858.

[72] a) T. Luu, E. Elliott, A. D. Slepkov, S. Eisler, R. McDonald, F. A. Hegmann, R. R. Tykwinski, *Org. Lett.* **2005**, *7*, 51–54; b) S. Eisler, A. D. Slepkov, E. Elliott, T. Luu, R. McDonald, F. A. Hegmann, R. R. Tykwinski, *J. Am. Chem. Soc.* **2005**, *127*, 2666–2676.

[73] M. M. Haley, B. L. Langsdorf, *Chem. Commun.* **1997**, 1121–1122.

[74] W. Krätschmer, L. D. Lamb, K. Fostiropoulos, D. R. Huffman, *Nature* **1990**, *347*, 354–358.

[75] F. Bohlmann, *Chem. Ber.* **1953**, *86*, 657–667.

[76] A. Lucotti, M. Tommasini, D. Fazzi, M. Del Zoppo, W. A. Chalifoux, M. J. Ferguson, G. Zerbi, R. R. Tykwinski, *J. Am. Chem. Soc.* **2009**, *131*, 4239–4244.

[77] S. Schrettl, E. Contal, T. N. Hoheisel, M. Fritzsche, S. Balog, R. Szilluweit, H. Frauenrath, *Chem. Sci.* **2015**, *6*, 564–574.

[78] S. M. E. Simpkins, M. D. Weller, L. R. Cox, *Chem. Commun.* **2007**, 4035–4037.

[79] B. Pigulski, N. Gulia, S. Szafert, *Eur. J. Org. Chem.* **2019**, 1420–1445.

[80] J. Zirzlmeier, S. Schrettl, J. C. Brauer, E. Contal, L. Vannay, É. Brémond, E. Jahnke, D. M. Guldi, C. Corminboeuf, R. R. Tykwinski, H. Frauenrath, *Nat. Commun.* **2020**, *11*, 4797.

[81] R. R. Tykwinski, T. Luu, *Synthesis* **2012**, *44*, 1915–1922.

[82] A. Ehnbom, M. B. Hall, J. A. Gladysz, *Org. Lett.* **2019**, *21*, 753–757.

[83] a) Y. Nagano, T. Ikoma, K. Akiyama, S. Tero-Kubota, *J. Am. Chem. Soc.* **2003**, *125*, 14103–

14112; b) D. Fazzi, F. Scotognella, A. Milani, D. Brida, C. Manzoni, E. Cinquanta, M. Devetta, L. Ravagnan, P. Milani, F. Cataldo, L. Lüer, R. Wannemacher, J. Cabanillas-Gonzalez, M. Negro, S. Stagira, C. Vozzi, *Phys. Chem. Chem. Phys.* **2013**, *15*, 9384–9391.

[84] G. N. Lewis, M. Calvin, *Chem. Rev.* **1939**, *25*, 273–328.

[85] a) H. Meier, U. Stalmach, H. Kolshorn, *Acta Polym.* **1997**, *48*, 379–384; b) S. Yang, M. Kertesz, *J. Phys. Chem. A* **2008**, *112*, 146–151.

[86] M. Weimer, W. Hieringer, F. D. Sala, A. Görling, *Chem. Phys.* **2005**, *309*, 77–87.

[87] a) L. Shi, P. Rohringer, M. Wanko, A. Rubio, S. Waßerroth, S. Reich, S. Cambré, W. Wenseleers, P. Ayala, T. Pichler, *Phys. Rev. Mater.* **2017**, *1*, 075601; b) M. Kertesz, C. H. Choi, S. Yang, *Chem. Rev.* **2005**, *105*, 3448–3481.

[88] C. D. Zeinalipour-Yazdi, D. P. Pullman, *J. Phys. Chem. B* **2008**, *112*, 7377–7386.

[89] S. Szafert, J. A. Gladysz, *Chem. Rev.* **2006**, *106*, PR1–PR33.

[90] S. Yang, M. Kertesz, V. Zólyomi, J. Kürti, *J. Phys. Chem. A* **2007**, *111*, 2434–2441.

[91] a) D. R. Dreyer, R. S. Ruoff, C. W. Bielawski, *Angew. Chem. Int. Ed.* **2010**, *49*, 9336–9344; b) E. Frackowiak, *Phys. Chem. Chem. Phys.* **2007**, *9*, 1774–1785; c) E. Frackowiak, F. Béguin, *Carbon* **2001**, *39*, 937–950; d) H. Shi, G. Wen, Y. Nie, G. Zhang, H. Duan, *Nanoscale* **2020**, *12*, 5261–5285; e) D. G. Papageorgiou, Z. Li, M. Liu, I. A. Kinloch, R. J. Young, *Nanoscale* **2020**, *12*, 2228–2267.

[92] L. Shi, P. Rohringer, K. Suenaga, Y. Niimi, J. Kotakoski, J. C. Meyer, H. Peterlik, M. Wanko, S. Cahangirov, A. Rubio, Z. J. Lapin, L. Novotny, P. Ayala, T. Pichler, *Nat. Mater.* **2016**, *15*, 634–640.

[93] C. Wang, H. Jia, H. Li, Y. Wang, *Jilin Huagong Xueyuan Xuebao* **2012**, *20*, 33–36.

[94] a) P. Sivaguru, Z. K. Wang, G. Zanoni, X. H. Bi, *Chem. Soc. Rev.* **2019**, *48*, 2615–2656; b) K. Wu, C. Song, D. Cui, *Chinese J. Org. Chem.* **2017**, *37*, 586–602; c) D. S. Kim, W. J. Park, C. H. Jun, *Chem. Rev.* **2017**, *117*, 8977–9015.

[95] Y. Li, C. Yang, X. Guo, *Acc. Chem. Res.* **2020**, *53*, 159–169.

[96] C. H. Hendon, D. Tiana, A. T. Murray, D. R. Carbery, A. Walsh, *Chem. Sci.* **2013**, *4*, 4278–4284.

[97] A. Goulet-Hanssens, F. Eisenreich, S. Hecht, *Adv. Mater.* **2020**, e1905966.

[98] A. Schlimm, R. Low, T. Rusch, F. Rohricht, T. Strunskus, T. Tellkamp, F. Sonnichsen, U. Manthe, O. Magnussen, F. Tuczek, R. Herges, *Angew. Chem. Int. Ed.* **2019**, *58*, 6574–6578.

[99] V. Walter, Y. Gao, N. Grzegorzek, M. Krempe, F. Hampel, N. Jux, R. R. Tykwinski, *Angew. Chem. Int. Ed.* **2019**, *58*, 494–498.

[100] M. Hammerich, R. Herges, *J. Org. Chem.* **2015**, *80*, 11233–11236.

Chapter 2

[1] A. Hirsch, *Nat. Mater.* **2010**, *9*, 868–871.

[2] K. Kaiser, L. M. Scriven, F. Schulz, P. Gawel, L. Gross, H. L. Anderson, *Science* **2019**, *365*, 1299–1301.

[3] a) M. D. Kilde, A. H. Murray, C. L. Andersen, F. E. Storm, K. Schmidt, A. Kadziola, K. V. Mikkelsen, F. Hampel, O. Hammerich, R. R. Tykwinski, M. B. Nielsen, *Nat. Commun.* **2019**,

10, 3714; b) D. Malko, C. Neiss, F. Viñes, A. Görling, *Phys. Rev. Lett.* **2012**, *108*, 086804.

[4]   X. Y. Wang, X. L. Yao, K. Mullen, *Sci. China Chem.* **2019**, *62*, 1099–1144.

[5]   H. Schwertfeger, A. A. Fokin, P. R. Schreiner, *Angew. Chem. Int. Ed.* **2008**, *47*, 1022–1036.

[6]   E. R. Darzi, R. Jasti, *Chem. Soc. Rev.* **2015**, *44*, 6401–6410.

[7]   a) W. A. Chalifoux, R. R. Tykwinski, *C. R. Chimie* **2009**, *12*, 341–358; b) R. R. Tykwinski, *Chem. Rec.* **2015**, *15*, 1060–1074; c) S. Szafert, J. A. Gladysz, *Chem. Rev.* **2006**, *106*, PR1–PR33; d) C. S. Casari, M. Tommasini, R. R. Tykwinski, A. Milani, *Nanoscale* **2016**, *8*, 4414–4435; e) F. Banhart, *ChemTexts* **2020**, *6*, 3–10.

[8]   M. Liu, V. I. Artyukhov, H. Lee, F. Xu, B. I. Yakobson, *ACS Nano* **2013**, *7*, 10075–10082.

[9]   a) Q. Zheng, J. C. Bohling, T. B. Peters, A. C. Frisch, F. Hampel, J. A. Gladysz, *Chem. Eur. J.* **2006**, *12*, 6486–6505; b) N. Weisbach, H. Kuhn, H. Amini, A. Ehnbom, F. Hampel, J. H. Reibenspies, M. B. Hall, J. A. Gladysz, *Organometallics* **2019**, *38*, 3294–3310.

[10] W. A. Chalifoux, R. R. Tykwinski, *Nat. Chem.* **2010**, *2*, 967–971.

[11] L. Shi, P. Rohringer, K. Suenaga, Y. Niimi, J. Kotakoski, J. C. Meyer, H. Peterlik, M. Wanko, S. Cahangirov, A. Rubio, Z. J. Lapin, L. Novotny, P. Ayala, T. Pichler, *Nat. Mater.* **2016**, *15*, 634–639.

[12] B. Pigulski, N. Gulia, S. Szafert, *Eur. J. Org. Chem.* **2019**, 1420–1445.

[13] a) C. Wang, A. S. Batsanov, M. R. Bryce, S. Martín, R. J. Nichols, S. J. Higgins, V. M. García-Suárez, C. J. Lambert, *J. Am. Chem. Soc.* **2009**, *131*, 15647–15654; b) D. C. Milan, M. Krempe, A. K. Ismael, L. D. Movsisyan, M. Franz, I. Grace, R. J. Brooke, W. Schwarzacher, S. J. Higgins, H. L. Anderson, C. J. Lambert, R. R. Tykwinski, R. J. Nichols, *Nanoscale* **2017**, *9*, 355–361.

[14] P. Moreno-Garcia, M. Gulcur, D. Z. Manrique, T. Pope, W. J. Hong, V. Kaliginedi, C. C. Huang, A. S. Batsanov, M. R. Bryce, C. Lambert, T. Wandlowski, *J. Am. Chem. Soc.* **2013**, *135*, 12228–12240.

[15] C. Wang, H. Jia, H. Li, Y. Wang, *Jilin Huagong Xueyuan Xuebao* **2012**, *20*, 33–36.

[16] M. Krempe, R. Lippert, F. Hampel, I. Ivanovic-Burmazovic, N. Jux, R. R. Tykwinski, *Angew. Chem. Int. Ed.* **2016**, *55*, 14802–14806.

[17] a) W. A. Chalifoux, R. McDonald, M. J. Ferguson, R. R. Tykwinski, *Angew. Chem. Int. Ed.* **2009**, *48*, 7915–7919; b) T. Gibtner, F. Hampel, J. P. Gisselbrecht, A. Hirsch, *Chem. Eur. J.* **2002**, *8*, 408–432.

[18] S. M. E. Simpkins, M. D. Weller, L. R. Cox, *Chem. Commun.* **2007**, 4035–4037.

[19] X. Yi, J. Chen, X. Xu, Y. Ma, *Synth. Commun.* **2017**, *47*, 872–877.

[20] a) A. C. Spivey, T. Fekner, S. E. Spey, *J. Org. Chem.* **2000**, *65*, 3154–3159; b) O. S. Tee, M. Paventi, *Can. J. Chem.* **1983**, *61*, 2556–2562.

[21] L. Robke, T. Rodrigues, P. Schröder, D. J. Foley, G. J. L. Bernardes, L. Laraia, H. Waldmann, *Tetrahedron* **2018**, *74*, 4531–4537.

[22] C. Eidamshaus, H.-U. Reissig, *Eur. J. Org. Chem.* **2011**, 6056–6069.

[23] J. Ranta, T. Kumpulainen, H. Lemmetyinen, A. Efimov, *J. Org. Chem.* **2010**, *75*, 5178–5194.

[24] a) D. N. Coventry, A. S. Batsanov, A. E. Goeta, J. A. Howard, T. B. Marder, R. N. Perutz, *Chem. Commun.* **2005**, 2172–2174; b) A. G. Crawford, Z. Liu, I. A. Mkhalid, M. H. Thibault,

N. Schwarz, G. Alcaraz, A. Steffen, J. C. Collings, A. S. Batsanov, J. A. Howard, T. B. Marder, *Chem. Eur. J.* **2012**, *18*, 5022–5035.

[25] Y. Hashikawa, M. Murata, A. Wakamiya, Y. Murata, *J. Am. Chem. Soc.* **2017**, *139*, 16350–16358.

[26] H.-J. Knops, L. Born, *Tetrahedron Lett.* **1983**, *24*, 2973–2976.

[27] X. Nie, G. Wang, *J. Org. Chem.* **2006**, *71*, 4734–4741.

[28] M. Turlington, Y. Du, S. G. Ostrum, V. Santosh, K. Wren, T. Lin, M. Sabat, L. Pu, *J. Am. Chem. Soc.* **2011**, *133*, 11780–11794.

[29] S. J. Havens, P. M. Hergenrother, *J. Org. Chem.* **1985**, *50*, 1763–1765.

[30] A. S. Hay, *J. Org. Chem.* **1962**, *27*, 3320–3321.

[31] G. Eglinton, A. R. Galbraith, *Chem. Ind. (London)* **1956**, 737–738.

[32] T. R. Johnson, D. R. M. Walton, *Tetrahedron* **1972**, *28*, 5221–5236.

[33] H. Amini, Z. Baranova, N. Weisbach, S. Gauthier, N. Bhuvanesh, J. H. Reibenspies, J. A. Gladysz, *Chem. Eur. J.* **2019**, *25*, 15896–15914.

[34] P. Bichler, W. A. Chalifoux, S. Eisler, A. L. K. Shi Shun, E. T. Chernick, R. R. Tykwinski, *Org. Lett.* **2009**, *11*, 519–522.

[35] S. Eisler, A. D. Slepkov, E. Elliott, T. Luu, R. McDonald, F. A. Hegmann, R. R. Tykwinski, *J. Am. Chem. Soc.* **2005**, *127*, 2666–2676.

[36] R. R. Tykwinski, W. Chalifoux, S. Eisler, A. Lucotti, M. Tommasini, D. Fazzi, M. Del Zoppo, G. Zerbi, *Pure Appl. Chem.* **2010**, *82*, 891–904.

[37] a) L. D. Movsisyan, M. Franz, F. Hampel, A. L. Thompson, R. R. Tykwinski, H. L. Anderson, *J. Am. Chem. Soc.* **2016**, *138*, 1366–1376; b) M. Franz, J. A. Januszewski, F. Hampel, R. R. Tykwinski, *Eur. J. Org. Chem.* **2019**, 3503–3512.

[38] R. R. Tykwinski, T. Luu, *Synthesis* **2012**, *44*, 1915–1922.

[39] a) J.-L. Bredas, *Mater. Horiz.* **2014**, *1*, 17–19; b) J. Zirzlmeier, S. Schrettl, J. C. Brauer, E. Contal, L. Vannay, É. Brémond, E. Jahnke, D. M. Guldi, C. Corminboeuf, R. R. Tykwinski, H. Frauenrath, *Nat. Commun.* **2020**, *11*, 4797.

[40] a) A. Milani, M. Tommasini, G. Zerbi, *J. Raman Spectrosc.* **2009**, *40*, 1931–1934; b) M. Kertesz, C. H. Choi, S. Yang, *Chem. Rev.* **2005**, *105*, 3448–3481.

[41] L. Shi, P. Rohringer, M. Wanko, A. Rubio, S. Waßerroth, S. Reich, S. Cambré, W. Wenseleers, P. Ayala, T. Pichler, *Phys. Rev. Mater.* **2017**, *1*, 075601.

[42] R. Hoffmann, *Angew. Chem. Int. Ed. Engl.* **1987**, *26*, 846–878.

[43] a) L. D. Movsisyan, M. D. Peeks, G. M. Greetham, M. Towrie, A. L. Thompson, A. W. Parker, H. L. Anderson, *J. Am. Chem. Soc.* **2014**, *136*, 17996–18008; b) D. Fazzi, F. Scotognella, A. Milani, D. Brida, C. Manzoni, E. Cinquanta, M. Devetta, L. Ravagnan, P. Milani, F. Cataldo, L. Lüer, R. Wannemacher, J. Cabanillas-Gonzalez, M. Negro, S. Stagira, C. Vozzi, *Phys. Chem. Chem. Phys.* **2013**, *15*, 9384–9391; c) Y. Nagano, T. Ikoma, K. Akiyama, S. Tero-Kubota, *J. Am. Chem. Soc.* **2003**, *125*, 14103–14112.

[44] R. Dembinski, T. Bartik, B. Bartik, M. Jaeger, J. A. Gladysz, *J. Am. Chem. Soc.* **2000**, *122*, 810–822.

[45] W. A. Chalifoux, M. J. Ferguson, R. McDonald, F. Melin, L. Echegoyen, R. R. Tykwinski,

J. Phys. Org. Chem. **2012**, *25*, 69–76.

[46] H. Meier, U. Stalmach, H. Kolshorn, *Acta Polym.* **1997**, *48*, 379–384.

[47] R. E. Martin, F. Diederich, *Angew. Chem. Int. Ed.* **1999**, *38*, 1350–1377.

[48] A. Lucotti, M. Tommasini, D. Fazzi, M. Del Zoppo, W. A. Chalifoux, M. J. Ferguson, G. Zerbi, R. R. Tykwinski, *J. Am. Chem. Soc.* **2009**, *131*, 4239–4244.

[49] M. Nishio, *Phys. Chem. Chem. Phys.* **2011**, *13*, 13873–13900.

[50] K. Fahsi, J. Deschamps, K. Chougrani, L. Viau, B. Boury, A. Vioux, A. van der Lee, S. G. Dutremez, *CrystEngComm* **2013**, *15*, 4261–4279.

[51] R. L. Gieseking, C. Risko, J.-L. Brédas, *J. Phys. Chem. Lett.* **2015**, *6*, 2158–2162.

[52] C. D. Zeinalipour-Yazdi, D. P. Pullman, *J. Phys. Chem. B* **2008**, *112*, 7377–7386.

[53] S. Yang, M. Kertesz, *J. Phys. Chem. A* **2006**, *110*, 9771–9774.

[54] N. R. Agarwal, A. Lucotti, D. Fazzi, M. Tommasini, C. Castiglioni, W. A. Chalifoux, R. R. Tykwinski, *J. Raman Spectrosc.* **2013**, *44*, 1398–1410.

[55] L. Shi, P. Rohringer, K. Suenaga, Y. Niimi, J. Kotakoski, J. C. Meyer, H. Peterlik, M. Wanko, S. Cahangirov, A. Rubio, Z. J. Lapin, L. Novotny, P. Ayala, T. Pichler, *Nat. Mater.* **2016**, *15*, 634–640.

Chapter 3

[1] A. L. K. Shi Shun, R. R. Tykwinski, *Angew. Chem. Int. Ed.* **2006**, *45*, 1034–1057.

[2] J. A. Marsden, G. J. Palmer, M. M. Haley, *Eur. J. Org. Chem.* **2003**, 2355–2369.

[3] X. Gao, H. B. Liu, D. Wang, J. Zhang, *Chem. Soc. Rev.* **2019**, *48*, 908–936.

[4] S. E. Allen, R. R. Walvoord, R. Padilla-Salinas, M. C. Kozlowski, *Chem. Rev.* **2013**, *113*, 6234–6458.

[5] a) W. A. Chalifoux, R. R. Tykwinski, *C. R. Chimie* **2009**, *12*, 341–358; b) R. R. Tykwinski, W. Chalifoux, S. Eisler, A. Lucotti, M. Tommasini, D. Fazzi, M. Del Zoppo, G. Zerbi, *Pure Appl. Chem.* **2010**, *82*, 891–904.

[6] C. Glaser, *Ber. Dtsch. Chem. Ges.* **1869**, 422–424.

[7] G. Eglinton, A. R. Galbraith, *Chem. Ind. (London)* **1956**, 737–738.

[8] A. S. Hay, *J. Org. Chem.* **1962**, *27*, 3320–3321.

[9] W. Chodkiewicz, P. Cadiot, *C. R. Hebd. Seances Acad. Sci.* **1955**, *241*, 1055–1057.

[10] a) W. A. Chalifoux, M. J. Ferguson, R. McDonald, F. Melin, L. Echegoyen, R. R. Tykwinski, *J. Phys. Org. Chem.* **2012**, *25*, 69–76; b) W. A. Chalifoux, R. McDonald, M. J. Ferguson, R. R. Tykwinski, *Angew. Chem. Int. Ed.* **2009**, *48*, 7915–7919; c) S. Eisler, A. D. Slepkov, E. Elliott, T. Luu, R. McDonald, F. A. Hegmann, R. R. Tykwinski, *J. Am. Chem. Soc.* **2005**, *127*, 2666–2676.

[11] T. Gibtner, F. Hampel, J. P. Gisselbrecht, A. Hirsch, *Chem. Eur. J.* **2002**, *8*, 408–432.

[12] a) P. Sivaguru, Z. K. Wang, G. Zanoni, X. H. Bi, *Chem. Soc. Rev.* **2019**, *48*, 2615–2656; b) L. Souillart, N. Cramer, *Chem. Rev.* **2015**, *115*, 9410–9464; c) C. H. Jun, *Chem. Soc. Rev.* **2004**, *33*, 610–618.

[13] C. T. To, K. S. Chan, *Eur. J. Org. Chem.* **2019**, 6581–6591.

[14] a) W. Zhou, W. Y. Fan, Q. J. Jiang, Y. F. Lang, N. Jiao, *Org. Lett.* **2015**, *17*, 2542–2545; b) C.

Tang, N. Jiao, *Angew. Chem. Int. Ed.* **2014**, *53*, 6528–6532; c) A. Maji, S. Rana, Akanksha, D. Maiti, *Angew. Chem. Int. Ed.* **2014**, *53*, 2428–2432; d) X. Huang, X. Li, M. Zou, S. Song, C. Tang, Y. Yuan, N. Jiao, *J. Am. Chem. Soc.* **2014**, *136*, 14858–14865; e) W. Zhou, Y. Yang, Y. Liu, G.-J. Deng, *Green Chem.* **2013**, *15*, 76–80; f) C. Zhang, P. Feng, N. Jiao, *J. Am. Chem. Soc.* **2013**, *135*, 15257–15262; g) L. Zhang, X. Bi, X. Guan, X. Li, Q. Liu, B. D. Barry, P. Liao, *Angew. Chem. Int. Ed.* **2013**, *52*, 11303–11307.

[15] J. P. Brand, J. Charpentier, J. Waser, *Angew. Chem. Int. Ed.* **2009**, *48*, 9346–9349.

[16] R. Frei, J. Waser, *J. Am. Chem. Soc.* **2013**, *135*, 9620–9623.

[17] R. A. Seburg, J. A. Hodges, R. J. McMahon, *Helv. Chim. Acta* **2009**, *92*, 1626–1643.

[18] a) K. Wu, C. Song, D. Cui, *Chinese J. Org. Chem.* **2017**, *37*, 586–602; b) D. S. Kim, W. J. Park, C. H. Jun, *Chem. Rev.* **2017**, *117*, 8977–9015.

[19] W. A. Chalifoux, R. R. Tykwinski, *Nat. Chem.* **2010**, *2*, 967–971.

[20] a) J. Wang, X. Cao, S. Lv, C. Zhang, S. Xu, M. Shi, J. Zhang, *Nat. Commun.* **2017**, *8*, 14625; b) I. V. Shishkov, F. Rominger, P. Hofmann, *Organometallics* **2009**, *28*, 1049–1059; c) B. F. Straub, P. Hofmann, *Angew. Chem.* **2001**, *113*, 1328–1330.

[21] F. Bohlmann, H. Schönowsky, E. Inhoffen, G. Grau, *Chem. Ber.* **1964**, *97*, 794–800.

Chapter 4

[1] J. Ranta, T. Kumpulainen, H. Lemmetyinen, A. Efimov, *J. Org. Chem.* **2010**, *75*, 5178–5194.

[2] a) D. N. Coventry, A. S. Batsanov, A. E. Goeta, J. A. Howard, T. B. Marder, R. N. Perutz, *Chem. Commun.* **2005**, 2172–2174; b) A. G. Crawford, Z. Liu, I. A. Mkhalid, M. H. Thibault, N. Schwarz, G. Alcaraz, A. Steffen, J. C. Collings, A. S. Batsanov, J. A. Howard, T. B. Marder, *Chem. Eur. J.* **2012**, *18*, 5022–5035.

[3] a) A. C. Spivey, T. Fekner, S. E. Spey, *J. Org. Chem.* **2000**, *65*, 3154–3159; b) O. S. Tee, M. Paventi, *Can. J. Chem.* **1983**, *61*, 2556–2562; c) L. Robke, T. Rodrigues, P. Schröder, D. J. Foley, G. J. L. Bernardes, L. Laraia, H. Waldmann, *Tetrahedron* **2018**, *74*, 4531–4537.

[4] C. Eidamshaus, H.-U. Reissig, *Eur. J. Org. Chem.* **2011**, 6056–6069.

[5] X. Yi, J. Chen, X. Xu, Y. Ma, *Synth. Commun.* **2017**, *47*, 872–877.

[6] C. D. Campbell, R. L. Greenaway, O. T. Holton, P. R. Walker, H. A. Chapman, C. A. Russell, G. Carr, A. L. Thomson, E. A. Anderson, *Chem. Eur. J.* **2015**, *21*, 12627–12639.

[7] X. Nie, G. Wang, *J. Org. Chem.* **2006**, *71*, 4734–4741.

[8] M. Turlington, Y. Du, S. G. Ostrum, V. Santosh, K. Wren, T. Lin, M. Sabat, L. Pu, *J. Am. Chem. Soc.* **2011**, *133*, 11780–11794.

[9] S. Eisler, N. Chahal, R. McDonald, R. R. Tykwinski, *Chem. Eur. J.* **2003**, *9*, 2542–2550.

[10] W. A. Chalifoux, R. R. Tykwinski, *Nat. Chem.* **2010**, *2*, 967–971.

[11] A. L. Spek, *Acta Crystallogr. C* **2015**, *71*, 9–18.

[12] K. Usami, E. Yamaguchi, N. Tada, A. Itoh, *Org. Lett.* **2018**, *20*, 5714–5717.

[13] J. P. Brand, J. Charpentier, J. Waser, *Angew. Chem. Int. Ed.* **2009**, *48*, 9346–9349.

[14] S. B. Kamptmann, R. Brückner, *Eur. J. Org. Chem.* **2013**, 6584–6600.

[15] R. Frei, J. Waser, *J. Am. Chem. Soc.* **2013**, *135*, 9620–9623.

[16] a) C. Eaborn, N. Farrell, J. L. Murphy, A. Pidcock, *J. Chem. Soc., Dalton Trans.* **1976**, 58–

67; b) P. M. Treichel, K. P. Wagner, W. J. Knebel, *Inorg. Chim. Acta* **1972**, *6*, 674–676.

[17] F. Morandini, G. Consiglio, O. Piccolo, *Inorg. Chim. Acta* **1982**, *57*, 15–19.

[18] M. Krempe, R. Lippert, F. Hampel, I. Ivanovic-Burmazovic, N. Jux, R. R. Tykwinski, *Angew. Chem. Int. Ed.* **2016**, *55*, 14802–14806.

[19] R. Pelagalli, I. Chiarotto, M. Feroci, S. Vecchio, *Green Chem.* **2012**, *14*, 2251–2255.

[20] N. R. Ayyangar, S. N. Naik, K. V. Srinivasan, *Tetrahedron Lett.* **1989**, *30*, 7253–7256.

[21] M. E. Moustafa, P. D. Boyle, R. J. Puddephatt, *Can. J. Chem.* **2014**, *92*, 706–715.

[22] J. Strueben, P. J. Gates, A. Staubitz, *J. Org. Chem.* **2014**, *79*, 1719–1728.

[23] L.-X. Liao, F. Stellacci, D. V. McGrath, *J. Am. Chem. Soc.* **2004**, *126*, 2181–2185.

[24] O. K. Farha, C. D. Malliakas, M. G. Kanatzidis, J. T. Hupp, *J. Am. Chem. Soc.* **2010**, *132*, 950–952.

[25] I.-Y. Wu, J. T. Lin, J. Luo, S.-S. Sun, C.-S. Li, K. J. Lin, C. Tsai, C.-C. Hsu, J.-L. Lin, *Organometallics* **1997**, *16*, 2038–2048.

[26] J. S. Lindsey, R. W. Wagner, *J. Org. Chem.* **1989**, *54*, 828–836.

[27] C. Wang, K. V. Shalyaev, M. Bonchio, T. Carofiglio, J. T. Groves, *Inorg. Chem.* **2006**, *45*, 4769–4782.

[28] V. Walter, Y. Gao, N. Grzegorzek, M. Krempe, F. Hampel, N. Jux, R. R. Tykwinski, *Angew. Chem. Int. Ed.* **2019**, *58*, 494–498.

[29] A. R. Waterloo, R. Lippert, N. Jux, R. R. Tykwinski, *J. Coord. Chem.* **2015**, *68*, 3088–3098.

Chapter 5

[1] a) M. Hammerich, R. Herges, *J. Org. Chem.* **2015**, *80*, 11233–11236; b) T. Muraoka, K. Kinbara, T. Aida, *Nature* **2006**, *440*, 512–515.

[2] a) A. S. Lubbe, W. Szymanski, B. L. Feringa, *Chem. Soc. Rev.* **2017**, *46*, 1052–1079; b) S. Samanta, A. A. Beharry, O. Sadovski, T. M. McCormick, A. Babalhavaeji, V. Tropepe, G. A. Woolley, *J. Am. Chem. Soc.* **2013**, *135*, 9777–9784; c) Q. Shao, B. Xing, *Chem. Soc. Rev.* **2010**, *39*, 2835–2846.

[3] a) A. Goulet-Hanssens, F. Eisenreich, S. Hecht, *Adv. Mater.* **2020**, *32*, e1905966; b) A. H. Heindl, J. Becker, H. A. Wegner, *Chem. Sci.* **2019**, *10*, 7418–7425.

[4] a) C. Zong, Y. Zhao, H. Ji, X. Han, J. Xie, J. Wang, Y. Cao, S. Jiang, C. Lu, *Angew. Chem. Int. Ed.* **2016**, *55*, 3931–3935; b) S. Venkataramani, U. Jana, M. Dommaschk, F. D. Sönnichsen, F. Tuczek, R. Herges, *Science* **2011**, *331*, 445–448; c) B. Baisch, D. Raffa, U. Jung, O. M. Magnussen, C. Nicolas, J. Lacour, J. Kubitschke, R. Herges, *J. Am. Chem. Soc.* **2009**, *131*, 442–443.

[5] a) E. Merino, *Chem. Soc. Rev.* **2011**, *40*, 3835–3853; b) F. Hamon, F. Djedaini-Pilard, F. Barbot, C. Len, *Tetrahedron* **2009**, *65*, 10105–10123.

[6] M. H. Davey, V. Y. Lee, R. D. Miller, T. J. Marks, *J. Org. Chem.* **1999**, *64*, 4976–4979.

[7] N. R. Ayyangar, S. N. Naik, K. V. Srinivasan, *Tetrahedron Lett.* **1989**, *30*, 7253–7256.

[8] C. Zhang, N. Jiao, *Angew. Chem. Int. Ed.* **2010**, *49*, 6174–6177.

[9] a) C. R. Crecca, A. E. Roitberg, *J. Phys. Chem. A* **2006**, *110*, 8188–8203; b) C. J. Brown, *Acta Crystallogr.* **1966**, *21*, 146–152.

[10] A. Mostad, C. Rømming, *Acta Chem. Scand.* **1971**, *25*, 3561–3568.

[11] H. M. Bandara, S. C. Burdette, *Chem. Soc. Rev.* **2012**, *41*, 1809–1825.

[12] A. Schlimm, R. Low, T. Rusch, F. Rohricht, T. Strunskus, T. Tellkamp, F. Sonnichsen, U. Manthe, O. Magnussen, F. Tuczek, R. Herges, *Angew. Chem. Int. Ed.* **2019**, *58*, 6574–6578.

[13] T. R. Rusch, M. Hammerich, R. Herges, O. M. Magnussen, *Chem. Commun.* **2019**, *55*, 9511–9514.

[14] S. Mohnani, D. Bonifazi, *Coord. Chem. Rev.* **2010**, *254*, 2342–2362.

[15] a) C. B. Kc, F. D'Souza, *Coord. Chem. Rev.* **2016**, *322*, 104–141; b) S. M. Law, D. Chen, S. L. Chan, X. Guan, W. M. Tsui, J. S. Huang, N. Zhu, C. M. Che, *Chem. Eur. J.* **2014**, *20*, 11035–11047.

[16] J. M. Kamm, C. P. Iverson, W. Y. Lau, M. D. Hopkins, *Langmuir* **2016**, *32*, 487–495.

[17] V. Walter, Y. Gao, N. Grzegorzek, M. Krempe, F. Hampel, N. Jux, R. R. Tykwinski, *Angew. Chem. Int. Ed.* **2019**, *58*, 494–498.

[18] a) C. Schutt, G. Heitmann, T. Wendler, B. Krahwinkel, R. Herges, *J. Org. Chem.* **2016**, *81*, 1206–1215; b) M. Dommaschk, C. Schutt, S. Venkataramani, U. Jana, C. Nather, F. D. Sonnichsen, R. Herges, *Dalton Trans.* **2014**, *43*, 17395–17405.

[19] a) W. Huang, S. K. Lee, Y. M. Sung, F. Peng, B. Yin, M. Ma, B. Chen, S. Liu, S. R. Kirk, D. Kim, J. Song, *Chem. Eur. J.* **2015**, *21*, 15328–15338; b) L. J. Esdaile, P. Jensen, J. C. McMurtrie, D. P. Arnold, *Angew. Chem. Int. Ed.* **2007**, *46*, 2090–2093; c) T. Yamamura, A. Momotake, T. Arai, *Tetrahedron Lett.* **2004**, *45*, 9219–9223; d) S. Tsuchiya, *J. Am. Chem. Soc.* **1999**, *121*, 48–53; e) H. K. Hombrecher, K. Lüdtke, *Tetrahedron* **1993**, *49*, 9489–9494.

[20] a) T. Hirose, F. Helmich, E. W. Meijer, *Angew. Chem. Int. Ed.* **2013**, *52*, 304–309; b) S. Dey, S. A. Ikbal, S. P. Rath, *New J. Chem.* **2014**, *38*, 1458–1470; c) J. Otsuki, E. Seki, T. Taguchi, M. Asakawa, K. Miyake, *Chem. Lett.* **2007**, *36*, 740–741; d) O. Tsutsumi, H. Sato, K. Takeda, T. Ogawa, *Thin Solid Films* **2006**, *499*, 219–223; e) J. Otsuki, K. Narutaki, *Bull. Chem. Soc. Jap.* **2004**, *77*, 1537–1544; f) J. Otsuki, K. Harada, K. Araki, *Chem. Lett.* **1999**, *28*, 269–270; g) V. Marvaud, J. P. Launay, *Inorg. Chem.* **1993**, *32*, 1376–1382.

[21] a) D. R. Reddy, B. G. Maiya, *J. Phys. Chem. A* **2003**, *107*, 6326–6333; b) D. R. Reddy, B. G. Maiya, *Chem. Commun.* **2001**, 117–118.

[22] S. Yao, Y. Yan, K. L. Wong, K. S. Chan, Z. Shen, *J. Porphyrins Phthalocyanines* **2018**, *22*, 918–924.

[23] R. Pelagalli, I. Chiarotto, M. Feroci, S. Vecchio, *Green Chem.* **2012**, *14*, 2251–2255.

[24] R. R. Tykwinski, *Angew. Chem. Int. Ed.* **2003**, *42*, 1566–1568.

[25] O. Zenkina, M. Altman, G. Leitus, L. J. W. Shimon, R. Cohen, M. E. van der Boom, *Organometallics* **2007**, *26*, 4528–4534.

[26] L.-X. Liao, F. Stellacci, D. V. McGrath, *J. Am. Chem. Soc.* **2004**, *126*, 2181–2185.

[27] O. K. Farha, C. D. Malliakas, M. G. Kanatzidis, J. T. Hupp, *J. Am. Chem. Soc.* **2010**, *132*, 950–952.

[28] I.-Y. Wu, J. T. Lin, J. Luo, S.-S. Sun, C.-S. Li, K. J. Lin, C. Tsai, C.-C. Hsu, J.-L. Lin, *Organometallics* **1997**, *16*, 2038–2048.

[29] J. S. Lindsey, R. W. Wagner, *J. Org. Chem.* **1989**, *54*, 828–836.

[30] C. Wang, K. V. Shalyaev, M. Bonchio, T. Carofiglio, J. T. Groves, *Inorg. Chem.* **2006**, *45*, 4769–4782.

[31] A. R. Waterloo, R. Lippert, N. Jux, R. R. Tykwinski, *J. Coord. Chem.* **2015**, *68*, 3088–3098.

[32] K. Chichak, N. R. Branda, *Chem. Commun.* **1999**, 523–524.

[33] a) M. Krempe, R. Lippert, F. Hampel, I. Ivanovic-Burmazovic, N. Jux, R. R. Tykwinski, *Angew. Chem. Int. Ed.* **2016**, *55*, 14802–14806; b) K. Campbell, R. McDonald, N. R. Branda, R. R. Tykwinski, *Org. Lett.* **2001**, *3*, 1045–1048.

[34] S. Crespi, N. A. Simeth, B. Koinig, *Nat. Rev. Chem.* **2019**, *3*, 133–146.

[35] a) N. Shafizadeh, S. Boye-Peronne, S. Soorkia, B. K. Cunha de Miranda, G. A. Garcia, L. Nahon, S. Chen, A. de la Lande, L. Poisson, B. Soep, *Phys. Chem. Chem. Phys.* **2018**, *20*, 11730–11739; b) K. Ishii, S.-i. Hoshino, N. Kobayashi, *Inorg. Chem.* **2004**, *43*, 7969–7971; c) M. Hoshino, Y. Kashiwagi, *J. Phys. Chem.* **1990**, *94*, 673–678.

[36] a) H. Iwamoto, K. Hori, Y. Fukazawa, *Tetrahedron* **2006**, *62*, 2789–2798; b) Y. Uemori, A. Nakatsubo, H. Imai, S. Nakagawa, E. Kyuno, *Inorg. Chem.* **1992**, *31*, 5164–5171; c) R. J. Abraham, S. C. M. Fell, K. M. Smith, *Org. Magn. Reson.* **1977**, *9*, 367–373.

[37] A. Stanger, *J. Phys. Chem. A* **2019**, *123*, 3922–3927.

[38] A reasonable definition is required to establish when $\Delta\delta_\infty$ has been achieved. Assuming that the accuracy of the NMR measurements is ± 0.001 ppm, $\Delta\delta_\infty$ is defined by fulfilment of the relationship $\Delta\delta r - \Delta\delta r' \leq 0.001$ ppm, i.e., $\Delta\delta_\infty$ has been achieved if the difference in chemical shifts at two distances, r and r' cannot be resolved by the NMR measurement.

[39] a) R. A. Al-Balushi, A. Haque, M. Jayapal, M. K. Al-Suti, J. Husband, M. S. Khan, J. M. Skelton, K. C. Molloy, P. R. Raithby, *Inorg. Chem.* **2016**, *55*, 10955–10967; b) N. Masaru, R. Masahiro, W. Masayoshi, S. Kohei, O. Naoya, *Bull. Chem. Soc. Jap.* **1997**, *70*, 737–744.

[40] a) N. Fukui, H. Yorimitsu, A. Osuka, *Chem. Eur. J.* **2016**, *22*, 18476–18483; b) N. Yoshida, T. Ishizuka, A. Osuka, D. H. Jeong, H. S. Cho, D. Kim, Y. Matsuzaki, A. Nogami, K. Tanaka, *Chem. Eur. J.* **2003**, *9*, 58–75.

[41] K. Ghebreyessus, S. M. Cooper, *Organometallics* **2017**, *36*, 3360–3370.

[42] S. J. Carrington, I. Chakraborty, J. R. Alvarado, P. K. Mascharak, *Inorg. Chim. Acta* **2013**, *407*, 121–125.

[43] Thermal reversion was also minimal upon standing at room temperature, although the experiment was not quantified.

[44] Photophysical studies of multiporphyrin arrays incorporating Ru-metalloporphyrins bearing a CO ligand suggested that these systems would be stable under mild irradiation (see ref. 32), while decarbonylation is well known under strong irradiation (refs. 20g, 35b, 35c). In the present case, no attempt was made to identify the product(s) of decarbonylation given the small amounts that were produced in the experiments.

Chapter 6

[1] W. A. Chalifoux, R. R. Tykwinski, *Nat. Chem.* **2010**, *2*, 967–971.

[2] M. Denis, S. M. Goldup, *Nat. Rev. Chem.* **2017**, *1*, 0061.

[3] a) M. Franz, J. A. Januszewski, F. Hampel, R. R. Tykwinski, *Eur. J. Org. Chem.* **2019**, 3503–

3512; b) L. D. Movsisyan, M. Franz, F. Hampel, A. L. Thompson, R. R. Tykwinski, H. L. Anderson, *J. Am. Chem. Soc.* **2016**, *138*, 1366–1376; c) M. Franz, J. A. Januszewski, D. Wendinger, C. Neiss, L. D. Movsisyan, F. Hampel, H. L. Anderson, A. Gorling, R. R. Tykwinski, *Angew. Chem. Int. Ed.* **2015**, *54*, 6645–6649.

[4]   E. T. Chernick, R. R. Tykwinski, *J. Phys. Org. Chem.* **2013**, *26*, 742–749.

[5]   A. Jolly, D. Miao, M. Daigle, J. F. Morin, *Angew. Chem. Int. Ed.* **2020**, *59*, 4624–4633.

[6]   B. Pigulski, N. Gulia, S. Szafert, *Eur. J. Org. Chem.* **2019**, 1420–1445.

[7]   T. Luu, R. McDonald, R. R. Tykwinski, *Org. Lett.* **2006**, *8*, 6035–6038.

[8]   a) W. Yang, R. Bam, V. J. Catalano, W. A. Chalifoux, *Angew. Chem. Int. Ed.* **2018**, *57*, 14773–14777; b) W. Yang, J. H. S. K. Monteiro, A. de Bettencourt-Dias, V. J. Catalano, W. A. Chalifoux, *Angew. Chem. Int. Ed.* **2016**, *55*, 10427–10430.

[9]   a) K. B. Jorgensen, *Molecules* **2010**, *15*, 4334–4358; b) F. B. Mallory, C. S. Wood, J. T. Gordon, *J. Am. Chem. Soc.* **1964**, *86*, 3094–3102.

[10]   C. S. Casari, M. Tommasini, R. R. Tykwinski, A. Milani, *Nanoscale* **2016**, *8*, 4414–4435.

[11]   X. Zhao, C. Huang, M. Gulcur, A. S. Batsanov, M. Baghernejad, W. Hong, M. R. Bryce, T. Wandlowski, *Chem. Mater.* **2013**, *25*, 4340–4347.

[12]   a) B. S. Basel, R. M. Young, M. D. Krzyaniak, I. Papadopoulos, C. Hetzer, Y. Gao, N. T. La Porte, B. T. Phelan, T. Clark, R. R. Tykwinski, M. R. Wasielewski, D. M. Guldi, *Chem. Sci.* **2019**, *10*, 11130–11140; b) A. Kunzmann, M. Gruber, R. Casillas, R. R. Tykwinski, R. D. Costa, D. M. Guldi, *Nanoscale* **2018**, *10*, 8515–8525; c) C. Hetzer, D. M. Guldi, R. R. Tykwinski, *Chem. Eur. J.* **2018**, *24*, 8245–8257; d) B. S. Basel, J. Zirzlmeier, C. Hetzer, S. R. Reddy, B. T. Phelan, M. D. Krzyaniak, M. K. Volland, P. B. Coto, R. M. Young, T. Clark, M. Thoss, R. R. Tykwinski, M. R. Wasielewski, D. M. Guldi, *Chem* **2018**, *4*, 1092–1111.

[13]   I. Papadopoulos, Y. Gao, C. Hetzer, R. R. Tykwinski, D. M. Guldi, *ChemPhotoChem* **2020**, *4*, 5168–5174.

[14]   Y. Gao, V. Walter, M. J. Ferguson, R. R. Tykwinski, *Chem. Eur. J.* **2020**, *DOI: 10.1002/chem.202002030*.

[15]   A. Mostad, C. Rømming, *Acta Chem. Scand.* **1971**, *25*, 3561–3568.

Chapter 7

[1]   J. Ranta, T. Kumpulainen, H. Lemmetyinen, A. Efimov, *J. Org. Chem.* **2010**, *75*, 5178–5194.

[2]   a) D. N. Coventry, A. S. Batsanov, A. E. Goeta, J. A. Howard, T. B. Marder, R. N. Perutz, *Chem. Commun.* **2005**, 2172–2174; b) A. G. Crawford, Z. Liu, I. A. Mkhalid, M. H. Thibault, N. Schwarz, G. Alcaraz, A. Steffen, J. C. Collings, A. S. Batsanov, J. A. Howard, T. B. Marder, *Chem. Eur. J.* **2012**, *18*, 5022–5035.

[3]   a) A. C. Spivey, T. Fekner, S. E. Spey, *J. Org. Chem.* **2000**, *65*, 3154–3159; b) O. S. Tee, M. Paventi, *Can. J. Chem.* **1983**, *61*, 2556–2562; c) L. Robke, T. Rodrigues, P. Schröder, D. J. Foley, G. J. L. Bernardes, L. Laraia, H. Waldmann, *Tetrahedron* **2018**, *74*, 4531–4537.

[4]   C. Eidamshaus, H.-U. Reissig, *Eur. J. Org. Chem.* **2011**, 6056–6069.

[5]   X. Yi, J. Chen, X. Xu, Y. Ma, *Synth. Commun.* **2017**, *47*, 872–877.

[6]   C. D. Campbell, R. L. Greenaway, O. T. Holton, P. R. Walker, H. A. Chapman, C. A. Russell,

G. Carr, A. L. Thomson, E. A. Anderson, *Chem. Eur. J.* **2015**, *21*, 12627–12639.

[7] X. Nie, G. Wang, *J. Org. Chem.* **2006**, *71*, 4734–4741.

[8] M. Turlington, Y. Du, S. G. Ostrum, V. Santosh, K. Wren, T. Lin, M. Sabat, L. Pu, *J. Am. Chem. Soc.* **2011**, *133*, 11780–11794.

[9] S. Eisler, N. Chahal, R. McDonald, R. R. Tykwinski, *Chem. Eur. J.* **2003**, *9*, 2542–2550.

[10] W. A. Chalifoux, R. R. Tykwinski, *Nat. Chem.* **2010**, *2*, 967–971.

[11] A. L. Spek, *Acta Crystallogr. C* **2015**, *71*, 9–18.

[12] K. Usami, E. Yamaguchi, N. Tada, A. Itoh, *Org. Lett.* **2018**, *20*, 5714–5717.

[13] J. P. Brand, J. Charpentier, J. Waser, *Angew. Chem. Int. Ed.* **2009**, *48*, 9346–9349.

[14] S. B. Kamptmann, R. Brückner, *Eur. J. Org. Chem.* **2013**, 6584–6600.

[15] R. Frei, J. Waser, *J. Am. Chem. Soc.* **2013**, *135*, 9620–9623.

[16] a) C. Eaborn, N. Farrell, J. L. Murphy, A. Pidcock, *J. Chem. Soc., Dalton Trans.* **1976**, 58–67; b) P. M. Treichel, K. P. Wagner, W. J. Knebel, *Inorg. Chim. Acta* **1972**, *6*, 674–676.

[17] F. Morandini, G. Consiglio, O. Piccolo, *Inorg. Chim. Acta* **1982**, *57*, 15–19.

[18] M. Krempe, R. Lippert, F. Hampel, I. Ivanovic-Burmazovic, N. Jux, R. R. Tykwinski, *Angew. Chem. Int. Ed.* **2016**, *55*, 14802–14806.

[19] R. Pelagalli, I. Chiarotto, M. Feroci, S. Vecchio, *Green Chem.* **2012**, *14*, 2251–2255.

[20] N. R. Ayyangar, S. N. Naik, K. V. Srinivasan, *Tetrahedron Lett.* **1989**, *30*, 7253–7256.

[21] M. E. Moustafa, P. D. Boyle, R. J. Puddephatt, *Can. J. Chem.* **2014**, *92*, 706–715.

[22] J. Strueben, P. J. Gates, A. Staubitz, *J. Org. Chem.* **2014**, *79*, 1719–1728.

[23] L.-X. Liao, F. Stellacci, D. V. McGrath, *J. Am. Chem. Soc.* **2004**, *126*, 2181–2185.

[24] O. K. Farha, C. D. Malliakas, M. G. Kanatzidis, J. T. Hupp, *J. Am. Chem. Soc.* **2010**, *132*, 950–952.

[25] I.-Y. Wu, J. T. Lin, J. Luo, S.-S. Sun, C.-S. Li, K. J. Lin, C. Tsai, C.-C. Hsu, J.-L. Lin, *Organometallics* **1997**, *16*, 2038–2048.

[26] J. S. Lindsey, R. W. Wagner, *J. Org. Chem.* **1989**, *54*, 828–836.

[27] C. Wang, K. V. Shalyaev, M. Bonchio, T. Carofiglio, J. T. Groves, *Inorg. Chem.* **2006**, *45*, 4769–4782.

[28] V. Walter, Y. Gao, N. Grzegorzek, M. Krempe, F. Hampel, N. Jux, R. R. Tykwinski, *Angew. Chem. Int. Ed.* **2019**, *58*, 494–498.

[29] A. R. Waterloo, R. Lippert, N. Jux, R. R. Tykwinski, *J. Coord. Chem.* **2015**, *68*, 3088–3098.